

# Shear in Reinforced Concrete Slabs under Concentrated Loads close to Supports

E.O.L. Lantsoght

# Propositions

Accompanying the Ph.D. Thesis

*Shear in Reinforced Concrete Slabs under Concentrated Loads close to Supports*

E.O.L. Lantsoght

1. The two-dimensional shear-carrying behaviour of one-way slabs under concentrated loads close to supports should be treated differently than the one-dimensional shear-carrying behaviour of beams.
2. By combining two-way quadrants and one-way strips, the Modified Bond Model bridges the gap between the one-way and two-way shear approaches.
3. The very large redistribution capacity of slabs is demonstrated, amongst others, by carrying out experiments on severely damaged and locally failed specimens that led, on average, to a capacity of about 80% of a virgin specimen.
4. The shear capacity of reinforced concrete members near to continuous supports is at least equal to the shear capacity near to simple supports, contrarily to the recommendations of NEN 6720:1995.
5. I can live with doubt, and uncertainty, and not knowing. I think it's much more interesting to live not knowing than to have answers which might be wrong. (Richard Feynman)
6. The educational system should support its students in their development as critical thinkers, not turn into a manufacturing line that spits out unidirectional individuals. Therefore, requesting a secondary school education based mostly on exact sciences as a prerequisite for engineering and science studies is utter nonsense.
7. The divide between Flanders and Wallonia can be observed in the media, where more attention is given to the US presidential elections than to the results of the local elections of the other half of the country.
8. Engineers need to master at least 3 languages: writing (action), math (quantity) and drawing (substance). (E.M. Hines, ASCE Structures Congress 2011)
9. The value of experimental work should not be evaluated purely economically, but should be weighed by taking into account its impact and spin-off on the field of study.
10. I have data, therefore I exist. (inspired by René Descartes)

*These propositions are regarded as opposable and defensible, and have been approved as such by the supervisor Prof. dr. ir. Dr.-Ing. e.h. J.C. Walraven*

# Stellingen

Behorende bij het proefschrift

*Shear in Reinforced Concrete Slabs under Concentrated Loads close to Supports*

E.O.L. Lantsoght

1. Het tweedimensionale afschuifdraagvermogen van in één richting dragende platen onder geconcentreerde belastingen nabij de opleggingen moet anders behandeld worden dan het eendimensionale afschuifdraagvermogen van balken.
2. Door in twee richtingen dragende kwadranten te combineren met stroken die in één richting dragen overbrugt het Modified Bond Model de kloof tussen de methodes voor pons en dwarskracht.
3. Het zeer grote vermogen tot herverdeling van platen is onder andere aangetoond door proeven uit te voeren op zwaar beschadigde en lokaal bezweken platen, waarbij gemiddeld een capaciteit van ongeveer 80% van een onbeschadigd proefstuk gehaald werd.
4. De dwarskrachtcapaciteit van gewapend betonnen elementen nabij doorgaande opleggingen is minstens gelijk aan de capaciteit nabij vrije opleggingen, in tegenstelling tot het NEN 6720:1995 voorschrift.
5. Ik kan leven met twijfel, en onzekerheid, en niet weten. Ik denk dat het veel interessanter is te leven met het niet weten dan met antwoorden die misschien verkeerd zijn. (Richard Feynman)
6. Het onderwijssysteem moet zijn studenten ondersteunen in hun ontwikkeling tot kritische denkers en mag niet veranderen in een fabriek voor eenzijdige individuen. Het vereisen van een middelbare schoolopleiding op basis van hoofdzakelijk wis- en wetenschappen als voorkennis voor een ingenieurs- of wetenschapsopleiding is daarom absolute nonsens.
7. De kloof tussen Vlaanderen en Wallonië kan gezien worden in de media, waarin meer aandacht besteed wordt aan de Amerikaanse presidentsverkiezingen dan aan de resultaten van de lokale verkiezingen in de andere helft van het land.
8. Ingenieurs moeten 3 talen beheersen: schrijven (actie), wiskunde (hoeveelheid) en tekenen (substantie). (E.M. Hines, ASCE Structures Congress 2011)
9. De waarde van experimenteel werk mag niet enkel zuiver economisch geëvalueerd worden, maar moet ook gewogen worden naar de impact en spin-off op de beschouwde discipline.
10. Ik heb data dus ik ben. (vrij naar René Descartes)

*Deze stellingen worden opponeerbaar en verdedigbaar geacht en zijn als zodanig goedgekeurd door de promotor Prof. dr. ir. Dr.-Ing. e.h. J.C. Walraven*

# **Shear in Reinforced Concrete Slabs under Concentrated Loads close to Supports**

*Het denken mag zich nooit onderwerpen,  
noch aan een dogma,  
noch aan een partij,  
noch aan een hartstocht,  
noch aan een belang,  
noch aan een vooroordeel,  
noch aan om het even wat,  
maar uitsluitend aan de feiten zelf,  
want zich onderwerpen betekent het einde van alle denken.*

(Henri Poincaré, 1909)

# **Shear in Reinforced Concrete Slabs under Concentrated Loads close to Supports**

## **Proefschrift**

ter verkrijging van de graad van doctor  
aan de Technische Universiteit Delft,  
op gezag van de Rector Magnificus prof.ir. K.C.A.M. Luyben,  
voorzitter van het College voor Promoties,  
in het openbaar te verdedigen

op vrijdag 14 juni 2013 om 12:30 uur  
door

**Eva Olivia Leontien LANTSOGHT**

Burgerlijk Ingenieur Bouwkunde, Vrije Universiteit Brussel  
Master of Science in Structural Engineering, Georgia Institute of Technology  
geboren te Lier, België

Dit proefschrift is goedgekeurd door de promotor:

Prof. dr. ir. J.C. Walraven

Copromotor: Dr. ir. C. van der Veen

Samenstelling promotiecommissie:

Rector Magnificus,	voorzitter
Prof. dr. ir. J.C. Walraven,	Technische Universiteit Delft, promotor
Dr. ir. C. van der Veen,	Technische Universiteit Delft, copromotor
Prof. dr. ir. D.A. Hordijk,	Technische Universiteit Delft
Prof. dr. P.E. Regan,	University of Westminster
Prof. ir. A.C.W.M. Vrouwenfelder,	Technische Universiteit Delft
Dr. ir. A. de Boer,	Rijkswaterstaat
Prof. Dr.-Ing. J. Hegger,	Rheinisch-Westfälische Technische Hochschule Aachen
Prof. dr. ir. J.G. Rots	Technische Universiteit Delft, reservelid

ISBN 978-90-8891-632-8

Printed by Uitgeverij BOXPress

Cover design: Uitgeverij BOXPress

Published by: Uitgeverij BOXPress, 's-Hertogenbosch



© 2013 E.O.L. Lantsoght. Some rights reserved.

*This work is licensed under a Creative Commons Attribution-NonCommercial-ShareAlike 3.0 Unported License. You are free to share and to remix, under the conditions of attribution (you must attribute the work to the author), non-commercial (you may not use this work for commercial purposes) and share alike (if you alter, transform, or build upon this work, you may distribute the resulting work only under the same or similar license to this one), with the understanding that any of the above conditions can be waived if you get permission from the copyright holder.*

## **Summary**

### **Shear in Reinforced Concrete Slabs under Concentrated Loads close to Supports**

In this thesis, the shear capacity of reinforced concrete slabs under concentrated loads near to supports is investigated based on a review of the literature, a series of experiments and the statistical analysis thereof and a theoretical study. The goal is to apply the insights of the research to the assessment practice for reinforced concrete slab bridges subjected to composite dead load and live loads. Therefore, the application to existing slab bridges is studied. Additional attention is paid to the horizontal load distribution of concentrated loads on slabs, to determine over which width (the so-called effective width in shear) the shear force can be distributed at the support.

The literature review in Chapter 2 introduces the problem of beam shear in the way it has been studied in beams, and punching shear as it has been studied on slab-column models. Both shear mechanisms are studied, as the problem of a one-way slab under concentrated loads close to supports occurs in the transition zone between beam shear and punching shear. The concept of an effective width for wide beams and slabs in shear is introduced, and different strategies for determining the effective width from practice and from the literature are cited. The literature review chapter serves as a basis for the slab shear database that is developed as a part of this research, and can be found in Annex 1. An overview of 215 experiments on slabs and wide beams in shear under concentrated loads as well as line loads is gathered in this database.

The experiments are described in Chapter 3 and discussed in Chapter 4. A total of 38 specimens (26 slabs of  $2,5\text{m} \times 5\text{m} \times 0,3\text{m}$  and 12 slab strips with a variable width and  $5\text{m} \times 0,3\text{m}$ ) are tested, resulting in 156 reported experiments. In Chapter 3, the test setup, the measurement frame and the boundary conditions are described. The properties of the specimens, with regard to the reinforcement layout and the cube concrete compressive strength at the age of testing, are given. The maximum loads, resulting shear force at the support and observed failure mode of all experiments are tabulated. A selection of experiments is described in further detail. These results are then analysed with regard to the tested parameters in Chapter 4.

The observations from the experiments are compared in Chapter 4 to the knowledge of shear in beams from the literature, and used as a starting point to describe the behaviour of slabs under a concentrated load close to the support failing in shear. The geometric properties are found to have the largest influence on the capacity: the size of the loading plate, the distance between the load and the support and the overall width. Surprisingly, the capacity of heavily damaged and locally failed slabs is still on average  $\pm 80\%$  of the capacity of an undamaged specimen. The moment distribution in the shear span influences the shear capacity, resulting in higher observed capacities at a continuous

## *Summary*

support. In slabs reinforced with plain bars, anchorage failures could occur and in slabs supported by flexible bearings, punching of the support was a possible failure mechanism. No conclusions can be given with regard to the role of the concrete compressive strength, as over the tested range no significant influence on the shear capacity could be observed. The hypothesis of superposition for concentrated loads over their effective width to distributed loads over the full slab width is experimentally verified.

Based on the Bond Model for concentric punching shear as developed by Alexander and Simmonds (1992), the Modified Bond Model is developed in Chapter 5, as a mechanical model for determining the capacity of one-way slabs under concentrated loads near to supports. The Modified Bond Model is applicable as well to non-concentric, non-axis-symmetric conditions, to loads close to the support, near the edge, and to slabs not supported over their full width. By studying two-way shear force transfer on quadrants, influenced by their geometry, and one-way shear transfer on strips, the Modified Bond Model combines elements of one-way and two-way shear as necessary for one-way slabs under a concentrated load. To take into account the lower bond capacity in slabs reinforced with plain bars (as used in the existing Dutch slab bridges built before 1963), an empirical factor is introduced. Another element of empiricism is that the shear capacity of the strips is expressed based on the inclined cracking shear load from the ACI 318-08 code, as in the original Bond Model. The comparison of the Modified Bond Model to the experimental results shows a better agreement between the theory and the experiments and a better performance over the ranges of important tested parameters than when using NEN-EN 1992-1-1:2005. A study of the distribution of the results shows that the 5% lower bound of the ratio between the experimental shear capacities and the maximum loads predicted by the Modified Bond Model is still at the safe side, and thus the method can be applied for design.

A comparison between the experimental results and design codes is given in Chapter 6, along with parameter studies that address how the tested parameters are taken into account in the codes and if this corresponds to the experiments. A traditional statistical analysis, based on the assumption of a normal distribution, is carried out for the ratio of the experimental results to the predicted values. This comparison shows that the method for one-way slabs under a concentrated load close to the support as developed by Regan (1982), the Modified Bond Model and NEN-EN 1992-1-1:2005 with an effective width based on the assumption of load spreading from the far side of the loading plate to the face of the support lead to the best results. Subsequently, a statistical analysis is executed based on the cumulative distribution function of the experimental to calculated results. A lognormal distribution is shown to most closely resemble the distribution function from this ratio in the experiments. Monte Carlo simulations, in which the ratio of test values to predicted results as well as the material properties are considered as random variables, are used to propose an extension to the formula from NEN-EN 1992-1-1:2005. The required

## *Summary*

reliability level used for the repair level of assessment as defined by NEN 8700:2011 is  $\beta_{rel} = 3,8$  (and 3,6 for bridges built before April 1<sup>st</sup> 2012). The resulting code extension proposal follows the basic assumptions of the Eurocodes.

The application to existing reinforced concrete slab bridges that have an insignificant skew angle is treated in Chapter 7. This chapter first outlines how the prescribed composite dead load (self-weight and wearing surface) and live loads (distributed lane load and truck loads) are implemented into a “Quick Scan” method “QS-EC2”, based on the analysis of the experiments with regard to NEN-EN 1992-1-1:2005 and the resulting recommendations. This method is then used for determining the “unity check” (ratio of design shear force over design shear capacity) of nine cases of solid slab bridges owned by the Dutch Ministry of Infrastructure and the Environment, an example case from the Manual of Bridge Evaluation and a set of existing frame bridges from the United States (in Annex 5). For comparison, a Quick Scan based on the Dutch recommendations for concrete structures NEN 6720:1995 “QS-VBC” and the North American practice (AASHTO LRFD and AASHTO LRFR) “QS-AASHTO” are developed as well. The improvement in the filtering capacity of the Quick Scan when implementing the recommendations from the research is shown.

An extensive overview of all conclusions from this research, its original contributions, the resulting recommendations and possibilities for future research are given in Chapter 8.

## *Summary*

## **Samenvatting**

### **Afschuiving in gewapend betonnen platen onder geconcentreerde belastingen nabij opleggingen**

In dit proefschrift is de afschuifcapaciteit van gewapend betonnen platen onder geconcentreerde belastingen nabij de opleggingen onderzocht op basis van een literatuurstudie, op basis van een serie experimenten en de statistische verwerking hiervan, en op basis van een theoretische studie. Het doel is om de inzichten van het onderzoek toe te passen in de praktijk van het beoordelen van bestaande betonnen plaatbruggen belast met het eigengewicht, de rustende belasting en de mobiele lasten. De toepassing op bestaande plaatbruggen is dan ook onderzocht. Bijkomende aandacht is besteed aan de horizontale lastspreiding van geconcentreerde belastingen op platen, om de breedte te bepalen (de zogenaamde effectieve breedte voor afschuiving) waarover de schuifkracht aan de oplegging gespreid kan worden bij het ontwerp.

De literatuurstudie in Hoofdstuk 2 leidt het probleem in van afschuiving in balken zoals het tot heden in balkproeven bestudeerd is, en het probleem van pons zoals het in plaat-kolomverbindingen bestudeerd is. Deze beide mechanismen van afschuiving zijn bestudeerd, omdat het probleem van afschuiving in platen onder geconcentreerde belastingen nabij opleggingen zich bevindt in het overgangsgebied tussen afschuiving (in één richting) en pons (afschuiving in twee richtingen). Het principe van de effectieve breedte voor brede balken en platen belast op afschuiving is geïntroduceerd, en verschillende mogelijkheden om de effectieve breedte te bepalen uit de praktijk en de literatuur zijn geciteerd. Het hoofdstuk met de literatuurstudie vormt de basis voor de database van platen en brede balken belast op afschuiving, welke als onderdeel van dit onderzoek opgesteld is, en die in Annex 1 opgenomen is. Een overzicht met 215 proeven op platen en brede balken belast op afschuiving door geconcentreerde lasten en lijnlasten is gegeven in deze database.

De experimenten zijn in Hoofdstuk 3 beschreven en besproken in Hoofdstuk 4. In totaal zijn 38 proefstukken (platen van  $2,5\text{m} \times 5\text{m} \times 0,3\text{m}$  en plaatstroken met een variabele breedte en  $5\text{m} \times 0,3\text{m}$ ) getest in 156 proeven. Hoofdstuk 3 beschrijft de proefopstelling, de metingen en de randvoorwaarden. De eigenschappen van de proefstukken zijn weergegeven, en in het bijzonder de wapening en de kubusdruksterkte van het beton op het ogenblik van beproeven. De maximale last, de resulterende schuifkracht aan de oplegging en de bezwijkvorm voor alle proeven zijn in tabellen opgenomen. Een selectie van proeven is uitgebreider besproken. Deze resultaten zijn vervolgens in Hoofdstuk 4 geanalyseerd in het licht van de beproefde parameters.

De waarnemingen gedaan tijdens de experimenten zijn in Hoofdstuk 4 vergeleken met de kennis van afschuiving in balken uit de literatuur, en deze vormen het vertrekpunt om het gedrag te beschrijven van op afschuiving bezwijkende platen onder geconcentreerde

## *Samenvatting*

belastingen nabij de opleggingen. De geometrische eigenschappen blijken de grootste invloed op de capaciteit te hebben: de grootte van de lastplaat, de afstand tussen de last en de oplegging en de totale breedte. Het wekte verbazing dat het draagvermogen van zwaar beschadigde en lokaal bezwaken platen onderworpen aan herbelasting met een andere belastingscombinatie gemiddeld  $\pm 80\%$  bedraagt van de capaciteit van een onbeschadigd proefstuk. De momentenverdeling tussen de belasting en de oplegging beïnvloedt de afschuifcapaciteit, wat leidt tot hogere capaciteiten in afschuiving aan de doorgaande oplegging dan aan de vrije oplegging. In platen met gladde staven werd bezwijken van de verankering waargenomen en voor de platen op rubberen oplegblokken werd bezwijken door het ponsen van een oplegpunt waargenomen. Over de invloed van de betondruksterkte op de afschuifcapaciteit kunnen geen conclusies gegeven worden, omdat voor de beproefde betondruksterkteklassen geen significante invloed op het draagvermogen waargenomen werd. De hypothese van superpositie voor geconcentreerde belastingen over hun effectieve breedte met verdeelde belastingen over de volledige breedte van de plaat is bevestigd met de proefresultaten.

Gebaseerd op het Bond Model voor concentrische pons dat door Alexander en Simmonds (1992) ontwikkeld werd, is in Hoofdstuk 5 het Modified Bond Model ontwikkeld voor het bepalen van het draagvermogen van in één richting dragende platen belast met geconcentreerde belastingen nabij opleggingen. Het Modified Bond Model is toepasbaar voor excentrische belastingen, asymmetrische randvoorwaarden, belastingen nabij de oplegging, nabij de vrije zijde en voor platen die niet over de volledige breedte ondersteund zijn. Het Modified Bond Model combineert elementen van afschuiving in één en twee richtingen zoals benodigd voor in één richting dragende platen onder een geconcentreerde belasting. Deze combinatie is verwerkt in het Modified Bond Model door het beschrijven van de afschuiving in twee richting op kwadranten, bepaald door hun geometrie, en door het beschrijven van de afschuiving in één richting op stroken. Om de ondergrens van het draagvermogen te bepalen voor platen die gewapend zijn met gladde staven (zoals toegepast in de bestaande betonnen plaatbruggen die voor 1963 gebouwd zijn), is een empirische factor bepaald. Een bijkomend element van empirie is dat het afschuifdraagvermogen van de stroken uitgedrukt wordt op basis van de dwarskracht bij het ontstaan van de dwarskrachtscheur zoals deze in de ACI 318-08 norm gegeven is. Deze aanpak werd ook in het originele Bond Model toegepast. De vergelijking tussen het Modified Bond Model en de proefresultaten toont een betere overeenkomst alsook een betere weergave van de beschouwde parameters dan wanneer NEN-EN 1992-1-1:2005 gebruikt wordt. Een analyse van de verdeling van de resultaten toont dat de 5% ondergrens van de verhouding tussen de proefresultaten en de waarde berekend met het Modified Bond Model aan de veilige kant is, en dat de methode dus voor ontwerp toegepast kan worden.

Een vergelijking tussen de proefresultaten en de resultaten verkregen met de rekenmethodes en normen is gegeven in Hoofdstuk 6, als ook een overzicht van de manier

## Samenvatting

waarop de beproefde parameters in de beschouwde rekenmethodes verwerkt zijn, en hoe dit overeenstemt met de invloed van deze parameters zoals deze in de proeven waargenomen is. Een traditionele statistische analyse, gebaseerd op de aanname van een normaalverdeling voor de verhouding tussen de proefresultaten en de berekende waarden, is uitgevoerd. Deze vergelijking toont dat de beste resultaten gevonden worden met Regan's methode (1982) voor het bepalen van het afschuifdraagvermogen van een plaat onder geconcentreerde belastingen nabij opleggingen, met het Modified Bond Model en met NEN-EN 1992-1-1:2005 in combinatie met een effectieve breedte gebaseerd op een aanname voor de horizontale lastspreiding van de verre zijde van de lastplaat tot de dag van de oplegging. Vervolgens is een statistische analyse uitgevoerd op basis van de cumulatieve verdelingsfunctie van de verhouding tussen de proefresultaten en de berekende waarden. Een lognormaalverdeling sluit het best aan bij de gevonden verdelingsfunctie op basis van deze verhouding uit de proeven. Monte Carlo simulaties, waarin de verhouding van de proefresultaten tot de berekende waarden en de materiaaleigenschappen als stochasten beschouwd zijn, zijn gebruikt om een uitbreiding van de afschuifformule van NEN-EN 1992-1-1:2005 voor te stellen. De vereiste betrouwbaarheidsindex voor het verbouwniveau voor het beoordelen van bestaande constructies zoals gedefinieerd in NEN 8700:2011 bedraagt  $\beta_{rel} = 3,8$  (en 3,6 voor kunstwerken gebouwd voor 1 april 2012). De voorgestelde uitbreidingsformule is in lijn met de aannames en veiligheidsfilosofie van de Eurocodes.

De toepassing van de inzichten van het onderzoek op quasi-rechte bestaande betonnen plaatbruggen is opgenomen in Hoofdstuk 7. Dit hoofdstuk legt eerst uit hoe de voorgeschreven belastingen (eigengewicht, rustende belasting, verdeelde verkeersbelasting en aslasten) toegepast worden in de "Quick Scan" methode "QS-EC2", gebaseerd op de vergelijking tussen de proefresultaten en NEN-EN 1992-1-1:2005 en de daaruit volgende aanbevelingen. Deze methode is vervolgens gebruikt voor het bepalen van een "unity check" (verhouding tussen de schuifspanning ten gevolge van de voorgeschreven belastingen en het afschuifdraagvermogen) voor negen gevallen van bestaande plaatbruggen beheerd door Rijkswaterstaat, een voorbeeld uit de Noord-Amerikaanse Manual of Bridge Evaluation en een aantal bestaande raamwerkbruggen uit de Verenigde Staten (in Annex 5). Ter vergelijking met de vroegere Nederlandse praktijk is "QS-VBC" gebaseerd op het vroegere Nederlandse voorschrift voor betonconstructies NEN 6720:1995 ontwikkeld. Bovendien is "QS-AASHTO" ontwikkeld, gebaseerd op de Noord-Amerikaanse praktijk (AASHTO LRFD en AASHTO LRFR). Het vermogen van de Quick Scan om dwarsdoorsnedes die mogelijk kritiek zijn voor afschuiving aan te duiden is verbeterd indien de aanbevelingen uit het onderzoek toegepast worden.

Een uitgebreid overzicht van alle conclusies uit dit onderzoek, de originele bijdragen en de voorgestelde aanbevelingen als ook mogelijkheden voor toekomstig onderzoek zijn weergegeven in Hoofdstuk 8.

## *Samenvatting*

**Table of Contents**

Summary..... i  
    Shear in Reinforced Concrete Slabs under Concentrated Loads close to Supports ..... i  
Samenvatting ..... v  
    Afschuiving in gewapend betonnen platen onder geconcentreerde belastingen nabij opleggingen..... v  
Table of Contents..... ix  
List of notations ..... xv  
    Greek lower case ..... xv  
    Greek upper case ..... xviii  
    Roman lower case ..... xviii  
    Roman upper case ..... xxiii  
    Abbreviations ..... xxviii  
1 Introduction ..... 1  
    1.1 Background ..... 1  
    1.2 Scope of the research: the shear problem ..... 1  
    1.3 Aim of the research ..... 2  
    1.4 Research strategy and thesis outline ..... 2  
    1.5 Impact of the research ..... 5  
2 Shear capacity of reinforced concrete members without shear reinforcement ..... 9  
    2.1 Introduction ..... 9  
    2.2 Scope ..... 9  
        2.2.1 Slab bridges..... 9  
        2.2.2 Forces in slabs..... 10  
        2.2.3 Existing concrete bridges ..... 10  
        2.2.4 Wheel loading ..... 10  
    2.3 Mechanisms of shear transfer ..... 11  
        2.3.1 Concrete compression zone ..... 11  
        2.3.2 Residual tension at crack ..... 12  
        2.3.3 Aggregate interlock..... 12  
        2.3.4 Dowel action ..... 14  
        2.3.5 Arching action/ Strut action ..... 15  
        2.3.6 Discussion..... 16  
    2.4 Shear in slabs..... 16  
        2.4.1 One-way shear models ..... 16  
        2.4.2 Two-way shear models ..... 21  
        2.4.3 Similarities, transition zone and distinction ..... 28  
        2.4.4 Effective width in wide beams and slabs ..... 29  
    2.5 Experiments and database ..... 31

## *Table of Contents*

2.6	Code provisions .....	33
2.7	Conclusions .....	34
2.7.1	Summary .....	34
2.7.2	Discussion .....	35
2.7.3	Conclusions and outlook .....	36
3	Experiments .....	39
3.1	Introduction .....	39
3.2	Test setup .....	39
3.2.1	Slabs under a concentrated load .....	39
3.2.2	Slabs under a combination of loads .....	42
3.3	Specimens .....	43
3.4	Results .....	48
3.4.1	Overview of experimental results .....	48
3.4.2	Description of selected experiments .....	56
3.5	Conclusions .....	61
4	Parameter analysis .....	63
4.1	Introduction .....	63
4.2	Size of the loading plate .....	63
4.2.1	Background .....	63
4.2.2	Experimental observations .....	64
4.2.3	Explanation .....	65
4.3	Effect of predamaging .....	66
4.3.1	Role of precracking on bearing capacity of structural concrete elements as found in literature .....	66
4.3.2	Experimental observations .....	66
4.3.3	Explanation .....	68
4.4	Transverse flexural reinforcement .....	68
4.4.1	Background .....	68
4.4.2	Experimental observations .....	68
4.4.3	Explanation .....	70
4.5	Moment distribution at support .....	70
4.5.1	Background .....	70
4.5.2	Experimental observations .....	71
4.5.3	Explanation .....	72
4.6	Distance between load and support .....	73
4.6.1	Background .....	73
4.6.2	Experimental observations .....	74
4.6.3	Explanation .....	76
4.7	Concrete compressive strength .....	76

*Table of Contents*

4.7.1	Background.....	76
4.7.2	Experimental observations.....	77
4.7.3	Explanation.....	78
4.8	Overall width and effective width.....	79
4.8.1	Background.....	79
4.8.2	Experimental observations.....	79
4.8.3	Explanation.....	81
4.9	Reinforcement type.....	82
4.9.1	Background.....	82
4.9.2	Experimental observations.....	82
4.9.3	Explanation.....	83
4.10	Line supports compared to elastomeric bearings.....	85
4.10.1	Background.....	85
4.10.2	Experimental observations.....	85
4.10.3	Explanation.....	87
4.11	Combination of loads.....	87
4.11.1	Background.....	87
4.11.2	Experimental observations.....	89
4.11.3	Explanation.....	91
4.12	Conclusions.....	92
5	Modified Bond Model.....	95
5.1	Introduction.....	95
5.2	Alexander’s Bond Model.....	96
5.2.1	Motivation.....	96
5.2.2	Description of the Bond Model.....	98
5.3	Development of the Modified Bond Model.....	109
5.3.1	Concentrated loads close to the support.....	109
5.3.2	Loads close to the continuous support.....	116
5.3.3	Loads at and close to the edge.....	119
5.3.4	Application to slabs on bearings.....	124
5.3.5	Extension to plain bars.....	130
5.3.6	Resulting Modified Bond Model.....	133
5.3.7	Verification with S19 – S26 and extension for slabs under a combination of loads.....	137
5.4	Comparison between experimental results and Modified Bond Model.....	145
5.4.1	General comparison.....	145
5.4.2	Comparison with existing methods.....	146
5.4.3	Verification with experiments from the literature.....	148
5.4.4	Parameter analysis.....	150

## *Table of Contents*

5.5	Discussion of Modified Bond Model .....	154
5.5.1	Discussion of scope .....	154
5.5.2	Advantages of the Modified Bond Model.....	157
5.5.3	Limitations of the Modified Bond Model .....	158
5.6	Conclusions .....	160
6	Statistical Evaluation of Design Methods .....	161
6.1	Introduction .....	161
6.2	Comparison to design methods.....	161
6.2.1	Comparison between experimental results and design methods .....	161
6.2.2	Comparison between experimental results from database and Eurocode 2	177
6.3	Influence of parameters on design methods .....	180
6.3.1	Size of the loading plate.....	180
6.3.2	Loading sequence .....	181
6.3.3	Transverse flexural reinforcement .....	181
6.3.4	Moment distribution at support.....	183
6.3.5	Distance between load and support.....	184
6.3.6	Concrete compressive strength .....	186
6.3.7	Overall width and effective width.....	186
6.3.8	Reinforcement type.....	187
6.3.9	Line supports compared to elastomeric bearings .....	187
6.3.10	Combination of loads .....	187
6.4	Probabilistic approach .....	187
6.4.1	Introduction.....	187
6.4.2	Studied limit state function .....	188
6.4.3	Assumed distributions.....	189
6.4.4	Results from simulations.....	194
6.4.5	Code extension proposal .....	195
6.4.6	Applicability of Modified Bond Model for design .....	201
6.5	Conclusions .....	204
7	Application to slab bridges and case studies .....	207
7.1	Introduction .....	207
7.2	Loads and load factors.....	207
7.2.1	Self-weight and superimposed loads.....	207
7.2.2	Live loads.....	210
7.2.3	Load factors .....	213
7.2.4	Static indeterminacy.....	214
7.2.5	Influence of skew angle .....	215
7.3	Quick Scan approach.....	217
7.3.1	Background.....	217

## *Table of Contents*

7.3.2	Overview of model assumptions.....	217
7.3.3	Overview of geometric and material assumptions .....	222
7.3.4	Comparison to Quick Scan approach according to other codes .....	224
7.4	Results from 10 selected cases .....	226
7.4.1	Introduction.....	226
7.4.2	Results according to QS-EC2 .....	226
7.4.3	Comparison to results according to QS-VBC and QS-AASHTO.....	228
7.4.4	Conclusions.....	231
7.5	Conclusions .....	232
7.5.1	Summary .....	232
7.5.2	Recommendations and outlook for practicing engineers .....	233
8	Conclusions and Outlook .....	235
8.1	Overview of main contributions to knowledge on shear in one-way slabs .....	235
8.2	Summary of conclusions and research findings .....	235
8.2.1	Force transfer in slab bridges .....	235
8.2.2	Development of the slab shear database .....	237
8.2.3	Slab shear experiments .....	237
8.2.4	Influence of parameters on shear capacity of slabs.....	239
8.2.5	The Modified Bond Model .....	240
8.2.6	Comparison between methods and experimental results .....	241
8.2.7	Code extension proposal based on statistical analysis .....	242
8.2.8	Application to practice: Quick Scan approach.....	243
8.3	Recommendations for assessment and design .....	244
8.4	Future work .....	247
8.4.1	Future experimental work.....	247
8.4.2	Future theoretical research.....	247
8.4.3	Future improvement of the assessment practice .....	248
	References .....	249
	Annex 1: Slab Shear Database.....	265
	Annex 2: Example application of the Modified Bond Model.....	277
	Annex 3: Comparison between experiments and design methods .....	285
	Annex 4: Comparison between experiments from slab shear database and NEN-EN 1992-1-1:2005 .....	291
	Annex 5: Results of North American slab bridges checked by the Quick Scan .....	299
	Acknowledgements.....	301
	Curriculum Vitae .....	303

*Table of Contents*

**List of notations**

**Greek lower case**

$\alpha_{AS}$	angle of inclination of the shear strut in the three-dimensional strut-and-tie model
$\alpha_{DL}$	correction factor on the shear stress for the statical indeterminacy on the dead load
$\alpha_{Gumbel}$	factor that determines the Gumbel distribution
$\alpha_{MBM}$	the factor from the Modified Bond Model to reduce the capacity of a strip influenced by the geometry
$\alpha_M$	correction factor on moment for statical indeterminacy
$\alpha_{MDL}$	correction factor on moment for statical indeterminacy for self-weight
$\alpha_{MUDL}$	correction factor on moment for statical indeterminacy for the distributed lane load
$\alpha_{Qi}$	the factor for the design truck or tandem in the $i$ -th lane as given in NEN-EN 1991-2:2003
$\alpha_{qi}$	the factor for the lane load in the $i$ -th lane as given in NEN-EN 1991-2:2003
$\alpha_{Regan}$	factor that increases the punching capacity at the continuous support in Regan's method
$\alpha_{red}$	reduction factor for the case of a combination of loads, when using the Modified Bond Model
$\alpha_{rel}$	reduction factor for required reliability level in case of different load or resistance situations
$\alpha_{Trucki}$	correction factor for the statical indeterminacy on the AASHTO design truck in the $i$ -th lane
$\alpha_{TSi}$	correction factor for the statical indeterminacy on the design truck in the $i$ -th lane
$\alpha_{UDL}$	correction factor on the shear stress for the statical indeterminacy on the uniformly distributed lane load
$\beta$	the reduction factor on the loads to take direct load transfer into account
$\beta_{new}$	the reduction factor on the loads to take direct load transfer into account for concentrated loads on slabs
$\beta_{nolim}$	the reduction factor on the loads to take direct load transfer into account in which the lower bound at $d/2$ is omitted
$\beta_{rel}$	the reliability index
$\beta_{Theoret}$	factor used to determine the influence of the skew angle as used by Theoret et al. (2012)
$\beta_{400}$	the reduction factor for $a = 400\text{mm}$

### List of notations

$\beta_{600}$	the reduction factor for $a = 600\text{mm}$
$\gamma_c$	the material factor for concrete = 1,5
$\gamma_{DL}$	the load factor for the dead load = 1,15
$\gamma_{LL}$	the load factor for the live load = 1,3
$\gamma_m$	the material factor for concrete
$\gamma_1$	the skewness of the distribution of a series of data
$\gamma_2$	the kurtosis of the distribution of a series of data
$\varepsilon$	the standard deviation of the natural logarithm of a series of data
$\varepsilon_c$	the strain in the concrete
$\varepsilon_{ct}$	the strain at maximum tension, after the peak
$\varepsilon_{ctu}$	the tensile strain in the concrete
$\lambda$	the mean value of the natural logarithm of a series of data
$\lambda_v$	the shear slenderness as used in NEN 6720:1995
$\lambda_r$	the reduction factor for slabs not supported over their full width
$\mu$	the mean value of a series of data
$\theta$	tangential axis in polar coordinates
$\xi_{MBM}$	factor that takes direct load transfer into account in the Modified Bond Model
$\xi_s$	the size effect factor
$\xi_{prop}$	the proposed enhancement factor
$\rho$	the reinforcement ratio for the layer of reinforcement considered ( $\rho_l$ or $\rho_t$ )
$\rho_l$	the longitudinal reinforcement ratio
$\rho_{lbot}$	the bottom longitudinal reinforcement ratio
$\rho_{ltop}$	the top longitudinal reinforcement ratio
$\rho_{neg}$	the reinforcement ratio of the sagging moment reinforcement in the load-carrying strip (Modified Bond Model)
$\rho_{neg,x}$	the reinforcement ratio of the sagging moment reinforcement in the $x$ -direction strip
$\rho_{neg,y}$	the reinforcement ratio of the sagging moment reinforcement in the $y$ -direction strip
$\rho_{pos}$	the reinforcement ratio of the hogging moment reinforcement in the load-carrying strip (Modified Bond Model)
$\rho_{pos,x}$	the reinforcement ratio of the hogging moment reinforcement in the $x$ -direction strip
$\rho_{pos,y}$	the reinforcement ratio of the hogging moment reinforcement in the $y$ -direction strip
$\rho_t$	the transverse flexural reinforcement ratio
$\rho_{tot}$	the total reinforcement ratio, as the geometric mean of the reinforcement in the longitudinal and transverse direction

### List of notations

$\sigma$	the normal stress
$\sigma_c$	the stress in the concrete
$\sigma_{cp}$	the axial stress on the cross-section
$\sigma_{pu}$	the normal stress at the contact surface between the aggregate and the matrix material
$\sigma_s$	the standard deviation of a set of data
$\tau$	the shear stress
$\tau_{ACI}$	the shear capacity determined based on ACI 318-08
$\tau_{add}$	the shear stress due to the self-weight of the slab and the prestressing force
$\tau_{calc}$	the calculated shear capacity
$\tau_{combination}$	the shear stress for an experiment under a combination of loads, $\tau_{conc} + \tau_{line}$
$\tau_{conc}$	the contribution of the concentrated load to the shear stress at the support
$\tau_d$	the shear stress at the support resulting from the composite dead load and the live loads according to NEN 8701:2011
$\tau_{exp}$	the shear stress at the support at failure
$\tau_{exp,beff1}$	the shear stress at the support, resulting from shear stress due to the concentrated load distributed over $b_{eff1}$ , superposed to the shear stress due to the self-weight, force in the prestressing bars, line load and self-weight of the line load distributed over the full width $b$
$\tau_{exp,EC,beff1}$	the shear stress at the support, resulting from shear stress due to the concentrated load distributed over $b_{eff1}$ , superposed to the shear stress due to the self-weight, force in the prestressing bars, line load and self-weight of the line load distributed over the full width $b$ , in which the contribution of loads close to the support is reduced by $\beta = a\sqrt{2}d_l$
$\tau_{exp,EC,beff2}$	the shear stress at the support, resulting from shear stress due to the concentrated load distributed over $b_{eff2}$ , superposed to the shear stress due to the self-weight, force in the prestressing bars, line load and self-weight of the line load distributed over the full width $b$ , in which the contribution of loads close to the support is reduced by $\beta = a\sqrt{2}d_l$
$\tau_{line}$	the contribution of the line load to the shear stress
$\tau_{tot,cl}$	the shear stress for an experiment under a concentrated load, taking into account distributed loads such as the self-weight, $\tau_{conc} + \tau_{add}$
$\tau_{tot,cl,corr}$	the corrected value of $\tau_{tot,cl}$ that takes into account the difference in the concrete compressive strength of the tested specimens
$\tau_{pu}$	the shear stress at the contact surface between the aggregate and the matrix material
$\tau_u$	the shear capacity resulting from NEN 6720:1995, used in the Quick Scan

### *List of notations*

$\tau_{VBC}$	the shear capacity determined based on NEN 6720:1995, used in the experiments
$\phi$ or $\phi$	the diameter of the reinforcement bar
$\phi_{top}$	diameter of the top reinforcement
$\phi_{AASHTO}$	the resistance factor used in AASHTO LRFD
$\chi_i$	the reduction factor from the Modified Bond Model to take into account the influence of the geometry on the capacity of the considered strip, depending on the factors $\alpha_{MBM}$
$\psi$	rotation of slab
$\psi(s)$	slab rotations as a function of the distance along the control perimeter

### **Greek upper case**

$\Delta$	the shear displacement or slip
$\Phi$	normal distribution function

### **Roman lower case**

$a$	the centre-to-centre distance between the load and the support
$a/d_l$	the shear span-to-depth ratio
$a_{i,j}$	the centre-to-centre distance between the support and the tyre contact area from the $j$ -th axle of the $i$ -th design truck
$a_{Beta}$	factor that determines the interval on which the general Beta distribution is described
$a_v$	the clear shear span, the face-to-face distance between the load and the support
$a_v/d_l$	the clear shear span-to-depth ratio
$a_{vi,j}$	the face-to-face distance between the support and the tyre contact area from the $j$ -th axle of the $i$ -th design truck
$a_{v400}$	the clear shear span that is associated with $a = 400\text{mm}$
$a_{v600}$	the clear shear span that is associated with $a = 600\text{mm}$
$a_x$	contact area between aggregate and matrix material, $x$ -direction
$a_y$	contact area between aggregate and matrix material, $y$ -direction
$b$	the member width
$b_5$	the effective width based on the measurements of the reaction force at failure – failure was the fifth identified step in time during the analysis, hence the subscript “5”
$b_{5st}$	the effective width based on the measurements of the reaction force at failure for slabs supported by steel bearings
$b_{5el}$	the effective width based on the measurements of the reaction force at failure for slabs supported by elastomeric bearings

### *List of notations*

$b_{Beta}$	factor that determines the interval on which the general Beta distribution is described
$b_{edge}$	the width of the edge of the viaduct
$b_{eff}$	the effective width in shear
$b_{eff1}$	the effective width based on the load spreading method as used in Dutch practice
$b_{eff2}$	the effective width based on the load spreading method as used in French practice
$b_{eff,axle}$	the effective width associated with the entire axle
$b_{eff,i,j}$	the effective width associated with the $i$ -th truck, $j$ -th axle
$b_{eff,load1}$	the effective width associated with the first wheel load of the axle
$b_{eff,load2}$	the effective width associated with the second wheel load of the axle
$b_{load}$	the width of the load; taken in the span direction
$b_{max}$	the maximum effective width based on the measurements of the reaction force
$b_{maxst}$	the maximum effective width based on the measurements of the reaction force for slabs supported by steel bearings
$b_{maxel}$	the maximum effective width based on the measurements of the reaction force for slabs supported by elastomeric bearings
$b_{meas}$	threshold effective width as based on the series of experiments with different widths
$b_r$	the distance between the free edge and the centre of the load along the width
$b_{rebar}$	the total distance between the first reinforcing bars on either side of the strip (Modified Bond Model)
$b_{rebar,x}$	the total distance between the first reinforcing bars on either side of the $x$ -direction strip
$b_{rebar,y}$	the total distance between the first reinforcing bars on either side of the $y$ -direction strip
$b_{side}$	the edge distance to the side of the first tyre contact area, minimum 600mm
$b_{sup}$	the width of the support, this distance is taken in the span direction
$b_w$	the web width of the section
$c$	the width of the strip
$c_{cover}$	the concrete cover
$c_l$	the column width determining the first considered strip
$d$	the effective depth to the considered layer of reinforcement ( $d_l$ or $d_t$ )
$d_{agg}$	the size of the aggregates
$d_{asphalt}$	thickness of the asphalt layer

### List of notations

$d_l$	the effective depth to the longitudinal (main flexural) reinforcement
$d_{pos,x}$	the effective depth to the hogging moment reinforcement in the $x$ -direction
$d_{pos,y}$	the effective depth to the hogging moment reinforcement in the $y$ -direction
$d_t$	the effective depth to the transverse flexural reinforcement
$e$	eccentricity
$f_b$	the tensile strength of the concrete as determined in NEN 6720:1995
$f_c'$	the specified concrete strength as used in ACI 318-08
$f_{c,combi}$	the concrete compressive strength in the case of the experiments from the second series (specimens S19 - S26)
$f_{c,conc}$	the concrete compressive strength in the case of the experiments from the first series (specimens S1 - S18)
$f_{ck}$	the characteristic cylinder compressive strength of concrete
$f_{ck,calc}$	the calculated characteristic cylinder compressive strength of concrete: $f_{c,meas,28} - 8$ MPa
$f_{ck,cube}$	the characteristic cube compressive strength of concrete
$f_{c,cyl,meas}$	the measured cylinder compressive strength of the concrete at the age of testing
$f_{c,mean}$	the mean cylinder concrete compressive strength
$f_{c,meas}$	the measured cube compressive strength of the concrete at the age of testing
$f_{c,meas,28}$	the cylinder compressive strength of the concrete at an age of 28 days
$f_{ct}$	tensile strength of concrete
$f_{ctm}$	maximum tensile stress in the concrete
$f_{ct,meas}$	measured tensile splitting strength of the concrete at the age of testing
$f_{ctk}$	the characteristic tensile splitting strength of the concrete
$f_s$	the stress in the reinforcement steel
$f_{yk}$	the characteristic yield strength of steel
$f_{ym}$	the average yield strength of steel
$f_{um}$	the average ultimate strength of steel
$g$	limit state function
$g(x)$	variable end span height
$g_\lambda$	a parameter that determines $k_\lambda$ in NEN 6720:1995
$h$	the height of the specimen
$h(x)$	variable mid-span height
$h_1$	the cross-sectional height at the support
$h_2$	the cross-sectional height at mid span
$h_{min}$	the cross-sectional height at the end support

### List of notations

$h_{max}$	the cross-sectional height at the mid support
$i$	running index
$j$	running index
$k$	the size effect factor
$k_{\lambda}$	the factor that takes the direct load transfer into account in NEN 6720:1995
$k_l$	0,15 (in NEN-EN 1992-1-1:2005)
$k_{Frechet}$	factor that determines the Frechet distribution
$k_h$	size effect factor from NEN 6720:1995
$k_{MBM}$	the size effect factor that is proposed to be used in combination with the Modified Bond Model
$k_r$	a factor that takes the proportion of the hogging moment reinforcement into account when a continuous support provides rotational restraint
$l_{bearing,i}$	the length of the $i$ -th bearing, taken perpendicularly to the span direction
$l_{load}$	the length of the load; this distance is taken perpendicularly to the span direction
$l_{span}$	the span length of the specimen, taken as the centre-to-centre distance between two supports
$l_{strip}$	the length of the strip in the Bond Model (Alexander and Simmonds, 1992)
$l_{sup}$	the support length
$l_w$	the length of the loaded area in the Bond Model and the Modified Bond Model
$m$	moment on a concrete tooth
$m_e$	the median of a series of data
$m_n$	bending moment
$m_{rr}$	the radial moment on a slab section
$m_t$	torsional moment
$m_{\theta\theta}$	the tangential moment on a slab section
$n_{bearings}$	the number of bearings
$q$	distributed load applied directly to the load-carrying strip
$q_{Beta}$	factor that determines the shape of the general Beta distribution
$q_{DL}$	the distributed self-weight
$q_{ik}$	the design lane load
$q_{perm}$	the distributed permanent load
$r$	ribbed reinforcement bars are used
$r$	radial axis in polar coordinates
$r_{Beta}$	factor that determines the shape of the general Beta distribution

### *List of notations*

$r_e$	location of the intersection between the rebar and the straight-line compression strut
$r_i$	location where bar force gradient starts
$r_o$	location where bar force gradient ends
$s$	crack spacing = distance between centre of gravity of reinforcement and root of concrete tooth
$s_{rebar}$	the reinforcement spacing
$s_{jack}$	the displacement at the jack
$u$	perimeter for punching shear
$u_1$	the remainder of the punching perimeter, not in the vicinity of the support (Regan, 1982)
$u_2$	the part of the punching perimeter parallel and closest to the support (Regan, 1982)
$u_{Frechet}$	factor that determines the Frechet distribution
$u_{Gumbel}$	factor that determines the Gumbel distribution
$u_{EC2}$	unity check based on QS-EC2
$u_{VBC}$	unity check based on QS-VBC
$v$	shear stress
$v(x)$	shear stress over the width
$v_c$	the ultimate design shear stress
$v_{c,AASHTO}$	the shear capacity resulting from AASHTO LRFD
$v_E$	the shear stress over the punching perimeter from NEN-EN 1992-1-1:2005
$v_{Ed}$	the shear stress at the face of the support due to the composite dead load and the live loads
$v_{Ed,wheel}$	the distributed shear stress over the support due to a wheel load
$v_{min}$	the lower bound of the shear capacity
$v_{max}$	the maximum shear stress in $v(x)$
$v_{pu}$	the punching shear capacity as defined in NEN-EN 1992-1-1:2005
$v_R(s)$	nominal punching strength as a function along the control perimeter
$v_{R,c}$	the shear stress capacity determined based on NEN-EN 1992-1-1:2005
$v_{Rd,c}$	the design shear stress capacity determined based on NEN-EN 1992-1-1:2005
$v_u$	a given maximum shear stress
$v_{u,AASHTO}$	the shear stress at the support due to the composite dead load and the live loads according to AASHTO LRFD and AASHTO LRFR
$v_x$	shear in $x$ -direction
$v_y$	shear in $y$ -direction

### *List of notations*

$w$	the loading term in the (Modified) Bond Model, this is the uniformly distributed load on the strips
$w_x$	the loading term in the (Modified) Bond Model on an $x$ -direction strip
$w_y$	the loading term in the (Modified) Bond Model on a $y$ -direction strip
$w_{ACI}$	the loading term in the (Modified) Bond Model based on the shear stress limits from ACI 318-08
$w_{ACI,x}$	the loading term in the (Modified) Bond Model based on the shear stress limits from ACI 318-08 for the $x$ -direction strips
$w_{ACI,x,plain}$	the loading term in the (Modified) Bond Model based on the shear stress limits from ACI 318-08 for the $x$ -direction strips for slabs reinforced with plain bars
$w_{ACI,y}$	the loading term in the (Modified) Bond Model based on the shear stress limits from ACI 318-08 for the $y$ -direction strips
$w_{ACI,y,plain}$	the loading term in the (Modified) Bond Model based on the shear stress limits from ACI 318-08 for the $y$ -direction strips for slabs reinforced with plain bars
$w_{crack}$	crack width
$w_{th,i}$	the width of the $i$ -th notional lane
$w_0$	crack width over which stress cannot be transferred
$w_1$	the loading term on the first considered strip
$w_2$	the loading term on the second considered strip
$x$	horizontal Cartesian axis
$y$	vertical Cartesian axis
$z$	moment arm
$z_l$	moment arm with respect to the longitudinal reinforcement
$z_{pos,x}$	moment arm with respect to the longitudinal hogging moment reinforcement
$z_{pos,y}$	moment arm with respect to the transverse hogging moment reinforcement
$z_t$	moment arm with respect to the transverse reinforcement
$z_{load}$	the size of the square loading plate

### **Roman upper case**

$A_0$	the size parameter determined by the size of the load or the size of the support in NEN 6720:1995
$A_s$	the area of the longitudinal reinforcement steel
$A_{s,bottom}$	the area of the bottom longitudinal reinforcement steel
$A_{s,top}$	the area of the top longitudinal reinforcement steel

### *List of notations*

$A_{sT}$	the total cross-sectional area of top steel within the strip plus half the area of the first top bar on either side of the strip
$A_{sB}$	the total cross-sectional area of bottom steel within the strip plus half the area of the first top bar on either side of the strip
$C$	the compression in the concrete
$C_{Rd,c}$	calibration factor in the shear formula from NEN-EN 1992-1-1:2005: $0,18/\gamma_c$
$C_{Rd,c,test}$	calibration factor in the shear formula for comparison with experimental results: 0,15
$C_{VD95\%}$	design value with a 95% confidentiality level for the skew factor on the dead load
$C_{VL95\%}$	design value with a 95% confidentiality level for the skew factor on the live load
$D$	the dowel force
$D_{load}$	the diameter of the circle on which the loads transferred through each half strip are considered
$F$	applied force
$F_b'$	the force increment in the reinforcement bar
$F_{conc}$	the applied concentrated force
$F_{min}$	the lower bound of the increased contribution of the first lane load
$F_{pres}$	the sum of the forces on the prestressing bars as measured by the load cells
$F_{pres,1}$	the force on prestressing bar 1 as measured by the load cell
$F_{pres,2}$	the force on prestressing bar 2 as measured by the load cell
$F_{pres,3}$	the force on prestressing bar 3 as measured by the load cell
$F_{test}$	the maximum load as applied during the experiment
$G_F$	the fracture energy
$K_1$	non-dimensional constant to study the validity of the Bond Model
$K_2$	non-dimensional constant to study the validity of the Bond Model
$M_1$	the larger moment in the shear span
$M_2$	the smaller moment in the shear span
$M_{CR}$	the maximum moment at shear failure
$M_{DL}$	the moment due to the dead load
$M_{Ed}$	the design moment
$M_{FL}$	the theoretical flexural failure moment
$M_{neg}$	the flexural capacity of the tensile reinforcement
$M_{neg,x}$	the flexural capacity of the tensile reinforcement in an $x$ -direction strip
$M_{neg,y}$	the flexural capacity of the tensile reinforcement in a $y$ -direction strip
$M_{pos}$	the flexural capacity of the compression reinforcement

*List of notations*

$M_{pos,x}$	the flexural capacity of the compression reinforcement in an $x$ -direction strip
$M_{pos,y}$	the flexural capacity of the compression reinforcement in a $y$ -direction strip
$M_r$	radial moment on a slab section
$M_s$	the flexural moment capacity
$M_{s,x}$	the flexural moment capacity in an $x$ -direction strip
$M_{s,y}$	the flexural moment capacity in a $y$ -direction strip
$M_{s1}$	the flexural moment capacity of the first considered strip
$M_{s2}$	the flexural moment capacity of the second considered strip
$M_{span}$	the moment at the location of the concentrated load
$M_{sup}$	the moment at the support
$M_{t1}$	the torsional moment capacity of the first considered strip
$M_{t2}$	the torsional moment capacity of the second considered strip
$M_\theta$	the tangential moment
$N$	number of samples in a Monte Carlo simulation
$P$	applied point load
$P\{\}$	the probability of the expression between $\{ \}$
$P_1$	the capacity of the first considered strip
$P_2$	the capacity of the second considered strip
$P_{AS}$	the concentric punching shear capacity as determined by Alexander and Simmonds (1992)
$P_{DL}$	total load due to the dead load
$P_{exp}$	point load at failure in experiment
$P_f$	the failure probability
$P_{f,req}$	the required failure probability
$P_{line}$	the maximum force applied on the line load during the experiment (second series only, specimens S19 – S26)
$P_{MBM}$	the capacity as determined with the Modified Bond Model, all strips
$P_{MBM,s}$	the capacity of the $x$ -direction strip assuming loading close to the edge
$P_{MBM,slabstrip}$	the reduced capacity according to the Modified Bond Model for a slab strip with $b_{load}/b > 0,2$ .
$P_{MBM,ss}$	the capacity of the $x$ -direction strip between the load and the support assuming loading near the edge
$P_{MBM,sup}$	the capacity of the strip between the load and the support in the Modified Bond Model
$P_{MBM,x}$	the capacity of an $x$ -direction strip in the Modified Bond Model
$P_{MBM,y}$	the capacity of a $y$ -direction strip in the Modified Bond Model

### *List of notations*

$P_{R1}$	the resistance of the remainder of the perimeter, not influenced by the vicinity of the support (Regan, 1982)
$P_{R2}$	the resistance of the part of the perimeter parallel and closest to the support (Regan, 1982)
$P_{Regan}$	the maximum load determined based on Regan's method (Regan, 1982)
$P_{s1}$	the capacity of the first considered strip according to the simplified model
$P_{s2}$	the capacity of the second considered strip according to the simplified model
$P_u$	the maximum concentrated load during the experiment
$Q_{ik}$	the design truck or design tandem
$R$	the resistance
$R_d$	the design resistance
$R_{load}$	the reaction force of the wheel load
$R_{sup}$	the reaction force at the support
$R_{support}$	the force vector of the distributed shear stress over the support
$S$	the load
$T$	the tension in the reinforcement
$V$	the sectional shear force
$V_a$	the shear force carried by aggregate interlock
$V_{ACI}$	the shear capacity determined based on ACI 318-08 and $b_{effl}$
$V_{add}$	the shear force at failure at the location of the largest $V_{exp}$ when the slab is considered as a beam on two supports, taking into account self-weight and the force due to the prestressing bars, and -in the second series of experiments- the line load and the self-weight of the line load
$V_{addlane}$	the increased contribution of the lane load in the first lane assuming a triangular distribution over the width
$V_c$	the shear capacity obtained in an experiment for residual shear capacity
$V_{calc}$	the calculated shear capacity
$V_{ct}$	the shear force carried by the concrete through residual tension at the crack tip
$V_{cz}$	the shear force carried by the concrete compression zone
$V_{conc}$	the contribution of the concentrated load to the shear force
$V_{conc,EC}$	the shear force at the support as a result of the concentrated load only, taking into account $\beta = a_v/2d_l$
$V_d$	the shear force carried by dowel action
$V_{DL}$	the shear due to the dead load
$V_{db}$	the ultimate shear force as from the experiments in the slab database from Annex 1
$V_{Ed}$	the design shear force

### List of notations

$V_{exp}$	the calculated shear force at failure when the slab is considered a beam on two supports, taking into account self-weight, the concentrated load, the force due to the prestressing bars and -for the second series of experiments- the line load and the self-weight of the line load; also: shear force at support at failure in an experiment
$V_{exp,400}$	the shear force at failure in an experiment with $a = 400\text{mm}$
$V_{exp,600}$	the shear force at failure in an experiment with $a = 600\text{mm}$
$V_{exp,CS}$	the shear force at failure in an experiment at the continuous support
$V_{exp,EC}$	the shear force at the support, resulting from the concentrated load, self-weight, force in the prestressing bars, for which the loads close to the support are reduced by $\beta = a/\sqrt{2}d_i$
$V_{exp,SS}$	the shear force at failure in an experiment at the simple support
$V_{line}$	the contribution of the line load to the shear force
$V_{perm}$	the shear force due to the permanent loads
$V_{R,c}$	the average shear capacity of the concrete
$V_{Rd}$	the design shear capacity
$V_{Rd,c}$	the design shear capacity of the concrete
$V_{R,c,eff1}$	the resulting shear capacity from NEN-EN 1992-1-1:2005 using the effective width $b_{eff1}$ based on load spreading from the centre of the load to the support
$V_{Rd,c,eff1}$	the resulting design shear capacity from NEN-EN 1992-1-1:2005 using the effective width $b_{eff1}$ based on load spreading from the centre of the load to the support
$V_{R,c,eff2}$	the resulting shear capacity using the effective width $b_{eff2}$ based on load spreading from the far side of the load to the support
$V_{Rd,c,eff2}$	the resulting design shear capacity using the effective width $b_{eff2}$ based on load spreading from the far side of the load to the support
$V_{Rd,c,prop}$	the proposed formula for the design shear capacity
$V_{test}$	the resulting maximum sectional shear force
$V_{TU}$	the ultimate shear force as observed in the Delft University of Technology experiments
$V_u$	maximum theoretical shear capacity
$V_{u,exp,\beta}$	the expected shear force when using the factor $\beta_{nolim}$ on an experimental result obtained at a larger $a/d_i$
$V_{uncr}$	the shear capacity obtained in a shear capacity experiment on an undamaged slab
$V_{VBC}$	the shear capacity determined based on NEN 6720:1995 and $b_{eff1}$
$W$	corresponds to a distribution of shear and is a function of the basic control perimeter $u$

*List of notations*

**Abbreviations**

A	anchorage failure
AASHTO	American Association of State Highway and Transportation Officials
ACI	American Concrete Institute
age	the age at the time of the first experiment on the specimen
ASCE	American Society of Civil Engineers
AVG	average
B	failure as a beam in shear with a noticeable shear crack at the side
B'	beam shear failure away from the support, typically between the concentrated load and the line load, only observed in the second series of experiments
BS	specimen of 0,5m wide
BM	specimen of 1,0m wide
BL	specimen of 1,5m wide
BX	specimen of 2m wide
c	experiment on a locally failed and heavily cracked specimen
c, OK	additional experiments in the vicinity of a local failure that resulted in a useful test result
cantilever	a cantilever slab
Char	characteristic value, 5% lower bound assuming a normal distribution
Char,LN	characteristic value, 5% lower bound assuming a lognormal distribution
CSA	Canadian Standards Association
COV	coefficient of variation
CS	the load is placed near to the continuous support
DT	diagonal tension failure (as reported in report)
E	loading with the concentrated load close to the edge of the width
el	elastomeric bearings at the support
GEV	generalized extreme value distribution
LRFD	load and resistance factor design
LRFR	load and resistance factor rating
M	loading with the concentrated load in the middle of the width
MBE	Manual of Bridge Evaluation
mode	the observed failure mode determined on pictures and cracking patterns from the original reference
n	the number of loads, either one number (number of loads at the same distance to the support), or two numbers separated by // when loads at multiple distances to the support are used (database Annex 1)
n	number of experiments carried out on the specimen (Chapter 3)
nn	pictures, descriptions or crack patterns are not available

*List of notations*

p	plain reinforcement bars are used
P	punching shear failure: punching off of a (partial) perimeter is visible on the bottom/top face
PCI	Precast Concrete Institute
QS-AASHTO	Quick Scan based on AASHTO LRFD and AASHTO LRFR
QS-EC2	Quick Scan based on the Eurocodes, NEN 8700 series and recommendations based on the experimental research
QS-VBC	Quick Scan based on NEN 6720:1995 and loading from NEN 8701:2011
QR24	plain rebar with a yield strength of 240 MPa
real bridge	experiment on an existing decommissioned bridge
Ref	the (abbreviated) author-date reference in which the experiments are reported
$R^2$	coefficient of correlation
SF	punching failure around the support
slab, SS	a simply supported slab or wide beam
slab, CS	a continuously supported slab or wide beam
S	specimen of 2,5m wide
SS	the load is placed near to the simple support
SS'	the load is placed at the north side of the slab, but without prestressing
st	steel bearings at the support
STD	standard deviation
sup	the support or support type
Test	the name of the experiment as used in the original reference
type	the category of experiment
uc	the unity check value
uncr	experiment on an undamaged or uncracked specimen
var	this parameters has been varied in the experiments on this specimen
VBC	“Voorschrift Betonnen Constructies”, Dutch concrete code before introduction of the Eurocode
WB	wide beam shear failure: inclined cracks fanning out from the load towards the support are visible on the bottom/top face

*List of notations*

## **1 Introduction**

### **1.1 Background**

Together with the expansion of the road network in the years between the end of the Second World War and 1975, a large number of bridges in the Netherlands were designed and built in the 1960s and 1970s. These bridges are still in service, and subjected to the current traffic loads and volumes, which are significantly larger than those at the time of design. To verify whether the existing concrete bridges under the current live loads still can be deemed satisfactory, an initial assessment round was organized. Different categories of bridge types and details were studied.

The results of this initial assessment indicated, among others, that there was reason for concern with regard to the shear capacity of reinforced concrete solid slab bridges. However, the assessment was carried out based on simplified design rules that do not take all load-bearing mechanisms into account. Several possible additional mechanisms were indicated, and it was decided to investigate the sources of residual capacity to better assess the shear capacity of solid slab bridges. In particular, the ability for transverse load distribution in slabs was identified as needing further study.

### **1.2 Scope of the research: the shear problem**

The scope of this research work is to study the behaviour of reinforced concrete slabs subjected to concentrated loads close to supports failing in shear for the application to slab bridges under wheel loads.

The typical existing slab bridges were designed for flexure, and checked according to the less stringent requirements for shear and punching of that era. Nowadays the requirements for shear are sometimes not met for these structures for two reasons:

- 1) due to an increase in traffic loads, heavier design truck loads are used in the live load models found in current codes;
- 2) the shear provisions in the current codes are more conservative than in previously used national codes.

When a reinforced concrete slab subjected to a concentrated load is checked for shear, two shear-related failure mechanisms need to be considered. The slab can fail in one-way shear (or beam shear), according to which a shear crack between the load and the support occurs and finally results in failure of the element. A slab under a concentrated load can also fail in two-way shear (or punching shear), according to which both radial and tangential cracks occur first, followed by punching through of a concrete cone.

In the current codes, the beam shear and punching shear capacity of elements without shear reinforcement is determined based on semi-empirical expressions. For one-way shear, the results of a large database of experiments on beams failing in shear have

been used to derive formulas that are able to predict the shear capacity of beams similar to those that have been tested. The typical shear test beams are small (in dimensions), heavily reinforced, simply supported and loaded in four-point bending. These results cannot directly be used for slabs subjected to a concentrated load. Slabs have a large width, which might allow for redistribution of forces in the transverse direction.

In beams, the web width is one of the parameters used to determine the shear capacity. In slabs, not the entire width can be used when the slab is loaded in the vicinity of the support under a concentrated load. A certain effective width at the support over which the shear force is supposed to be carried needs to be determined in the calculation. To determine this effective width, a method for the horizontal spreading of the load from its location towards the support should be offered; it should be possible to determine how the load fans out towards the support and which part of the width of the slab is activated.

Within the scope of this project, an experimental investigation of the shear capacity of reinforced concrete slabs under concentrated loads near to supports was carried out. In this thesis the shear capacity of reinforced concrete slabs subjected to concentrated loads close to supports is explored based on the analysis of the experiments, and the comparison with the shear assessment practice of existing solid slab bridges.

### ***1.3 Aim of the research***

***The aim of this research is to determine the shear capacity of reinforced concrete slabs subjected to concentrated loads close to supports, and the associated effective width at the support based on a model for horizontal load spreading.***

This research question is tackled by using two strategies: the development of a mechanical model that predicts the capacity of a slab under a concentrated load near to the support, and the statistical analysis of the data according to the basic assumptions of the Eurocodes so that a code extension proposal can be developed that takes into account the additional bearing capacity of slabs as compared to beams.

As the origin of this research is a consequence of the uncertainty about the bearing capacity of existing bridges in the Netherlands, an important part is directly linked to cases of existing Dutch bridges. The suggested recommendations resulting from the experimental work as discussed in this thesis and the analysis of the experimental results are implemented into a practical first-order approach that can be used for identifying the bridges that need further study.

### ***1.4 Research strategy and thesis outline***

This thesis contains eight chapters. After the first, introductory chapter, a survey of the literature is given along with a database of experiments on slabs and wide beams failing in shear. A description of the experimental research is given in Chapter 3, and a study of the parameters is reported in Chapter 4. Chapter 5 contains the theoretical modelling of slabs in

shear under concentrated loads near to supports. The connection with the codified methods and the statistical analysis of the test results is made in Chapter 6, after which in Chapter 7 the application to slab bridges is given. Finally, Chapter 8 contains the conclusions and outlook. A sketch of the thesis outline is given in Fig. 1.1.

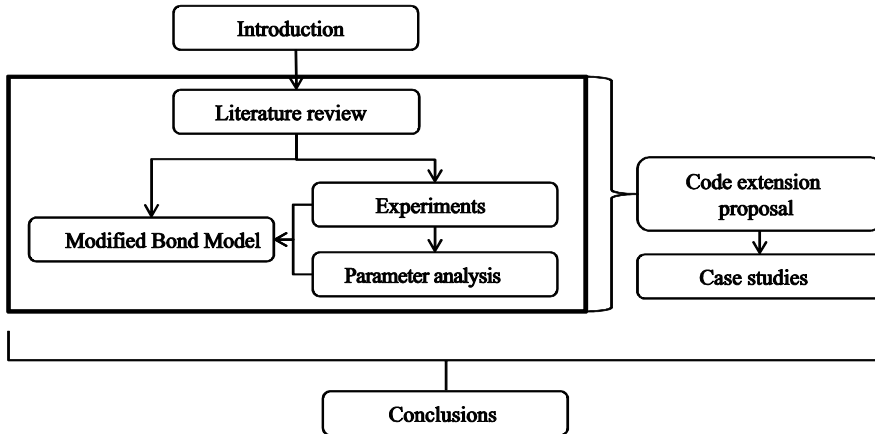


Fig. 1.1: Overview of the contents and structure

The literature review in Chapter 2 introduces the problem of beam shear in the way it has been studied for beams, and punching shear as it has been studied for slab-column connections. The differences and similarities between slabs and beams are highlighted. It is necessary to study both mechanisms, as the problem of a one-way slab under concentrated loads close to supports occurs in the transition zone between beam shear and punching shear. To fully grasp the behaviour of a slab under this loading case, both types of shear mechanisms should be understood. The concept of an effective width for wide beams and slabs loaded in shear is introduced, and different strategies for determining the effective width from the literature are cited. But the literature review chapter does not only contain a survey; it also contains a slab shear database. The database consists of 215 experiments on slabs and wide beams in shear under concentrated loads as well as under line loads. Its development, categories and implications are further explained in Chapter 2.

Chapter 3 gives the experimental results. An overview of the test setup is given, with the boundary conditions as used in the experiments. The properties of the 38 tested specimens (26 slabs and 12 slab strips) are summarized, along with the results of the 156 experiments that have been carried out. Additional attention is paid to the method of measuring the deformations with lasers and the layout of the reinforcement. As the failure mode of a slabs under a concentrated loads close to supports can show similarities with wide beam shear (beam shear failure as observed in elements of large width), beam shear and punching shear, the observations of the failure mode are also presented.

## *Introduction*

Chapter 4 contains a parameter analysis of the test data. Sets of experimental results in which one parameter is varied are used to study the influence of this parameter. The following parameters are regarded:

- the size of the loading plate representing the tyre contact area;
- the loading sequence and the influence of local failure and existing cracks on the ultimate residual capacity and the capacity for redistribution;
- the amount of transverse flexural reinforcement;
- the moment distribution in the shear span and thus the difference between loading close to the continuous support or close to the simple support;
- the distance between the load and the support to study the direct transfer of the load between its area of application and the support;
- the concrete compressive strength to study the difference between the behaviour in normal strength concrete and high strength concrete slabs;
- the overall slab width (or slab width to depth ratio) to study the transition from beam behaviour to slab behaviour;
- the type of reinforcement to study the difference in behaviour between slabs reinforced with plain bars and slabs reinforced with deformed bars;
- the support layout to study the difference between slabs on line supports and slabs on flexible bearings;
- the difference between slabs under a concentrated load only and slabs under a combination of a concentrated load and a distributed (line) load.

The trends that are reflected by the experiments are also compared to the results of beams in shear or slabs in punching known from the literature. The differences in the behaviour of slabs and beams in shear are highlighted, and indicated as a starting point for modelling the physical behaviour.

Chapter 5 contains the theoretical modelling of the behaviour of slabs in shear under concentrated loads near to supports. The Bond Model for concentric punching shear by Alexander and Simmonds (1992) is studied and modified so that it becomes applicable to different geometries of slabs, non-axis-symmetric conditions and loading close to the support. An empirical factor is introduced to take into account the reduced bond capacity of plain bars. The proposed model, the Modified Bond Model, combines aspects of one-way (beam) shear and two-way (punching) shear by modelling the slab as quadrants that carry load into two directions towards strips that carry the load by arching action into one direction. A comparison between the experimental results and the calculated values according to the Modified Bond Model shows a very good correspondence between the model and the experiments. The results according to the Modified Bond Model and according to NEN-EN 1992-1-1:2005 are compared to the experimental results. This comparison shows that the Modified Bond Model gives a better prediction of the capacity,

## *Introduction*

and reflects the influence of the important parameters that determine the shear capacity in a better way. It is shown that the Modified Bond Model leads to safe results for design.

In Chapter 6 the experimental results are compared to the results obtained with the existing codes as well as with the Modified Bond Model. It is verified whether the parameters studied in the experiments are correctly represented in the code methods and the proposed model. To quantify the increased level of safety in slabs subjected to concentrated loads near to supports as compared to beams, a probabilistic approach is followed. This approach is based on the cumulative distribution function of the ratio between the experimental results and the capacities calculated from NEN-EN 1992-1-1:2005. By means of Monte Carlo simulations, the variability in the material properties and in the ratio of the experimental shear capacity to the shear capacity as determined based on NEN-EN 1992-1-1:2005 is simulated. The requirements for the reliability index are taken as prescribed by NEN 8700:2001 for assessment at the repair level. This method results in a code extension proposal that is fully in line with the basic assumptions and safety philosophy of the Eurocodes as outlined in NEN-EN 1990:2002.

Chapter 7 introduces a method for assessment based on the Eurocodes, extended by taking into account the recommendations resulting from this research. The stress distribution of the prescribed live loads over the width and the depth is studied. The method is then used to assess the shear capacity of existing solid slab bridges based on a “unity check”: the ratio between the design shear stress at the edge of the support as a result of composite dead load (self-weight and load due to the wearing surface) and the live loads on one hand and the design shear resistance as determined in the code on the other hand. The results are compared to the unity checks obtained from the Dutch Code NEN 6720:1995 without the proposed recommendations to investigate the benefit from this research. A comparison to North American practice (AASHTO LRFD and LRFR) is included as well.

Chapter 8 contains an overview of the main conclusions of the thesis. Special attention is paid to the original contributions that result from the research work. A separate overview of the recommendations for practice is given, and finally possibilities for future research are discussed.

### ***1.5 Impact of the research***

While the research purely aims at determining the shear capacity of reinforced concrete slabs under concentrated loads near to supports for the assessment of reinforced concrete solid slab bridges under a combination of composite dead load and live loads, the impact of the research is larger than just its effect on the assessment practice. The entire impact should be measured in terms of the economic, environmental and social implications, which can be summed together as the impact on sustainability.

By better estimating the shear capacity of the existing slab bridges, it is expected that their service life can be prolonged. To assess the impact of prolonging the service life

## Introduction

of slab bridges in the Netherlands on sustainability, all aspects of the economic impact, environmental impact and impact on society should be addressed, Fig. 1.2. Additional attention to the influence on climate change and use of resources are considered in the Sustainability Index for Bridges as used in the United Kingdom (Hendy and Petty, 2012). As the current study comprises a group of about 2300 existing structures, of which 1000 are solid slab bridges, the impact on sustainability can only be discussed in **qualitative terms**. More detailed calculations of the individual structures should determine which of these can remain in service, and lead to a quantification of the impact of a prolonged service life of this specific structure. However, not all attributes can be described by a **quantitative system** (Hendy and Petty, 2012). The challenge for bridge owners and designers therefore lies in combining methodologies from different disciplines and weighing their importance before opting for a certain repair or replacement scheme.

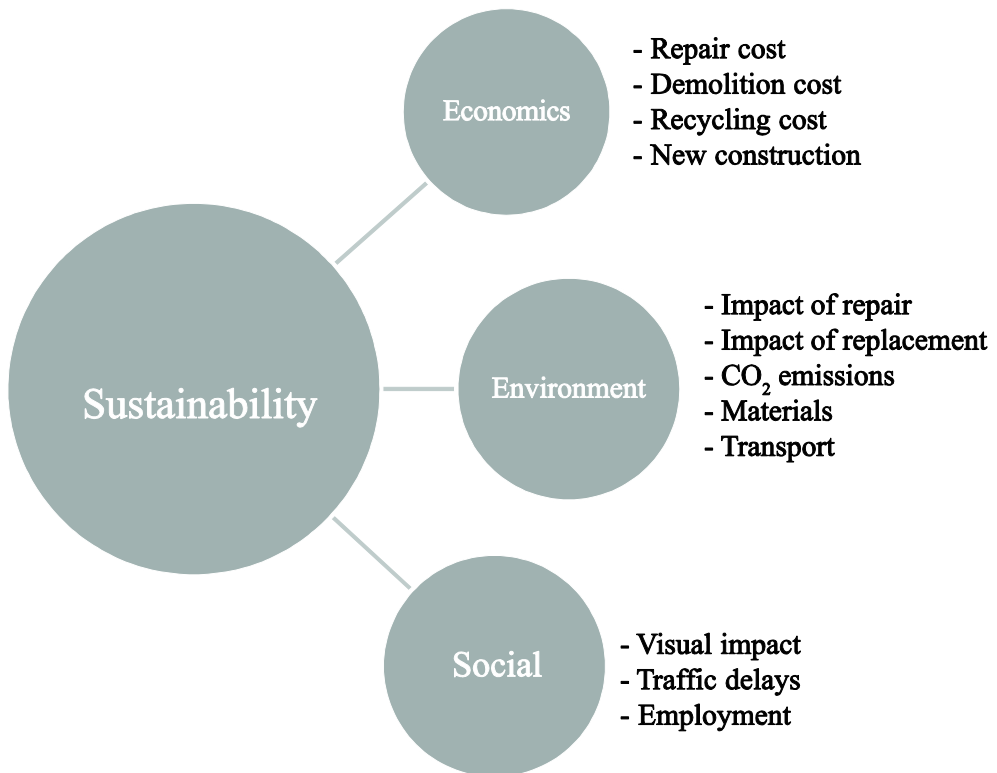


*Fig. 1.2: Impact of choices with regard to repair and replacement on sustainability.*

The economic impact of prolonging the service life of a slab bridge depends on the repair costs, or alternatively the end-of-life costs combined with the cost of replacing the

## *Introduction*

respective bridge. For a first idea of the economic impact of replacing one slab superstructure, an existing Dutch slab bridge is considered. The superstructure is a three-span continuous slab with an end span of 10m and a mid-span of 13m. The cross-sectional depth is 0,5m and the width is 19,2m. Assuming a cost of 800 – 1000 €/m<sup>2</sup> leads to an initial cost of 500000 - 640000€ for the concrete deck only.

The environmental impact is related amongst others to the avoidance of the impact associated with repairing the existing structure or building a new structure. Revisiting the three-span solid slab bridge, and studying the impact of the 320m<sup>3</sup> concrete deck from the superstructure requires assessing the carbon footprint of an estimated 91 tons of concrete and 30 tons of steel. The calculated associated fossil CO<sub>2</sub> emission equals 136 tons for Portland limestone cement based on the Carbon Calculator for Construction Activities (Environment Agency, 2012). This value is almost three times the annual carbon footprint of a household in the USA (i.e. 48 tons per year). For Portland slag cement the CO<sub>2</sub> emission becomes 122 tons and for blast furnace cement (as typically used in the Netherlands) the emissions are reduced to 74 tons.

The social dimension comprises a large number of aspects such as visual impact, time delays, job opportunities and more (Zinke et al., 2012). The impact is mostly quantified based on the driver delay costs that are associated with the refurbishment of the existing structure or with the demolition of the existing structure and placement of the new structure. These costs depend on the location of the structure and should be studied case by case. It is however very important to study these effects, as it is shown by Zinke et al. (2012) that the external costs can exceed the direct, economic costs by far. For a case study from Zinke et al. (2012), the social impact due to delay costs was about 9 times higher than the direct costs in the construction phase. In a densely populated country like the Netherlands, considering the broader cost by means of the social impact is thus of the utmost importance.

Through this qualitative description of the impact of repairing or replacing a large number of the existing solid slab bridges in the Netherlands because of their lack of shear capacity, it can be understood that the implications of the current research are larger than just adding a new perspective on the long-standing issue of the shear capacity of concrete structures.

## *Introduction*

## **2 Shear capacity of reinforced concrete members without shear reinforcement**

### **2.1 Introduction**

This chapter gives an overview of the relevant literature with regard to the studied problem of shear in reinforced concrete slabs subjected to concentrated loads close to supports, for the application to slab bridges subjected to wheel loads. In this chapter, a summary can be found of the findings from the full literature studies on the shear capacity of reinforced concrete slab bridges under wheel loads close to supports (Lantsoght, 2012b) and of punching shear in reinforced concrete slabs (Lantsoght, 2009). In a first subsection, an introduction to solid slab bridges and live loads is given. The subsequent subsection deals with the mechanisms of shear transfer, which are commonly used as a basis for modelling both one-way and (to a lesser extent) two-way shear. Then, an overview of the knowledge on beam shear, punching shear and the similarities, differences and transition between the failure modes is given. For wide beams and slabs, the effective width in shear is highlighted. On the basis of the extensive survey of past experimental research, a database of slab shear experiments is compiled. This database is explained in subsection 5 and is given in Annex 1. At the end of the chapter, reference to the code provisions used in this dissertation is made, and a discussion and conclusions are provided.

### **2.2 Scope**

#### **2.2.1 Slab bridges**

Typical reinforced concrete slab bridges have spans up to 18m and widths between 9m and 20m. The majority of the existing solid slab bridges in the Netherlands have 3 to 4 spans and a constant slab depth. The average main span of these structures is 13,5m and the average end span is 10,1m. The average edge distance is 0,67m and the average total road width is 11,87m, resulting in an average slab width of 13,2m.

Solid slab bridges have a larger residual capacity as compared to their design capacity than other types of bridges (Aktan et al., 1992), as was shown by a limited number of experiments on existing decommissioned slab bridges (Azizinamini et al., 1994). The Manual of Bridge Evaluation (2011), as used for assessment in North America, does not require shear checks for concrete slabs and slab bridges designed according to the AASHTO specifications. In the Netherlands, existing slab bridges are nowadays checked for shear based on a Quick Scan method (Chapter 7), which is a spreadsheet-based method to analyse a large database of viaducts. The Quick Scan sheet results in a “unity check” value for assessment: the ratio of the design shear force resulting from composite dead load, including the superimposed load due to the wearing surface, and live loads (lane loads and wheel loads) to the design shear capacity. The goal of the Quick Scan is to indicate which

## *Shear capacity of reinforced concrete members without shear reinforcement*

viaducts need a more detailed analysis for shear. If the criterion of the Quick Scan is not met, other methods, such as a finite element analysis, need to be used for further analysis.

### *2.2.2 Forces in slabs*

According to NEN-EN 1992-1-1:2005, a slab is a member with a minimum width  $b$  larger than 5 times its overall depth,  $h$ :  $b \geq 5h$ . A slab has an extra dimension in which load can be carried as compared to a beam and is therefore statically multiply indeterminate. According to Marti (1999), the principal and diaphragm shear forces are essential to understanding the internal force flow in slabs.

In French practice (Coin and Thonier, 2007) the lower bound for the shear stress  $v_{min}$  in slabs is allowed to be up to 3,43 times higher than the lower bound shear stress in beams, provided that the slab benefits from transverse load redistribution under the load case considered. This claim, however, is only supported by a limited number of experimental results (Iyengar et al., 1988), yet contested by other experiments (Kani et al., 1979).

### *2.2.3 Existing concrete bridges*

Within the scope of the current study, the only pre-existing damage to a slab bridge that is covered by the discussed methods is minor flexural cracking. This cracking can be the result of the considered bridge being in service for several decades. However, the influence of corrosion and deterioration on the shear capacity of existing concrete bridges and the required maintenance schemes (with repairs estimated at 40% of the total construction contract cost; Pearson-Kirk, 2010) are not studied.

### *2.2.4 Wheel loading*

As a result of the new code provisions (Eurocodes NEN-EN 1991-2:2003 and NEN-EN 1992-1-1:2005), shear can become the governing failure mode because of the larger sectional shear forces due to the more concentrated and heavier wheel loads as compared to the previous national codes (Rombach and Velasco, 2005). The shear stress over the width of the support line is determined from the sectional shear force at the support. The distribution of shear stresses over the support due to wheel loading is dependent on the size of the tyre contact area. In Load Model 1 of NEN-EN 1991-2:2002 the equivalent tyre contact area is prescribed as 400mm × 400mm with an axle load of maximum 300kN. Live loads are further discussed in Chapter 7.

Naumann (2010) predicted an 80% increase in transport of goods over the road network between 2010 and 2025, with an increasing share of heavy goods transport (Unger and Empelmann, 2012). For the Netherlands, the increase of transport of goods is estimated, depending on the scenario, between 15% and 80% between 2000 and 2020 (Ministry of Infrastructure and the Environment, 2004).

## *Shear capacity of reinforced concrete members without shear reinforcement*

To study wheel loading in laboratory experiments, steel plates are used. The rubber pneumatic tyres of vehicles in practice provide a more favourable load distribution and thus improve the load bearing capacity of the slab (Kirkpatrick et al., 1984; Vaz Rodrigues, 2007). This beneficial effect is not further taken into account in this research.

### **2.3 Mechanisms of shear transfer**

A number of shear carrying mechanisms contribute to the shear capacity of a member. An overview is given in Fig. 2.1, in which the following symbols are used:

- $V_{cz}$  the shear force carried by the concrete compression zone;
- $V_a$  the shear force carried by aggregate interlock;
- $V_{ct}$  the shear force carried by the concrete through residual tension at the crack tip;
- $V_d$  the shear force carried by dowel action;
- $T$  the tension in the reinforcement;
- $C$  the compression force in the concrete;
- $R_{sup}$  the reaction force at the support.

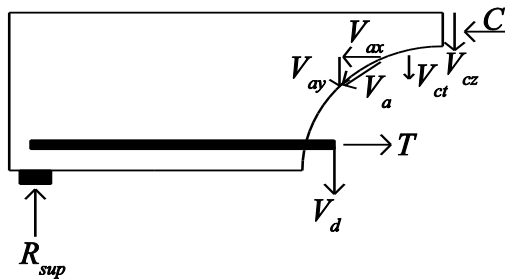


*Fig. 2.1: Forces acting at an inclined crack*

#### **2.3.1 Concrete compression zone**

The first models for shear attributed the shear carrying capacity of the concrete entirely to the capacity of the concrete compression zone (Baker et al., 1969; Kani et al., 1979). Assuming that all shear force is carried by the concrete compression zone and that the moment due to the tension in the reinforcement  $T$  is fully carried by flexure at the root of the tooth in between two flexural cracks, results in flexural stresses at the tooth root that are too high to be resisted by the concrete (Taylor, 1973). The parameters determining the shear carrying capacity of the concrete compression zone are: the depth and the width of the compression zone and the concrete compressive strength (Taylor, 1972). The shear carrying capacity of the concrete compression zone can be determined by integrating the shear stresses over the depth of the compression zone (Reineck, 1991).

The contribution of the concrete compression zone to the total shear carrying capacity is estimated to range between 20% (Fenwick and Paulay, 1968) and 40% (Kani et

al., 1979). Hamadi and Regan (1980) note that beams with expanded clay aggregates have a relatively larger contribution of the concrete compression zone than beams with natural gravel aggregates. This observation shows the interdependence between the shear carrying mechanisms. As clay aggregates have a lower aggregate interlock capacity, a relatively larger part of the shear capacity needs to be carried by the concrete compression zone.

### 2.3.2 Residual tension at crack

As a crack in concrete is not a “clean break” and small pieces of concrete are bridging the crack, the residual tension over the crack contributes to the shear capacity. In fracture mechanics approaches to the shear capacity, these residual tensile stresses are seen as the primary shear transfer mechanism (ASCE-ACI committee 445, 1998). For small beams, this mechanism is more important than for larger elements (Reineck, 1992; Rombach et al., 2009). The residual tension is studied in the zone in which the tensile strain,  $\epsilon_{ctu}$ , exceeds the strain at maximum tension,  $\epsilon_{ct}$ , (associated stress  $f_{ctm}$ ): the tension-softening zone (Pruijssers, 1986). This zone consists of concrete intersected by micro-cracks. The mean shear stiffness of the tension-softening zone is 40% of the shear stiffness of the compression zone, Fig. 2.2.

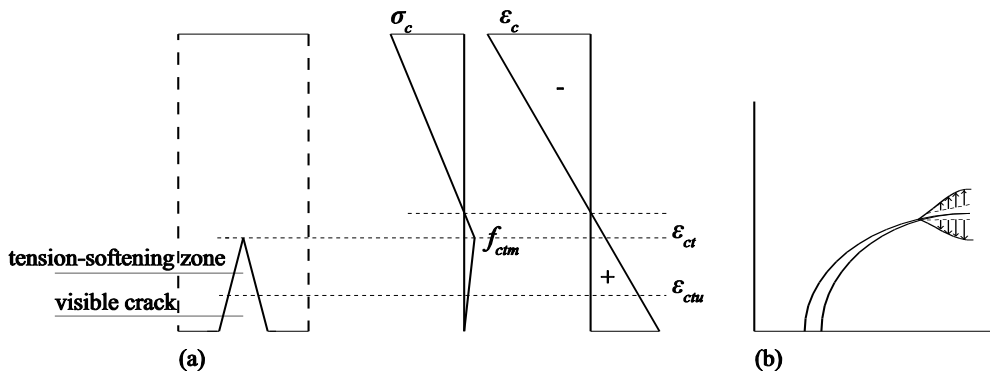


Fig. 2.2: The fracture zone: (a) flexural crack (modified from: Pruijssers, 1986) and state of stress  $\sigma_c$  and strain  $\epsilon_c$  in the cross-section; (b) applied to a shear crack.

### 2.3.3 Aggregate interlock

The shear capacity from aggregate interlock is a result of the friction in a crack caused by its rough surface. Aggregate interlock is directly related to the way a crack is formed in concrete. Because the strength of the hardened cement paste in most concretes is lower than the strength of the aggregate particles, cracks intersect the cement paste along the edges of the aggregate particles. So the aggregate particles, extending from the crack faces, “interlock” with the opposite face and resist shear displacements (Walraven, 1980, 1981a, b). The factors influencing the aggregate interlock capacity are: the concrete microstructure, the fracture energy of the concrete (Ghazavy-Khorasgany and Gopalaratnam, 1993), the

aggregate size (Sherwood et al., 2007) and the type of aggregate (Regan et al. 2005), with limestone and clay aggregates resulting in low aggregate interlock capacities. As the aggregate interlock capacity depends on the concrete microstructure and chosen mixture, several types of concrete with lower aggregate interlock capacities can be identified: mixtures with less coarse aggregates (the influence of the particle diameter is given by Walraven, 1980, 1981a) like some self-consolidating concretes (Hassan et al. 2010), lightweight concrete (Taylor, 1973; Vaz Rodrigues, 2007) and high strength concrete (Vintzileou, 1997), in which the shear crack intersects the aggregates because of their low strength as compared to the matrix material.

Walraven (1980, 1981a, b) developed a model for aggregate interlock in which concrete is considered as a two-phase material consisting of stiff aggregate particles embedded in an ideally-plastic matrix. Earlier measurements on beams had shown that cracks open and shear simultaneously. Therefore, both the shear stress and normal stress have to be taken into account as essential components in the equilibrium of forces. The shear stress  $\tau$  and the normal stress  $\sigma$  are functions of the crack width  $w_{crack}$  and the shear displacement  $\Delta$ . The fundamental model for aggregate interlock is based on a statistical analysis of the crack structure and the associated contact areas between the crack faces as a function of the displacements,  $w_{crack}$  and  $\Delta$ , and the composition of the concrete mix. Two fundamental modes of behaviour characterize the aggregate interlock:

1. sliding at the contact area between particles and matrix at opposite sides of the crack (“overriding”), and
2. irreversible deformation of the matrix by a high contact stress.

For the matrix material, a rigid-plastic stress-strain relation is used.

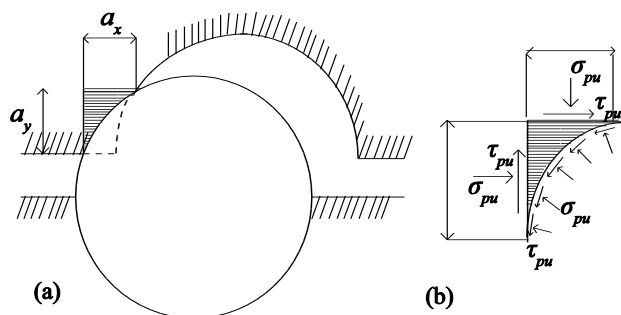


*Fig. 2.3:(a) Contact area (expressed as  $a_x$  and  $a_y$ ) between matrix and aggregate; (b) stress conditions: normal stress  $\sigma_{pu}$  and shear stress  $\tau_{pu}$ . (based on: Walraven 1980)*

Experiments that study the shear-friction (or in other words aggregate interlock) behaviour have often been carried out on concrete push-off specimens (Hofbeck et al., 1969; Walraven et al., 1987; Kahn and Mitchell, 2002). In those experiments, the crack opening path is influenced by the external restraint stiffness. For larger restraint stiffness, the crack

### *Shear capacity of reinforced concrete members without shear reinforcement*

opening path becomes stiffer. For reinforced concrete, the restraining force is introduced internally by the reinforcement and depends on the bond properties between the reinforcement and the concrete and on the yield strength. The contribution of aggregate interlock to the shear capacity in beams is estimated between 33% (Taylor, 1973) and 70% (Sherwood et al., 2007).

#### *2.3.4 Dowel action*

Dowel action is the resistance of a reinforcing bar, crossing a crack, to shear displacement. The deflection of a bar, subjected to a dowel force, is partially the result of the deformation of the concrete around the bar and partially of the deformation of the steel over a free length (Walraven, 1980). The dowel action capacity is typically small as the maximum shear stress to be carried by dowel action is limited by the tensile strength of the concrete cover supporting the dowel (Lubell, 2006). Cope (1985) reported that dowel action in slabs is less significant than in beams because the shear crack will not open over the entire member width and because of the continuity provided by bars in two directions, so that the dowel will not be activated as much as in a narrow beam failing in shear. Ghazavy-Khorasgany and Gopalaratnam (1993) on the other hand claim that there is some evidence that dowel action is quite effective in slabs.

Since this mechanism relies on shear deformations at the level of the tension steel, bond characteristics and concrete stiffness around the bars play an important role. Taylor (1973) related the dowel splitting force to the side cover of the bars, the distance between the bars, the splitting tensile strength and the bar diameter.

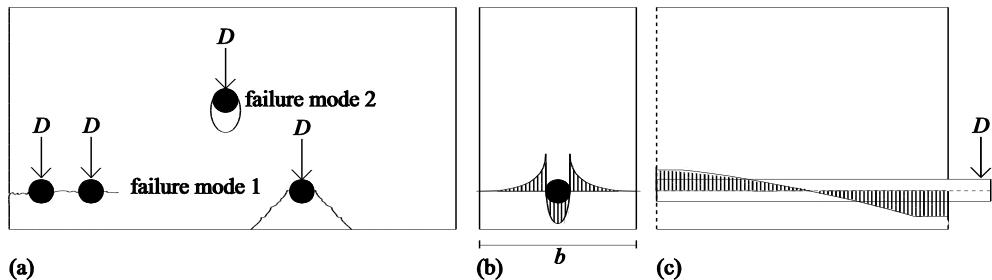


*Fig. 2.4: Dowel action: (a) failure modes of the mechanism due to the dowel force  $D$ ; (b) stress distribution over the width  $b$  within a section; (c) stress distribution along a dowel (schematic), (based on: Vintzileou, 1997).*

Models for dowel action are based on a linear elastic stress distribution over the reinforcing bar (Fenwick and Paulay, 1968) or plastic approaches (Dulacska, 1972; Chana, 1988; Bhide and Collins, 1989), Fig. 2.4. Vintzileou (1997) distinguishes 2 possible failure modes of dowel action, Fig. 2.4: splitting failure of the side or/and bottom concrete cover (mode 1) or crushing of the concrete under the dowel and yielding of the bar (mode 2).

### *Shear capacity of reinforced concrete members without shear reinforcement*

The contribution of dowel action to the shear carrying capacity of concrete members is estimated between 15% (Taylor, 1973) and 30% (for punching in slabs, Long, 1975).

#### *2.3.5 Arching action/ Strut action*

For loads close to the support, direct transfer of the load from its point of application to the support by means of a compressive strut (concentrated loads) or arch (distributed loads) results in an increase in the shear capacity.

The shear force  $V$  can be written as the sum of the contribution of “beam action” (a constant moment arm but a difference in the reinforcement tension due to bond) and arching action (a constant tension in the reinforcement, but a changing moment arm as shown in Fig. 2.5) (Bažant and Kim, 1984; Alexander and Simmonds, 1992):

$$V = \frac{d(Tz)}{dx} = \frac{d(T)}{dx} z + \frac{d(z)}{dx} T \quad (2.1)$$

The following elements are shown in Fig. 2.5:

- $T$  the tensile force in the reinforcement;
- $z$  the internal lever arm in the cross-section;
- $x$  location along axis in the span-direction;
- $C$  the compressive force in the concrete compression zone;
- $F$  applied concentrated load;
- $q$  applied distributed load;
- $R_{sup}$  the reaction force in the support.

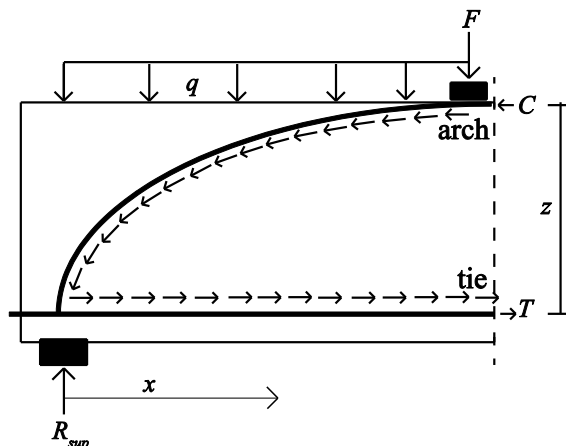


*Fig. 2.5: Modelling of inclined compression cord or arching action carrying the compressive force  $C$ . The tensile force in the reinforcement,  $T$ , the applied load,  $F$ , and the reaction force,  $R_{sup}$ , are also shown.*

### *Shear capacity of reinforced concrete members without shear reinforcement*

The shape of the resulting strut or arch depends on the loading configuration, with a general combination shown in Fig. 2.5. Expressions for the compressive force path are developed by Kim and Jeong (2011). The capacity of arching action can be estimated based on stress trajectories (Kani, 1966, 1969) or empirically from strain readings in experiments (Kim et al., 1999). The parameters influencing arching action are: the layout of the reinforcement, with layering resulting in a smaller depth for arching action, the anchorage of the tie (Rafla, 1971; Ghazavy-Khorasgany and Gopalaratnam, 1993), the crack shape (influenced by the  $a/d_t$  ratio, with  $a$  the centre-to-centre distance between the load and the support and  $d_t$  the effective depth to the longitudinal reinforcement) that defines the remaining uncracked compression zone (Reineck, 1997) and the type of reinforcement - with plain bars facilitating arching action more than ribbed bars, in which the force in the tension chord decreases due to bond (Reineck, 1990, Feldman and Bartlett, 2005; Feldman and Bartlett, 2008).

Olonisakin and Alexander (1998) measured the strains in the main flexural reinforcement in order to quantify the beam and arch action in wide beam shear tests and concluded that it is conceptually incorrect to assign all load to beam action.

#### *2.3.6 Discussion*

As the mechanisms of shear transfer are interrelated, the results from experiments that study these mechanisms separately can be questionable. The cited percentages of the contribution of each shear-carrying mechanism to the total shear capacity should thus be treated with due consideration (Swamy and Andriopoulos, 1973). Moreover, as arching or strut action is dependent on the position of the load and only delivers a considerable contribution to the shear carrying capacity for loads close to the support, some authors (e.g. Adebar, 2000) argue that this mechanism should be omitted from analysis.

Not all models for the behaviour of an element in shear are based on the sum of the contributions of the shear carrying mechanisms. Fracture mechanics models, in which a new and sudden shear crack is assumed to develop, crossing previously developed cracks, offer a different method to study elements in shear (Ehmann, 2006; Zararis and Papadakis, 2001).

## ***2.4 Shear in slabs***

When slabs under point loads fail as wide beams with a distinct shear crack at the side, the failure mode is denoted as “one-way shear”. When slabs under point loads fail locally with a conical failure face, the failure mode is denoted as punching or “two-way shear”, Fig. 2.6.

### *2.4.1 One-way shear models*

Shear failure in beams has been a research topic for more than 110 years. Since the first truss model for beams with stirrups by Ritter (1899) and Mörsch (1908) and the seminal

### *Shear capacity of reinforced concrete members without shear reinforcement*

beam shear experiments by Talbot (1904, 1905, 1906, 1908, 1909) and Mörsch (1908), researchers worldwide have studied the topic from many different points of view. The complex internal force system in a cracked concrete member is one of the main causes for the on-going debate (Joint Committee on Concrete and Reinforced Concrete, 1916; Zararis and Papadakis, 2001, Balažs, 2010). An implicit challenge is the biaxial stress state in the concrete (Clark, 1951; ASCE-ACI Committee 426, 1973; Leonhardt, 1978). Moreover, the diagonal direction of shear failure requires designers to think out of the scope of the traditional cross-sectional analysis (Lubell, 2006). As a result of the debate in the early days of shear research whether horizontal shear or diagonal tension is the cause of a shear failure, the following formula (reported by van den Berg (1962) and earlier researchers) that is nowadays used in design was developed for the expression for the shear stress  $v$ :

$$v = \frac{V}{bd_l} \quad (2.2)$$

with:

- $V$  the sectional shear force;
- $b$  the member width (or web width for non-rectangular sections, or effective width for wide beams and slabs);
- $d_l$  the effective depth to the longitudinal reinforcement of the member.

In codified design methods, this calculated shear stress is then compared to a maximum design stress that is not to be exceeded in members without stirrups.

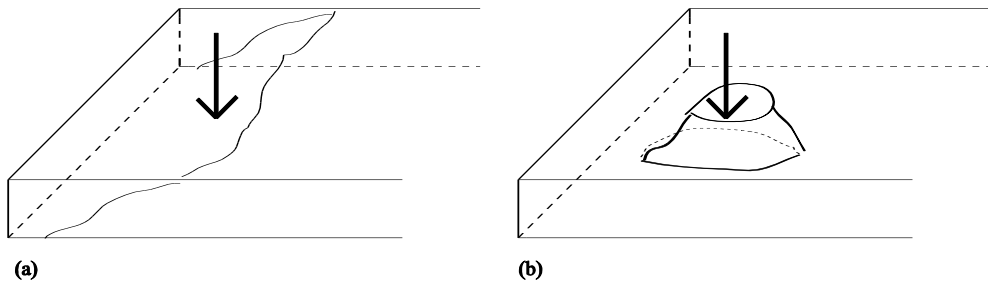


*Fig. 2.6: (a) one-way shear, (b) two-way shear.*

Over the past decades, a multitude of analytical methods have been developed. The first discussed approach is the **compression field theory** for elements with shear reinforcement. Originally developed for shear-reinforced concrete in pure torsion (Mitchell and Collins, 1974), this method (Collins, 1978) is based on stress-strain relationships for cracked concrete. After cracking, the concrete is assumed not to carry tension, resulting in a diagonal compression field. Average stresses and strains are used. The use of average stress-strain relations is a major simplification, as in reality cracked concrete transmits stresses in a complex manner of opening and closing of existing cracks, forming new

cracks, aggregate interlocking forces and variations of the bond stresses. Another main assumption of the method is that the directions of the largest compressive stress and strain coincide. The observed tendency is for the direction of the principal stress to lag behind the direction of the principal strain (Vecchio, 2000; Sun and Kuchma, 2007). The failure criterion is determined by yielding of the reinforcement or reaching the limiting compressive strength in the concrete (smaller than the uniaxial compressive strength, as the stress is transferred through severely cracked and deformed concrete) (Collins and Mitchell, 1980). Taking into account the contribution of the residual tensile stresses, the **modified compression field theory (MCFT)** was developed (Vecchio and Collins, 1986), based on experimental research on concrete panels subjected to in-plane shear and axial stresses, resulting in expressions for the tension- and compression-softening behaviour of cracked concrete with shear reinforcement. Originally developed for members with stirrups, the theory is expanded for use in members without shear reinforcement by Adebar and Collins (1996) by introducing concrete tension ties resulting from aggregate interlock action perpendicular to the compression struts. The expressions are developed assuming that the ability of cracked concrete to transmit shear is primarily governed by the width of the diagonal cracks, thus excluding the influence of shear slip. Average crack widths, as a product of the principal tensile strain and the crack spacing, over the crack surface are used. The assumed crack spacing, however, is not found to correspond to experimental results (Sun and Kuchma, 2007). Researchers at the University of Houston (Labib et al., 2009) are testing concrete panels reinforced in two directions in a three-dimensional panel tester, to expand the scope of smeared crack models (**fixed-angle softened-truss models**, corresponding to the observations in girder experiments, and the simplified approach of **rotating-angle softened-truss models**, Hsu, 1996) to account for three-dimensional loading effects. A hybrid between a fully rotating and a fixed-angle crack model expansion of the MCFT is also available: the **disturbed stress field model** (Vecchio, 2000). The design method based on the MCFT is the **simplified modified compression field theory** (Bentz and Collins, 2006; Bentz et al., 2006), which is the basis of the design method for members with and without shear reinforcement in Model Code 2010 (*fib*, 2012). The disadvantage of the compression field approaches is that these are developed for members with shear reinforcement, and then modified for the application to members without shear reinforcement, for which larger scatter on test to predicted values can be observed (Bentz, 2010).

A second approach that has been thoroughly researched is the **critical shear crack theory (CSCT)**, developed since 1985 to estimate both the ultimate beam shear and punching shear capacities of concrete members (Muttoni, 2003). The basic assumption of this theory is that the shear strength of members without transverse reinforcement is governed by the width and roughness of a shear crack, which develops through the inclined compression strut carrying the shear. The critical zone is assumed at a cross-section located

at  $0,5d_l$  from the load and at  $0,6d_l$  from the extreme compression fibre. The width of the critical shear crack  $w_{crack}$  is proportional to the strain  $\varepsilon$  at a control depth for one-way members (Muttoni, 2008) and is influenced by the aggregate size and the spacing between the layers of reinforcement.

A third approach is a general **plasticity-based approach**. The strut-and-tie models, discussed separately here, form a **lower bound plasticity approach**, in which a statically admissible safe stress field is constructed. Alternatively, in an **upper bound plasticity approach** a yield line (for shear, a critical crack) is studied (Nielsen, 1984; Nielsen and Hoang, 2011). The advantage of plasticity-based approaches is the wide applicability of the theory of plasticity. The disadvantages of the plasticity models are: the assumption of the crack location (upper bound approaches), the necessity of redistribution and ductility which is not always available in shear and the need for effectiveness factors to determine the compressive strength of the concrete. These factors are not the same for all load cases and cannot be physically explained.

A fourth approach and application of the plasticity approach is the use of **strut-and-tie models** (Schlaich et al, 1987); mechanical models using the lower bound theorem of plasticity and representing the force flow in a concrete member by compressive struts and tension ties (reinforcing bars, prestressing tendons or concrete tensile stress fields in members without stirrups). Stress fields as determined from finite element models can be used to select a strut-and-tie model (Fernandez Ruiz and Muttoni, 2007). Since loads follow the path that requires the least forces and deformations, and reinforcement ties are much more deformable than concrete struts, the model with the least and shortest ties is the best. The structure adapts itself to the assumed internal structural system. The failure criteria are yielding of the reinforcement or obtaining the effective concrete compressive strength. The effective concrete compressive strength is lower than the uniaxial compressive strength as the compressive capacity of the concrete is largely influenced by the multi-axial stress-state and the disturbances from cracks and reinforcement. To calculate the effective concrete compressive strength, the use of an effectiveness factor is required. A point of criticism (Gastbled and May, 2001) is that the assumed failure mechanism in a strut-and-tie model for members without shear reinforcement differs from the experimentally observed failure mechanism.

A fifth approach is the use of **mechanical models**. A first example is the **tooth model**, in which the zone between two flexural cracks is a “tooth”, a concrete cantilever fixed in the compression zone and loaded by horizontal forces resulting from bond (Kani, 1964), Fig. 2.7. This model correctly links the beam shear capacity (the capacity of the concrete teeth) and the capacity of the remaining arch (Fig. 2.5) to the experimentally observed “valley of diagonal failure” (Kani, 1964). A weakness of the model is the need to assume a spacing for the cracks. Reineck (1991, 1997) extended the tooth model approach by studying the influence of all shear carrying mechanisms on a concrete tooth, in which

### Shear capacity of reinforced concrete members without shear reinforcement

the acting forces are determined based on stress fields. While this approach relies on discrete cracks, the compression field approaches use smeared cracks (Reineck, 2002). However, both methods consider the aggregate interlocking capacity as the most important mechanism in determining the shear strength of members without transverse reinforcement (ASCE-ACI committee 445, 1998).

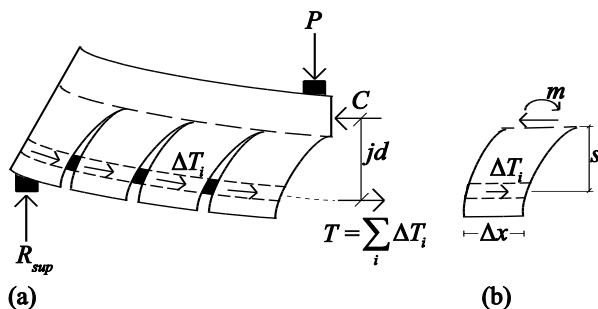


Fig. 2.7: Kani's tooth model: (a) beam under a point load  $P$  and bond forces  $\Delta T_i$ ; (b) simplified model of a typical concrete tooth, showing acting moment,  $m$ , and distance  $s$  between the centre of gravity of the reinforcement and the root of the concrete tooth.

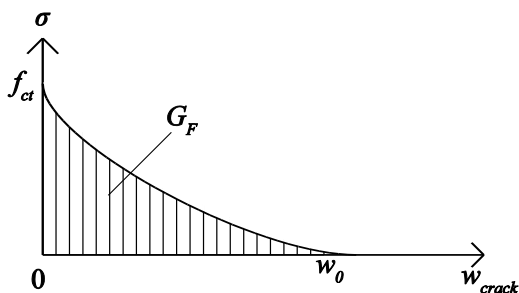


Fig. 2.8: Tension softening curve ( $\sigma - w_{crack}$ ), with  $f_{ct}$  = tensile strength of concrete and  $w_0$  = crack width over which stress cannot be transferred. The area underneath the curve is the fracture energy  $G_F$ .

As a sixth group of methods, **fracture mechanics-based approaches** can be mentioned, which provide, in addition to the stress-strain relations, tensile stress-crack opening relations (Niwa, 1997), such as the relation based on the fictitious crack model (Gustaffson and Hillerborg, 1988), Fig. 2.8. The approaches use the fracture energy  $G_F$ , as a function of the concrete compressive strength and the maximum aggregate size (Walraven, 2007). The peak tensile stress near the crack and the tension-softening in the cracked zone are regarded. The fracture is assumed to propagate with a relatively large fracture process zone ahead of the crack tip in which progressive micro-cracking gradually reduces the tensile stress to zero (Mihashi and Nomura, 1993). Gastebled and May (2001) developed a model

based on the assumption that the release of the main reinforcement by splitting controls the opening and the extension of the diagonal crack. Once splitting has begun, the steel bar is released from its concrete encasement. The drastically reduced stiffness in tension allows for the diagonal crack to open and extend, while a rotation about the tip of the diagonal crack occurs. The fundamental relation of fracture mechanics is then used as a criterion for splitting failure. This model, however, requires assumptions of the location and shape of the crack, as well as the use of empirical factors. While this approach initially assumes the bond fracture to be a mode I fracture (normal stresses), a correction for mode II fracture (shear) has been developed (Xu and Reinhardt, 2005).

As the mechanics of the shear problem are still not fully understood, many **empirical expressions** have been developed as well. These one-way shear models are developed based on statistical evaluations of laboratory tests on beams (for example: Zsutty, 1971; Regan, 1987; König and Fischer, 1995; Tureyen and Frosch, 2004).

#### 2.4.2 *Two-way shear models*

Just like one-way shear failure, two-way shear or punching shear has been a topic of research for the past 100 years, since the first experiments by Talbot (1913) and Talbot and Slater (1916). The behaviour of the failure region in punching is complex, because of the combined flexural and diagonal tensile cracking, the three-dimensional nature of the problem (Park and Gamble, 1999), and the variable depth of the compression zone (Theodorakopoulos and Swamy, 2002).

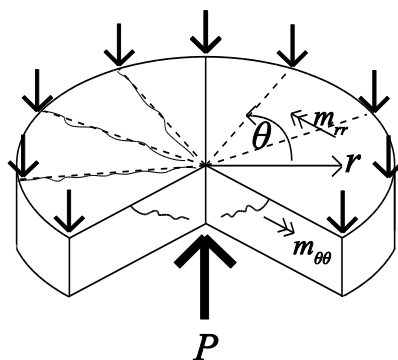


*Fig. 2.9: Slab-column connection: tangential  $m_{\theta\theta}$  and radial  $m_{rr}$  moments, shear cracks – in polar coordinates  $(r, \theta)$ .*

Most available punching test data come from slab-column tests, consisting of a slab-column specimen with the slab piece extending up to the line of contra-flexure. The behaviour of slab-column specimens differs from the real behaviour of a slab, since in-plane forces cannot develop. Likewise, Rombach et al. (2009) note the difference between flat floor slabs and bridge deck slabs under concentrated loads: the principal shear forces and

### *Shear capacity of reinforced concrete members without shear reinforcement*

moments are rotationally symmetric around the load in flat floor slabs, while in bridge deck slabs a different flow of forces occurs.

Fig. 2.9 shows the distribution of cracks due to the occurring moment in a slab-column connection. The radial moment  $m_{rr}$  decreases at a rapid rate with the distance from the loaded area. It causes yielding of the steel first at the perimeter of the loaded area. Meanwhile, a tangential moment  $m_{\theta\theta}$  will counteract any rotation at the inclined crack (ASCE-ACI Committee 426, 1974).  $m_{\theta\theta}$  leads to cracks on lines radiating from the centre of the loaded area and divides the slab into sectors.  $m_{rr}$  leads to inclined cone-shaped internal cracks. Most punching failures do not occur until aggregate interlock effects are markedly diminished by yielding in both the  $r$  and  $\theta$  direction.

Models for punching shear can be divided into four categories (Lantsoght, 2009): models based on a limiting shear stress, strut-and-tie models and mechanical models, beam analogy models and plate analysis models (solved for example by using finite elements methods).

Most models since the seminal work by Moe (1961) rely upon **the limitation of a shear stress on a critical perimeter**. The perimeter is determined at a certain distance from the loaded area, which is typically related to the experimentally observed inclination of the punching failure cone. The inclination, however, indicates the influence of flexure on the failure mode, with inclination angles of about  $30^\circ$  indicating predominantly shear and angles of  $90^\circ$  indicating pure flexure. Two approaches for the determination of limiting shear stress are possible: physical models, based on the internal non-isotropic structure of the material, and phenomenological models, based on the external behaviour under different stress combinations. The physical models are mathematically complicated and the phenomenological models, using Mohr's theory of failure, do not give a reliable criterion of failure under all circumstances. The original shear stress approaches limit the shear stress on the perimeter so that the slab will always fail in flexure (Moe, 1961). Alexander and Simmonds (1986) question the validity of basing a theory on the observed diagonal cracks, as test observations have shown cracks developing at 50-70% of the ultimate loading. The slab in that cracked state is very stable since it can be unloaded and reloaded without affecting the ultimate capacity.

For slabs subjected to concentrated loads, **three-dimensional strut-and-tie models** can be developed. For the punching of edge columns, Alexander and Simmonds (1986, 1987) developed a three-dimensional strut-and-tie model, with two types of compression struts (in-plane or anchoring struts as illustrated in Fig. 2.11a and out-of-plane or shear struts as in Fig. 2.11b). The anchoring struts are balanced by two mutually perpendicular reinforcing bars. The shear struts are similar to the direct compression struts for loads close to the support (for example, as in the strut-and-tie model used for corbel design), but the point of load application does not coincide with the junction of the tensile and compressive force, and as a result the angle of inclination of the shear strut,  $\alpha_{AS}$ , is not

*Shear capacity of reinforced concrete members without shear reinforcement*

pre-set. Likewise, the vertical component of the compression strut is no longer equilibrated at the junction by the applied load. There exists a force component out of the plane of the slab that must be balanced by some tension field in the concrete, resulting in a three-dimensional truss, Fig. 2.10. These tension fields were not shown nor considered in the original model by Alexander and Simmonds (1986, 1987), as the tension was assumed to be dispersed over the surrounding slab material. Three failure criteria are used: failure of the tension tie, failure of the compression strut and failure due to the out-of-plane component (Fig. 2.11b) of the compression strut exceeding the confining strength of the slab. Yielding of the flexural reinforcement is assumed at failure. The angle of the shear strut,  $\alpha_{AS}$ , is empirically determined.

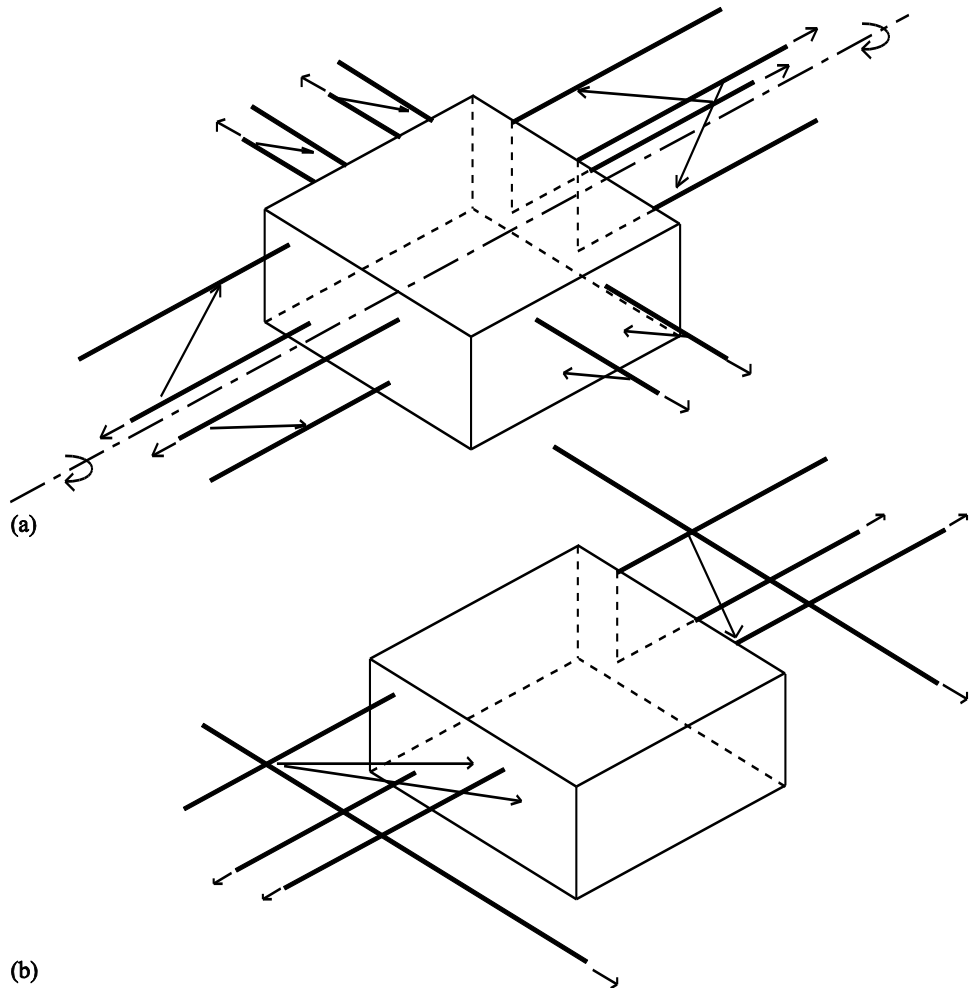


*Fig. 2.10: 3D strut-and-tie model (Alexander and Simmonds, 1987), showing only the types of struts for clarity purposes (a) struts working on a vertical plane (out-of-plane struts); (b) struts working on a horizontal plane (anchoring struts).*

A **mechanical model** for punching in slabs is the **Bond Model** (Alexander and Simmonds, 1992), which combines arching action and the concept of a critical shear stress on a critical section. Tests showed that the out-of-plane compression struts from the three-dimensional strut-and-tie model are actually curved and parallel to the reinforcement in plan. The geometry of the curved arch is assumed to be governed by the interaction between the arch and the adjacent quadrants of the slab. The shear is carried through these arches from the load towards a position of zero shear. A disadvantage of this approach is the requirement of axis-symmetrical conditions, such as at an inner column in a flat slab structure. This method is studied in more detail in Chapter 5 and forms the basis for the proposed Modified Bond Model.

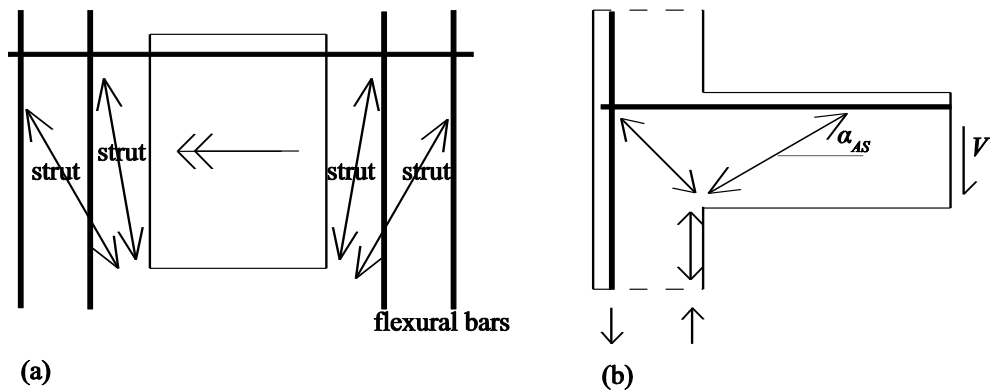


*Fig. 2.11: Types of struts that are used in the three-dimensional strut-and-tie model (a) In-plane or anchoring struts, top view of slab with central column (b) out-of-plane or shear strut, situation with edge column (Alexander and Simmonds, 1986).*

A more recent mechanical model is the **critical shear crack theory** (CSCT) for two-way shear, in which the width of the critical shear crack  $w_{crack}$  is proportional to the slab rotation  $\psi$  (Muttoni, 2003, 2008), Fig. 2.12. This method is used in the Model Code 2010 (*fib*, 2012) for punching shear. The CSCT can be used in the case of deck slabs of bridges, where the shear field and developed rotations around the wheel loads differ from residential flat slabs supported by columns. Then, the nonlinear load-rotation relationship should be calculated by integrating the moment-curvature relation of the slab. For this application, Sagaseta et al. (2011) extended the CSCT to cases of non-axis-symmetrical punching. The nominal punching strength  $v_R(s)$  is then non-uniform along the control perimeter. Some parts of the perimeter will reach their ultimate strength, whereas others will still have a potential strength capacity. The redistribution of shear stresses along the perimeter increases the punching capacity and the slab rotations. In this approach, the punching strength is determined by integrating the nominal shear strength along the control perimeter. The method can be simplified by assuming that the rotations  $\psi(s)$  are constant along the straight

### *Shear capacity of reinforced concrete members without shear reinforcement*

segments of the control perimeter. By estimating the rotations along with the punching shear capacity, the designer gains a better insight in the ductility of the structure (Muttoni and Fernandez Ruiz, 2010a, b). However, the necessity of a good description of the rotations  $\psi(s)$  can also be seen as a downside of this method, as for cases of bridge decks under wheel loads, non-linear finite element calculations are necessary (e.g. Falbr, 2011), so that the method becomes less suitable for design and assessment.

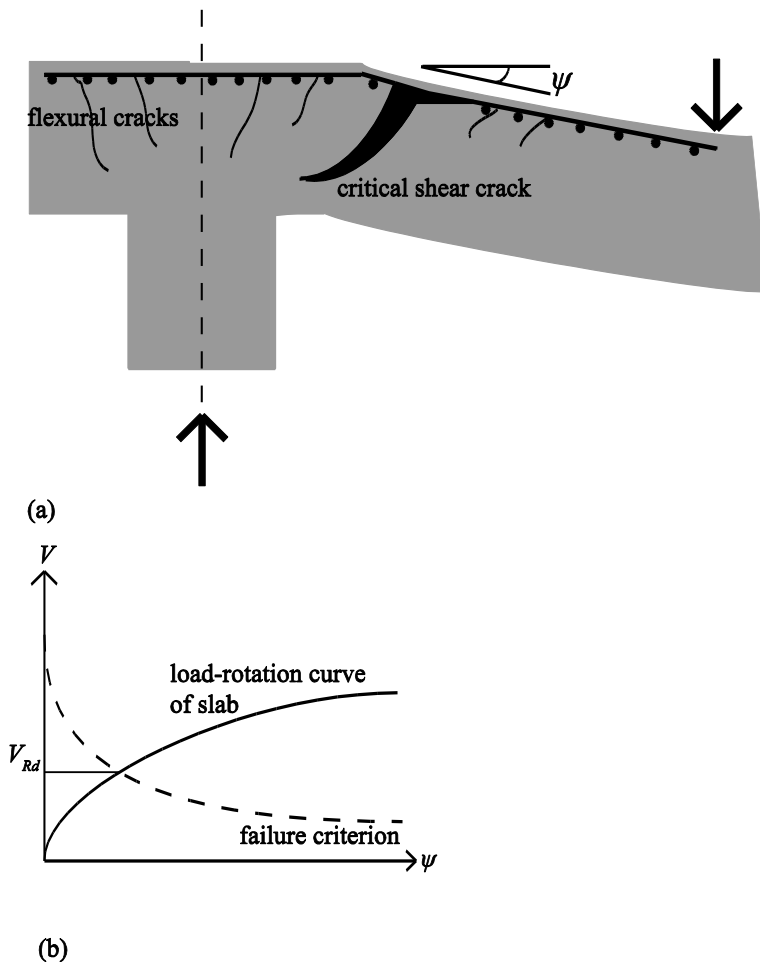


Fig. 2.12: (a) Slab deflection during punching test interpreted according to the critical shear crack theory; and (b) design procedure to check the punching strength of a slab (based on Guandalini, Burdet and Muttoni, 2009).

A **plasticity-based mechanical model** for punching shear was developed by Kinnunen and Nylander (1960). This model assumes that the slab portion outside the shear crack, bound

by this crack, radial cracks, and the circumference of the slab, can be regarded as a rigid body, which is rotated under load action around the root of the shear crack. Three failure modes are considered: shear failure, failure of the concrete cone between the shear crack and the column, and concrete compression failure in a tangential direction. The Kinnunen and Nylander model (1960) was further developed by Hallgren (1996) to incorporate a failure criterion based on non-linear fracture mechanics.

Another approach is the use of **plate theory and finite element methods** ranging from simple elastic plate models to sophisticated nonlinear models that account for cracking and plastic behaviour. Reinforcement should be modelled as discrete bars with plastic behaviour. The bond properties of the interface between the concrete and the reinforcement need to be adequately modelled. Taking into account tension-softening behaviour, Fig. 2.8, improves the model. Finite element solutions can be time-consuming and require a very good understanding of the material behaviour and the software. The user needs to be aware of the limitations of the material models, element types and calculation techniques used. For complex cases, finite element models that succeed to realistically display the behaviour from first loading until failure are still the subject of research.

In the past, **beam analogy methods** have been developed for shear in slabs. In these models, slab strips (beams) are subjected to a bending moment, a torsional moment and a shear force. Redistribution of these actions is able to occur between the beams. Each beam is assumed to be able to develop its ultimate bending moment, torsional moment, and shear force, and interaction effects can be taken into account. The total strength is the sum of the contributions of the strength of the beams. Failure occurs when at least three beams reach their ultimate strength (Park and Gamble, 1999). However, the large number of possible limiting strength combinations makes the application complex. Moreover, sufficient ductility is tacitly assumed.

The **empirical expressions** for punching shear are the result of experiments on small-scale slab-column connections and are based on a limiting shear stress. Of all empirical expressions that are available in the literature, Regan's approach (Regan, 1982) is of most interest as it was developed for slabs under concentrated loads near to supports. It is based on the definition of a critical perimeter around the concentrated load, Fig. 2.13. The resistance  $P_{R2}$  of the part  $u_2$  of the perimeter parallel and closest to the support (Fig. 2.13) is defined as ( $f_{ck,cube}$  in [MPa];  $d$  in [mm];  $u_2$  in [m];  $P_{R2}$  in [kN]):

$$P_{R2} = \left( \frac{2d_l}{a_v} \right) \xi_s v_c u_2 d_l < \frac{\sqrt{f_{ck,cube}}}{\gamma_m} u_2 d_l \quad (2.3)$$

$$\xi_s = \sqrt[4]{\frac{500}{d}} \quad (2.4)$$

$$v_c = \frac{0,27}{\gamma_m} \sqrt[3]{100\rho f_{ck,cube}} \quad (2.5)$$

## Shear capacity of reinforced concrete members without shear reinforcement

with:

- $d$  the effective depth to the considered layer of reinforcement ( $d_t$  or  $d_l$ );
- $a_v$  the clear shear span, the face-to-face distance between the load and the support;
- $f_{ck,cube}$  the cube compressive strength of the concrete;
- $\xi_s$  the size effect factor;
- $\rho$  the reinforcement ratio for the layer of reinforcement considered ( $\rho_l$  or  $\rho_t$ );
- $\gamma_m$  the material factor for concrete;
- $v_c$  the ultimate design shear stress.

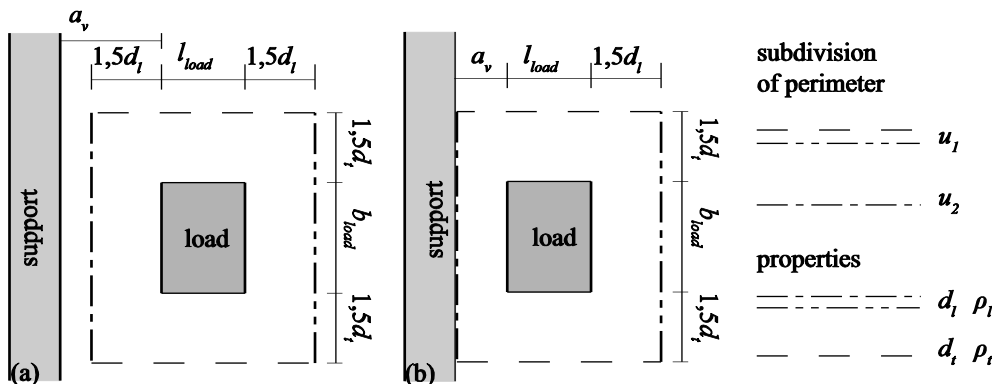


*Fig. 2.13: Subdivision of perimeter and slab properties to be used for parts of the perimeter: (a) for  $2d_l > a_v > 1,5d_b$ , (b) for  $a_v < 1,5d_b$ . Drawing based on Regan (1982).*

The resistance  $P_{R1}$  of the remainder ( $\Sigma u = u_l$ ) of the perimeter (Fig. 2.13) is defined as:

$$P_{R1} = \sum \xi_s v_c u d \quad (2.6)$$

For each part of the calculation, the local values of the effective depth  $d$  ( $d_t$  to the transverse reinforcement and  $d_l$  to the main flexural reinforcement) and the ratio of flexural reinforcement  $\rho$  ( $\rho_t$  and  $\rho_l$ ) as indicated in Fig. 2.13 are used. The contributions of  $P_{R2}$  from Eq. (2.3) and  $P_{R1}$  from Eq. (2.6) are summed to give the total resistance against shear failure,  $P_{Regan}$ . At a continuous support, the total shear resistance is multiplied with a factor  $\alpha_{Regan} > 1$  depending on the larger moment at the end of the shear span,  $M_1$ , and the smaller moment,  $M_2$  ( $M_1$  and  $M_2$  as absolute values).

$$\alpha_{Regan} = \sqrt{\frac{M_1 + M_2}{M_1}} \quad (2.7)$$

*2.4.3 Similarities, transition zone and distinction*

Olonisakin and Alexander (1999) measured the force increment in one-way and two-way slabs and found that the values are very similar, suggesting a fundamental link between one- and two-way shear.

In intermediate cases between one- and two-way shear, shear forces develop neither parallel nor radially (Vaz Rodrigues et al., 2008). The strength for these cases is not covered by current codes of practice. Vaz Rodrigues (2007) argues that one-way shear and two-way shear are confusing terms, as shear is inherently unidirectional as a mechanical quantity (it can be represented as a vector). At any location, shear equilibrium is ensured by two components ( $v_x$  and  $v_y$ ). As a result, there is only one direction for principal shear, and not two directions as for moments, which are a tensorial quantity of a higher level, and have at each location two principal directions. Shear is thus exclusively carried in the direction of the principal shear, with no perpendicular shear transfer. In that sense, two-way shear is a physical impossibility. Based on the flow of shear forces, however, the concept of one-way and two-way shear can be explained. Zones in which one-way shear is acting, are the areas where the principal shear lines run parallel to one another. Zones in which two-way shear is acting are those in which the principal shear lines are not running in parallel, for example around a concentrated load.

Close to the support, the three-dimensional force flow of the punching mechanism interacts with the force flow from one-way shear and the modes cannot be treated independently (Lubell, 2006), Fig. 2.14. Similarly, when the size of the loaded area increases relative to the slab thickness and when the direction of the reinforcement more closely parallels the direction of the maximum moment when there is essentially one-way action, a slab can fail in shear as a wide beam.

A first difference between shear in beams and slabs is noted by Elstner and Hognestad (1956), revealing the link between the width and the failure mode. The behaviour of slab strip specimens was observed not to reflect the behaviour and mode of failure of a corresponding slab and slab strips were deemed unsuitable to evaluate the punching strength of slabs even though they were successfully used to model the flexural behaviour of slabs. Likewise, Hawkins and Mitchell (1979) differentiate between wide beam shear failure and punching shear failure based on the influence of flexure on the failure mode. For wide beam shear failure the shear strength is independent of the stiffness and therefore of the flexural strength of the slab. Contrarily, for punching failure the shear strength decreases as the stiffness of the connection decreases. Inclined cracking develops at about the same shear stress for either a wide beam or punching shear failure. However, for punching those cracks cannot open until there is a marked decrease in the tangential stiffness of the slab. A two-way reinforcement pattern or in-plane restraints will maintain stiffness and permit development of an ultimate capacity considerably greater than the beam shear capacity. Another difference (Criswell and Hawkins, 1973) lies in the inclined

### *Shear capacity of reinforced concrete members without shear reinforcement*

crack location. For punching, the inclined crack is confined to a region immediately adjacent to the perimeter of the loaded area. The crack is less free to develop at the weakest section than in a slender beam. Moreover, the stress conditions at the apex of the inclined crack are different. In a slab under a concentrated load, the concrete at the apex of the inclined crack is subjected to complex tri-axial stress conditions. The biaxial bending moments in the slab create orthogonal compressive stresses in a horizontal plane and the concentrated load causes compressive stresses in the vertical plane.

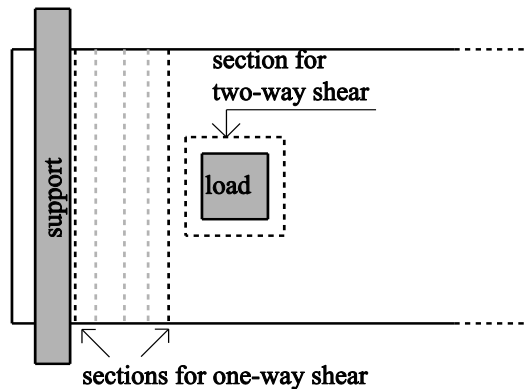


Fig. 2.14: Critical sections for shear.

#### 2.4.4 Effective width in wide beams and slabs

The effective width is determined from the stress distribution over the width of the slab (Goldbeck and Smith, 1916; Goldbeck, 1917) and is defined so that the resisting action due to the maximum stress distributed over the effective width equals the resisting action due to the variable stresses over the entire width, Fig. 2.15. For flexure, the effective width as a result of a wheel load on a slab can be found in the literature (Westergaard, 1930; Amer et al., 1999).

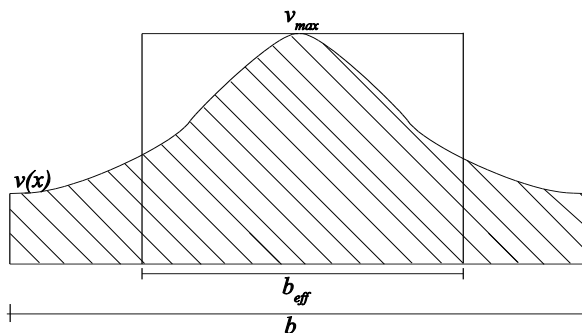


Fig. 2.15: Principle of effective width,  $b_{eff}$ : the area underneath the curve  $v(x)$  of the shear stresses over the width  $b$  equals the area of the maximum shear stress  $v_{max}$  over  $b_{eff}$ .

### *Shear capacity of reinforced concrete members without shear reinforcement*

For bridges, other than beam-and-slab, very little information on the shear distribution is available (Zokaie, 1992). The design methods to determine the effective width result from local practice. In Dutch practice, a  $45^\circ$  horizontal load spreading method from the centre of the load is used to determine the effective width at the face of the support (Fig. 2.16(a)) and in French practice the load spreading is taken from the farthest side of the load (Fig. 2.16(b)). In the Model Code 2010 (*fib*, 2012) guidelines for the determination of the effective width are given as indicated in Fig. 2.17. For simply supported slabs the angle of horizontal load spreading is taken as  $60^\circ$  and for clamped slabs  $45^\circ$ , as based on the Swiss Code SIA 162 (1968). Moreover, the shear stress is checked in a cross-section at a distance  $x = d_l$  provided that  $d_l \leq a_v/2$ .

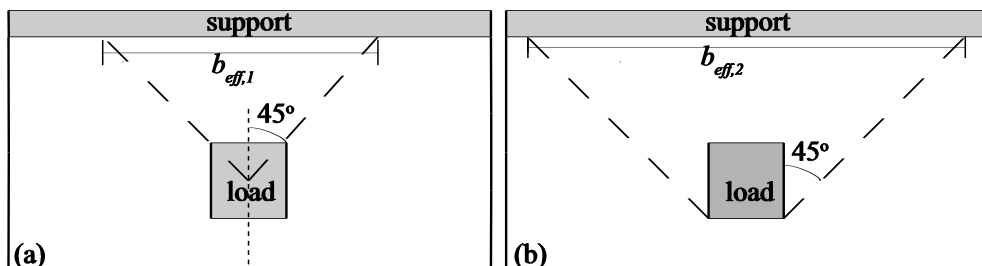


Fig. 2.16: (a) Load spreading under  $45^\circ$  and the resulting effective width as used in Dutch practice, (b) Load spreading and the resulting effective width as used in French practice, Chauvel et al. (2007).

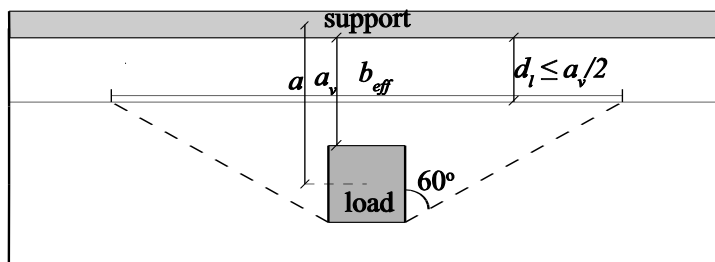


Fig. 2.17: Location and length of the control section,  $b_{eff}$ , for the determination of the shear resistance of slabs with point loads located close to a support line; simple edge support (*fib*, 2010).

In German practice (Grasser and Thielen, 1991), a formula is used, which results in much lower values for the effective width than when using the load spreading methods from Fig. 2.16 and Fig. 2.17. In the literature, additional methods for calculating the effective width for well-defined cases are suggested, none of which appears to be suitable for extrapolation towards a more general use (Taylor et al., 2003; Diaz de Cossio, 1962; Graf, 1933; Regan and Rezai-Jorabi, 1988).

## **2.5 Experiments and database**

The extended literature review (Lantsoght, 2012b) gives an overview of shear experiments on slabs and wide beams as reported in the literature. The resulting full database is provided as a table in Annex 1. The following columns can be found in the database:

Ref	the (abbreviated) author-date reference in which the experiments are reported;
Test	the name of the experiment as used in the original reference;
type	the category of experiment:
slab, SS	a simply supported slab or wide beam;
slab, CS	a continuously supported slab or wide beam;
cantilever	a cantilever slab;
real bridge	experiment on an existing decommissioned bridge;
n	the number of loads, either one number (number of loads at the same distance to the support), or two numbers separated by // when loads at multiple distances to the support are used;
$b$	the specimen width;
$f_{ck}$	the cylinder compressive strength of the concrete: when cube compressive strengths are reported in the original reference, the cylinder strength is assumed as 0,82 times the cube strength;
$a$	the centre-to-centre distance between the load or the centre of gravity of multiple loads and the support;
$b_r$	the distance between the free edge and the centre of the load along the width;
$b_{sup}$	the width of the support; this distance is taken in the span direction;
$l_{load}$	the length of the load; this distance is taken perpendicularly to the span direction;
$b_{load}$	the width of the load; taken in the span direction;
$\rho_l$	the reinforcement ratio in the span direction;
$\rho_t$	the ratio of the transverse flexural reinforcement;
$d_l$	the effective depth to the longitudinal reinforcement;
$d_t$	the effective depth to the transverse flexural reinforcement;
$a_v$	the clear shear span: the face-to-face distance between the concentrated load and the support;
$b_{eff1}$	the effective width based on the load spreading method from Fig. 2.16(a);
$b_{eff2}$	the effective width based on the load spreading method from Fig. 2.16(b);
mode	the observed failure mode determined on pictures and cracking patterns from the original reference:
WB	wide beam shear failure: inclined cracks fanning out from the load towards the support are visible on the bottom/top face;

### *Shear capacity of reinforced concrete members without shear reinforcement*

P	punching shear failure: punching off of a (partial) perimeter is visible on the bottom/top face;
nn	pictures, descriptions or crack patterns are not available;
DT	diagonal tension failure (as reported);
$F_{test}$	the maximum load as applied during the experiment;
$V_{test}$	the resulting maximum sectional shear force.

In the last columns of the database, a few checks are carried out, resulting in the value “1” if true and the value “0” if not true:

- $b_{eff1} < b$ : if the effective width is larger than the specimen width, three-dimensional load spreading as in a wide beam or slab is not assumed to occur;
- $b_{eff2} < b$ : similar criterion for the other studied horizontal load spreading method;
- $a/d_1 > 2,5$ ?: is there an influence of direct transfer from the load to the support by means of a compressive strut?
- $e$ ?: is the load placed in the middle of the slab width (0) or towards the edge (1)?

The database contains a total of 215 experiments from the literature. Some of these experiments are taken from the database by Reineck et al. (2003), which contains the results of 702 experiments on beams without shear reinforcement. Additional relevant experiments from the literature are used as well. From the experiments in the database from Annex 1, only 22 experiments on slabs ( $b_{eff2} < b$ ) close to the support ( $a/d_1 < 2,5$ ) are available, most of which are executed on small specimens ( $h \leq 150\text{mm}$ ). Practical slab bridges have a height of  $h \approx 600\text{mm}$ . The results of small specimens might not be fully representative for existing structures due to the size effect in shear. The size effect in shear leads to relatively smaller shear capacities for larger cross-sectional depths. Moreover, most of the 22 experiments are isolated experiments. Only Regan (1982) tested a series of experiments that can give some insight in the relative influence of the varied parameters. Therefore, there is a necessity for a comprehensive series of experiments using a larger cross-sectional height and varying systematically the important parameters that influence the shear capacity.

A remarkable observation is that for the results of Ekeberg et al. (1982) for punching failures in an existing building floor slab, in which lateral restraint was likely to activate compressive membrane forces, a minimum capacity is obtained for  $a/d_1 = 7,3$  while for beam shear laboratory experiments this minimum typically is observed to be around  $a/d_1 = 2,5$  (Kani, 1964).

The database shows crowding in the region with small cross-sectional depths and a relatively large reinforcement percentage, as observed in all shear databases available. A knowledge-based system using artificial neural networks, which uses a database of prior knowledge in combination with a method that mimics the problem-solving strategy of the human brain (Jung and Kim, 2008) could be used to analyse the database, taking its non-uniform distribution over the parameter ranges into account.

## *Shear capacity of reinforced concrete members without shear reinforcement*

When comparing results from a database to a suggested method, the variability of the material should be taken into account. Reineck (1997a) points out that different control specimens could yield differences in the tensile strength of more than 20% and up to 30%. Therefore, similar scatter can be expected in shear experiments. However, Walraven et al. (2012) show a good repeatability of beam shear tests under short-term loading.

### **2.6 Code provisions**

The following code provisions for beam shear and punching shear are studied in the full report of the literature review: NEN 6720:1995, NEN-EN 1992-1-1:2005 (+ French National Annex and Cortade, 2007), ACI 318-08 and Model Code 2010. Since these codes all use very different expressions for the shear capacity, these provisions reflect the lack of consensus on the shear capacity of members without shear reinforcement. NEN 6720:1995, NEN-EN 1992-1-1:2005 and ACI 318-08 are based on (semi-)empirical approaches, while Model Code 2010 is based on the Modified Compression Field Theory for one-way shear and on the Critical Shear Crack Theory for two-way shear. The aim of a code should be to give transparent models, based as much as possible on physical reality, verified by suitable tests and representative for the majority of the practical situations that the designer might encounter.

The code extension proposal in Chapter 6 and the Quick Scan method in Chapter 7 are based on the Eurocodes. Therefore, the beam shear provisions of NEN-EN 1992-1-1:2005 are repeated here. According to NEN-EN 1992-1-1:2005 §6.2.2 (1) the shear resistance for a structural member without stirrups is calculated as follows:

$$V_{Rd,c} = \left( C_{Rd,c} k (100 \rho_l f_{ck})^{1/3} + k_1 \sigma_{cp} \right) b_w d_l \geq (v_{min} + k_1 \sigma_{cp}) b_w d_l \quad (2.8)$$

$$k = 1 + \sqrt{\frac{200}{d_l}} \leq 2,0 \quad (2.9)$$

with:

- $V_{Rd,c}$  the design shear capacity in [kN];
- $k$  the size effect factor, with  $d_l$  in [mm];
- $\rho_l$  the flexural reinforcement ratio;
- $f_{ck}$  the characteristic cylinder compressive strength of the concrete in [MPa];
- $k_1$  0,15;
- $\sigma_{cp}$  the axial stress on the cross-section in [MPa];
- $b_w$  the web width of the section, or for slabs the effective width in [m];
- $d_l$  the effective depth to the main flexural reinforcement in [mm].

According to the Eurocode procedures, the values of  $C_{Rd,c}$  and  $v_{min}$  may be chosen nationally. The default values are  $C_{Rd,c} = 0,18/\gamma_c$  with  $\gamma_c=1,5$  in general and  $v_{min} (f_{ck}$  in [MPa]):

## *Shear capacity of reinforced concrete members without shear reinforcement*

$$v_{min} = 0,035k^{3/2}f_{ck}^{1/2} \text{ in [MPa]} \quad (2.10)$$

In the French National Annex (Chauvel et al., 2007) a different approach is used with regard to  $v_{min}$ . For slabs benefiting from transverse redistribution under the considered load case  $v_{min}$  is defined as ( $f_{ck}$  in [MPa]):

$$v_{min} = 0,34f_{ck}^{1/2} \text{ in [MPa]} \quad (2.11)$$

and for beams and slabs other than those described by Eq. (2.11) ( $f_{ck}$  in [MPa]):

$$v_{min} = 0,053k^{3/2}f_{ck}^{1/2} \text{ in [MPa]} \quad (2.12)$$

Note that when  $k = 2$ , the value of  $v_{min}$  according to Eq. (2.11) is 3,43 times larger than according to Eq. (2.10). NEN-EN 1992-1-1:2005 §6.2.2 (6) accounts for the influence of the shear span to depth ratio on direct load transfer. The contribution of a load applied within a distance  $0,5d_l \leq a_v \leq 2d_l$  from the edge of a support to the shear force  $V_{Ed}$  may be multiplied by the reduction factor  $\beta = a_v/2d_l$ . In that clause of the code, the distance  $a_v$  is considered the distance between the face of the load and the face of the support, or the centre of the support for flexible supports.

## **2.7 Conclusions**

### **2.7.1 Summary**

Slab bridges are robust structures, typically designed to fail in flexure instead of in shear. A small number of experiments on decommissioned solid slab bridges shows that these structures can typically carry loads that are significantly larger than their design loads. Another aspect of slabs is that, due to the extra dimension as compared to beams, transverse load redistribution should be considered. As the recently adopted Eurocodes use heavier live loads than previous national codes and more conservative shear provisions, wheel loadings resulting in increased sectional shear forces need to be considered for design and assessment.

An overview of the research on beam shear and punching shear from the past decades was given. First, the general mechanisms of shear transfer were discussed. Next, an overview of the existing models for beam shear and punching shear was given. For slabs under concentrated loads close to supports, the only available model in the literature is Regan's method (1982). Consequently, the differences and similarities between and the transition from beam shear to punching shear were studied. An overview of past research on the effective width of wide beams and slabs in shear was also given. A limited number of guidelines exist to give an estimate of the effective width in shear and the origins of these guidelines and national practices seem to be based on tradition and rules of thumb rather than on experiments or theoretical work. The only code that gives guidelines for the determination of the effective width in shear is Model Code 2010.

### *Shear capacity of reinforced concrete members without shear reinforcement*

A database with relevant test results is given in Annex 1. In this database, a distinction is made between punching shear failures and one-way shear failures. The database is subdivided into different categories, as not all design approaches are suitable for all cases. As most databases, the constructed database shows crowding in the small size and relatively large reinforcement percentage region. Only 22 experiments on slabs benefiting from transverse redistribution with the load placed close to the support are available.

The on-going debate in the literature on how to deal with shear in concrete members is also reflected by the code provisions. The studied codes (Dutch Code NEN 6720:1995, NEN-EN 1992-1-1, ACI 318 and Model Code 2010) all recommend very different approaches that result in different design shear capacities and take the parameters affecting the shear capacity into account in a different way.

#### *2.7.2 Discussion*

Most of our knowledge on shear is the result of experiments on small, heavily reinforced slender beams subjected to two concentrated loads, and most of our knowledge on punching shear is the result of experiments on centrally loaded unconfined slab-column connection specimens. It might be questionable to extrapolate this knowledge to the case of slab bridges under live loads.

Another point of discussion is the breakdown of shear into the shear carrying mechanisms. It is difficult to experimentally investigate these mechanisms separately, and to prove that the total shear capacity is the result of the sum of the capacities of these mechanisms.

Within the developed models for shear, a multitude of different approaches is available. However, a closer look at most of the theories shows more similarities and commonly shared assumptions than initially expected. Most theories use a formulation that is related to a plasticity-based approach, in which the traditional failure modes are considered: yielding of the reinforcement or failure of the concrete in compression, typically expressed by the concrete reaching a concrete compressive strength limit that is lower than the uniaxial compressive strength as a result of the multi-axial stress state. None of the studied models is developed for the application of concrete slab bridges under a wheel load close to the support line, and therefore all methods contain some major drawbacks. The Modified Compression Field Theory has not been derived or expanded for the application to slabs, and is therefore less suitable for slabs subjected to concentrated loads close to the support, and cannot be applied to the problem of punching. It is questionable if this method can adequately model the transitional problem of shear in one-way slabs under a concentrated load. The Critical Shear Crack Theory uses formulas that are in the same format for one-way shear as well as for two-way shear, although the underlying assumptions are different. However, in the case of a concentrated load close to the support, the non-axis-symmetrical layout needs to be taken into account, and finite

### *Shear capacity of reinforced concrete members without shear reinforcement*

element programs are necessary to determine the moment-curvature relation and the stress distribution along the punching perimeter. Strut-and-tie models can be applied for the problem of a concentrated loads on slabs. There is however an art in selecting the right strut-and-tie model, which might make the approach not suitable for the assessment practice. Both plasticity-based and fracture mechanics models need to be considered with regard to the assumptions on which the models are based. These assumptions are a simplification of reality and may not always be applicable to the problem under study. For example, the ductility requirement for using plasticity-based models is not always fulfilled for shear failures. Ideally, the empirical code formulas should be replaced by calculation methods with a theoretical basis.

The distinction between one-way and two-way shear in slabs is not clear and there seems to be a transition zone between these two failure mechanisms. Also, there seems to be no consensus in the literature on how to determine the failure mode based on pictures and the cracking pattern as observed in experiments.

So far, the only code that gives recommendations for the determination of the effective width in shear is Model Code 2010. While the approaches from the existing codes generally lead to safe designs with a satisfactory margin of safety, they are by definition not suitable for assessing the shear capacity of an existing structure when additional load-carrying mechanisms need to be taken into account.

#### *2.7.3 Conclusions and outlook*

Up to date, none of the existing theoretical approaches for one-way shear or two-way shear seem to be able to fully explain the mechanics behind the problem of shear failure. For the problem of a one-way slab under a concentrated load, the additional dimension of the slab needs to be taken into account, thus further complicating the mechanics behind the failure mechanism. For design, therefore, simplified methods need to be used. The only method tailored for the problem of shear in slabs under concentrated loads close to the support is the empirical approach developed by Regan (1982).

A database of existing test results is compiled. This database shows that a very limited amount of experimental results on slabs under concentrated loads close to the support is available in the literature. Most of the available results are based on small-scale specimens in which the size effect might have resulted in higher shear capacities as compared to slabs in practice.

There is a significant distinction between the design practice, which needs a good tool to guarantee a safe design, on the one hand and on the other hand the analysis and assessment practice, which needs a model to accurately describe the behaviour of a slab bridge under wheel loads in shear. The first need seems to be satisfied with code provisions that work adequately well in practice. The second need is not fulfilled, as none of the

*Shear capacity of reinforced concrete members without shear reinforcement*

discussed models explain the behaviour of or can be extrapolated to slabs under concentrated loads close to supports.

Therefore, experiments on slabs under concentrated loads close to supports are necessary to gain a better understanding of the problem. These experiments are described in the following chapter and discussed with respect to the studied parameters in Chapter 4.

*Shear capacity of reinforced concrete members without shear reinforcement*

### **3 Experiments**

#### **3.1 Introduction**

In this chapter, an overview of the experiments on reinforced concrete slabs subjected to concentrated loads and their results is given. The setup for the experiments is described and additional attention is given to the measuring devices. Also, the tested specimens are described with regard to their material properties and reinforcement layout. Then, all results of the experiments are given in terms of the maximum load, the maximum calculated sectional shear at the support, the maximum occurring force on the vertical prestressing bars restraining the rotation of the cantilevering end of the slab (Fig. 3.1) and the failure mode.

#### **3.2 Test setup**

##### **3.2.1 Slabs under a concentrated load**

Slabs of  $5\text{m} \times 2,5\text{m} \times 0,3\text{m}$  and slab strips of  $5\text{m} \times 0,3\text{m}$  with a variable width are tested. The slabs are a half-scale model of a continuous solid slab bridge. A sketch of the test setup in top view is given in Fig. 3.1 and a side view is given in Fig. 3.2. The load can be applied at different positions along the width and close to support 1 (sup 1 in Fig. 3.1) or close to support 2 (sup 2 in Fig. 3.1). The load is applied by a displacement-controlled hydraulic jack (Fig. 3.2). The distance between the load and the support is varied. Loading plates of  $200\text{mm} \times 200\text{mm}$  and  $300\text{mm} \times 300\text{mm}$  are used.

Line supports as well as three elastomeric bearings per side are used as support conditions. The line support consists of an HEM 300 beam (width of 300mm), a layer of plywood and a layer of felt of 100mm wide (Fig. 3.1a). Alternatively, three elastomeric bearings of  $350\text{mm} \times 280\text{mm} \times 45\text{mm}$  per support line are placed on a steel HEM 300 beam (Fig. 3.1b). The bearings contain 3 layers of 8mm natural rubber, 4 layers of 4mm steel S235 and 2 layers of 2,5mm chloroprene, resulting in a compression stiffness of 2361kN/mm. The properties of the plywood and felt are described by Prochazkova and Lantsoght (2011).

Support 1 (sup 1) is a simple support and support 2 (sup 2) is considered as a continuous support. Prestressing bars, anchored to the laboratory floor, are used to restrain the rotation at support 2 (sup 2) and thus create a moment over support 2 (sup 2). The prestress is applied before the start of every test, initially compensating for the self-weight of the slab. Due to the deformation of the felt and plywood and the elongation of the prestressing bars, some rotation could occur at support 2. The force in the prestressing bars is measured by load cells, so that the moment over support 2 is known at any time during the experiment.





## Experiments

### 3.2.2 *Slabs under a combination of loads*

In the second series of experiments, slabs of  $5\text{m} \times 2,5\text{m} \times 0,3\text{m}$  are tested. A sketch of the top view of the setup is shown in Fig. 3.4. A frame consisting of HEM 1000 beams (1000mm wide) was necessary to support the loading jacks for this series of experiments as the combination of loads induces large moments into the frame. The concentrated load can be applied at different locations along the width and close to support 1 (sup 1 in Fig. 3.4) or close to support 2 (sup 2 in Fig. 3.4). The distance between the concentrated load and the support can be altered as well, while the distance between the line load and the support is fixed at 1,2m. The size of the loading plate is taken as  $300\text{mm} \times 300\text{mm}$ . The support consists of an HEM 300 beam (300mm wide) and 7 bearings (steel or elastomeric) on hinges and load cells. When steel bearings are used for the support, 7 strips of steel of  $100\text{mm} \times 350\text{mm} \times 15\text{mm}$  and felt strips of  $100\text{mm} \times 350\text{mm} \times 5\text{mm}$  are used on top of the steel bearings. As in the first series of experiments, support 1 (sup 1 in Fig. 3.4) is considered as a simple support and support 2 (sup 2 in Fig. 3.4) as a continuous support. An overview of the locations of the lasers that measure the deflections is shown in Fig. 3.5.

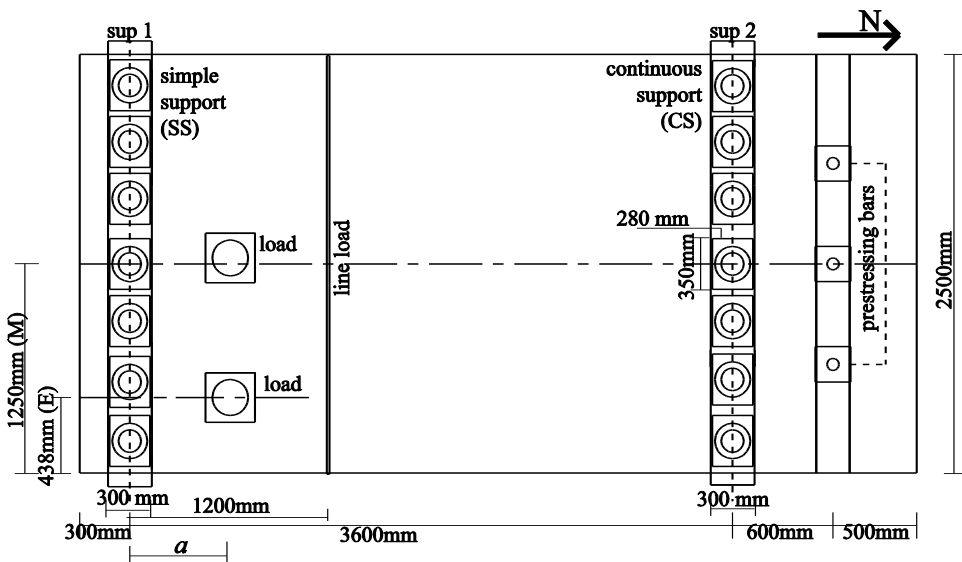


Fig. 3.4: Top view of setup used for slabs under a combination of loads. Units: [mm].

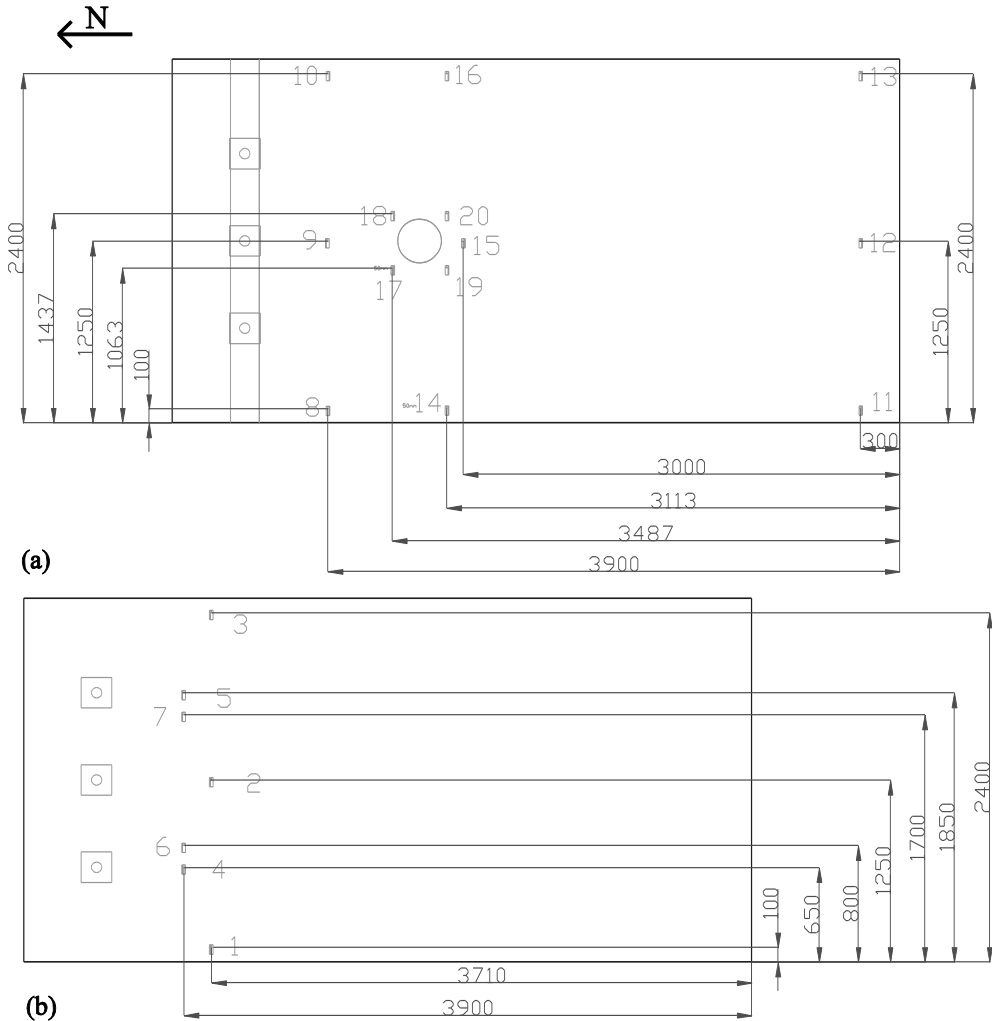


Fig. 3.5: Locations of lasers in second series of experiments: (a) top; (b) bottom. Units: [mm].

### 3.3 Specimens

An overview of the properties of the 26 slabs (S-series) and 12 slab strips (B-series) is given in Table 3.1, with:

- $b$  the specimen width;
- $d_l$  the effective depth to the longitudinal reinforcement;
- $d_t$  the effective depth to the transverse reinforcement;
- $f_{c,meas}$  the measured cube compressive strength of the concrete at the age of testing;
- $f_{ct,meas}$  the measured tensile splitting strength of the concrete at the age of testing;
- $\rho_l$  the amount of main flexural reinforcement;

## Experiments

- $\rho_t$  the amount of transverse flexural reinforcement;
- r/p the type of reinforcing bars: ribbed (r) or plain (p);
- $a$  the centre-to-centre distance between the load and the support;
- $a/d_t$  the ratio of the distance between the load and the support (or shear span) to the effective depth;
- n number of experiments carried out on the specimen;
- $z_{load}$  the size of the square loading plate;
- M/E the location of the load along the width of the slab: in the middle (M) or near the edge (E);
- sup the type of support that is used: “line” (line support using plywood and felt), “3 el” (3 elastomeric bearings per support line), “7 st” (7 steel bearings per support line), “7st\*” (7 steel bearings plus strip of steel and felt) or “7 el” (7 elastomeric bearings);
- age the age at the time of the first experiment on the specimen;
- var this parameter has been varied in the experiments on this specimen.

The maximum aggregate size is 16mm for all specimens. Glacial river aggregates were used. The reinforcement layout of S1 and S2 is shown in Fig. 3.7(a) en Fig. 3.7(b), of S3, S5 – S10 and S19 – S26 in Fig. 3.7(c) and of S4 in Fig. 3.7(d). The reinforcement layout of the slabs with plain reinforcement (S11 – S14) is shown in Fig. 3.8(a, b) and of the slabs on elastomeric bearings (S15 – S18) in Fig. 3.9(a, b). For the slab strips (BS1 – BX3), the reinforcement of the BS series is shown in Fig. 3.6 and all other slab strips are reinforced in a similar, yet proportional, way. Deformed bars of steel S500 (measured properties for  $\phi 20\text{mm}$ :  $f_{ym} = 542\text{MPa}$  yield strength;  $f_{um} = 658\text{MPa}$  ultimate strength and for  $\phi 10\text{mm}$ :  $f_{ym} = 537\text{MPa}$ ;  $f_{um} = 628\text{MPa}$ ) are used. Plain bars of steel 52.3K (measured properties for  $\phi 20\text{mm}$ :  $f_{ym} = 601\text{MPa}$ ;  $f_{um} = 647\text{MPa}$  and for  $\phi 10\text{mm}$ :  $f_{ym} = 635\text{MPa}$ ;  $f_{um} = 700\text{MPa}$ ) are used.

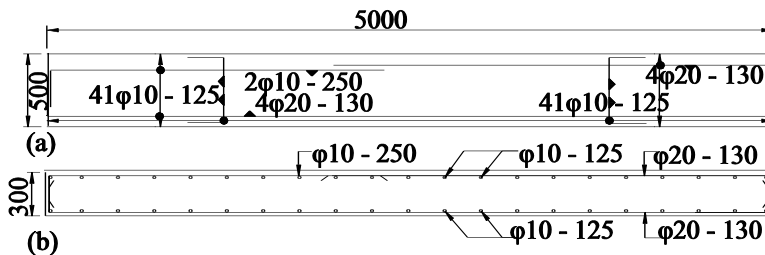


Fig. 3.6: Reinforcement layout for slab strips: (a) top view of BS1; (b) cross-section of BS1.

Table 3.1: Properties of the studied specimens<sup>1</sup>

Slab nr.	b (m)	d <sub>t</sub> (m)	d <sub>t</sub> (m)	f <sub>concr</sub> (MPa)	f <sub>concr</sub> (MPa)	ρ <sub>t</sub> (%)	ρ <sub>t</sub> (%)	r/p	a (m)	a/d <sub>t</sub>	n	M/E	z <sub>load</sub> (mm)	sup	age	
line support normal strength concrete	S1	2,5	0,265	0,250	35,8	3,1	0,996	0,132	r	0,6	2,26	6	M	200	line	28
	S2	2,5	0,265	0,250	34,5	2,9	0,996	0,132	r	0,6	2,26	6	M	300	line	56
	S3	2,5	0,265	0,250	51,6	4,1	0,996	0,258	r	0,6	2,26	5	M	300	line	63
	S4	2,5	0,265	0,250	51,7	4,2	0,996	0,182	r	0,6	2,26	6	E	300	line	76
	S5	2,5	0,265	0,250	48,2	3,8	0,996	0,258	r	0,4	1,51	5	M	300	line	31
	S6	2,5	0,265	0,250	50,6	3,9	0,996	0,258	r	0,4	1,51	6	E	300	line	41
high strength concrete	S7	2,5	0,265	0,250	82,1	6,2	0,996	0,258	r	0,6	2,26	6	E	300	line	83
	S8	2,5	0,265	0,250	77,0	6,0	0,996	0,258	r	0,6	2,26	3	M	300	line	48
	S9	2,5	0,265	0,250	81,7	5,8	0,996	0,258	r	0,4	1,51	6	M	200	line	77
	S10	2,5	0,265	0,250	82,4	5,8	0,996	0,258	r	0,4	1,51	7	E	200	line	90
plain rebars	S11	2,5	0,265	0,250	54,9	4,2	1,375	0,358	p	0,6	2,26	6	M	200	line	90
	S12	2,5	0,265	0,250	54,8	4,2	1,375	0,358	p	0,6	2,26	6	E	200	line	97
	S13	2,5	0,265	0,250	51,9	4,2	1,375	0,358	p	0,4	1,51	6	M	200	line	91
	S14	2,5	0,265	0,250	51,3	4,2	1,375	0,358	p	0,4	1,51	6	E	200	line	110
rubber bearings	S15	2,5	0,255	0,233	52,2	4,2	1,035	1,078	r	0,6	2,35	5	M	200	3 el	71
	S16	2,5	0,255	0,233	53,5	4,4	1,035	1,078	r	0,6	2,35	6	E	200	3 el	85
	S17	2,5	0,255	0,233	52,5	3,7	1,035	1,078	r	0,4	1,57	6	M	200	3 el	69
	S18	2,5	0,255	0,233	52,1	4,5	1,035	1,078	r	0,4	1,57	6	E	200	3 el	118
+ line load	S19	2,5	0,265	0,250	56,9	4,7	0,996	0,258	r	0,6	2,26	2	M	300	7 st	89
	S20	2,5	0,265	0,250	60,5	4,7	0,996	0,258	r	0,6	2,26	5	M	var	7 st	176
	S21	2,5	0,265	0,250	56,8	4,5	0,996	0,258	r	0,6	2,26	6	M	300	7 st*	187

<sup>1</sup> For slab S25, experiments are carried out with the concentrated load at a = 0,6m and with the concentrated load at a = 0,4m.

Experiments

Slab nr.	<i>b</i> (m)	<i>d<sub>1</sub></i> (m)	<i>d<sub>2</sub></i> (m)	<i>f<sub>c,meas</sub></i> (MPa)	<i>f<sub>c,meas</sub></i> (MPa)	<i>ρ<sub>t</sub></i> (%)	<i>ρ<sub>t</sub></i> (%)	<i>r/p</i>	<i>a</i> (m)	<i>a/d<sub>1</sub></i>	<i>n</i>	M/E	<i>z<sub>load</sub></i> (mm)	sup	age	
+ line load	S22	2,5	0,265	0,250	58,0	4,5	0,996	0,258	r	0,6	2,26	4	E	7 st*	188	
	S23	2,5	0,265	0,250	58,9	4,7	0,996	0,258	r	0,6	2,26	2	M	7 el	197	
	S24	2,5	0,265	0,250	58,9	4,7	0,996	0,258	r	0,6	2,26	4	E	7 el	183	
	S25	2,5	0,265	0,250	58,6	4,5	0,996	0,258	r	var	var	5	M	7 st*	170	
	S26	2,5	0,265	0,250	58,6	4,5	0,996	0,258	r	0,4	1,51	5	M&E	7 st*	174	
	BS1	0,5	0,265	0,250	81,5	6,1	0,996	0,258	r	0,6	2,26	2	M	300	line	55
slab strips	BM1	1,0	0,265	0,250	81,5	6,1	0,996	0,258	r	0,6	2,26	2	M	300	line	62
	BL1	1,5	0,265	0,250	81,5	6,1	0,996	0,258	r	0,6	2,26	2	M	300	line	189
	BS2	0,5	0,265	0,250	88,6	5,9	0,996	0,258	r	0,4	1,51	2	M	200	line	188
	BM2	1,0	0,265	0,250	88,6	5,9	0,996	0,258	r	0,4	1,51	2	M	200	line	188
	BL2	1,5	0,265	0,250	94,8	5,9	0,996	0,258	r	0,4	1,51	2	M	200	line	180
	BS3	0,5	0,265	0,250	91,0	6,2	0,996	0,258	r	0,6	2,26	2	M	300	line	182
	BM3	1,0	0,265	0,250	91,0	6,2	0,996	0,258	r	0,6	2,26	2	M	300	line	182
	BL3	1,5	0,265	0,250	81,4	6,2	0,996	0,258	r	0,6	2,26	2	M	300	line	171
	BX1	2,0	0,265	0,250	81,4	6,0	0,996	0,258	r	0,6	2,26	2	M	300	line	47
	BX2	2,0	0,265	0,250	70,4	5,8	0,996	0,258	r	0,4	1,51	2	M	200	line	39
	BX3	2,0	0,265	0,250	78,8	6,0	0,996	0,258	r	0,6	2,26	2	M	200	line	40

Experiments

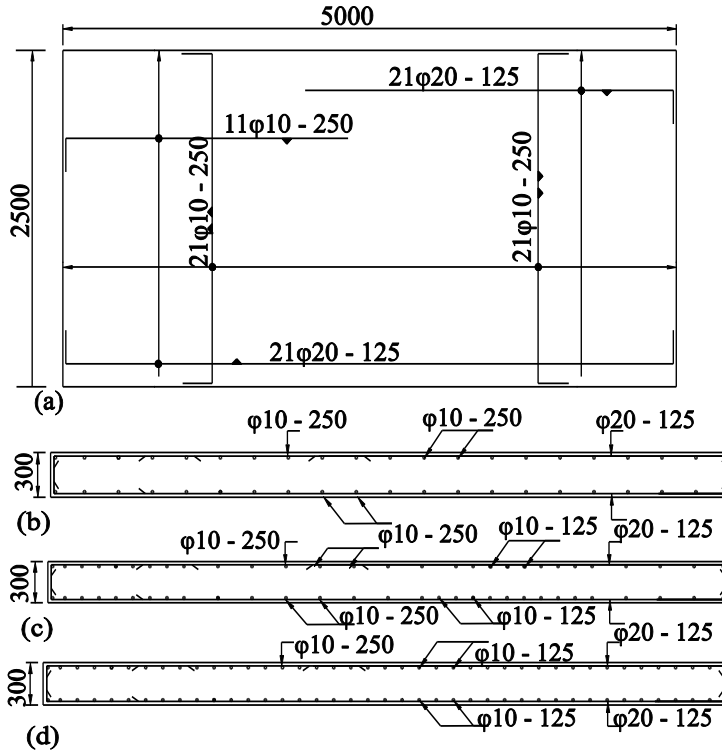


Fig. 3.7. Reinforcement layout (a) top view of S1 and S2; (b) cross-section of S1 and S2; (c) cross-section of S3, S5-S10 and S19-S26; (d) cross-section of S4. Note the difference in transverse reinforcement in (b), (c) and (d).

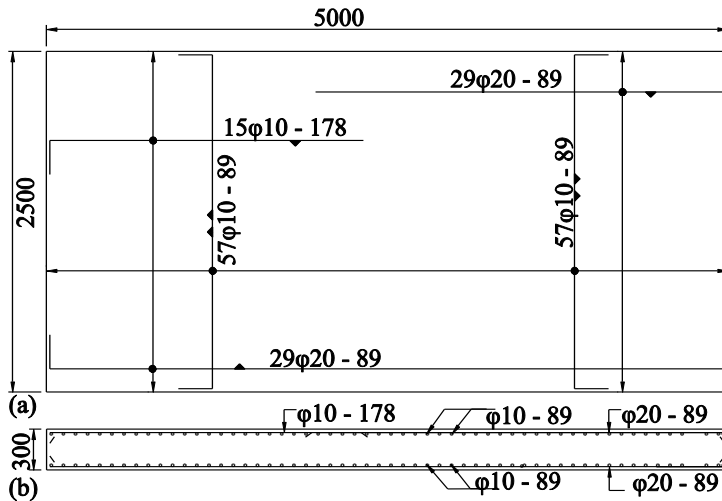


Fig. 3.8: Reinforcement layout for slabs with plain reinforcement S11-S14: (a) top view; (b) cross-section.

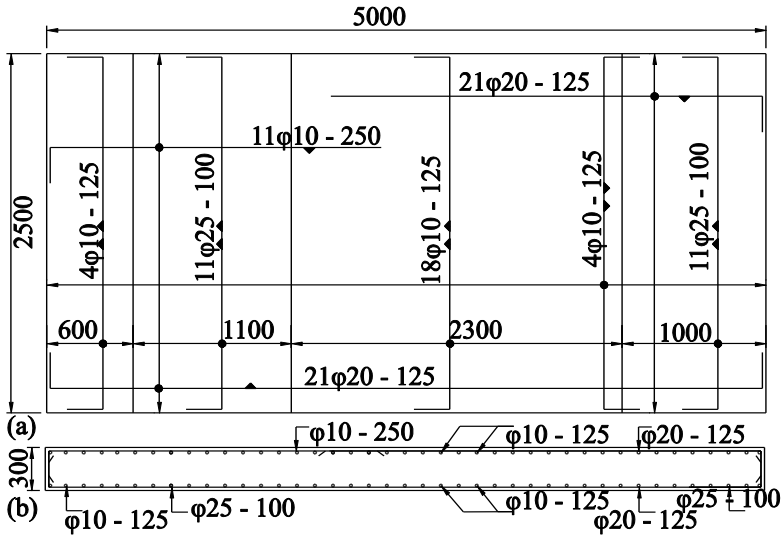


Fig. 3.9: Reinforcement layout for slabs on bearings S15-S18; (a) top view; (b) cross-section.

### 3.4 Results

#### 3.4.1 Overview of experimental results

The results of all experiments (127 in the first series and 29 in the second series) are summarised in Table 3.2 for the first series and in Table 3.3 for the second series, with:

$a/d_l$  the ratio between the shear span (the distance between the load and the support) and the effective depth to the longitudinal reinforcement;

$b_r$  the distance between the edge and the centre of the load, along the width;

SS/CS load placed near to the simple support (SS, sup 1 in Fig. 3.1) or the continuous support (CS, sup 2 in Fig. 3.1);

uncr/c experiment on an undamaged or uncracked (uncr) specimen or on a locally failed and heavily cracked (c) specimen;

$P_u$  the maximum concentrated load during the experiment;

$P_{line}$  the maximum force applied on top of the line load during the experiment (second series only);

Mode the observed failure mode:

- failure as a wide beam in shear with cracks at an angle to the axis of the span direction, denoted as “inclined cracks at the bottom” (WB, Fig. 3.10a);
- beam shear failure away from the support, typically between the concentrated load and the line load, only observed in the second series of experiments (B', Fig. 3.10b);

## *Experiments*

- punching failure around the discrete (Fig. 3.1b) support (SF, Fig. 3.10c);
- anchorage failure (A, Fig. 3.10d);
- failure as a beam in shear with a noticeable shear crack at the side (B, Fig. 3.10e); or
- development of a partial punching surface on the bottom face (P, Fig. 3.10f);

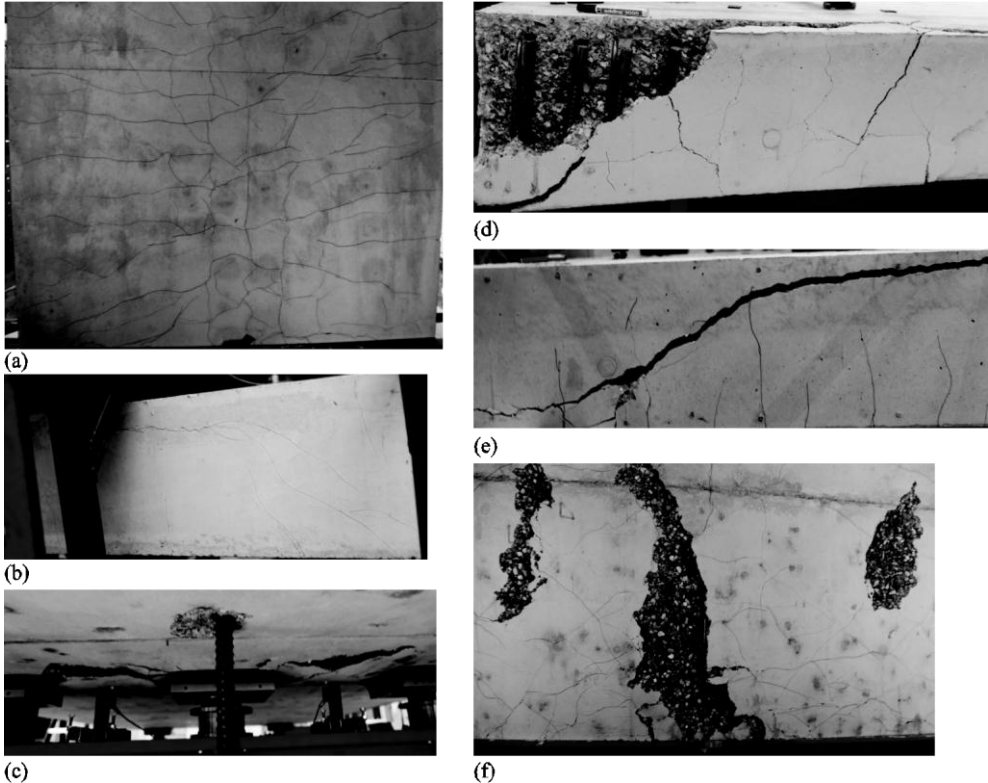


*Fig. 3.10: (a) WB crack pattern: inclined cracks at the bottom face (BL3T1); (b) B': shear crack at the side face away from the support (S21T1); (c) SF: failure at the support (S17T1); (d) A: Anchorage failure (S11T3); (e) B: shear crack at the side face (BL3T1); (f) P: partial punching at the bottom face (S14T6).*

- $F_{pres}$  the sum of the forces on the prestressing bars as measured by the load cells;
- $V_{exp}$  the shear force at failure when the slab is considered as a beam on two supports, taking into account self-weight, the concentrated load, the force due to the prestressing bars and –for the second series of experiments- the line load and the self-weight of the line load;
- $V_{add}$  the shear force at failure at the cross-section of the largest  $V_{exp}$  when the slab is considered a beam on two supports, taking into account self-weight and the force

## Experiments

due to the prestressing bars and -for the second series of experiments- the line load and the self-weight of the line load;

$V_{conc}$  the shear force at failure due to the concentrated load at the cross-section of the largest  $V_{exp}$  when the slab is considered a beam on two supports.

The loading sequence as executed on a slab in the first series of experiments is explained taking S5 as an example in Fig. 3.11. The first experiment (S5T1) is executed on a specimen without any damage (uncracked, uncr). As a result of this experiment, the slab will have failed locally and will be heavily damaged. The next experiment (S5T2) in the vicinity of the previous failure gives an indication of the remaining capacity of a heavily cracked (c) and locally failed slab. Consecutively, experiments are carried out at the other support (for S5, sup 1) where again the first experiment (S5T4) is considered to be executed on an undamaged specimen and the next experiments (S5T5 and S5T6) as influenced by the failure of S5T4.

In the second series, the application of the line load resulted in cracks over the full width upon damaging the specimen. Only some additional experiments in the vicinity of a local failure resulted in a useful test result, which have been denoted as “c, OK” in Table 3.3. In such a test, a new shear crack developed between the load in a new position and the support, while in other experiments (“c”) an existing crack opened and no new information could be obtained. Tests at the north side of the slab (Fig. 3.11), but without prestressing have been denoted by SS’ in the second series of experiments.

A complete description of the experiments can be found in the full test reports (Lantsoght, 2011a, b for the first series and Lantsoght, 2012c for the second series).

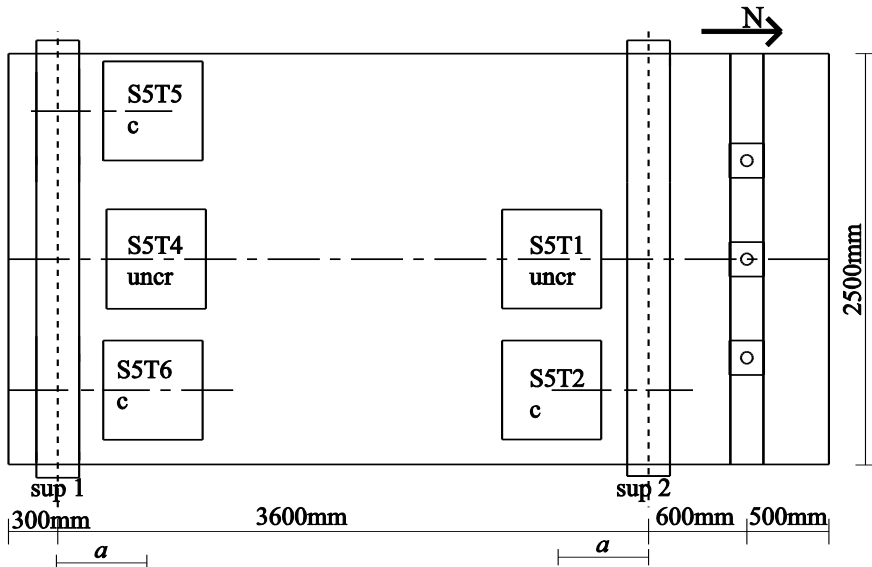


Fig. 3.11: Loading sequence on a slab, taking S5 as an example.

Experiments

Table 3.2: Results of first series of experiments

Test	$d_l$ (m)	$d_t$ (m)	$a$ (m)	$b_r$ (mm)	SS/CS	uncr/c	$P_{exp}$ (kN)	Mode	$F_{pres}$ (kN)	$V_{exp}$ (kN)	$V_{add}$ (kN)	$V_{conc}$ (kN)
S1T1	0,265	0,250	0,60	1250	SS	uncr	954	WB	163	799	4	795
S1T2	0,265	0,250	0,60	1250	CS	uncr	1023	WB	138	912	60	853
S1T3	0,265	0,250	0,62	438	CS	c	758	WB + B	87	683	51	632
S1T4	0,265	0,250	0,60	438	CS	c	731	WB + B	100	663	53	609
S1T5	0,265	0,250	0,60	438	SS	c	851	WB + B	147	716	6	709
S1T6	0,265	0,250	0,60	438	SS	c	659	WB + B	145	556	7	549
S2T1	0,265	0,250	0,60	1250	SS	uncr	1374	WB + P	280	1129	-16	1145
S2T2	0,265	0,250	0,60	438	SS	c	1011	WB + B	228	835	-7	843
S2T3	0,265	0,250	0,60	438	SS	c	844	WB + B	248	693	-11	703
S2T4	0,265	0,250	0,60	1250	CS	uncr	1421	WB	330	1276	92	1184
S2T5	0,265	0,250	0,60	438	CS	c	805	WB + B	153	733	62	671
S2T6	0,265	0,250	0,60	438	CS	c	957	WB + B	177	864	66	798
S3T1	0,265	0,250	0,60	1250	SS	uncr	1371	WB	252	1131	-11	1143
S3T2	0,265	0,250	0,60	438	SS	c	993	WB + B	245	818	-10	828
S3T3	0,265	0,250	0,60	438	SS	c	705	WB + B	190	587	-1	588
S3T4	0,265	0,250	0,60	1250	CS	uncr	1337	WB + B	287	1199	84	1114
S3T5	0,265	0,250	0,60	438	CS	c	852	WB + B	128	768	58	710
S4T1	0,265	0,250	0,60	438	SS	uncr	1160	WB + B	203	964	-3	967
S4T2	0,265	0,250	0,60	438	SS	uncr	1110	WB + B	187	925	0	925
S4T3	0,265	0,250	0,60	1250	SS	c	1016	WB	227	840	-7	847
S4T4	0,265	0,250	0,60	438	CS	c	861	WB + B	158	781	63	718
S4T5	0,265	0,250	0,60	438	CS	c	1014	WB + B	185	913	68	845
S4T6	0,265	0,250	0,60	1250	CS	c	994	WB	147	889	61	828
S5T1	0,265	0,250	0,40	1250	CS	uncr	1804	WB + B	235†	1679	76	1604
S5T2	0,265	0,250	0,40	438	CS	c	1395	WB + B	162†	1304	64	1240
S5T4	0,265	0,250	0,40	1250	SS	uncr	1755	WB + B	280†	1544	-16	1560
S5T5	0,265	0,250	0,40	438	SS	c	1295	WB + B	227†	1144	-7	1151
S5T6	0,265	0,250	0,40	438	SS	c	1286	WB + B	170†	1146	3	1143
S6T1	0,265	0,250	0,40	438	CS	uncr	1446	WB + B	183†	1353	67	1285
S6T2	0,265	0,250	0,40	438	CS	uncr	1423	WB + B	213†	1337	72	1265
S6T3	0,265	0,250	0,40	1250	CS	c	1897	WB	313†	1775	89	1686
S6T4	0,265	0,250	0,40	438	SS	uncr	1366	WB + B	195†	1213	-2	1214
S6T5	0,265	0,250	0,40	438	SS	uncr	1347	WB + B	245†	1187	-10	1197
S6T6	0,265	0,250	0,40	1250	SS	c	1384	WB	270†	1216	-14	1230

*Experiments*

Test	$d_l$ (m)	$d_t$ (m)	$a$ (m)	$b_r$ (mm)	SS/CS	uncr/c	$P_{exp}$ (kN)	Mode	$F_{pres}$ (kN)	$V_{exp}$ (kN)	$V_{add}$ (kN)	$V_{conc}$ (kN)
<b>S7T1</b>	0,265	0,250	0,60	438	SS	uncr	1121	WB + P + B	217	929	-5	934
<b>S7T2</b>	0,265	0,250	0,60	438	CS	uncr	1172	WB + P + B	197	1046	69	977
<b>S7T3</b>	0,265	0,250	0,60	438	CS	uncr	1136	WB + P + B	227	1021	74	947
<b>S7T4</b>	0,265	0,250	0,60	1250	CS	c	1128	WB + P	188	1008	68	940
<b>S7T5</b>	0,265	0,250	0,60	438	SS	uncr	1063	WB + P + B	157	891	5	886
<b>S7T6</b>	0,265	0,250	0,60	1250	SS	c	1011	WB + P	443	799	-43	843
<b>S9T3</b>	0,265	0,250	0,40	438	SS	c	1089	WB + P + B	178	969	1	968
<b>S9T4</b>	0,265	0,250	0,40	1250	CS	uncr	1842	WB + P	255	1717	79	1637
<b>S9T5</b>	0,265	0,250	0,40	438	CS	c	1287	WB + B	138	1204	60	1144
<b>S9T6</b>	0,265	0,250	0,40	438	CS	c	1128	WB + B	87	1054	51	1003
<b>S10T1</b>	0,265	0,250	0,40	438	SS	uncr	1320	WB + P + B	162	1177	4	1173
<b>S10T2</b>	0,265	0,250	0,40	438	SS	uncr	1116	WB + P + B	173	994	2	992
<b>S10T3</b>	0,265	0,250	0,40	1250	SS	c	1326	WB + P	320	1156	-23	1179
<b>S10T4</b>	0,265	0,250	0,40	438	CS	uncr	1511	WB + (B)	252	1422	79	1343
<b>S10T4B<sup>2</sup></b>	0,265	0,250	0,40	438	CS	c	1058	WB + B	165	1005	64	940
<b>S10T5</b>	0,265	0,250	0,40	438	CS	uncr	1454	WB + B	235	1368	76	1292
<b>S10T6</b>	0,265	0,250	0,40	1250	CS	c	1431	WB	233	1348	76	1272
<b>S11T1</b>	0,265	0,250	0,60	1250	SS	uncr	1194	WB + P	165	998	3	995
<b>S11T2</b>	0,265	0,250	0,60	438	SS	c	869	P	162	728	4	724
<b>S11T3</b>	0,265	0,250	0,60	438	SS	c	890	WB + P + B + A	253	730	-11	742
<b>S11T4</b>	0,265	0,250	0,60	1250	CS	uncr	958	WB + P	307	886	88	798
<b>S11T5</b>	0,265	0,250	0,60	438	CS	c	566	WB + B	180	538	67	472
<b>S11T6</b>	0,265	0,250	0,60	438	CS	c	492	WB + B	147	471	61	410
<b>S12T1</b>	0,265	0,250	0,60	438	SS	uncr	931	WB + B + P	162	780	4	776
<b>S12T2</b>	0,265	0,250	0,60	438	SS	uncr	1004	P	173	839	2	837
<b>S12T3</b>	0,265	0,250	0,60	1250	SS	c	1053	WB + P	193	876	-1	878
<b>S12T4</b>	0,265	0,250	0,60	438	CS	uncr	773	WB + P + B	147	705	61	644
<b>S12T5</b>	0,265	0,250	0,60	438	CS	uncr	806	WB + B	158	735	63	672
<b>S12T6</b>	0,265	0,250	0,60	1250	CS	c	683	WB + P	107	624	54	569

<sup>2</sup> Repeated test of S10T4, during which at the moment of reaching the maximum load, the loading plate started to slide away from underneath the jack and the experiment was aborted.

*Experiments*

Test	$d_l$ (m)	$d_t$ (m)	$a$ (m)	$b_r$ (mm)	SS/CS	uncr/c	$P_{exp}$ (kN)	Mode	$F_{pres}$ (kN)	$V_{exp}$ (kN)	$V_{add}$ (kN)	$V_{conc}$ (kN)
S13T1	0,265	0,250	0,40	1250	SS	uncr	1404	WB + P	157	1253	5	1248
S13T2	0,265	0,250	0,40	438	SS	c	1253	WB + P + B	137	1122	8	1114
S13T3	0,265	0,250	0,40	438	SS	c	916	WB + P + B	183	815	0	814
S13T4	0,265	0,250	0,40	1250	CS	uncr	1501	WB + P	240	1411	77	1334
S13T5	0,265	0,250	0,40	438	CS	c	1062	WB + B	150	1006	62	944
S13T6	0,265	0,250	0,40	438	CS	c	1023	WB + B	150	971	62	909
S14T1	0,265	0,250	0,40	438	SS	uncr	1214	WB + P + B	133	1088	9	1079
S14T2	0,265	0,250	0,40	438	SS	uncr	1093	WB + P + B	162	975	4	972
S14T3	0,265	0,250	0,40	1250	SS	c	1385	WB + B	230	1224	-8	1231
S14T4	0,265	0,250	0,40	438	CS	uncr	1282	WB + P + B	187	1207	68	1140
S14T5	0,265	0,250	0,40	438	CS	uncr	1234	WB + P + B	142	1157	60	1097
S14T6	0,265	0,250	0,40	1250	CS	c	1304	WB + B	145	1220	61	1159
S15T1	0,255	0,233	0,60	1250	CS	uncr	1040	WB + B + SF	245	944	78	867
S15T2	0,255	0,233	0,60	438	CS	c	555	WB + B + SF	102	516	54	463
S15T4	0,255	0,233	0,60	1250	SS	uncr	1127	WB + SF	158	944	4	939
S15T5	0,255	0,233	0,60	438	SS	c	863	WB + B + SF	145	726	7	719
S15T6	0,255	0,233	0,60	438	SS	c	804	WB + B	155	675	5	670
S16T1	0,255	0,233	0,60	438	SS	uncr	932	WB + B	188	776	-1	777
S16T2	0,255	0,233	0,60	438	SS	uncr	815	WB + B	208	675	-4	679
S16T3	0,255	0,233	0,60	1250	SS	c	593	WB + SF	327	471	-24	494
S16T4	0,255	0,233	0,60	438	CS	uncr	776	WB + B + SF	235	723	76	647
S16T5	0,255	0,233	0,60	438	CS	uncr	700	WB + B + SF	198	653	70	583
S16T6	0,255	0,233	0,40	1250	CS	c	570	WB + SF	182	542	67	475
S17T1	0,255	0,233	0,40	1250	CS	uncr	1365	WB + SF	208	1285	71	1213
S17T2	0,255	0,233	0,40	438	CS	c	715	WB + B + SF	77	685	49	636
S17T3	0,255	0,233	0,40	438	CS	c	812	WB + B + SF	157	785	63	722
S17T4	0,255	0,233	0,40	1250	SS	uncr	1235	WB + SF	118	1109	11	1098
S17T5	0,255	0,233	0,40	438	SS	c	847	WB + B + SF	115	765	12	753
S17T6	0,255	0,233	0,40	438	SS	c	875	WB	117	789	11	778

*Experiments*

Test	$d_t$ (m)	$d_i$ (m)	$a$ (m)	$b_r$ (mm)	SS/CS	uncr/c	$P_{exp}$ (kN)	Mode	$F_{pres}$ (kN)	$V_{exp}$ (kN)	$V_{add}$ (kN)	$V_{conc}$ (kN)
<b>S18T1</b>	0,255	0,233	0,40	438	SS	uncr	1157	WB + B + SF	170	1031	3	1028
<b>S18T2</b>	0,255	0,233	0,40	438	SS	uncr	1079	WB + B	213	954	-5	959
<b>S18T3</b>	0,255	0,233	0,40	1250	SS	c	967	WB	280	844	-16	860
<b>S18T4</b>	0,255	0,233	0,40	438	CS	uncr	1122	WB + B + SF	167	1062	64	997
<b>S18T5</b>	0,255	0,233	0,40	438	CS	uncr	1104	WB + B + SF	190	1050	68	981
<b>S18T6</b>	0,255	0,233	0,60	1250	CS	c	995	WB + P + SF	185	952	68	884
<b>BS1T1</b>	0,265	0,250	0,60	250	SS	uncr	290	B	37	242	0	242
<b>BS1T2</b>	0,265	0,250	0,60	250	CS	uncr	623	B	212	562	43	519
<b>BS2T1</b>	0,265	0,250	0,40	250	SS	uncr	633	B	100	552	-11	563
<b>BS2T2</b>	0,265	0,250	0,40	250	CS	uncr	976	B	267	919	52	868
<b>BS3T1</b>	0,265	0,250	0,60	250	SS	uncr	356	B	57	293	-3	297
<b>BS3T2</b>	0,265	0,250	0,60	250	CS	uncr	449	B	107	399	25	374
<b>BM1T1</b>	0,265	0,250	0,60	500	CS	uncr	923	WB + B	160	811	41	769
<b>BM1T2</b>	0,265	0,250	0,60	500	SS	uncr	720	WB + B	127	591	-9	600
<b>BM2T1</b>	0,265	0,250	0,40	500	SS	uncr	1212	WB + B	167	1062	-15	1077
<b>BM2T2</b>	0,265	0,250	0,40	500	CS	c	1458	WB + B	262	1354	58	1296
<b>BM3T1</b>	0,265	0,250	0,60	500	SS	uncr	735	WB + B	110	607	-6	613
<b>BM3T2</b>	0,265	0,250	0,60	500	CS	uncr	895	WB + B	183	791	45	746
<b>BL1T1</b>	0,265	0,250	0,60	750	SS	uncr	1034	WB + B	215	844	-17	862
<b>BL1T2</b>	0,265	0,250	0,60	750	CS	uncr	1252	WB + B	320	1119	75	1043
<b>BL2T1</b>	0,265	0,250	0,40	750	SS	uncr	1494	WB + B	212	1311	-17	1328
<b>BL2T2</b>	0,265	0,250	0,40	750	CS	uncr	1708	WB + B	277	1586	68	1518
<b>BL3T1</b>	0,265	0,250	0,60	750	SS	uncr	1114	WB + B	242	907	-22	928
<b>BL3T2</b>	0,265	0,250	0,60	750	CS	uncr	1153	WB + B	312	1035	74	961
<b>BX1T1</b>	0,265	0,250	0,60	1000	SS	uncr	1331	WB + P	325	1080	-30	1109
<b>BX1T2</b>	0,265	0,250	0,60	1000	CS	uncr	1596	WB + B + P	335	1415	85	1330
<b>BX2T1</b>	0,265	0,250	0,40	1000	SS	uncr	1429	WB + B + P	217	1259	-11	1270
<b>BX2T2</b>	0,265	0,250	0,40	1000	CS	uncr	1434	WB + P	167	1332	57	1275
<b>BX3T1</b>	0,265	0,250	0,60	1000	SS	uncr	1141	WB + P	245	935	-16	951
<b>BX3T2</b>	0,265	0,250	0,60	1000	CS	uncr	1193	WB + B	210	1059	64	994

† The initial prestressing was  $3 \times 50\text{kN}$ .

Experiments

Table 3.3: Results from second series of experiments

Test	$d_l$ (m)	$d_t$ (m)	$a$ (m)	$b_r$ (mm)	SS/CS	uncr/c	$P_{exp}$ (kN)	$P_{line}$ (kN)	Mode	$F_{pres}$ (kN)	$V_{exp}$ (kN)	$V_{add}$ (kN)	$V_{conc}$ (kN)
S19T2	0,265	0,250	0,60	1250	SS	uncr	1484	0	WB	112	1249	132	1237
S19T1	0,265	0,250	0,60	1250	CS	uncr	1568	0	WB	217	1379	237	1307
S20T1	0,265	0,250	0,60	1250	SS	uncr	1542	603	B	870	1579	294	1285
S20T2	0,265	0,250	0,60	1250	CS	c	1273	602	B	1408	1739	678	1061
S20T2b <sup>3</sup>	0,265	0,250	0,60	1250	CS	uncr	1552	601	WB	678	1657	493	1164
S20T3	0,265	0,250	0,60	438	CS	uncr	1337	601	WB + B	643	1487	484	1003
S20T4	0,265	0,250	0,60	438	CS	uncr	1449	601	WB + B	637	1569	482	1087
S21T1	0,265	0,250	0,60	1250	CS	uncr	1165	602	WB + B + B'	343	1472	501	971
S21T2	0,265	0,250	0,60	1250	SS	uncr	1386	603	WB + B'	297	1544	389	1155
S21T3	0,265	0,250	1,39	438	SS' <sup>4</sup>	c	730	0	B	0	479	31	448
S21T4	0,265	0,250	1,39	438	SS'	c	753	0	B	0	493	31	462
S21T5	0,265	0,250	0,87	438	SS'	c, OK <sup>5</sup>	853	0	WB + B + B'	0	678	31	647
S21T6	0,265	0,250	1,13	438	SS'	c	785	0	B'	0	569	31	539
S22T1	0,265	0,250	0,60	438	CS	uncr	984	602	WB + B	335	1320	500	820
S22T2	0,265	0,250	0,60	438	CS	uncr	961	602	WB + B	323	1298	498	801
S22T3	0,265	0,250	0,60	438	SS	uncr	978	603	WB + B	195	1221	406	815
S22T4	0,265	0,250	0,60	438	SS	uncr	895	604	WB + B	252	1143	397	746
S23T1	0,265	0,250	0,60	1250	CS	uncr	1386	601	WB + B + B'	332	1653	498	1155
S23T2	0,265	0,250	0,60	1250	SS	uncr	1132	602	WB + B	230	1343	400	943
S24T1	0,265	0,250	0,60	438	CS	uncr	1358	601	WB + B'	327	1629	497	1132
S24T2	0,265	0,250	0,60	438	CS	uncr	1182	601	WB + B	295	1477	492	985
S24T3	0,265	0,250	0,60	438	SS	uncr	995	602	WB + B'	190	1235	406	829
S24T4	0,265	0,250	0,60	438	SS	uncr	784	602	WB + B	262	1048	394	653
S25T1	0,265	0,250	0,60	1250	SS	uncr	1461	0	WB + P	203	1214	224	1218
S25T2	0,265	0,250	0,40	1250	CS	uncr	1620	601	WB + B	372	1945	505	1440
S25T3	0,265	0,250	0,40	438	CS	c	1563	602	WB + B	358	1893	503	1389
S25T4	0,265	0,250	0,87	438	SS'	c, OK	854	0	WB + B	0	678	31	648
S25T5	0,265	0,250	1,13	438	SS'	c, OK	968	0	WB + B	0	695	31	664

<sup>3</sup> S20T2b is the repeated test of S20T2, which failed by further opening the shear crack of S20T1. For S20T2b, a temporary support was constructed so that the span length was reduced to 2,4 m.

<sup>4</sup> SS' experiments are carried out at the north side of the specimen (CS) but without applying the prestressing force. For the SS' experiments, no moment occurred over the support.

<sup>5</sup> For "c, OK" experiments, the influence of previous cracks did not influence the failure mode, while for the "c" experiments it was observed that a previous shear crack would open and result in an earlier failure.

## Experiments

Test	$d_l$ (m)	$d_t$ (m)	$a$ (m)	$a/d$	$b_r$ (mm)	SS/CS	uncr/c	$P_{exp}$ (kN)	$P_{line}$ (kN)	Mode	$F_{pres}$ (kN)	$V_{exp}$ (kN)	$V_{add}$ (kN)	$V_{conc}$ (kN)
S26T1	0,265	0,250	0,42	1,51	438	SS	uncr	1448	602	WB + B'	187	1686	407	1279
S26T2	0,265	0,250	0,42	1,51	438	SS	uncr	1324	602	B	238	1568	398	1170
S26T3	0,265	0,250	0,40	1,51	1250	CS	uncr	1555	602	WB + B	418†	1896	513	1382
S26T4	0,265	0,250	0,40	1,51	438	CS	c	1363	602	B	418†	1725	513	1212
S26T5	0,265	0,250	0,40	1,51	438	CS	c	1451	602	WB + B	422†	1804	514	1290

† The initial prestressing was  $3 \times 50$ kN.

‡ The initial prestressing was  $3 \times 80$ kN. The span length was reduced to 2,4m.

### 3.4.2 Description of selected experiments

To give an insight in the formation of the cracks and the failure patterns, four experiments are selected and discussed further, each with a different failure pattern. These experiments are the following:

- S3T1 failing in wide beam shear (WB);
- S9T1, failing in punching (P) and wide beam shear (WB);
- BS2T1 failing in beam shear (B); and
- S21T1 failing in a combination of wide beam shear (WB), beam shear (B) and beam shear away from the support (B').

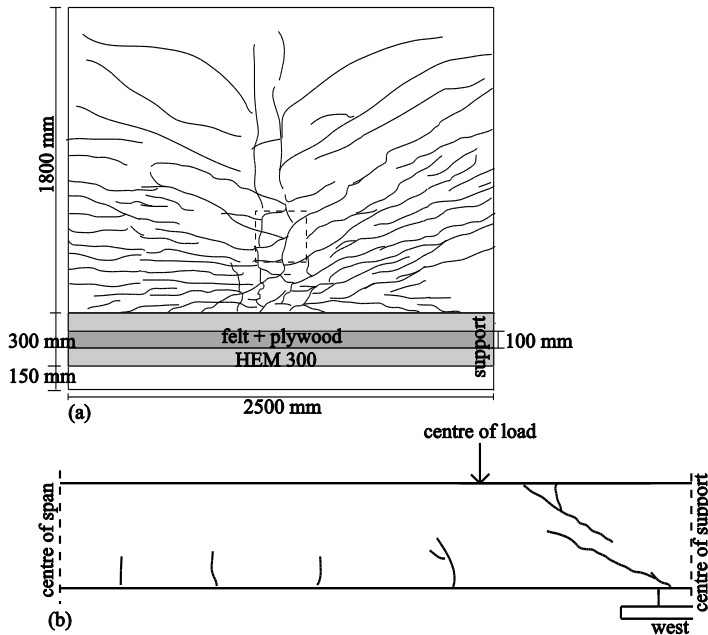


Fig. 3.12: Cracks after failure of S3T1: (a) bottom face, (b) west side face.

## Experiments

In S3T1, the first flexural cracks were visible at a concentrated load of 200kN. At 600kN, cracks appeared at the front face of the slab specimen, and slightly inclined cracks were visible at the side face, indicating flexure-shear. Inclined cracks between the load and the support were also observed on the bottom face. These cracks developed further and opened up until failure occurred at a concentrated load of 1371kN, which was accompanied by a loud noise indicating the release of energy within the slab. After the peak, at 1240kN, shear cracks appeared at the side face (Fig. 3.12b). The measured crack widths after the experiment were 3mm for a crack in the middle of the bottom face (Fig. 3.12), 0,35mm for a crack towards the support on the bottom face, 2mm for the crack in the middle of the front face and 0,9 – 1mm for the cracks at the side face.

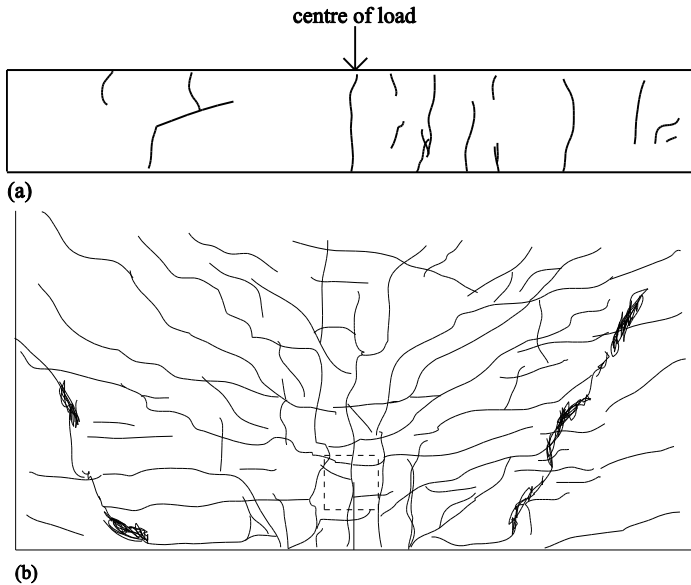


Fig. 3.13: Cracks after failure of S9T1: (a) front face; (b) bottom face.

In S9T1, the first flexural cracks were observed at the bottom face, side face and at the front face at a concentrated load of 400kN. Before failure, the largest crack width was 1,5mm for a crack at the front face (Fig. 3.13a). Failure occurred upon reaching a concentrated load of 1523kN. After failure, the largest measured crack widths were 1mm at the front face, 10mm for the punching surface and 0,4mm for cracks on the bottom face (Fig. 3.13b).

In BS2T1, the first flexural cracks were observed at a concentrated load of 100kN. An inclined crack indicating flexure-shear was observed at 200kN. All cracks at the bottom face developed in the transverse direction. The shear crack was clearly visible at 400kN. Failure occurred at a concentrated load of 633kN. The crack widths after the experiments were the following: 5mm for the shear crack at the east side face (Fig. 3.14c); 4mm for the shear crack at the west side face (Fig. 3.14b); 2mm for a flexural crack at the bottom face

## Experiments

close to the location of the concentrated load (Fig. 3.14a) and 3mm for the largest flexural crack at the west side face.

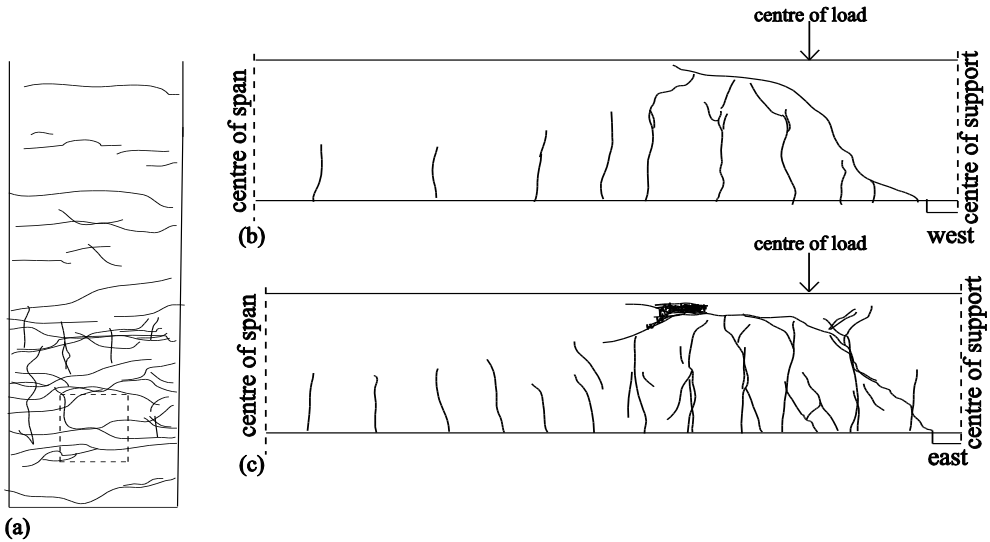


Fig. 3.14: Cracks after failure of BS2T1: (a) bottom face; (b) west side face; (c) east side face.

In S23T1, the line load was applied first up to a jack load of 600kN and thus a line load of 240kN/m, after which flexural cracks were observed at the side faces. Then, the concentrated load was applied. A shear crack developed at a concentrated load of 900kN. Failure occurred at a concentrated load of 1386kN. The following crack widths were registered after failure of the specimen: 0,5mm for a shear crack between the concentrated load and the support at the east side (Fig. 3.15), 0,05mm for the shear crack between the support and the line load (Fig. 3.15) and 0,05mm for the flexural cracks at the bottom face (Fig. 3.16a). A cracking pattern also developed on the top face (Fig. 3.16b). Generally, very few cracks were visible at the bottom face after this experiment.

No saw cuts of the specimens were made, but the cracking patterns can be used to sketch an assumed three-dimensional cracking pattern for the three main failure mechanisms that will be further discussed: beam shear (B), wide beam shear (WB) and punching shear (P). Note that these failure modes are drawn separately in the three figures presented, while it can be seen in the experimental results that in reality the failure mode is a combined mode.

Experiments

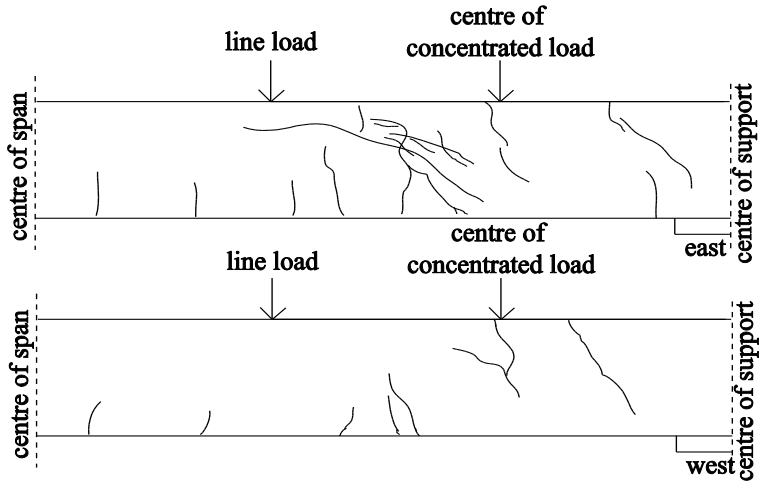


Fig. 3.15: Cracks after failure of S23T1 at the east and west side faces.

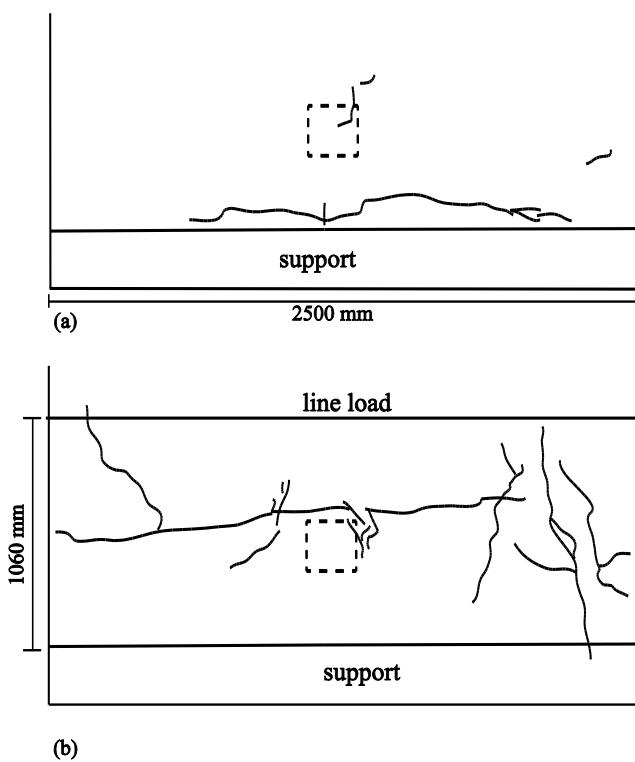
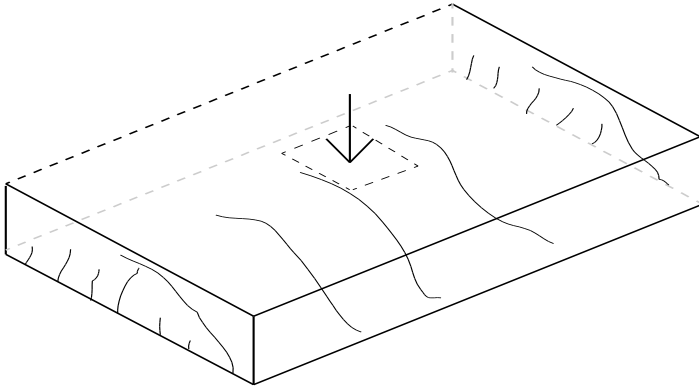
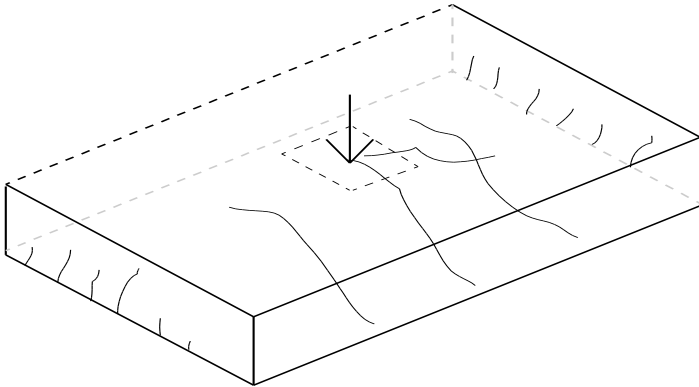


Fig. 3.16: Cracks after failure of S23T1: (a) bottom face; (b) top face.

*Experiments*



*Fig. 3.17: Assumed three-dimensional cracking pattern for beam shear failure (B).*



*Fig. 3.18: Assumed three-dimensional cracking pattern for wide beam shear failure (WB).  
Note that for this case, the shear crack is not visible at the side face of the slab.*

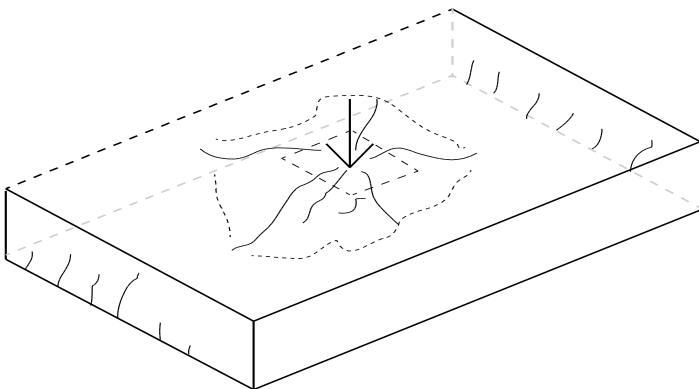


*Fig. 3.19: Assumed three-dimensional cracking pattern for punching shear failure (P)*

### **3.5 Conclusions**

In this chapter, the experiments have been briefly described, while the complete description can be found in the full test reports (Lantsoght 2011a, b, 2012c). In total, 156 experiments on 38 specimens have been carried out. The most important parameters for slabs under a concentrated load in shear have been varied, and 6 different failure modes have been observed. In the following chapters, these experimental results will be further analysed.

## *Experiments*

## 4 Parameter analysis

### 4.1 Introduction

The goal of this chapter is to analyse the experimental results from Chapter 3 with regard to the parameters under study. Each section discussing a parameter is divided into three parts. The first part introduces how the considered parameter is dealt with in the literature. These observations are typically based on beam shear tests or slab-column connection punching tests. The second part discusses the influence of the parameter under study as observed in the experiments. In a third part, the experimental observations are explained, compared to knowledge from the literature and related to theoretical principles.

### 4.2 Size of the loading plate

#### 4.2.1 Background

The size of the loading plate represents the size of the tyre contact area, which is not a constant but depends on the vehicle type. For design purposes however, the size of the tyre contact area used for road bridges is prescribed in the code provisions as a fixed value. The tyre contact area as prescribed by NEN-EN 1991-2:2003 is 400mm × 400mm in Load Model 1, which covers most of the effects of trucks and cars and 600mm × 350mm in Load Model 2, a single axle load. In AASHTO LRFD 2007 the tyre contact area is 510mm × 250mm for design truck and tandem. For other design vehicles, the tyre contact area should be determined by the engineer.

It was noted previously (Sherwood et al., 2006), based on limited test data (Sherwood et al., 2006; Serna-Ros et al., 2002; Leonhardt and Walther, 1962), that loads and supports narrower than the specimen width may have a small reducing effect on the shear capacity of a one-way spanning member. The reference for this conclusion was a one-way slab under a line load over the full specimen width, not supported over its full width, behaving as a beam, a situation that may not be representative for a slab under a concentrated load.

Test results from the literature, compared on the basis of the size of the loading plate in Table 4.1 show an increasing shear capacity for an increasing width of the loading plate. The increase in loaded area as compared to the loaded area of the experiment on the previous row in the table, and the increase in ultimate capacity as compared to the ultimate capacity of the experiment on the previous row are shown. For example, the increase in measured ultimate load for A-20-10 as compared to A-10-10 is 16%, while the area of the load was doubled. It is remarkable that the increase in ultimate capacity becomes larger for the largest tested loading plates, while the increase in size of these loading plates is percentage-wise smaller than for the smaller tested loading plates. For smaller  $a/d_1$  distances, smaller increases in capacity are reported than for loads applied further away

### Parameter analysis

from the support. In the experiments compared in Table 4.1, one dimension of the loading plate is constant, leading to an increasing ratio between the width and length of the load.

*Table 4.1: Increase in ultimate load for an increasing size of the loading plate as reported in literature.*

Reference	Nr	$a/d_l$	$l_{load} \times b_{load}$ (mm × mm)	increase load size	$P_{exp}$ (kN)	increase $P_{exp}$
Furuuchi et al. 1998	A-10-10	1,75	100 × 50		294	
	A-20-10		200 × 50	100%	340	16%
	A-30-10		300 × 50	50%	450	32%
	C-10-10	1,25	100 × 50		480	
	C-20-10		200 × 50	100%	525	9%
	C-30-10		300 × 50	50%	626	19%
	C-50-10		500 × 50	67%	811	30%
Regan 1982	2SS	2,16	100 × 100		130	
	5SS		200 × 100	100%	190	46%
	3SS	1,68	100 × 100		195	
	7SS		200 × 100	100%	200	3%

#### 4.2.2 Experimental observations

*Table 4.2: Measured increase in ultimate shear capacity for an increase in the size of the loading plate from 200mm × 200mm to 300mm × 300mm, with  $a/d_l = 2,26$ .*

Specimens	$b$ (m)	Average increase $V_u$
BS1 – BS3	0,5	11,5%
BM1 – BM3	1,0	0,1%
BL1 – BL3	1,5	0,6%
BX1 – BX3	2,0	24,6%
S1 – S2	2,5	40,6%

To study the influence of the size of a square loading plate on the shear capacity of one-way slabs and slab strips, the results of S1 and S2 can be compared, as well as BS1 and BS3, BM1 and BM3, BL1 and BL3 and BX1 and BX3. The slabs are made of normal strength concrete and the slab strips of high strength concrete. The results of the comparison of the experiments are shown in Table 4.2, displaying the measured average increase in shear capacity for an increase in size of the loading plate from 200mm × 200mm to 300mm × 300mm. The span to depth ratio  $a/d_l$  is constant at 2,26. The results of the specimens with widths of 1m to 2,5m in Table 4.2 show an increasing influence of the loading plate size as

the overall width of the specimen increases. The scatter on the results with a width of 0,5m (BS-series) is rather large (Lantsoght, 2012a).

#### 4.2.3 Explanation

The influence of the size of the loading plate representing the size of the tyre contact area can be explained based on the transverse load redistribution capacity in slabs. When considering the load distribution from the concentrated load towards the support in a slab as a three-dimensional problem in which compression struts occur over the depth and the width of the slab, it is clear that a larger loading plate provides a larger base from which the compressive struts can fan out. As these compressive struts develop over a larger area, more material is activated to carry the load and thus the shear capacity is increased.

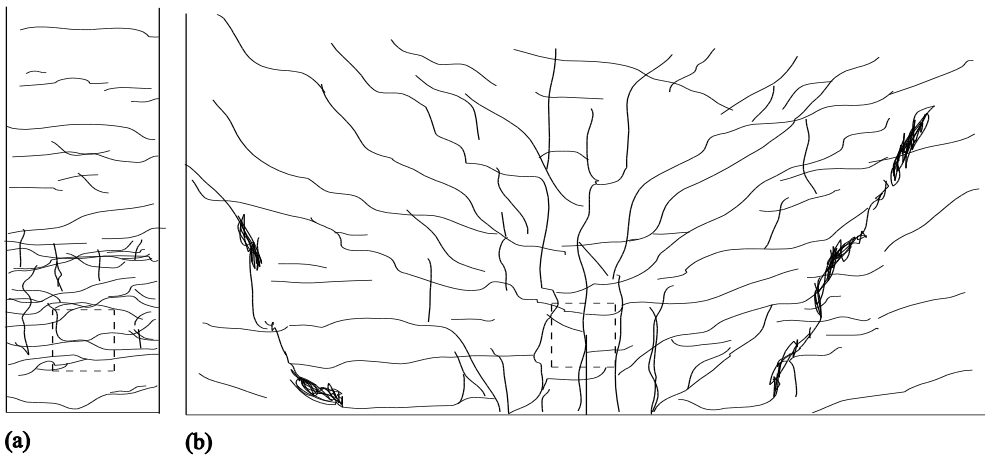


*Fig. 4.1: Difference in cracking pattern between a beam and a slab: (a) cracking pattern at bottom face after BS2T1, (b) cracking pattern at bottom face after S9T1. The dashed lines denote the location of the loading plate. Bolder lines in (b) denote areas of punching damage. Note that the cracks further than the inner face of the support are not drawn in this sketch.*

Regan (1988) suggested that the difference in shear capacity from the narrow to full width conditions as observed in experiments on slabs under concentrated loads at larger distances to the support is the result of an interaction between the one-way and two-way shear modes. This idea is supported by the observation of the cracking patterns at the bottom face of the specimens, showing the differences between one-dimensional beam behaviour and two-dimensional slab behaviour. The specimens of smaller width (BS and BM series) show a cracking pattern at the bottom face, consisting mainly of straight cracks parallel to the support, Fig. 4.1(a). In the wider specimens, a different more grid-like pattern is visible, Fig. 4.1(b). These observations correspond to the concept of transverse load redistribution in slabs. For members with a smaller width, transverse load redistribution hardly takes

place and the load is carried directly from its point of application to the support. In this case, the size of the loading plate should not influence the capacity of the member too much. However, for a wider member, load spreading in the transverse direction becomes more important. For a larger loading plate, a larger surface is available out of which the load can be carried through the previously mentioned three-dimensional struts towards the support.

### **4.3 Effect of predamaging**

#### **4.3.1 Role of precracking on bearing capacity of structural concrete elements as found in literature**

A limited number of experimental data concerning the shear capacity of precracked or locally failed (by an earlier test) concrete beams, or the punching capacity of precracked concrete slabs is available. For aggregate interlock, Hofbeck et al. (1969) argument that, if a crack exists in the shear plane of a push-off specimen before the application of shear, the slip at all stages of loading will be larger than would have occurred if the crack had not been present. In their push-off experiments, the existence of a crack in the shear plane reduced the ultimate shear strength. Yang (2011) observed similar inclined cracking strengths for precracked beams but lower ultimate strengths, as the precracked beams failed upon the formation of the inclined crack.

Hamadi and Regan (1980) carried out shear experiments on beams precracked in bending. None of the beams tested in this way showed any unusual distress. Another test series by Regan (1971) also studied the influence of predamage: elements were subjected to centric tension, resulting in large cracks. The shear tests carried out afterwards showed only a marginal effect of the pre-cracks. Azad et al. (1993) studied the influence of crack damage on the punching shear capacity. For cracks under a degree of 20 to 30°, the existing crack had a detrimental effect on the punching shear capacity, which became about 54% of the punching shear capacity of a specimen without an existing crack.

Executing an experiment on a slab in the vicinity of a local failure can give a lower bound of the shear capacity of bridge slabs that are fully cracked in bending after being in service for several decades. The influence of predamaging until failure is a lower bound, as the case in which a local failure has occurred will never occur in practice. From the literature, it is expected that in general a local failure near to the area of load application will have a negative effect on the bearing capacity of the slab.

#### **4.3.2 Experimental observations**

For slabs S3 to S18, always two specimens have been tested with all parameters similar except the loading sequence. The only exception is the set S3 – S4, where the ratio of transverse flexural reinforcement in S3 equals 0,258% and in S4 0,182% (as the overall

### Parameter analysis

transverse reinforcement ratio for considering the number of bars provided over the entire specimen length), Table 3.1. However, within the shear span the same transverse reinforcement layout is applied for both slabs. To study the effect of predamage, the results of an experiment on an undamaged specimen are compared to the results of an experiment carried out with the load in the vicinity of a local failure. It was observed that the width of cracks from previous tests increased during testing for residual capacity. S6T3 gave a 5% higher residual capacity than S5T1 and S13T2 gave a 3% higher capacity than S14T2; all other comparisons gave lower residual capacities for the experiments on the damaged slabs, as expected. The results per pair of slabs are given in Table 4.3, in which:

$V_c$  the shear capacity obtained in an experiment for residual shear capacity;

$V_{uncr}$  the shear capacity obtained in a shear capacity experiment on an undamaged (virgin) slab.

The slabs are either tested initially in the middle (M) or near the edge (E), as indicated in Table 4.3. The overall average is a residual capacity of 81% of the undamaged shear strength. This ratio is surprisingly high, as it was not expected that slabs that had been tested up to their ultimate bearing capacity and showed cracks of sometimes 20mm to 30mm wide (Fig. 4.2) would be able to resist again considerable levels of loading when loaded at a different location nearby.

*Table 4.3: Comparison of shear capacity between undamaged specimen  $V_{uncr}$  and locally failed specimen,  $V_c$ , as average value for the experiments tested on the considered specimens.*

Slab	$\rho_t$ (%)	M/E	$V_c/V_{uncr}$
S3	0,182	M	80%
S4	0,258	E	
S5	0,258	M	95%
S6	0,258	E	
S7	0,258	E	77%
S8	0,258	M	
S9	0,258	M	81%
S10	0,258	E	
S11	0,258	M	80%
S12	0,258	E	
S13	0,258	M	90%
S14	0,258	E	
S15	0,258	M	75%
S16	0,258	E	
S17	0,258	M	74%
S18	0,258	E	

### 4.3.3 Explanation

The high residual bearing capacity of slabs under concentrated loads close to supports in shear indicates the large redistribution capacity of slabs. In the case of an experiment in the vicinity of a local failure, an alternative load-carrying path around the local failure can be found, resulting in redistribution of forces over the width.

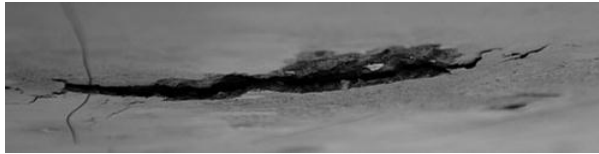


Fig. 4.2: Punching damage at the bottom of a slab after an experiment.

## 4.4 Transverse flexural reinforcement

### 4.4.1 Background

The influence of the transverse flexural reinforcement is not considered in one-way shear. The methods to calculate one-way shear are developed based on experiments on beams, typically not provided with transverse flexural reinforcement, as no moments occur in the transverse direction. Sherwood et al. (2006) show no influence of the transverse flexural reinforcement<sup>6</sup> on the shear resistance of one-way slabs under line loads. This observation agrees with the idea that one-way slabs under line loads behave as wide beams. Two-way shear (punching shear) provisions are developed based on experiments on slabs with flexural reinforcement in both directions.

The amount of flexural reinforcement is not considered in the punching shear expression of ACI 318-08 (§11.11.2.1). The punching formula from NEN-EN 1992-1-1:2005 §6.4.4. (1), formula (6.47), gives a relation to the 1/6<sup>th</sup> power between the transverse flexural reinforcement and the punching capacity.

### 4.4.2 Experimental observations

To study the influence of the amount of transverse reinforcement, three different layouts of transverse reinforcement are tested in S2 ( $\rho_t = 0,132\%$ ), S4 ( $\rho_t = 0,182\%$ ) and S3 ( $\rho_t = 0,258\%$ ), as shown in Fig. 3.7b, c and d respectively. The transverse reinforcement is anchored with hooks to provide sufficient anchorage length. The concrete compressive strength of S2 (34,5 MPa) differs from S3 and S4 (51,6 MPa), even though in both cases a mixture for normal strength concrete C28/35 was delivered. S2 and S3 are loaded in the middle of the width, while S4 is loaded close to the edge.

---

<sup>6</sup> Sherwood et al. (2006) referred to the transverse flexural reinforcement as temperature and shrinkage reinforcement, as they tested slabs subjected to line loads, acting purely as one-way slabs.

### Parameter analysis

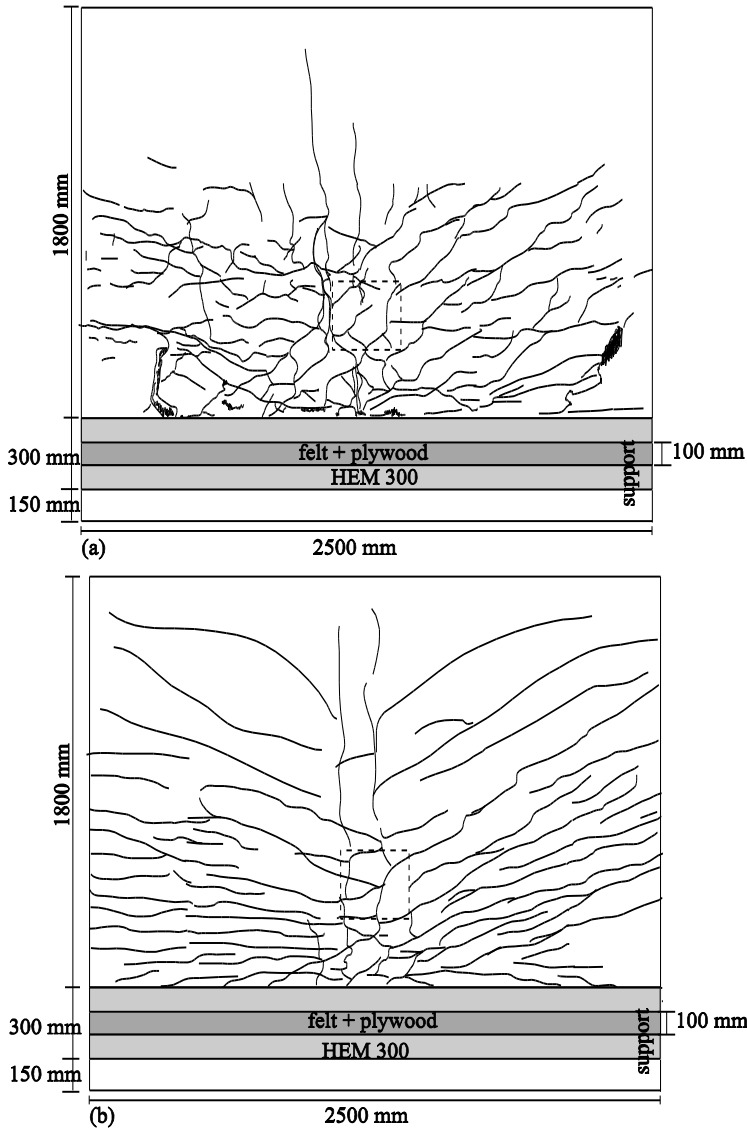


Fig. 4.3: Influence of the amount of transverse flexural reinforcement on the cracking pattern at the bottom face of the specimen, (a) S2T1 with  $\rho_t = 0,132\%$ , (b) S3T1 with  $\rho_t = 0,258\%$ . Loading plate is indicated with dashed lines. Note that the cracks further than the inner face of the support are not drawn in this sketch.

A difference in cracking pattern between a slab with less transverse reinforcement (e.g. S2) and a slab with more transverse reinforcement (e.g. S3) is observed, Fig. 4.3. In the tests S2T1 and S3T1 the load is applied near to the simple support. The cracks at the bottom face after testing S2T1 (Fig. 4.3a) do not cover the same part of the slab width as the cracks at

## *Parameter analysis*

the bottom face after testing S3T1 (Fig. 4.3b). These observations indicate that the transverse flexural reinforcement helps at distributing the cracks in the transverse direction.

In the tests S2T4 and S3T4 the load is applied close to the continuous support. The shear failure in S3T4 extends over the full width of the specimen (bottom and side faces), while in S2T4 inclined cracks are only observed at the bottom face (Lantsoght, 2011a, b). Fewer cracks are observed at the front face in S3 as compared to S2 as a result of the increased moment resistance in the transverse direction. No influence of the transverse reinforcement is found on the ultimate shear capacity.

### *4.4.3 Explanation*

In one-way slabs under concentrated loads, moments occur in the span direction as well as in the transverse direction. Under these loading conditions a one-way slab does not behave like a beam. The transverse reinforcement is activated due to the transverse moments, and shear is carried to a certain extent over the width of the slab.

The cracking patterns confirm the idea of transverse load-carrying action and indicate that more transverse flexural reinforcement leads to a better distribution of the load over the width of the slab. However, an influence on the shear capacity is not observed, as more transverse reinforcement seems to result in shear failure at the side face of the 2,5m wide specimens, thus slightly altering the failure mode. The cracking patterns in the experiments show that in the slabs with more transverse flexural reinforcement, a larger part of the load is carried in the transverse direction, leading to a less localised cracking pattern on the bottom of the slab. With the cracks occurring over an increasing portion of the width for specimens with more transverse flexural reinforcement, it is understood that from a certain amount of transverse flexural reinforcement, the shear failure will be visible at the side face (Fig. 3.17) while for smaller amounts of transverse flexural reinforcement the shear crack will be inside the concrete mass of the slab (Fig. 3.18).

## *4.5 Moment distribution at support*

### *4.5.1 Background*

Research from the 60s and 70s indicates a lower shear capacity at continuous supports than at end supports. Rafla (1971) attributed this observation to what he described as the lower bond quality of the top reinforcement<sup>7</sup> and the combination of larger moments and larger shears. As a result, according to the provisions from NEN 6720:1995, an increase in bearing capacity as a result of direct load transfer can only be accounted for in the case of loads close to the end supports or when no change in the sign of the moment occurs in the shear span (CUR 1994).

---

<sup>7</sup> Most likely, this effect was caused by the insufficient anchorage length of the top reinforcing bars.

### Parameter analysis

Early experimental research by Rodriguez et al. (1959) showed similar failure modes in continuously supported slabs as in simply supported slabs. Van den Berg (1962) described the shear cracks as a function of the ratio between the span and support moments. Leonhardt (1965) pointed out that the system of internal forces in continuous beams is generally assumed to be similar to a simply supported beam between the points of contraflexure. However, he observed experimentally that for rectangular beams or T-beams with thick webs, the inclined compression strut extends directly to the support, provided that the bottom reinforcement is partially extended towards the support.

Regan (1982), §2.4.2, predicts an increase of the shear capacity at the continuous support with:

$$\alpha_{Regan} = \sqrt{\frac{M_1 + M_2}{M_1}}$$

in which  $M_1$  and  $M_2$  are the larger respectively the smaller moment at the end of the shear span. These moments are illustrated in Fig. 4.4. Regan (1982) explains that the strength of a short continuous shear span is expected to be higher than that for a simple span of equal length. Near the continuous support, the width of the compressive strut becomes wider as a result of the activated load-carrying behaviour of the top reinforcement. For the experiments reported by Regan (1982), an increase in shear capacity<sup>8</sup> at the continuous support of 55% is measured, while the calculated increase based on  $\alpha_{Regan}$  is only 14%.

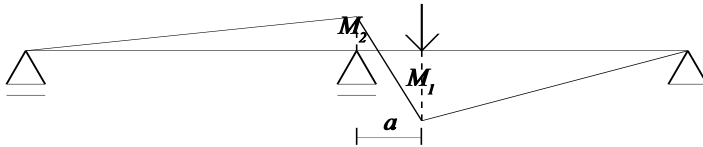


Fig. 4.4: Illustration of the moments that are used to determine  $\alpha_{Regan}$  at a continuous support.

#### 4.5.2 Experimental observations

All slabs are tested at the simple and continuous support. As the force in the vertical prestressing bars close to the continuous support (Fig. 3.2) is only applied at the beginning of every test, the moment over the continuous support is on average only about 26% of the moment in a fully clamped support for the slabs under a concentrated load, 31% for the slab strips, 38% for the slabs under a combination of loading with an initial force on the prestressing bars of  $3 \times 15\text{kN}$  and 52% for the slabs under a combination of loading with an initial force on the prestressing bars of  $3 \times 50\text{kN}$ . This observation shows that adding a line

---

<sup>8</sup> For Regan's experiments (1982) the sectional shear force at failure is calculated based on a statically indeterminate beam with a clamped support (continuous support) and a hinged support (simple support)

### Parameter analysis

load over the width of the slab facilitates the development of the support moment since the initial decrease in prestressing force, as observed in the experiments on slabs under a concentrated load only, is inhibited. The execution procedure of the experiments is different from that by Regan (1982) in which the rotation at the continuous support was fully restrained.

The experimental results are summarized in Table 4.4, showing the average (AVG) increase of the shear capacity when an experiment at the continuous support,  $V_{exp,CS}$ , is compared to an identical experiment at the simple support,  $V_{exp,SS}$ , as well as the associated standard deviation (STD) and coefficient of variation (COV). The expected increase based on Regan's proposed factor  $\alpha_{Regan}$  is also given. The results in Table 4.4 show that the shear capacity at the continuous support is indeed larger than the shear capacity at the simple support. The factor  $\alpha_{Regan}$  as proposed by Regan (1982) reasonably reflects the influence of the moment distribution at the support. The results show that the influence of the moment distribution at the support decreases with an increase in the slab width.

Table 4.4: Comparison between ultimate shear capacity at simple and continuous support

Experiments	$b$ (m)	$\alpha_{Regan}$	AVG $V_{exp,CS}/V_{exp,SS}$	STD	COV
BS	0,5	1,263	1,783	0,492	28%
BM	1,0	1,149	1,329	0,069	5%
BL	1,5	1,191	1,225	0,093	8%
BX	2,0	1,134	1,167	0,130	11%
S1 – S10	2,5	1,150	1,112	0,133	12%
plain bars	2,5	1,169	1,015	0,140	14%
slabs on bearings	2,5	1,196	1,031	0,085	8%
combination of loads	2,5	1,178	1,163	0,152	13%
slab strips	---	1,184	1,376	0,337	24%

The measurements of the distribution of the reaction at the support for the slabs under a combination of loads give a smaller width over which the force is carried at the continuous support as compared to the simple support (Lantsoght 2012c). Similarly, Model Code 2012 (*fib* 2012) allows a larger effective width at the simple support ( $60^\circ$  load spreading, Fig. 2.16) than at the continuous or clamped support ( $45^\circ$  load spreading)

#### 4.5.3 Explanation

The experimental results indicate that for slabs, the increase in capacity at the continuous support is smaller than for beams. This observation indicates that for slabs the influence of the transverse moment should be taken into account. It is thus necessary to investigate the

combination of longitudinal and transverse moment to assess the influence of the moment distribution at the support.

Moreover, the effective width calculated from the measured reaction forces over the width of the slab is smaller at the continuous than at the simple support. The effective width from reaction forces at the support in linear finite element models (Lantsoght 2012a, c) is also smaller at the continuous support than at the simple support. As this observation results from a linear model, no influence of cracking but solely the action of forces and moments is at the basis of the smaller effective width at the continuous support. A sharper peak is thus observed in the shear stress distribution over the continuous support than over the simple support.

## 4.6 Distance between load and support

### 4.6.1 Background

From shear tests on reinforced concrete beams it is known that the distance between the load and the support, expressed as the shear span to depth ratio ( $a/d_l$ ) is an important parameter influencing the shear capacity and was identified as such in early research on shear in beams (Talbot 1909; Richart 1927; Clark 1951). Kani (1964) showed the influence of the  $a/d_l$  ratio on the ratio of maximum moment to theoretical flexural failure moment  $M_{CR}/M_{FL}$  and the failure mode, resulting in the so-called valley of shear failure.

When the load is placed close to the support, the formation of a concrete compressive strut between the load and the support provides an alternative load bearing path, satisfying equilibrium requirements after inclined cracking occurs. This mechanism allows for a considerable increase of the load upon the formation of an inclined crack. As a result, decreasing the  $a/d_l$  ratio from about 2,5 to 0,5 increases the shear resistance because a steeper compression strut can carry a higher load. To take this into account, NEN-EN 1992-1-1:2005 allows for the reduction of loads applied within a face-to-face distance<sup>9</sup>  $a_v$  of  $2d_l$  to  $d_l/2$  with a factor  $\beta = a_v/2d_l$  in §6.2.2. (6). This value is determined from beam shear tests (Regan 1998) and provides a lower bound for the increase in capacity as  $a_v/d_l$  decreases.

In the case of slabs under concentrated loads, the influence of the span to depth ratio ( $a/d_l$ ) is not well understood. A 45° load spreading in the horizontal plane as shown in Fig. 2.16 leads to a decreasing effective width for a decreasing distance to the support. For a given maximum shear capacity  $v_u$ , a smaller effective width leads consequently to a smaller maximum theoretical sectional shear force  $V_u = v_u b_{eff} d$ . For slabs, the increase resulting from direct load transfer is theoretically counteracted by a decrease in effective width. The influence of the shear span to depth ratio as observed in experiments from the

---

<sup>9</sup> Note that for flexible supports the distance  $a_v$  for the determination of  $\beta$  is prescribed as the distance from the face of the load to the centre of the support.

### Parameter analysis

literature is shown in Table 4.5 and compared to the expected shear capacity  $V_{u,exp,\beta}$  based on the factor  $\beta$  from NEN-EN 1992-1-1:2005, not limited to  $d/2$ :  $\beta_{nolim}$ . To calculate  $V_{u,exp,\beta}$ , the value of  $V_{exp}$  from the previous row is multiplied by the expected increase. This increase is the ratio between  $\beta_{nolim}$  on the previous row and  $\beta_{nolim}$  of the considered experiment. These results show lower increases in the shear capacity for slabs with a decrease of the distance between the load and the support than expected based on the factor  $\beta$  from NEN-EN 1992-1-1:2005:  $V_{exp}$  is in all cases smaller than  $V_{u,exp,\beta}$ , with the exception of C-10-10 by Furuuchi et al. (1998).

*Table 4.5: Increase in capacity for a decreasing distance to the support as reported in literature compared to factor  $\beta_{nolim}$  from NEN-EN 1992-1-1:2005, not limited for  $d/2$ .*

Reference	Nr	$a/d_1$	$a\sqrt{d_1}$	$\beta_{nolim}$	$V_{exp}$ (kN)	$V_{u,exp,\beta}$ (kN)
Regan 1982	2SS	2,93	0,96	0,48	110	
	3SS	2,46	0,48	0,25	171	211
	4SS	1,98	0,24	0,12	206	356
Furuuchi et al. 1998	D-10-10	2,25	1,94	0,97	179	
	A-10-10	1,75	1,44	0,72	186	242
	C-10-10	1,25	0,94	0,47	320	285
Graf 1933	1244b2	2,16	0,72	0,36	123	
	1244b1	1,68	0,24	0,12	137	369
	1245b2	2,12	0,71	0,35	173	
	1245b1	1,65	0,24	0,12	172	505
Cullington et al. 1996	lab 1	2,00	1,32	0,66	620	
	lab 2	1,00	0,32	0,16	1000	2558

#### 4.6.2 Experimental observations

To study the influence of the distance between the load and the support ( $a/d_1$ ) experimentally S3, S4, S11, S12, S15, S16, S21, S22, BS3, BM3, BL3 and BX3 are loaded with a concentrated load at  $a = 600\text{mm}$  and S5, S6, S13, S14, S17, S18, S25, S26, BS2, BM2, BL2 and BX2 with the load at  $a = 400\text{mm}$ . It should be emphasized that the size of the loading plate for slabs S1 – S8, S19 – S26 is  $300\text{mm} \times 300\text{mm}$  and for the slab strips and slabs S9 – S18 it is  $200\text{mm} \times 200\text{mm}$ , Table 3.2. The experimental observations are summarized in Table 4.6, showing the measured average ratio of the shear capacity for  $a = 400\text{mm}$ ,  $V_{exp,400}$ , to the shear capacity for  $a = 600\text{mm}$ ,  $V_{exp,600}$ . The results in Table 4.6 show a clear increase in shear capacity with decreasing distance to the support as well as a clear influence of the overall member width  $b$  on the quantity of this increase. The last column of Table 4.6 shows the expected average ratio of the shear capacity for  $a = 400\text{mm}$  as compared to the shear capacity for  $a = 600\text{mm}$  based on the factor  $\beta$  from NEN-EN 1992-1-

Parameter analysis

1:2005. For S17 and S18 the value of  $a_v/2d_l$  equals  $a_v/2d_l = 0,314$ , which results in  $\beta = 0,5$ . Therefore, the expected increase in capacity is given based on the comparison of  $a_{v400}/a_{v600}$  (2,25) and based on  $\beta_{400}/\beta_{600}$  (1,41). Comparing this column to the column with the experimental average increase shows that the observed increase in shear resistance for slabs is less than obtained with the factor  $\beta$  given by NEN-EN 1992-1-1:2005 for beam shear.

Table 4.6: Influence of the decrease in the shear span from 600mm to 400mm on the observed increase of the shear capacity.

Specimens	$b$ (m)	AVG $V_{exp,400}/V_{exp,600}$	standard deviation	coefficient of variation	NEN-EN 1992-1-1 $V_{exp,400}/V_{exp,600}$
BS2 – BS3	0,5	2,09	0,297	14,2%	1,8
BM2 – BM3	1,0	1,73	0,027	1,6%	1,8
BL2 – BL3	1,5	1,49	0,061	4,1%	1,8
BX2 – BX3	2,0	1,30	0,063	4,8%	1,8
S3 – S6	2,5	1,42	0,172	12,1%	2
S11 – S14	2,5	1,45	0,213	14,7%	1,8
S15 – S18	2,5	1,39	0,145	10,4%	2,25 // 1,41
S21 – S26	2,5	1,35	0,037	2,7%	2

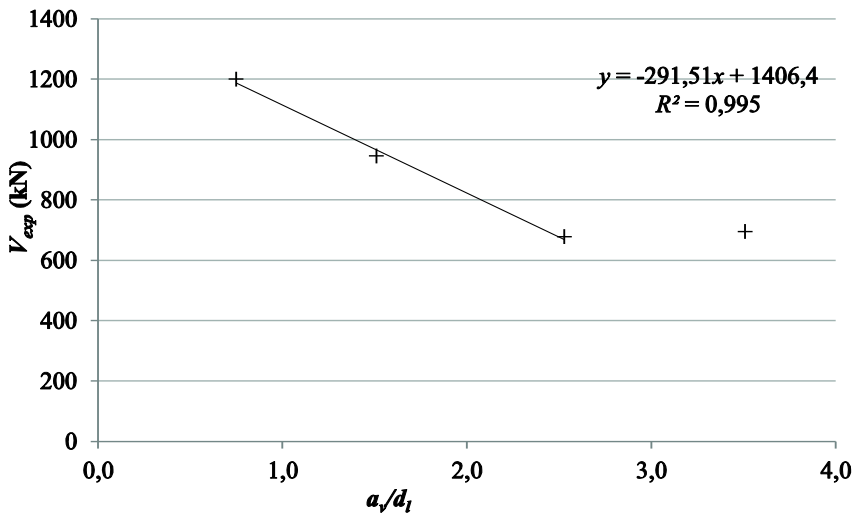


Fig. 4.5: Influence of  $a_v/d_l$  on shear capacity as observed in experiments. The results of S25T5, S25T4, the average of S4T1 and S4T2 and the average of S6T4 and S6T5 are used.

The main goal of the experimental research was to study the behaviour of slabs under concentrated loads close to the support ( $a/d_l < 2,5$ ). A few additional experiments at a larger

distance to the support were carried out with the concentrated load close to the edge and in the vicinity of a failure induced by a previous experiment. The results of the influence of  $a_v/d_l$  on the shear capacity  $V_{exp}$  are shown graphically in Fig. 4.5, indicating an initial linear decrease for the shear capacity as a function of  $a/d_b$ , followed by a constant shear capacity for values  $a_v \geq 2d_l$ . This resembles the behaviour of beams with loads near to supports.

#### 4.6.3 Explanation

The lower increase in capacity for a decrease in the shear span to depth ratio  $a/d_l$  as observed for slabs can be explained when studying the compressive struts in slabs under concentrated loads. While for beams, a clearly defined strut develops over the distance  $a$  (or  $a_v$ ), in slabs a fan of struts can develop. A plan view of these struts is shown in Fig. 4.6. This sketch also shows the influence of the slab width and the resulting transverse redistribution of the load. In beams, only the straight strut ( $a/d_l = 1$  in Fig. 4.6) can develop. In slabs, the resulting  $a/d_l$  will depend on the fan of struts and their resulting load path, which is on average longer than the direct straight strut. This larger average  $a/d_l$  can thus explain the smaller influence of the distance between the load and the support in slabs than in beams. The experimental results show the difference in behaviour between the beams or slab strips with mainly two-dimensional load-carrying behaviour and slabs with mainly three-dimensional load-carrying behaviour.

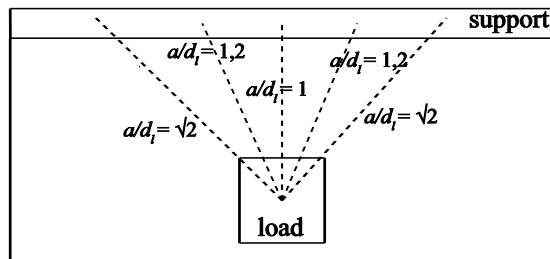


Fig. 4.6: Larger average  $a/d_l$  ratio for slabs as compared to beams.

## 4.7 Concrete compressive strength

### 4.7.1 Background

Traditionally, the concrete tensile strength is considered the most important factor influencing the shear resistance of beams and the punching strength of slabs. For design purposes, the tensile strength is calculated from the concrete compressive strength with a square root (e.g. ACI 318-08) or cube root (e.g. NEN-EN 1992-1-1:2005) relationship.

The relationship between the concrete compressive strength and the beam shear resistance is determined based on a statistic evaluation of an extensive database of shear tests, for example in König and Fischer (1995) and Regan (1987), both for  $a/d_l \geq 3$ .

### *Parameter analysis*

Mitchell, Cook and Dilger (2005) compared the influence of the square and cube root of the concrete compressive strength with experimental data for slabs failing in punching, showing that the overall trend in the capacity is reasonably well presented by both a square root and a cube root relationship.

The concrete compressive strength influences the shear capacity of beams because it directly influences the concrete tensile strength, the dowel capacity limited by the tensile strength of the concrete cover supporting the dowel, the aggregate interlock capacity and the strength of the compression zone.

No influence of the concrete compressive strength was experimentally observed in large, lightly reinforced beams by Angelakos et al. (2001) in which the concrete compressive strength was varied between 21MPa and 98MPa and the shear span to depth ratio was  $a/d_l = 2,92$ . Kani postulated in 1967 that: “The influence of concrete strength on the so-called shear resistance of rectangular reinforced concrete beams without web reinforcement is negligible and can be omitted in strength analysis.”

#### *4.7.2 Experimental observations*

To quantify the influence of the concrete compressive strength on the one-way shear resistance of slabs, the results of S2, S3, S4, S7 and S8 are compared. S2, S3 and S4 are produced with normal strength concrete, while S7 and S8 are produced with high strength concrete, Table 3.2. All tests were carried out at  $a/d_l = 2,26$ . For the tested mixtures, no increase in shear capacity with increasing compressive strength was observed, Fig. 4.7. The measured average increase in shear resistance for S3 and S4 versus S7 and S8 is 0,6% for an increase in concrete cube compressive strength of 54%. The expected increase in capacity is 24% for a square root relationship between the concrete compressive strength and the tensile strength and 15% for a cube root relationship. The measured splitting tensile strength increased with 47%, as shown in Table 3.2. In Fig. 4.7, the results from the experiments are shown, as well as the lines with the expected values assuming a cube root relationship, as prescribed by NEN-EN 1992-1-1:2005. For the slabs with the load in the middle of the width (M), the cube root relationship is based on the average of the experimental results of S3T1 and S3T4 as a reference. For the slabs with the load close to the edge (E), the cube root relationship is based on the average of the experimental results of S4T1, S4T2, S4T4 and S4T5 as a reference. The discrepancy between the curve of expected shear capacities assuming a cube root relationship and the measured shear capacities is reasonable considering the small number of experiments: the coefficient of variation between the experimental results and the curve is 16% for the slabs with the load in the middle of the width (M) and 8% for the slabs with the load near to the edge (E).

4.7.3 Explanation

The experimental data do not agree with the theoretically expected increase in capacity. Sherwood et al. (2007) suggest that 70% of the shear resistance is carried by aggregate interlock. For high strength concrete the aggregate interlock capacity is reduced. The aggregate itself is then the weakest element through which the shear crack passes. Failure of the aggregates is observed in S7 and S8. The reduced aggregate interlock capacity of the high strength concrete might explain why no increase in shear resistance is observed for an increasing concrete strength. However, for the glacial river aggregates used in the experiments under consideration, failure of the aggregates only occurs for compressive strengths larger than 65MPa. Therefore, an increase in capacity up to 65MPa would be expected – this increase is not observed for the series with the load in the middle of the width, but can be seen for the series with the load near to the edge.

A possible explanation for the negligible observed influence of the concrete compressive strength for slabs subjected to a concentrated load close to the support is that, in this loading case, a three-dimensional load carrying mechanism develops that depends more on the geometric properties of the slab, the load and the supports than on the concrete material properties.

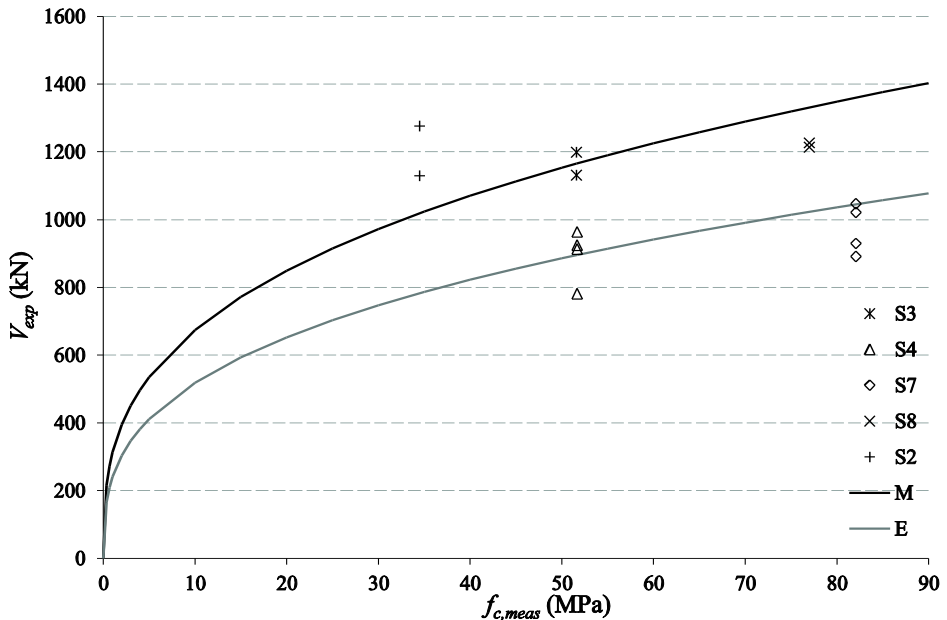


Fig. 4.7: Influence of concrete compressive strength on measured shear capacity.

## 4.8 Overall width and effective width

### 4.8.1 Background

If the concept of an effective width can be applied to concrete slabs loaded in shear, then the shear capacity should cease to increase as the width is increased after reaching a threshold value, the effective width. As long as the element width is smaller than the effective width, increasing widths lead to increasing shear capacities. When the element width is larger than the effective width, only the effective width at the support can be activated to carry the shear load, and further increasing of the element width will not result in an increase in the shear carrying capacity.

Previous research (Regan and Rezai-Jorabi, 1988) showed increasing maximum shear capacities for increasing widths (0,4m to 1,2m) up to a certain value (1m) for slabs with a concentrated load placed at such a location that  $a/d_l = 5,42$  after which the maximum shear capacity remained around the same value. Reißen and Hegger (2012) tested slabs of increasing widths, but a threshold value cannot be observed from this series of tests.

From the results of experiments on slabs under a concentrated load close to the support from the literature, only A-10-10 and B-10-10 (Furuuchi et al. 1998) can be compared. Load spreading based on the traditional load spreading method, Fig. 2.16a, results in an effective width of  $b_{eff1} = 510\text{mm}$ , limited to  $b_{eff1} = b = 500\text{mm}$  for A-10-10 by its full width  $b$ . The French load spreading method, Fig. 2.16b results in an effective width of  $b_{eff2} = 660\text{mm}$ , limited by the specimen width of  $b_{eff2} = b = 500\text{mm}$  for A-10-10 and to  $b_{eff2} = b = 650\text{mm}$  for B-10-10. As a result, the expected increase in capacity based on the traditional load spreading is 2% and based on the French load spreading method is 30%. The experimental results show an increase in capacity of 25%. Thus, the French load spreading method agrees best with these experimental data. The validity of these conclusions, based on a very small number of experiments, could be questioned.

Another aspect related to the overall width is the transverse redistribution capacity around local weaknesses. According to this concept, larger widths lead to larger capacities. In wide elements such as slabs, disturbances caused by local weaknesses are expected to be smoothed out. Experiments with regard to this phenomenon are reported by Yang (2012).

### 4.8.2 Experimental observations

To study the influence of the overall width on the shear capacity, the results of S8 (2,5m) and S9 (2,5m) are compared to the results of the series of slab strips (BS1/0,5m – BX3/2m), all of which are made with high strength concrete, Table 3.2. The results of the series of experiments with an increasing width are shown in Fig. 4.8. The trendlines through datapoints that are at widths smaller than the threshold value are shown together with the lines of constant shear capacities. The intersection of these lines for a data series determines the measured threshold from a series of specimens with varying widths. These results show

### Parameter analysis

that the concept of using an effective width for slabs is indeed valid as the shear capacity does not increase linearly for larger widths. In Fig. 4.8 the shear capacity increases linearly for the results of BS, BM and BL. Comparing the test results of BL, BX and S8/S9 shows that the increase in shear capacity for these slab widths is rather small, indicating that the threshold value for this load configuration is achieved.

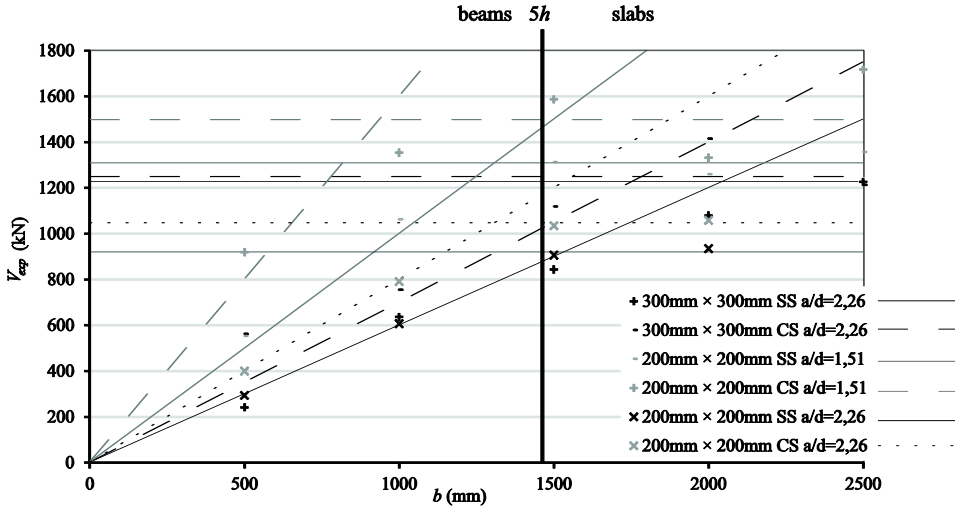


Fig. 4.8: Influence of overall width on shear capacity. Test results for BS, BM, BL, BX, S8 and S9 are shown.

In Fig. 4.8, the line of  $5h$  is also marked, which according to NEN-EN 1992-1-1:2005 is the lower bound for a structural element to be considered as a slab. Note that the line is slightly shifted to the left to keep the datapoints of the graph visible.

The results for the calculated threshold effective width based on the experimental results are given in Table 4.7 and compared to the calculated widths based on the load spreading methods from Fig. 2.16a and Fig. 2.16b with:

$b_{meas}$  effective width as the calculated threshold value from the series of experiments with different widths;

$b_{eff1}$  effective width based on the Dutch load spreading method;

$b_{eff2}$  effective width based on the French load spreading method.

The results from Table 4.7 show a difference between loading at the simple (SS) and continuous (CS) support. Consistently, lower effective widths are found at the continuous support as compared to the simple support (§4.5.3).

The results from Table 4.7 also show a different effective width depending on the size of the loading plate. As previously discussed, load spreading from the centre of the load towards the support would not imply an influence of the size of the loading plate on

### Parameter analysis

the effective width or the overall shear capacity. The results of this series of experiments show the influence of the size of the loading plate on the effective width. The size of the loading plate is also taken into account in the French load spreading method.

Moreover, the results from Table 4.7 show that the effective width becomes smaller as the  $a/d_l$  ratio decreases, which corresponds to the idea of horizontal load spreading from the load towards the support at a certain angle. The results in the last two columns of Table 4.7 show that the experimental effective width corresponds best to the effective width based on the French load spreading method.

*Table 4.7: Effective width as calculated from the experimental results.*

<b>Series</b>	<b><math>b_{meas}</math> (m)</b>	<b><math>b_{eff1}</math> (m)</b>	<b><math>b_{eff2}</math> (m)</b>	<b><math>b_{meas}/b_{eff1}</math></b>	<b><math>b_{meas}/b_{eff2}</math></b>
300mm × 300mm, SS, $a/d_l = 2,26$	2,0	1,1	1,7	1,86	1,20
300mm × 300mm, CS, $a/d_l = 2,26$	1,8	1,1	1,7	1,62	1,05
200mm × 200mm, SS, $a/d_l = 1,51$	1,3	0,7	1,1	1,87	1,19
200mm × 200mm, CS, $a/d_l = 1,51$	0,9	0,7	1,1	1,34	0,85
200mm × 200mm, SS, $a/d_l = 2,26$	1,5	1,1	1,5	1,39	1,02
200mm × 200mm, CS, $a/d_l = 2,26$	1,3	1,1	1,5	1,19	0,87

#### 4.8.3 Explanation

The idea behind the effective width as explained in the background section §4.8.1, is reflected by the experimental results. For the smaller specimens, increasing the width results in an increasing shear capacity. After reaching a threshold effective width, the shear capacity fluctuates around a certain value. The threshold effective width was also observed in the experiments.

The moment distribution in the shear span is observed to influence the load spreading mechanism that occurs in the slab. This observation corresponds to the measurements of the reaction forces in the experiments on slabs under a combination of loads and the results from the linear finite element analysis, indicating the relation to the transverse moment, as discussed in §4.5.3.

The results of this series of experiments show the influence of the size of the loading plate on the effective width: a larger loading plate leads to a larger effective width and thus a wider mechanism of load spreading. As previously discussed, load spreading from the centre of the load towards the support does not imply an influence of the size of the loading plate on the effective width or the overall shear capacity. The results of this series of experiments show the influence of the size of the loading plate on the effective width: a larger loading plate leads to a larger effective width and thus a wider mechanism of load spreading. This observation can be explained by the larger area from which the compression struts are distributed.

The importance of the distance between the load and the support is reflected by both horizontal load spreading methods as well as the measured effective widths based on the series of slab strips. Indeed, at smaller distances between the load and the support, the compressive struts cannot fan out over the width as much as at larger distances.

## **4.9 Reinforcement type**

### **4.9.1 Background**

Shear tests on beams with plain bars typically show a larger shear capacity as compared to beams with deformed bars (Kani, 1964; Muttoni and Ruiz, 2008; Leonhardt and Walther, 1962). However, for beams with loads close to the support and smaller reinforcement ratios, lower shear capacities with plain bars than with deformed bars have been reported (Regan, 2000; Iyengar et al., 1988). For this loading case, the action of direct load transfer is dominant, and this action is the same in beams with deformed bars and beams with plain bars.

The higher shear capacity for beams with plain bars as observed in most beam shear experiments is attributed to the absence of a force increment (Fig. 2.5) over the reinforcement. As a result, no interlock forces and no compression increment can result, but the member will behave as a tied arch with a constant force in the reinforcement and a constant compression force at a variable depth (Lubell, 2006). While for a beam with deformed bars, the inclined crack develops through the theoretical compression strut and reduces the strength of the beam, in beams with plain bars only a limited part of the inclined crack develops through the theoretical strut due to the reduced bond strength of the bar (Muttoni and Ruiz, 2008). Olonisakin and Alexander (1999) tested beams in shear, reinforced with ribbed bars with bond and epoxy coated bars without bond. The authors were surprised that there was no obvious correlation between the magnitude of the force increment and the presence or absence of an epoxy coating. A possible explanation is that adhesion bond was not significant in these experiments. Alternatively, factors other than the force increment may have had a more significant effect.

### **4.9.2 Experimental observations**

To study the difference in shear capacity for slabs reinforced with plain bars or deformed bars, the results of S1 (deformed bars) and S11 (plain bars) are compared, the reinforcement layout of which is shown in Fig. 3.7 and Fig. 3.8 respectively. The loading conditions are identical, but a difference in the measured concrete cube compressive strength and reinforcement layout should be noted, see Table 3.1. The results are shown in Fig. 4.9. The experiments mainly show a difference in the cracking pattern, with the slabs reinforced with plain bars developing significantly less flexural cracks, Fig. 4.10.

### Parameter analysis

Anchorage failure can occur in slabs reinforced with plain bars. Low residual shear capacities were observed in some experiments for the slabs with plain bars.

#### 4.9.3 *Explanation*

The absence of bond between the plain reinforcement bars and the concrete leads to a continuous force in the longitudinal reinforcement. As a result, fewer flexural cracks are observed.

The possibility of anchorage failure can as well be explained by the fact that the entire reinforcing bar will carry the same tensile force, leading to higher forces for plain bars close to their anchorage as compared to deformed bars.

Taking into account that the reinforcement ratio of slab S1 was larger than that of S11, it can be concluded that there is no significant difference in shear capacity between specimens reinforced with plain bars and those reinforced with deformed bars. This can be explained by the fact that for loads close to the support, arching action is governing over beam action. Arching action and direct load transfer are not influenced by the bond properties of the reinforcement.

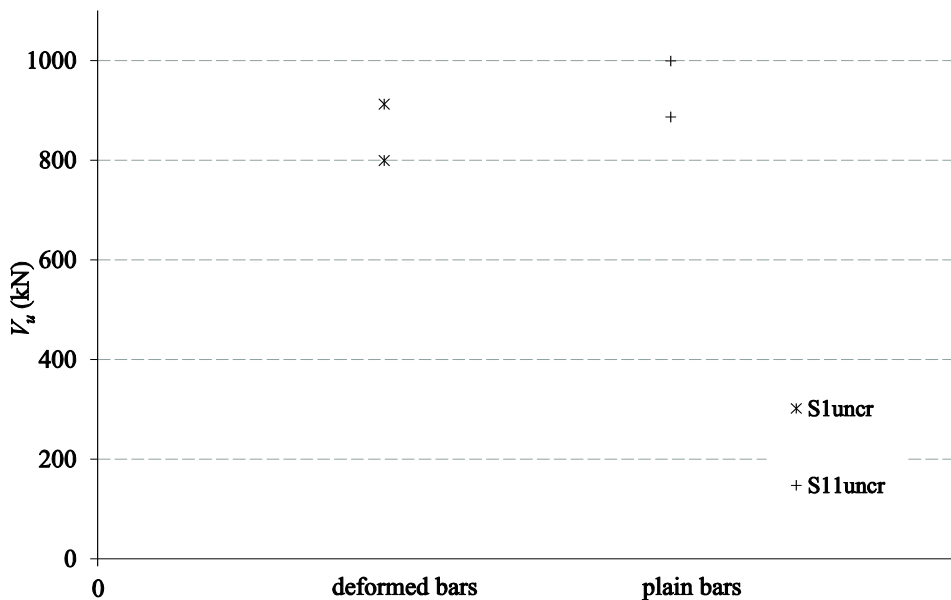
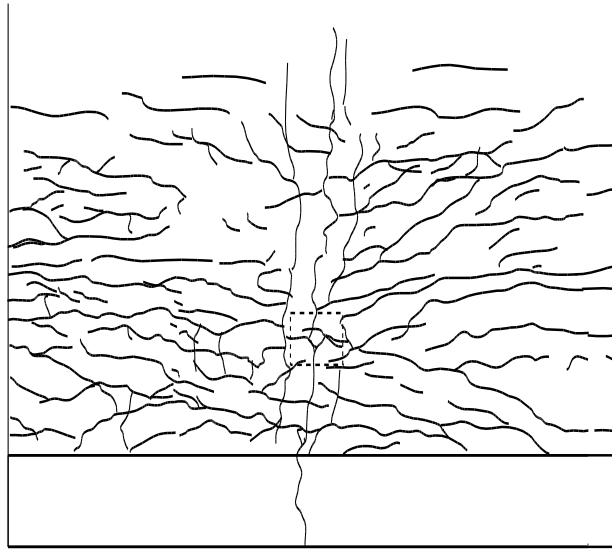


Fig. 4.9: Comparison of test results for deformed reinforcing bars (S1) and for plain reinforcing bars (S11) with  $a/d_1 = 2,26$ ; size of the loading plate  $200\text{mm} \times 200\text{mm}$ ; C28/35.

Parameter analysis



(a)



(b)

Fig. 4.10: Observed cracking at the bottom face to compare cracks in a slab with deformed bars to cracks in a slab with plain bars: (a) after failure of S1T1 (deformed bars). Flexural cracks form a grid-like pattern and inclined cracks between the load and the support indicate wide beam shear failure; (b) after failure of S11T1 (plain bars). Mostly inclined cracking is observed and the majority of the cracks occur close to the support and towards the edge.

#### 4.10 Line supports compared to elastomeric bearings

##### 4.10.1 Background

In the literature (Chapter 2) and developed database (Annex 1), no series of experiments is found in which a comparison can be made between slabs on rigid line supports and slabs on elastomeric bearings. In NEN-EN 1992-1-1:2005 § 6.2.2. (6) direct load transfer between the load and the support is taken into account by  $\beta = a_v/2d_l$ . The distance  $a_v$  is defined as the distance between the face of the support and the face of the load. However, for the case of elastomeric bearings (flexible supports), the distance  $a_v$  is taken to the centre of the support. For the same position of the load, a smaller capacity would thus be expected for a slab supported by elastomeric bearings.

##### 4.10.2 Experimental observations

In the first series of experiments, four slabs (S15 – S18) supported by three elastomeric bearings per support line are tested (Fig. 3.1b), as compared to the rigid line supports in all other experiments. In the second series of experiments, two slabs (S23 - S24) are tested on elastomeric bearings, as compared to steel bearings in all other cases, Table 3.3.

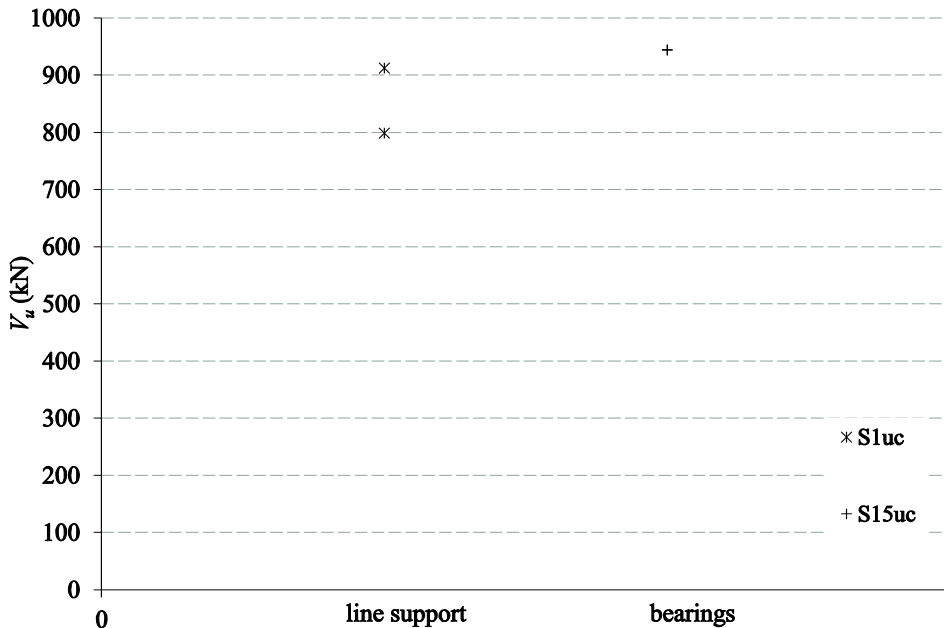


Fig. 4.11: Results of slabs on rigid line supports as compared to slabs on elastomeric bearings; results from S1 and S15 ( $a/d_l = 2,26$ ; size of the loading plate  $200\text{mm} \times 200\text{mm}$ ; C28/35).

### Parameter analysis

To study the difference between a rigid line support and elastomeric bearings, the results of S1 and S15 can be compared, as these slabs are loaded under similar conditions. It should be noted that a different measured concrete cube compressive strength is reported for these slabs and that the reinforcement layout is different, as in the slabs on bearings a hidden transverse beam is used over the support, resulting in a lower effective depth ( $d_l = 255\text{mm}$ ), Table 3.1. The results are shown in Fig. 4.11, showing approximately similar results for S1 and S15. For S15 as compared to S1 the capacity remains about constant (0,3% decrease) for the undamaged slabs. As reported in Table 3.2, in the slabs on elastomeric bearings, punching shear failure around the bearings was a possible failure mechanism. For the locally failed specimens, low values of the ultimate capacity were found.

To study the difference between slabs on steel bearings and slabs on elastomeric bearings, the results of S23 and S24 (elastomeric bearings) are compared to the results of S21 and S22 (steel bearings). It should be noted that the same centre-to-centre distance  $a$  between the load and the support was used for these experiments, but that the support width is different, leading to a different face-to-face distance  $a_v$ . The results are summarised in Table 4.8, in which the comparison is based on the shear force at failure at the support ( $V_{exp}$ ), the shear stress at failure at the support ( $\tau_{exp}$ ), the effective width based on the measurements of the reaction forces at failure ( $b_s$ ) and the maximum effective width based on the measurements of the reaction forces ( $b_{max}$ )<sup>10</sup>. The subscript “st” is used for the steel bearings and “el” for the elastomeric bearings. These results show similar capacities for slabs with steel bearings as compared to slabs with elastomeric bearings. However, the observed effective widths based on the measurements of the reaction force, are clearly larger for slabs on steel bearings. This observation can also be made by looking at the distribution of the reaction forces over the width, as shown in Fig. 4.13 for S22T4 supported by steel bearings and S24T3 supported by elastomeric bearings. Moreover, it is observed in the experiments that slabs on elastomeric supports show a failure mode with more warning behaviour than slabs on steel bearings. This observation is reflected in the load-displacement diagrams (Fig. 4.12).

*Table 4.8: Comparison of the test results for slabs on steel bearings and slabs on elastomeric bearings.*

	$V_{st}/V_{el}$	$\tau_{st}/\tau_{el}$	$b_{sst}/b_{sel}$	$b_{maxst}/b_{maxel}$
<b>AVG</b>	0,968	0,899	1,074	1,180
<b>STD</b>	0,132	0,141	0,130	0,109
<b>COV</b>	0,137	0,156	0,121	0,092

---

<sup>10</sup> The effective width is determined from the reaction forces, so that the total reaction due to the maximum reaction over the effective width equals the total reaction from the measured force profile over the full width.

### 4.10.3 Explanation

As shown in Fig. 4.13, the measurements of the reaction forces are not uniform, but disturbed by the geometry of the slab, which is not perfectly flat. As the results in Table 4.8 for the effective width are around 1, no significant influence of the support material on the way the load is distributed over the support can be seen. The differences in capacity for  $\tau_{st}/\tau_{el}$  can be attributed to the difference in the support width, resulting in a larger distance  $a_v$  for the slabs supported by steel bearings than for the slabs supported by elastomeric bearings.

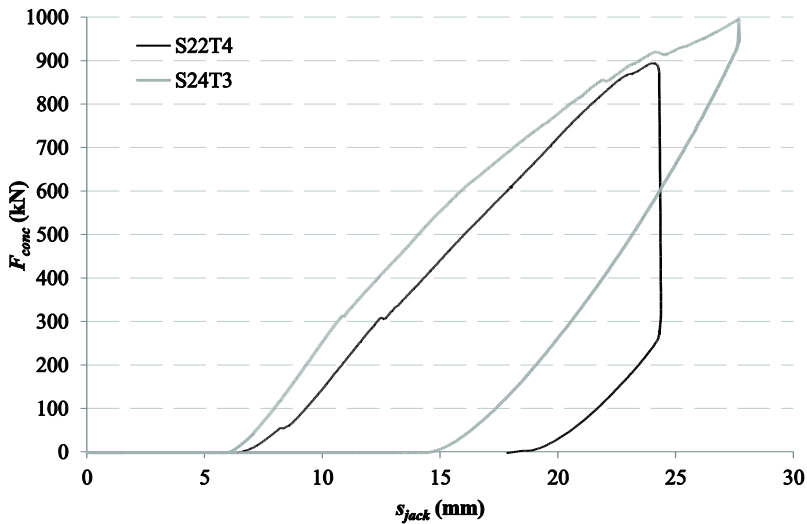


Fig. 4.12: Load-displacement ( $F_{conc}$  vs.  $s_{jack}$ ) diagram of S22T4 (steel bearings) compared to S24T3 (elastomeric bearings).

## 4.11 Combination of loads

### 4.11.1 Background

In the literature (Chapter 2) and resulting slab shear database (Annex 1), no report is made of experiments on slabs under a combination of concentrated and distributed loads. The only exceptions are the experiments by Reißer and Hegger (2012) and Rombach and Latte (2009), in which a small line load representing an edge load is applied at the tip of a cantilevering deck. Reißer and Hegger (2012) tested two double T-beams at the cantilevering ends, both with a concentrated load only and with a combination of a concentrated load and a line load. The ratios between the shear stress at the support from the experiment with a line load and a concentrated load  $\tau_{combination}$  to the shear stress of the experiment with a concentrated load only  $\tau_{tot,cl}$  are  $\tau_{combination}/\tau_{tot,cl} = 1,42$  and  $\tau_{combination}/\tau_{tot,cl} = 1,41$ , indicating a higher shear stress at failure for the slabs with a combination of loads.

Parameter analysis

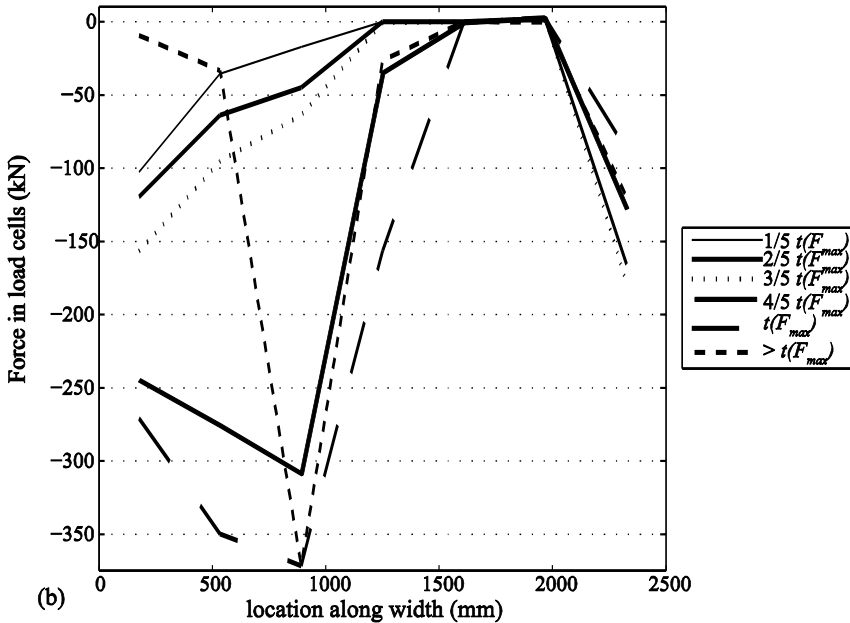
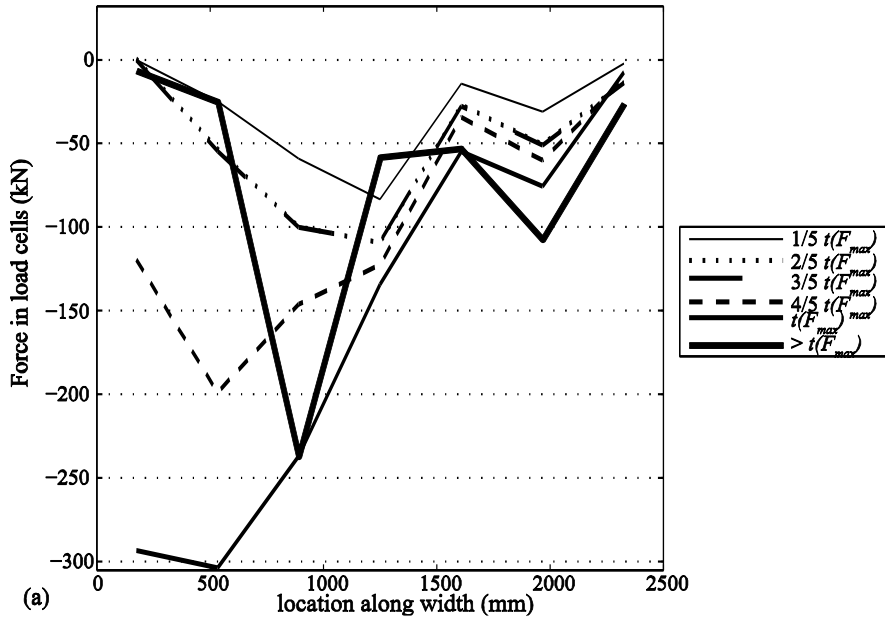


Fig. 4.13: Reaction forces at different moments during the experiments as a function of different points in time expressed as a fraction of the time of failure  $t(F_{max})$  measured by the loads cells that indicate how the shear stresses at the support are distributed: (a) S22T4 (steel bearings) compared to (b) S24T3 (elastomeric bearings).

### Parameter analysis

When a concentrated load on a slab is distributed over a certain effective width, and thus a certain amount of transverse redistribution over the width of the slab is allowed, it is not known if this contribution of the concentrated load can be added to the contribution of the distributed load when assessing the shear capacity. The concept is sketched in Fig. 4.14. If the hypothesis of superposition is valid, then the sum  $\tau_{combination}$  of the shear stress due to the concentrated load over the effective width  $\tau_{conc}$  and the shear stress due to the distributed load at failure over the full width  $\tau_{line}$  should be larger than or equal to the ultimate shear stress in an experiment with a concentrated load only,  $\tau_{tot,cl}$ .

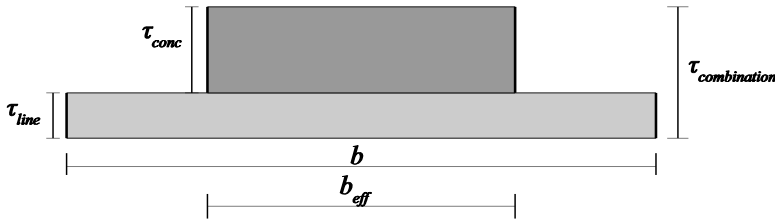


Fig. 4.14: Superposition of the shear stress due to a concentrated load over the effective width with the distributed load over the full slab width.

#### 4.11.2 Experimental observations

To verify the hypothesis of superposition, the shear stresses over the support at ultimate from the second series of tests are compared to the shear stresses at ultimate in a similar experiment from the first series. If the principle of superposition holds true, then the shear stress (calculated over  $b_{eff2}$ ) of the experiment with a concentrated load only,  $\tau_{tot,cl}$ , should be smaller than or equal to the sum of the shear stress due to the loads that act over the full width  $b$  (line load, dead load and vertical prestressing load),  $\tau_{line}$ , with the shear stress due to the concentrated load acting over  $b_{eff2}$ ,  $\tau_{conc}$ : the requirement can thus be expressed as  $\tau_{combination} = \tau_{line} + \tau_{conc} \geq \tau_{tot,cl}$ .

In Fig. 4.15, the total shear stress at failure at the support in the experiments with a combination of loads is compared to the ultimate shear stress obtained in a similar experiment with a concentrated load only. As can be seen in Table 3.1 there is a difference in the cube compressive strengths of the concrete used in the experiments with combined loading and the experiments with a concentrated load only. Therefore, a correction has been made by multiplying  $\tau_{tot,cl}$  with the cube root (as used in NEN-EN 1992-1-1:2005) of the ratio between these compressive strengths  $(f_{c,combi}/f_{c,conc})^{1/3}$ . This correction led to the results denoted “compare, corr” in Fig. 4.15, as opposed to the results indicated with “comparison” in which no correction for the difference in the concrete compressive strength was applied. It should be noted that S15 to S18 are supported by three elastomeric bearings, forming point supports, while S23 and S24 are supported by seven elastomeric bearings, almost forming a line support. As shown in Table 3.2 punching failure around the bearings is a

*Parameter analysis*

failure mode occurring in the first series of experiments. Therefore the comparison based on the results of S15 to S18 compared to S23 and S24 is omitted from Fig. 4.15.

*Table 4.9: Results of the experiments used to study the hypothesis of superposition.*

<b>Test</b>	$\tau_{conc}$ (MPa)	$\tau_{line}$ (MPa)	$\tau_{combination}$ (MPa)	<b>Test</b>	$\tau_{conc}$ (MPa)	$\tau_{add}$ (MPa)	$\tau_{tot,cl}$ (MPa)	$\tau_{tot,cl,corr}$ (MPa)
S21T1	2,16	0,76	2,91	S3T1	2,54	-0,02	2,52	2,60
S21T2	2,56	0,59	3,15	S3T4	2,47	0,13	2,60	2,68
S22T1	2,40	0,75	3,16	S4T1	2,77	0,00	2,77	2,88
S22T2	2,35	0,75	3,10	S4T2	2,77	0,00	2,77	2,88
S22T3	2,39	0,61	3,00	S4T4	2,29	0,10	2,39	2,49
S22T4	2,19	0,60	2,79	S4T5	2,29	0,10	2,39	2,49
S20T1	2,85	0,44	3,30	S19T2	2,75	0,02	2,76	2,82
S20T2b	2,58	0,74	3,33	S19T1	2,90	0,11	3,01	3,07
S20T3	2,94	0,73	3,67	S4T4	2,29	0,10	2,39	2,52
S20T4	3,19	0,73	3,91	S4T5	2,29	0,10	2,39	2,52
S25T2	4,18	0,76	4,94	S5T1	4,66	0,11	4,77	5,09
S25T3	4,77	0,76	5,52	S6T1	4,37	0,11	4,48	4,70
S26T1	4,46	0,61	5,08	S6T4	4,18	-0,01	4,17	4,38
S26T2	4,08	0,60	4,68	S6T5	4,18	-0,01	4,17	4,38
S26T3	4,01	0,77	4,79	S5T1	4,66	0,11	4,77	5,09
S26T4	4,20	0,77	4,98	S6T1	4,42	0,11	4,53	4,75
S26T5	4,47	0,78	5,25	S6T2	4,42	0,11	4,53	4,75

The results that are shown in Fig. 4.15 are based on the shear stresses that are determined from the experiments as given in Table 4.9. In this table, the following symbols are used:

- $\tau_{conc}$  the shear stress due to the concentrated load distributed over  $b_{eff2}$ ;
- $\tau_{line}$  the shear stress due to the line load, the self-weight of the line load (HEM 1000) and of the slab and the prestressing force;
- $\tau_{combination}$   $\tau_{conc} + \tau_{line}$ ;
- $\tau_{add}$  the shear stress due to the self-weight of the slab and the prestressing force;
- $\tau_{tot,cl}$   $\tau_{conc} + \tau_{add}$ ;
- $\tau_{tot,cl,corr}$  the corrected value of  $\tau_{tot,cl}$  that takes into account the difference in the concrete compressive strength of the tested specimens.

## Parameter analysis

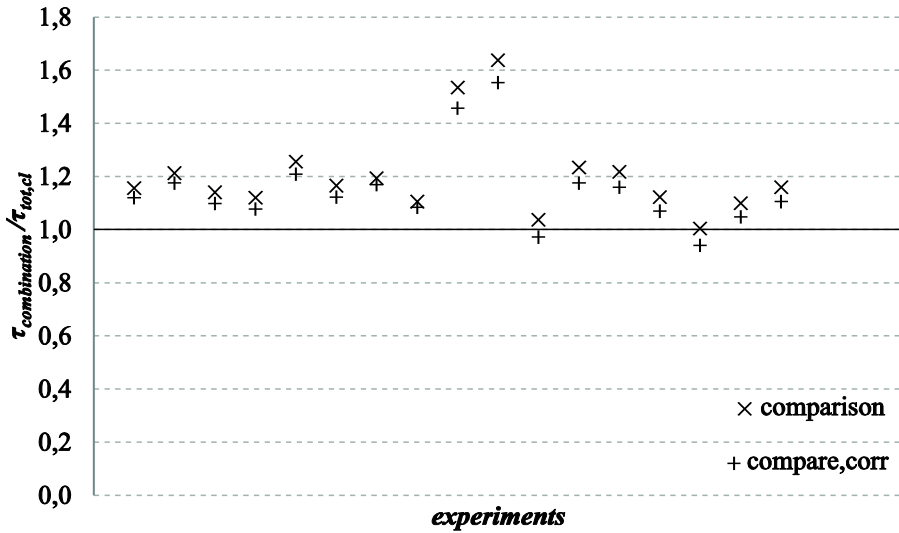


Fig. 4.15: Results of experiments verifying the hypothesis of superposition.

### 4.11.3 Explanation

The results in Fig. 4.15 confirm the hypothesis of the superposition of a reduced concentrated load over an effective width with a line load representing the distributed load. Typically, as can be seen in Fig. 4.15, higher shear stresses can be attained when combining different loads as compared to the experiments in which only a concentrated load is applied. These results show that the hypothesis of superposition of the concentrated load over the effective width to the distributed load is a safe assumption.

Reißen and Hegger (2012) contribute the larger capacity in the experiments with a combination of loads to the changed moment lines in the cantilevered specimens. The contribution of the line load in these experiments is rather small, as it was aimed at representing an edge load and not the contribution of the distributed load.

Another possible explanation is that the assumed shear stress distribution at the support as shown in Fig. 4.14 is disturbed at failure and that redistribution occurs so that more of the shear stress due to the distributed loads is taken by the extremities of the slab width and less of this shear stress is taken by the part of the width that serves as effective width for the concentrated load.

It should be mentioned that the combination of a distributed load and a concentrated load is just one of the many interesting load combinations that can be studied. The influence of additional concentrated loads, as for example the two axes with two wheel loads for the design truck in Load Model 1 from NEN-EN 1991-2:2003, would also be

interesting to study. Currently, the effective width is determined per axle, combining the two concentrated loads. To further analyse how the effective width should be determined when multiple concentrated loads are used, additional experiments are recommended.

#### **4.12 Conclusions**

Reinforced concrete slabs loaded with a concentrated load close to the support show a three-dimensional behaviour that is distinctly different from the two-dimensional shear carrying behaviour in beams. This statement is supported by the following observations from the parameter analysis:

- The increase in shear capacity at the continuous support as compared to the simple support is smaller for elements with a larger width.
- The influence of the size of the loading plate becomes larger for specimens of a larger width.
- The influence of the distance between the load and the support becomes smaller as a result of the average resulting loading path for specimens with a larger width.
- The influence of the concrete compressive strength is found to be smaller in slabs than observed in beam shear experiments from the literature.
- The overall width of the specimen significantly influences the capacity, cracking behaviour and dependence on the aforementioned parameters.

The test results have indicated that the important parameters for the shear capacity of slabs under concentrated loads close to the support are:

- the size of the loading plate,
- the distance between the load and the support, and
- the overall width of the member.

This indicates that the shear capacity of slabs under concentrated loads close to supports mainly depends on the geometrical properties of the slab and the load. The following parameters did not affect the shear capacity substantially:

- the amount of transverse flexural reinforcement,
- the concrete compressive strength,
- the type of reinforcement (plain bars or deformed bars), and,
- the material of the bearing (steel or rubber) when using a line of bearings.

The experimental results show the large residual capacity of slabs after a locally occurring failure, and a more ductile failure mechanism than observed in typical beam shear experiments. At the bottom face or the side face of the slabs, inclined cracks are observed already at 70% of the value of the ultimate load, illustrating the ability of a slab to warn for shear distress.

The shear capacity at the continuous support is at least equal to, and on average larger than, the shear capacity at the simple support, unlike previously stated in the Dutch code NEN 6720:1995.

### *Parameter analysis*

In the slabs reinforced with plain bars, anchorage failure can occur and in the slabs supported on three bearings, failure by punching around the support can occur, so that a direct comparison with other experiments might be obstructed by the differences in the failure modes.

The results show that the concentrated load can be distributed over an effective width based on the horizontal load spreading method as used in French practice. Experiments on slabs under a combination of loads demonstrated that the hypothesis of superposition of the shear stress due to concentrated loads over their effective width with the shear stress due to distributed loads over the full width is a safe and valid assumption.

*Parameter analysis*

## **5 Modified Bond Model**

### **5.1 Introduction**

The goal of this chapter is to develop a theoretical model that describes the load-bearing behaviour of slabs under concentrated loads close to supports. The proposed model is a combination of load-bearing quadrants and strips, and is based on the Bond Model by Alexander and Simmonds (1992). The original Bond Model was developed for concentric punching shear. In this chapter, it is extended for the application to slabs under concentrated loads close to supports. The resulting Modified Bond Model, developed as part of this research, can be considered a mechanical model, in which the concept of a limiting one-way shear stress is incorporated. Where most beam shear and punching shear models make a strict distinction between these two modes of failure, the Bond Model considers the shear-carrying behaviour as an action of two-way quadrants and one-way strips. As such, it is the most suitable model for the case of one-way slabs under concentrated loads close to supports, in which shear failure occurs as a combination of one-way shear and two-way shear.

There are a number of advantages that can be attributed to the Modified Bond Model to determine the capacity of slabs under concentrated loads. First, the Modified Bond Model shows the essential link between one-way and two-way shear failure modes by breaking down the shear-carrying behaviour of a slab subjected to a concentrated load into the load carried in two directions through beam action shear in the quadrants and the load carried by arching action in the strips. As such, the model allows for studying failure mechanisms that are in the transition zone between one-way and two-way shear, as observed in the experiments. One-way and two-way shear are separated into beam action shear and arching action shear, elements that occur regardless of whether shear or punching is studied. Second, as the Modified Bond Model is inspired by methods that are based on the lower bound theorem of plasticity as well as by Regan's (1982) approach for punching in slabs subjected to concentrated loads close to supports, the influence of the geometry of the slab, load and supports is taken into account by defining reduction factors in a similar way as in a plasticity model, such as Hillerborg's strip method (1996). Third, the Modified Bond Model takes direct load transfer into account by increasing the capacity of one of the load-bearing strips, and is thus applicable to slabs under concentrated loads close to supports. Fourth, the Modified Bond Model is an engineering model that can be used in a hand calculation, but leads to good and safe results.

The starting point for the development of the theory was the search for a method that could fully take into account the geometry of the slab, the load and the support, as these parameters were found in the experiments to determine the shear capacity of a slab subjected to a concentrated load. The ability of the Modified Bond Model to take into account the geometry is thus one of the major advantages of the model. Another basic

requirement of the model was that it should be easy to use and not require the use of nonlinear finite element analysis to determine parameters, such as the moment-curvature diagram when using the Critical Shear Crack Theory or the eccentricity of the load when using the full punching analysis from NEN-EN 1992-1-1:2005.

In this chapter the improvement of the Modified Bond Model as compared to NEN-EN 1992-1-1:2005 for determining the ultimate load is highlighted with respect to the experimental results. Moreover, the improved incorporation of the main parameters determining the shear capacity in the experiments is discussed.

## 5.2 Alexander's Bond Model

### 5.2.1 Motivation

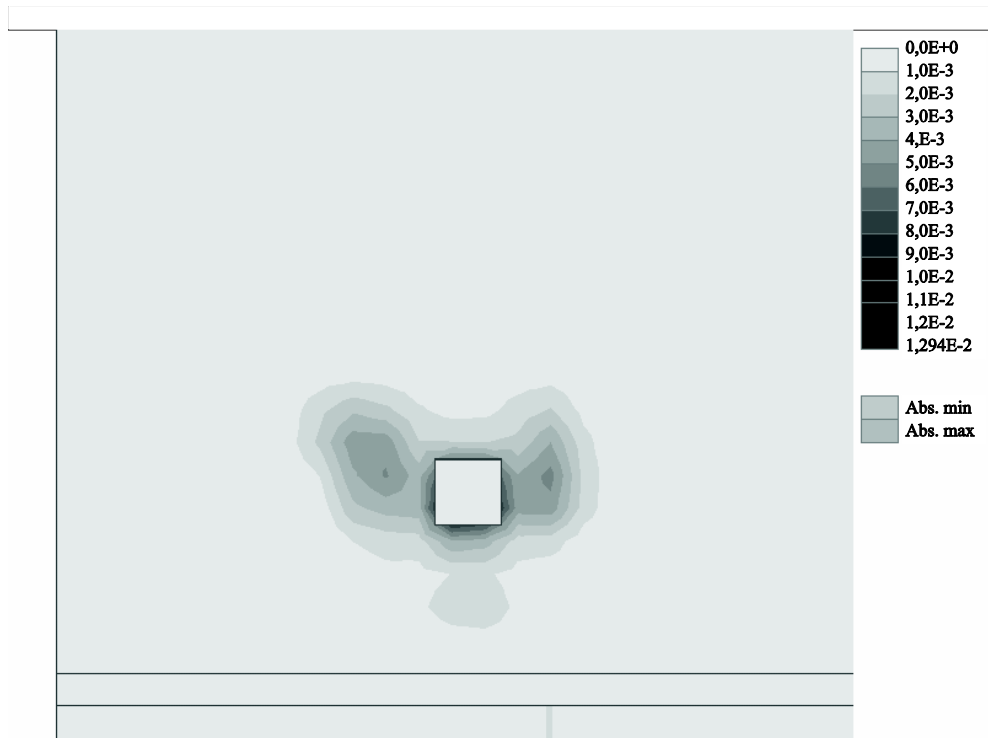


*Fig. 5.1: Strain profile around the load (modified from Prochazkova, 2012), for the experiment SIT1 near failure.*

The results of the parameter analysis in Chapter 4 indicate that the geometry of the load, the position of the load, the geometry of the slab and the moment distribution in the shear span, varying from the support moment  $M_{sup}$  to the span moment  $M_{span}$  as shown in Fig. 4.4, are the most important parameters to determine the shear capacity of a slab under a

concentrated load close to the support. A mechanical model that aims at describing the experiments should have a strong focus on the geometry.

As highlighted in Chapter 2, mechanical models for axis-symmetric punching shear typically study the equilibrium of forces on a segmental part of the slab portion outside of the shear crack (Kinnunen and Nylander, 1960; Hallgren, 1996). To describe the stress and strain states, these models (in polar coordinates) assume an inversely proportional relation between the tangential strains and the distance to the load along the radial axis. Nonlinear finite element models (adapted from: Prochazkova, 2012) indicate however a disturbed pattern of the strains in the experiments on slabs under concentrated loads close to supports, Fig. 5.1. Thus, the assumption of inversely proportional strains cannot be used in a mechanical model representing the studied slabs, as the presence of the support disturbs the strain pattern.

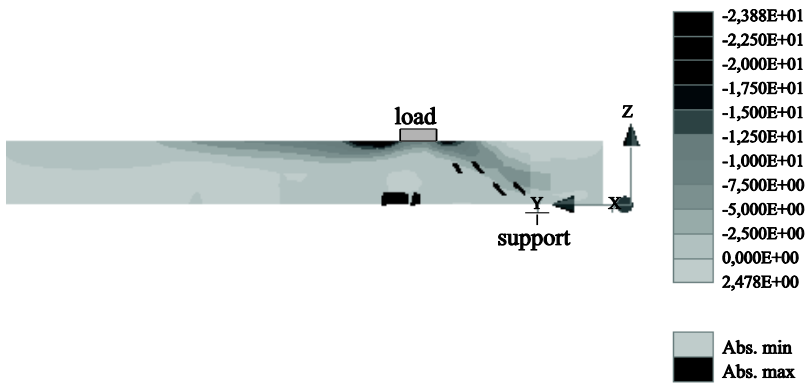


Fig. 5.2: Cut along the span showing the compressive strut (stresses) and cracks between the load and the support, for the experiment SITI near failure.

An important load-carrying mechanism for slabs loaded close to the support is the direct load transfer through thrust action (arching action). In the nonlinear finite element models of the experiments, the stresses are studied on sections to verify if a compressive strut or arch can be identified as a load-carrying mechanism in slabs under a concentrated load close to the support. A clear compressive strut is indeed observed in the models, Fig. 5.2. When studying a cut along the width at the location of the load, some arching in the transverse direction can also be identified, however much less pronounced than in the longitudinal direction, Fig. 5.3. Observing these compression struts identified three-dimensional strut-and-tie models, and their derivatives such as the Bond Model (Alexander and Simmonds, 1992) as suitable models for the studied slabs.

The mechanical model to describe the experiments should also allow for a combination of principles of one-way shear and two-way shear. It is observed in nonlinear finite element models (Doorgeest, 2012) that the experiments under study have a failure

### Modified Bond Model

mode that is a combination of one-way shear and two-way shear. One of the few mechanical models that describes shear in slabs as a combination of one-way and two-way shear is the Bond Model by Alexander (1990). This model is chosen as a starting point for the development of a mechanical model that describes the experiments on slabs under concentrated loads close to supports.

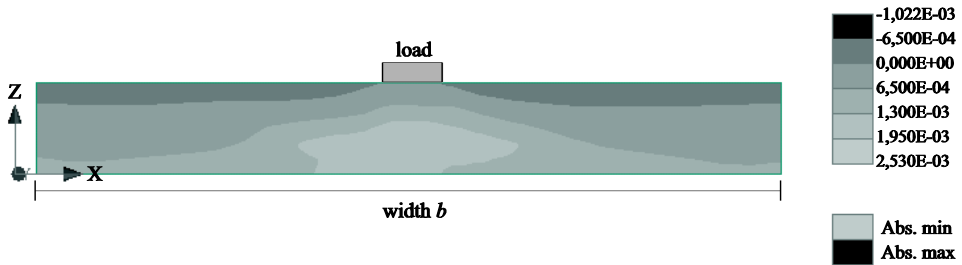


Fig. 5.3: Cut along the width at the location of the load showing the strains, for the experiment SIT1 near failure.

#### 5.2.2 Description of the Bond Model<sup>11</sup>

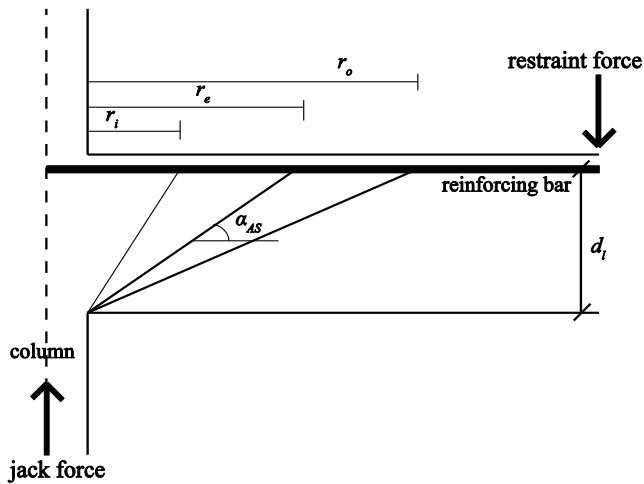


Fig. 5.4: Geometry of straight-line compression strut (Alexander, 1990), showing one symmetrical half of a slab-column specimen as used in the experiments by Alexander (1990).

<sup>11</sup> As the Bond Model is not commonly used to determine the punching capacity of a slab, the model is introduced in this section, and is largely cited from Alexander and Simmonds (1992).

### Modified Bond Model

Alexander and Simmonds (1986, 1987) originally developed a three-dimensional strut-and-tie model to describe punching in slab-column connections with external moment acting on the connection as occurs in edge and corner columns. To verify this theory, experimental studies were carried out in which the strains at the reinforcing bars were measured (Alexander, 1990). These experiments and measurements indicated that the radial compression struts in the vertical plane are curved and not straight as assumed in the three-dimensional strut-and-tie model, requiring fundamental changes to the mechanics of the strut-and-tie model. The assumed geometry of a straight-line strut as used in the three-dimensional strut-and-tie model is shown in Fig. 5.4. The strut acts as a straight-line compression member, at a distance  $r_e$  away from the face of the column. The distances  $r_i$  and  $r_o$  mark the length over which the bar force is expected to decline to zero<sup>12</sup>. The length of  $r_e$  is calculated based on the measured forces:

$$r_e = \frac{d_i}{\tan(\alpha_{AS})} \quad (5.1)$$

with  $\tan(\alpha_{AS})$  the ratio of the central column load to the force of the strut steel acting at yield. The distances  $r_i$  and  $r_o$  are estimated on the basis of measured bar force profiles. For a straight-line compression strut, it is expected that  $r_i$  be less than  $r_e$ . From the results of the bar force profiles, it was found that the straight-line idealization of the concrete compression fan is not adequate. Therefore, another way to describe the three-dimensional strut-and-tie model was sought.

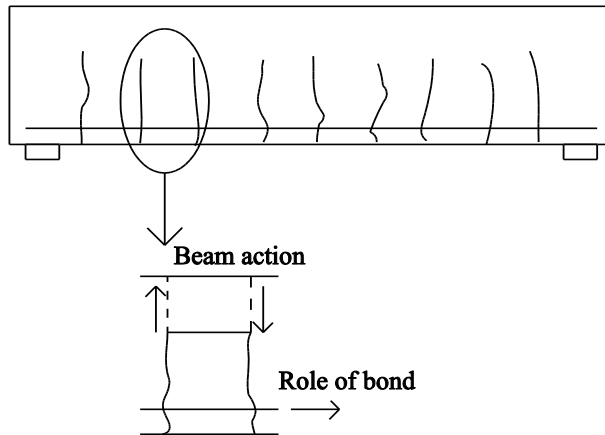
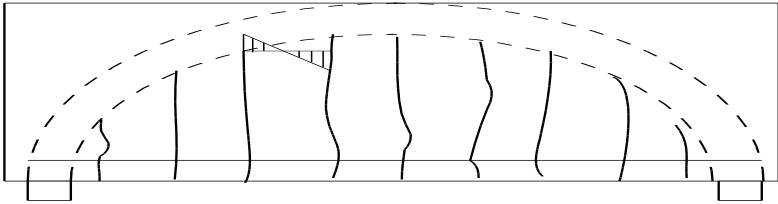


Fig. 5.5: Detailed sketch of beam action and its connection to the role of bond.

<sup>12</sup> In the experiments of Alexander, a slab-column connection with a central jack force and restraint forces at the edges was tested. Strain gages were used on the reinforcement bars. These measurements were used to determine the distances  $r_i$  (position of yield in the bar) and  $r_o$ .

### *Modified Bond Model*

The result of the modifications of the three-dimensional strut-and-tie model is the Bond Model for concentric punching shear (Alexander, 1990; Alexander and Simmonds, 1992), a mechanical model that explains the transfer of load between the plate and the column by combining radial arching action and the concept of a critical shear stress. It is based on force increments in the reinforcement, and as force increments are transferred by bond, the model is named the Bond Model. The model gives a design value of the ultimate slab shear strength, based on a combination of the strut-and-tie model with the concept of a limiting one-way shear stress. The Bond Model describes a mechanism of shear transfer for orthogonally reinforced slab-column connections that is consistent with the test observations by Alexander (1990).



*Fig. 5.6: Detailed sketch of arch action for which bond is not necessary.*

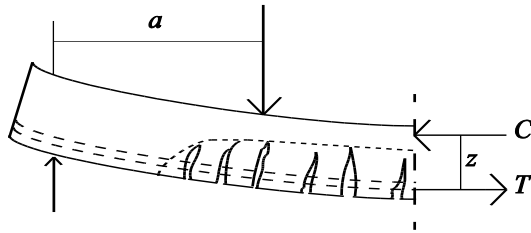


*Fig. 5.7: Comb-like model of cracked beam in which shear is carried through beam action and arching action. Note that both  $z$  and  $T$  vary through the shear span. Illustration based on Kani (1964).*

In a reinforced concrete flexural member, the bending moment is calculated as the product of the steel force  $T$  and the effective lever arm  $z$ . Shear, or moment gradient, results wherever the magnitude of the force or the lever arm varies along the length of the member. It can thus be said that shear is carried through beam action (requiring strong bond forces, Fig. 5.5) and arching action (requiring only remote anchorage of the reinforcement, Fig. 5.6). This concept can be expressed as given in Eq. (2.1), and is repeated here:

$$V = \frac{d(Tz)}{dx} = \frac{d(T)}{dx} z + \frac{d(z)}{dx} T \quad (5.2)$$

The concept of shear being carried by beam action and by arching action is also shown in Fig. 5.7, which indicates the compatibility of these shear-carrying mechanisms. The force in the reinforcement changes by  $\Delta T$  in every concrete tooth (element between two flexural

### *Modified Bond Model*

cracks). The length of the moment arm  $z$  between the compressive force  $C$  and the steel tension force  $T$  also changes in the shear span.

One of the key assumptions of the Bond Model is that the beam shear capacity is governed by the limiting force increment in the reinforcement, and that these concepts are interchangeable. It is known that some combination of beam and arching action is responsible for shear transfer at the connection between the plate and the column. The slab-column connection can be studied based on a wedge-shaped element between the radial cracks, as done in the mechanical punching model by Kinnunen and Nylander (1960). In this model, expressed in polar coordinates, it is assumed that arching action, expressed by the radial compression strut, is the dominant mechanism in the radial direction. Therefore, it is assumed that the load is distributed in the radial directions from the column or the point of application of the concentrated load by arching action. In the Bond Model, four strips branching out from the column work in arching action.

Although the Bond Model is a modification of the three-dimensional strut-and-tie model as developed by Alexander and Simmonds (1987), in the Bond Model as well as in a three-dimensional strut-and-tie model, a location loaded under a concentrated load is considered as an assembly of steel tension ties and concrete compression struts. Therefore, there is an essential link and similarity between the original three-dimensional strut-and-tie model and the Bond Model.

Strain measurements on the reinforcing steel (Alexander, 1990) showed that the geometry of the curved arch, replacing the straight compression strut that was used in the strut-and-tie model, is not governed by conditions at the intersection of the arch and the reinforcement tying the arch, but rather by the interaction between the arch and the adjacent quadrants of the slab. In plan, the arch is parallel to the reinforcement. As in the three-dimensional strut-and-tie model, the horizontal component of the arch is equilibrated by the tension in the reinforcement. For concentric punching shear, four strips, the “radial strips”<sup>13</sup>, are considered to extend from the column parallel to the reinforcement, Fig. 5.8. The strips separate the column from the slab so that all load reaching the column must be carried by the strips. The length of the strips is determined from the column (or concentrated load) to a remote end, a position of zero shear, Fig. 5.8. In the case of a plate supported by a single, central column, the zero shear position is at the edge of the specimen. For a continuous plate with multiple column supports, the location of maximum positive radial moment close to the centre of the span corresponds to the position of zero shear. In the Bond Model (Alexander and Simmonds, 1992), the strips are loaded in shear on their side faces only. Any load reaching the column must pass through one of the four strips. The

---

<sup>13</sup> Alexander and Simmonds (1992) call these four strips the radial strips. However, this name is slightly misleading, as from the center of the column a large number of radial strips could be drawn. Therefore, these four strips are further denoted as “strips”, and –where possible- they are indicated as  $x$ -direction strips or  $y$ -direction strips.

### *Modified Bond Model*

original Bond Model is limited to the joints between columns and orthogonally reinforced concrete slabs.

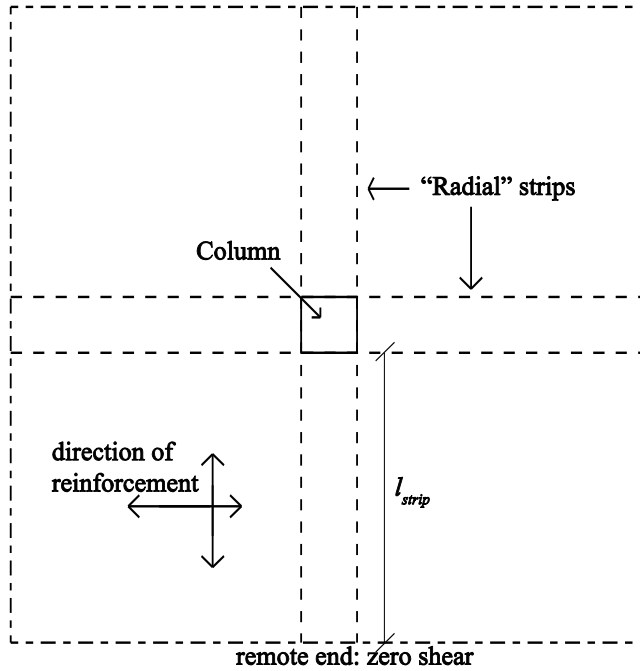


*Fig. 5.8: Layout of strips, Alexander and Simmonds (1992).*

In the Bond Model, shear is assumed to be carried in a strip to the column by a curved, radial compression arch. The horizontal force component of the arch is taken as constant, and thus, the shear carried by the arch varies from maximum at the face of the column (location of the concentrated load), where the slope of the arch is large, to a minimum, or perhaps zero, at the intersection of the arch and the reinforcing steel, where the slope is small. The curvature of the arch is related to the rate of the dissipation of the shear, and is equal to:

$$\frac{d^2 z}{dx^2} = \frac{dV}{T} \quad (5.3)$$

The shear that is carried within the strip by arching action at the face of the column must be dissipated in a direction perpendicular to the strip at some distance away from the column. The rate at which shear is dissipated determines the curvature of the arch.

Taking the considerations with regard to the strip into account, it is assumed (as shown in Fig. 5.9) that the strip can be described as a cantilever beam. Fig. 5.9 shows the static scheme of one of the four strips, showing that not the full length  $l_{strip}$  is considered

### Modified Bond Model

as the loaded length  $l_w$ . This cantilever beam has negative and positive moment capacities of  $M_{neg}$  and  $M_{pos}$  that can be combined into  $M_s$ , the total flexural capacity of the strip. The strip supports all the loads by acting as a cantilever beam. At the side of the column, the maximum load  $P_{AS,l}$  is acting and at the outermost edges of the strip, the moments  $M_{neg}$  and  $M_{pos}$ , determined from the reinforcement, are acting.

In the strip, the length  $l_w$  is the loaded length of the strip, and  $w$  the uniformly distributed load. The strip is loaded on each side face by an internal shear generated by the adjacent quadrant of the two-way plate (Fig. 5.8). The loading term  $w$  is an estimate of the shear that can be delivered by the adjacent quadrant of the slab to one side face of the strip. For a strip with two side faces, and with an equal capacity at each side, the total uniformly distributed load on the strip is  $2w$ . This load is distributed to maximise the total load on the strip and still satisfy flexural equilibrium in the strip<sup>14</sup>.

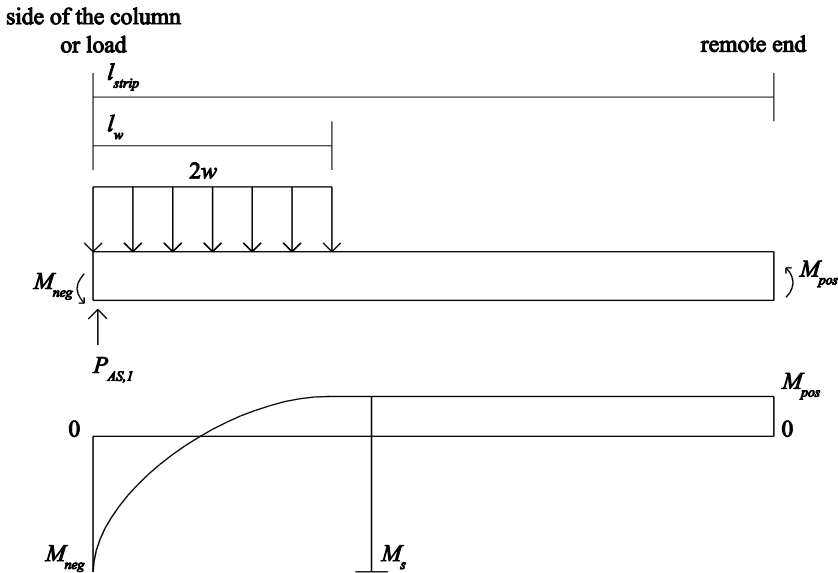


Fig. 5.9: Equilibrium of strip, Alexander and Simmonds (1992).

Using force and moment equilibrium of the cantilever strip (Fig. 5.9) results in:

$$M_s = \frac{2wl_w^2}{2} \quad (5.4)$$

$$P_{AS,l} = 2wl_w \quad (5.5)$$

Solving Eq. (5.4) for the unknown loaded length  $l_w$  and substituting this into Eq. (5.5) results in the shear capacity of a single strip:

---

<sup>14</sup> Note that the expressions by Alexander and Simmonds (1992) focus on the equilibrium of the strip, while the behaviour of the other zones of the slab is not studied in further detail.

### Modified Bond Model

$$P_{AS,l} = 2\sqrt{M_s w} \quad (5.6)$$

The unknown loaded length  $l_w$  is an auxiliary parameter that has been replaced to express the maximum load  $P_{AS,l}$  as a function of the moment capacity  $M_s$  at yield. Through  $l_w$  the loading of the strips is optimised with regard to maximising the total load. Note that this assumption is not inherently conservative and almost certainly violates conditions of compatible deformations within the plates, therefore the boundary conditions are important.

For four strips, the capacity of all four strips can be summed. The concentric punching capacity  $P_{AS}$  is then expressed as:

$$P_{AS} = 8\sqrt{M_s w} \quad (5.7)$$

The loaded length  $l_w$  is determined as the maximum loaded length for which the flexural equilibrium is satisfied. The loading term  $w$  represents an estimate of the maximum shear load that may be delivered to one side of a strip by the adjacent quadrant of the slab. Because each strip of an interior column-slab connection has two adjacent quadrants of the two-way plate, the total line load is  $2w$ . For an edge or corner column, there will be strips at the free edge that have only one adjacent quadrant. For these strips, the total line load is  $w$ .

The flexural capacity depends upon the amount of reinforcement that effectively acts within the strip and is composed of the negative  $M_{neg}$  and positive  $M_{pos}$  moment capacity (Alexander and Simmonds, 1992).

$$M_{neg} = \rho_{neg} f_{yk} z d c \quad (5.8)$$

$$M_{pos} = k_r \rho_{pos} f_{yk} z d c \quad (5.9)$$

In these equations<sup>15</sup>, the following symbols are used:

$\rho_{neg} = \frac{A_{sT}}{b_{rebar} d_{top}}$  the negative effective reinforcing ratio;

$\rho_{pos} = \frac{A_{sB}}{b_{rebar} d_{bottom}}$  the positive effective reinforcing ratio;

$A_{sT}$  the total cross-sectional area of top steel within the strip plus half the area of the first top bar on either side of the strip;

$A_{sB}$  the total cross-sectional area of bottom steel within the strip plus half the area of the first top bar on either side of the strip;

$b_{rebar}$  the total distance between the first reinforcing bars on either side of the strip;

$d$  the effective depth to the considered reinforcement layer, indicated by the subscript “top” or “bottom”;

$z$  the internal moment arm;

---

<sup>15</sup> Note that these expressions are for slab-column connections, and that the top and bottom bars are thus different from the case of a slab under a wheel load. The main ideas are however related to the notions of positive and negative moment reinforcement.

### Modified Bond Model

- $c$  the width of the strip;
- $f_{yk}$  the yield stress of the reinforcement;
- $k_r$  a factor that accounts for the proportion of the bottom steel that can be developed by the rotational restraint at the remote end of the strip. This value is zero if the remote end is simply supported.

Alexander and Simmonds (1992) note that  $M_{pos}$  is not necessarily calculated for the section at the remote end of a strip. The bending moment diagram in Fig. 5.9 shows that the value of  $M_{pos}$  is constant from the end of the loaded length  $l_w$  to the remote end of the strip, at a distance  $l_{sup}$  from the column.

A free body diagram of one-half of a strip is given in Fig. 5.10. The far side face lies on an axis of symmetry of the plate. Under centric loading, both shear and torsion on this face are zero. The bending moment applied to the far side face of the half-strip is equal and opposite to the bending moment on the near side face. The half-strip carries the combined effect of any external load applied directly to the strip  $q$  and the internal shears and moments developed on the side faces of the strip by the adjacent quadrants of the two-way plate. The near side face of the half-strip is loaded by the internal shear and moments developed on the side faces of the strip by the adjacent quadrants of the slab: shear  $v$ , torsion  $m_t$  and bending  $m_n$ . Two approximations are made: the direct load  $q$  and the torsional shear are neglected.

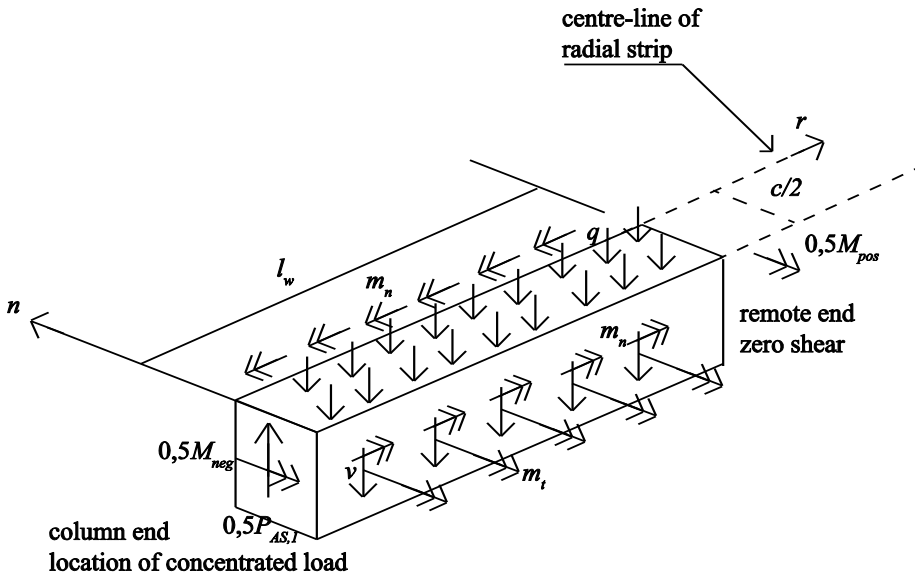


Fig. 5.10: Free-body diagram of one-half strip, Alexander and Simmonds (1992), axis showing  $r$  (radial direction) and  $n$  (perpendicular direction).

### Modified Bond Model

The shear and torsion on the side face of the radial half-strip is replaced by its statically equivalent line load  $\bar{v}$ , the Kirchhoff shear, at an internal plate boundary, with axes  $n$  and  $r$  as defined in Fig. 5.10 :

$$\bar{v} = \frac{\partial m_n}{\partial n} + 2 \frac{\partial m_t}{\partial r} \quad (5.10)$$

The Kirchhoff shear has its origins in plate theory as a way of satisfying equilibrium at a free or simply supported edge of a plate. As the slab is here considered as separated into strips and quadrants, the interface between the strip and the quadrants can be considered as a free edge with the loads from the quadrants. In Eq. (5.10) the first term is the bending moment gradient in a circumferential direction  $n$ , the primary shear. In a region dominated by beam action, bending moment gradients and force gradient in the reinforcement are equivalent. The internal moment arm  $z$  does not change much in the circumferential direction. Thus, the primary shear requires a force increment in the reinforcement perpendicular to the strip. This gradient is known from Eq. (5.2) to be the result of beam action, (depending on bond between the reinforcement and the concrete) and may be expressed in terms of a force increment in the reinforcement perpendicular to the strip:

$$\frac{\partial m_n}{\partial n} = \frac{z}{s_{rebar}} \frac{\Delta T}{s} \quad (5.11)$$

with

- $z$  the internal lever arm,
- $s_{rebar}$  the reinforcement spacing,
- $\Delta T$  the force increment in a reinforcement bar<sup>16</sup>,
- $s$  the crack spacing.

For very lightly reinforced slabs, the behaviour near ultimate load is characterised by widespread yielding of the reinforcement at increasing distances from the loaded area. Under such circumstances, the maximum force gradient at the edge of the strip may be limited by the spread of yielding, rather than bond.

The second term in Eq. (5.10) is the gradient in the radial direction of the twisting moment along the side face of the strip, the torsional shear. The factors governing the magnitude of the torsional moment and the torsional moment gradient are not known, nor is it clear how these quantities should be measured. Torsional shear is assumed to affect only the distribution of Kirchhoff shear along the length of the strip. As a result, primary shear is assumed to be the root source of all shear loading on the side face of a strip. For the development of the Bond Model, the torsional shear was neglected, which is a conservative assumption. Note that the concentrated shear forces, running in the edge direction of the adjacent plate quadrants are also not regarded anymore when torsion is neglected.

---

<sup>16</sup> In the original expression by Alexander and Simmonds (1992), the gradient in the reinforcement bar was expressed as  $F_b'$ . To link back to Kani's tooth model, Fig. 2.7,  $F_b'$  is replaced here by  $\Delta T/s$ .

### *Modified Bond Model*

Alexander (1990) discusses the assumption of neglecting the torsional shear. The effect of torsional shear is to redistribute primary shear so that the net loading of each strip is applied closer to the column, thereby increasing the total load that may be carried by each strip. The torsional shear can be estimated experimentally, on the basis of how much the ultimate loads exceed the Bond Model predictions. In Alexander's experiments (1990), large deflections occurred in some cases, which may favour the development of torsional shear and which reduces the primary shear capacity. For those cases, the effects of torsional shear and primary shear may not be entirely additive. To estimate the torsional shear contribution, the experiments in which torsional shear developed while primary shear was maintained close to the column, are studied by Alexander (1990). This criterion of developing torsional shear and maintaining primary shear is assumed to be satisfied when the value of the force increment over the second interval of the perimeter bar is maintained at or near its maximum value through failure. For three experiments that fulfil this requirement, it is assumed that the effects of primary and torsional shear were fully additive. For these experiments, the measured ultimate test load to the calculated punching load  $P_{exp}/P_{AS}$  is used as an experimental measure of the combined effects of primary shear and torsional shear to primary shear alone. Alexander (1990) found by this reasoning that the contribution of torsional shear is about 29% of the Bond Model load based on primary shear alone.

The loads  $v$  and  $q$  are carried by the strip. The direct load  $q$  is neglected, which can be justified by noting that the total area of the slab quadrants is large relative to the area of the strips. With these assumptions, the loading term  $2w$  on the strip results from primary shear, and equals:

$$2w = 2 \left( \frac{\partial m_n}{\partial n} \right) \quad (5.12)$$

There are two ways to estimate the maximum value of the loading term that the slab-column connection can carry:

1. According to Eq. (5.11), the bending moment difference and thus the load  $w$  can be found based on the maximum force increment in the reinforcing bars perpendicular to the strip. A direct way to quantify the force increment in the reinforcing bars is by directly estimating the bond strength of the reinforcement as governed by the unconfined splitting failure of the concrete. The lack of confinement perpendicular to the plane of the slab makes splitting failure the most likely bond failure mechanism.
2. The equivalence between the maximum value of the beam action shear and a limiting nominal one-way shear stress as prescribed by the codes can be used.

In the development of the Bond Model, Alexander and Simmonds (1992) explored these different approaches. The best results were obtained when the loading term is described based on the one-way shear capacity that defines the inclined cracking shear capacity from

### *Modified Bond Model*

ACI 318 that is defined as the inclined cracking load from a large number of test results (Morrow and Viest, 1957).  $w_{ACI}$  is given in [kN/m] with  $f_{ck}$  in [MPa] and  $d$  in [mm]. Note that  $d$  can be the effective width to the longitudinal reinforcement  $d_l$  or the effective width to the transverse reinforcement  $d_t$ , depending on the considered strip.

$$w_{ACI} = 0,166d\sqrt{f_{ck}} \quad (5.13)$$

Values of critical nominal shear stress for one-way beams are well established in design codes. Primary shear may be estimated on the basis of code values for critical nominal shear stress<sup>17</sup>. In this way, the Bond Model provides a link between code provisions for the design of one-way and two-way members. Afhami et al. (1998) found with a finite element analysis that the shear on the side face of the strips can be approximated by a rectangle in a region near the column, and has a maximum value that is about the value of the critical one-way shear according to ACI 318. In Eq. (5.13), a size effect factor is not used. The expression can however easily be adapted to take into account a size effect factor, see §5.3.1.

By using the connection between the force transfer in the reinforcing bars, and bond between concrete and the reinforcement on the one hand, and the beam shear capacity on the other hand, the chosen name for the model as a “Bond Model” is in fact slightly misleading as the concept of bond is replaced by the concept of shear.

The free body diagram of Fig. 5.10 suggests that it is necessary to check as well the moments at the sides of the strips and the shear resistance of the strips themselves. However, the load-carrying mechanism is assumed as the combination of the two-way quadrants and the one-way shear strips, and it is, in this model, precisely the sides of the strips, where shear loading is transferred from the two-way quadrants to the one-way strips, that form the most critical location of the Bond Model. Therefore, following the ideas of the Bond Model, the cruciform failure surface is to replace the critical perimeter that is typically used to determine the punching capacity. While the punching perimeter more closely resembles the punching cone that is observed in experiments, the use of strips enables the incorporation of arching action and beam action into a punching model. The importance of arching action was measured by Alexander (1990) in punching experiments.

Moreover, the depth of a punching perimeter in the code approaches determines the location of a critical section, taken perpendicularly to the radial direction. This would be a valid assumption if beam action in the radial direction were to determine the punching capacity. However, Alexander’s measurements (1990) indicated that arching action is the primary load-carrying mechanism in the radial direction. In a strip in the Bond Model, shear is carried by a vertical component of a curved compression strut or arch. Slab shear

---

<sup>17</sup> The square root relationship between the shear capacity and the concrete compressive strength can be used for concrete up to class C55/65. Note that the high strength concrete slabs that were tested were concrete C55/65 (Chapter 3).

## *Modified Bond Model*

failure can be expressed as the loss of moment gradient and hence shear capacity in the vicinity of the column (or loaded area). It can thus be considered as the result of the limited ability of the adjacent quadrants of the slab to deliver shear loading to the strips.

The Bond Model is limited to slabs with a value  $c/d_l$  (with  $c$  the size of the column determining the strip width) larger than 0,66 as small column dimensions and small strips could be governed by splitting of the strip rather than the shear capacity of the adjacent quadrants of the plate (Alexander and Simmonds, 1992). This limitation does not affect the application of the Bond Model to the slab shear experiments from Chapter 3 ( $c/d_l = 0,75$  for  $c = 200\text{mm}$ ).

Afhami et al. (1998) found that the Bond Model is suitable for most tests on interior connections as reported in the literature. For these cases, the ratio of the test load to the prediction according to the Bond Model is greater than one. These experiments are typically so that all the strips are loaded to their maximum capacity and that the torsional moments along the side faces of the strips are in the same direction as the flexural moments. Under certain conditions, however, the strips of an interior connection might not be loaded in proportion to their nominal capacities. These connections punch when the strips in only one direction reach their maximum capacity. Along the side faces of these strips, the torsional moments are in the same direction as the flexural moments. However, along the side faces of strips not loaded to their nominal capacity, the resultant of the torsional moments is in the opposite direction of the flexural moments.

### **5.3 Development of the Modified Bond Model**

#### **5.3.1 Concentrated loads close to the support**

Translating the approach from the Alexander and Simmonds Bond Model (1992) so that it is not only applicable for concentric punching shear, but also for the case of slabs under concentrated loads near to supports requires taking direct load transfer between the load and the support into account. For the three strips that are not influenced by the vicinity of the support, the original approach is extended so that a differentiation between the load-carrying behaviour in the span-direction and in the transverse direction can be made, Fig. 5.11.

In the Bond Model, as well as in the Modified Bond Model, a failure mechanism is described that is based on two compatible components that carry shear: beam shear action in the quadrants, requiring bond between reinforcement and concrete, and arching action in the strips, requiring only remote anchorage.

The Bond Model is developed for concentric punching shear, and considers the four strips as cantilevering strips that are supported by the column in a slab-column connection. The problem of the punching capacity is the inverse problem of a slab subjected to a concentrated load. For this case, as in the Bond Model, the strips are assumed

### Modified Bond Model

to cantilever from the point of application of the load. The situation of punching for a slab-column connection is thus mentally turned upside down, and might be harder to imagine than the case of the column with its cantilevering strips. The four cantilevering strips that depart from the location of the load can be studied together to sketch the moment distribution that is assumed, as shown in Fig. 5.11. The  $x$ -direction strip between the load and the simple support is subjected to the action of the load  $P_{MBM,sup}$  (increased capacity due to direct load transfer) and the sagging moment capacity  $M_{neg,x}$  that is determined by the reinforcement. The  $x$ -direction strip between the load and the continuous support is loaded over  $l_w$  and subjected to the action of the load  $P_{MBM,x}$  (capacity of the  $x$ -direction strip) and the moments  $M_{pos,x}$  and  $M_{neg,x}$ . To determine the capacity according to the Modified Bond Model for loading close to the simple support, the contribution of the hogging moment capacity  $M_{pos,x}$  is not taken into account. The  $y$ -direction strips are loaded by  $P_{MBM,y}$  and  $M_{neg,y}$  as it is determined by the capacity of the transverse reinforcement.

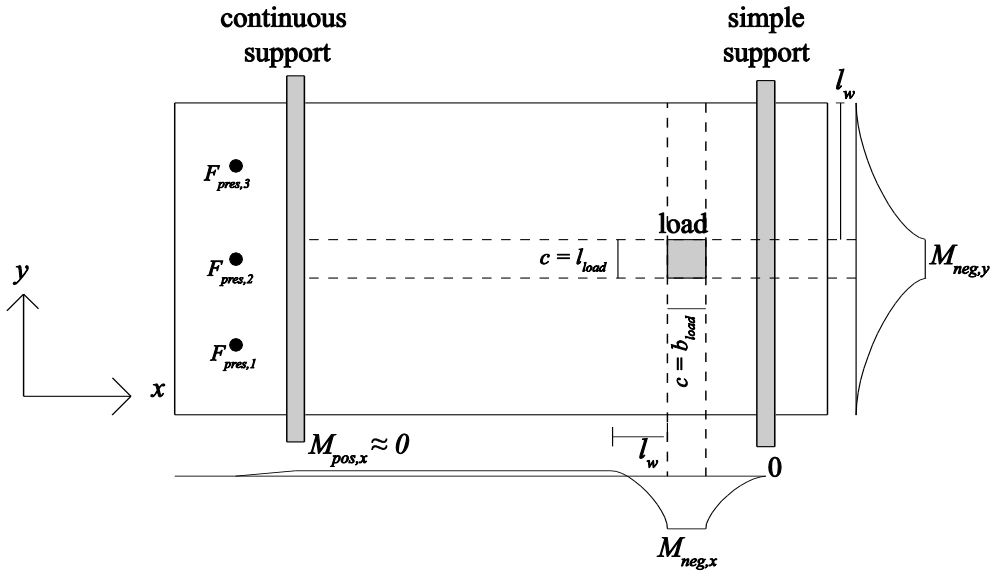


Fig. 5.11: Sketch of application of Bond Model to slabs under a concentrated load close to the support.

For the strips into the span direction and towards the free edges, the maximum load can be expressed as  $P_{MBM,y}$  for the capacity of the  $y$ -direction strips and  $P_{MBM,x}$  for the capacity of the  $x$ -direction strips ( $x$ - and  $y$ -direction as defined in Fig. 5.11):

$$\begin{aligned}
 P_{MBM,y} &= 2\sqrt{M_{s,y}w_y} \\
 P_{MBM,x} &= 2\sqrt{M_{s,x}w_x}
 \end{aligned}
 \tag{5.14}$$

### Modified Bond Model

Note that in Eq. (5.14) a distinction is made between the  $x$ - and  $y$ -direction. In Alexander's Bond Model (1990), concentric punching shear was studied and the reinforcement ratios in both directions were identical. For the case of a one-way slab under a concentrated load in shear, typically the reinforcement in the  $y$ -direction is only 20% of the reinforcement in the main longitudinal  $x$ -direction. Therefore, the capacity of the strips in the  $x$ - and  $y$ -directions is studied separately. Also, the moments are expressed as  $M_{s,x}$  and  $M_{s,y}$ . The first experiments that are analysed are all carried out with the load close to the simple support (the situation shown in Fig. 5.11), so that here  $M_{s,x} \approx M_{neg,x}$  and  $M_{s,y} \approx M_{neg,y}$ .

The load  $w$  in the Bond Model is defined as the lower bound estimate of the maximum shear that can be delivered by the adjacent quadrant to one side-face of the strip, Fig. 5.9. As a result, every strip is loaded with  $2w$ .

The flexural capacity of the strip results from the sum of the negative and positive moment capacities. Using both moment capacities for loads near to the continuous support is further investigated in §5.3.2, while for this case, as shown also in Fig. 5.11, the influence of the prestressing bars causing a moment over the continuous support is very small. Therefore, for the case of an experiment with the concentrated load close to the simple support  $M_{pos,x}$  and  $M_{pos,y}$  are assumed to be zero.

For the strip between the concentrated load and the support, direct load transfer between the load and the support needs to be taken into account. Regan (1982) described the punching capacity of a slab under a concentrated load close to the support by considering the 4 sides of the punching perimeter separately, §2.4.2. The capacity of the side of the punching perimeter at the support was enhanced to take into account the beneficial influence of direct transfer of the load from its point of application to the support by multiplying the capacity of the part of the perimeter at the support with the following factor:

$$\frac{2d_l}{a_v} \text{ for } a_v < 2d_l$$

Similarly, it is proposed to enhance the capacity of the  $x$ -direction strip<sup>18</sup> between the load and the support by multiplying the original capacity  $P_{MBM,x}$  with the following factor:

$$\frac{2d_l}{a_v} \text{ for } 0,5d_l < a_v < 2d_l \text{ and } 4 \text{ for } a_v \leq 0,5d_l$$

This method is to be preferred to take direct load transfer into account for application with the Modified Bond Model (Lantsoght, 2012f). It is not equivalent to the treatment of short shear spans of beams according to NEN-EN 1992-1-1:2005, where the full capacity is multiplied by a factor  $2d_l/a_v$ . For this case, only one of the four strips is influenced by the support. Similarly, in Regan's method (1982), only the capacity of one of the four sides of

---

<sup>18</sup> Here, the  $x$ -direction strip between the load and the support is still considered as a cantilevering strip. Another option would be to take the upward reaction force into account.

### Modified Bond Model

the punching perimeter is enhanced by  $2d/a_v$ . The chosen method assumes an increased arching action capacity in the strip between the load and the support. It is tacitly assumed that the horizontal force action on the strip at or close to the support will be provided by the reinforcing bars outside of the strip.

The width of the strip depends on the size of the loading plate through the parameter  $c$ , as also indicated in Fig. 5.11. This width is incorporated into the model, as also observed in the experiments, §4.2.2.

As in a strut-and-tie model, the layout of the reinforcement is important:  $A_{sT}$  and  $A_{sB}$  are determined as the top and bottom steel within a strip, plus one-half the area of the first top or bottom bar at either side of the strip to make the resulting reinforcement ratio less dependent on the precise location of the bar. In S1T1, the size of the loading plate is 200mm × 200mm. The main longitudinal reinforcement is  $\phi$  20mm – 125mm. Thus, in a strip, 2 bars can be used, and then half of the bottom bar on each side of the strip is added. In total, 3 bars  $\phi$  20mm are used, so that  $A_{sB} = 942\text{mm}^2$ . The distance between the outermost bars is  $b_{rebar,x} = 375\text{mm}$ . With  $d_l = 265\text{mm}$ , a reinforcement ratio  $\rho_{neg} = 0,95\%$  is found for the  $x$ -direction strips. The first results of the Modified Bond Model, taking the stronger strip towards the support into account are given in Table 5.1. A subset of experiments is selected close to the simple support with the load in the middle of the width. In Table 5.1, the following symbols are used:

$f_{c,cyl,meas}$  the measured cylinder compressive strength of the concrete at the age of testing;

$M_{neg,x}$  the flexural capacity of the sagging moment reinforcement in an  $x$ -direction strip, determined as follows<sup>19</sup>:

$$M_{neg,x} = \rho_{neg,x} f_{yk} z_t d_l l_{load} \quad (5.15)$$

$M_{neg,y}$  the flexural capacity of the sagging moment reinforcement in a  $y$ -direction strip, determined as follows:

$$M_{neg,y} = \rho_{neg,y} f_{yk} z_t d_l b_{load} \quad (5.16)$$

$w_x$  the loading term in the (Modified) Bond Model on an  $x$ -direction strip;

$w_y$  the loading term in the (Modified) Bond Model on a  $y$ -direction strip;

$P_{MBM,x}$  the capacity of an  $x$ -direction strip in the Modified Bond Model;

$$P_{MBM,x} = 2\sqrt{M_{s,x} w_x} \quad (5.17)$$

For the situation of a concentrated load close to the simple support,  $P_{MBM,x}$  is determined as follows:

$$P_{MBM,x} = 2\sqrt{M_{neg,x} w_x} \quad (5.18)$$

---

<sup>19</sup> Note that, while the (Modified) Bond Model assumes that the reinforcement will locally yield at shear failure, a check of the flexural capacity of the slab is never considered in this model. Only the shear capacity of slabs subjected to concentrated loads is studied.

### Modified Bond Model

$P_{MBM,y}$  the capacity of a  $y$ -direction strip in the Modified Bond Model;

$$P_{MBM,y} = 2\sqrt{M_{s,y}w_y} \quad (5.19)$$

For the situation of a concentrated load close to the simple support,  $P_{MBM,y}$  is determined as follows:

$$P_{MBM,y} = 2\sqrt{M_{neg,y}w_y} \quad (5.20)$$

$P_{MBM,sup}$  the capacity of the strip between the load and the support in the Modified Bond Model;

$$P_{MBM,sup} = 2\sqrt{M_{s,x}w_x} \left( \frac{2d_l}{a_v} \right) \text{ for } 0,5d_l < a_v < 2d_l \text{ and} \quad (5.21)$$

$$P_{MBM,sup} = 8\sqrt{M_{s,x}w_x} \text{ for } a_v \leq 0,5d_l \quad (5.22)$$

For the situation of a concentrated load close to the simple support,  $P_{MBM,sup}$  is determined as follows:

$$P_{MBM,sup} = 2\sqrt{M_{neg,x}w_x} \left( \frac{2d_l}{a_v} \right) \text{ for } 0,5d_l < a_v < 2d_l \text{ and} \quad (5.23)$$

$$P_{MBM,sup} = 8\sqrt{M_{neg,x}w_x} \text{ for } a_v \leq 0,5d_l \quad (5.24)$$

$P_{MBM}$  the capacity of a slab under a concentrated load according to the Modified Bond Model, expressed as the maximum concentrated load.

$$P_{MBM} = 2P_{MBM,y} + P_{MBM,x} + P_{MBM,sup} \quad (5.25)$$

The loading on the strips,  $w_x$  and  $w_y$ , is determined from  $w_{ACI}$ , as given in Eq. (5.13), as Alexander and Simmonds (1992) found this expression to lead to the best results. A difference has been made between  $w_{ACI}$  on the  $x$ -direction strips and the  $y$ -direction strips:

$$w_{ACI,x} = 0,166d_l \sqrt{f_{ck}} \quad (5.26)$$

$$w_{ACI,y} = 0,166d_t \sqrt{f_{ck}} \quad (5.27)$$

In Eq. (5.26) and Eq. (5.27),  $f_{ck}$  is in [MPa],  $d_l$  and  $d_t$  in [mm] and the resulting  $w_{ACI,x}$  and  $w_{ACI,y}$  are in [kN/m]. It is not surprising that  $w_{ACI}$  leads to the best results. Other important parameters for the shear capacity, such as the reinforcement ratio, are incorporated in expressions for the inclined cracking load (for example, the shear expression from NEN-EN 1992-1-1:2005) based on a statistical analysis. In the Modified Bond Model, however, this parameter is taken into account in a rational way through the definition of the moment capacity in the strip  $M_s$  that defines the arching action. For comparison, the shear capacity  $v_{Rd}$  from NEN-EN 1992-1-1:2005, as given in Eq. (2.8), was also evaluated as a replacement for  $w_{ACI}$ , as well as the expressions for the bond capacity from NEN-EN 1992-1-1:2005 and the *fib* Model Code 2010. The best results are still obtained for  $w_{ACI}$ , as was earlier concluded by Alexander and Simmonds (1992).

### Modified Bond Model

The disadvantage of  $w_{ACI}$  is that it does not incorporate a size effect factor directly. Expanding the formula to take the size effect into account is easily done. All experiments that are carried out have a height  $h = 300\text{mm}$ . Based on the experiments, it is not possible to propose a size effect factor. Therefore, it is suggested to use a factor that is similar to the size effect factor from NEN-EN 1992-1-1:2005, and that equals 1 for all considered experiments.

$$k_{MBM} = \frac{1 + \sqrt{\frac{300}{d_l}}}{2} \leq 1 \quad \text{with } d_l \text{ in [mm] and } k_{MBM} \text{ in [-]} \quad (5.28)$$

The expression from Eq. (5.28) is based on the experiments from Chapter 3, in which local yielding of the reinforcement occurs. The size effect factor from NEN-EN 1992-1-1:2005 however is based on beam shear experiments in which yielding does not occur. It might be expected that the influence of the size effect factor becomes less when yielding occurs. There are however no experimental results to use as a basis for such a size effect factor, and therefore the expression from NEN-EN 1992-1-1:2005 is just modified so that it equals 1 for the tested slabs. Further experiments on slabs of different depths to study the size effect on slabs in shear are highly recommended. As can be seen in Table 3.2, the failure mechanism of the experiments is a combination of one-way and two-way shear. The choice for a punching model that incorporates elements from one-way shear and that shows the essential link between both failure modes, is thus a rational decision. Moreover, the experiments also showed significant bending distress and the influence of the occurring moments. This is taken into account in the Modified Bond Model by linking the moment and force capacities.

To evaluate the chosen model, and the approximation according to the configuration from Fig. 5.11, the resulting values of  $l_w$  are studied. For the experiments in Table 5.1, it is found that typically the value of  $l_w$  for the  $x$ -direction strips is 0,6 m and for the  $y$ -direction strips 0,24 m. As indicated in Fig. 5.11, this implies that, for the considered experiments on slabs subjected to a concentrated load, the loaded length  $l_w$  in the transverse direction covers almost the entire width, so that the location of zero moment can be drawn at the edge. For the  $x$ -direction strips, these results imply that the strip between the concentrated load and the support is loaded over its full length, so that the location of zero moment coincides with the simple support and that the strip between the concentrated load and the continuous support has a loaded length  $l_w$  that is much smaller than the strip length  $l_{strip}$ .

Modified Bond Model

Table 5.1: Comparison between experimental results and Bond Model with fortified strip towards the support.

Test	$f_{c-cyl,meas}$ (MPa)	$M_{neg-x}$ (kNm)	$M_{neg-y}$ (kNm)	$w_x$ (kN/m)	$w_y$ (kN/m)	$P_{MBM,x}$ (kN)	$P_{MBM,y}$ (kN)	$a_y$ (mm)	$P_{MBM,sup}$ (kN)	$P_{MBM}$ (kN)	$P_{exp}$ (kN)	$P/P_{exp}$ $P_{MBM}$
S1T1	29	65	8	240	226	249	87	450	293	716	954	1,33
S2T1	28	97	12	235	222	302	105	400	400	912	1374	1,51
S3T1	42	100	25	288	272	340	164	400	451	1119	1371	1,23
S5T4	40	100	25	278	262	333	161	200	883	1539	1755	1,14
S8T1	63	103	25	352	332	381	182	400	504	1249	1481	1,19
S9T1	67	69	17	362	342	316	151	250	669	1287	1523	1,18
											<b>AVG</b>	<b>1,26</b>
											<b>STD</b>	<b>0,14</b>
											<b>COV</b>	<b>0,11</b>

5.3.2 Loads close to the continuous support

To extend the Bond Model for application to all experiments, further development is required. A first expansion is aimed at determining how to apply the Modified Bond Model close to the continuous support. Alexander (1990) proposes using a factor  $k_r$  on the positive moment capacity. The factor  $k_r$  ranges from 0 (for simply supported edges) to 1 (for fully restrained cases), but was not further dealt with in the original Bond Model. For the application to continuous slabs under a concentrated load, it is necessary to better define the parameter  $k_r$  and to study on which strips it can be applied. The factor  $k_r$  can be defined as:

$$k_r = \frac{M_{sup}}{M_{span}} \quad (5.29)$$

with  $M_{sup}$  being the moment at the support and  $M_{span}$  the moment at the location of the concentrated load, Fig. 5.12.

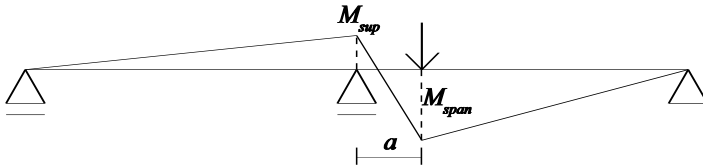


Fig. 5.12: Illustration of the moments at continuous support.

The contribution of the hogging moment reinforcement can be taken into account on three strips: all strips facing or directly reaching the support. These strips are adjacent to the quadrants that are situated between the load and the support. In these quadrants, the influence of the moment distribution that changes from the negative support moment to the positive span moment is noticeable. The load-bearing principle is shown in Fig. 5.13, with the factor  $k_r$  drawn in the three strips onto which it is applied. The force in the three prestressing bars is shown in Fig. 5.13 as  $F_{pres,i}$ , and these forces are known at every moment in the experiment by the measurements with the load cells. In Fig. 5.13, the factors in the quadrants that determine the capacity of the strip are also shown. Note that for the basic case of the Bond Model for concentric punching shear, all strips are loaded with  $2w_{ACI}$ .

The results in Table 5.2 show that applying  $k_r$  to the three strips carrying the load from the two quadrants between the load and the support leads to good results. The experiments considered in Table 5.2 are experiments with the load in the middle of the width, near to the continuous support. In Table 5.2, the following symbols are used, in addition to those used in Table 5.1:

### Modified Bond Model

- $M_{pos,x}$  the flexural capacity of the hogging moment reinforcement in an  $x$ -direction strip<sup>20</sup>;
- $M_{pos,y}$  the flexural capacity of the hogging moment reinforcement in a  $y$ -direction strip.

The value of  $k_r$  is based on the resulting  $M_{sup}$  of the sum of the three prestressing bars  $F_{pres,i}$ . In the experiments, the force in the prestressing bars was not the same for all three of the bars. For the sake of simplification however, the sum of the three forces is considered. It is shown that this simplification gives adequate results.

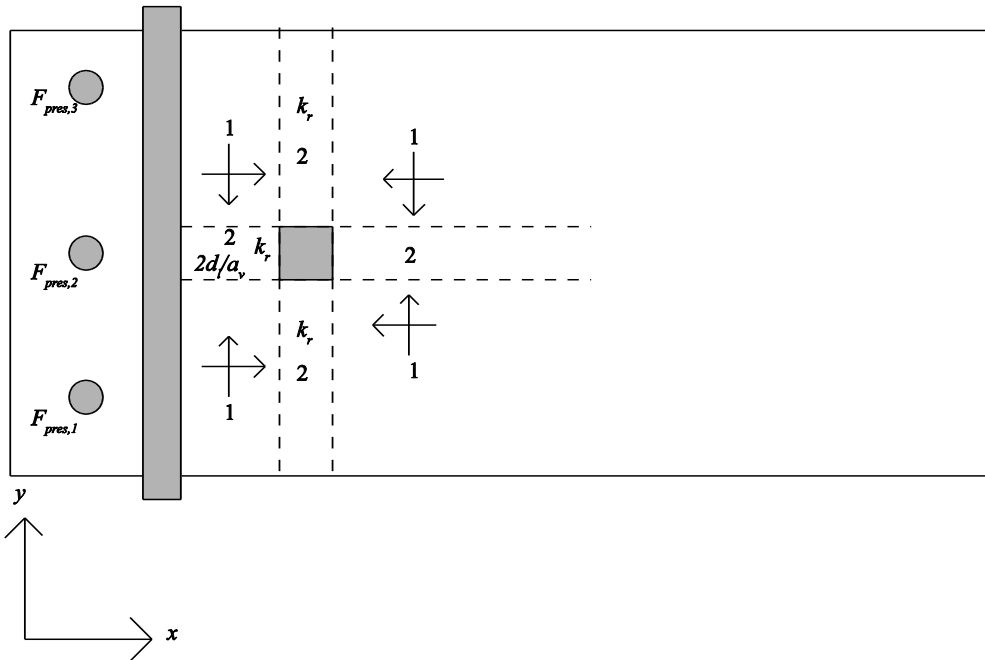


Fig. 5.13: Application of the Bond Model for loads close to the continuous support (a moment is applied over the support by three prestressing bars,  $F_{pres,i}$ ). The influence of the positive moment capacity is taken into account by  $k_r$  for three strips.

<sup>20</sup> Note that this reinforcement works as compression reinforcement at the location of the concentrated load, where the maximum load is determined, and as tension reinforcement at the support.

Modified Bond Model

Table 5.2: Comparison between Modified Bond Model and experimental results close to the continuous support.

Test	$f_{c-cyl,mean}$ (MPa)	$M_{neg,x}$ kNm	$M_{neg,y}$ kNm	$w_x$ kN/m	$w_y$ kN/m	$P_{MRM,x}$ kN	$P_{MRM,y}$ kN	$k_r$	$M_{pos,x}$ kNm	$M_{pos,y}$ kNm	$P_{MRM,exp}$ kN	$P_{MRM}$ kN	$P/P_{exp}$ $P_{MRM}$
S1T2	29	65	8	238	225	248	95	0,21	64	8	321	760	1,35
S2T4	28	97	12	234	221	301	123	0,38	96	12	467	1014	1,40
S3T4	42	100	25	286	270	339	190	0,34	100	25	520	1239	1,08
S5T1	40	100	25	277	261	332	183	0,29	99	25	1001	1700	1,06
S8T2	63	103	25	350	330	379	209	0,33	102	25	579	1376	0,99
S9T4	67	69	17	360	340	315	173	0,32	68	17	765	1425	1,29
												<b>AVG</b>	<b>1,19</b>
												<b>STD</b>	<b>0,17</b>
												<b>COV</b>	<b>0,15</b>

5.3.3 Loads at and close to the edge

To extend the Bond Model for application to rectangular slabs under concentrated loads, the method also needs to be suitable for loads near the edge. For punching shear, the unbalanced moments at the corner and edge need to be taken into account. With the Modified Bond Model, the concept of quadrants and strips can be used as a simplification.

The first situation that is studied is a slab under a concentrated load at the edge. The procedures from NEN-EN 1992-1-1:2005 would result in a punching perimeter with three sides, as indicated in Fig. 5.14a. The load can only be carried on the perimeter that is indicated, and the unsupported edge itself does not contribute to the load-carrying capacity.

For the application of the Modified Bond Model to the situation of a load placed directly at the edge, the strips and quadrants are used to carry the load. When the load is applied directly at the edge, it is clear that only three strips can be used, two of which have only half the capacity of a strip as defined by the Bond Model and one that has its full strip capacity, Fig. 5.14b. Equal shares of the load are assumed to be carried in the quadrants in the  $x$ -direction and the  $y$ -direction. For the case with the load at the edge, only two quadrants are defined, from which load is carried to the strips. This situation is represented by factors in the quadrants that are carried to the strips. The  $y$ -direction strip is assumed to be a cantilever strip, with the moment due to the torsional restraint from the  $x$ -direction strips providing the clamping moment. The sum of the factors on the strips is then used to determine the capacity of the strips. As a result, the  $x$ -direction strips are loaded with “1” and the  $y$ -direction strip with “2”, Fig. 5.14b. This configuration results in larger amounts of torsion than in the case of concentric punching.

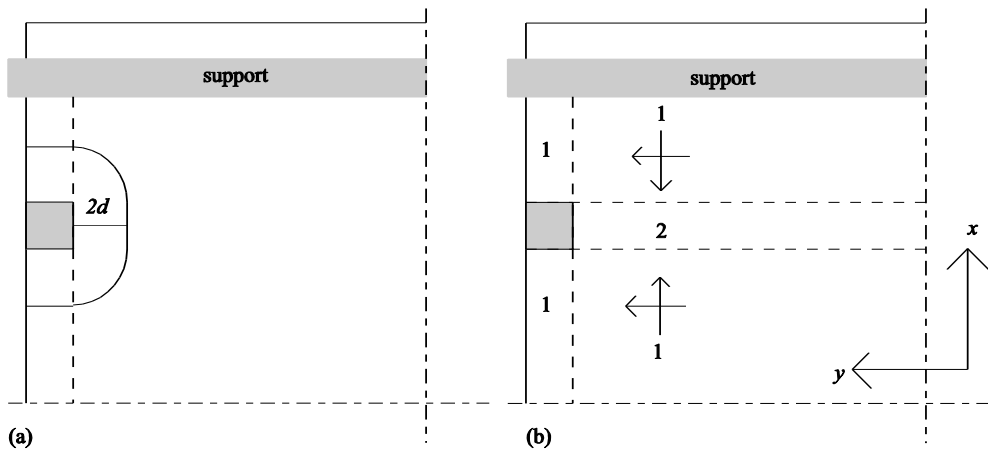


Fig. 5.14: Case of loading at the edge: (a) Punching perimeter as prescribed by NEN-EN 1992-1-1:2005, (b) Application of Bond Model to load at the edge.

### Modified Bond Model

To translate the approach of a slab supported by a column, as used in the original Bond Model to the case of a concentrated wheel load on a slab, it is necessary to imagine the situation to be reversed. Similarly, the Modified Bond Model could be considered a reverse model. While most equilibrium models study the way in which load is carried from its point of application to the support, the Modified Bond Model studies the elements that contribute to the maximum capacity, and for this purpose, reverts this flow and looks at how capacity can be built from the quadrants via the strips to the maximum load that can be applied. Therefore, an alternative explanation would be to use Hillerborg's strip method (1996) to study the strips from Fig. 5.14b, as shown in Fig. 5.15. The  $y$ -direction strip (light grey) is assumed to be carried by the dark grey  $x$ -direction strip, as well as by all  $x$ -direction strips parallel to the dark grey strip. The  $y$ -direction strip is assumed to be supported by the  $x$ -direction strips that can be represented by a series of springs. Another advantage of this explanation is that the torsional moment of the  $x$ -direction strips is not necessary for the support of the  $y$ -direction strip, which is now supported by a series of springs. However, to be able to fully draw the analogy with the Modified Bond Model, it needs to be verified if there exists a link between the loaded length  $l_w$  and the deflection of the  $y$ -direction strip supported by springs. The connection between the Modified Bond Model and the equilibrium models such as Hillerborg's strip method (1996) is recommended to be studied in future research.

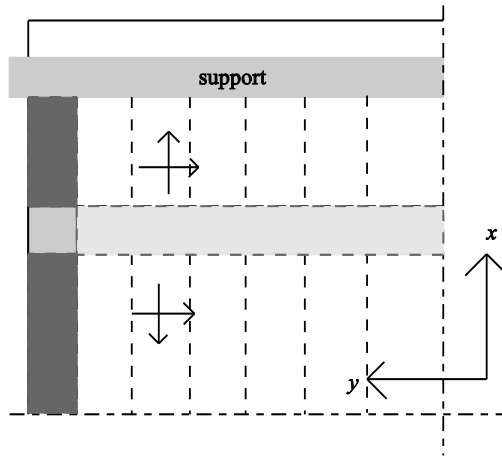


Fig. 5.15: Exploring the link between the Modified Bond Model and an equilibrium strip model.

The next case that is studied is the case in which the load is placed in the vicinity of the edge but not directly at the edge. In the punching approach from NEN-EN 1992-1-1:2005, three sides of the perimeter would be used as indicated by the method sketched in Fig. 5.14a, with two sides longer so that they reach up to the free edge. When applying the Modified Bond Model to this case, and translating the situation into load-bearing quadrants

### Modified Bond Model

and strips, it would be a safe assumption to consider as well just the three strips and two quadrants as shown in Fig. 5.14b. However, to consider all types of loading that are eccentric from the centre line of the slab width, the quadrants between the  $x$ -direction strips and the free edge should be considered. Some load transfer can occur in these slab quadrants, Fig. 5.16, but the associated strips will have a smaller capacity. First, it is assumed that in a quadrant not affected by the vicinity of the free edge, the strips reach their full capacity  $P_{AS,1} = 2\sqrt{M_s w}$ , as used in Alexander's Bond Model (1990). Then, the theory can be extended by assuming that in the quadrants between the  $x$ -direction strips and the free edge, a reduced capacity can be expected for the strips in the vicinity of the edge. This reduction can be expressed by the factor  $\alpha_{MBM}$ , with  $\alpha_{MBM} < 1$ . Therefore, the reduced capacity of the strips can be expressed in terms of  $\alpha_{MBM}$ . For the strips in the  $x$ -direction, the factor  $\chi_1 \leq 2$  is:

$$\chi_1 = (1 + \alpha_{MBM}) \quad (5.30)$$

with  $2 \geq \chi_1 > 1$ . For the strip between the load and the free edge, the reduction factor is:

$$\chi_2 = 2\alpha_{MBM} \quad 0 \leq \chi_2 \leq 1 \quad (5.31)$$

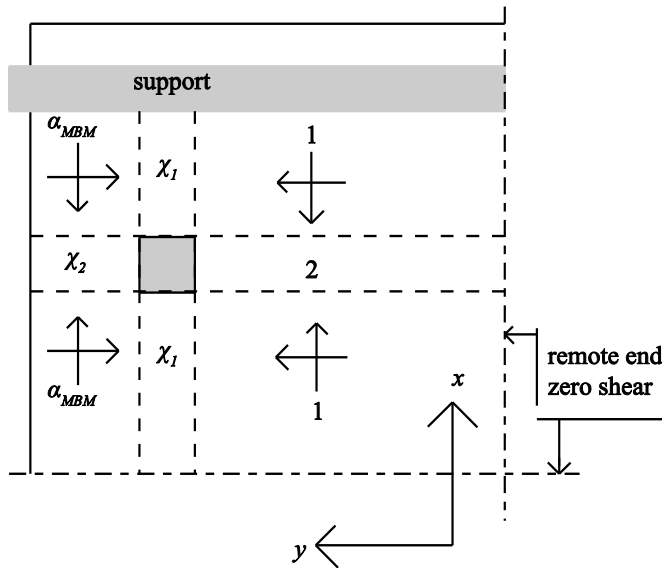


Fig. 5.16: Modified Bond Model for a load in the vicinity of the edge, showing the factors to be used to determine the factor  $\chi$  to assess the capacity of the considered strip.

It is observed in the experiments that geometrical considerations have a large influence on the resulting shear capacity. Therefore, for the experiments with the centre of the concentrated load at 438mm from the edge, the factor  $\alpha_{MBM}$  can be based on the geometry of the position along the width. A simple ratio expressing the eccentricity of the load along

### Modified Bond Model

the width is sufficient to express the influence of the reduced capacity for loads in the vicinity of the edge, linking the influence of the geometry to the Modified Bond Model. The factor  $\alpha_{MBM}$  is determined as:

$$\alpha_{MBM} = \frac{2b_r}{b} \leq 1 \quad (5.32)$$

with

$b_r$  the distance between the free edge and the centre of the load along the width;

$b$  the member width.

In the tested experiments, the full slab width is 2,5m and the centre of the load is placed at 438mm from the edge in the case of loading in the vicinity of the edge. For this case:

$$\alpha_{MBM} = \frac{2 \times 438mm}{2500mm} = 0,35$$

The load on the strips is determined by  $w_{ACI,x}$  as given in Eq. (5.26) and  $w_{ACI,y}$  as given in Eq. (5.27). Taking into account the reduction due to the geometry, the capacity of the strips can be determined as:

for the  $x$ -direction strip:  $P_{MBM,x} = \chi_1 \sqrt{M_{s,x} w_x}$

for both  $y$ -direction strips<sup>21</sup>:  $P_{MBM,y} = (\chi_2 + 2) \sqrt{M_{s,y} w_y}$

for the  $x$ -direction strip between the load and the support:  $P_{MBM,sup} = \left( \frac{2d_l}{a_v} \right) \chi_1 \sqrt{M_{s,x} w_x}$  for

$0,5d_l \leq a_v \leq 2d_l$ .

These strip capacities are reduced with respect to the original capacity determined by Alexander and Simmonds (1992). The capacity as determined from the Modified Bond Model is then:

$$P_{MBM} = P_{MBM,x} + P_{MBM,y} + P_{MBM,sup}$$

To compare this approach to the experimental results, a subset of experiments at the simple support and with the load near to the edge is selected. A comparison between the experimental results from this subset and the proposed method is given in Table 5.3. Again, an excellent agreement between the experimental results and the proposed Modified Bond Model is found.

---

<sup>21</sup> Note that the capacity of both  $y$ -direction strips is given here, and thus  $2 \leq \chi_2 + 2 \leq 4$ .

Modified Bond Model

Table 5.3: Comparison between proposed Modified Bond Model for loads near the edge and the experimental results.

Test	$f_{c\text{-of-max}}$ (MPa)	$a_y$ (m)	$P_{exp}$ (kN)	$M_{neg,x}$ kNm	$M_{neg,y}$ kNm	$w_x$ kN/m	$w_y$ kN/m	$P_{MBM,x}$ kN	$P_{MBM,y}$ kN	$P_{MBM,sup}$ kN	$P_{MBM}$ kN	$P/P_{MBM}$ $P_{exp}$
S4T1	42	0,4	1160	100	25	286	270	229	221	410	860	1,35
S4T2	42	0,4	1110	100	25	286	270	229	221	410	860	1,29
S6T4	41	0,2	1366	100	25	283	267	228	220	814	1261	1,08
S6T5	41	0,2	1347	100	25	283	267	228	220	814	1261	1,07
S7T1	67	0,4	1121	103	25	361	341	261	249	466	976	1,15
S7T5	67	0,4	1063	103	25	361	341	261	249	466	976	1,09
S10T1	68	0,25	1320	69	17	362	341	213	204	609	1026	1,29
S10T2	68	0,25	1116	69	17	362	341	213	204	609	1026	1,09
											<b>AVG</b>	<b>1,18</b>
											<b>STD</b>	<b>0,11</b>
											<b>COV</b>	<b>0,10</b>

### *Modified Bond Model*

These results indicate that the approach from the Modified Bond Model, in which an expression based on the geometry is used to reduce the capacity of the strips that are influenced by the quadrants between the  $x$ -direction strips and the free edge, is sufficiently accurate to take into account the reduced shear and punching capacity near to the edge.

The case as shown in Fig. 5.14b corresponds to the simplification in which torsion is neglected, and is an interpretation of the Bond Model. For the Modified Bond Model, the additional influence of the quadrants between the  $x$ -direction strips and the edge is taken into account. By doing so, the initial safe assumption of neglecting the torsion is not fully met, but the results in Table 5.3 show that taking the quadrants between the free edge and the  $x$ -direction strips into account still leads to safe estimates of the maximum concentrated load on a slab.

#### *5.3.4 Application to slabs on bearings*

When a slab is supported by bearings, not the entire length of the support can be used to carry the load. For slabs under a concentrated load in the vicinity of the edge, in §5.3.3 the geometry was taken as a measure to reduce the capacity of the strips that border the quadrants close to the free edge. For a slab supported by bearings, as simulated in the tests, the Modified Bond Model is further extended. Again, the solution is found by reducing the contribution of the strips bordering the quadrants near the support line based on the geometry of the support. This effect of the geometry can be expressed in terms of the reduced supported length. Since the support length is reduced when bearings are used instead of a line support and smaller maximum concentrated loads occurred in the experiments, further modification of the Bond Model is required.

For loads in the vicinity of the edge, the eccentricity of the load, measured with respect to the middle of the slab as given in Eq. (5.32), was used as a measure for the geometry. The geometry was used to express a reduction factor  $\chi$  for the capacity of the strips, Fig. 5.16.

A similar approach can be followed for slabs on bearings. Here, the influence of the reduced load-bearing capacity of the quadrants between the  $y$ -direction strips and the support can be considered. This reduction can be based on the geometry, as the parameter studies in Chapter 4 have indicated the geometry as most decisive for the shear capacity of slabs under concentrated loads close to supports.

The factor  $\alpha_{MBM}$  reduces the capacity of the strips influenced by the quadrants between the  $y$ -direction strips and the support, and can be expressed as the ratio of the length of the support to the entire width of the slab. For the case of a line support, the full slab width is supported and the factor equals 1. When a reduced support length is used, the factor  $\alpha_{MBM}$  can be expressed as:

### Modified Bond Model

$$\alpha_{MBM} = \frac{\sum_{i=1}^{n_{bearings}} l_{bearing,i}}{b} \leq 1 \quad (5.33)$$

with:

$n_{bearings}$  the number of bearings;  
 $l_{bearing,i}$  the length of the  $i$ -th bearing, taken perpendicular to the span direction, as indicated in Fig. 5.17

In the series of experiments, S15 to S18 were supported by three elastomeric bearings of 280mm × 350mm. As a result, the influence of the quadrants on the factor determining the reduced strip capacity can be expressed as:

$$\alpha_{MBM} = \frac{\sum_{i=1}^3 l_{bearing,i}}{b} = \frac{3 \times 350mm}{2500mm} = 0,42$$

Note that the sum of the coefficients on the strips does not equal “8” anymore, as in the basic case, Fig. 5.11. The geometry is taken into account by reducing the capacities of the strips that border quadrants that are influenced by the short distance to the free edge or reduced support length.

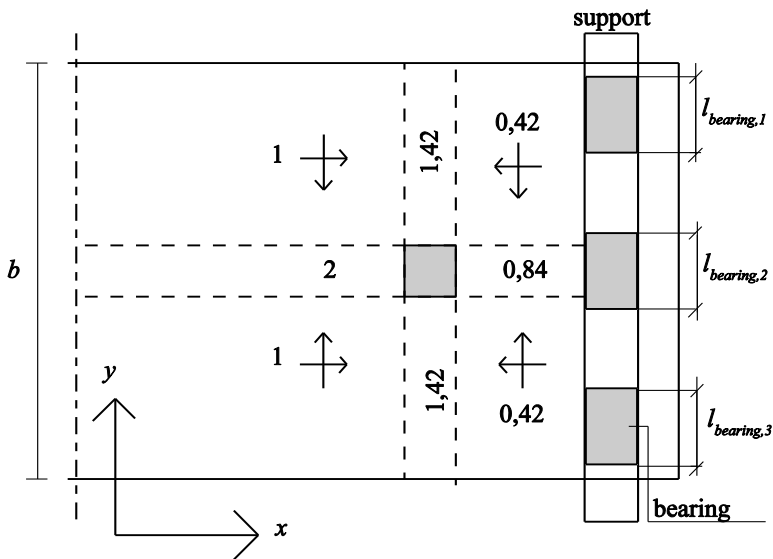


Fig. 5.17: Application of the Modified Bond Model to slabs on bearings.

For concentrated loads near to the edge on a slab supported by bearings, the initial approach is a combination of the method sketched in Fig. 5.16 and the method for slabs on bearings from Fig. 5.17. The vicinity of the free edge, combined with the reduced support length, results in an effect of the geometry on three out of the four considered quadrants, Fig. 5.18.

### Modified Bond Model

As a result, all four strips have a reduced capacity, and this reduction results in a lower total concentrated load that can be carried. To summarize, for this case, two factors that reduce the load-bearing capacity of the quadrants should be taken into account:

1. the influence of the free edge for the quadrants between the  $x$ -direction strips and the free edge, and
2. the influence of the reduced support length for the quadrants between the  $y$ -direction strips and the support.

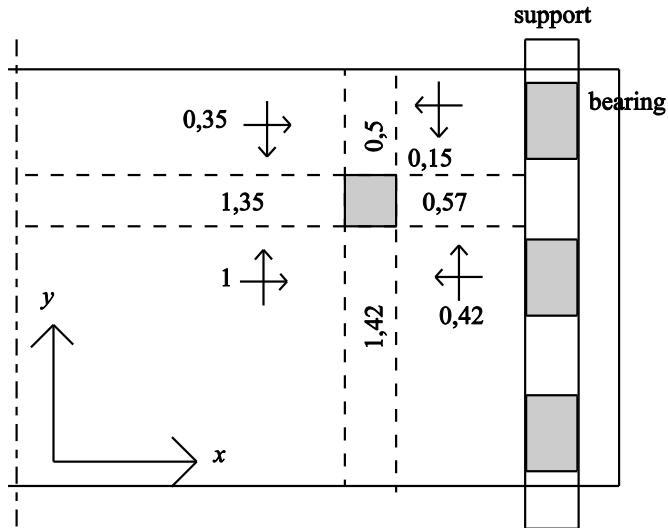


Fig. 5.18: Application of the Modified Bond Model to slabs on bearings with the load close to the edge.

As a result, the quadrant that borders the support and the free edge is influenced by the free edge as well as by the reduced support length. To take both reductions into account, it is proposed to combine the effect of the free edge as well as of the reduced support length by multiplying the reduction due to the free edge ( $\alpha_{MBM} = 0,35$ ; Fig. 5.16) with the reduction due to the reduced support length ( $\alpha_{MBM} = 0,42$ ; Fig. 5.17). The resulting factor for the quadrant bordering the edge and the support is then expressed as  $0,35 \times 0,42 = 0,15$ . This approach is shown in Fig. 5.18. The reduction factor for the capacity of the strips is determined as the sum of the capacity that is carried in each direction of the quadrants, as indicated in Fig. 5.18. For example: the quadrant that borders the support and the free edge carries 0,15 instead of 1 to two strips:

1. The  $x$ -direction strip between the load and the support. This strip also receives 0,42 (instead of 1) from the quadrant that borders the line of bearings. In total, the reduced capacity of the strip is expressed by using  $\chi = 0,57$  instead of  $\chi = 2$ .

### Modified Bond Model

2. The y-direction strip between the load and the free edge. This strip also receives 0,35 from the quadrant that borders the free edge. In total, the reduced capacity of the strip is expressed by using  $\chi = 0,5$  instead of  $\chi = 2$

However, the stiff x-direction strip between the load and the support is assumed to have a larger capacity than the value for  $P_{MBM,sup}$  that results from this approach:

$$P_{MBM,sup} = \left( \frac{2d_l}{a_v} \right) 0,57 \sqrt{M_{s,x} w_x}$$

This small capacity of the stiff strip is the result of the previously discussed approach as shown in Fig. 5.18.

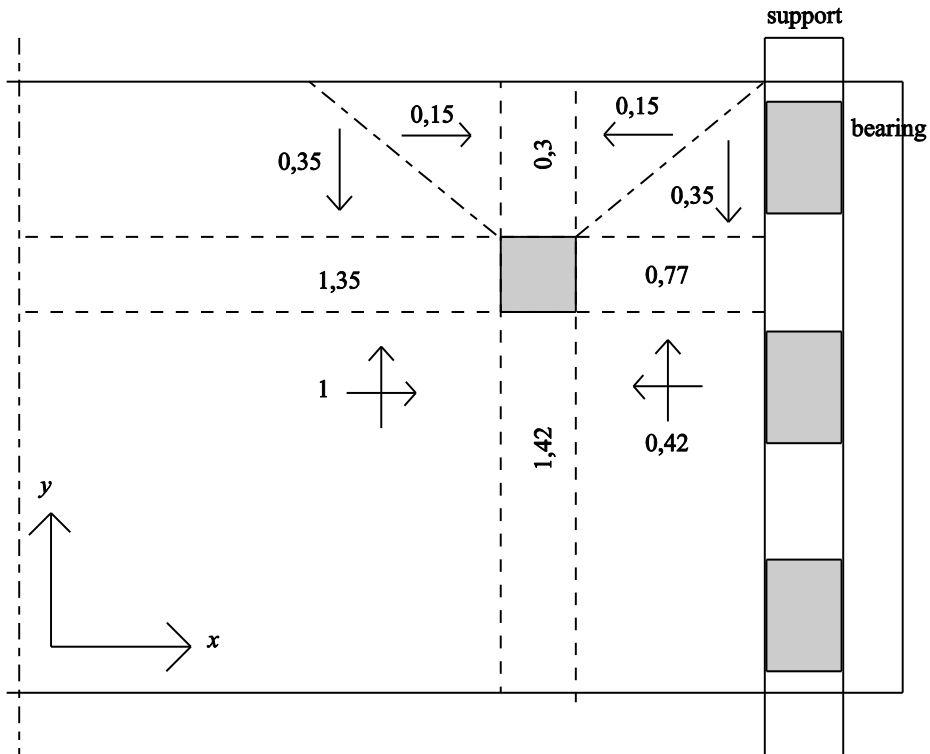


Fig. 5.19: Proposed application of the Modified Bond Model to slabs on bearings with the load close to the edge, taking redistribution into account.

Therefore, the quadrants close to the edge are considered from a different point of view: in the strong direction (x-direction), only the influence of the edge is taken into account, with  $\alpha_{MBM} = 0,35$  to express the contribution in the x-direction, while the combined effect of the edge and the bearings ( $\alpha_{MBM} = 0,15$ ) is used in the y-direction, Fig. 5.19. Note that the sum of the factors  $\chi$  on the strips is still the same, but the stiff strips in the x-direction now carry

### *Modified Bond Model*

a relatively larger proportion while the strips in the  $y$ -direction have a larger reduction in their shear-carrying capacity. Since the Modified Bond Model is a mechanical model that is inspired by plasticity theory, the application of redistribution is according to the principles of its basic assumptions. Note that the contribution of the  $x$ -direction strip in the span (1,35) is larger than the contribution of the strip between the load and the support (0,77). It is observed in the experiments that significant cracking also occurs in the span at a larger distance to the support than the position of the load, indicating that this area is activated. Moreover, the contribution of the strip between the load and the support is in fact  $0,77 \times 2d/a_v$ , which equals at least 1,32 for  $a = 600\text{mm}$  in the experiments.

All results of experiments on undamaged slabs S15 to S18 (Table 3.2) are used for comparison to the Modified Bond Model: slabs at the simple and continuous support, and slabs loaded near the edge and in the middle of the width. The properties of S15 to S18 and the results of the comparison between the Modified Bond Model and the experiments are given in Table 5.4, in which the following symbols are used in addition to those from Table 5.2:

$P_{MBM,s}$                     the capacity of the  $x$ -direction strip assuming loading close to the edge;  
 $P_{MBM,ss}$                     the capacity of the  $x$ -direction strip between the load and the support assuming loading close to the edge.

For experiments with the concentrated load near to the continuous support, the influence of the top reinforcement is taken into account by applying the factor  $k_r$  on three strips. The capacity based on the Modified Bond Model is then determined in Table 5.4 as:

$$P_{MBM} = P_{MBM,x} + 2P_{MBM,y} + P_{MBM,sup} \text{ for loading in the middle of the width, and}$$

$$P_{MBM} = P_{MBM,s} + \left( \frac{\chi_3 + \chi_4}{\chi_3} \right) P_{MBM,y} + P_{MBM,ss} \text{ for loading near the edge.}$$

In Table 5.4,  $P_{MBM,y}$  is defined as the capacity of the  $y$ -direction strip that is not influenced by the free edge. The value of  $\chi_3$  is  $\chi_3 = 1,42$  for the considered slab experiments, and this factor is also used for the  $y$ -direction strips for the case of loading in the middle of the width. The value of  $\chi_4$  is determined by the influence of the free edge, and equals  $\chi_4 = 0,3$  (as shown in Fig. 5.19).

Modified Bond Model

Table 5.4: Comparison between Modified Bond Model and experimental results of slabs on bearings.

Test	$b_r$ m	$a_v$ m	$P_{exp}$ kN	$M_{neg,x}$ kNm	$M_{neg,y}$ kNm	$w_x$ kN/m	$w_y$ kN/m	$k_r$	$M_{pos,x}$ kNm	$M_{pos,y}$ kNm	$P_{MBM,x}$ kN	$P_{MBM,y}$ kN	$P_{MBM,up}$ kN	$P_{MBM,s}$ kN	$P_{MBM,ss}$ kN	$P_{MBM}$ kN	$P_{exp}/P_{MBM}$		
S15T1	1,25	0,36	1040	64	104	277	253	0,39	64	16	267	237	187	180	172	928	1,12		
S15T4	1,25	0,36	1127	64	104	277	253	0,19	9	17	267	230	159	180	151	886	1,27		
S16T1	0,438	0,36	932	64	105	280	256	0,27	9	17	269	232	160	181	152	615	1,52		
S16T2	0,438	0,36	815	64	105	280	256	0,34	9	17	269	232	160	181	152	615	1,33		
S16T4	0,438	0,36	776	64	105	280	256	0,55	64	16	269	242	199	181	189	663	1,17		
S16T5	0,438	0,36	700	64	105	280	256	0,50	64	16	269	241	196	181	187	660	1,06		
S17T1	1,25	0,16	1365	64	104	278	253	0,36	64	16	267	237	418	180	398	1159	1,18		
S17T4	1,25	0,16	1235	64	104	278	253	0,19	9	17	267	231	358	180	341	1086	1,14		
S18T1	0,438	0,16	1157	64	104	277	252	0,28	9	17	267	230	357	180	340	799	1,45		
S18T2	0,438	0,16	1079	64	104	277	252	0,37	9	17	267	230	357	180	340	799	1,35		
S18T4	0,438	0,16	1122	64	104	277	252	0,36	64	16	267	236	416	180	396	862	1,30		
S18T5	0,438	0,16	1104	64	104	277	252	0,43	64	16	267	237	426	180	406	874	1,26		
																	AVG	1,26	
																		STD	0,14
																		COV	0,11

### *Modified Bond Model*

It is shown in Table 5.4 that a good agreement between the experimental results and the predictions from the Modified Bond Model is achieved. This result might be surprising, as some generalizing assumptions have been made in order to take the different layouts of the geometry into account. The method of the Modified Bond Model seems to be very flexible for adaptation, like most mechanical approaches, and good results can still be obtained after significant modifications. In the original Bond Model, the load on the strips is assumed to be purely from internal loading, and torsion is neglected, Fig. 5.9. Alexander (1990) calculated that the influence of torsion allows for about 29% more capacity, as shown in §5.2.2, and therefore omitting the torsion leads to safe results. For the comparison between the Modified Bond Model and the experimental results, on average also 20% to 30% more capacity is found in the experiments. This observation indicates that also for these cases neglecting the effect of torsion is a safe assumption.

#### *5.3.5 Extension to plain bars*

The next step in the development of the Modified Bond Model is the application to the slabs reinforced with plain bars S11 to S14. Here, it should be repeated that the original Bond Model considers the contribution of arching action (no bond required) and beam shear action (bond is necessary). As the bond properties of plain bars are different, the impact on the Modified Bond Model is expected to be large. Plain bars are assumed not to transfer forces to the reinforcement by means of bond, and thus the force in the reinforcement remains constant. Following this logic, it is expected that for slabs with plain bars, only the contribution of arching action can be taken into account. Since arching action does not depend on force transfer through bond between the concrete and the reinforcement, the influence of the bond properties is not important for the strips. One of the assumptions of the Bond Model is that, in the quadrants, one-way shear is transferred via beam action, a mechanism that depends on the force increment in the reinforcement as a result of bond between the reinforcement and the concrete. Therefore, the influence of the bond properties and the type of reinforcement should be incorporated in the loading term  $w$ , which determines the loading that is carried by one-way shear and bond action in the quadrants.

In the Modified Bond Model, the distinction between the strips and the quadrants is clear: the quadrants carry one-way shear via bond to the strips, and the strips carry this load through arching action. These load-carrying mechanisms are illustrated in Fig. 5.5 for beam action, Fig. 5.6 for arching action and Fig. 5.7 for the combined load-carrying mechanism. The Modified Bond Model, however, is just a schematization and simplification of the physical behaviour of a slab under a concentrated load. In reality, the shear-carrying mechanisms are interdependent and cannot be simply separated into quadrants and strips. The relative importance of the shear-carrying mechanisms also

### Modified Bond Model

depends on the properties of the slab. For example, in a slab with plain bars, arching action will carry a relatively larger percentage of the load.

In Dutch practice (NEN 6720:1995), the bond capacity of plain bars is considered as 0,5 times the bond capacity<sup>22</sup> of ribbed bars. This factor (0,5) cannot be directly applied onto the loading term  $w$  for the aforementioned reasons. For slabs reinforced with plain bars an empirical reduction factor of 0,8 on the loading term  $w_{ACI}$  in the Modified Bond Model can be used to take into account the reduced capacity to carry shear by means of beam action. The resulting expressions for the load on the strips are then:

$$w_{ACI,x,plain} = 0,8 \times 0,166d_l \sqrt{f_{ck}} = 0,8w_{ACI,x} \quad (5.34)$$

$$w_{ACI,y,plain} = 0,8 \times 0,166d_l \sqrt{f_{ck}} = 0,8w_{ACI,y} \quad (5.35)$$

with  $f_{ck}$  in [MPa],  $d_l$  and  $d_t$  in [mm] and  $w_{ACI,x,plain}$  and  $w_{ACI,y,plain}$  in [kN/m]. Although this factor 0,8 is determined empirically, it can be explained by reflecting on the shear transfer mechanisms that are used in the Modified Bond Model. As a result, the capacity of the strips can be determined as:

for the  $x$ -direction strip:  $P_{MBM,x} = \chi_1 \sqrt{M_{s,x} 0,8w_x}$

for both  $y$ -direction strips:  $P_{MBM,y} = (\chi_3 + \chi_4) \sqrt{M_{s,y} 0,8w_y}$

for the  $x$ -direction strip between the load and the support:  $P_{MBM,sup} = \left( \frac{2d_l}{a_v} \right) \chi_2 \sqrt{M_{s,x} 0,8w_x}$ .

The total capacity according to the Modified Bond Model is then determined as:

$P_{MBM} = P_{MBM,x} + 2P_{MBM,y} + P_{MBM,sup}$  for loading in the middle of the width, and

$P_{MBM} = P_{MBM,s} + \left( \frac{\chi_3 + \chi_4}{\chi_3} \right) P_{MBM,y} + P_{MBM,ss}$  for loading near the edge.

In Table 5.5,  $P_{MBM,y}$  is defined as the capacity of the  $y$ -direction strip that is not influenced by the free edge.

The properties and experimental results of S11 to S14 as compared to the Modified Bond Model are given in Table 5.5. In Table 5.5 the loading terms  $w_x$  and  $w_y$  are multiplied by 0,8 – effectively showing  $w_{ACI,x,plain}$  and  $w_{ACI,y,plain}$ . Again, good agreement is found between the experimental results and the Modified Bond Model.

---

<sup>22</sup> The influence of the bond capacity on the beam shear capacity is also a function of the concrete compressive strength. For low strength concrete (eg. C20/25), the difference in behaviour of beams with plain bars and with deformed bars tested in shear is more significant than for normal strength concrete, as was used in the experiments.

Modified Bond Model

Table 5.5: Overview of the comparison between the Modified Bond Model and the experimental results from S11 to S14 with plain bars.

Test	$b_f$ (mm)	$a_v$ (mm)	$P_{exp}$ (kN)	$M_{neg-x}$ kNm	$M_{neg-y}$ kNm	$w_x$ kN/mm	$w_y$ kN/mm	$k_r$	$M_{pos-x}$ kNm	$M_{pos-y}$ kNm	$P_{MDM-x}$ kN	$P_{MDM-y}$ kN	$P_{MDM,exp}$ kN	$P_{MDM,s}$ kN	$P_{MDM,ss}$ kN	$P_{MDM}$ kN	$P_{exp} / P_{MDM}$		
S11T1	SS	1,25	0,45	1194	101	27	236	223	0,19	15	308	156	363	208	245	983	1,21		
S11T4	CS	1,25	0,45	958	101	27	236	223	0,59	101	308	156	458	208	309	1077	0,89		
S12T1	SS	0,438	0,45	931	101	27	236	223	0,23	15	308	156	363	208	245	663	1,40		
S12T2	SS	0,438	0,45	1004	101	27	236	223	0,23	15	308	156	363	208	245	663	1,51		
S12T4	CS	0,438	0,45	773	101	27	236	223	0,31	101	308	156	416	208	280	699	1,11		
S12T5	CS	0,438	0,45	806	101	27	236	223	0,32	101	308	156	417	208	282	700	1,15		
S13T1	SS	1,25	0,25	1404	100	27	230	217	0,21	15	303	153	643	205	434	1252	1,12		
S13T4	CS	1,25	0,25	1501	100	27	230	217	0,38	100	303	153	755	205	510	1365	1,10		
S14T1	SS	0,438	0,25	1214	100	27	228	215	0,21	15	302	153	640	204	432	842	1,44		
S14T2	SS	0,438	0,25	1093	100	27	228	215	0,28	15	302	153	640	204	432	842	1,30		
S14T4	CS	0,438	0,25	1282	100	27	228	215	0,34	100	302	153	742	204	501	911	1,41		
S14T5	CS	0,438	0,25	1234	100	27	228	215	0,26	100	302	153	720	204	486	896	1,38		
																	AVG	1,25	
																		STD	0,18
																		COV	0,15

### 5.3.6 Resulting Modified Bond Model

The Modified Bond Model is based on the Bond Model by Alexander and Simmonds (1992) for concentric punching shear. The following alterations are made:

- For one-way slabs, the  $x$ - and  $y$ -direction strips are considered separately to take into account the different reinforcement layout in both directions.
- The capacity of the  $x$ -direction strip between the load and the support is increased by the factor  $2d_v/a_v$ , which takes direct load transfer into account.
- To take into account the support moment at the continuous support, the factor  $k_r$  is determined to be the ratio between the support moment and the span moment. The factor  $k_r$  is applied on both  $y$ -direction strips, and on the  $x$ -direction strip between the load and the support, as these strips are affected by the quadrants in which the sign of the moment changes.
- For loads at the edge, three strips are used.
- For loads in the vicinity of the edge or away from the centre of the width, a factor  $\alpha_{MBM}$  is defined,  $\alpha_{MBM} < 1$ , as given in Eq. (5.32):

$$\alpha_{MBM} = \frac{2b_r}{b} \leq 1$$

- When not the full width of the slab is supported, a factor  $\alpha_{MBM}$  is defined,  $\alpha_{MBM} < 1$ , as given in Eq. (5.33):

$$\alpha_{MBM} = \frac{\sum_{i=1}^{n_{bearings}} l_{bearing,i}}{b} \leq 1$$

- Redistribution of loads can be applied, and the different stiffness in the  $x$ - and  $y$ -direction strips can be taken into account, as shown for the case of a slab supported by bearings under a concentrated load in the vicinity of the edge.
- For slabs with plain bars, an empirical reduction factor on the loading term  $w_{ACI}$  of 0,8 is used.

To calculate the shear capacity of a slab under a concentrated load near to the support according to the Modified Bond Model, the following steps are taken:

1. Gather the relevant information:
  - the cylinder compressive strength of the concrete,
  - the geometry of the slab,
  - the geometry of the load,
  - the position of the load along the width and along the span,
  - the geometry of the support, and
  - if loading occurs near a simple or continuous support.

### *Modified Bond Model*

2. Sketch an  $xy$  plane with the load, support and slab. Draw the four strips that extend from the load in the  $x$ - and  $y$ -direction, Fig. 5.20a. Only when the load is placed directly at the edge, 3 strips are used.
3. Study the reduction due to the geometry in the four (when four strips are used) resulting quadrants. If the geometric conditions do not penalize the quadrant, a value of “1” is carried in two directions. If the load is placed eccentric from the middle of the width, the loading term in the quadrants between the  $x$ -direction strips and the free edge is reduced by  $\alpha_{MBM}$  with:

$$\alpha_{MBM} = \frac{2b_r}{b} \leq 1.$$

If not the full width of the slab is supported, the loading term in the quadrants between the  $y$ -direction strips and the support is  $\alpha_{MBM}$  with:

$$\alpha_{MBM} = \frac{\sum_{i=1}^{n_{bearings}} l_{bearing,i}}{b} \leq 1.$$

If a quadrant is influenced by both conditions, both factors  $\alpha_{MBM}$  can be multiplied for that quadrant, Fig. 5.20b.

4. Calculate the factors  $\chi_i$  for the capacities of the strips by adding the  $\alpha_{MBM}$  terms that are transferred to the strips, Fig. 5.20c, onto the factor for the reduction of the capacity of the strip  $\chi_i$ .
5. If the amount of reinforcement in the  $x$ -direction strips is considerably larger than in the  $y$ -direction strips, plastic load redistribution towards the stiff strip between the load and the support can occur, resulting in larger load coefficients on the stiffer strip and smaller load coefficients on the more flexible strip, for example see Fig. 5.19.
6. Gather the required information about the reinforcement in the strips and the geometry of the reinforcement: the effective depth to the longitudinal  $d_l$  and transverse reinforcement  $d_t$ , the yield strength  $f_{yk}$  of the bars and the layout of the reinforcement.
7. Count the number of bars per strip, and add  $\frac{1}{2}$  bar on every side of the strip. The distance between these bars is  $b_{rebar,x}$  for the longitudinal bars and  $b_{rebar,y}$  for the transverse flexural bars.

Modified Bond Model

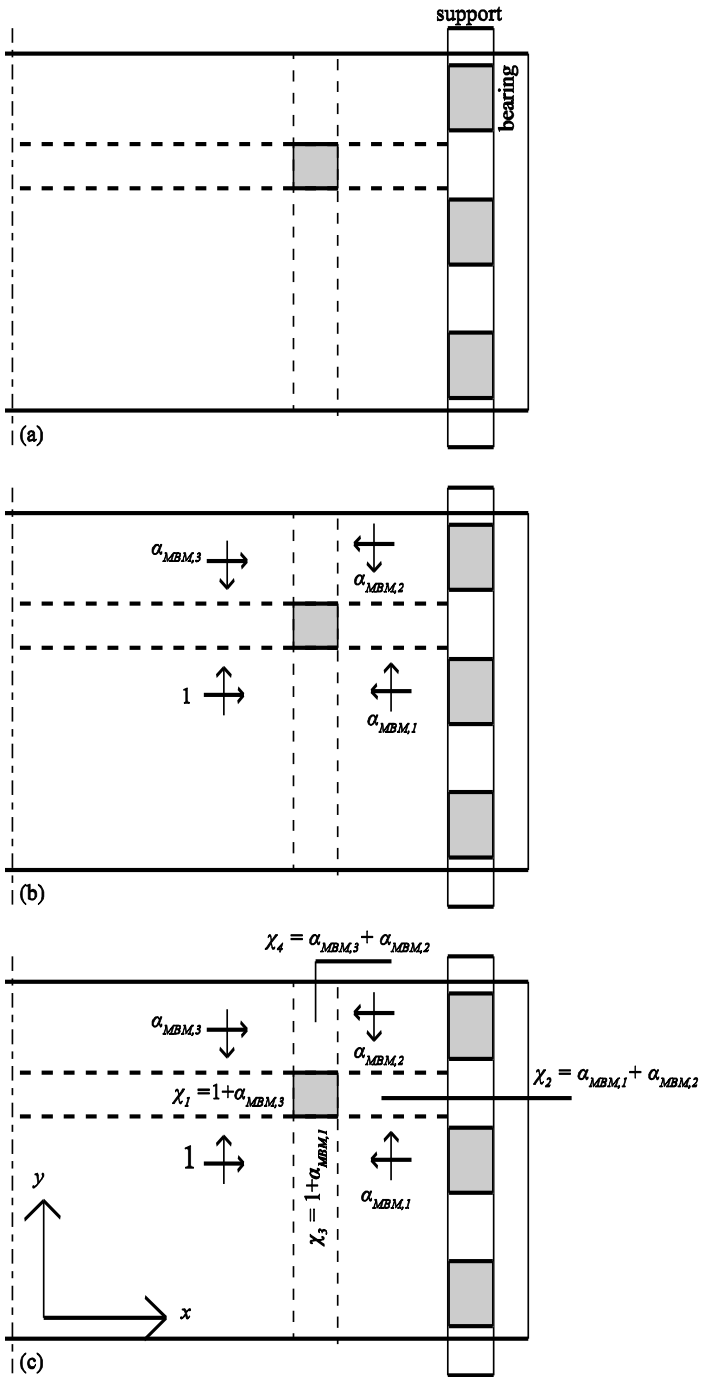


Fig. 5.20: Step-by-step approach showing how to develop the model to determine the load factors  $\chi_i$  on the strips with the Modified Bond Model

### Modified Bond Model

8. Determine the reinforcement area  $A_{sx}$  and  $A_{sy}$  of the bars over  $b_{rebar,x}$  and  $b_{rebar,y}$ . The percentage of reinforcement to be considered is determined as:

$$\rho_{neg,x} = \frac{A_{sB,x}}{b_{rebar,x}d_l} \text{ and } \rho_{neg,y} = \frac{A_{sB,y}}{b_{rebar,y}d_y} \cdot^{23}$$

9. The moment capacity of the longitudinal and transverse reinforcement is:

$$M_{neg,x} = \rho_{neg,x} f_{yk} z_l d_l l_{load} \text{ and } M_{neg,y} = \rho_{neg,y} f_{yk} z_l d_l b_{load} \cdot$$

10. If the load is placed near a continuous support, determine  $k_r$ :

$$k_r = \frac{M_{sup}}{M_{span}}$$

with  $M_{sup}$  the moment at the support and  $M_{span}$  the moment at the location of the concentrated load, Fig. 5.12.

11. If the load is placed close to a continuous support, the reinforcement activated by the support moment should be taken into account as described in steps 5 to 8,

$$\text{resulting in } M_{pos,x} = \rho_{pos,x} f_y z_{pos,x} d_{pos,x} l_{load} \text{ and } M_{pos,y} = \rho_{pos,y} f_y z_{pos,y} d_{pos,y} b_{load} \cdot$$

12. If the load is placed close to a continuous support, then  $M_{s,x} = M_{neg,x} + k_r M_{pos,x}$  and  $M_{s,y} = M_{neg,y} + k_r M_{pos,y}$ . For loads close to the simple support,  $k_r = 0$ . The support moment and span moment influence the quadrants between the load and the support. Therefore, for loads near to the continuous support  $k_r$  is applied as  $> 0$  to the  $x$ -direction strip between the load and the support and the  $y$ -direction strips.

13. The loading term is determined to be  $w_{ACI,x} = 0,166d_l \sqrt{f_{ck}}$  in the  $x$ -direction and

$w_{ACI,y} = 0,166d_t \sqrt{f_{ck}}$  in the  $y$ -direction for ribbed bars, with  $f_{ck}$  in [MPa],  $d_l$  and  $d_t$  in [mm] and  $w_{ACI,x}$  and  $w_{ACI,y}$  in [kN/m]. A reduction factor of 0,8 is applied to  $w$  for plain bars. A size effect factor can be applied as :

$$k_{MBM} = \frac{1 + \sqrt{\frac{300}{d_l}}}{2} \leq 1 \text{ with } d_l \text{ in [mm] and } k_{MBM} \text{ in [-].}$$

14. Determine the capacity of the 4 strips:

- for the  $x$ -direction strip from the load towards the span:

$$P_{MBM,x} = \chi_1 \sqrt{w_{ACI,x} M_{neg,x}}, \text{ with } \chi_1 \text{ the result of the factors from the geometry affecting the considered strip, Fig. 5.20.}$$

---

<sup>23</sup> Note that top and bottom refers here to the layout for the experiments of slabs under a concentrated load, which is different from the slab-column experiments that served as a basis for the original Bond Model by Alexander and Simmonds (1992).

### *Modified Bond Model*

- for the  $x$ -direction strip between the load and the support:

$$P_{MBM,sup} = \chi_2 \sqrt{w_{ACI,x} M_{s,x}} \frac{2d_l}{a_v}, \text{ with } \chi_2 \text{ the result of the factors from}$$

geometry affecting the considered strip.

- for the  $y$ -direction strips:  $P_{MBM,y} = (\chi_3 + \chi_4) \sqrt{w_{ACI,y} M_{s,y}}$ , with  $\chi_3$  and  $\chi_4$  the resulting factors from geometry affecting the  $y$ -direction strips.

15. The shear capacity of a slab under a concentrated load near to the support according to the Modified Bond Model is:<sup>24</sup>

$$P_{MBM} = P_{MBM,x} + P_{MBM,sup} + P_{MBM,y}.$$

An example calculation of an experiment with the Modified Bond Model can be found in Annex 2.

#### 5.3.7 Verification with S19 – S26 and extension for slabs under a combination of loads

As the Modified Bond Model is flexible, it can be applied without further modification on the experiments from the second series on slabs S19 – S26 in which only a concentrated load is applied. Some of these experiments are also carried out at a larger distance to the support. Therefore, the expression for the capacity of the  $x$ -direction strip between the load and the support is extended to:

$$\begin{aligned} P_{MBM,sup} &= \chi_2 \sqrt{w_{ACI,x} M_{s,x}} \frac{2d_l}{a_v} \text{ for } 0,5d_l \leq a_v \leq 2d_l \\ P_{MBM,sup} &= \chi_2 \sqrt{w_{ACI,x} M_{s,x}} \text{ for } a_v > 2d_l \end{aligned} \quad (5.36)$$

The results of the comparison are given in Table 5.6, showing an excellent agreement between the proposed model and the experimental results. It is noteworthy to point out the uniform behaviour of the Modified Bond Model over the larger range of shear spans that are tested in these experiments.

For the experiments on slabs under a combination of a concentrated load and a line load, the Modified Bond Model can again be adapted, as it was adapted in the previous sections to take into account changes in the geometry. When an additional load is applied to a slab subjected to a concentrated load, the following questions should be considered:

1. In which direction does the additional load act?
2. Which quadrants does the additional load affect?
3. As a result, which strips does the additional load affect?

---

<sup>24</sup> Note that  $P_{MBM,y}$  is the sum of the capacities of both  $y$ -direction strips.

Modified Bond Model

Table 5.6: Overview of the comparison between the Modified Bond Model and the experimental results from S19 to S26 under a concentrated load only.

Test	$b_y$ (m)	$a_y$ (m)	$P_{exp}$ (kN)	$M_{neg,x}$ kNm	$M_{neg,y}$ kNm	$w_x$ kN/m	$w_y$ kN/m	$k_r$	$M_{pos,x}$ kNm	$M_{pos,y}$ kNm	$P_{MBM,x}$ kN	$P_{MBM,y}$ kN	$P_{MBM,avg}$ kN	$P_{MBM,s}$ kN	$P_{MBM,ss}$ kN	$P_{MBM}$ kN	$P_{exp} / P_{MBM}$	
S19T2	SS	1,25	0,31	1484	101	25	301	284	0	14	26	349	166	584	235	393	1265	1,17
S19T1	CS	1,25	0,31	1568	101	25	301	284	0,21	101	25	349	183	642	235	432	1356	1,16
S25T1	SS	1,25	0,4	1461	101	25	305	288	0	14	26	352	167	456	237	307	1143	1,28
S25T4	SS'	0,438	0,67	854	101	25	305	288	0	101	25	352	167	344	237	232	695	1,23
S25T5	SS'	0,438	0,93	968	101	25	305	288	0	101	25	352	167	344	237	232	695	1,39
S21T3	SS'	0,438	1,19	730	100	25	272	256	0	100	25	329	158	322	222	217	652	1,12
S21T4	SS'	0,438	1,19	753	100	25	272	256	0	100	25	329	158	322	222	217	652	1,15
S21T5	SS'	0,438	0,67	853	100	25	272	256	0	100	25	329	158	322	222	217	652	1,31
S21T6	SS'	0,438	0,93	785	100	25	272	256	0	100	25	329	158	322	222	217	652	1,20
																	AVG	1,22
																	STD	0,09
																	COV	0,07

### Modified Bond Model

For the line load of 240 kN/m that is applied in the experiments on S19 to S26, the questions can be answered as follows:

1. The line load is applied in one direction only, over the  $y$ -direction of the slab, as shown in Fig. 3.4.
2. Two quadrants are affected by the presence of the line load: the quadrants between the line load and the concentrated load, as shown in Fig. 5.21. However, the line load is applied in the  $y$ -direction only. As a result, in the quadrant, the reduced load is only carried in the  $x$ -direction. The reduction factor is given as  $\alpha_{red}$ .
3. Since the effect of the line load only is taken into account in the  $x$ -direction in the affected quadrants, both  $y$ -direction strips are affected. The multiplication factors  $\chi_3$  and  $\chi_4$  for the resulting load on the  $y$ -direction strip are then found by summing the resulting factors from the quadrants, Fig. 5.21.

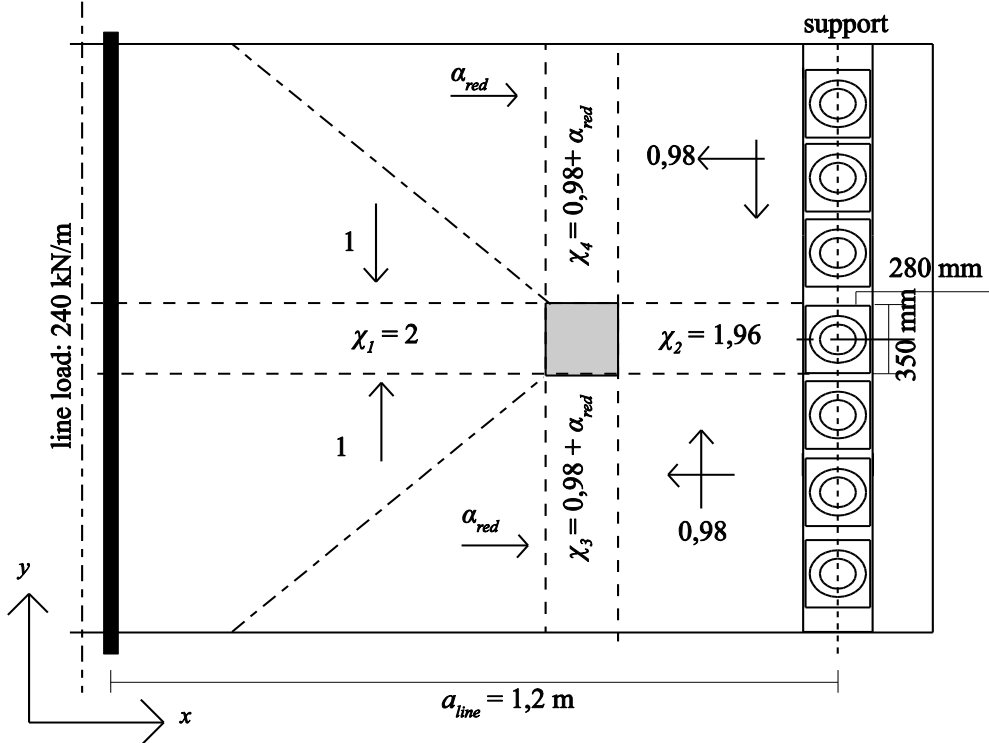


Fig. 5.21: Application of the Modified Bond Model to slabs under a combination of a line load and a concentrated load, as applied in slabs S19 to S26.

For application of the combination of the concentrated load close to the edge and close to the support with a line load, the resulting Modified Bond Model factors are shown in Fig.

5.22. For a concentrated load close to the edge, the influence of the edge is again taken into account as proposed by Eq. (5.32):

$$\alpha_{MBM} = \frac{2b_r}{b} = 2 \frac{438\text{mm}}{2500\text{mm}} = 0,35$$

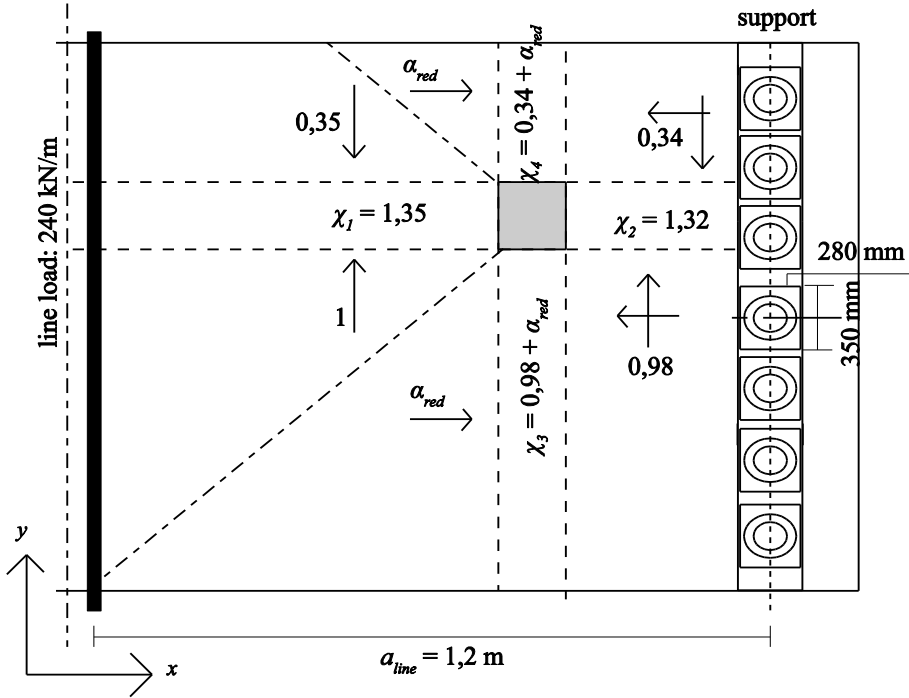


Fig. 5.22: Application of the Modified Bond Model to slabs under a combination of a line load and a concentrated load near to the edge, as applied in slabs S19 to S26.

Moreover, the quadrants between the concentrated load and the support are influenced by the reduced support length. In the second series on slabs S19 to S26, the slabs are supported by 7 bearings of 350mm length. The reduction factor is then given by Eq. (5.33):

$$\alpha_{MBM} = \frac{\sum_{i=1}^{n_{bearings}} l_{bearing,i}}{b} = \frac{7 \times 350\text{mm}}{2500\text{mm}} = 0,98$$

For concentrated loads near to the edge, the quadrant that borders the free edge and the support takes into account the combined effect of the reduced support length and the vicinity of the edge:  $\alpha_{MBM} = 0,35 \times 0,98 = 0,34$ .

Now that it has been explained how the reduction factors are determined and how the loads on the four strips are found, further attention is given to the determination of the factor  $\alpha_{red}$  that takes the influence of the line load into account. Due to the fact that the line

### Modified Bond Model

load only acts over the y-direction, it already became clear that only the capacity of the y-direction strips is reduced. To quantify the effect, the shear force due to the line load is used to determine the reduction factor. The maximum shear capacity at the contact surface between a quadrant and a strip is defined by the one-way shear capacity  $w_{ACI}$ . Therefore, the reduction factor  $\alpha_{red}$  is based on the reduced one-way shear capacity due to the shear force from the line load. The factor  $\alpha_{red}$  is thus expressed as:

$$\alpha_{red} = \frac{1}{w_{ACI}} \left( w_{ACI} - \frac{P_{line}}{b} \frac{l_{span} - a_{line}}{l_{span}} \right) \leq 1 \quad (5.37)$$

with:

$w_{ACI}$  the lower bound of the inclined cracking load, as given by Eq. (5.13);

$P_{line}$  the applied jack force on the line load, as given in Table 3.3;

$b$  the full slab width over which the line load is applied;

$l_{span}$  the span length between the two considered supports;

$a_{line}$  the distance between the support and the line load, which equals 1,2m for all experiments under consideration, see Fig. 5.21 and Fig. 5.22.

After the determination of the reduction factors, the procedure of the Modified Bond Model is repeated without further modifications. The moment capacity is determined as explained previously, and the influence of the support moment is taken into account on three strips if the concentrated load is placed near to the continuous support. The capacity of the four strips is then given as:

- for the x-direction strip from the load towards the span:  $P_{MBM,x} = \chi_1 \sqrt{w_{ACI,x} M_{neg,x}}$ , where  $\chi_1$  is the result of the factors regarding the geometry of the strip under consideration. The factors  $\chi_1$  are now 2 for the load in the middle of the width and 1,35 for the load in the vicinity of the edge.

- for the x-direction strip between the load and the support:

$$P_{MBM,sup} = \chi_2 \sqrt{w_{ACI,x} M_{s,x}} \frac{2d_l}{a_v} \text{ for } 0,5d_l \leq a_v \leq 2d_l, \text{ where } \chi_2 \text{ represents the result of}$$

the factors from geometry for the strip under consideration. For these experiments, the influence of the reduced support length is taken into account by  $\alpha_{MBM} = 0,98$ . The factors  $\chi_2$  are 1,96 for the load in the middle of the width and 1,32 for the load in the vicinity of the edge.

- for the y-direction strips:  $P_{MBM,y} = (\chi_3 + \chi_4) \sqrt{w_{ACI,y} M_{s,y}}$ , where  $\chi_3$  and  $\chi_4$  are the resulting factors from geometry for the y-direction strips and taking the influence of the line load into account. For the case with the load in the middle of the width  $\chi_3 = \chi_4 = 0,98 + \alpha_{red}$ . For the case with the load in the vicinity of the edge, the factors are  $\chi_4 = 0,98 + \alpha_{red}$  and  $\chi_3 = 0,34 + \alpha_{red}$ .

### *Modified Bond Model*

The shear capacity of a slab under a concentrated load near to the support according to the Modified Bond Model is:  $P_{MBM} = P_{MBM,x} + P_{MBM,sup} + P_{MBM,y}$ .

A comparison between the experimental results of S19 to S26<sup>25</sup> for the tests in which a concentrated load and a line load are used, and the results from the proposed extension of the Modified Bond Model is given in Table 5.7. The same symbols are used as in the previous overview tables, only a column with  $\alpha_{red}$  has been added. The results in Table 5.7 show again a good agreement between the test results and the proposed extension of the Modified Bond Model.

The main idea of the followed approach is the superposition of the effects arising from the two load systems and comparing the resultants with limit values defined by the details of the slab. In essence, the shear due to the line load is added to the shear due to the concentrated load to determine  $\alpha_{red}$ . The reduction expresses the amount of shear capacity that is consumed by the line load.

It is important to note that the Modified Bond Model, which was basically developed for a single concentrated load on a slab, can easily be expanded to include additional loads. The versatility of the proposed model is thus a noteworthy beneficial feature.

---

<sup>25</sup> Note that the results of S20T2 are not used, as S20T2 failed by further opening the shear crack from S20T1.

Modified Bond Model

Table 5.7: Overview of the comparison between the Modified Bond Model and the experimental results from S19 to S26 under a combination of a concentrated load and a line load

Test	$b_f$ (m)	$a_v$ (m)	$P_{exp}$ (kN)	$M_{neg,x}$ kNm	$M_{neg,y}$ kNm	$w_x$ kN/m	$w_y$ kN/m	$\alpha_{red}$	$k_r$	$M_{pos,x}$ kNm	$M_{pos,y}$ kNm	$P_{MM,x}$ kN	$P_{MM,y}$ kN	$P_{MM,exp}$ kN	$P_{MM,s}$ kN	$P_{MM,ss}$ kN	$P_{MM}$ kN	$P/P_{exp}$
S20T1	1,25	0,31	1542	102	25	310	292	0,45	0,00	14	26	355	122	594	239	400	1193	1,29
S20T2b	1,25	0,36	1552	68	17	310	292	0,59	0,73	68	17	290	144	550	195	370	1127	1,38
S20T3	0,438	0,31	1337	102	25	310	292	0,59	0,81	102	25	355	180	799	239	538	1064	1,26
S20T4	0,438	0,31	1449	102	25	310	292	0,59	0,72	102	25	355	176	780	239	525	1044	1,39
S21T1	1,25	0,4	1165	101	25	300	283	0,43	0,33	101	25	348	137	521	235	351	1143	1,02
S21T2	1,25	0,4	1386	101	25	300	283	0,43	0,00	14	26	348	118	452	235	305	1038	1,34
S22T1	0,438	0,4	984	101	25	303	286	0,44	0,37	101	25	350	140	532	237	359	812	1,21
S22T2	0,438	0,4	961	101	25	303	286	0,44	0,36	101	25	350	140	531	237	357	810	1,19
S22T3	0,438	0,4	978	101	25	303	286	0,44	0,00	14	26	350	120	455	237	307	728	1,34
S22T4	0,438	0,4	895	101	25	303	286	0,44	0,00	14	26	350	120	455	237	307	728	1,23
S23T1	1,25	0,31	1386	101	25	306	288	0,44	0,27	101	25	352	136	665	238	448	1289	1,08
S23T2	1,25	0,31	1132	101	25	306	288	0,44	0,00	14	26	352	121	590	238	397	1183	0,96
S24T1	0,438	0,31	1358	101	25	306	288	0,44	0,27	101	25	352	136	665	238	448	896	1,52
S24T2	0,438	0,31	1182	101	25	306	288	0,44	0,27	101	25	352	136	665	238	448	896	1,32
S24T3	0,438	0,31	995	101	25	306	288	0,44	0,00	14	26	352	121	590	238	397	822	1,21
S24T4	0,438	0,31	784	101	25	306	288	0,44	0,00	14	26	352	121	590	238	397	822	0,95

Test	$b_r$ (m)	$a_v$ (m)	$P_{exp}$ (kN)	$M_{neg,x}$ kNm	$M_{neg,y}$ kNm	$w_x$ kN/m	$w_y$ kN/m	$\alpha_{red}$	$k_r$	$M_{pos,x}$ kNm	$M_{pos,y}$ kNm	$P_{MBM,x}$ kN	$P_{MBM,y}$ kN	$P_{MBM,exp}$ kN	$P_{MBM,s}$ kN	$P_{MBM,ss}$ kN	$P_{MBM}$ kN	$P_{exp}/P_{MBM}$	
S25T2	CS	1,25	0,2	1620	101	25	305	288	0,44	0,43	101	25	352	144	1093	237	736	1732	0,94
S25T3	CS	0,438	0,2	1563	101	25	305	288	0,44	0,43	101	25	352	144	1091	237	735	1195	1,31
S26T1	SS	0,438	0,22	1448	101	25	305	288	0,44	0,00	14	26	352	120	830	237	559	983	1,47
S26T2	SS	0,438	0,22	1324	101	25	305	288	0,44	0,00	14	26	352	120	830	237	559	983	1,35
S26T3	CS	1,25	0,2	1555	101	25	305	288	0,44	0,53	101	25	352	149	1129	237	761	1778	0,87
S26T4	CS	0,438	0,2	1363	101	25	305	288	0,44	0,62	101	25	352	153	1160	237	781	1256	1,09
S26T5	CS	0,438	0,2	1451	101	25	305	288	0,44	0,58	101	25	352	151	1148	237	773	1244	1,17
																	AVG	1,21	
																	STD	0,18	
																	COV	0,15	

## 5.4 Comparison between experimental results and Modified Bond Model

### 5.4.1 General comparison

To study the overall performance of the Modified Bond Model, all results of the experiments on uncracked slabs S1 to S18 are compared to the results obtained with the Modified Bond Model<sup>26</sup>. The maximum concentrated load in the experiment is compared to the maximum capacity obtained with the Modified Bond Model. The evaluation showed an average ratio  $P_{exp}/P_{MBM} = 1,24$  with a standard deviation of 0,15 and a coefficient of variation of 12%. Considering that the problem regarded is a shear problem with a multitude of parameters that have been varied, the resulting statistical results are excellent. The average value is at the conservative side, and therefore the Modified Bond Model is suitable for a safe application in design or assessment within its limits of application. The results are shown graphically in Fig. 5.23.

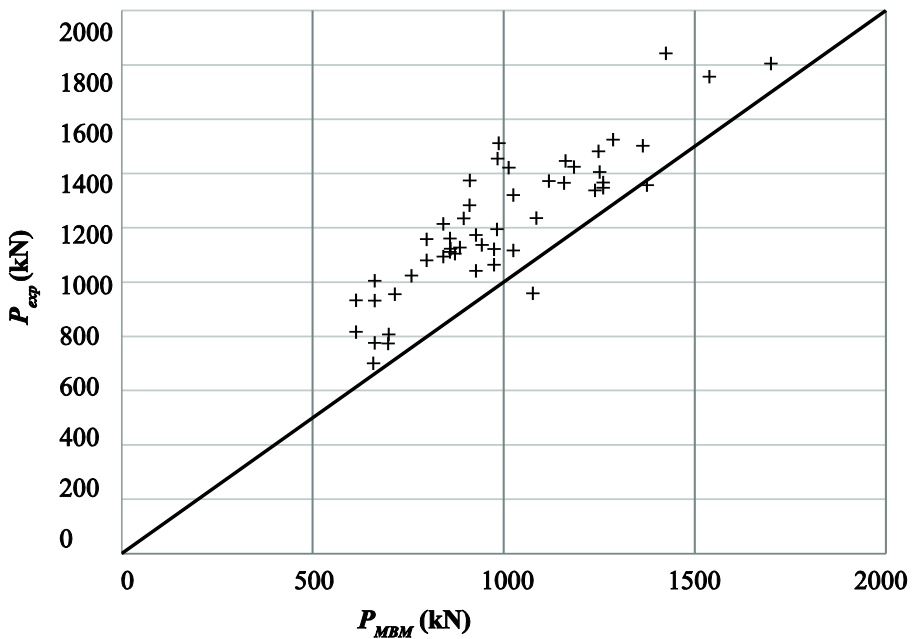


Fig. 5.23: Comparison between experimental results of S1 – S18 and the capacity according to the Modified Bond Model

<sup>26</sup> The analysis of the results of BS1 – BX3 and S19T1 – S26T5 is discussed in more detail in Chapter 6. Similar conclusions can be drawn from the results of BS1 – BX3, S19T1 – S26T5 as those given here for the experiments on S1 to S18.

### Modified Bond Model

To study the distribution of  $P_{exp}/P_{MBM}$ , as will be further dealt with in Chapter 6, this ratio is shown in a histogram in Fig. 5.24. The histogram shows that the shape of the distribution is not a normal distribution, but more a lognormal distribution. The 5% lower bound, which can be used as a measure for the characteristic strength, should not be smaller than 1 to guarantee a safe application of the proposed method. The cumulative distribution function in Fig. 5.24 shows that the 5% lower bound is about 1,06. This result means that the Modified Bond Model has sufficient inherent safety for design applications, and is sufficiently accurate to predict the capacity of one-way slabs subjected to concentrated loads within its limits of application.

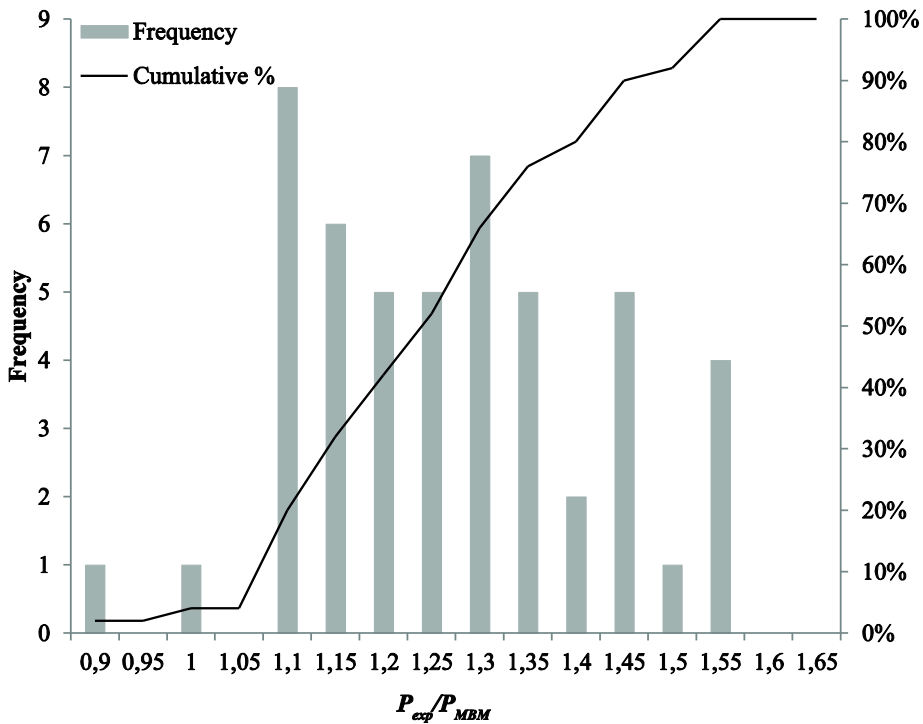


Fig. 5.24: Histogram of  $P_{exp}/P_{MBM}$ .

#### 5.4.2 Comparison with existing methods

In this section, the performance of the Modified Bond Model is compared to the performance of the shear provisions from NEN-EN 1992-1-1:2005 based on the ratio of the experimental result to the predicted value. Note that the Modified Bond Model predicts a maximum load and NEN-EN 1992-1-1:2005 a maximum sectional shear force.

For all experiments on the uncracked slabs S1 to S18, the values of the experimental sectional shear force compared to the shear capacity according to NEN-EN

### Modified Bond Model

1992-1-1:2005 are shown in Fig. 5.25. The comparison shows the resulting shear capacity using the effective width  $b_{eff1}$ , Fig. 2.16a, based on load spreading from the centre of the load to the support  $V_{R,c,eff1}$  and using the effective width  $b_{eff2}$ , Fig. 2.16b, based on load spreading from the far side of the loading plate,  $V_{R,c,eff2}$ . Using  $V_{R,c,eff2}$  is the preferable method as shown by research based on the slab shear experiments (see §4.8 and Chapter 7). The statistical properties for  $V_{exp,EC}/V_{R,c,eff2}$  are the following:

- the average value is 1,92;
- the standard deviation is 0,26; and
- the coefficient of variation is 14% .

The 45° line in Fig. 5.25 indicates experimental shear capacities that are exactly as predicted by NEN-EN 1992-1-1:2005 combined with the two load spreading assumptions resulting in  $b_{eff1}$  and  $b_{eff2}$ . For a good representation of the experimental results, the family of test results is expected to lie parallel with and above the 45° line. When using NEN-EN 1992-1-1:2005 to compare to the experimental results, however, the results show increasing conservatism with increasing shear capacities<sup>27</sup>, contrary to the results obtained with the Modified Bond Model, Fig. 5.23.

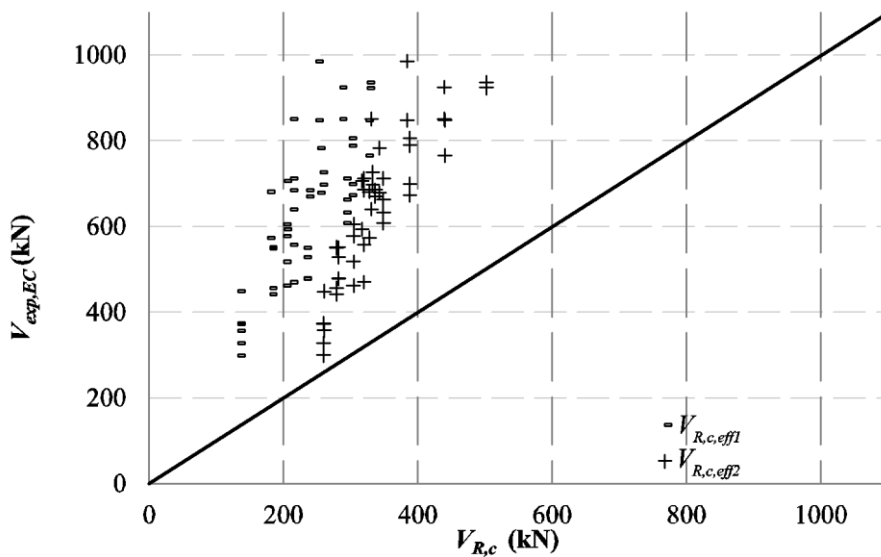


Fig. 5.25: Comparison of experiments on virgin slabs S1 to S18 with NEN-EN 1992-1-1:2005 based on the traditional load spreading method  $V_{R,c,eff1}$  and the French load spreading method  $V_{R,c,eff2}$ .

<sup>27</sup> These results might indicate that a larger angle for the load spreading method can be chosen or that an enhancement factor can be used. The development of this enhancement factor is discussed in §6.4.

**5.4.3 Verification with experiments from the literature**

To further validate the Modified Bond Model, experiments from four different series from the literature are chosen for which  $b_{load}/b < 0,2$ . The following experiments are analysed:

- from Reißen and Hegger (2011): experiments on specimens S25B, S35B, S35A and S35C;
- all experiments from Regan (1982);
- from Coin and Thonier (2007) experiments 3bis, 7 and 7bis;
- from Rombach et al. (2009) VK3V3 and VK4V3.

The comparison between these experiments and the Modified Bond Model is given in Table 5.8. The Modified Bond Model seriously overestimates the capacity of the experiments by Reißen and Hegger (2011). The assumption of yielding of the reinforcement is not valid for these experiments. The reinforcement that was used in the experiments by Reißen and Hegger (2011) is high strength steel with a yield strength  $f_{ym} = 900\text{MPa}$ . Measurements of the strain in the reinforcement show the maximum strain that is reached in the experiments from which the stress in the reinforcement at failure is determined. The steel stress  $f_s$  at failure varies between 334MPa for S35A and 594MPa for S35C. When the measured values for  $f_s$  are used instead of  $f_{ym}$ , the Modified Bond Model shows a better correspondence with the experiments, as shown for the results of the series “Reißen and Hegger (2011),  $f_s$ .” For this comparison, a better coefficient of variation is obtained. The average value of the measured to predicted capacities, is however still smaller than 1. This observation indicates that the Modified Bond Model is not suitable for slabs that are over-designed in bending.

The limitation of the Modified Bond Model to slabs in which local yielding of the reinforcement occurs before shear failure has no implications for practice, as a good slab design will not result in over-reinforced sections. Therefore, the requirement for local yielding in combination with the Modified Bond Model can be expressed as follows:

$$\rho_{tot} \frac{f_{ym}}{f_{c,mean}} < 0,135 \tag{5.38}$$

with

- $\rho_{tot}$  the total reinforcement ratio, as the geometric mean of the reinforcement in the longitudinal and transverse direction  $\rho_{tot} = \sqrt{\rho_l \rho_t}$  ;
- $f_{ym}$  the average yield strength of steel;
- $f_{c,mean}$  the mean cylinder concrete compressive strength.

This requirement is based on the experiments from Chapter 3, as it is known that the requirements for the Modified Bond Model are fulfilled in these experiments. Additional experiments and research are necessary to further refine Eq. (5.38).

The three experiments from Coin and Thonier (2007) indicate that for this case, the Modified Bond Model overestimates the capacity. However, interpreting the

### *Modified Bond Model*

reinforcement drawings of the experiments by Coin and Thonier (2007) is not a straightforward task, and therefore, the number of bars in the strips might have been overestimated, leading to an overestimation of the maximum load. Slab 7 by Coin and Thonier (2007) also does not satisfy the requirements from Eq. (5.38). The scope of the experiments by Coin and Thonier (2007) was flat slabs as used for buildings. In the experiments by Rombach et al. (2009), the slab was the central part of a double T-girder, of which the behaviour might be significantly different than of a slab bridge. The experiments on the middle parts of the double T-beams were not discussed in detail in the report by Rombach et al. (2009).

*Table 5.8: Comparison between results from the literature and the Modified Bond Model*

<b>Series</b>		<b><math>P_{exp}/P_{MBM}</math></b>
Reißen and Hegger (2011)	AVG	0,654
	STD	0,091
	COV	0,139
$f_s$ Reißen and Hegger (2011)	AVG	0,903
	STD	0,109
	COV	0,120
Regan (1982)	AVG	1,304
	STD	0,222
	COV	0,170
Coin and Thonier (2007)	AVG	0,983
	STD	0,052
	COV	0,053
Rombach et al. (2009)	AVG	1,122
	STD	0,139
	COV	0,124
All	AVG	1,122
	STD	0,249
	COV	0,222

Overall, it can be concluded that, when the assumptions of the Modified Bond Model such as yielding of the reinforcement are met, good results are obtained for the experiments from the literature. This statement can best be seen when the experiments by Regan (1982) are compared to the predicted capacity using the Modified Bond Model. The resulting values of the statistical parameters are similar to the results that are obtained when comparing the slab shear experiments from Chapter 3 to the Modified Bond Model. The average of the experimental to predicted value is slightly larger than observed in the comparison between the experiments from Chapter 3, and this observation is expected on the basis of the influence of the size effect. The size effect in shear results in relatively larger capacities for

cross-sections with a small depth and smaller capacities for cross-sections with a larger depth. The slabs tested by Regan (1982) had a depth  $h = 100$  mm while the slabs from Chapter 3 had a depth  $h = 300$  mm.

When the results that fulfil Eq. (5.38) are combined with the results of the experiments on S1 to S26, it can be found that these results all belong to the same distribution. The overall average of the ratio between the experimental load and the maximum load according to the Modified Bond Model equals 1,237 with a standard deviation of 0,164 and a coefficient of variation of 13%. The resulting histogram is shown in Fig. 5.26. When this histogram is compared to Fig. 5.24, it becomes clear that the results from the literature can be regarded as samples taken from the same distribution.

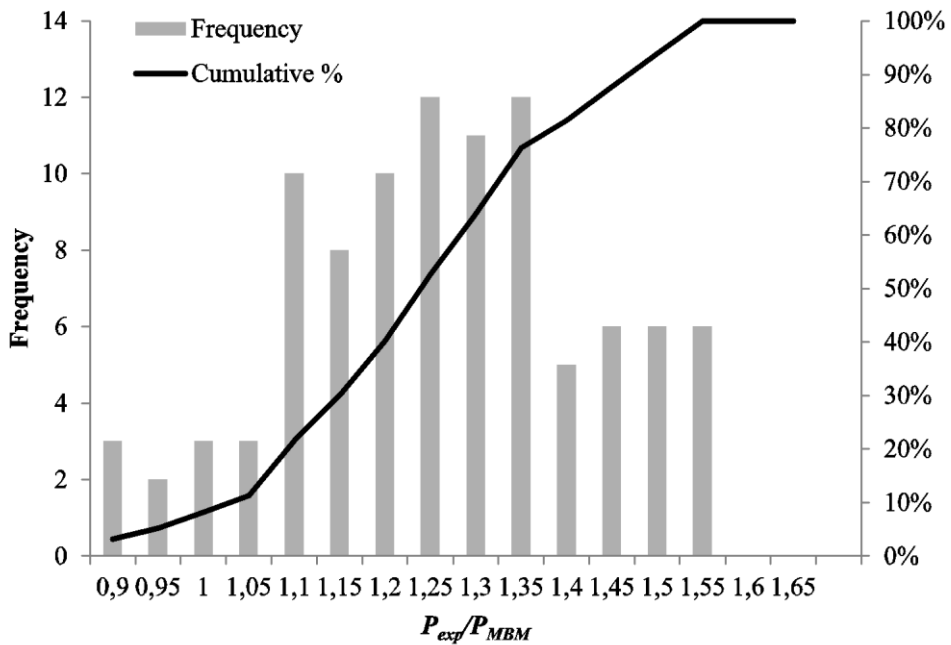


Fig. 5.26: Histogram of  $P_{exp}/P_{MBM}$  for S1 to S26 and results from the literature that fulfil the requirement from Eq. (5.38).

#### 5.4.4 Parameter analysis

The following parameters are determined from the analysis in Chapter 4 to have a large influence on the shear capacity of slabs under a concentrated load near to the support:

- the size of the loading plate,
- the moment distribution in the shear span, and
- the distance between the load and the support.

### Modified Bond Model

These parameters are also taken into account in the method according to the Modified Bond Model. In this section, attention is paid to the influence of the concrete compressive strength, the distance between the load and the support (expressed as  $a/d_l$  and  $a_v/d_l$ ) and the size of the loading plate.

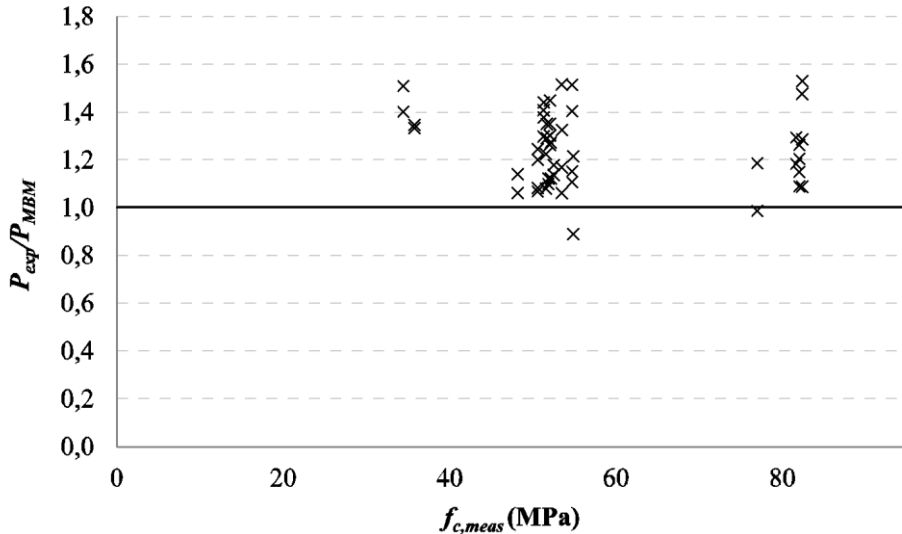


Fig. 5.27: Results of comparison  $P_{exp}/P_{MBM}$  between experiments and Modified Bond Model as a function of the measured concrete cube compressive strength,  $f_{c,meas}$

The first parameter to be discussed is the concrete compressive strength. In traditional approaches for shear and punching, the concrete compressive strength is (one of) the most important parameter(s) in the expression for the capacity. In Chapter 4 section §4.7.2, the expected dependence of the shear capacity of slabs under a concentrated load close to the support on the concrete compressive strength could not be observed from the small number of experiments that was carried out. In the Modified Bond Model, the concrete compressive strength influences the loading term  $w_{ACI}$ . The relationship between the concrete compressive strength and the capacity of the strips is to the power  $1/4$ . The influence of the concrete compressive strength in the Modified Bond Model is therefore not as pronounced as in traditional approaches that use a square or cube root relationship between the concrete compressive strength and the shear capacity. The ratio of the experimental result to the calculated capacity according to the Modified Bond Model  $P_{exp}/P_{MBM}$  is plotted as a function of the measured average cube compressive strength  $f_{c,meas}$  at the age of testing in Fig. 5.27. This figure does not show a variation of  $P_{exp}/P_{MBM}$  over the different concrete compressive strengths that were applied in the series of experiments. Therefore, it can be

concluded that the Modified Bond Model adequately takes the concrete compressive strength into account.

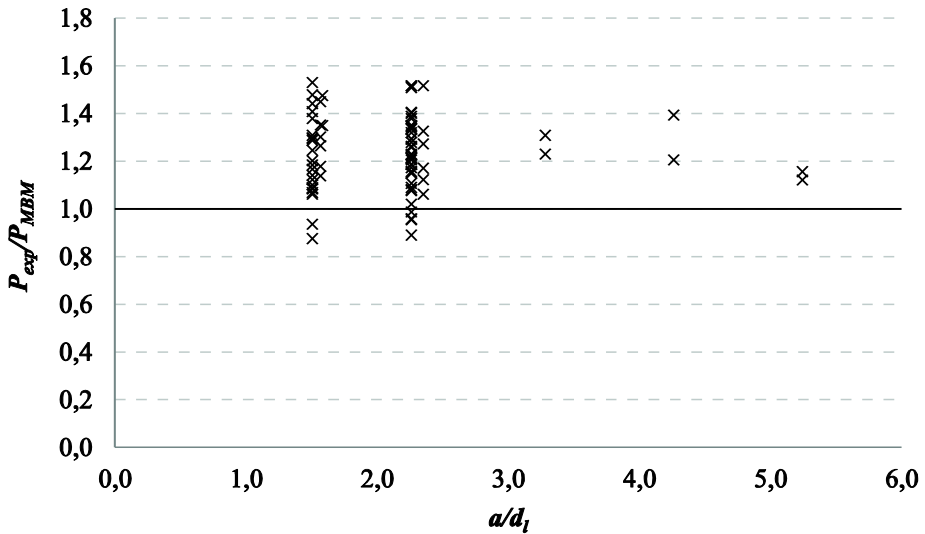


Fig. 5.28: Results of comparison between experiments on S1 to S26 and Modified Bond Model as a function of the distance between the load and the support expressed as  $a/d_l$ .

The second parameter for which the performance of the Modified Bond Model is studied, based on the experimental results, is the distance between the load and the support. In Chapter 4 section §4.6.2 the influence of the distance between the load and the support was determined as an important factor for the shear capacity of a slab under a concentrated load close to the support. In the expression for the shear capacity from NEN-EN 1992-1-1:2005, the influence of the distance between the load and the support is taken into account by reducing the contribution of loads applied within a face-to-face distance from the load  $a_v$  smaller than  $2d_l$  with a reduction factor  $\beta$ :

$$\beta = \frac{a_v}{2d_l} \text{ for } 0,5d_l \leq a_v \leq 2d_l.$$

In the Modified Bond Model, the distance between the load and the support is taken into account by increasing the capacity of the strip between the load and the support with the enhancement factor  $\zeta_{MBM}$ :

$$\zeta_{MBM} = \frac{2d_l}{a_v} \text{ for } 0,5d_l \leq a_v \leq 2d_l$$

$$\zeta_{MBM} = 4 \text{ for } a_v < 0,5d_l$$

### Modified Bond Model

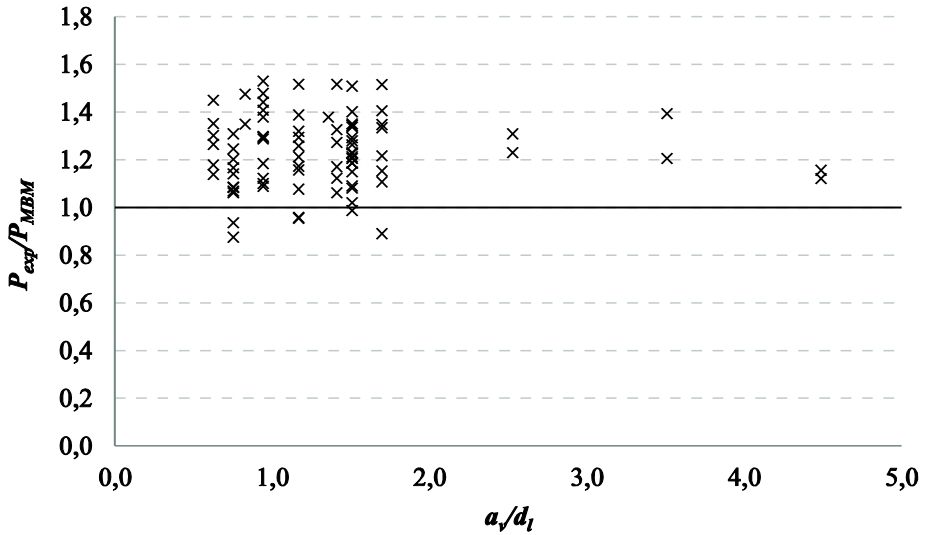


Fig. 5.29: Results of comparison between experiments on S1 to S26 and Modified Bond Model as a function of the distance between the load and the support expressed as  $a/d_t$ .

The difference between the Modified Bond Model and the approach from NEN-EN 1992-1-1:2005 is that in the Modified Bond Model the influence between the load and the support is only taken into account for the strip between the load and the support and not in all 4 strips that determine the entire capacity. Therefore, the influence of the distance between the load and the support on the capacity according to the Modified Bond Model is smaller than when using the shear expressions from NEN-EN 1992-1-1:2005. The ratio of the experimental results to the calculated capacity according to the Modified Bond Model  $P_{exp}/P_{MBM}$  is plotted as a function of the distance between the load and the support based on the centre-to-centre distance  $a$  and the face-to-face distance  $a_v$  in Fig. 5.28 and Fig. 5.29, respectively. In these figures, the results of the second series of experiments, on S19 to S26, are also given, as a few additional experiments on larger distances to the support were carried out in this series. These figures show a uniform performance of the Modified Bond Model expressed in terms of  $P_{exp}/P_{MBM}$  over the range of distances between the load and the support that were applied in the series of experiments. Note that the results of the experiments in which the load was placed at a larger distance to the support are consistently as good as the results for the experiments with the concentrated load close to the support. Therefore, it can be concluded that the Modified Bond Model adequately takes the distance between the load and the support into account.

The last important parameter is the size of the loading plate. The size of the loading plate determines the size of the punching perimeter when the punching capacity is determined according to NEN-EN 1992-1-1:2005 and determines the effective width when

## Modified Bond Model

load spreading according to French practice from the far side of the loading plate to the support,  $b_{eff2}$  (Fig. 2.16b) is used. As shown in Chapter 4, §4.2.2, the shear capacity of slabs under a concentrated load close to the support is clearly influenced by the size of the loading plate. In the Modified Bond Model, the size of the loading plate determines the width and arching capacity of the strips. The ratio of the experimental result to the calculated capacity according to the Modified Bond Model  $P_{exp}/P_{MBM}$  is plotted as a function of the size of a side  $b_{load}$  of the square loading plate in Fig. 5.30. This figure again shows similar results for  $P_{exp}/P_{MBM}$  when considering a loading plate of 200mm × 200mm or a loading plate of 300mm × 300mm. The Modified Bond Model thus takes the size of the loading plate correctly into account.

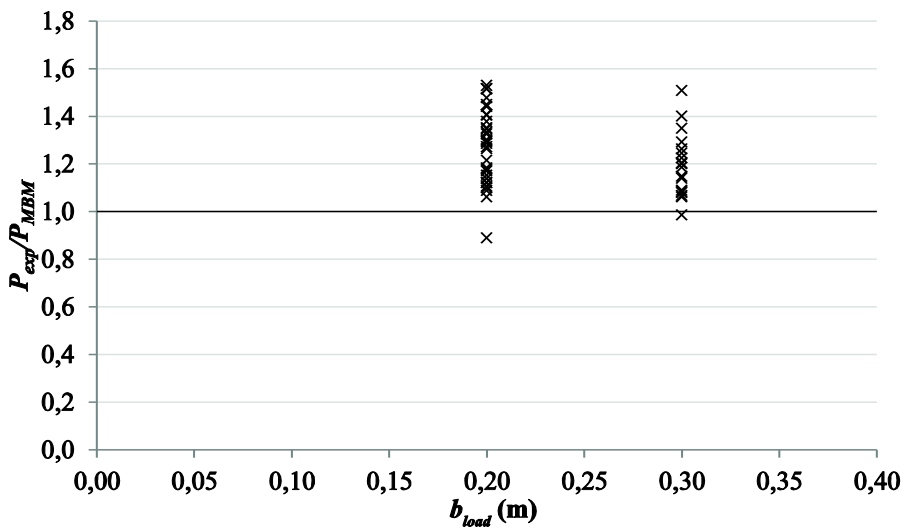


Fig. 5.30: Results of comparison between experiments and Modified Bond Model as a function of the size of the loading plate.

## 5.5 Discussion of Modified Bond Model

### 5.5.1 Discussion of scope

Afhami et al (1998) pointed out that the Bond Model provides a lower bound estimate for the shear capacity of a single radial strip, because the equilibrium and the boundary condition of the strip is satisfied, and both the flexural capacity of the strip and the shear capacity of the adjacent quadrants that load the strip are not exceeded. However, the Bond Model does not necessarily provide a lower bound estimate of the capacity of a column-slab connection. It is possible to have cases in which the strips are not all loaded to their

### *Modified Bond Model*

nominal capacities. In such cases, called non-proportional behaviour, the share of the load being applied to each strip cannot be determined solely by the equations of equilibrium. Compatibility of deformations must also be considered. Afhami et al. (1998) subsequently developed the Strip Model that takes into account the torsional moments. When relatively large negative torsion occurs along the side faces of the strips, the Bond Model (and thus Modified Bond Model) does not give a lower bound prediction. The relation between the loads transferred through a half strip in the  $x$ -direction and  $y$ -direction can be expressed based on a circle, Fig. 5.31. In Fig. 5.31a, the general case is shown, and the value of  $D$  is determined as<sup>28</sup>

$$D = \sqrt{M_{s1}w_1 + M_{s2}w_2 + 2(M_{t1}w_1 + M_{t2}w_2)} \quad (5.39)$$

with  $M_{t1}$  and  $M_{t2}$  as the torsional moments, and this can be simplified to:

$$D = \sqrt{M_{s1}w_1 + M_{s2}w_2} \quad (5.40)$$

because the overall effect of torsion is so that it always adds to the capacity of the connection. Therefore, neglecting the contribution of the torsion ( $M_{t1} + M_{t2} = 0$ , and assuming that  $w_1 \approx w_2$ ) results in a conservative estimate. The situation that is considered in Fig. 5.31b is the assumption of the (Modified) Bond Model, in which all strips are loaded to their nominal capacities. In that case, the strip capacities are determined as:

$$P_1 = P_{s1} = \sqrt{M_{s1}w_1} \text{ and } P_2 = P_{s2} = \sqrt{M_{s2}w_2} . \quad (5.41)$$

A maximum capacity is obtained, as shown in Fig. 5.31c, when  $P_1 = P_2$ . The values of  $P_1$  and  $P_2$  are then also larger than  $P_{s1}$  and  $P_{s2}$ . A minimum estimate can be found when it is assumed that one of the strips reaches its full capacity (here  $P_1$ ) and that the other strip is limited to:

$$P_2 = \frac{c_1 w_1}{2} \quad (5.42)$$

If non-proportional behaviour occurs, the capacity of the second strip  $P_2$  should be calculated according to Eq. (5.42). Based on Fig. 5.31a, the relation between  $P_1$  and  $P_2$  can be expressed as:

$$P_1^2 + P_2^2 = M_{s1}w_1 + M_{s2}w_2 \quad (5.43)$$

When the capacity of  $P_2$  is assumed as the minimum capacity, the value for the capacity of the other strip  $P_1$  can be determined.

---

<sup>28</sup> In the notations of Afhami et al. (1998),  $x$ -direction and  $y$ -direction are replaced by directions 1 and 2. This choice is preserved here.

Modified Bond Model

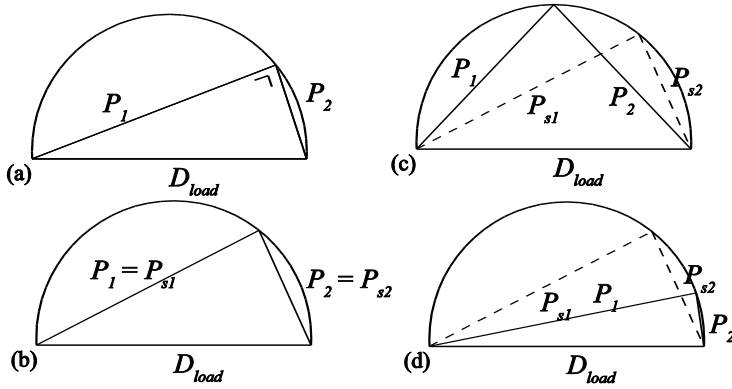


Fig. 5.31: Relation between loads transferred through each half strip: (a) general case; (b) the Bond Model; (c) maximum estimate; (d) minimum estimate, based on Afhami et al. (1998).

The analysis by Afhami et al. (1998) determined for which cases non-proportional behaviour occurs. If the capacity of both strips is the same, the Bond Model and the maximum estimate in the Strip Model are the same. Afhami et al. (1998) expressed the bounds for non-proportional behaviour by studying the following two non-dimensional constants:

$$K_1 = \frac{M_{s2}w_2}{M_{s1}w_1} = \left( \frac{P_{s2}}{P_{s1}} \right)^2 \quad (5.44)$$

$$K_2 = \frac{c_1w_1}{2\sqrt{M_{s1}w_1}} = \frac{c_1w_1}{2P_{s1}} \quad (5.45)$$

According to Afhami et al. (1998), if the capacity of both strips is the same ( $K_1 = 1$ ), the Bond Model and the Strip Model give equal results. When the behaviour is non-proportional, the capacity of the connection may be overestimated by the Bond Model by 25%. Using the subset from Table 5.1, it is found that the value of  $K_1$  ranges between 1/8 and 1/4 and for  $K_2$  the value equals  $K_2 = 1/10$ . For this case, the Bond Model is expected to overestimate the capacity by more than 15%. However, the results in Table 5.1 indicate that the (Modified) Bond Model leads to safe results for these cases. Therefore, the modifications of the Modified Bond Model seem to cover non-proportionality within the scope of the studied experiments.

The size effect is currently taken into account through  $k_{MBM}$  which is used to expand the expression for  $w_{ACI}$ . However, experimental results to quantify the size effect on slabs in shear under concentrated loads close to supports are not available, and the factor equals  $k_{MBM} = 1$  for all studied experiments.

Following the ideas of the Bond Model, the cruciform failure surface is to replace the critical perimeter that is typically used to determine the punching capacity. While the

### *Modified Bond Model*

punching perimeter more closely resembles the punching cone that is observed in experiments, the use of strips enables the incorporation of arching action into a punching and shear model. The importance of arching action was measured by Alexander (1990) in punching experiments.

For cases of slabs that are beyond the scope of the Modified Bond Model, it is recommended to use the recommendations from NEN-EN 1992-1-1:2005 or *fib* Model Code 2012. In Chapter 6, an additional code extension proposal is provided for all cases of slabs subjected to concentrated loads close to supports.

#### *5.5.2 Advantages of the Modified Bond Model*

The results in §5.4 have shown the improvement that results from the Modified Bond Model as compared to NEN-EN 1992-1-1:2005 to determine the shear capacity of slabs under concentrated loads close to supports. The improvement can be seen from comparing Fig. 5.23 to Fig. 5.25, from the statistical properties of  $P_{exp}/P_{MBM}$  as compared to those of  $V_{exp}/V_{R,c,eff2}$  and from the consistently good performance of the Modified Bond Model as a function of the studied range of the concrete compressive strength, the distance between the load and the support and the two tested loading plate sizes.

As the width of the strips depends on the size of the loading plate, the influence of this important parameter is taken into account in the Modified Bond Model. The Modified Bond Model correctly reflects the influence of the concrete compressive strength, which was experimentally found to have a small influence on the shear capacity of slabs under concentrated loads. The influence of the distance between the load and the support is taken into account by increasing the capacity of the strip between the load and the support,  $P_{MBM,sup}$ , as a function of  $a\sqrt{2}d_l$  which again leads to uniform results over the range of values of  $a/d_l$  or  $a\sqrt{2}d_l$  that are tested.

Another advantage of the proposed model is that it shows the essential link between one-way and two-way shear for the case of a slab under a concentrated load in shear, by using strips and quadrants. While the quadrants work in two-way shear, this behaviour is in fact considered as two directions of one-way shear. The elements of one-way shear (beam shear and arching action) are then used to construct the model. Therefore, the two-way shear-carrying behaviour is split up into its essential one-way shear components.

The Modified Bond Model with strips and quadrants is suitable for a large number of different geometries. The strips and the quadrants used in the Modified Bond Model can be sketched when the loading situation is known, and the geometry in the quadrants is taken into account to determine the capacity of the strips. This procedure is thus easy to adapt to different geometric situations. This mechanical method allows for a range of solutions depending on the geometry of the problem and is easily used for the determination of the maximum load. The geometry of the slab, the load and the support were found to be the most important parameters to determine the one-way shear capacity of slabs subjected to

### *Modified Bond Model*

concentrated loads. Therefore, it should be emphasized that the ability of the Modified Bond Model to incorporate a vast variety of different geometries is one of the major strengths of the method.

An additional advantage of the Modified Bond Model is that it can be used for hand calculations. Where the punching capacity according to NEN-EN 1992-1-1:2005 requires the use of nonlinear finite element analysis to determine the eccentricity of the load, or the use of oversimplified factors, the Modified Bond Model takes the influence of the geometry easily into account by using the reduction factors in the determination of the capacity of the strips.

The comparison to the experimental results shows that the Modified Bond Model is sufficiently accurate to determine the shear capacity of a one-way slab subjected to a concentrated load. Because the 5% lower bound of the ratio between the experimental result and the predicted capacity is larger than 1, the Modified Bond Model also results in safe estimates.

#### *5.5.3 Limitations of the Modified Bond Model*

Currently, empiricism is involved in the model with respect to two aspects:

1. the choice of the loading term as originally used by Alexander and Simmonds (1992),  $w_{ACI}$ , could be seen as a more empirical decision, which however leads to better results than other expressions for the one-way shear capacity or bond capacity; and,
2. the reduction factor of 0,8 to be used on  $w_{ACI}$  for plain bars is empirical as well.

It should be noted however that all current codes have levels of empiricism involved in their expressions for the shear capacity. The most important parameters are related to the geometry of the slab and the load, and these parameters are fully modelled by the Modified Bond Model.

The reduction factor 0,8 for plain bars has a physical background, as beam action and arching action are in reality interdependent mechanisms for shear transfer. In the Modified Bond Model, the distinction is made by subdividing the slab into quadrants and strips. It is known that elements reinforced with plain bars carry shear in arching action. In slabs with plain bars, the capacity for beam action shear is almost fully lost because of the lack of bond transfer between the concrete and the reinforcement. More of the capacity thus needs to be carried by arching action. In the Modified Bond Model, this behaviour is covered by reducing the contribution from beam action shear.

A comparison with experiments from the literature shows that the Modified Bond Model is valid when the assumptions of the model are met. When the stress in the steel is only a fraction of the yield stress of the steel, the Modified Bond Model will overestimate the maximum load that can be carried by the slab. Local yielding of the reinforcement is necessary to activate the mechanism that is assumed in the Modified Bond Model. For

### *Modified Bond Model*

practice, this requirement does not have significant implications, as slab designs will not result in over-reinforced sections. Sections are designed so that robustness and safety are guaranteed in practice, which typically results in designs that will show significant flexural distress before a brittle failure mode, such as shear or punching shear, can occur. The Modified Bond Model does not cover slabs that fail prematurely in punching before local yielding of the reinforcing steel can occur. When comparing to experiments however, test slabs can be over-reinforced for flexure to ensure a shear failure in the experiment. Therefore, a limitation is formulated on the mechanical reinforcement ratio. The mechanical reinforcement ratio needs to fulfil the following requirement:

$$\rho_{tot} \frac{f_{ym}}{f_{c,mean}} < 0,135 .$$

For the experiments from Chapter 3, it was shown in finite element models that indeed local yielding was achieved at the location of the concentrated load at failure (Falbr, 2011; Doorgeest, 2012).

Another assumption used in the Modified Bond Model is that the reinforcement is distributed over the slab, so that the reinforcement ratio in the strips corresponds to the reinforcement ratio in the considered quadrants. For slab bridges, this condition is always met, as the location of the wheel load is variable. However, for the application to punching of slab-column connections, the (Modified) Bond Model will overestimate the capacity when the reinforcement is concentrated over the column. The reinforcement ratio in the considered strips then becomes too high. Regan and Braestrup (1985) showed that rearrangement of the reinforcement to a pattern involving concentration is not beneficial, as excessive banding leaves larger radial sectors almost unreinforced. As these results are known from the literature, and the scope of this research is slab bridges subjected to wheel loads, this limitation is not considered a constraint on the application of the Modified Bond Model.

As the equilibrium is studied on the interface between the two-way quadrants and the one-way strips, the structural behaviour of the parts of the slab outside of the cross-shaped region have no influence on defining the critical case for determining the maximum concentrated load. The actions that are considered on the free-body diagram of half a strip as shown in Fig. 5.10 imply that the actions are similar along the interfaces for the different considered slab strips. In reality, the shear will be higher for the strip close to the support. Also, the assumed lines of zero shear as shown in Fig. 5.8 do not completely correspond for the case of concentric punching shear as compared to the case of a concentrated load on a one-way slab. However, the use of the described factors that take into account the effects of the geometry of the slab, load and the support compensate for this discrepancy.

The Modified Bond Model follows the approach of a method to determine the maximum punching capacity. As a result, a maximum load is found. For the application to slab bridges under composite dead load and live loads, a limiting shear stress should be

used to assess the shear capacity. A combination of loads can also be studied by using the Modified Bond Model, as demonstrated in §5.3.7. For assessment purposes, the Modified Bond Model could thus be used to determine the maximum truck load that can be applied on a bridge, when all other loads are considered according to the code. This approach is however not as straight-forward as a shear check at the support.

## **5.6 Conclusions**

A model for the shear capacity of reinforced concrete slabs under concentrated loads close to supports is proposed: the Modified Bond Model. Direct transfer of the load between its point of application and the support through a compressive strut or arching action is determined as an important shear-carrying mechanism for the situation under study. Studying direct load transfer resulted in adapting the Bond Model by Alexander and Simmonds (1992) for concentric punching shear so that it is applicable to rectangular slabs with different amounts of reinforcement in the  $x$ - and  $y$ -direction and with the concentrated load close to the support. The Modified Bond Model is also applicable for loads near to the edge, near to a continuous support, for slabs with plain bars and for slabs not supported over their entire width.

This chapter showed in detail how the Modified Bond Model is constructed to be applicable to a wide range of loading situations. The experimental results are used to show the influence of the proposed approach on the Modified Bond Model. To conclude, an overview of the improvements from the Bond Model by Alexander and Simmonds (1992) to the proposed Modified Bond Model is listed, and a step-by-step guide is given of the actions that should be followed to determine the shear capacity according to the Modified Bond Model. The experiments on slabs under a concentrated load only from the second series of experiments (S19 – S26) are used to verify the method, indicating excellent agreement between the experimental results and the maximum loads predicted by the Modified Bond Model. Furthermore, the method is extended to take into account additional loads that occur, by studying the experiments on S19 to S26 under a combination of loads.

The improvement of the calculated punching shear capacity according to the Modified Bond Model to determine the maximum load on the slab as compared to the calculated shear capacity according to NEN-EN 1992-1-1:2005 to determine the maximum sectional shear is shown graphically, based on statistical properties and by studying the performance of the Modified Bond Model over the range of the tested parameters. In all cases it is clear that, within its limitations, the Modified Bond Model results in an improved determination of the shear capacity of slabs under concentrated loads.

## **6 Statistical Evaluation of Design Methods**

### **6.1 Introduction**

This chapter compares the experimental results with the results of the design methods, and aims at determining the safety associated with using the design methods for the determination of the shear capacity of a slab under concentrated loads close to supports. In section 6.2 “Comparison to design methods”, the comparison is based on a traditional statistical analysis based on the assumption of a normal distribution, by evaluating the mean, standard deviation and coefficient of variation of the ratio between the experimental and predicted shear capacity. The characteristic value, or 5% lower bound, is then determined as the average value minus 1,64 times the standard deviation of this ratio. The design methods under study are the shear and punching provisions from NEN-EN 1992-1-1:2005, NEN 6720:1995, ACI 318-08, Regan’s method (Regan, 1982) and the Modified Bond Model.

Next, the parameters studied in Chapter 4 are revisited to analyse if the way in which these parameters are included in the design methods corresponds to the experimental observations. The differences between the beam shear provisions and the observations from the experiments are discussed.

Finally, a code extension proposal for the code currently used in the Netherlands NEN-EN 1992-1-1:2005 is developed based on requirements with regard to the failure probability. For existing structures, the required reliability index  $\beta_{rel}$  for the repair level (NEN 8700:2011), as used for the assessment of existing structures, is determined as 3,8 (and 3,6 for bridges built before April 1<sup>st</sup> 2012). Other load levels and requirements are discussed in Chapter 7. The code extension proposal comprises the enhancement of the shear capacity of slabs subjected to concentrated loads close to supports. The enhancement factor is expressed as a function of the concrete compressive strength as observed in the experiments. The proposal also includes a method to reduce the effective width when the support length is smaller than the full slab width.

### **6.2 Comparison to design methods**

#### **6.2.1 Comparison between experimental results and design methods**

In this section, the results of the experiments are compared to relevant design methods for one-way shear. The following methods are analysed: NEN-EN 1992-1-1:2005 with  $b_{eff1}$  (Fig. 2.16a), NEN-EN 1992-1-1:2005 with  $b_{eff2}$  (Fig. 2.16b), NEN 6720:1995, ACI 318-08, Regan’s method (Regan, 1982) and the Modified Bond Model. The results of the comparison between the experimental values and the predictions from NEN-EN 1992-1-1:2005 are emphasized, as this design method is used for the recommendations for

concentrated loads on slab bridges as discussed in Chapter 7. The predictions according to NEN-EN 1992-1-1:2005 are based on the following assumptions:

- The contribution of loads close to supports with  $0,5d_l \leq a_v \leq 2d_l$  to the shear force at the support can be reduced by  $\beta = a_v/2d_l$ ;
- Mean material properties are used;
- All partial factors are equal to 1,0 for the comparison to the experiments;
- $C_{Rd,c,test} = 0,15^{29}$  for comparison with experimental results (Regan, 1987).

The expression for the shear capacity is given in Eq. (2.8), in which  $b_w$  is replaced with the effective width, either  $b_{eff1}$  or  $b_{eff2}$ . The contribution of loads close to supports to the shear force at the support is reduced with  $\beta$ , resulting in the reduced sectional shear  $V_{exp,EC}$ . For the considered experiments, the contribution of the concentrated load is reduced, and, depending on the size of the support, the contribution of the force due to the prestressing bars.

Additionally, a comparison to the punching shear provisions from NEN-EN 1992-1-1:2005 is given, based on the following assumptions:

- The distance to the perimeter is taken as  $a_v$ , according to NEN-EN 1992-1-1:2005 §6.4.4, provided that  $0,5d_l \leq a_v \leq 2d_l$ ;
- Mean material properties are used;
- All partial factors are equal to 1,0 for the comparison to the experiments;
- $C_{Rd,c,test} = 0,18$  is used as prescribed by the code, this value corresponds reasonably well with experiments (Walraven, 2002);
- The punching capacity  $v_{pu}$  is determined based on NEN-EN 1992-1-1:2005 §6.4.4.(2) Eq. (6.50):

$$v_{pu} = 0,18k(100\rho f_{ck})^{1/3} \times \frac{2d}{a_v} \text{ with } \rho = \sqrt{\rho_l \rho_t} \quad (6.1)$$

with  $f_{ck}$  in [MPa] and  $v_{pu}$  in [MPa];

- The minimum perimeter length for a perimeter with four sides, three sides (and a free edge) and two sides (for the slab strips with a small width) is determined;
- Only the concentrated load is regarded; self-weight and clamping force of the prestressing bars are not taken into account;
- For eccentric loading, the value of  $v_E$  is determined based on NEN-EN 1992-1-1:2005 §6.4.4.(2) Eq. (6.51):

---

<sup>29</sup> As pointed out by Yang and Den Uijl (2012), König and Fischer (1995) used a more balanced database to calibrate the equation for the shear formula, and the resulting mean value of the shear capacity predicted by Regan's formula is about 0,92 of the experimental data. For more accurate predictions based on the König and Fischer (1995) database,  $C_{Rd,c,test}$  should be  $0,15/0,92 = 0,163$ . However, Yang (2012) found the calibration factor to be  $C_{Rd,c,test} = 0,144$  for shear experiments on continuous beams as carried out in the Stevin Laboratory. Regan (1987) suggested  $C_{Rd,c,test} = 0,135$  and noted that the proposed expression (with  $C_{Rd,c,test} = 0,15$ ) was much more accurate than previous code provisions. Therefore, the value of  $C_{Rd,c,test}$  is taken as 0,15 for the current comparison.

$$v_E = \frac{P}{ud} \left( 1 + k_{pu} e_{pu} \frac{u}{W} \right) \quad (6.2)$$

and the perimeter  $u$  is based on the distance  $a_v$ .

- The value of  $k_{pu}$  equals 0,6 as  $b_{load} = l_{load}$ ;
- The eccentricity ratio  $e_{pu}$  from NEN-EN 1992-1-1:2005 §6.4.4.(2) Eq. (6.51) is determined by the eccentricity between the centre of the load and the centre of gravity of the area within the perimeter<sup>30</sup>;
- The value of  $W$  is based on NEN-EN 1992-1-1:2005 §6.4.3.(3) Eq. (6.41) for a rectangular column, in which the original distance to the perimeter  $2d$  is replaced by the reduced distance  $a_v$ :

$$W = \frac{l_{load}^2}{2} + l_{load} b_{load} + 2b_{load} a_v + 4a_v^2 + \pi a_v l_{load} \quad (6.3)$$

The predictions according to previous Dutch Code NEN 6720:1995 are based on the following assumptions:

- Mean material properties are used;
- All partial factors are taken equal to 1,0;
- The effective width resulting from load spreading from the centre of the load towards the face of the support,  $b_{eff}$  (Fig. 2.16a) is used as this method is typically used in Dutch practice;
- The moments and shear forces at failure in the experiment are used to determine  $k_\lambda$ , in which  $k_\lambda$  is the factor that takes direct load transfer at the simple support into account;
- At the continuous support,  $k_\lambda = 1$ ;
- The long-term tensile strength is used, as prescribed by NEN 6720:1995 and further explained in CUR 94-13 (1994);
- The cube concrete compressive strength is limited to 65MPa, as prescribed by CUR 97 (2004).

The shear capacity according to NEN 6720:1995,  $V_{VBC}$  is determined based on the governing shear stress  $\tau_{VBC}$  for a section without shear reinforcement.

$$\tau_{VBC} = 0,4 f_b k_\lambda k_h \sqrt[3]{\rho_l} \geq 0,4 f_b \quad (6.4)$$

with

$$f_b \quad \text{the concrete tensile strength defined as } f_b = 1,4 \times 0,7 \left( 1,05 + 0,05 f_{c,meas} \right) \quad (6.5)$$

with  $f_{c,meas}$  in [MPa] and  $f_b$  in [MPa].

$k_\lambda$  the enhancement factor for direct load transfer, only applied at the simple support, defined as

---

<sup>30</sup> This approach is an approximation. To determine the true eccentricity, it is necessary to carry out a nonlinear finite element analysis.

$$k_{\lambda} = \frac{12}{g_{\lambda}} \sqrt[3]{\frac{A_0}{bd_l}} \geq 1 \quad (6.6)$$

for corbels and members at end supports where a compression strut develops between the load and the support

$g_{\lambda}$  factor for determining  $k_{\lambda}$ :

$$g_{\lambda} = 1 + \lambda_v^2 \text{ if } \lambda_v \geq 0,6; \quad \text{with } \lambda_v = \frac{M_{span}}{d_l V_{exp}}$$

$$g_{\lambda} = 2,5 - 3\lambda_v \text{ if } \lambda_v < 0,6.$$

$A_0$  is the smallest value of the area of the load or support, not exceeding  $bd_l$

$k_h$  is the size effect factor  $k_h = 1,6 - h \geq 1,0$  ( $h$  in [m]);

The shear capacity according to NEN 6720:1995 is then defined as:

$$V_{VBC} = \tau_{VBC} b_{eff1} d_l \quad (6.7)$$

For the predicted values based on ACI 318-08, the following assumptions are used:

- Mean material properties are used;
- The full formula from §11.2.2.1 Eq. 11-5 is used;
- All partial factors are taken equal to 1,0;
- The effective width based on load spreading from the centre of the load towards the support,  $b_{eff1}$  (Fig. 2.16b) is used;
- The moments and sectional shear forces at failure in the experiment are used to determine  $V_{exp}$  and  $M_{span}$ .

The shear capacity from ACI 318-08 is given for normal weight concrete as:

$$V_{ACI} = \left( 0,16\sqrt{0,82f_{c,meas}} + 17\rho_l \frac{V_{exp}d_l}{M_{span}} \right) b_{eff1}d_l \leq 0,29\sqrt{0,82f_{c,meas}} b_{eff1}d_l \quad (6.8)$$

with  $f_{c,meas}$  in [MPa],  $b_{eff1}$  in [m],  $d_l$  in [mm] and  $V_{ACI}$  in [kN].

The maximum concentrated load according to Regan's method (Regan, 1982) (§2.4.2) is determined from the expressions from Eq. (2.3) and Eq. (2.6) and is based on the following assumptions:

- Mean material properties are used;
- All partial factors are taken equal to 1,0;
- For loads near to the edge, three sides of the perimeter can be used and for loads on specimens with a small width, two sides of the perimeter can be used, Fig. 6.1;
- To determine the enhancement factor  $\alpha_{Regan}$ , which increases the capacity at the continuous support, the moments at failure from the experiment are used;
- As Regan's method determines the magnitude of the point load, the influence of the self-weight is not taken into account for this method;
- The force due to the prestressing bars is only taken into account at the continuous support by  $\alpha_{Regan}$ ;

- The maximum load in Regan's method is determined for a single concentrated load on a slab – this method is therefore not applied to the case of a combination of loads on a slab.

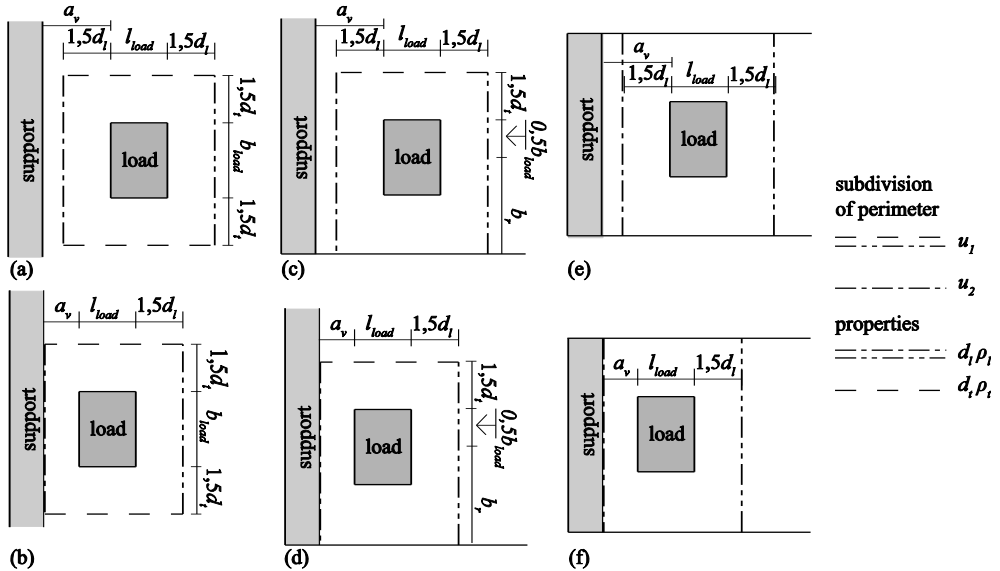


Fig. 6.1: Definition of the perimeter in Regan's method: (a, b) four sides of the perimeter for the load in the middle of the width; (c, d) three sides of the perimeter for the load near the edge; (e, f) two sides of the perimeter for specimens with a small width.

The maximum concentrated load according to the Modified Bond Model is based on the following set of assumptions:

- Mean material properties are used;
- The procedure as described in Chapter 5 §5.3.6 is used.
- The strips to a remote end are only taken into account if their length can be at least 200mm. This requirement does not hold for the strip between the load and the support, as this strip is an essential load-bearing path for the transfer of load between its point of application and the support.
- To determine the factor  $k_r$  for the contribution of the top reinforcement, the moments at failure in the experiment  $M_{span}$  and  $M_{sup}$  are used;
- As the Modified Bond Model determines the magnitude of the point load, the influence of the self-weight is not taken into account for this method;
- The force due to the prestressing bars is only taken into account at the continuous support by  $k_r$ ;

- The maximum load in the Modified Bond Model is determined for a single concentrated load on a slab. An extension for the application to the case of slabs under a combination of loads is however available in §5.3.7.

In Annex 3, the results of the calculations for the considered methods are given for every single experiment. An overview of the results of the first series of experiments is given in Table 6.1 and of the second series of experiments in Table 6.2, in which different subsets of the experimental results are considered. The considered subsets are all taken from experiments on an undamaged specimen. The following subsets are given:

- S1 – S18: all experiments on the slabs from the first series of experiments;
- S1 – S6: all experiments on the slabs supported by line supports, with normal strength concrete and with deformed bars (reference subset);
- S7 – S10: all experiments on the slabs with high strength concrete;
- S11 – S14: all experiments on the slabs with plain bars;
- S15 – S18: all experiments on the slabs supported by elastomeric bearings;
- BS1 – BX3: all experiments on the slab strips ( $b \leq 2\text{m}$ );
- S19 – S26, all: all experiments from the second series, including reference tests and experiments with the concentrated load at a larger  $a/d_i$ ;
- S19 – S26, combi: experiments from the second series in which the slab is subjected to a line load and a concentrated load.

The comparisons in Table 6.1 and Table 6.2 are based on a traditional statistical analysis assuming normal distributions. For all subsets, the following values are determined:

- AVG: the average value of the ratio between the experimental and predicted value;
- STD: the associated standard deviation;
- COV: the coefficient of variation =  $\text{STD}/\text{AVG}$ ;
- Char: the characteristic value, the 5% lower bound value assuming a normal distribution for which it holds that  $\text{Char} = \text{AVG} - 1,64 \times \text{STD}$ . As this expression does not take into account the sometimes limited number of experiments under consideration, it would be more appropriate to consider “Char” as a best estimate for the characteristic value.

The results in Table 6.1 and Table 6.2 summarize the findings from the full analysis reports (Lantsoght, 2012a; 2012d), with regard to the comparison between the experiments and the design methods. The summary is based on the following parameters:

$V_{exp,EC}$	the shear force at the support, resulting from the concentrated load, self-weight, force in the prestressing bars, for which the loads close to the support are reduced by $\beta = a_i/\sqrt{2}d_i$ ;
$V_{R,c,beff1}$	the shear capacity determined based on the combination of NEN-EN 1992-1-1:2005 and $b_{eff1}$ (Fig. 2.16a);
$V_{R,c,beff2}$	the shear capacity determined based on the combination of NEN-EN 1992-1-1:2005 and $b_{eff2}$ (ref Fig. 2.16b);

### Statistical Evaluation of Design Methods

$v_E$	the shear stress over the punching perimeter from NEN-EN 1992-1-1:2005;
$v_{pu}$	the punching shear capacity as defined in NEN-EN 1992-1-1:2005;
$V_{exp}$	the shear force at the support, resulting from the concentrated load, self-weight, force in the prestressing bars;
$V_{VBC}$	the shear capacity determined based on NEN 6720:1995 and $b_{eff1}$ (Fig. 2.16a);
$V_{ACI}$	the shear capacity determined based on ACI 318-08 and $b_{eff1}$ (Fig. 2.16a);
$V_{calc}$	the calculated shear capacity (in Fig. 6.4);
$P_{exp}$	the maximum concentrated load;
$P_{Regan}$	the maximum load determined based on Regan's method;
$P_{MBM}$	the maximum load determined based on the Modified Bond Model;
$\tau_{exp,EC,b_{eff1}}$	the shear stress at the support, resulting from shear stress due to the concentrated load distributed over $b_{eff1}$ , superposed to the shear stress due to the self-weight, force in the prestressing bars, line load and self-weight of the line load distributed over the full width $b$ , in which the contribution of loads close to the support is reduced by $\beta = a\sqrt{2d_i}$ ;
$\tau_{exp,EC,b_{eff2}}$	the shear stress at the support, resulting from shear stress due to the concentrated load distributed over $b_{eff2}$ , superposed to the shear stress due to the self-weight, force in the prestressing bars, line load and self-weight of the line load distributed over the full width $b$ , in which the contribution of loads close to the support is reduced by $\beta = a\sqrt{2d_i}$ ;
$v_{R,c}$	the shear capacity determined based on NEN-EN 1992-1-1:2005;
$\tau_{exp,b_{eff1}}$	the shear stress at the support, resulting from the shear stress due to the concentrated load distributed over $b_{eff1}$ , superposed to the shear stress due to the self-weight, force in the prestressing bars, line load and self-weight of the line load distributed over the full width $b$ ;
$\tau_{VBC}$	the shear capacity determined based on NEN 6720:1995;
$\tau_{ACI}$	the shear capacity determined based on ACI 318-08;
$\tau_{calc}$	the calculated shear capacity (in Fig. 6.4).

The results are also presented graphically in Fig. 6.2, Fig. 6.3, Fig. 6.4, Fig. 6.5 and Fig. 6.6.

Table 6.1: Comparison between experimental results of first series and predictions from design methods.

Series		$V_{exp,EC}/V_{R,c,beffI}$	$V_{exp,EC}/V_{R,c,beff2}$	$v_p/v_{pu}$	$V_{exp}/V_{VBC}$	$V_{exp}/V_{ACI}$	$P_{exp}/P_{Regen}$	$P_{exp}/P_{MBM}$
<b>S1 – S18</b>	AVG	2,793	1,874	1,138	2,886	2,710	0,968	1,245
	STD	0,480	0,292	0,237	1,426	1,091	0,182	0,151
	COV	0,172	0,156	0,208	0,494	0,403	0,188	0,121
	Char	2,005	1,396	0,749	0,547	0,920	0,669	0,998
<b>S1 – S6</b>	AVG	3,087	2,023	1,325	3,295	2,954	1,144	1,238
	STD	0,443	0,259	0,182	1,714	1,077	0,134	0,140
	COV	0,144	0,128	0,137	0,520	0,364	0,117	0,113
	Char	2,360	1,598	1,026	0,484	1,188	0,924	1,008
<b>S7 – S10</b>	AVG	2,851	1,951	1,240	2,831	2,339	1,012	1,228
	STD	0,520	0,283	0,135	1,491	0,823	0,074	0,156
	COV	0,182	0,145	0,109	0,527	0,352	0,074	0,127
	Char	1,999	1,486	1,019	0,385	0,989	0,890	0,971
<b>S11 – S14</b>	AVG	2,600	1,863	1,131	2,576	2,468	0,923	1,252
	STD	0,411	0,182	0,137	1,259	0,998	0,136	0,184
	COV	0,158	0,098	0,121	0,489	0,404	0,147	0,147
	Char	1,926	1,565	0,907	0,512	0,831	0,700	0,950
<b>S15 – S18</b>	AVG	2,585	1,634	0,823	2,775	3,038	0,762	1,262
	STD	0,393	0,298	0,099	1,202	1,362	0,111	0,136
	COV	0,152	0,182	0,120	0,433	0,448	0,146	0,108
	Char	1,940	1,146	0,661	0,803	0,805	0,579	1,038

Table 6.2: Comparison between experimental results of second series and predictions from design methods.

Series	$V_{exp,RC} / N_{R,c,eff1}$	$V_{exp,RC} / N_{R,c,eff2}$	$v/v_{ps}$	$V_{exp} / N_{VBC}$	$V_{exp} / N_{ACI}$	$P_{exp} / P_{MBM}$	$P_{exp} / P_{RC}$
AVG	2,463	1,950	1,158	2,344	1,807	0,968	0,902
STD	0,636	0,418	0,206	1,299	0,812	0,122	0,257
COV	0,258	0,215	0,178	0,554	0,449	0,126	0,285
Char	1,420	1,264	0,819	0,215	0,476	0,768	0,480

Series	$\tau_{exp,RC,eff1} / v_{R,c}$	$\tau_{exp,RC,eff2} / v_{R,c}$	$\tau_{exp,eff1} / \tau_{VBC}$	$\tau_{exp,eff1} / \tau_{ACI}$	$P_{exp} / P_{MBM}$
AVG	2,574	1,926	2,157	2,924	1,215
STD	0,361	0,252	0,852	0,796	0,156
COV	0,140	0,131	0,395	0,272	0,129
Char	1,983	1,513	0,760	1,618	0,958
AVG	2,674	2,021	2,326	3,136	1,211
STD	0,289	0,176	0,832	0,650	0,178
COV	0,108	0,087	0,358	0,207	0,147
Char	2,200	1,733	0,962	2,069	0,920

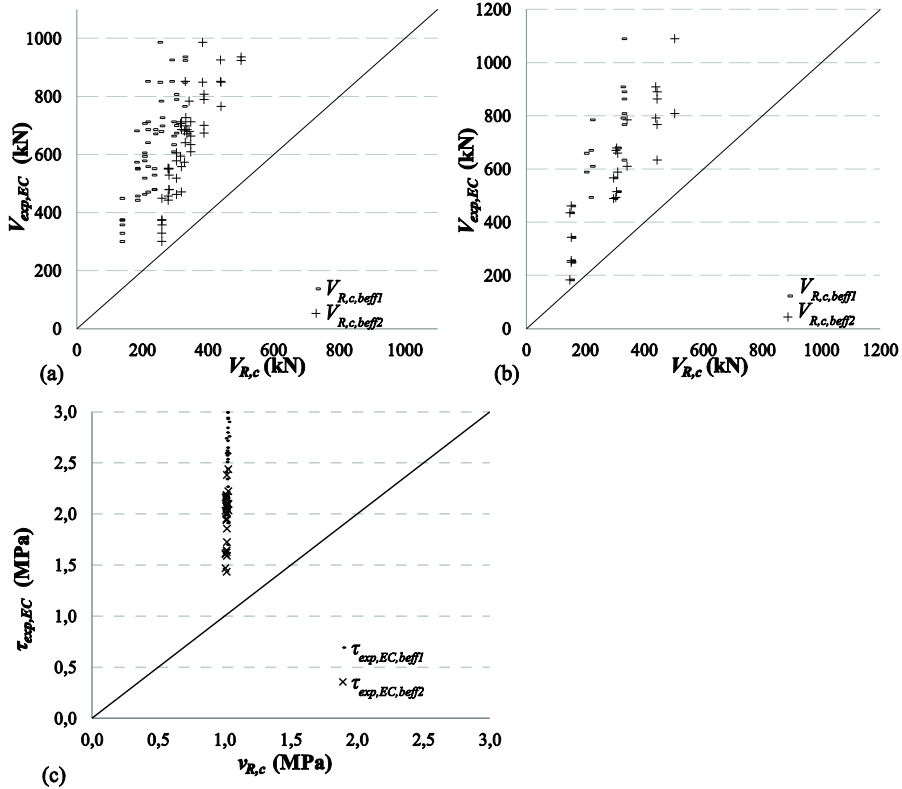


Fig. 6.2: Graphical comparison between experimental results and predicted values for shear according to NEN-EN 1992-1-1:2005 with  $b_{eff1}$  and  $b_{eff2}$ : (a) for all experiments on undamaged slabs S1 – S18; (b) for all experiments on the slab strips BS1 – BX3; (c) for all results of the second series of experiments S19 – S26.

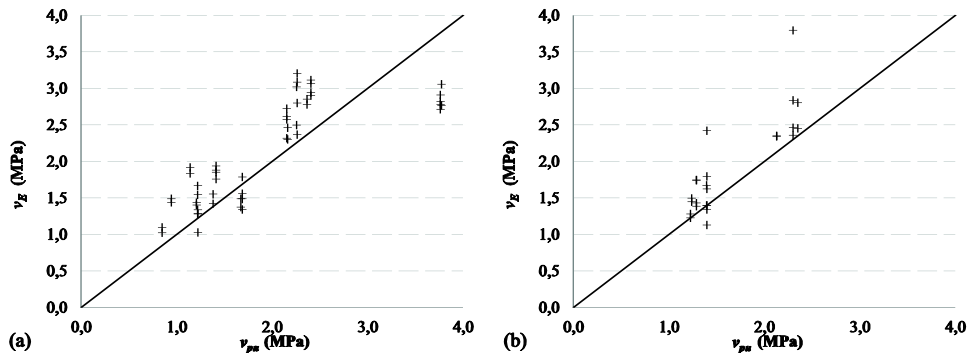


Fig. 6.3: Graphical comparison between experimental results and predicted punching capacities according to NEN-EN 1992-1-1:2005 (a) for all experiments on undamaged slabs S1 – S18; (b) for all experiments on the slab strips BS1 – BX3.

Statistical Evaluation of Design Methods

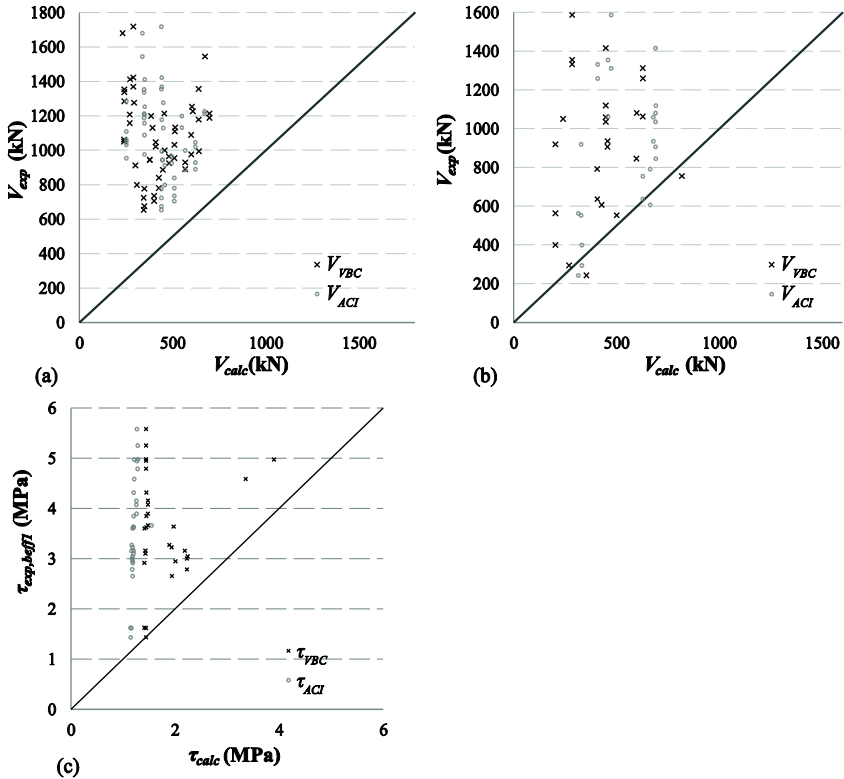


Fig. 6.4: Graphical comparison between experimental results and predicted values according to ACI 318-08 and NEN 6720:1995: (a) for all experiments on undamaged slabs S1 – S18; (b) for all experiments on the slab strips BS1 – BX3; (c) for all results of the second series of experiments S19-S26.

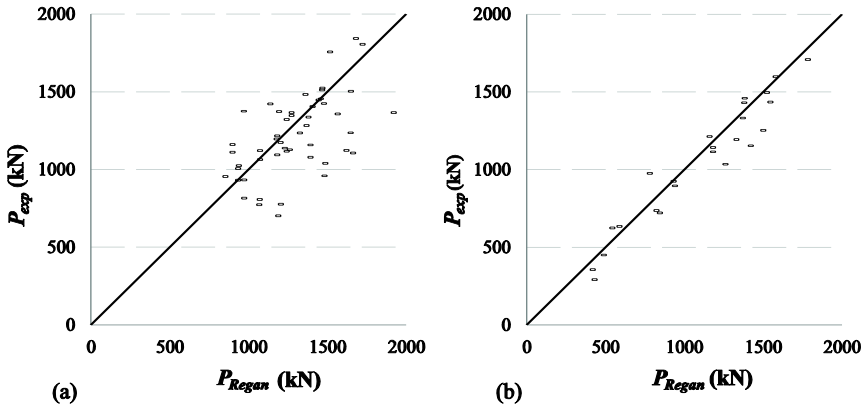


Fig. 6.5: Graphical comparison between experimental results and predicted values according to Regan's method: (a) for all experiments on undamaged slabs S1 – S18; (b) for all experiments on the slab strips BS1 – BX3.

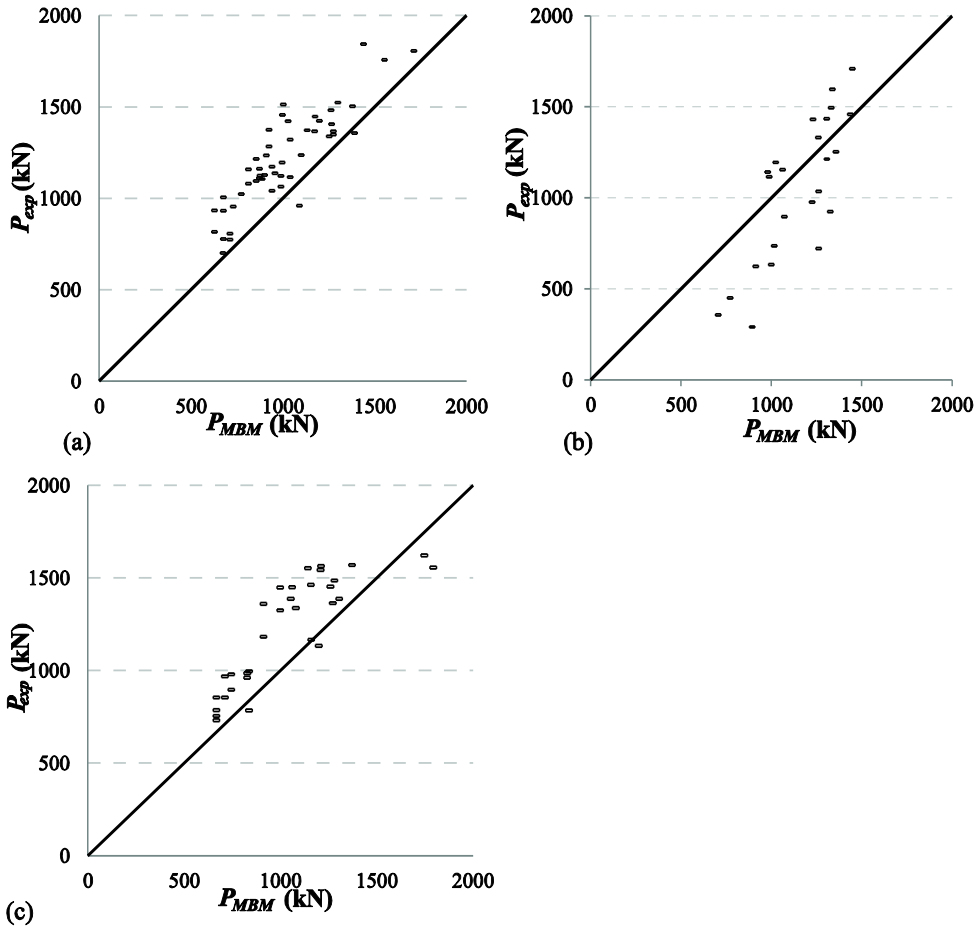


Fig. 6.6: Graphical comparison between experimental results and predicted values according to the Modified Bond Model: (a) for all experiments on undamaged slabs S1 – S18; (b) for all experiments on the slab strips BS1 – BX3; (c) for all results of the second series of experiments S19 – S26.

The results from Table 6.1 and Table 6.2 can be used to highlight the major conclusions from the full analysis reports (Lantsoght, 2012a; 2012d). When looking at the results from the slabs under a concentrated load only (S1 – S18), the best results are obtained when comparing the experimental results to the Modified Bond Model. Good results and a small coefficient of variation for the ratio between the experimental and calculated values are also found for calculated values based on NEN-EN 1992-1-1:2005 with  $b_{eff2}$  and Regan’s method. The predicted punching capacities according to NEN-EN 1992-1-1:2005 are close to the experimental results. However, it must be noted that the wide beam shear capacity is found to be governing for these experiments, and not the

punching capacity. The average value of the ratio between the experimental and calculated value is near 1,0 for Regan's method, indicating that Regan's method is more suitable for predicting the maximum load during an experiment (average values) than as a design method (characteristic values). Regan's method leads to good predictions as well, as can be seen from the relatively small values for the coefficient of variation that are obtained for  $P_{exp}/P_{Regan}$ . Similarly, the differences that are observed in Fig. 6.5 and Fig. 6.6 indicate that -as expected- Regan's method (Regan 1982) predicts an average test value, while the Modified Bond Model determines a value that is suitable for design. The results from comparing the experiments to the Modified Bond Model indicate that a margin of safety is built into the model in such a way that it can be used for design. Further discussion with regard to the quantification of this margin of safety can be found in §6.4.6. The coefficient of variation of the ratio between experimental and calculated values is high for the calculated values according to NEN 6720:1995 and ACI 318-08. When looking at the ratio between the experimental and calculated values for NEN-EN 1992-1-1:2005 with the calculated values resulting from  $b_{eff1}$  as compared to  $b_{eff2}$ , it is clear that  $b_{eff2}$  leads to better results: the average value becomes less conservative and the coefficient of variation becomes smaller.

The reference subset (S1 – S6) has for all design methods under study (except the Modified Bond Model) the largest average value for the ratio between the experimental and calculated value, and is as well the subset with one of the smallest standard deviations and coefficients of variation on all test to predicted values. This reference subset can be used for comparison to the other subsets. It can be seen in Table 6.1 that the Modified Bond Model leads to an average  $P_{exp}/P_{MBM}$  that does not change significantly for the different subsets. The same observation is made in Chapter 5 where the development of the Modified Bond Model is discussed with regard to the different parameters that determine the shear capacity.

The subset with the high strength concrete slabs (S7 – S10) has in all cases a smaller average value for the experimental to predicted value. The decrease in average is smallest when applying the Modified Bond Model and Regan's method. This observation indicates that most analysed methods overestimate the influence of the concrete compressive strength on the shear capacity of slabs under concentrated loads.

The subset with the slabs reinforced with plain bars (S11 – S14) shows again a smaller average value of the ratio of the experimental to the predicted value than for the reference subset. It should be noted, however, that the reinforcement ratio did not remain the same: the longitudinal reinforcement ratio for S11 to S14 is  $\rho_l = 1,375\%$  and for S1 to S10  $\rho_l = 0,996\%$ . The observed difference is thus either due to an overestimation of the influence of the amount of reinforcement by the design methods, or a result of the different load-carrying mechanism in slabs reinforced with plain bars. In the Modified Bond Model, which takes beam action shear and arching action shear into account, the average reduced

ability for beam shear transfer as a result of the lower bond between the reinforcing bars and the concrete is taken into account by reducing the calculated value of  $w_{ACI}$ . Note that a smaller capacity for beam shear transfer does not immediately indicate a smaller shear capacity, as in elements reinforced with plain bars, a percentage-wise larger share of the shear capacity will be carried by arching action. As a result, the Modified Bond Model gives good results for slabs reinforced with plain bars.

The subset with the results from slabs supported by elastomeric bearings (S15 – S18) shows as well a smaller average value for the ratio of the experimental to the predicted value as compared to the reference subset. Again, two possible causes can be identified:

- 1) the support length has become smaller as only three bearings support the slab at each side, and
- 2) the reinforcement layout is altered, as a virtual beam of reinforcement is applied at the support to carry the loads to the bearings.

The punching capacity from NEN-EN 1992-1-1:2005 overestimates the load in the experiment, most likely due to the reinforcement layout. As the Modified Bond Model is developed to be able to take the change in geometry from a slab on line supports to a slab on elastomeric bearings into account, the comparison between the experimental results and the Modified Bond Model leads to good results.

When comparing the statistical results of the ratio between the experimental and calculated capacities of the series of slab strips to the reference subset, the results are different per considered method. For the approaches based on the shear provisions from NEN-EN 1992-1-1:2005 it can be observed that the coefficient of variation of the ratio of the experimental to predicted value is increased. This observation indicates a discrepancy between the behaviour of the slab strips of small width (not benefiting from transverse load redistribution) as compared to the slab strips of larger width (benefiting from transverse load redistribution). Another observation with regard to the predictions based on the shear provisions from NEN-EN 1992-1-1:2005 is that the average ratio of experimental to predicted values is smaller than for the reference subset when  $b_{eff1}$  is used, while the average becomes larger when  $b_{eff2}$  is used. This observation can be explained by the fact that the effective width has the full specimen width as its upper bound, and the upper bound is reached for more specimen widths for  $b_{eff2}$ . With the full width  $b$  as an upper bound for the effective width  $b_{eff2}$ , the calculated shear capacity will be smaller based on  $b$  than on  $b_{eff2}$ . As a result, a larger ratio of the experimental to the predicted values is found. For the slab strips, ACI 318-08 and NEN 6720:1995 both result in smaller average values for the ratio between the experimental and predicted values as compared to the reference subset. The specimens with a small width do not benefit from transverse load redistribution and thus lead to smaller shear capacities. Regan's method (1982) results in similar statistical results for the slab strips as compared to the reference subset. This observation indicates

that reducing the perimeter to two or three sides when necessary (Fig. 6.1) leads to appropriate results.

For the Modified Bond Model, it was already taken into account that strips to a remote end should be at least  $\pm 200\text{mm}$  long in order for the strip to be considered for the capacity. However, the results indicate that the method is not suitable for the slab strips with a small width, as shown in Fig. 6.7 and in Table 6.1. This observation is studied in more detail to set an expression for the lower bound for which the Modified Bond Model can be applied. It can be seen in Fig. 6.7 that the values of  $P_{exp}/P_{MBM}$  cover a rather large range of values for every specimen width studied. One of the important parameters that is varied as well is the size of the loading plate  $b_{load}$ . Therefore, the results of  $P_{exp}/P_{MBM}$  are studied as a function of  $b_{load}/b$ , Fig. 6.8. These results show a more uniform trend for  $P_{exp}/P_{MBM}$  as a function of  $b_{load}/b$  than as a function of  $b$ . It can thus be concluded that the Modified Bond Model can only be applied for slabs with  $b_{load}/b < 0,2$ . It is assumed that a two-dimensional load-carrying mechanism can develop when this criterion is fulfilled. Alternatively, it can be seen in Fig. 6.8 that the decrease in capacity can be expressed as a logarithmic function, which can be found as a trendline through the datapoints:

$$P_{MBM,slabstrip} = \left( -0,41 \ln \frac{b_{load}}{b} + 0,25 \right) P_{MBM} \quad \text{for } \frac{b_{load}}{b} > 0,2 \quad (6.9)$$

It is however deemed prudent to advise that the Modified Bond Model should be used solely for slabs ( $b \geq 5h$ ), and when  $b_{load}/b < 0,2$  and that for beams (with a smaller width) the known shear expressions should be used, for example the shear provisions from NEN-EN 1992-1-1:2005.

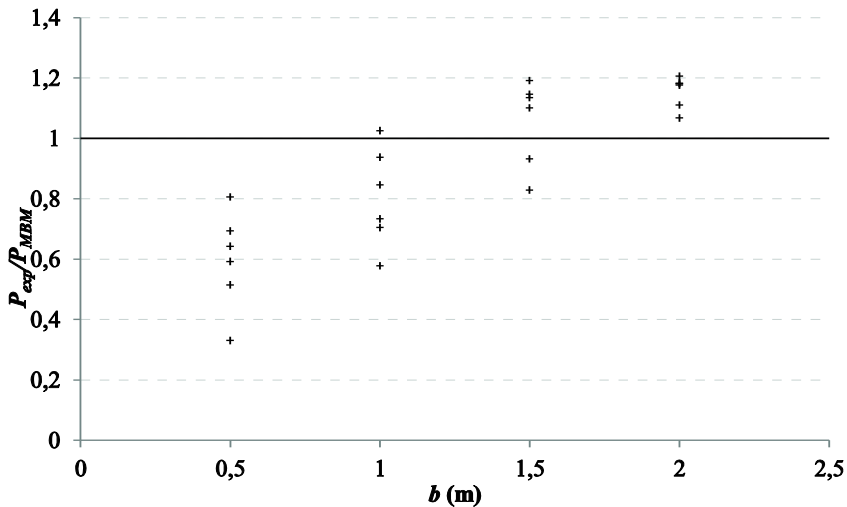


Fig. 6.7: Results of comparison between the experiments on slab strips BS1 – BX3 and the capacity according to the Modified Bond Model as a function of the specimen width  $b$ .

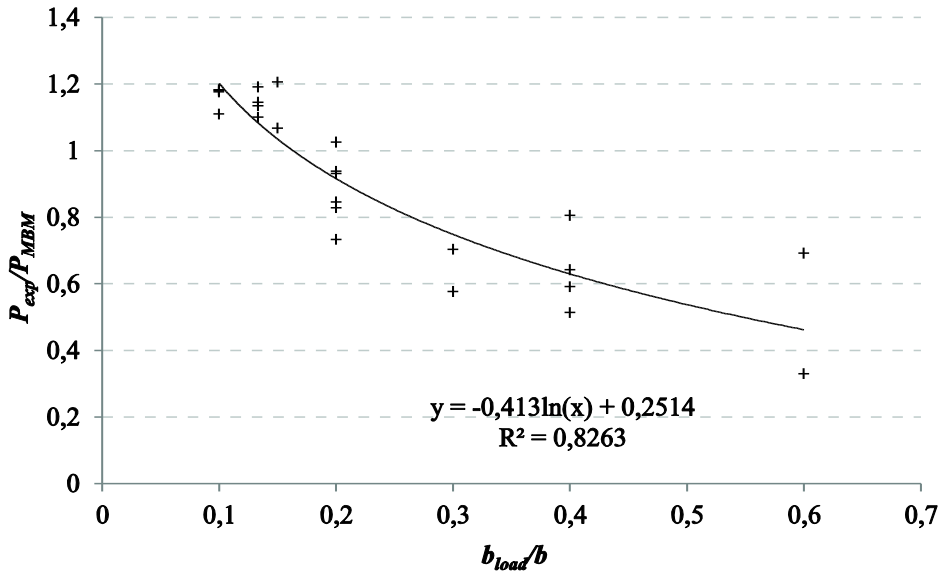


Fig. 6.8: Results of comparison between the experiments on slab strips BS1 – BX3 and the capacity according to the Modified Bond Model as a function of the ratio  $b_{load}/b$  expressing the geometry.

The results from the subset with all experiments from the second series of experiments are comparable to the results obtained from the reference subset. It should be noted that the subset with all results from the second series also includes the reference tests with slabs under a concentrated load only, and the experiments in which the concentrated load was placed at a larger distance to the support, resulting in a larger  $a/d_1$  value. When these experiments are eliminated, the subset “S19 – S26, combi” results, in which only experiments on slabs subjected to the combination of a line load and a concentrated load are considered. For this subset, again, the best statistical results are obtained when the experimental value is predicted by using the Modified Bond Model and by using NEN-EN 1992-1-1:2005 combined with the effective width from the French load spreading method,  $b_{eff2}$ . The coefficient of variation of the ratio  $P_{exp}/P_{MBM}$  for S19 to S26 is similar to the coefficient of variation of  $\tau_{exp,EC,b_{eff2}}/\nu_{R,c}$ , but the average value and characteristic 5% lower bound are much less conservative for  $P_{exp}/P_{MBM}$ . The Modified Bond Model underestimates the capacity of slabs under a concentrated load less than EN 1992-1-1:2005 and is thus more suitable. Only for the subset “S19 – S26, combi” the coefficient of variation of  $P_{exp}/P_{MBM}$  is not the smallest of the studied methods, as the coefficient of variation of  $\tau_{exp,EC,b_{eff2}}/\nu_{R,c}$  is found to be smaller. This observation could indicate that adding the line load results in more one-way shear behaviour in the slabs under study, so that a model that combines one-way and two-way shear models like the Modified Bond Model gives less accurate results than a shear prediction based solely on one-way shear, such as the shear

provisions from NEN-EN 1992-1-1:2005. However, it should be noted that the average value of  $P_{exp}/P_{MBM}$  is still significantly better and closer to unity than the average value of  $\tau_{exp,EC,b_{eff}2}/\nu_{R,c}$ .

In Chapter 7, an enhancement factor of 1,25 is used for the shear capacity of slabs under concentrated loads close to supports (Lantsoght, 2012a) in combination with NEN-EN 1992-1-1:2005,  $b_{eff2}$  and a minimum effective width of  $4d_l$ . It can be seen in Table 6.1 that the characteristic value (5% lower bound according to a normal distribution) of the ratio between the experimental and predicted value according to NEN-EN 1992-1-1:2005 for all results of undamaged specimens on line supports (S1 – S14) is about 1,5. However, this result is found for  $C_{Rd,c,test} = 0,15$  which is not directly related to the code value of  $C_{Rd,c} = 0,18/\gamma_c = 0,12$  with  $\gamma_c = 1,5$ . The value of  $C_{Rd,c,test} = 0,15$  corresponds to the average value as found when comparing beam shear experiments to the proposed formula that became the expression from NEN-EN 1992-1-1:2005 without the factor  $C_{Rd,c,test}$  (Regan, 1987; König and Fischer, 1995). However, an additional conservative assumption is to fully adhere to the text of the code and to compare the experimental results to the predicted values from NEN-EN 1992-1-1:2005 with  $C_{Rd,c} = 0,18$  and then take the 5% lower bound assuming a normal distribution for the ratio between the experimental and predicted values. This approach leads to the factor 1,25, which is used to take transverse load redistribution in slabs under concentrated loads into account for the case of the assessment of the shear capacity of existing solid slab bridges.

### 6.2.2 Comparison between experimental results from database and Eurocode 2

A comparison between the experiments from the database in Annex 1 and the Eurocode provisions for shear and punching is given in this subsection. Many of the experiments from Annex 1 failed in a combined mode of shear and/or punching and flexure. In order not to confuse the results with the influence of flexural failure, the experiments with flexural failure are omitted from the comparison to NEN-EN 1992-1-1:2005 for shear. The flexural failure check is carried out based on the rectangular stress block diagram, and only for the moment associated with the main flexural reinforcement. The internal lever arm  $z$  is assumed to be  $0,9d_l$  and so the height of the rectangular stress block is assumed as  $0,2d_l$ . As a result of this control for flexure the experiments from the following references are selected for further analysis with regard to shear and punching:

- Reißer and Hegger, 2011
- Regan, 1982
- Sherwood et al., 2006
- Vaz Rodrigues et al., 2006
- Jäger 2002, 2005, 2007
- Graf, 1933
- Richart & Kluge, 1939

*Statistical Evaluation of Design Methods*

- de Cossio, 1962: experiments A50-25A and A50-25B
- Rajagopalan and Ferguson, 1968
- Aster and Koch, 1974
- Heger and McGrath, 1980
- Cullington et al., 1996
- Coin and Thonier, 2007: experiments 3bis, 6bis, 7 and 7bis
- Olonisakin and Alexander, 1999
- Rombach and Latte, 2008, 2009: all experiments except VK4V3.

The results of these calculations are given in Annex 4.

*Table 6.3: Comparison between results from a selected subset of 118 experiments from the literature as given in Annex 1 and predictions based on the shear and punching shear provisions from NEN-EN 1992-1-1:2005.*

<b>Subset</b>		$V_{exp,EC}/V_{R,c,beff1}$	$V_{exp,EC}/V_{R,c,beff2}$	$v_E/v_{pu}$
WB and P 118 experiments	AVG	1,837	1,404	1,447
	STD	0,983	0,518	1,220
	COV	0,535	0,369	0,843
	Char	0,224	0,555	-0,553
	Char,LN	0,762	0,807	0,423
WB 87 experiments	AVG	1,518	1,265	
	STD	0,745	0,340	
	COV	0,491	0,269	
	Char	0,296	0,707	
	Char,LN	0,759	0,826	
P 21 experiments	AVG			1,250
	STD			0,498
	COV			0,399
	Char			0,433
	Char,LN			0,578

In the experiments reported by Ekeberg et al. (1982), compressive membrane action is assumed to have had a significant influence on the test results, and therefore these experiments are not considered in the comparison to NEN-EN 1992-1-1:2005. In total, 118 experiments of the database of 215 experiments are further analysed with respect to shear and punching shear. An overview of the results is given in Table 6.3, and a graphical comparison is shown in Fig. 6.9 and Fig. 6.10. In Table 6.3, the average (AVG), standard deviation (STD), coefficient of variation (COV), characteristic value assuming a normal distribution (Char) and the characteristic value assuming a lognormal distribution (Char,LN) are given. The experiments that were identified as wide beam shear failure are

then separated into the WB subset (87 experiments) and the experiments that were identified as punching into the P subset (21 experiments). In Table 6.3, the subset of the 87 (wide) beam shear failures is only used to study the shear provisions from NEN-EN 1992-1-1:2005 and the subset of the 21 punching failures is used to study the punching provisions from NEN-EN 1992-1-1:2005. Therefore, the results of  $v_E/v_{pu}$  are left blank for the subset with the WB failures and the results of  $V_{exp,EC}/V_{R,c,b_{eff1}}$  and  $V_{exp,EC}/V_{R,c,b_{eff2}}$  are left blank for the P failures. For the P failures subset, the results of the comparison between the experiments by Graf (1933) and the punching provisions from NEN-EN 1992-1-1:2005 are omitted. In some of these experiments, the load was placed so close to the support that part of the loading plate overlapped with the support, resulting in a virtually negative distance  $a_v$  (see Annex 1). This special case of loading gives capacities much in excess of the predicted capacity, and distorts the statistical parameters.

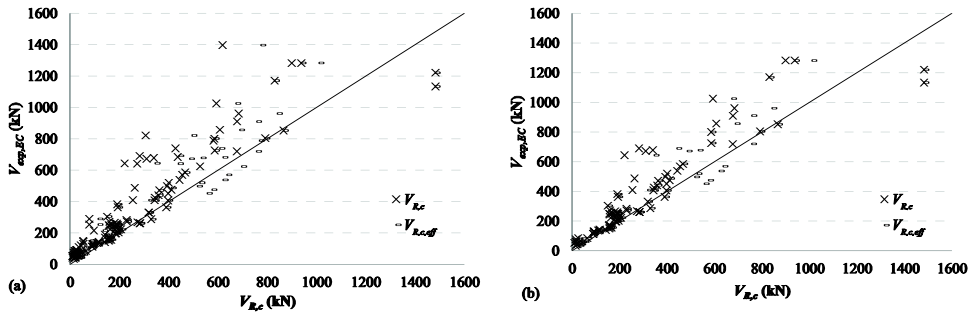


Fig. 6.9: Graphical comparison between results from Annex 1 and predicted values for shear according to NEN-EN 1992-1-1:2005 with  $b_{eff1}$  and  $b_{eff2}$ : (a) for all 118 experiments that did not fail in flexure; (b) for 87 experiments that were reported to fail in (wide) beam shear.

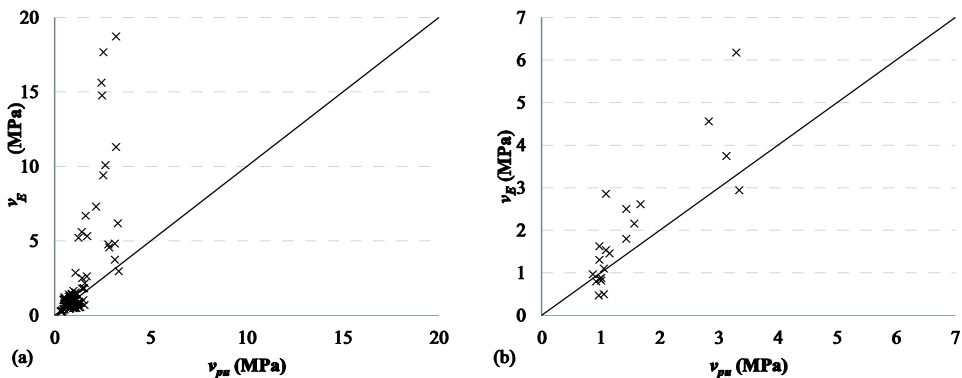


Fig. 6.10: Graphical comparison between results from Annex 1 and predicted values for punching according to NEN-EN 1992-1-1:2005: (a) for all 118 experiments that did not fail in flexure; (b) for 21 experiments that were reported to fail in punching.

In Fig. 6.9, two experiments fall far below the 45° line. These results are from experiments AT-1-East and AT-1-West from Sherwood et al. (2006). These specimens are the deepest cross-sections of the 118 tests, with a height of  $h = 1\text{m}$ . This observation might indicate that the shear provisions from NEN-EN 1992-1-1:2005 underestimates the influence of the size effect in shear. In Fig. 6.10b, the experiments that are far below the 45° are the experiments TB2 1TV and TB2 2TV from Reißer and Hegger (2012), that failed in a combined mode of punching shear and wide beam shear.

The results in Table 6.3 show that overall the wide beam shear capacity better predicts the experimental capacity, as  $V_{exp,EC}/V_{R,c,b_{eff2}}$  leads to the smallest average value between the experimental and predicted values and the smallest corresponding coefficient of variation. This observation, however, can be the result of the fact that more WB failures are observed in the database than P failures. When comparing the results of  $V_{exp,EC}/V_{R,c,b_{eff1}}$  and  $V_{exp,EC}/V_{R,c,b_{eff2}}$ , it is clear that using the effective width  $b_{eff2}$  based on the French method for horizontal load distribution is to be preferred. Another observation from Table 6.3 is that the statistical results become significantly better as subsets for the different classes of failure are made. Therefore, when gathering experimental results in a database, it is important to note down the observed failure mode from the reported photographs and crack patterns, and to create thoughtfully selected subsets.

### **6.3 Influence of parameters on design methods**

#### **6.3.1 Size of the loading plate**

The size of the loading plate is implemented as a parameter in some of the design methods that are discussed. For NEN-EN 1992-1-1:2005, the size of the loading plate is only taken into account when the effective width  $b_{eff2}$  resulting from the French load spreading method is used. For this load spreading method, horizontal load spreading from the far side of the loading plate towards the support is assumed. As a result, the size of the loading plate influences the resulting effective width, and thus the predicted shear capacity. The influence of the two different load spreading methods from Fig. 2.16 is observed on the ratio of experimental to calculated value. While the average and standard deviation of this ratio increase for the calculated values with  $b_{eff1}$ , the results when using  $b_{eff2}$  are less influenced by the change in size of the loading plate. This observation supports the previous conclusion that the effective width as determined based on the French load spreading method  $b_{eff2}$  leads to better results. An improvement of the results is observed as the French load spreading method takes into account the size of the loading plates and thus the enhanced transverse load redistribution capacity for the case of a slab under a larger concentrated load than under a smaller concentrated load.

For NEN 6720:1995, the size of the loading plate is only reflected in the use of the parameter  $A_0$  in the expression for  $k_\lambda$  for specimens loaded near to the simple support. The

influence of this parameter on the shear capacity is found to be smaller than the influence as observed in the experiments. Furthermore, it is observed that the standard deviations become larger for the ratio of the experimental to predicted values according to NEN 6720:1995 if the size of the loading plate is increased (Lantsoght, 2012a). This result indicates that the beam shear provisions of NEN 6720:1995 become less suitable as the size of the loading plate increases and more transverse load redistribution capacity is activated.

For Regan's method (Regan, 1982), the size of the loading plate is directly related to the size of the punching perimeter around the load. The ratio between the experimental and calculated results according to Regan's method is observed to increase as the size of the loading plate increases. This observation indicates that Regan's method becomes more conservative for larger concentrated loads.

In Chapter 5 §5.4.4 it is shown that the Modified Bond Model adequately represents the influence of the size of the loading plate, since this size determines the width of the strips in the model and their resulting arching capacity.

### 6.3.2 Loading sequence

As none of the design methods that are discussed aimed at determining the shear capacity of a specimen with damage from previous testing or a structure with severe cracking as a result of being several years in service, the influence of the loading sequence and resulting cracking is not further discussed.

### 6.3.3 Transverse flexural reinforcement

The influence of the transverse flexural reinforcement is taken into account when the experimental results are compared to the predictions based on Regan's method, which accounts for the longitudinal and transverse reinforcement at their respective parts of the perimeter and when the experimental results are compared to the predictions based on the Modified Bond Model. The results of the ratio of the experimental to calculated values according to Regan's method (Lantsoght, 2012a) show a clear decrease for an increasing transverse reinforcement ratio. This observation could also explain the smaller average value of the ratio between the experimental and predicted values according to Regan's method for the slabs with plain reinforcement and the slabs supported by bearings, as these specimens had larger amounts of transverse reinforcement. The importance of this observation with respect to the transition from one-way to two-way shear should be highlighted, Fig. 6.12. For the slab shear experiments the transverse parts of the punching perimeter do not contribute as much as the longitudinal parts, which carry a higher percentage of the load (Fig. 6.12b). According to Regan's method, the capacity of the four parts of the perimeter is related to their respective transverse ( $d_t, \rho_t$ ) or longitudinal ( $d_l, \rho_l$ ) properties, Fig. 6.1. When one-way action is dominant, the longitudinal parts of the perimeter carry the entire load (Fig. 6.12a). On the other hand, when shear is carried by

two-way action (Fig. 6.12c), both longitudinal and transverse parts of the perimeter have equal shear capacities. The transient situation is shown in Fig. 6.12b. The cracking pattern in some experiments (Fig. 3.10), with punching of only the transverse parts of the perimeter, confirms this idea. As the transverse part of the perimeter has a smaller capacity, this part of the perimeter tends to be more prone to punching failure.

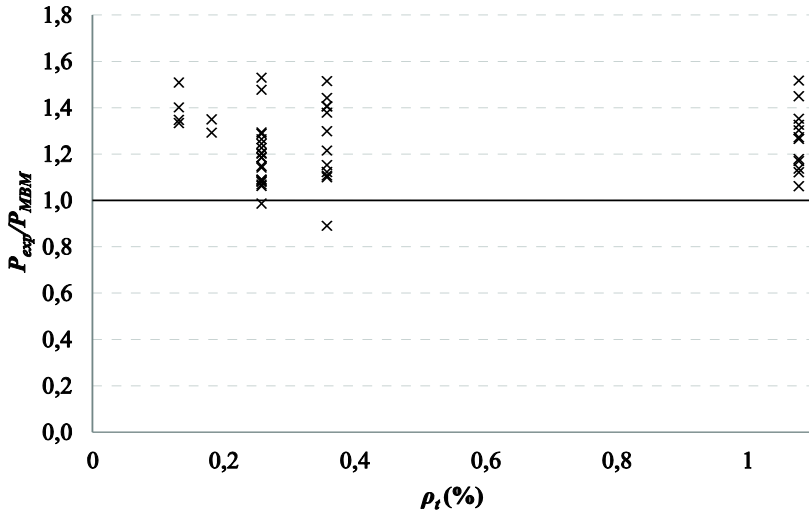


Fig. 6.11: Influence of the transverse reinforcement ratio on the ratio of the experimental to the calculated results according to the Modified Bond Model.

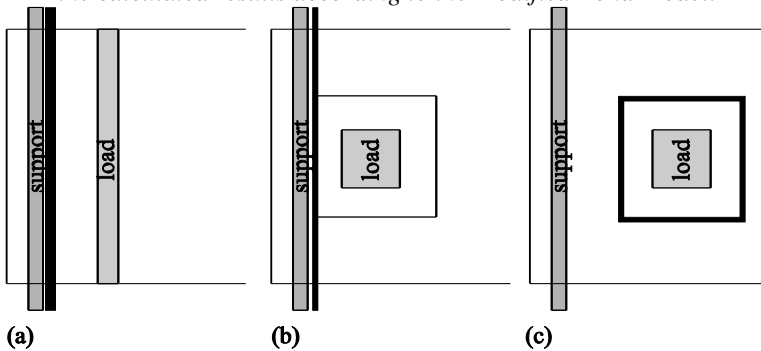


Fig. 6.12: Sketch of the governing sections and load transfer methods for different cases; the line width at the support and of the punching perimeter indicates the distribution of the load-carrying capacity over these different parts: (a) pure one-way shear: all shear is carried over the support; (b) transition from one-way to two-way shear: more shear is carried at the support than on the punching perimeter around the load; (c) pure two-way shear: all shear is carried equally on the punching perimeter around the load.

The results of the comparison between the experiments and the capacity according to the Modified Bond Model are studied as a function of the transverse reinforcement ratio  $\rho_t$ , Fig.

6.11. The Modified Bond Model takes the influence of the transverse reinforcement into account in its calculation of the moment capacity of the y-direction strips. It is shown in Fig. 6.11 that the transverse reinforcement is properly taken into account by the Modified Bond Model.

#### 6.3.4 *Moment distribution at support*

The influence of the moment distribution at the support is only taken into account by ACI 318-08, Regan's method and the Modified Bond Model. In ACI 318-08, the factor  $M_{span}/V_{exp}d_l$  is used to take into account the influence of direct load transfer between the load and the support. This factor allows a wider range of applications than the factor  $a/d_l$  or  $a_v/d_l$  as used in NEN-EN 1992-1-1:2005 for the reduction of concentrated loads close to the support. The shear capacities calculated according to ACI 318-08, however, are barely influenced by this factor.

According to Regan's method, the increase in shear capacity close to the continuous support is taken into account directly through the factor  $\alpha_{Regan}$ , which is determined as:

$$\alpha_{Regan} = \sqrt{\frac{M_1 + M_2}{M_1}} \quad (6.10)$$

with  $M_1$  being the larger bending moment in the shear span and  $M_2$  the smaller moment as shown in Fig. 4.4. The comparison of the ratio between the experimental and predicted values according to Regan's method indicates different behaviour for slabs and slab strips (Lantsoght, 2012a). A larger decrease in average  $P_{exp}/P_{Regan}$  is observed for slabs than for slab strips, which show similar statistical properties for  $P_{exp}/P_{Regan}$  at the simple and continuous support. This observation indicates an overestimation of the influence of the moment distribution at the support quantified through  $\alpha_{Regan}$ . For the slab strips, the average of the test to predicted values for the experiments at the continuous support increases. As already mentioned in §4.5.2, the influence of the moment distribution at the support becomes smaller as the specimen width, and thus the influence of the transverse flexural moment, increases. The results of the experiments indicate that the factor  $\alpha_{Regan}$  leads to an overestimation of the maximum concentrated load at the continuous support for slabs.

In the analysis report (Lantsoght, 2012a) the comparison of the ratio between the experimental value and the predicted value according to NEN-EN 1992-1-1:2005 is studied at the simple and continuous support. When the enhancement factor  $\alpha_{Regan}$  is applied to the predicted shear capacity for loading close to the continuous support, an improvement in the results is observed. It is important to point out that the shear capacity at the continuous support is at least equal to the shear capacity at the simple support. This observation is unlike the requirement from NEN 6720:1995, in which the enhancement due to direct load transfer is only applicable at the simple support.

The Modified Bond Model takes the influence of the support moment into account through the factor  $k_r$ . This factor partially adds the contribution of the hogging moment capacity to the capacity of the sagging moment to determine the arching capacity of the strips that border the quadrants over which the sign of the moment changes from support moment  $M_{sup}$  to span moment  $M_{span}$ . It is shown in Fig. 6.13 that this approach leads to results that are equally good at the simple and at the continuous support.

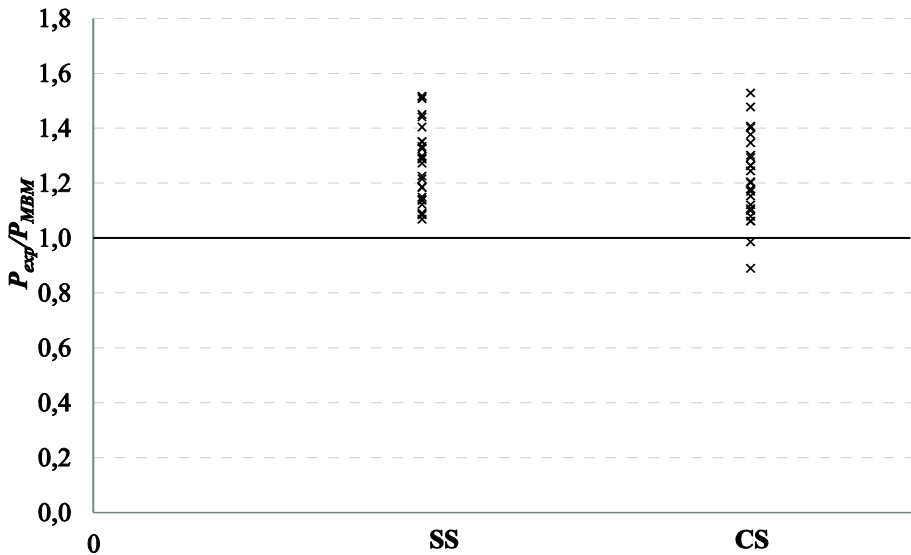


Fig. 6.13: Performance of the Modified Bond Model expressed as the ratio of the experimental to the calculated results at the simple support as compared to the ratio at the continuous support.

### 6.3.5 Distance between load and support

The influence of the distance between the load and the support is considered in the calculation procedures from the design methods in the following ways:

- in the calculation according to NEN-EN 1992-1-1:2005 through the reduction factor  $\beta = a/\sqrt{2}d_l$  on the contribution of loads close to the support to the shear force at the support and through the effective width;
- in the calculation according to NEN 6720:1995 at the simple support through the enhancement factor  $k_i$ ;
- in the calculation according to ACI 318-08 through  $M_{span}/V_{exp}d_l$ ;
- in the calculation according to Regan's method in the enhancement factor  $a/\sqrt{2}d_l$  on the part of the perimeter at the support and on the length of the transverse parts of the perimeter, Fig. 6.1.; and

- in the calculation according to the Modified Bond Model on the capacity of the  $x$ -direction strip between the load and the support.

As noted in §6.3.4, the influence of the factor  $M_{span}/V_{exp}d_l$  on the calculated shear capacity according to ACI 318-08 is negligible. NEN 6720:1995 only takes the distance between the load and the support into account for loads close to the simple support, which is shown in §6.3.4 not to correspond well with the experimental observations.

When the ratio of experimental to predicted values according to NEN-EN 1992-1-1:2005 is studied as a function of the decreasing distance between the load and the support, it is found that in combination with  $b_{eff1}$  a small increase in the average ratio is found and in combination with  $b_{eff2}$  a small decrease, Fig. 6.14 (Lantsoght, 2012a).

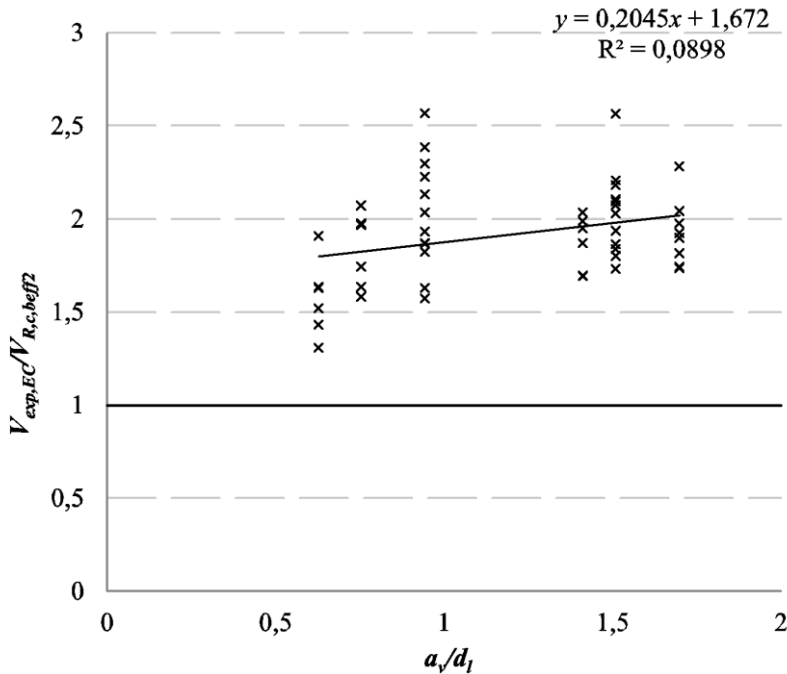


Fig. 6.14: Influence of distance between load and support on the ratio of the experimental value to the predicted value according to NEN-EN 1992-1-1:2005 with  $b_{eff2}$ .

NEN-EN 1992-1-1:2005 prescribes that for elastomeric bearings the distance  $a_v$  should be taken from the face of the load to the **centre** of the flexible support. In the comparison between the predicted capacities according to NEN-EN 1992-1-1:2005 and the experimental results, however, optimal results are found when the distance  $a_v$  is taken as the face-to-face distance between the load and the support for slabs supported by bearings.

The influence of the distance between the load and the support on the ratio of the experimental to the predicted value according to Regan's method is found to be small. A

slight decrease in average ratio is found for a decreasing  $a_v/d_l$ . Regan's method is developed for loads with  $a_v/d_l \leq 2$ , and it is observed in the ratio of experimental to predicted values that the results for the smallest values of  $a_v/d_l$  show the least scatter.

For the Modified Bond Model it was shown in Fig. 5.28 that the distance between the load and the support is taken correctly into account by increasing the capacity of the strip between the load and the support with the enhancement factor  $2d/a_v$ . As the influence is taken only for the strip between the load and the support, and not on the full capacity, the Modified Bond Model gives a smaller increase in capacity for a decrease in distance between the load and the support than NEN-EN 1992-1-1:2005. It is discussed in Chapter 4 §4.6.3 that transverse load redistribution results in a smaller influence of the distance between the load and the support, a concept that is properly taken into account by the Modified Bond Model.

### 6.3.6 Concrete compressive strength

As can be seen in Table 6.1, the ratio of the experimental to the predicted value is smaller for the subset with high strength concrete (S7 – S10) than for the subset with normal strength concrete (S1 – S6). This observation indicates that for the design methods studied the influence of the concrete compressive strength is overestimated or that not enough experimental results are available to assess the influence of the concrete compressive strength. As shown in §4.7.2, the influence of the concrete compressive strength on the shear capacity of slabs under concentrated loads is smaller than the influence of the parameters defining the geometry of the slab, the load and the support. In the design methods, however, the concrete compressive strength is considered the most influential parameter. In ACI 318-08 a square root relationship between the shear capacity and the concrete compressive strength is assumed. In NEN 6720:1995, a linear fraction relationship is assumed. In NEN-EN 1992-1-1:2005 and Regan's method (1982) a cube root relationship is assumed. As shown in Fig. 5.27 the influence of the concrete compressive strength on the capacity according to the Modified Bond Model is smaller, as a  $\frac{1}{4}$  power relation between the punching capacity and the concrete compressive strength is used. Therefore, the Modified Bond Model better represents the observations from the experiments.

### 6.3.7 Overall width and effective width

Limited attention is paid to determining the effective width in shear in the design methods. In the *fib* Model Code 2010, recommendations for the load spreading method and resulting effective width (as shown in Fig. 2.17) are given, which can be highlighted as a positive evolution.

### **6.3.8 Reinforcement type**

None of the design methods discussed differentiate between the shear capacity of an element reinforced with plain bars and an element reinforced with deformed bars, except for the Modified Bond Model. However, in the Modified Bond Model the influence of the reduced capacity for beam shear transfer due to the smaller bond between the reinforcement and the concrete is determined empirically (see §5.3.5). Therefore, the influence of the reinforcement type on the ratio of the experimental to predicted value is not discussed in more detail.

### **6.3.9 Line supports compared to elastomeric bearings**

The influence of the support type on the shear capacity is only mentioned in NEN-EN 1992-1-1:2005 through the definition of the distance  $a_v$  that is used for the reduction factor for loads close to the support  $\beta = a_v/2d$ . The distance  $a_v$  is taken as the face-to-face distance between the load and the support for stiff bearing materials and as the distance between the face of the load and the centre of the support for flexible bearing materials. As discussed in §6.3.5, the experimental results do not support this statement. In the Modified Bond Model a reduced support length for slabs supported by individual bearings is taken into account as this model determines the influence of the geometry on the capacity of the strips.

### **6.3.10 Combination of loads**

None of the studied design methods provides advice on how to superpose the contributions of different types of loading. As a result, the second series of experiments is executed to investigate if a concentrated load over an effective width can be superimposed to a distributed load over the full specimen width, a hypothesis which turned out to be valid, §4.11.2.

## **6.4 Probabilistic approach**

### **6.4.1 Introduction**

The semi-empirical expression for the shear capacity  $V_{Rd,c}$  from NEN-EN 1992-1-1:2005 is based on a statistical analysis. Therefore, the extension of the code formula that takes into account the enhancement of the shear capacity in slabs under concentrated loads close to supports as a result of transverse redistribution, should be based upon a similar statistical analysis, and should satisfy the same requirements with regard to the failure probability. For this purpose, the ratio between the experimental and predicted value based upon the beam shear formula of NEN-EN 1992-1-1:2005 is treated as a random variable in a statistical analysis.

Typically, in a reliability analysis, the variability of the loads and elements of the resistance is studied. When analysing experimental results to extend a codified approach, a

different technique is required, as the load is not variable. The limit state that is studied in this case is based on a probabilistic comparison between the test results and the design shear capacity. To take into account the variability of the material properties and the variation on the ratio between the experimental results and the predicted results, Monte Carlo simulations are used. These simulations are carried out for different subsets, resulting in a code extension proposal. The background and complete description of this procedure can be found in the full research report (Lantsoght, 2012e). Lastly, the applicability of the Modified Bond Model for design is investigated based on the resulting probability density function and cumulative distribution function.

#### 6.4.2 Studied limit state function

To compare the experimental results to the design shear capacity from NEN-EN 1992-1-1:2005, the approach used to determine the factor for the bending moment resistance of steel beams (Yura et al., 1978; Ravindra and Galambos, 1978) is used as an inspiration. In this approach, the quantity of the ratio between the experimental result and its prediction is treated as a random variable, which is added as a parameter to the formula for predicting the capacity. This ratio is expressed as:

$$\frac{\text{Test Capacity}}{\text{Prediction}}$$

The limit state function is defined as:

$$g = R - S \quad (6.11)$$

and failure occurs when  $g < 0$ , or when the load  $S$  exceeds the resistance  $R$ . This requirement can be expressed as seeking the chance that the experimental resistance is smaller than the design shear resistance:

$$P_f = P\{R < R_d\} \quad (6.12)$$

The requirement that must be satisfied is given in NEN-EN 1990:2002 Annex C, 8b as:

$$P\{R < R_d\} = \Phi(-\alpha_{rel}\beta_{rel}) \quad (6.13)$$

The function  $\Phi$  is the standard Gaussian function. The factor  $\alpha_{rel}$  depends on the loading conditions and  $\beta_{rel}$  is the required reliability index. The value of  $\alpha_{rel}$  equals  $\alpha_{rel} = 0,8$  according to NEN-EN 1990:2003.

For the comparison with the test data, the following expressions are used for  $R$  and  $R_d$  (replacing  $S$  in this case), based on the shear capacity expression<sup>31</sup> from NEN-EN 1992-1-1:2005 §6.2.2 (6):

---

<sup>31</sup> As recommended by EN 1992-1-1:2005 §6.2.2(6), the influence of direct load transfer for loads applied at a distance  $0,5d_l \leq a_v \leq 2d_l$  is taken into account by reducing the contribution of these loads to the shear force at the support with the factor  $\beta = a_v/2d_l$ .

*Statistical Evaluation of Design Methods*

$$R_d = \frac{C_{Rd,c}}{\gamma_c} k (100\rho_l f_{ck,calc})^{1/3} b_w d_l \quad (6.14)$$

$$R = \frac{\text{Test}}{\text{Prediction}} \times C_{Rd,c,test} k (100\rho_l f_{c,meas,28})^{1/3} b_w d_l \quad (6.15)$$

In which:

$C_{Rd,c}$  0,18 as default value for NEN-EN 1992-1-1:2005;

$\gamma_c$  1,5 for concrete;

$k$  the size factor;

$\rho_l = \frac{A_s}{bd_l}$  the ratio of longitudinal steel;

$A_s$  the area of longitudinal steel;

$b$  the member width;

$d_l$  the effective depth to the longitudinal reinforcement;

$\frac{\text{Test}}{\text{Prediction}}$ <sup>32</sup> the ratio of the tested value to the predicted mean value according to

NEN-EN 1992-1-1:2005 taking into account the effective width  $b_{eff2}$  based on the French load spreading method with a minimum value of  $4d_l$ ;

$f_{ck,calc}$  the characteristic concrete cylinder compressive strength;

$C_{Rd,c,test}$  0,15 for the comparison with test data;

$f_{c,meas,28}$  the mean cylinder concrete compressive strength;

$b_w$  the web width, or for slabs the effective width in shear, which is determined here based on the French load spreading method,  $b_{eff2}$ , Fig. 2.16b.

The expression for the limit state is then:

$$g = \left[ \frac{\text{Test}}{\text{Prediction}} C_{Rd,c,test} (f_{c,meas,28})^{1/3} - \frac{C_{Rd,c}}{\gamma_c} (f_{ck,calc})^{1/3} \right] k b_w d_l (100\rho_l)^{1/3} \quad (6.16)$$

The governing criterion is thus:

$$\left[ \frac{\text{Test}}{\text{Prediction}} C_{Rd,c,test} (f_{c,meas,28})^{1/3} - \frac{C_{Rd,c}}{\gamma_c} (f_{ck,calc})^{1/3} \right] < 0 \quad (6.17)$$

This limit state function is used for the Monte Carlo simulations.

### 6.4.3 Assumed distributions

In Eq. (6.17), the following random variables can be distinguished:

- Test/Prediction
- $f_{c,meas,28}$

---

<sup>32</sup> The distributions of the random variables are discussed in detail in §6.4.3.

-  $f_{ck,calc}$

The distributions of these random variables are based on experimental results and on the guidelines of the JCSS Probabilistic Model Code (JCSS, 2000, 2001, 2002).

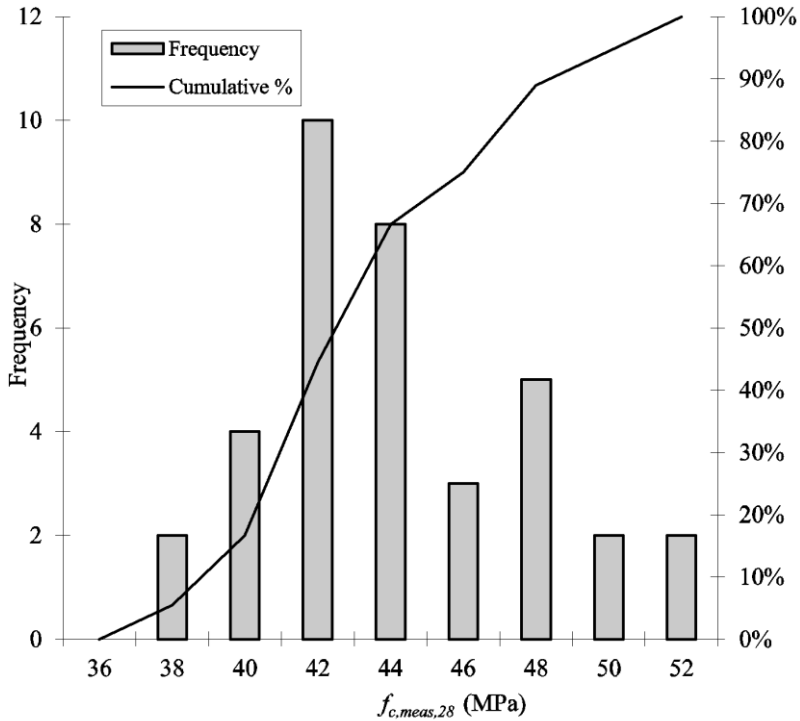


Fig. 6.15: Distribution of the cube compressive strength for C28/35: histogram resulting from 36 cubes from different casts tested at 28 days.

The variability of the concrete compressive strength of the mixture used for the slabs is determined from the cube compressive strengths measured at 28 days in the laboratory, for C28/35 (as used in S1 – S6, S11 – S26) and C55/65 (as used for the slab strips and for S7 – S10). According to the JCSS Probabilistic Model Code, the cube concrete compressive strength follows a lognormal distribution. Thus, the experimental results of the cubes at 28 days are analysed to determine the input values  $\lambda$  and  $\varepsilon$  for a lognormal distribution (Melchers, 1999). The number of test specimens was 36 cubes for C28/35 and 14 cubes for C55/65. Assuming a lognormal distribution, the constants defining the distribution are for C28/35:

- $\lambda = 3,762$  the mean value of the natural logarithm of the cube compressive strength of the concrete in [MPa];
- $\varepsilon = 0,084$  the associated standard deviation in [MPa].

The histogram of the cube compressive strength resulting for C28/35 at 28 days is shown in Fig. 6.15. It can be seen from this histogram that the probability density function has the skewed shape typical of a lognormal distribution.

For C55/65 these constants are:

$\lambda = 4,293$  the mean value of the natural logarithm of the cube compressive strength of the concrete in [MPa];

$\varepsilon = 0,047$  the associated standard deviation in [MPa].

To find the distribution of the characteristic concrete compressive strength, it is assumed that  $f_{ck,calc} = f_{c,meas,28} - 8\text{MPa}$  as used in NEN-EN 1992-1-1:2005 Table 3.1. This assumption is more conservative than calculating the characteristic concrete compressive strength based on the standard deviation from the experiments on the concrete cubes:  $3,68\text{MPa} \times 1,64 = 6,04\text{MPa}$ .

To study the enhancement of the shear capacity for slabs subjected to concentrated loads close to supports as compared to beams, the following subsets of experiments (uncracked specimens only) are used:

- S1 to S6: this subset is the reference case;
- S7 to S10: this subset is used to study the influence of the concrete compressive strength;
- S11 to S14: this subset is used to study the influence of plain reinforcement;
- S15 to S18: this subset is used to study the influence of a reduced support length;
- S19 to S26, combi: this subset is used to verify the code extension proposal;
- Selected results from the database from Annex 1: this subset is used to study the case of concentrated loads on a slab with  $a_s/d_l > 2,5$ .

The ratios between the experimental result and the predicted capacity according to NEN-EN 1992-1-1:2005 are used here to determine the appropriate distribution function for the subset with the experiments from the uncracked specimens S1 to S6. The predicted value is determined from NEN-EN 1992-1-1:2005 with the effective width as based on the French load spreading method and with a minimum effective width of  $4d_l$ . To describe distributions other than the normal distribution, the following input parameters are used:

$\mu = 2,023$  the mean value of the experimental shear force to the predicted shear force;

$\sigma_s = 0,259$  the associated standard deviation;

$m_e = 2,025$  the median of the experimental to predicted shear forces;

$\gamma_1 = 0,098$  the skewness of the distribution;

$\gamma_2 = 0,483$  the kurtosis of the distribution;

$\lambda = 0,697$  the mean value of the natural logarithm of the ratio of the experimental and predicted shear force;

$\varepsilon = 0,130$  the associated standard deviation.

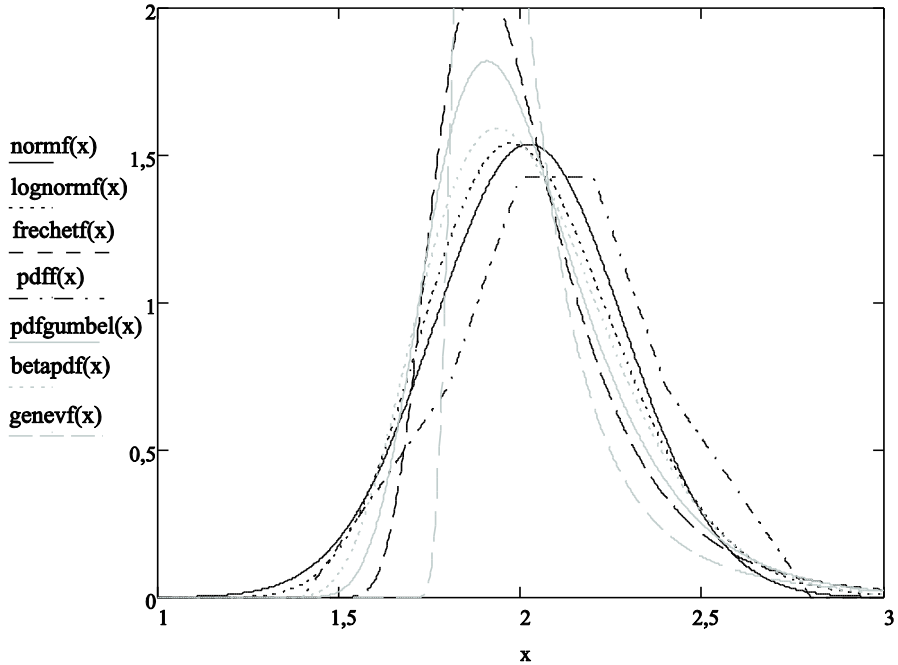


Fig. 6.16: Probability density function of the ratio of the experimental to the calculated value (Test/Predicted), for a normal distribution,  $\text{normf}(x)$ , lognormal distribution,  $\text{lognormf}(x)$ , Frechet distribution,  $\text{frechetf}(x)$ , the measured distribution,  $\text{pdff}(x)$ , the generalized extreme value distribution,  $\text{genevf}(x)$ , the Gumbel distribution,  $\text{pdfgumbel}(x)$  and the Beta distribution,  $\text{betapdf}(x)$ .

In a designated MathCad sheet, the following distributions are studied:

- a lognormal distribution, with input parameters  $\lambda$  and  $\varepsilon$ ;
- a Frechet distribution, with constants  $u_{\text{Frechet}}$  and  $k_{\text{Frechet}}$  that can be found from the given mean  $\mu$  and standard deviation  $\sigma_s$ ;
- a generalized extreme value distribution, with three constants (a scale factor, shape factor and location constant) that can be found from the mean  $\mu$ , variance  $\sigma_s^2$  and the median  $m_e$ ;
- a Gumbel distribution, with the mode of the distribution  $u_{\text{Gumbel}}$  and the measure of the dispersion  $\alpha_{\text{Gumbel}}$  that can be found from the mean  $\mu$  and the variance  $\sigma_s^2$ ;
- a Beta distribution, with 4 constants ( $a_{\text{Beta}}$  and  $b_{\text{Beta}}$  defining the interval on which the general beta distribution is defined; and  $q_{\text{Beta}}$  and  $r_{\text{Beta}}$  determining the shape of the distribution) that can be found with the mean  $\mu$ , the standard deviation  $\sigma_s$ , the skewness  $\gamma_1$  and the kurtosis  $\gamma_2$ ;
- a normal distribution, defined by the mean value  $\mu$  and the standard deviation  $\sigma_s$ .

The detailed expressions and determinations of these distributions are given in the full research report (Lantsoght, 2012e).

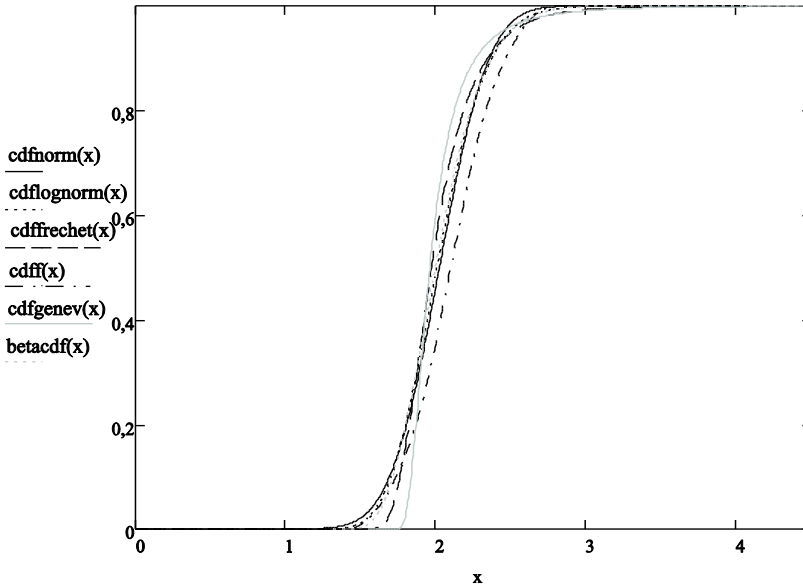


Fig. 6.17: Cumulative distribution function of the ratio of the experimental to the calculated values (*Test/Predicted*), for a normal distribution,  $cdfnorm(x)$ , lognormal distribution,  $cdflognorm(x)$ , Frechet distribution,  $cdffrechet(x)$ , the measured distribution,  $cdff(x)$ , the generalized extreme value distribution,  $cdfgenev(x)$  and Beta distribution,  $betacdf(x)$ .

The suggested distributions are then compared to the density function that results from the histogram. This probability density function of the ratio between the experimental to predicted value consists of stepwise linear parts over every bin interval. The results of the comparison for the probability density function are given in Fig. 6.16 and for the cumulative distribution function in Fig. 6.17. To compare the results of the proposed distributions to the measured distribution, the 5% lower bound and the median (50% value in the cumulative distribution function) from the distributions are given in Table 6.4. As the failure probabilities are governed by the results in the left tail, the 5% lower bounds of the ratio between the experimental result and the prediction are more closely studied to determine the most suitable distribution. The results in Fig. 6.16, Fig. 6.17 and Table 6.4 show that the left tail is best described by a lognormal distribution or a beta distribution. The lognormal distribution is more conservative than the data from the measured distribution, while the beta distribution slightly overestimates the value of the 5% lower bound. Therefore, the lognormal distribution is used in the Monte Carlo simulations. An overview of the considered random variables is given in Table 6.5.

Table 6.4: Results for the 5% lower bound and median (50%) of the experimental to calculated values (Test/Predicted), for the suggested distributions and the measured distribution of the data. GEV is used for the generalized extreme value distribution.

<b>Distribution</b>	<b>5%</b>	<b>50%</b>
<b>data</b>	1,637	2,100
<b>normal</b>	1,597	2,023
<b>lognormal</b>	1,621	2,008
<b>Frechet</b>	1,720	1,970
<b>GEV</b>	1,813	1,958
<b>Beta</b>	1,649	1,995

Table 6.5: Overview of considered random variables and statistical properties.

<b>Random variable</b>	<b>distribution</b>	$\mu$	$\sigma_s$	$\lambda$	$\varepsilon$
Test/Prediction	lognormal	2,02	0,26	0,70	0,13
$f_{c,meas,28}$	lognormal	43,20 MPa	3,68 MPa	3,76 MPa	0,08 MPa
$f_{ck,calc}$	lognormal	35,20 MPa	3,68 MPa	3,56 MPa	0,10 MPa

#### 6.4.4 Results from simulations

As the amount of random variables studied in the simulations is limited, the chosen approach is a brute force Monte Carlo simulation technique. The number of samples  $N$  required for a Monte Carlo simulation equals (Waarts, 2000):

$$N > \frac{3}{P_f} \quad (6.18)$$

For the case where  $\beta_{rel} = 4$ , the required number of samples is  $N > 10^5$ . For the case where  $\beta_{rel} = 3,6$ , the number of samples is  $N > 18856$ , and therefore  $10^5$  runs are typically used.

To quantify the enhancement due to transverse load redistribution on the safety of slabs as compared to beams, an enhancement factor  $\xi_{prop}$  is sought for which the limit state:

$$g = \left[ \frac{\text{Test}}{\text{Prediction}} C_{Rd,c,test} (f_{c,meas,28})^{1/3} - \xi_{prop} \frac{C_{Rd,c}}{\gamma_c} (f_{ck,calc})^{1/3} \right] kb_w d_l (100\rho_l)^{1/3} < 0 \quad (6.19)$$

results in a reliability index  $\beta_{rel}$  of 3,6. This given reliability index is the required safety level for existing structures built before April 1<sup>st</sup> 2012 for the “repair” level (Steenbergen et al., 2012) for structures of Consequences Class 3, as this class is defined in NEN-EN 1990:2002. This requirement is used by the Dutch Ministry of Infrastructure and the Environment for the assessment of existing slab bridges, Chapter 7. In the Monte Carlo simulations, a probability of failure  $P_f$  is found. The reliability index  $\alpha_{rel}\beta_{rel}$  can be expressed as a function of the failure probability  $P_f$  by using the inverse normal distribution function:

$$\alpha_{rel}\beta_{rel} = \Phi^{-1}(1 - P_f) \quad (6.20)$$

The value of  $\alpha_{rel}$  here equals  $\alpha_{rel} = 0,8$  (NEN-EN 1990:2002 C.8b). Combining this with the required reliability index  $\beta_{rel} = 3,8$  (3,6 for bridges built before April 1<sup>st</sup> 2012), results in the requirement for the probability of failure to be  $P_{f,req} = 1,988 \cdot 10^{-3}$ . The different values that are studied for the enhancement factor  $\xi_{prop}$  with their resulting reliability index  $\beta_{rel}$ , probability of failure  $P_f$  and number of trials can be found in the background report (Lantsoght, 2012e).

For the sake of comparison, the resulting required enhancement factor is determined as well for the assumption that the random variable of the ratio between the experimental results and the prediction based on NEN-EN 1992-1-1:2005 follows a normal distribution. Comparing the resulting enhancement factor assuming a lognormal distribution for the ratio of the experimental to predicted values to the resulting enhancement factor assuming a normal distribution for this ratio (values given in background report, Lantsoght, 2012e), shows that for larger reliability levels, the associated enhancement factors show a larger difference. For the required  $\alpha_{rel}\beta_{rel} = 2,88$  the resulting enhancement factor assuming a lognormal distribution equals  $\zeta_{prop} = 1,76$  and assuming a normal distribution  $\zeta_{prop} = 1,71$ . For basic cases of slabs under a concentrated load near to the support, the shear capacity can be increased with a factor  $\xi_{prop} = 1,76$ .

The previous analysis is carried out assuming the concrete compressive strength as the random variable described by the properties from Table 6.5. However, according to Vrouwenvelder et al. (2002), the coefficient of variation of concrete is about 0,17<sup>33</sup> for ready mixtures delivered to the construction site. When this coefficient of variation is used in the Monte Carlo simulation assuming  $\xi_{prop} = 1,76$ , then the resulting reliability  $\alpha_{rel}\beta_{rel}$  becomes 2,61 which implies a  $\beta_{rel}$  of 3,26  $\approx$  3,3 the limit for the “unfit for use” level. When the variation of the concrete compressive strength is larger than assumed in Table 6.5, it is necessary to use a smaller enhancement factor  $\xi_{prop}$ . For example, for a coefficient of variation of 0,17 it is found that the enhancement factor  $\xi_{prop}$  equals 1,68. An enhancement factor based on the procedures from NEN-EN 1990:2002 Annex D (Design assisted by testing) is given in the background report of this analysis (Lantsoght, 2012e).

#### 6.4.5 Code extension proposal

The enhancement factor  $\xi_{prop} = 1,76$  for the basic case (based on the results from the subset with the experiments on the undamaged specimens S1 to S6) is now used as a starting point to study the other subsets that are identified in §6.4.3. As the expected influence of the concrete compressive strength on the resistance of slabs under concentrated loads in shear was not clearly observed experimentally (§4.7.2), it is deemed conservative and prudent to

---

<sup>33</sup> Note that the recommendations from the Probabilistic Model Code prescribe that the logarithm of the concrete compressive strength should be described by a student distribution.

reduce the allowed enhancement factor for larger concrete compressive strengths. As the formula from NEN-EN 1992-1-1:2005 takes into account the concrete compressive strength by a cube root relationship (as discussed in §6.3.6), which seems to overestimate the influence of the concrete compressive strength for slabs subjected to concentrated loads close to supports, it is thus found necessary to reduce the enhancement factor for higher strength concrete. For this purpose, the subset with results from the experiments on undamaged specimens S7 to S10 is used. Again, the enhancement factor  $\xi_{prop}$  for which the probability of failure of the limit state in Eq. (6.19) is about  $P_{f,req} = 1,988 \cdot 10^{-3}$  or the reliability index  $\alpha_{rel}\beta_{rel} = 2,88$  needs to be determined. An analysis of the ratio between the experimental results and the predicted values based on NEN-EN 1992-1-1:2005, leads to the following statistical properties:

- $\mu = 1,951$  the mean value of the experimental shear force to the predicted shear force;
- $\sigma_s = 0,283$  the associated standard deviation;
- $\lambda = 0,659$  the mean value of the natural logarithm of the ratio of the experimental and predicted shear force;
- $\varepsilon = 0,143$  the associated standard deviation.

Again, a lognormal distribution is assumed for the ratio between the experimental results and the predicted value based on NEN-EN 1992-1-1:2005. With  $10^5$  simulations, it is found that for S7 – S10 the enhancement factor can be determined as  $\xi_{prop} = 1,64$ .

As only two concrete strength classes are tested in the experiments, a linear dependence of the enhancement factor on the concrete compressive strength is assumed. As the code extension proposal is aimed at a design formula, the relation is given as a function of the characteristic cylinder compressive strength of the concrete  $f_{ck}$ . The resulting relation, based on linear interpolation, is:

$$\xi_{prop}(f_{ck}) = 1,884 - \frac{f_{ck}}{225} \text{ with } f_{ck} \text{ in [MPa] and } 28 \text{ MPa} \leq f_{ck} \quad (6.21)$$

Slabs S11 to S14 are reinforced with plain steel bars. The results of the experiments on the undamaged specimens S11 and S14 are studied as a separate subset. An analysis of the ratio between the experimental results and the predicted value based on NEN-EN 1992-1-1:2005, leads to the following statistical properties:

- $\mu = 1,863$  the mean value of the experimental shear force to the predicted shear force;
- $\sigma_s = 0,182$  the associated standard deviation;
- $\lambda = 0,618$  the mean value of the natural logarithm of the ratio of the experimental to the predicted shear force;
- $\varepsilon = 0,098$  the associated standard deviation.

To determine the required enhancement factor  $\xi_{prop}$  for  $\alpha_{rel}\beta_{rel}$  to be  $\alpha_{rel}\beta_{rel} = 2,88$ , Monte Carlo simulations are used. The required enhancement factor is now 1,82. For the code

extension proposal, it is suggested not to distinguish between slabs with plain bars and deformed bars. In most structures nowadays regular deformed bars are applied, while the results from slabs reinforced with plain bars are more interesting for existing structures. Therefore, it suffices to note that the proposed enhancement factor leads to safe results for slabs with plain bars. It is interesting to note that a full statistical analysis shows a larger shear enhancement for slabs with plain bars as compared to slabs with deformed bars. This result is similar to the observations from experiments on beams with plain bars failing in shear (§4.9.2), but this result is not reflected clearly by a regular analysis of the experimental results as compared to NEN-EN 1992-1-1:2005, §6.3.8 and Table 6.1.

A last subset for the code extension proposal studies the results from the experiments on the undamaged specimens S15 to S18. These slabs are supported by three elastomeric bearings of 280mm × 350mm per side, resulting in a total supported length of 1,05m per side. Even though only 42% of the full width of  $b = 2,5\text{m}$  is supported, the reduction in the shear capacity is found to be less pronounced, yet significant enough to be studied in further detail through a probabilistic analysis. Assuming that only the bearing pads contribute to the effective width at the support is too conservative. A linear expression to reduce the effective width for a reduction in the support length needs to be determined. This expression is determined by comparing the statistical properties of S15 to S18 to those of the reference subset S1 to S6. An analysis of the ratio between the experimental results and the predicted value based on NEN-EN 1992-1-1:2005, leads to the following statistical properties for S15 to S18:

- $\mu = 1,634$             the mean value of the experimental shear force to the predicted shear force;
- $\sigma_s = 0,298$         the associated standard deviation;
- $\lambda = 0,475$          the mean value of the natural logarithm of the ratio of the experimental to the predicted shear force;
- $\varepsilon = 0,189$         the associated standard deviation.

A lognormal distribution is used for the ratio between the experimental results and the predicted value based on NEN-EN 1992-1-1:2005. The results show that the enhancement factor is now  $\zeta_{prop} = 1,23$ , indicating an important reduction of the shear capacity as the supported length is decreased. This reduction can be expressed by the factor  $\lambda_r$ . The factor  $\lambda_r$  is applied to the effective width from the French load spreading method  $b_{eff2}$  and reduces the effective width when less than the full slab width is supported. As only two support layouts are tested in the experiments, a linear dependence between the supported length and the resulting reduction of the effective width is used. This relation, based on linear interpolation, is:

$$\lambda_r\left(\frac{l_{sup}}{b}\right) = 0,52\frac{l_{sup}}{b} + 0,48 \quad \text{with } l_{sup} = \sum_{i=1}^{n_{bearings}} l_{bearing,i} \quad (6.22)$$

with

$l_{sup}$	the supported length;
$l_{bearing,i}$	the length of the considered bearing, taken perpendicularly to the span;
$n_{bearings}$	the total number of bearings;
$b$	the full width of the slab.

The proposed formula for the shear capacity of slabs under a concentrated load close to the support can be summarized as:

$$V_{Rd,c,prop} = C_{Rd,c} k (100 \rho_l f_{ck})^{1/3} b_{eff,2} d_l \left( 1,884 - \frac{f_{ck}}{225} \right) \left( 0,52 \frac{l_{sup}}{b} + 0,48 \right) \quad (6.23)$$

with  $l_{sup} = \sum_{i=1}^{n_{bearings}} l_{bearing,i}$ , and with  $f_{ck}$  in [MPa],  $b_{eff2}$  in [m],  $d_l$  in [mm] and  $V_{Rd,c,prop}$  in [kN].

Note that Eq. (6.23) is based on the shear expression from NEN-EN 1992-1-1:2005, and thus  $C_{Rd,c} = 0,18/\gamma_c$  with  $\gamma_c = 1,5$ . This formula is applicable for the design of slabs under a concentrated load, and  $b_{eff}$  is determined based on the French load spreading method, Fig. 2.16b. The large enhancement factor indicates the large additional capacity of slabs under a concentrated load close to the support. The influence of the distance between the load and the support  $a/d$  is taken into account by using the factor  $\beta = a/\sqrt{2}d_l$  to reduce the contribution of loads close to the support to the total shear load at the support. The shear capacity  $V_{Rd,c,prop}$  is thus to be compared to  $V_{exp,EC}$ .

The results from the slabs under a combination of loads in the second series of experiments are now used to verify the proposed code extension for slabs under concentrated loads. In the second series of experiments, the slab is loaded with a concentrated load as well as with a line load at a fixed distance of 1,2m from the centre of the support. The code extension proposal is only valid for concentrated loads on slabs benefiting from transverse redistribution. Therefore, the shear stress at the support due to the concentrated load need to be considered separately from the shear stress at the support due to the distributed loads. Only the contribution of the concentrated load to the shear stress at the support is influenced by transverse load redistribution as described by the enhancement factor  $\xi_{prop}$ . The contribution of the concentrated load to the shear stress is thus expressed as (with  $f_{ck}$  in [MPa]):

$$\tau_{conc} = \frac{V_{conc,EC}}{b_{eff,2} d_l \xi_{prop}} \text{ with } \xi_{prop} = \left( 1,884 - \frac{f_{ck}}{225} \right) \left( 0,52 \frac{l_{sup}}{b} + 0,48 \right) \quad (6.24)$$

with

$V_{conc,EC}$	the shear force at the support as a result of the concentrated load only, taking into account $\beta = a/\sqrt{2}d_l$ ;
$b_{eff}$	the effective width resulting from the French load spreading method with a lower bound of $4d_l$ ;
$d_l$	the effective depth;

$l_{sup}$  the supported length (full width or length of bearings).  
 $l_{sup} = \sum_{i=1}^{n_{bearings}} l_{bearing,i}$

The contribution of the distributed loads and the line load to the shear stress at the support is then (not taking the enhancement factor into account):

$$\tau_{line} = \frac{V_{line}}{bd_l} \quad (6.25)$$

with

$V_{line}$  the shear force at the support as a result of all distributed loads;

$b$  the full width;

$d_l$  the effective depth.

For the case under consideration, a concrete class C28/35 is used and the support length is 2,45m (7 bearings of 280mm × 350mm per side). Based on Eq. (6.24) the value of  $\xi_{prop}$  equals 1,74. The predicted shear capacity according to NEN-EN 1992-1-1:2005 at the support is then:

$$v_{R,c} = 0,15 \left( 100 \rho_l f_{c,cyl,meas} \right)^{1/3} \quad (6.26)$$

The comparison between the total shear stress at the support ( $\tau_{conc} + \tau_{line}$ ) and the predicted shear stress at the support ( $v_{R,c}$ ) results in the following statistical properties for the ratio between the experimental values and the predicted values:

$\mu = 1,351$  the mean value of the experimental shear stress to the predicted shear stress;

$\sigma_s = 0,232$  the associated standard deviation;

$\lambda = 0,284$  the mean value of the natural logarithm of the quotient of the experimental and predicted shear stress;

$\varepsilon = 0,196$  the associated standard deviation.

These values appear to be lower than the previous sets of values, but in this case, the enhancement factor of 1,74 is already taken into account on the contribution of the concentrated load to the shear stress at the support. A set of  $5.10^5$  simulations with the assumptions of the described approach results in a probability of failure  $P_f = 2,078.10^{-3}$  and thus a reliability index  $\beta_{rel} = 2,8661$ . The resulting reliability index is thus mostly the same as the required  $\beta_{rel} = 2,88$ . This result is deemed satisfactory and the method can be used.

A final subset with results from the slab shear database from Annex 1 is used to verify if this method can also be applied for concentrated loads on slabs with  $a_v > 2,5d_l$ . To gather relevant data for a subset from the slab shear database, the following filters are applied onto the database:

- results for  $a_v/d_l > 2,5$
- results for C20/25: the bounds for  $f_{c,mean}$  are determined to be 20MPa – 36MPa
- $b_{eff} < b$  to ensure that transverse load redistribution can be activated.

In total only 13 experiments satisfy the filter criteria. The results of the variability for the material and the comparison between the experimental results and the calculated values are summarized in Table 6.6.

Table 6.6: Statistical properties of concrete strength and the ratio of the experimental to predicted values for 13 selected experiments from the slab shear database (Annex 1)

	$f_{c,mean}$	$f_{c,k}$	$\frac{\text{Test}}{\text{Prediction}}, \xi_{prop}$	$\frac{\text{Test}}{\text{Prediction}}$
$\mu$	27,0MPa	19,0MPa	1,109	2,006
$\sigma$	6,2	6,2	0,647	1,195
$\lambda$	3,270MPa	2,887MPa	-0,050	0,537
$\varepsilon$	0,246	0,371	0,570	0,581

The results of the Monte Carlo simulations, taking into account the enhancement factor  $\xi_{prop}$ , lead to  $P_f = 0,3039$  and  $\beta_{rel} = 0,5132$ . When the enhancement factor is not taken into account,  $P_f = 0,069$  and  $\beta_{rel} = 1,4830$ . This high failure probability is the result of the large standard deviation on the results, which indicates that the subset resulting from filtering on three criteria from the database is not suitable for this type of analysis. When the results from this subset are plotted in a histogram, Fig. 6.18, it becomes clear that the data from this subset do not form a distribution that can be studied. In fact, an even smaller subset should be extracted, but then the number of experiments becomes insufficient to carry out a relevant Monte Carlo simulation. Therefore, the enhancement factor cannot be used for slabs under concentrated loads with  $a_v > 2,5d_l$ .

As the proposed enhancement factor in Eq. (6.23) suggests a level of accuracy that cannot be achieved in reality with respect to shear experiments, it is suggested to simplify the expression as:

$$V_{Rd,c,prop} = C_{Rd,c} k (100 \rho_l f_{ck})^{1/3} b_{eff,2} d_l \left( 1,9 - \frac{f_{ck}}{225} \right) \left( 0,5 \frac{l_{sup}}{b} + 0,5 \right) \quad (6.27)$$

with  $l_{sup} = \sum_{i=1}^{n_{bearings}} l_{bearing,i}$ , and with  $f_{ck}$  in [MPa],  $b_{eff,2}$  in [m],  $d_l$  in [mm] and  $V_{Rd,c,prop}$  in [kN].

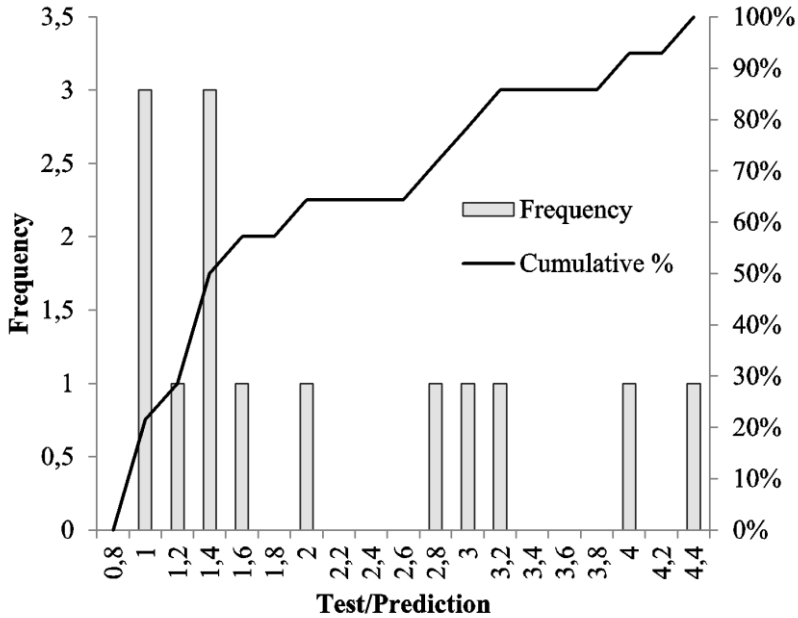


Fig. 6.18: Histogram of  $V_{exp}/V_{Rc,eff2}$  subset of data used to verify if the code extension proposal can be used for  $a_v > 2,5d_1$

#### 6.4.6 Applicability of Modified Bond Model for design

As briefly mentioned in Chapter 5, §5.4.1, the Modified Bond Model incorporates an adequate safety margin for design. In this paragraph, the full foundation for this claim can be found. The same methodology as in §6.4.3 is applied here to study the distribution of  $P_{exp}/P_{MBM}$ . As the Modified Bond Model takes into account the geometry, and is tailored to the precise geometric conditions under study, defining a suitable subset for an analysis that also takes into account the variability of the material properties, as shown in §6.4.4, results in a subset with only four experiments. This small number of experiments is not statistically relevant and therefore only the cumulative distribution function of  $P_{exp}/P_{MBM}$  is studied here. The requirement is that the 5% lower bound of  $P_{exp}/P_{MBM}$  has to be larger than 1 in order to make the method applicable for design.

To construct the distributions, the results of the ratio between the concentrated load from the experiment and the predicted capacity according to the Modified Bond Model, as described in Chapter 5, of all experiments from the uncracked specimens S1 to S18 are used. The Modified Bond Model as described in Chapter 5 is applied here. To determine the distributions, the following input parameters are used:

- $\mu = 1,245$             the mean value of the experimental maximum loads to the loads predicted by the Modified Bond Model;
- $\sigma_s = 0,151$         the associated standard deviation;

*Statistical Evaluation of Design Methods*

- |                       |  |
|-----------------------|--|
| $m_e = 1,235$         | the median of the experimental maximum load to the load predicted by the Modified Bond Model;  |
| $\gamma_1 = 0,109$    | the skewness of the distribution;  |
| $\gamma_2 = -0,554$   | the kurtosis of the distribution;  |
| $\lambda = 0,212$     | the mean value of the natural logarithm of the ratio of the experimental maximum loads to the loads predicted by the Modified Bond Model |
| $\varepsilon = 0,122$ | the associated standard deviation.   |

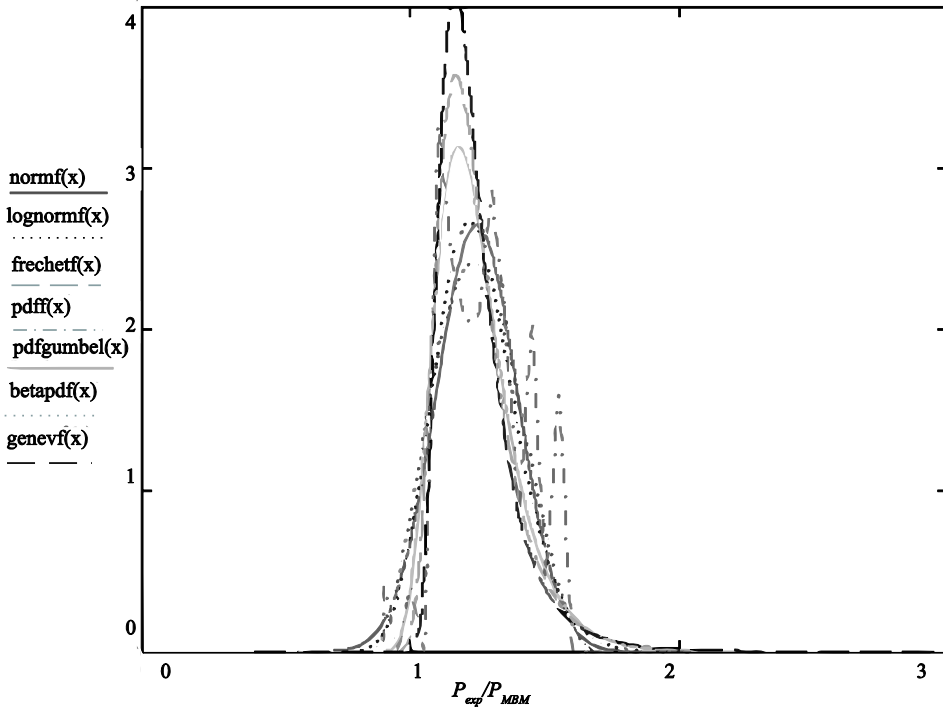


*Fig. 6.19: Probability density function of the ratio of the experimental to the calculated value (Test/Predicted), for a normal distribution,  $normf(x)$ , lognormal distribution,  $lognormf(x)$ , Frechet distribution,  $frechetf(x)$ , the measured distribution,  $pdff(x)$ , the generalized extreme value distribution,  $genevf(x)$ , the Gumbel distribution,  $pdfgumbel(x)$  and the Beta distribution,  $betapdf(x)$ .*

In a similar MathCad sheet as in §6.4.3, the following distributions are studied: a lognormal distribution, a Frechet distribution, a Gumbel distribution, a Beta distribution, a generalized extreme value distribution and a normal distribution. The results of the comparison for the probability density function are given in Fig. 6.19.

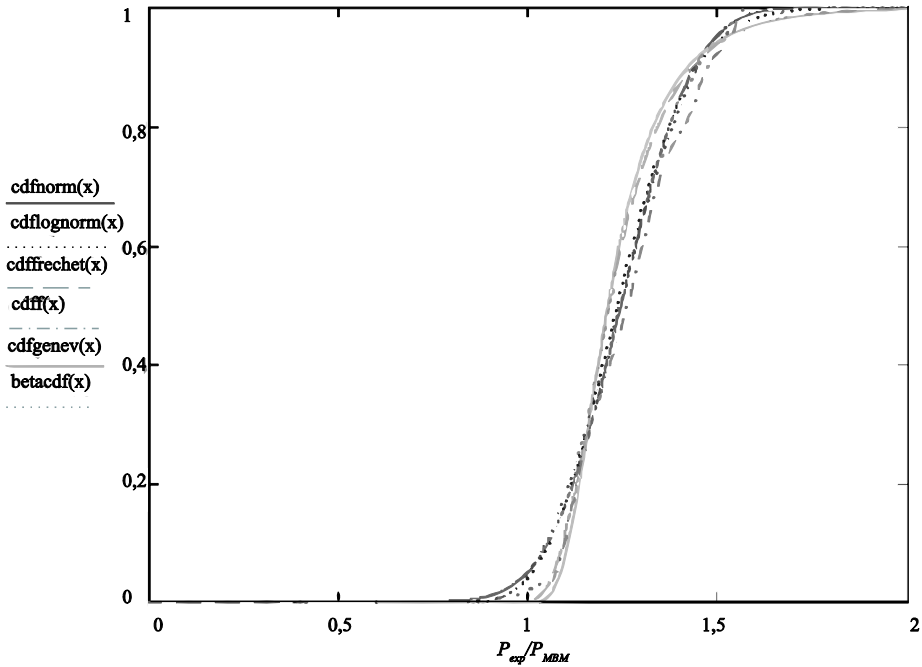


Fig. 6.20: Cumulative distribution function of the ratio of the experimental to the calculated value (Test/Predicted), for a normal distribution,  $cdfnorm(x)$ , lognormal distribution,  $cdflognorm(x)$ , Frechet distribution,  $cdffrechet(x)$ , the measured distribution,  $cdff(x)$ , the generalized extreme value distribution,  $cdfgenev(x)$  and Beta distribution,  $betacdf(x)$ .

These distributions are then compared with the density function that results from the histogram, constructed as explained in §6.4.3. The resulting cumulative distribution functions are shown in Fig. 6.17. To compare the results of the proposed distributions to the measured distribution, the 5% lower bound and the median from the distributions are given in Table 6.7. As the failure probabilities are governed by the results in the left tail, the 5% lower bounds of the ratio between the experimental result and the prediction are more closely studied to determine the most suitable distribution. The results in Table 6.7, Fig. 6.19 and Fig. 6.20 show that the lower bound is best described by a Frechet distribution or a generalized extreme value distribution. The results from the resulting distribution and all associated related distributions show that the 5% lower bound is larger than 1, and thus that the proposed method, the Modified Bond Model is suitable for application in design and assessment, regardless of the choice of distribution function to describe the results of  $P_{exp}/P_{MBM}$ . As indicated in §5.2.2 and §5.3.4, the assumption of neglecting the contribution of torsional shear leads to an underestimation of the capacity by 20% to 30%. This observation is also reflected by the median values of  $P_{exp}/P_{MBM}$ .

Table 6.7: Results of  $P_{exp}/P_{MBM}$  for the 5% lower bound and median (50%) of the cumulative distribution function of the experimental to calculated value (Test/Predicted), for different suggested distributions and the measured distribution.

<b>Distribution</b>	<b>5%</b>	<b>50%</b>
<b>data</b>	1,074	1,263
<b>normal</b>	0,997	1,245
<b>lognormal</b>	1,011	1,236
<b>frechet</b>	1,068	1,214
<b>GEV</b>	1,085	1,210
<b>Beta</b>	1,002	1,241

## 6.5 Conclusions

The general comparison between the experimental values and calculated values according to the design methods indicate that the preferable method for slabs subjected to concentrated loads close to supports is the Modified Bond Model. NEN-EN 1992-1-1:2005 with  $b_{eff2}$  and Regan's method lead to good results as well, with NEN-EN 1992-1-1:2005 being applicable to a wider range of loading situations, including combinations of loads. Regan's method is more suitable for predicting experimental results than for design, while the Modified Bond Model is shown to lead to safe predictions for design or assessment. Of the studied codified approaches, NEN-EN 1992-1-1:2005 with  $b_{eff2}$  leads to the best results for the 5% lower bound and is therefore used in the recommendations and verifications discussed in Chapter 7.

The results from the parameter analysis on the ratio of the experimental values to the calculated values according to the studied design methods can be summarized as follows:

- The size of the loading plate is taken into consideration when using the French load spreading method with NEN-EN 1992-1-1:2005 or the Modified Bond Model. These approaches reflect the increased ability for transverse load redistribution when a larger loading plate is used.
- Studying the influence of the amount of transverse reinforcement on the ratio between the experimental value and the predicted maximum load according to Regan's method shows that the experiments are at the transition between one-way and two-way shear, with more stresses transferred to the longitudinal sections of the punching perimeter or at the support and with a smaller contribution of the transverse sections to the capacity.
- The results of the influence of the distance between the load and the support  $a_v/d_l$  on the ratio of the experimental value to the predicted value according to NEN-EN 1992-1-1:2005 shows that the results are comparable for slabs on rigid and flexible bearings, unlike the provisions in NEN-EN 1992-1-1:2005. It is therefore

suggested to use  $\beta = a_v/2d_l$  as the reduction factor for the loads close to the supports with  $a_v$  the face-to-face distance between the load and the support for both rigid and flexible supports and to drop the code requirement of using the distance to the centre of the support in the case of flexible supports.

- Based on the tested range of concrete compressive strengths, this strength appears to be taken into account correctly in the Modified Bond Model by using the power  $1/4$  for the relation between the concrete compressive strength and the punching capacity.

Monte Carlo simulations are used to determine the enhancement factor for the shear capacity of slabs under concentrated loads close to the support in combination with the shear expressions from NEN-EN 1992-1-1:2005. The variability in material properties and the ratio of the experimental to predicted results is studied and lognormal distributions are considered. The expression is valid for assessment at the level of repair, with  $\beta_{rel} = 3,6$  as valid for all bridges built before April 1<sup>st</sup> 2012. The resulting expression for the shear capacity of slabs under concentrated loads near to the support benefiting from transverse load redistribution is determined to be:

$$V_{Rd,c,prop} = C_{Rd,c} k (100\rho_l f_{ck})^{1/3} b_{eff} d_l \left(1,9 - \frac{f_{ck}}{225}\right) \left(0,5 \frac{l_{sup}}{b} + 0,5\right)$$

with  $l_{sup} = \sum_{i=1}^{n_{bearings}} l_{bearing,i}$ , and with  $f_{ck}$  in [MPa],  $b_{eff}$  in [m],  $d_l$  in [mm] and  $V_{Rd,c,prop}$  in [kN].

This expression is verified with the results from the second series of experiments on slabs under a combination of loads and found to fulfil the reliability requirement. However, for slabs under concentrated loads with the position of the load at  $a_v > 2,5d_l$  no appropriate subset with experiments from the slab shear database could be found and the code extension proposal could not be verified for larger  $a_v/d_l$  distances.



## 7 Application to slab bridges and case studies

### 7.1 Introduction

As the incentive for this research on the shear capacity of reinforced concrete slabs under concentrated loads close to supports was given by the Dutch Ministry of Infrastructure and the Environment, part of the research has also been geared towards assessing the shear capacity of existing cases of slab bridges and developing practical techniques to take into account the results of the experimental research. In this chapter, the assumptions and background for a practical technique are given. This technique is implemented in the Quick Scan method. The Quick Scan method was originally developed by engineering firms as an assessment tool for the Ministry of Infrastructure and the Environment.

Then, the results of case studies for nine existing solid slab bridges from the Netherlands and one North-American slab bridge are given. First, the results of the Quick Scan approach for these cases with the recommendations based on the research are given. Next, these results are briefly compared to the Quick Scan results based on the previously used Dutch code NEN 6720:1995 and based on the North-American AASHTO codes. It should be noted that AASHTO does not require the shear capacity of reinforced concrete sections to be verified for rating purposes.

### 7.2 Loads and load factors

#### 7.2.1 Self-weight and superimposed loads

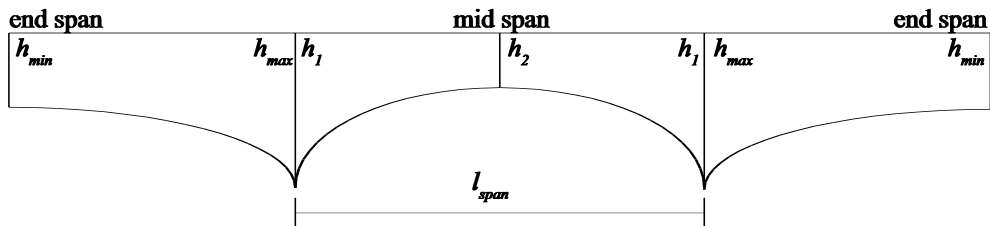


Fig. 7.1: Example of a three-span slab bridge with a parabolic height.

To determine the contribution of the self-weight to the design shear force, an approximate solution can be used. As several existing slab bridges in the Netherlands have a parabolic shape as shown in Fig. 7.1, the variable shape and resulting sectional forces can be determined based on the description of the parabolic height. The following expressions are used in the Quick Scan to describe the mid span (Fig. 7.2a) and the end span (Fig. 7.2b):

$$h(x) = \frac{4}{l_{span}^2} (h_1 - h_2) x^2 + \frac{4}{l_{span}} (h_2 - h_1) x + h_1 \text{ for the mid span} \quad (7.1)$$

$$g(x) = \frac{1}{l_{span}^2} (h_{max} - h_{min}) x^2 + h_{min} \text{ for the end span} \quad (7.2)$$

with

- $h_1$  the cross-sectional height at the support;
- $h_2$  the cross-sectional height at mid span;
- $h_{min}$  the cross-sectional height at the end support;
- $h_{max}$  the cross-sectional height at the mid support;
- $l_{span}$  the span length.

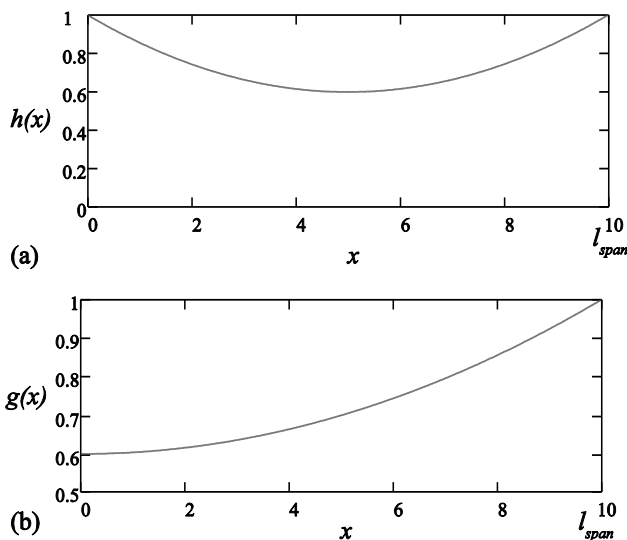


Fig. 7.2: Parabolic shape: (a) in the mid span; (b) in the end span. The height is unitless and scaled on the interval  $[0,1]$ , the length ( $x$ -axis) is taken for this example between  $0m$  and  $10m$ .

If the shear capacity is assessed according to NEN-EN 1992-1-1:2005, then the reduction factor  $\beta$  from NEN-EN 1992-1-1:2005 §6.2.2(6) for the contribution of the loads close to the support to the shear stress at the support can be expressed as:

$$\beta(x) = \begin{cases} 0,25 & \text{for } 0 \leq x \leq \frac{d_l}{2} \\ \frac{x}{2d_l} & \text{for } \frac{d_l}{2} \leq x \leq 2d_l \\ 1 & \text{for } x > 2d_l \end{cases} \quad (7.3)$$

The uniformly distributed self-weight is then expressed as:

$$q_{DL} = \begin{cases} bh(x)\beta(x) \times 25 \frac{\text{kN}}{\text{m}^3} & \text{for the mid span} \\ bg(x)\beta(x) \times 25 \frac{\text{kN}}{\text{m}^3} & \text{for the end span} \end{cases} \quad (7.4)$$

The resulting moment is taken as:

$$M_{DL} = \int_{\frac{d_l}{2}}^{\frac{l_{span}}{2} - \frac{d_l}{2}} q_{DL}(x)xdx \quad (7.5)$$

and the total load is:

$$P_{DL} = \int_{\frac{d_l}{2}}^{\frac{l_{span}}{2} - \frac{d_l}{2}} q_{DL}(x)dx \quad (7.6)$$

so that the shear force at the support due to the self-weight equals:

$$V_{DL} = \begin{cases} \frac{M_{DL}}{l_{span}} & \text{at the mid support} \\ P_{DL} - \frac{M_{DL}}{l_{span}} & \text{at the end support} \end{cases} \quad (7.7)$$

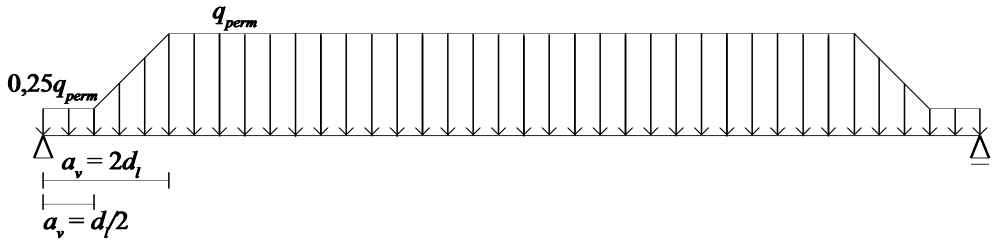


Fig. 7.3: Resulting distributed load for the wearing surface when  $\beta(x)$  is taken into account.

For the superimposed loads, a layer of  $d_{asphalt} = 120\text{mm}$  of asphalt as a wearing surface with  $q_{perm} = 23\text{kN/m}^3$  is assumed as required by the RBK (2012) guideline. To take into account the influence of  $\beta(x)$ , a distributed load as in Fig. 7.3 is used, in which the decrease in the contribution of loads close to the support is presented as a decrease in the uniformly distributed load. The shear force at the support due to the superimposed load (or permanent load) is then expressed as:

$$V_{perm} = q_{perm} b d_{asphalt} \left( \frac{l_{span}}{2} - 2d_l + \frac{1}{4} \frac{d_l}{2} + \frac{15}{16} d_l \right) \quad (7.8)$$

### 7.2.2 Live loads

In NEN-EN 1991-2:2003, a design truck or design tandem,  $Q_{ik}$ , is combined with a design lane load,  $q_{ik}$ . The design truck from Load Model 1 as prescribed in NEN-EN 1991-2:2003 has a tyre contact area of  $400\text{mm} \times 400\text{mm}$  and an axle load of  $\alpha_{Q1} \times 300\text{kN}$  (in the first lane), Fig. 7.4a. Vertical stress redistribution through the asphalt layer is assumed at a  $45^\circ$  angle, Fig. 7.5, resulting in a fictitious wheel print on the concrete surface of  $(400\text{mm} + 2d_{asphalt}) \times (400\text{mm} + 2d_{asphalt}) = 640\text{mm} \times 640\text{mm}$ . When multiple lanes are considered, a design truck with an axle load of  $\alpha_{Q2} \times 200\text{kN}$  is used in the second lane and of  $\alpha_{Q3} \times 100\text{kN}$  in the third lane. The value of all  $\alpha_{Qi} = 1$  in the Netherlands. The lane load from NEN-EN 1991-2:2003 Load Model 1 is applied over the full width of the lane and equals  $\alpha_{q1} \times 9\text{kN/m}^2$  for the first lane and  $\alpha_{qi} \times 2,5\text{kN/m}^2$  for all other lanes. The values of  $\alpha_{qi}$  are given in the National Annex. In the Netherlands, for bridges with three or more notional lanes, the value of  $\alpha_{q1}$  equals  $\alpha_{q1} = 1,15$  and for  $i > 1$  the value of  $\alpha_{qi}$  can be taken as  $\alpha_{qi} = 1,4$ .

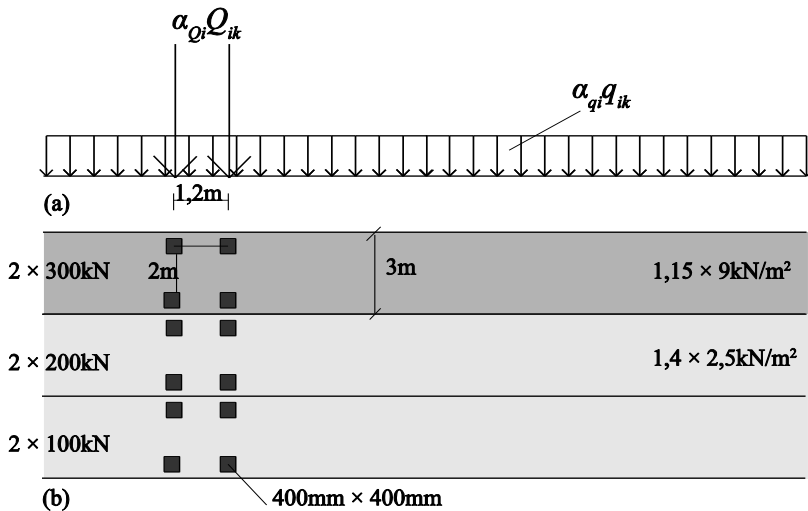


Fig. 7.4: Live loads according to NEN-EN 1991-2:2003: (a) side view; (b) top view.

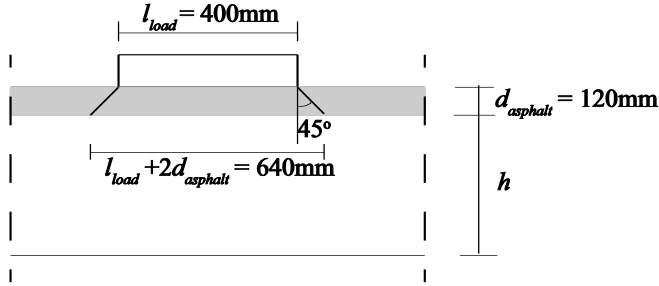


Fig. 7.5: Vertical load distribution of the wheel load through the wearing surface.

As shown in Fig. 7.4, the wheel print from Load Model 1 has a square shape. For the case of a truck with multiple wheels, and a resulting rectangular tyre contact area, the recommendations need to be verified with experiments in which a rectangular loading plate is used. As can be seen in Annex 1, a limited number of experiments from the literature cover this additional case.

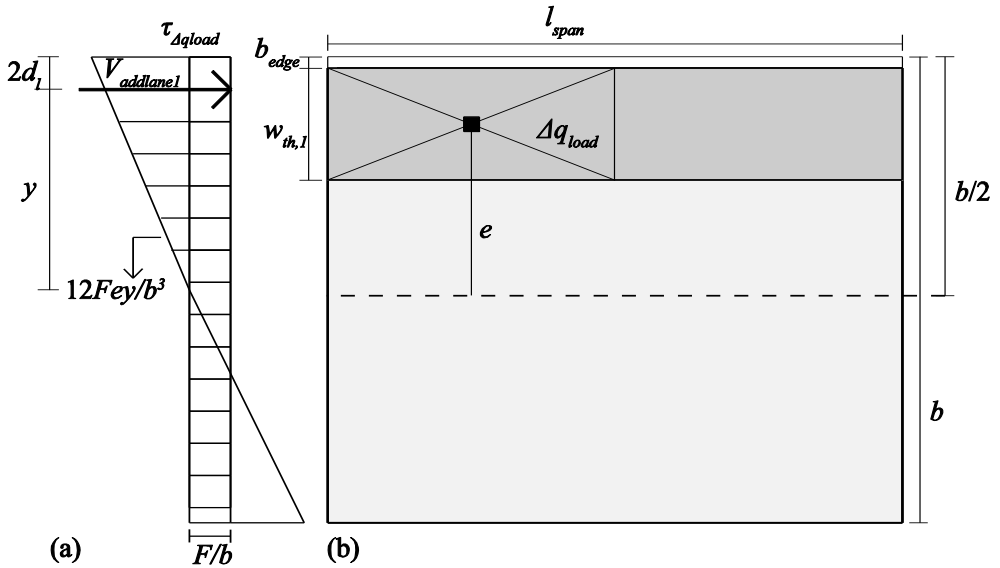


Fig. 7.6: Model for contribution of increased loading in the first heavily loaded lane as compared to other lanes assuming a triangular stress distribution over the support: (a) assumed stress distribution  $\tau_{\Delta q_{load}}$  due to load and moment from eccentricity of load; (b) sketch of top view with location of first heavily loaded lane

The increased contribution of the lane load in the first lane to the resulting shear stress can be approximated based on a triangular distribution as shown in Fig. 7.6. Moreover, the reduction  $\beta(x)$  from Eq. (7.3) of the distributed load close to the support as shown in Fig. 7.3 is also taken into account. The resulting shear force is then:

$$V_{\text{addlane1}} = \frac{F}{b} + \frac{(F.e)y}{\frac{1}{12}b^3} \quad (7.9)$$

with

$$F = \left( \alpha_{q1} \times 9 \frac{\text{kN}}{\text{m}^2} - \alpha_{q2} \times 2,5 \frac{\text{kN}}{\text{m}^2} \right) w_{th,1} \left( \frac{l_{span}}{2} - 2d_l + \frac{1}{4} \frac{d_l}{2} + \frac{15}{16} d_l \right) \quad (7.10)$$

$$e = \left( \frac{1}{2}b - b_{edge} - \frac{w_{th,1}}{2} \right) \quad (7.11)$$

$$y = \frac{1}{2}b - 2d_l \quad (7.12)$$

$$\Delta q_{load} = \alpha_{q1} \times 9 \frac{\text{kN}}{\text{m}^2} - \alpha_{q2} \times 2,5 \frac{\text{kN}}{\text{m}^2} \quad (7.13)$$

- $F$  the reaction force [kN/m];  
 $e$  the eccentricity of the load;  
 $w_{th,1}$  the width of the first notional lane (= 3m);  
 $b_{edge}$  the width of the edge;  
 $\Delta q_{load}$  the increased lane load in the first, heavily-loaded lane.

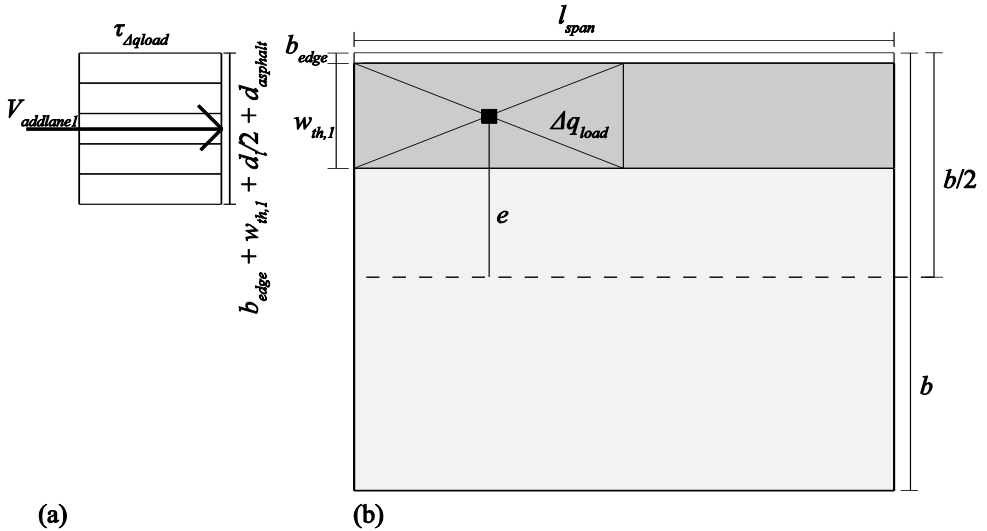


Fig. 7.7: Model for contribution of increased loading in the first heavily loaded lane as compared to other lanes assuming only vertical stress distribution over half the slab depth: (a) assumed stress distribution, note that the width is slightly larger than the lane width due to the vertical stress distribution to half the slab depth; (b) sketch of top view with location of first heavily loaded lane.

In the approach from Fig. 7.6, it is assumed that the slab is infinitely stiff in the transverse direction but weak in torsion. A slab bridge however also has torsional stiffness, which can be estimated with the approach of Guyon-Massonnet. The requirement for the proposed method from Fig. 7.6 is that it should give more conservative shear forces than the analysis based on the method of Guyon-Massonnet. To obtain this result, the maximum width  $b$  over which the triangular distribution is used, is limited to  $0,72l_{span}$  (Lantsoght et al., 2012a). If the viaduct width is larger, the full width  $b$  is replaced by the value of  $0,72l_{span}$ . A model factor of 1,1 should be used in combination with this approach. The lower bound of this approach is determined by vertical load distribution under an angle of  $45^\circ$  to half the slab depth  $d/2$ . This approach is shown in Fig. 7.7:

$$F_{min} = \left( \alpha_{q1} \times 9 \frac{\text{kN}}{\text{m}^2} - \alpha_{q2} \times 2,5 \frac{\text{kN}}{\text{m}^2} \right) \left( \min \left( b_{edge}, \frac{d_l}{2} + d_{asphalt} \right) + w_{th,1} + \frac{d_l}{2} + d_{asphalt} \right) \quad (7.14)$$

### 7.2.3 Load factors

Currently, the Eurocode suite only provides load factors for design. The Eurocodes for rating and assessment are still under development. To allow for assessment according to the basic assumptions and philosophy of the Eurocodes, in the Netherlands a set of national codes (NEN 8700:2011 for the basic rules, NEN 8701:2011 for actions, NEN 8702 (expected) for concrete structures, etc.) is developed. The load factors for the safety level “repair” are given in NEN 8700:2011 Table A1.2(B) and (C). The factors of the “repair” level correspond to a reliability index  $\beta_{rel} = 3,8$  (3,6 for bridges built before April 1<sup>st</sup> 2012) for Consequence Class 3 (Steenbergen and Vrouwenvelder, 2010). This Consequence Class is defined in NEN-EN 1990:2002 Table B1 as a class with a high consequence for the loss of human life or very great economic, social or environmental consequences. For the case of assessment at the repair level, a factor  $\gamma_{DL} = 1,15$  is used for all dead loads and  $\gamma_{LL} = 1,3$  for all live loads, provided that these bridges are built before April 1<sup>st</sup> 2012.

Other codes and national practices, such as the North American AASHTO LRFR Manual of Bridge Evaluation define similar load levels. An example of such a load level for rating purposes is the “design load at operating” level for AASHTO. Load ratings based on the operating rating level generally describe the maximum permissible live load to which the structure may be subjected. Allowing unlimited numbers of vehicles to use the bridge at operating level may shorten the life of the bridge. The description of the operating level is thus similar to the description of the repair level. However, the underlying assumption for the target reliability index for the determined load factors is found to be  $\beta_{rel} = 2,5$  for AASHTO at the operating rating level (Ghosn et al., 2010). This reliability level is significantly different from the requirements of NEN 8700:2011.

7.2.4 Static indeterminacy

The original Quick Scan method is developed for statically determinate structures. To expand the method to statically indeterminate structures, correction factors for the increased contributions of the loads to the shear force at the mid supports are defined. These factors result from a series of case studies (Lantsoght et al., 2012a) that cover the geometry as encountered in the studied slab bridges owned by the Dutch Ministry of Infrastructure and the Environment. From these case studies, the most conservative resulting factors are chosen for application within the Quick Scan based on the Eurocodes, NEN 8700 series and recommendations based on the experimental research, “QS-EC2”. These factors are to be used only within the scope of the QS-EC2, Table 7.1. The factors from Table 7.1 are applicable for end spans between  $0,7l_{span}$  and  $0,8l_{span}$  where  $l_{span}$  is the length of the mid span, for cross-sectional depths between 600mm and 1000mm and for edge distances  $b_{edge}$  between 300mm and 1400mm. For the distributed loads near to the mid supports, pattern loading is considered. The sections mentioned in Table 7.1 are shown in Fig. 7.8. In Table 7.1, the following symbols are used:

- $\alpha_{TS1}$  correction factor on the shear stress for the statical indeterminacy for the 1<sup>st</sup> design truck;
- $\alpha_{TS2}$  correction factor on the shear stress for the statical indeterminacy for the 2<sup>nd</sup> design truck;
- $\alpha_{TS3}$  correction factor on the shear stress for the statical indeterminacy for the 3<sup>rd</sup> design truck;
- $\alpha_{UDL}$  correction factor on the shear stress for the statical indeterminacy on the uniformly distributed lane load;
- $\alpha_{DL}$  correction factor on the shear stress for the statical indeterminacy on the dead load.

Table 7.1: Correction factors for statical indeterminacy for three or more spans to be used in combination with QS-EC.

Section	$\alpha_{TS1}$	$\alpha_{TS2}$	$\alpha_{TS3}$	$\alpha_{UDL}$	$\alpha_{DL}$
support 1-2	0,95	0,90	0,78	0,94	0,75
support 2-1	1,11	1,16	1,21	1,34	1,31
support 2-3	1,06	1,05	1,04	1,10	1,00
support 3-2	1,05	1,04	1,01	1,12	1,04

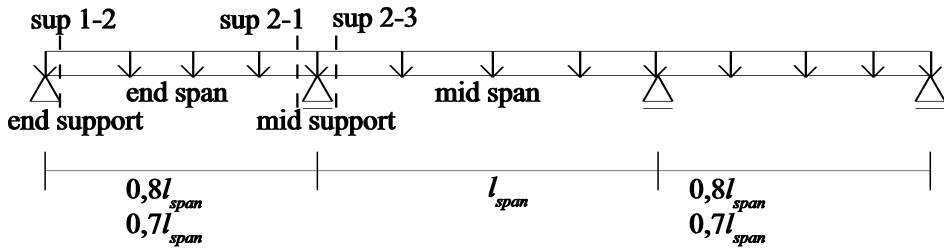


Fig. 7.8: Considered sections for a typical three-span bridge.

### 7.2.5 Influence of skew angle

As all slabs from the series of experiments are straight rectangular slabs, reference is made to the literature to provide recommendations with regard to the increased shear stresses that occur in skewed slabs. Cope et al. (1983) tested a series of slabs with an increasing skew angle of  $0^\circ$ ,  $30^\circ$  and  $45^\circ$ . As the slabs represented bridge decks, a load combination was used consisting of the following loads:

- two axes of an HB bogie load (concentrated wheel loads as used in the former British Standard) on the first lane;
- HA-loading (lane load as used in the former British Standard) on the second lane; and
- distributed loading to represent the larger contribution of the dead load for a full-scale model as compared to the scale models in the experiments.

The failure mode changed as the skew angle was varied; the straight slab failed in flexure (with some torsional distress), the  $30^\circ$  slab failed in wide beam shear and the  $45^\circ$  slab failed by punching at the support bearings. When using the shear and punching provisions from NEN-EN 1992-1-1:2005, it is found that the failure modes of shear and punching are both likely for the studied experiments (Lantsoght, 2012g). From this series of experiments, no conclusion with regard to the influence of the skew angle on the shear capacity could be made. Morrison and Weich (1987) tested two skewed slabs, one of which failed in flexure and one in punching shear. The second slab contained more flexural reinforcement. The results however cannot be used to study the influence of the skew angle on the shear capacity as only a skew angle of  $50^\circ$  was used for the specimens.

The experimental results from the literature cannot be used as a basis for a recommendation as none of the series showed the influence of the skew angle on the shear capacity. In the literature, recommendations based on the results of finite element calculations are available ('t Hart, 2012; Theoret et al., 2012). The skew factors by 't Hart (2012) are a function of the skew angle (straight or  $30^\circ$ ). In the results of a finite element analysis, the shear stress distribution at the support is studied. The results are obtained for the assumption of distributing the peak shear stress over  $2d_f$  and  $4d_f$ . The resulting skew factors are different for the dead load, the uniformly distributed load and the axle loads.

Quadratic summation of the shear stresses is shown to result in slightly smaller values for the skew factors and is used for comparison in Fig. 7.9. The method of Theoret et al. (2012) results in expressions for the design value of the skew factors  $C_{VD95\%}$  for the dead load and  $C_{VL95\%}$  for the live loads as a function of  $b$ ,  $l_{span}$  and the skew angle  $\theta$ :

$$\beta_{Theoret} = \frac{l_{span}}{b} \sin \theta \cos \theta \quad (7.15)$$

$$C_{VD95\%} = 1 + (0,095b + 0,25) \beta_{Theoret} \quad (7.16)$$

$$C_{VL95\%} = 1 + (0,095b - 0,125) \beta_{Theoret}$$

In the subscript of Eq. (7.16), “D” is used for the dead load, and “L” for the live load. The equations in (7.16) result in a design value with a 95% confidentiality level.

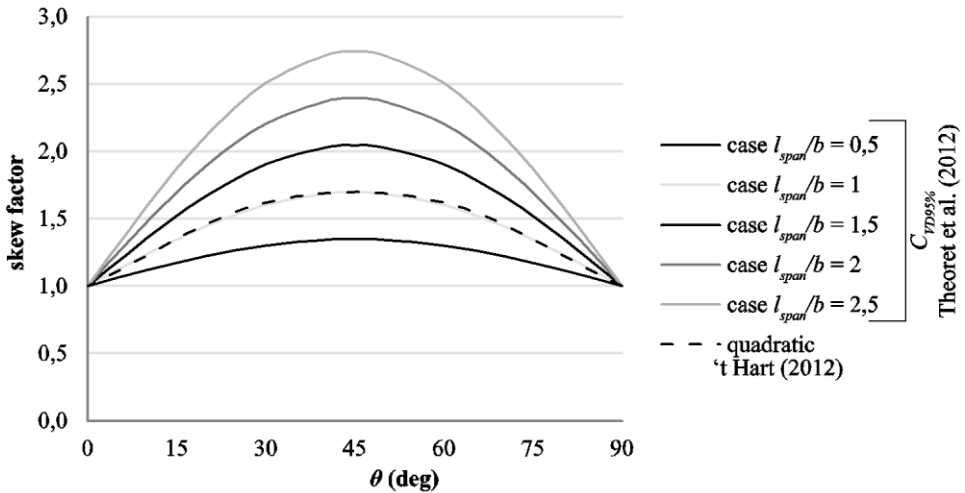


Fig. 7.9: Comparison between skew factors for the dead load from ‘t Hart (2012) and Theoret et al. (2012).

The resulting skew factors from the equations by Theoret et al. (2012) and ‘t Hart (2012) can be compared. However, as these methods take different variables into account, it depends on said parameters which method results in the smallest skew factors. A comparison between the resulting skew factors from ‘t Hart (2012) and Theoret et al. (2012) as a function of the skew angle  $\theta$ , assuming a fixed width  $b = 12\text{m}$  is shown in Fig. 7.9. Similar comparisons for different sets of parameters, covering the range of geometries as found in the cases of slab bridges owned by the Dutch Ministry of Infrastructure and the Environment, can be found in the full parameter studies (Lantsoght, 2012g). The resulting skew factors according to Theoret et al. (2012) become more conservative as the ratio  $l_{span}/b$  becomes larger and as the total width  $b$  becomes larger.

As a result of the lack of experimental results on the influence of the skew angle on the shear capacity of skewed slabs, no recommendation with sufficient confidence can be made with regard to the skew factors that should be used: the skew factor from 't Hart (2012) or Theoret et al. (2012). For the verification of the Quick Scan (QS-EC2), only viaducts with an insignificant skew angle are studied.

### **7.3 Quick Scan approach**

#### **7.3.1 Background**

In 2008, a first Quick Scan method was developed by Dutch structural engineering companies for the Ministry of Infrastructure and the Environment, based on the Dutch codes. For the current research, the Eurocodes and the NEN 8700 series for assessment as developed in the Netherlands were combined with the results of the experimental research and implemented into an updated version of the Quick Scan (QS-EC2), which will be discussed in the following paragraphs. The Quick Scan as used by the Dutch Ministry of Infrastructure and the Environment is a spreadsheet-based method providing an automated tool that can analyse a large number of viaduct sections at a time, and helps to decide which bridges should be given priority for a study in further detail. The Quick Scan method as developed for this research is a MathCad sheet in which all calculations and assumptions can be read, line by line. The Quick Scan results in a “unity check” value, which is the ratio of the design shear force as a result of the composite dead load (self-weight and wearing surface) and live loads (EN 1991-2:2003 Load Model 1) to the design shear capacity. The Quick Scan is based on the shear stress at the edge of the support, as Cope (1985) found this position to be the most critical for shear. Note that most assessment methods carry out a shear check at a distance  $d_l$  from the edge, while in the QS-EC2 the shear check is carried out at the face of the support.

#### **7.3.2 Overview of model assumptions**

The results of the experimental research are used in the Quick Scan sheet. The horizontal load spreading method to determine the effective width of the wheel loads, the minimum effective width, the influence of transverse stress redistribution, the hypothesis of superposition and the influence of flexure on the minimum shear capacity are discussed for application into the Quick Scan method in the following paragraphs.

To investigate which horizontal load spreading method is to be preferred, a comparison between all experimental results (from Table 3.2, Table 3.3 and Annex 1) and the values calculated with NEN-EN 1992-1-1:2005 taking into account  $b_{eff1}$  (Fig. 2.16a) and  $b_{eff2}$  (Fig. 2.16b) is carried out. As this comparison aims at analysing mean values of test data,  $C_{Rd,c,test}$  is taken as 0,15 and the mean material properties are used. For loads applied within a distance  $0,5d_l \leq a_v \leq 2d_l$  from the edge of a support, the contribution of this load to

the shear force  $V_{Ed}$  is multiplied by  $\beta = a_v/2d_v$ , according to §6.2.2.(6) from NEN-EN 1992-1-1:2005. The resulting statistical properties of the ratio between the experimental and calculated shear forces are summarized in Table 7.2, where

- $V_{TU}$  the ultimate shear force as observed in the Delft University of Technology experiments<sup>34</sup>;
- $V_{db}$  the ultimate shear force as from the experiments in the slab database from Annex 1;
- $V_{R,c,eff1}$  the shear force as calculated from NEN-EN 1992-1-1:2005 using  $b_{eff1}$ ;
- $V_{R,c,eff2}$  the shear force as calculated from NEN-EN 1992-1-1:2005 using  $b_{eff2}$ .

Table 7.2: Comparison between experimental results and values calculated according to NEN-EN 1992-1-1:2005 based on two assumptions for the horizontal load spreading method.

Comparison	Average	Standard deviation	Coefficient of variation
$V_{TU}/V_{R,c,eff1}$	3,401	0,890	26%
$V_{TU}/V_{R,c,eff2}$	2,382	0,522	22%
$V_{db}/V_{R,c,eff1}$	1,937	1,228	63%
$V_{db}/V_{R,c,eff2}$	1,570	0,659	42%

The statistical results from the comparison to NEN-EN 1992-1-1:2005 in Table 7.2 and the experimental results from the series of specimens with varying widths from Table 4.7 show that the horizontal load spreading method as used in French practice is to be preferred. The French load spreading method results in a smaller underestimation of the capacity when compared to the Delft experiments, and a significantly smaller coefficient of variation. Note that the scatter on the experiments from the slab shear database is large, as it comprises shear, punching and flexural failures. In §6.2.2, a more refined selection of the database was used, resulting in clearly smaller coefficients of variation as shown in Table 6.3. Therefore the results from the slab shear database are used here only in terms of the coefficient of variation to determine the preferable load spreading method.

Similarly, nonlinear finite element models (Falbr, 2011) showed that the effective width that results from the shear stress distribution at the support is closest to the effective width based on the French horizontal load spreading method. Doorgeest (2012) determined the effective width based on the stress distribution over the support for a series of models of slabs in TNO Diana with a variable width and a variable shear span. This analysis showed that the French load spreading method gives mostly a safe average of the effective width, although the increase of the effective width for an increasing shear span is smaller in the

---

<sup>34</sup> Note that all experiments are presented in terms of the ultimate shear force, and not the inclined cracking shear, which is difficult to observe in a slab shear experiment as the inclined crack can develop within the mass of the concrete slab.

models than as found when using the French load spreading method. Also, the effective width in the models by Doorgeest (2012) was found to be dependent on the overall slab width.

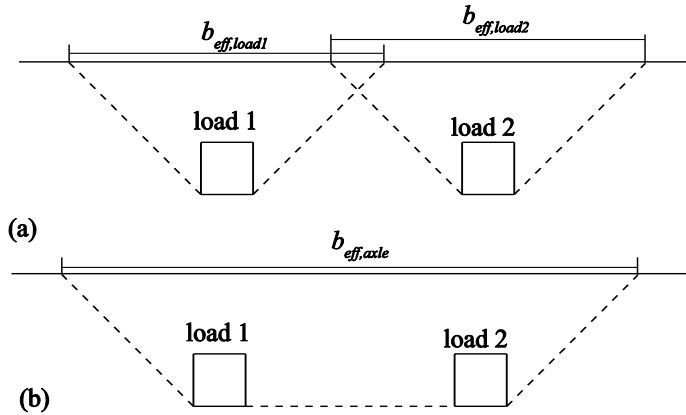


Fig. 7.10: Effective width applied to an axle from Load Model 1, top view: (a) effective width per concentrated load of the axle; (b) effective width of the entire axle.

As the French horizontal load spreading method results in overlapping effective widths when considering each wheel load separately, it is a conservative approach to determine the effective width of the entire axle (two wheel loads combined) (Lantsoght et al., 2012a). As in Load Model 1 always two wheel loads per axle are considered, using the effective width associated with the axle is a more conservative approach than using the effective width per concentrated load, Fig. 7.10. There are however no experimental results available to actually study the load-spreading behaviour for a slab subjected to two concentrated loads (one axle as drawn in Fig. 7.10), or four concentrated loads (two axles at 1,2 m distance of each other).

The minimum effective width can be taken as  $4d_l$ , provided that this value is a lower bound of the expression  $1,3(1,5b_{load} + d_l + b_r)$  (Lantsoght et al., 2012a) with:

$b_{load}$  the width of the load, taken in the span direction;

$b_r$  the distance between the free edge and the centre of the load.

This requirement results from comparing the expression for the asymmetric effective width for the case of a concentrated load near to the edge combined with the resulting  $V_{exp}/V_{R,c,eff2}$  from the experiments in this case to the lower bound  $4d_l$  combined with the general enhancement factor 1,25. The minimum effective width of  $4d_l$  becomes governing when the load is placed close to the support. The governing experiment is the case for which  $a/d_l = 1,51$  and the concentrated load is used near to the edge, as in: S6T1, S6T2, S6T4, S6T5, S10T1, S10T2, S10T4 and S10T5 (Table 3.2). For these cases, using an effective width of

$4d_l$  still provides conservative results when applied in combination with NEN-EN 1992-1-1:2005 (Lantsoght 2012a, Lantsoght et al., 2012a).

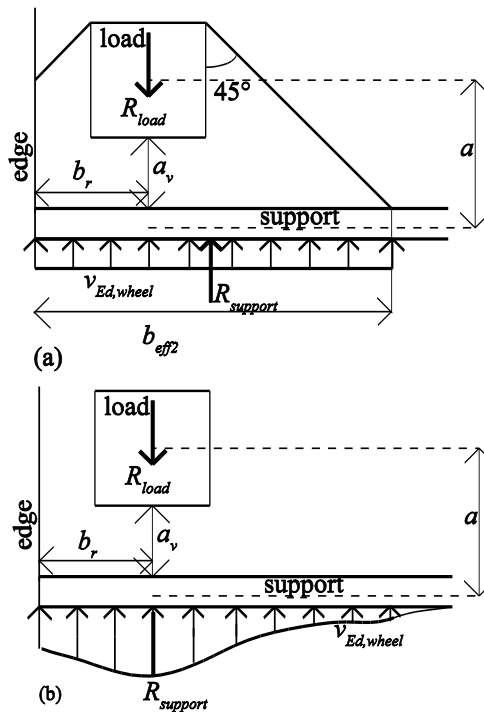


Fig. 7.11: Wheel load close to the edge: (a) Different location of resultant of shear force over support  $R_{support}$  and applied wheel load  $R_{load}$ ; (b) Real stress distribution at the support, in which the moment imbalance is not occurring anymore.

For loads close to the free edge of the slab, an asymmetric effective width can be chosen. For an asymmetric effective width, the reaction force of the wheel load  $R_{load}$  does not coincide horizontally with the force resultant  $R_{support}$  of the distributed shear stress over the support,  $v_{Ed,wheel}$ , Fig. 7.11a, creating an unbalanced moment. A statistical analysis (Lantsoght et al., 2012a) indicates a better correspondence between the experimental results and the shear capacities assuming an asymmetric effective width at the side than when a symmetric effective width is used. To further discuss this occurrence of the unbalanced moment as shown in Fig. 7.11a, it must be noted that the constant distribution of the shear stress at the support is mostly an assumption. The real shear stress distribution will have a peak at the location of the concentrated load and will then gradually decrease as the distance to the location of the load along the width becomes larger, Fig. 7.11b. The previous considerations thus show that for an approximate assessment method like the Quick Scan the assumption of an asymmetric effective width can be used.

Additional experiments on locally failed and heavily damaged slabs (S21T5, S21T6, S25T4, S25T5 given in Table 3.3) indicate that an asymmetric effective width can be used for loads with a clear shear span up to  $5,4d_l$  (Lantsoght et al., 2012a). For the tested slab, the effective width at a clear shear span of  $5,4d_l$  equals  $b_{eff2} = 2,32\text{m}$ , which almost corresponds to the full slab width of  $b = 2,5\text{m}$ .

To take into account the higher shear capacities of slabs as a result of transverse load distribution, the introduction of an additional enhancement factor is proposed (Lantsoght 2012d). The enhancement factor can be used in combination with NEN-EN 1992-1-1:2005 and an effective width based on the French load spreading method,  $b_{eff2}$ , assuming a minimum effective width of  $4d_l$ . To quantify the influence of transverse redistribution on the shear capacity, the results for  $V_{exp}/V_{R,c,eff2}$  with  $V_{R,c,eff2}$  determined assuming  $C_{Rd,c} = 0,18$  (as defined in NEN-EN 1992-1-1:2005, conservative approach<sup>35</sup> as discussed in §6.2) are studied. Assuming a normal distribution for  $V_{exp}/V_{R,c,eff2}$  results in a 5% lower bound for the enhancement factor of at least 1,25 (Lantsoght, 2012a).

All experiments were carried out to study the influence of the concentrated load close to the support. For  $a_v > 2,5d_l$  no results are available and data from the slab database needs to be evaluated. Therefore, a subset of the slab database for which  $b > b_{eff2}$  is used. Due to the large scatter on the database results, there is no proof for the use of the enhancement factor for  $a_v > 2,5d_l$  (Lantsoght et al., 2012a) based on the 5% lower bound of a normal distribution of the ratio between experimental and predicted values. Therefore, the enhancement factor can only be used in the vicinity of the support.

NEN-EN 1992-1-1:2005 §6.2.2(6) prescribes the use of the reduction factor  $\beta$ , Eq. (7.3) on loads close to supports with  $0,5d_l \leq a_v \leq 2d_l$  as  $\beta = a_v/2d_l$ . As the enhancement factor is also applicable only in the vicinity of the support, both factors can be combined into  $\beta_{new} = a_v/2,5d_l$  for the case of concentrated loads on slabs with  $0,5d_l \leq a_v \leq 2,5d_l$ . For distributed loads,  $\beta = a_v/2d_l$  is used as prescribed by NEN-EN 1992-1-1:2005 §6.2.2(6).

It was experimentally shown in Chapter 4, §4.11.2 that superposition of a concentrated load over the effective width,  $b_{eff2}$ , as determined based on the French load spreading method with the distributed loads over the full slab width can safely be used. This principle is applied in the Quick Scan approach: the contribution of the wheel loads to the shear stress, distributed over the effective width of the axle, is superposed to the shear stress due to the composite dead load and lane load, distributed over the full width of the viaduct.

NEN-EN 1992-1-1:2005 §6.2.2.(1) Eq. (6.3N) defines a lower bound for the shear capacity for elements without shear reinforcement, see Eq. (2.8). The lower bound defines the shear stress for which flexural failure will govern over shear failure, and assumes yielding of the longitudinal reinforcement at a characteristic yield strength  $f_{yk} = 500\text{MPa}$

---

<sup>35</sup> The following conservative assumptions are made:  $C_{Rd,c} = 0,18$ , using a normal distribution and taking the 5% lower bound to determine a characteristic increase.

(Walraven, 2002). However, reinforcing bars with a lower yield strength are commonly used in existing bridges. Before 1962, the standard reinforcement in the Netherlands was a type “QR24” with a yield strength  $f_{yk} = 240\text{MPa}$ . Therefore, the expression for  $v_{min}$  is derived again, as a function of the yield strength  $f_{yk}$ , which results in:

$$v_{min} = 0,772k^{3/2} f_{ck}^{1/2} f_{yk}^{-1/2} \quad (7.17)$$

The lower bound of the shear capacity is increased for elements reinforced with lower strength steel, as flexural failure will govern over shear failure for a larger range of shear stresses.

### 7.3.3 Overview of geometric and material assumptions

As not all geometric and material properties are known for existing bridges, some assumptions applicable to the bridges owned by the Dutch Ministry of Infrastructure and the Environment have to be made.

To assess the superimposed loads, the depth of the wearing surface is assumed to be 120mm (§7.2.1), leading to a fictitious tyre contact area of 640mm × 640mm as a result of vertical load distribution, Fig. 7.5. For the live loads, a combination of a lane load and the design vehicular loads (§7.2.2) is considered according to Load Model 1 from NEN-EN 1991-2:2003. A triangular stress distribution over the support, Fig. 7.6, is used for the additional uniformly distributed load in the first lane, with a lower bound based on vertical force redistribution, §7.2.2. All trucks are assumed to be centred in their fictitious lane.

The most unfavourable position of the vehicular loads to determine the maximum shear stress at the edge of the viaduct is obtained by placing the first design truck in such a way that the distance between the face of the support and the face of the fictitious tyre contact area equals  $2,5d_l$ . This distance is governing (§7.3.2) as the influence of direct load transfer is taken into account up to  $2,5d_l$ , provided that the slab depth is smaller than  $0,98\text{m}$ <sup>36</sup>. In the second and third lane, the design truck is placed in such a way that the effective width associated with the first axle reaches up to the edge of the viaduct. This concept is illustrated in Fig. 7.12 for the 2<sup>nd</sup> design truck. In Fig. 7.12 the following symbols are used:

- $a_{vi,j}$  the face-to-face distance between the support and the tyre contact area for the  $i^{\text{th}}$  truck and  $j^{\text{th}}$  axle;
- $b_{side}$  the edge distance to the side of the first tyre contact area, minimum 60cm;
- $a_{i,j}$  the centre-to-centre distance between the support and the tyre contact area for the  $i^{\text{th}}$  truck and  $j^{\text{th}}$  axle;
- $b_{load}$  the width of the tyre contact area;

---

<sup>36</sup> Changing the position of the wheel load influences the resulting shear force at the support, the effective width at the support and the reduction factor  $\beta$ . In a MathCad sheet, the most unfavourable position was determined by keeping the distance  $a_i$  as a variable.

- $l_{load}$  the length of the tyre contact area;  
 $w_{th,i}$  the width of the  $i^{th}$  notional lane = 3m;  
 $b_{eff,i,j}$  the effective width resulting from the French load spreading method for the  $i^{th}$  truck and  $j^{th}$  axle;  
 $i$  1.. 3, corresponding to the design truck under consideration;  
 $j$  1.. 2, corresponding to the axle of the design truck under consideration.

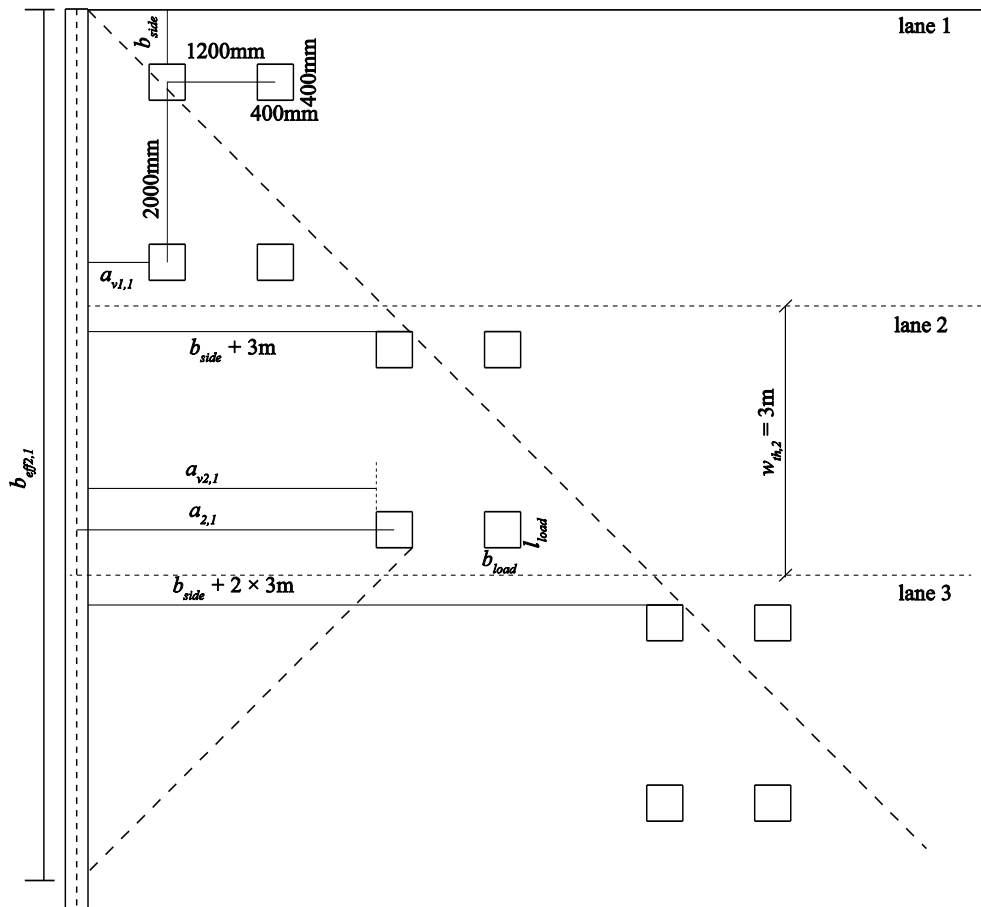


Fig. 7.12: Most unfavourable position of the design trucks.

Note that the position of the design trucks as shown in Fig. 7.12 is the most unfavourable condition for the largest shear stress at the edge of the support. For other failure modes, different arrangements of the design trucks need to be considered. For punching, for example, a relatively large force can result if two design trucks are placed at the same location in the span direction. The centre-to-centre distance between the wheel loads in the first lane and second lane is then only 1m, which is smaller than the distance between two

wheels of an axle (2m). A small punching perimeter should then be used around these two considered wheel loads.

To evaluate the concrete compressive strength of the slab bridges under study in the Netherlands and under the responsibility of the Ministry of Infrastructure and the Environment, material research was carried out. It was found that a minimum concrete cube compressive strength of 45MPa can safely be assumed when no strength determination on drilled cores is carried out (Steenbergen and Vervuurt, 2012; Vervuurt et al., 2012).

#### 7.3.4 Comparison to Quick Scan approach according to other codes

Similar approaches are followed to develop a Quick Scan method based on the Dutch Code NEN 6720:1995 (VBC), “QS-VBC”, and based on the North American practice (AASHTO LRFD and Manual of Bridge Evaluation AASHTO LRFR), “QS-AASHTO”. Vertical load redistribution through the wearing surface is assumed at a 45° angle for the axle loads in QS-VBC and QS-AASHTO. Additionally, in QS-VBC, vertical load redistribution is used to  $d/2$  for  $\Delta q_{load}$ , the increase in the lane load for the first, heavily-loaded lane.

For QS-AASHTO, the shear check is carried out at the face of the support (AASHTO LRFD §5.8.3.2), and the sheet selects whether the design tandem or design truck results in the largest shear forces. The QS-VBC uses the horizontal load spreading method as used in Dutch practice, while QS-AASHTO uses the load spreading method from French practice. For QS-AASHTO and QS-VBC the most unfavourable position of the vehicular loads to determine the maximum shear force at the edge of the viaduct is obtained by placing the first wheel load at such a location that the distance between the face of the support and the face of the tyre contact area equals  $a_v = d_t$ .

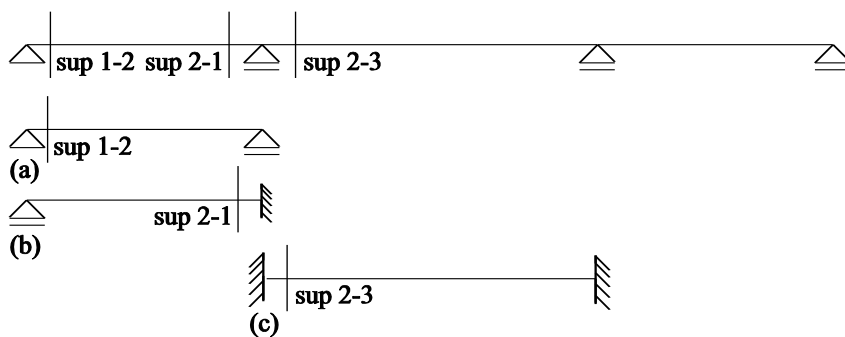


Fig. 7.13: Simplification of static scheme for the determination of the contribution of the concentrated wheel loads to the moment: (a) support 1-2 is simplified as pin-pin; (b) support 2-1 is simplified as fixed-pin; and (c) support 2-3 is simplified as fixed-fixed.

For application within the QS-AASHTO, factors for static indeterminacy applicable within the scope of the comparison are developed for the shear forces caused by the design truck, Table 7.3. In Table 7.3, the following symbols are used:

*Application to slab bridges and case studies*

- $\alpha_{Truck1}$  correction factor on the shear force due to the AASHTO design truck in the 1<sup>st</sup> lane at the support for the statical indeterminacy;
- $\alpha_{Truck2}$  correction factor on the shear force due to the AASHTO design truck in the 2<sup>nd</sup> lane at the support for the statical indeterminacy;
- $\alpha_{Truck3}$  correction factor on the shear force due to the AASHTO design truck in the 3<sup>rd</sup> lane at the support for the statical indeterminacy.

*Table 7.3: Correction factors for shear to account for statical indeterminacy for three or more spans, applicable to the AASHTO design trucks.*

Section	$\alpha_{Truck1}$	$\alpha_{Truck2}$	$\alpha_{Truck3}$
support 1-2	0,91	0,80	0,75
support 2-1	1,12	1,19	1,23
support 2-3	1,04	1,02	1,01
support 3-2	1,02	1,00	1,00

For the shear forces caused by the design tandem, lane load and permanent loads (QS-AASHTO) and for all loads applied in the QS-VBC, the values from Table 7.1 can be used. The AASHTO shear provisions are based on moments and shears. To determine the moments caused by the concentrated loads in a statically indeterminate structure, the static scheme is simplified to pin-pin for support 1-2 (Fig. 7.13a), to pin-fixed for support 2-1 (Fig. 7.13b), and to fixed-fixed for supports 2-3 and 3-2 (Fig. 7.13c). For the moments due to the dead loads and uniformly distributed lane load, the factors are based on a series of case studies comprising geometries within the scope of the Quick Scan. For the distributed loads near to the mid supports, pattern loading is considered. The maximum support moment is then expressed as:

$$\alpha_M q l_{span}^2 \tag{7.18}$$

with the values for  $\alpha_M$  as given in Table 7.4, in which:

- $\alpha_{MDL}$  correction factor for statical indeterminacy on the moment for the self-weight;
- $\alpha_{MUDL}$  correction factor for statical indeterminacy on the moment for the distributed lane load.

*Table 7.4: Factor  $\alpha_M$  as used in Eq. (7.18) for the maximum support moment for end spans between  $0,8l_{span}$  and  $0,7l_{span}$  and considering pattern loading for the lane load.*

Section	$\alpha_{MDL}$	$\alpha_{MUDL}$
support 2-1	0,08	0,09
support 2-3	0,08	0,09
support 3-2	0,09	0,10

The iterations based on AASHTO LRFD Table 5.8.3.4.2-2 to determine the shear capacity need to be carried out manually.

## **7.4 Results from 10 selected cases**

### **7.4.1 Introduction**

The resulting Quick Scan sheets are used to study ten selected cases: nine existing solid slab bridges from the Netherlands that have insignificant skew angles, an (almost) constant cross-sectional depth, no signs of deterioration and at least three spans; and a North-American example simple-span solid slab bridge from the Manual of Bridge Evaluation. For the nine cases from the Netherlands, the assumptions for the material and geometric properties valid for bridges owned and operated by the Ministry of Infrastructure and the Environment can be used. The continuous bridges are checked at minimum three different cross-sections, Fig. 7.2, and the simple-span bridge is checked at one cross-section. In Annex 5, the results of the QS-EC2 and QS-AASHTO for an additional set of 13 North American slab bridges is given as additional evidence for the conclusions in this section and for comparison to North American practice.

### **7.4.2 Results according to QS-EC2**

The geometry and the results of the Quick Scan calculations according to the Eurocodes, NEN 8700 series and the recommendations based on the experimental research (QS-EC2) are given in Table 7.5. In this table, the following symbols are used:

- $b$  width of the viaduct;
- $d_l$  effective depth to the longitudinal reinforcement;
- $l_{span}$  the length of the considered span;
- $f_{ck,cube}$  the characteristic cube compressive strength of the concrete: if no material research was carried out, this value is assumed to be 45MPa as explained in §7.3.3;
- $\rho_l$  the longitudinal reinforcement ratio;
- $v_{Ed}$  the shear stress at the face of the support due to the composite dead load and the live loads;
- $v_{Rd,c}$  the shear capacity from NEN-EN 1992-1-1:2005;
- uc EC the resulting unity check value according to QS-EC2.

According to the QS-EC2, for six out of ten viaducts the shear capacity should be studied in more detail. The Manual of Bridge Evaluation states for its example A7 that “concrete slabs and slab bridges designed in conformance with AASHTO specifications may be considered satisfactory for shear”, and “shear need not be checked for design load and legal load ratings of concrete members”.

Table 7.5: Geometry and results of Quick Scans QS-EC2 according to Eurocodes, NEN 8700 series and recommendations for 10 bridges.<sup>37</sup>

Section	$b$ (m)	$d_t$ (m)	$l_{span}$ (m)	$f_{ck,cube}$ (MPa)	$\rho_l$ (%)	$v_{Ed}$ (MPa)	$v_{Rd,c}$ (MPa)	uc EC
1 sup 1-2	9,6	0,791	9,5	45,0	0,443	0,267	0,450	0,595
1 sup 2-1	9,6	0,791	9,5	45,0	0,517	0,401	0,473	0,847
1 sup 2-3	9,6	0,791	13,0	45,0	0,517	0,449	0,473	0,948
1 sup 3-4	9,6	0,791	15,5	45,0	0,583	0,517	0,493	1,048
2 sup 1-1	14,5	0,331	7,0	45,0	1,045	0,533	0,715	0,746
2 sup 2-1	14,5	0,331	7,0	45,0	1,045	0,715	0,715	0,999
2 sup 2-3	14,5	0,331	8,4	45,0	1,045	0,727	0,715	1,018
3 sup 1-1	11,9	0,600	7,0	58,3	0,429	0,280	0,534	0,524
3 sup 2-1	11,9	0,600	7,0	58,3	0,429	0,401	0,534	0,750
3 sup 2-3	11,9	0,600	8,4	58,3	0,429	0,403	0,534	0,755
4 sup 1-1	11,9	0,360	7,0	70,6	0,716	0,453	0,725	0,625
4 sup 2-1	11,9	0,360	7,0	70,6	0,716	0,618	0,725	0,853
4 sup 2-3	11,9	0,360	8,4	70,6	0,716	0,629	0,725	0,868
5 sup 1-2	13,6	0,542	9,5	48,4	0,817	0,444	0,615	0,723
5 sup 2-1	13,6	0,542	9,5	48,4	0,909	0,626	0,615	1,018
5 sup 2-3	13,6	0,542	12,5	48,4	0,909	0,640	0,615	1,041
6 sup 1-2	19,2	0,457	10,0	49,6	0,934	0,525	0,670	0,783
6 sup 2-1	19,2	0,457	10,0	49,6	0,934	0,722	0,670	1,077
6 sup 2-3	19,2	0,457	13,0	49,6	0,934	0,738	0,670	1,102
7 sup 1-2	14,8	0,540	9,5	37,3	0,770	0,437	0,553	0,789
7 sup 2-1	14,8	0,540	9,5	37,3	1,284	0,606	0,656	0,924
7 sup 2-3	14,8	0,540	14,0	37,3	1,284	0,680	0,656	1,037
8 sup 1-2	13,4	0,590	12,0	66,4	1,366	0,439	0,798	0,550
8 sup 2-1	13,4	0,590	12,0	66,4	1,573	0,639	0,837	0,763
8 sup 2-3	13,4	0,590	15,1	66,4	1,573	0,638	0,837	0,762
9 sup 1-2	12,5	0,650	10,0	74,6	0,550	0,372	0,773	0,481
9 sup 2-1	12,5	0,650	10,0	74,6	1,092	0,543	0,773	0,703
9 sup 2-3	12,5	0,650	15,0	74,6	1,092	0,609	0,773	0,788
MBE A7	13,1	0,310	6,6	19,8	0,334	0,674	0,423	1,596

<sup>37</sup> The values of  $v_{Rd,c}$  highlighted in light grey are the cases for which  $v_{min}$  is governing. The unity check results highlighted in light grey are the values with  $1,0 \leq uc < 1,1$  and the results highlighted in grey are the values with  $1,1 \leq uc$ .

### Application to slab bridges and case studies

The results of the example AASHTO slab bridge (MBE-A7) according to the QS-EC2 are given on the last row of Table 7.5. According to QS-EC2, the example A7 from the Manual of Bridge Evaluation does not satisfy the NEN-EN 1992-1-1:2005 requirements for shear and results in the highest unity check value of the studied cross-sections. The statements from the Manual of Bridge Evaluation are thus not supported by the results of the Quick Scan according to the Eurocodes, NEN 8700 series and recommendations.

#### 7.4.3 Comparison to results according to QS-VBC and QS-AASHTO

For comparison to the QS-AASHTO, it is necessary to convert the cylinder compressive concrete strength  $f_{ck}$  into the specified concrete strength  $f_c'$  as defined by ACI 318-08 §5.3.2. The relation between the measured average concrete cylinder compressive strength and the specified concrete strength is based on the probability of 1% that the average of three consecutive tests is below the value of  $f_c'$ . As the standard deviation is not available for the material properties of the considered bridges, the average concrete compressive strength is transformed to  $f_c'$  by using Table 5.3.2.2 from ACI 318-08. To convert the characteristic cylinder compressive concrete strength as used in QS-EC2 into an average cylinder compressive strength, the relation between  $f_{cm}$  and  $f_{ck}$  from NEN-EN 1992-1-1:2005 Table 3.1 is used. Combining these expressions results in a relation between the cylinder compressive concrete strength  $f_{ck}$  and the specified concrete strength  $f_c'$  as follows:

$$f_c' = \frac{f_{ck} + 8\text{MPa} - 4,28\text{MPa}}{1,1} \quad (7.19)$$

The results of the unity checks according to the QS-AASHTO and the QS-VBC for the same ten cases of slab bridges, are given in Table 7.6, in which the following symbols are used:

$v_{u,AASHTO}$	the shear stress at the support due to the composite dead load and the live loads according to AASHTO LRFD and AASHTO LRFR;
$v_{c,AASHTO}$	the shear capacity resulting from AASHTO LRFD;
uc	the resulting unity check;
$\tau_d$	the shear stress at the support resulting from the composite dead load and the live loads according to NEN 8701:2011;
$\tau_u$	the shear capacity resulting from NEN 6720:1995.

Comparing the results of the calculations shows that the prescribed design loads (composite dead load and live loads as prescribed by the considered code) result in similar shear forces at the face of the support for both the Eurocode approach and the AASHTO approach (average of  $v_{u,AASHTO}/v_{Ed} = 1,01$  with a standard deviation of 0,10).

Table 7.6: Results of Quick Scans for 10 cases according to QS-AASHTO and QS-VBC<sup>38</sup>.

Section	$v_{u,AASHTO}$ (MPa)	$v_{c,AASHTO}$ (MPa)	uc AASHTO	$\tau_d$ (MPa)	$\tau_u$ (MPa)	uc VBC
1 sup 1-2	0,335	0,978	0,343	0,345	0,660	0,522
1 sup 2-1	0,452	0,812	0,557	0,485	0,660	0,735
1 sup 2-3	0,502	0,557	0,900	0,516	0,660	0,781
1 sup 3-4	0,580	0,557	1,041	0,583	0,660	0,883
2 sup 1-1	0,457	1,868	0,252	0,704	0,660	1,067
2 sup 2-1	0,603	1,105	0,559	0,921	0,660	1,396
2 sup 2-3	0,609	1,105	0,551	0,897	0,660	1,359
3 sup 1-1	0,310	1,237	0,250	0,386	0,793	0,487
3 sup 2-1	0,412	1,040	0,396	0,523	0,793	0,659
3 sup 2-3	0,398	1,040	0,382	0,506	0,793	0,638
4 sup 1-1	0,433	1,633	0,265	0,634	0,916	0,692
4 sup 2-1	0,554	1,398	0,408	0,834	0,916	0,910
4 sup 2-3	0,557	1,243	0,448	0,808	0,916	0,882
5 sup 1-2	0,454	1,379	0,329	0,533	0,694	0,768
5 sup 2-1	0,603	0,900	0,671	0,719	0,694	1,037
5 sup 2-3	0,640	0,782	0,819	0,731	0,694	1,053
6 sup 1-2	0,510	1,619	0,315	0,627	0,706	0,888
6 sup 2-1	0,684	1,095	0,624	0,841	0,706	1,192
6 sup 2-3	0,720	0,969	0,743	0,868	0,706	1,23
7 sup 1-2	0,444	1,297	0,343	0,524	0,583	0,899
7 sup 2-1	0,591	1,007	0,587	0,710	0,583	1,218
7 sup 2-3	0,699	0,846	0,826	0,770	0,583	1,321
8 sup 1-2	0,477	1,694	0,282	0,526	0,874	0,601
8 sup 2-1	0,656	1,316	0,499	0,731	0,874	0,836
8 sup 2-3	0,682	1,105	0,617	0,730	0,874	0,835
9 sup 1-2	0,407	1,390	0,293	0,450	0,956	0,471
9 sup 2-1	0,554	1,390	0,399	0,627	0,956	0,656
9 sup 2-3	0,657	1,016	0,647	0,686	0,956	0,717
MBE A7	0,576	0,853	0,675	0,855	0,451	1,894

However, two remarks should be made with respect to this observation:

<sup>38</sup> The unity check results highlighted in light grey are the values with  $1,0 \leq uc < 1,1$  and the results highlighted in grey are the values with  $1,1 \leq uc$ .

- 1) the shear force due to the AASHTO load already incorporates the resistance factor for shear  $\phi_{AASHTO} = 0,9$  while in the QS-EC2 a similar factor is incorporated into the expression for the shear capacity,  $v_{Rd,c}$ ; and
- 2) the load factors from NEN 8700:2011 result in higher reliability levels ( $\beta_{rel} = 3,6$  for the repair level for all bridges built before April 1<sup>st</sup> 2012) as compared to the load factors from AASHTO LRFR ( $\beta_{rel} = 2,5$  for the design load at operating level).

The demands on the level of “repair” from NEN 8700:2011 as compared to the level of “design-operating” from AASHTO LRFR are described similarly in words by the codes, but translated into a different requirement for the reliability index. Therefore, the limits of this comparison should be kept in mind.

Comparing the shear stress due to the prescribed design loads at the face of the support for both the QS-EC2 and the QS-VBC shows a smaller resulting shear stress for the QS-EC2 ( $v_{Ed}/\tau_d = 0,82$  with a standard deviation of 0,05). The decrease in the shear stress in the QS-EC2 is the result of the reduction factor  $\beta = a_v/2d_l$  for distributed loads with  $0,5d_l \leq a_v \leq 2d_l$  as shown in Fig. 7.3 and  $\beta_{new} = a_v/2,5d_l$  for concentrated loads with  $0,5d_l \leq a_v \leq 2,5d_l$ , as well as the larger effective width  $b_{eff2}$  resulting from the horizontal load spreading method used in French practice. It is thus important to highlight that, as a result of the recommendations from the experimental research, a decrease of 18% in the shear load that needs to be taken into consideration is obtained.

Comparing the resulting shear capacities  $v_{Rd,c}$  in QS-EC2 and  $v_{c,AASHTO}$  in QS-AASHTO shows that AASHTO LRFD allows for higher shear capacities than NEN-EN 1992-1-1:2005 (average of  $v_{c,AASHTO}/v_{Rd,c} = 1,78$  with a standard deviation of 0,41). Both methods take the size effect in shear into account, resulting in smaller shear capacities for larger depths. While the shear formula from NEN-EN 1992-1-1:2005 results in shear capacities of  $< 0,50\text{MPa}$  for low levels of flexural reinforcement ( $\rho_l < 0,6\%$ ), the influence on the calculated shear capacities according to AASHTO LRFD is smaller. The smallest shear capacity according to AASHTO LRFD of  $0,557\text{MPa}$  is obtained for a long span ( $l_{span}/d_l = 19,6$ ) with a cube concrete compressive strength of  $45\text{MPa}$ . The viaducts for which data from material research is available ( $f_{ck,cube} > 45\text{MPa}$ ), result in higher shear capacities according to AASHTO LRFD than NEN-EN 1992-1-1:2005, as AASHTO uses a square root for the relation between the compressive strength and the shear capacity while NEN-EN 1992-1-1:2005 uses a cube root. It should be noted that the Modified Compression Field Theory (Chapter 2, §2.4.1), on which the AASHTO provisions are based, reduces the size of the aggregate  $d_{agg}$  to 0mm for high strength concrete to take into account the reduced aggregate interlock capacity in high strength concrete. A similar limit is however not found in AASHTO LRFD.

Comparing the resulting shear capacities for QS-EC2 and the QS-VBC shows that NEN 6720:1995 allows for higher shear capacities than NEN-EN 1992-1-1:2005

( $\tau_d/v_{Rd,c} = 1,17$  with a standard deviation of 0,19). The NEN 6720:1995 formula is only a function of the compressive strength of the concrete. According to the Eurocode expression, low levels of flexural reinforcement and deep cross-sections have a smaller shear capacity.

The unity checks according to QS-AASHTO give lower results than QS-EC2. On average, the QS-AASHTO unity check value for shear is only 60% of the QS-EC2 unity check value (with a standard deviation of 0,16). In turn, the unity checks resulting from the QS-EC2 give smaller values than the unity checks resulting from the QS-VBC ( $uc_{EC2}/uc_{VBC} = 0,96$  with a standard deviation of 0,15). With the Eurocode Quick Scan, eight sections in six viaducts are identified as needing further investigations, with only two sections resulting in a unity check value  $> 1,1$ . With the QS-VBC, ten sections in five viaducts are identified as needing further investigations, with seven sections in four viaducts having a unity check  $> 1,1$ . With the AASHTO LRFR, only one section remains. The QS-EC2 meets its goal of providing an improved assessment tool as compared to the QS-VBC. As the QS-EC2 determines fewer cross-sections as shear-critical, fewer viaducts will require to be studied in further detail. As such, the QS-EC2 has a better selecting ability than the QS-VBC.

The example from the Manual of Bridge Evaluation A7 does not require shear to be checked according to the AASHTO provisions, which is reflected by the small unity check value in the QS-AASHTO. However, when calculating this example according to the European practice, a unity check value being almost 2,4 times larger is found for the QS-EC2 and of 2,8 times larger for the QS-VBC. Therefore, it can be concluded that it is justified to pay due attention to the problem of the shear capacity of existing bridges.

#### 7.4.4 Conclusions

The Quick Scan evaluation method is an approximate method to determine which bridges of a large set of reinforced concrete slab bridges should be further studied. The Quick Scan approach is based on checking a limited number of previously identified critical cross-sections. It is used as a first estimator to prioritize the efforts and is suitable for application by Departments or Ministries of Transportation or other organisations that own a large set of this type of bridges.

The QS-EC2 as developed based on the experimental results is used to study ten cases of bridges: nine existing, continuous reinforced concrete slab bridges from the Netherlands and one example from the Manual of Bridge Evaluation. The results of the QS-EC2 are compared to the QS-VBC, which is similar to the Quick Scan sheet that was used prior to application of NEN-EN 1992-1-1:2005 and the research findings, and to the QS-AASHTO, which is an application based on North-American practice and does not rely on the experimental results of shear in slabs. The results of these Quick Scans show a

refinement in the evolution from QS-VBC to QS-EC2 as a result of the change in the position of the design trucks and the larger effective width resulting from the French load spreading method. The unity check values as found by QS-AASHTO are significantly lower, but the comparison is based on rating levels that are described in similar words but for which the underlying assumptions of the reliability index and associated failure probability are different.

## **7.5 Conclusions**

### **7.5.1 Summary**

This chapter shows the practical applications of the research on shear in reinforced concrete slab bridges. To assess a large number of slab bridges, the research findings are implemented into an existing Quick Scan spreadsheet method. The loads used in this method are the composite dead load and the live loads. To optimize the contribution of the self-weight, the possibility of defining a parabolic shape is implemented. For the distributed loads, the reduction of the load close to the support through  $\beta = a_v/2d_l$  is implemented. For the live loads, Load Model 1 from NEN-EN 1991-2:2003 is used:

- for the wheel loads the most unfavourable location is found based on the research findings and,
- for the increased lane load in the first, heavily-loaded lane, a triangular stress distribution satisfying force and moment equilibrium is applied with a lower bound based on vertical stress distribution.

The load factors in the QS-EC2 are taken according to NEN 8700:2011, and based on a reliability index  $\beta_{rel} = 3,8$  (and 3,6 for bridges built before April 1<sup>st</sup> 2012). For comparison, note that rating according to the design – operating level from AASHTO LRFR as applied to QS-AASHTO is based on a reliability index  $\beta_{rel} = 2,5$ . As the Quick Scan method is used to indicate which viaducts need to be studied in more detail, an approximation is used to take static indeterminacy into account via the use of correction factors based on a series of case studies.

As the experimental research indicates that the transverse load redistribution and the direct load transfer of wheel loads near to the support increase the shear capacity, the QS-EC2 takes these research findings into account. These findings result in the following recommendations:

- Use the French horizontal load spreading method to determine the effective width in shear.
- Use a minimum effective width of  $4d_l$ .
- Use  $\beta_{new} = a_v/2,5d_l$  for wheel loads close to the support.
- Apply superposition of concentrated loads over their respective effective widths with distributed loads over the full slab width.

### *Application to slab bridges and case studies*

- Use Eq. (7.17) to take into account the influence of the yield strength of the reinforcement on the lower bound of the shear capacity,  $v_{min}$ .

To calculate the cases of existing bridges with the Quick Scan approach, a few assumptions can be made that are valid for the slab bridges owned by the Dutch Ministry of Infrastructure and the Environment. Material research has been carried out on a subset of these bridges. When comparing the results of the QS-EC2, QS-VBC and QS-AASHTO, it should also be noted that the procedure of the QS-EC2 is based upon and aligned with the research findings, while the QS-VBC and QS-AASHTO method are based upon the code provisions and the interpretation thereof. The results from the case studies of the ten slab bridges that are calculated with the Quick Scan spreadsheet show an improvement in the filtering ability of the QS-EC2 as compared to the QS-VBC, indicating the benefit of the application of the results from the experimental research. Moreover, the results from these cases indicate that the statement of AASHTO LRFR that shear should not be checked when rating reinforced concrete slabs and slab bridges, does not correspond to the findings of the verifications according to the QS-EC2 as well as the QS-VBC.

#### *7.5.2 Recommendations and outlook for practicing engineers*

To study the shear capacity of a reinforced concrete slab bridge subjected to the composite dead load and live loads, different levels of approximation can be used:

1. Use an initial spreadsheet-based or hand calculation-based approach to see if the considered cross-section might require further calculations. The QS-EC2 method, a tool to provide a first assessment, is found as the optimal approach.
2. If an initial assessment shows that further investigations are needed, refined models such as (non)-linear finite element models can be used.

Moreover, it is shown that the statement from the Manual of Bridge Evaluation that shear should not be checked in reinforced concrete slabs and slab bridges cannot be supported based on the QS-EC2, which implements the findings of the aforementioned experimental research. With the right tools, however, a quick check for shear can show that further levels of approximation to study the shear capacity are not required.

*Application to slab bridges and case studies*

## **8 Conclusions and Outlook**

### **8.1 Overview of main contributions to knowledge on shear in one-way slabs**

In this dissertation, the shear capacity of reinforced concrete slabs under concentrated loads close to supports is studied. This study is carried out by means of a literature review, an extensive series of experiments and case studies of existing solid slab bridges. The experimental results are used for a parameter analysis and for an extensive comparison to the code provisions as well as a statistical analysis thereof. Moreover, a series of existing slab bridges is studied to apply the research findings to the assessment practice. The research has resulted in the following original contributions to the body of knowledge on shear and slabs:

- the development of a database with shear tests on one-way slabs and wide beams (Chapter 2);
- results of experiments on slabs under concentrated loads close to supports ( $a_v < 2,5d_l$ ), as have not been carried out previously (Chapter 3);
- insight in the behaviour of one-way slabs under concentrated loads close to supports with regard to the different tested parameters (Chapter 4);
- a mechanical model, the Modified Bond Model, to assess the capacity of slabs subjected to concentrated loads close to supports (Chapter 5);
- a code extension proposal in line with the approach and philosophy of NEN-EN 1992-1-1:2005, based on a statistical analysis (Chapter 6);
- recommendations for the assessment of existing solid slab bridges based on this research and a study of the distribution of live loads, applied into the Quick Scan method (QS-EC2) for the Dutch Ministry of Infrastructure and the Environment (Chapter 7).

### **8.2 Summary of conclusions and research findings**

An overview of the main conclusions of the research is given in the following paragraphs.

#### **8.2.1 Force transfer in slab bridges**

Slab bridges are robust structures, designed to fail in flexure, as shear was not considered in the Dutch building codes from the post-war decades. However, in the recent years, more attention was paid to the shear capacity of the existing slab bridges, as concerns with regard to the shear capacity were raised. The reason for these concerns is twofold: larger live loads and smaller allowed shear capacities. The prescribed live loads in the newly implemented Eurocode 1 NEN-EN 1991-2:2003 are larger than used by the previous national codes. The heavier prescribed live loads include significantly heavier and more closely spaced wheel loads that result in increased sectional shear forces at the support. At the same time, the shear provisions from the recently implemented NEN-EN 1992-1-1:2005 are more

## *Conclusions and Outlook*

conservative, especially for deep cross-sections and low amounts of flexural reinforcement. Therefore, in the Netherlands it was decided to investigate the shear capacity of the existing reinforced concrete solid slab bridges. It should be kept in mind that the existing code provisions aim at limiting the shear stress so that ductile flexural failures occur before brittle shear failures. Also, the shear provisions are suitable to determine the shear capacity of beams and do not take the beneficial geometric properties of one-way slabs into account. While these approaches generally lead to safe designs, they are not suitable for assessing the real shear capacity of an existing structure.

To assess the existing bridges, it is interesting to take load transfer mechanisms into account that are typically neglected for design. An example of such a mechanism is transverse load distribution in slabs subjected to a concentrated load: a larger width than the width of the load will be activated to resist shear. Due to the extra dimension of the width in slabs as compared to beams, transverse load distribution can occur in slabs under a concentrated load. In this research, the transverse load distribution capacity of slabs under a concentrated load was studied experimentally for the first time.

A slab under a concentrated load fails in a failure mode that is not purely one-way (beam) shear or two-way (punching) shear. While for both one-way and two-way shear a multitude of approaches exist in the literature, the mechanics of the shear problem are still not fully understood. None of the studied models was developed for the application to concrete slab bridges under wheel loads close to support lines, and therefore all methods contain some major drawbacks. The Modified Compression Field Theory seems to be less suitable for loads close to the support, and cannot be applied to the problem of punching. Therefore, it is questionable if this method can adequately model the transitional problem of shear in one-way slabs under concentrated loads. The Critical Shear Crack Theory uses the same approach for one-way shear as well as for punching shear. However, in the case of a concentrated load close to the support, the non-axis-symmetrical layout needs to be taken into account, and finite element programs are needed to determine the load-rotation relationship and the stress distribution along the punching perimeter. Strut-and-tie models can be applied to the problem of a concentrated load on a slab. Due to the large number of possible models, however, this approach is deemed not suitable for the assessment practice.

The on-going debate in the literature on how to deal with shear in reinforced concrete members is also reflected by the code provisions. The studied codes (NEN 6720:1995, NEN-EN 1992-1-1:2005, ACI 318-08 and Model Code 2010) all recommend very different approaches and take the parameters affecting the shear capacity into account in different ways. Ideally, the empirical code formulas should be replaced by methods with a theoretical basis.

Most of our knowledge on shear is the result of experiments on small, heavily reinforced slender beams tested in four point bending, and most of our knowledge on punching shear is the result of experiments on centrally loaded slab-column connection

specimens. It might be questionable to extrapolate this knowledge to the case of a slab bridge under live loads. For the case of a slab under a concentrated load in shear, only Regan's empirical method (1982), based on a model for punching and combined with an enhancement factor from beam shear to take direct load transfer into account, is available in the literature.

For slabs and wide beams under a concentrated load, a certain effective width, that carries the load in shear, should be defined. This effective width is typically based on rules of thumb from local practice. The only code that gives guidelines for the determination of the effective width is the *fib* Model Code 2010. Until now, estimates of the effective width have been based on finite element results. The current research quantifies the effective width in shear experimentally for the first time.

### 8.2.2 Development of the slab shear database

While databases for beam shear and punching shear can be found in the literature, a database with experimental results of one-way slabs and wide beams failing in shear is compiled for the first time, including some experiments that are not commonly found in the existing databases. The developed database can be used to study the gaps in the current knowledge, to study trends in the data and to verify the recommendations that result from the experiments carried out as part of this research. The database can be found in Annex 1. A distinction is made between punching shear failures and one-way shear failures. This distinction is based on an interpretation of photographs and sketches of the cracking patterns. Different categories of experimental setups (simply supported slabs, continuously supported slabs, cantilevering decks or decommissioned bridges) are also identified and reported in the database.

The constructed database shows crowding in the small size and relatively large reinforcement percentage region. As most experiments are carried out on specimens with a small effective depth, the influence of the size effect cannot be studied from the database. Only 22 experiments on slabs benefiting from transverse redistribution ( $b_{eff2} < b$ ) with the load placed close to the support are available in this database of 215 experiments. Only one full series of small-sized slabs ( $h = 100\text{mm}$ ) subjected to concentrated loads close to supports has been carried out in the past (Regan, 1982). This small number of experiments demonstrates the need for an extensive series of experiments, as carried out for this research.

### 8.2.3 Slab shear experiments

A total of 26 slabs and 12 slab strips were tested in the Stevin II Laboratory of Delft University of Technology. Altogether 156 experiments were carried out, and the following parameters have been varied to study their influence on the shear capacity of reinforced concrete slabs under concentrated loads close to supports:

### *Conclusions and Outlook*

- the size of the loading plate, to study the influence of the wheel print as chosen in the load models and to study the different load spreading methods;
- the influence of predamageing<sup>39</sup>, to study if the shear capacity of a slab bridge that is cracked in flexure after many years of service is smaller;
- the amount of transverse flexural reinforcement, to study the influence of the reinforcement layout on the shear capacity and to study the contribution of the non-principal reinforcement direction to the shear capacity;
- the moment distribution at the support, to study the difference between loading close to the simple and continuous support;
- the distance between the load and the support, resulting in a different angle for the compression strut for direct load transfer;
- the concrete compressive strength, which is found to be one of the main parameters influencing the shear strength of reinforced concrete beams in experiments, by testing normal strength concrete and high strength concrete slabs;
- the overall width of the specimens by testing a series of slab strips with different widths, to study how the specimen width influences the failure mode and how the additional dimension of the width in the slabs is activated;
- the type of reinforcement (plain bars or ribbed bars), to study the influence of the reduced bond capacity of plain bars on the shear capacity of reinforced concrete slabs, as the existing bridges built before 1963 are reinforced with plain bars;
- the support layout (line supports or steel or elastomeric bearings), to study the influence of a reduced support length on the shear capacity of slabs and to study the difference between steel bearings and elastomeric bearings;
- the difference between loading with a concentrated load only and loading with a combination of a line load over the width and a concentrated load, as for the assessment of existing bridges a combination of the composite dead load (self-weight and wearing surface) and live loads (combination of distributed lane loads and concentrated wheel loads) is used.

The observed failure modes were:

- wide beam shear, with an inclined crack at the bottom face,
- beam shear failure at the side face between the load and the support,
- beam shear failure at the side face with an inclined crack at a distance away from the support,
- failure by punching of the support bearings (only observed for slabs supported by bearings),
- partial punching visible at the bottom face by a partial punching cone, and

---

<sup>39</sup> Note that the predamageing in the experiments was the result of a previous experiment up to failure (ultimate limit state), while cracking in existing bridges is never so severe as it remains within the bounds of the serviceability limit state.

- anchorage failure (only observed for slabs reinforced with plain bars).

A summary of the experimental results, with the loads at failure and the observed failure modes is given in Chapter 3. The full description of the tests is reported in the Stevin Reports of the experiments (Lantsoght 2011a, b; 2012c).

#### 8.2.4 *Influence of parameters on shear capacity of slabs*

The experimental results demonstrate that reinforced concrete slabs subjected to concentrated loads close to supports carry shear in a two-dimensional way that is distinctly different from the one-dimensional way in which shear is carried in beams. This statement is reflected in the results with regard to the following parameters:

- the size of the loading plate,
- the moment distribution in the shear span and its decreasing influence for increasing specimen widths,
- the distance between the load and the support,
- the concrete compressive strength and its smaller observed influence for slabs than for beams, and
- the overall specimen width.

The test results have indicated that the geometric properties of the slab, the support and the load are decisive for the shear capacity of reinforced concrete slabs under concentrated loads near to supports. This statement is supported by the results of the parameter analysis, indicating the following parameters to be important:

- the size of the loading plate,
- the distance between the load and the support, and
- the overall width of the member<sup>40</sup>.

On the other hand, the following parameters did not affect the shear capacity substantially:

- the amount of transverse flexural reinforcement,
- the concrete compressive strength,
- the type of reinforcement (plain bars or deformed bars), and,
- when using a line of bearings, the material of the bearing (steel or rubber).

The experimental results indicate a large residual capacity for severely damaged slabs. Also, slabs under concentrated loads close to supports fail in a more ductile mechanism than observed in typical beam shear experiments. Moreover, in the experiments on slabs, inclined cracks indicating imminent shear failure are observed at 70% of the failure load, indicating the ability of slabs to show warning behaviour before shear failure.

The experiments show that the shear capacity at the continuous support is at least equal to the shear capacity at the simple support. This observation is contrary to the previously used Dutch code (NEN 6720:1995), in which an increase due to direct load

---

<sup>40</sup> Note that the effective threshold width that is found depends on a number of parameters. According to NEN-EN 1992-1-1:2005, slab behaviour is expected for elements with  $b \geq 5h$ .

## *Conclusions and Outlook*

transfer for loads applied in the vicinity of the support was only allowed for loads close to simple supports.

From the series of slabs and slab strips with different widths, it became clear that the horizontal load spreading method that is used in French practice can be used to determine the effective width in shear.

The hypothesis of superposition was found to be a conservative assumption in the experiments on slabs subjected to a concentrated load and a line load. The contribution of the concentrated load over the effective width to the shear stress at the support can be added to the shear stress due to the distributed loads over the full width.

### *8.2.5 The Modified Bond Model*

The Modified Bond Model is developed as a mechanical model, inspired by the lower bound theorem of plasticity and Regan's method (1982) and combining elements from one-way and two-way shear. It is a tool for predicting the maximum load for reinforced concrete slabs under concentrated loads close to supports failing in shear. The load is carried by two-way quadrants and one-way strips that carry load through arching action, in the Modified Bond Model. In the strip between the load and the support, direct transfer of the load from its point of application to the support by means of a compressive strut or compressive arch is taken into account, resulting in an increased bearing capacity.

The original Bond Model for concentric punching shear by Alexander and Simmonds (1992) was extended in such a way that it is applicable to rectangular slabs with different reinforcement levels in the  $x$ - and  $y$ -directions and with loads close to supports. The resulting Modified Bond Model is also applicable for loads close to the edge, close to a continuous support, for slabs reinforced with plain bars and for slabs not supported over their entire width.

In Chapter 5, §5.3.6 a step-by-step guide is given on how to calculate the capacity for a slab under concentrated loads close to supports by using the Modified Bond Model. The proposed model strongly depends on the geometry of the slab, the load and the support, and requires sketching of the loading situation to understand how the load in two-way quadrants is transferred to the strips that carry load by means of arching. When the concentrated load is placed eccentric from the centre of the width, or when the supported length is smaller than the full slab width, reduction factors based on the geometry can be formulated. The layout of bottom and top reinforcement are important as well, and the top reinforcement (or hogging moment reinforcement) is activated in the strips that border the quadrants in which a sign change from the support moment to the span moment occurs. The moment distribution and reinforcement layout influence the flexural capacity  $M_s$ , which determines, together with the loading term  $w$ , the capacity of the strips. This loading term  $w_{ACI}$  is the same as in the original Bond Model, based on the ACI equation for the inclined cracking load, and can be considered as an element of empiricism in the proposed method.

## *Conclusions and Outlook*

As the Modified Bond Model considers cases that are non-axis-symmetrical, all four strips can be considered separately. In the original Bond Model for concentric punching shear, all four strips had equal capacities and were summed without further notice. The strength of the Modified Bond Model lies in its versatility: the strips are considered differently in all four directions, and the reduction of the capacity of the strips due to the geometry is taken into account by studying the changed loading term on the strips and the altered moment capacity.

It is shown that the results obtained with the Modified Bond Model give a better estimate of the maximum load on a slab than when using an existing method or when using a codified approach. The statistical analysis of the experimental results to the predicted values indicates that using the Modified Bond Model as compared to, amongst others, the shear provisions from NEN-EN 1992-1-1:2005 is to be preferred.

### 8.2.6 Comparison between methods and experimental results

To further evaluate the existing methods for shear and the proposed Modified Bond Model, a statistical comparison between the experimental results and the calculated values is carried out. The general comparison of the statistical properties of the ratio of experimental to predicted values shows that the preferred method for slabs under concentrated loads close to supports is the Modified Bond Model. Other methods that result in an acceptable coefficient of variation on  $V_{exp}/V_{calc}$  or  $P_{exp}/P_{calc}$  are the combination of NEN-EN 1992-1-1:2005 with an effective width  $b_{eff2}$  based on the French horizontal load spreading method, and Regan's modified punching approach (Regan, 1982). The advantage of using NEN-EN 1992-1-1:2005 is its applicability to a wider range of loading situations, as the shear stress at the support can be evaluated with respect to the codified shear capacity. For the assessment of existing bridges under live loads, the Eurocode approach is thus more applicable.

The combination of NEN-EN 1992-1-1:2005 with  $b_{eff2}$  based on the French load spreading method, takes into account the influence of the size of the loading plate on the effective width and thus the shear capacity. The Modified Bond Model takes into account the size of the loading plate, as this size determines the width and the moment capacity of the load-carrying strip. These methods reflect the increased ability for transverse load redistribution when a larger loading plate is used.

The amount of transverse reinforcement is not taken into account in a traditional one-way shear approach but can be used for a punching shear approach. When compared to Regan's method, based on punching shear, the experiments show that the influence of the transverse reinforcement is overestimated. The experiments are at the transition between one-way and two-way shear, with a larger shear capacity for the longitudinal sections and a smaller contribution for the transverse sections. In the Modified Bond Model, the transverse

## Conclusions and Outlook

reinforcement is taken into account in the strips in the  $y$ -direction of the slab, but redistribution of the loading to the stiffer  $x$ -direction strips is allowed for.

The moment at the continuous support is taken into account for the Modified Bond Model by applying the factor  $k_r = M_{sup}/M_{span}$  onto the flexural capacity  $M_s = M_{neg} + k_r M_{pos}$  for the strips that border the quadrants in which the sign of the moment changes. For NEN-EN 1992-1-1:2005, the same capacity at the simple and continuous support is assumed. In the experiments, it was found that the shear capacity at the continuous support is at least equal to the shear capacity at the simple support.

The experimental results showed the important influence of the distance between the load and the support  $a_v/d_l$  on the shear capacity of concrete slabs under concentrated loads. The influence on slabs is found to be smaller than the influence of beams. This observation is correctly taken into account for the Modified Bond Model, in which the influence of the distance between the load and the support only enhances the capacity of the  $x$ -direction strip between the load and the support. In NEN-EN 1992-1-1:2005, the distance between the load and the support leads to the reduction of the contribution of the considered load to the sectional shear at the support for loads with  $0,5d_l \leq a_v \leq 2d_l$ . The advantage here lies in the easy applicability to a combination of loads, which can consist of concentrated or distributed loads. The provisions from NEN-EN 1992-1-1:2005 state that for flexible supports the distance should be taken to the centre of the support and for rigid supports to the face of the support, but no experimental evidence could be found for this requirement.

All studied methods overestimate the influence of the concrete compressive strength as compared to the experiments. In the Modified Bond Model, a  $1/4$  power relation between the capacity of the strips and the concrete compressive strength is used, which results in a smaller predicted increase in capacity for an increasing concrete compressive strength. Plotting the experimental to predicted values  $P_{exp}/P_{MBM}$  according to the Modified Bond Model over the range of tested concrete compressive strengths shows that the influence of the concrete compressive strength in the model more closely parallels the tested behaviour.

### 8.2.7 Code extension proposal based on statistical analysis

As the preferred code method is found to be NEN-EN 1992-1-1:2005 in combination with the effective width  $b_{eff2}$  based on the French load spreading method, this Eurocode 2 approach is used as a basis to formulate a code extension proposal for reinforced concrete slabs under concentrated loads close to supports.

The code extension proposal is based on a statistical analysis that takes into account the safety philosophy and basic assumptions of the Eurocodes. Monte Carlo simulations are used, in which the material properties and distribution of the ratio of the experimental to predicted results are used as random variables, to determine the resulting reliability index. To study the parameters that are not (correctly) incorporated into the shear

## Conclusions and Outlook

provisions from NEN-EN 1992-1-1:2005, different subsets for the analysis are determined. The resulting expression for the shear capacity of slabs under concentrated loads close to the support benefiting from transverse load redistribution is determined to be:

$$V_{Rd,c,prop} = C_{Rd,c} k (100 \rho_l f_{ck})^{1/3} b_{eff} d_l \left( 1,9 - \frac{f_{ck}}{225} \right) \left( 0,5 \frac{l_{sup}}{b} + 0,5 \right)$$

with  $l_{sup} = \sum_{i=1}^{n_{bearings}} l_{bearing,i}$  and with  $f_{ck}$  in [MPa],  $b_{eff}$  in [m],  $d_l$  in [mm] and  $V_{Rd,c,prop}$  in [kN].

The proposed expression is an extension of the shear formula from NEN-EN 1992-1-1:2005 (for members without axial tension or axial compression):

$$V_{Rd,c} = C_{Rd,c} k (100 \rho_l f_{ck})^{1/3} b_w d_l \geq v_{min} b_w d_l$$

and with  $f_{ck}$  in [MPa],  $b_w$  in [m],  $d_l$  in [mm] and  $V_{Rd,c}$  in [kN]. The contribution of loads close to the support to the shear load at the support is reduced with  $\beta$ . This expression is applicable for slabs under concentrated loads with the position of the load at  $a_v \leq 2,5d_l$ . For larger distances between the load and the support, the code extension proposal could not be verified due to a lack of appropriate experimental data.

### 8.2.8 *Application to practice: Quick Scan approach*

As the research is initiated by the Dutch Ministry of Infrastructure and the Environment, and is aimed at the assessment of existing reinforced concrete solid slab bridges under dead loads and live loads, attention has been paid in the research to the practical applicability of the research findings.

To assess a large number of slab bridges, the research recommendations for transverse load distribution and direct load transfer are implemented into an existing Quick Scan spreadsheet method. The Quick Scan method is a first order approach that aims at indicating which bridges should be studied in more detail. It can be used to determine the capacity of an existing reinforced concrete slab bridge subjected to composite dead load (self-weight and a wearing surface of 120mm) as well as live loads prescribed by NEN-EN 1991-2:2003 Load Model 1, which combines a lane load, heavier in the first lane, with concentrated wheel loads.

The contribution of the self-weight to the shear stress at the support can be determined for straight and parabolic shapes in the span direction. For all distributed loads, the reduction of the load close to the support through  $\beta = a_v/2d_l$  is implemented. The most unfavourable location for the wheel loads from Load Model 1 occurs for a face-to-face distance between the load and the support of  $2,5d_l$ . For loads closer to the support, direct load transfer expressed as  $\beta_{new} = a_v/2,5d_l$  reduces the contribution of these loads to the shear stress at the support. For loads farther away in the span, the contribution becomes smaller as an increasing share will be carried to the opposite support and the effective width will increase so that the shear force can be distributed over a larger width and becomes smaller.

Load Model 1 also prescribes a heavier lane load for the first lane. The additional load in the first lane can be redistributed over the full width through a triangular stress distribution, which satisfies moment and force equilibrium.

The load factors in the QS-EC2 are taken according to NEN 8700:2011, and based on a reliability index  $\beta_{rel} = 3,6$  (for bridges built before April 1<sup>st</sup> 2012, otherwise  $\beta_{rel} = 3,8$ ), which corresponds to the load level of “repair”. For comparison it should be noted that rating according to the “design – operating” level from AASHTO LRFR is based on a reliability index  $\beta_{rel} = 2,5$ . While these codes seem to describe a similar loading level for assessment, the underlying safety requirements are very different.

The research findings indicate that QS-EC2 (NEN-EN 1992-1-1:2005 and NEN 8700:2011 combined with the recommendations from the experimental research) should be used to assess the existing bridges. However, for comparison of the implications of different codes (and their different sets of assumptions), a Quick Scan sheet (QS-VBC) according to the NEN 6720:1995 in combination with NEN 8701:2011 was developed as well as a Quick Scan sheet (QS-AASHTO) according to the North-American practice: the AASHTO LRFD code and the Manual of Bridge evaluation (AASHTO LRFR). In that regard, it should be noted that the procedure of the QS-EC2 is based upon and aligned with the research findings, while the QS-VBC and QS-AASHTO method are based upon the code provisions and the interpretation thereof.

The three resulting Quick Scan sheets were used to study nine existing slab bridges owned by the Dutch Ministry of Infrastructure and the Environment, 13 rigid frame bridges from North America and one example of a North-American slab bridge as given in the Manual of Bridge Evaluation. The nine existing Dutch slab bridges are chosen to represent the database of 1000 existing slab bridges. The results of these calculations on this subset show an improvement in the selection ability of the QS-EC2 as compared to the QS-VBC. The load (shear stress at the edge) that should be considered is 18% smaller in the QS-EC2 than in the QS-VBC as a result of the recommendations with regard to direct load transfer and transverse load distribution. This clearly demonstrates the benefit of the application of the results from the experimental research. Moreover, the results from these cases indicate that the statement of AASHTO LRFR that shear should not be checked when rating reinforced concrete slabs and slab bridges, does not correspond to the verifications according to the QS-EC2 as well as to QS-VBC.

### **8.3 Recommendations for assessment and design**

As the research was aimed at practical applications for the Dutch Ministry of Infrastructure and the Environment, one of the key accomplishments of the research is the formulation of recommendations that can be used for assessment. While the current Eurocode suite is aimed at design, a set of codes that follow the philosophy of the Eurocode suite are developed in the Netherlands for assessment: the NEN 8700 series. The use of this set of

## Conclusions and Outlook

codes can be recommended in combination with the Eurocode provisions for the assessment of structures.

Based on the comparison between the experimental results and the calculated shear capacity according to NEN-EN 1992-1-1:2005, the following recommendations for the determination of the shear capacity of slabs under concentrated loads close to supports can be formulated for assessment purposes:

- the effective width should be determined based on the French horizontal load spreading method: the load is distributed at an angle of  $45^\circ$  from the far side of the loading plate to the face of the support;
- the minimum effective width is taken as  $4d_l$  provided that this value is a lower bound of the expression  $1,3(1,5b_{load} + d_l + b_r)$ ;
- for concentrated loads near to the edge at a distance up to  $a_v = 5,4d_l$ , an asymmetric effective width can be assumed, limited by the edge distance on one side and at the other side determined by the  $45^\circ$  load spreading method;
- for concentrated loads close to the support, the reduction factor for the contribution of the load to the sectional shear force  $\beta = a_v/2d_l$  can be replaced by  $\beta_{new} = a_v/2,5d_l$  provided that the load is placed so that the face-to-face distance  $a_v$  is  $0,5d_l \leq a_v \leq 2,5d_l$ ;
- the influence of the yield strength on the minimum shear capacity is used into a new formulation for  $v_{min}$ ;
- the contribution of concentrated loads to the shear stress at the support, distributed over their respective effective widths can be superimposed to the contribution of distributed loads over the full slab width.

The evidence for the choice of the French horizontal load spreading method to determine the effective width is found in the series of experiments on slabs with a varying width, on the statistical properties of the ratio between the experimental to predicted values when using NEN-EN 1992-1-1:2005, based on measurements of the reaction forces with load cells in slabs S19 to S26 and based on non-linear finite element calculations in which the stress distribution over the support is analysed.

While the expression for the reduction factor  $\beta$  in NEN-EN 1992-1-1:2005 distinguishes between the use of rigid and flexible support materials, the experiments did not show a significant difference. The code prescribes to take  $\beta = a_v/2d_l$  as a reduction factor for loads close to the support, with  $a_v$  the face-to-face distance between the load and the support for rigid support materials, but for flexible support materials  $a_v$  is prescribed as the distance between the centre of the load and the face of the support. It is recommended to use  $a_v$  as the face-to-face distance between the load and the support for all types of support materials.

To determine a safe estimate of the maximum concentrated loads that can be applied to slabs in the vicinity of supports, the Modified Bond Model is recommended. It is

## Conclusions and Outlook

shown in the research that the Modified Bond Model represents the tested parameters in a better way than any other studied approach.

Based on a statistical analysis, an extension of the shear provisions of NEN-EN 1992-1-1:2005 is proposed, that follows the basic assumptions of the Eurocodes. The shear capacity of slabs under concentrated loads near to supports benefiting from transverse load redistribution can be determined as:

$$V_{Rd,c,prop} = C_{Rd,c} k (100 \rho_l f_{ck})^{1/3} b_{eff} d_l \left( 1,9 - \frac{f_{ck}}{225} \right) \left( 0,5 \frac{l_{sup}}{b} + 0,5 \right)$$

with  $l_{sup} = \sum_{i=1}^{n_{bearings}} l_{bearing,i}$  and with  $f_{ck}$  in [MPa],  $b_{eff2}$  in [m],  $d_l$  in [mm] and  $V_{Rd,c,prop}$  in [kN].

For the assessment of reinforced concrete slab bridges according to the Quick Scan method, the following assumptions can be made:

- Assessment is carried out at the “repair” level, which corresponds to a reliability index  $\beta_{rel} = 3,8$  (and  $\beta_{rel} = 3,6$  for all bridges constructed before April 1<sup>st</sup> 2012).
- For the distributed loads, the reduction factor  $\beta = a_v/2d_l$  can be applied for the part of the load with  $0,5d_l \leq a_v \leq 2d_l$  and for  $a_v \leq 0,5d_l$  the reduction factor is kept constant as  $\beta = 1/4$ .
- For the concentrated wheel loads, the reduction factor  $\beta_{new} = a_v/2,5d_l$  can be applied for the part of the load with  $0,5d_l \leq a_v \leq 2,5d_l$ .
- A fictitious wheel print can be used on the concrete surface, assuming vertical load spreading under  $45^\circ$  through the wearing surface.
- For the increased lane loading on the first, heavily-loaded lane, the additional load can be distributed assuming a triangular stress distribution over the support. A lower bound that corresponds to vertical load spreading under  $45^\circ$  to the mid-depth  $d_l/2$  of the slab is prescribed.
- In a Quick Scan approach, correction factors for statical indeterminacy can be used that take into account the reduced or increased shear forces at the supports in a continuous structure.
- Due to a lack of experimental data on the influence of the skew angle on the shear capacity of reinforced concrete slabs under concentrated loads close to supports, no clear recommendations for taking into account the skew angle can be formulated. Two methods from the literature are available for application.
- The wheel loads are placed in the most unfavourable way, resulting in the largest shear stresses close to the edge of the support. This situation occurs when the fictitious wheel print of the first axle of the first design truck is placed at a distance  $a_v = 2,5d_l$  from the support.

The Quick Scan method is a first-order approach that forms a first level of approach for bridge assessment. The following levels of approach are distinguished:

1. Use an initial spreadsheet-based or hand calculation-based approach to see if the considered cross-section might require further calculations. The QS-EC2 tool for initial assessment is recommended.
2. If an initial assessment shows that further investigations are needed, refined models such as non-linear finite element models can be used.

## **8.4 Future work**

### *8.4.1 Future experimental work*

When applying the experimental results and the recommendations that were formulated in the experiments, it is found that experimental data is lacking in a number of remaining areas of the problem of reinforced concrete slabs under concentrated loads. Therefore, it is recommended to carry out the following additional experiments:

- experiments on slabs with a different effective depth, to study how the size effect influences the shear capacity of concrete slabs under concentrated loads and to compare the influence of the size effect on beams and slabs;
- experiments on skewed slabs, in which it is aimed to determine the relation between the skew angle and the one-way shear capacity – none of the test series reported in the literature show a uniform failure mode;
- experiments on slabs with a larger distance between the load and the support, to verify if the proposed methods for slabs under concentrated loads near to the support are still valid for larger distances of the load;
- experiments on slabs subjected to multiple concentrated loads to represent the two wheel loads per axle and study the resulting effective width of the entire axle;
- experiments on slabs subjected to multiple concentrated loads to represent multiple axles and to verify the assumption that the effective width can be determined per axle;
- additional experiments on the influence of the concrete compressive strength on the shear capacity are recommended, to investigate the limitations to the code methods that depend on the concrete compressive strength as a determining parameter for the shear capacity;
- experiments to define the limits of application of the Modified Bond Model more accurately.

### *8.4.2 Future theoretical research*

To avoid the bias related to crowding of experimental results in the range of small depths and large reinforcement ratios, more advanced statistical techniques can be applied for the analysis of the database. Another way to study the slab shear database and the experimental results is by generating a purely empirical formula based on an artificial neural network.

## *Conclusions and Outlook*

Furthermore, the connection between the Modified Bond Model and the equilibrium models such as Hillerborg's strip method (1996) can be studied in more detail based on the concepts introduced in §5.3.3. A possible approach is to extend Hillerborg's strip method so that it also covers shear failures, along the lines of the research of Regan and Rezai-Jorabi (1988) and then link these results back to the Modified Bond Model.

### *8.4.3 Future improvement of the assessment practice*

The application of the experimental results to the assessment practice mostly focused on supporting the further development of the Quick Scan method. No attention was paid on how to further deal with the cases of viaducts that do not meet the unity check of the Quick Scan. Therefore, further research should focus on how to apply the knowledge that is gathered in the experiments to more advanced assessment procedures. A possible direction is by analysing the correspondence between the experimental behaviour and the results of nonlinear finite element models. By studying the experiments and computer models, an improvement of the models could be achieved and guidelines for the use of finite element models for the assessment of slab bridges can be given.

When further, more advanced, techniques still indicate that the viaduct under study does not meet the requirements, a decision with regard to repair, refurbishment or replacement should be made. To fully cover the topic of assessment and its application for the subject of the research, an integrated study of repair strategies, taking into account the economic, environmental and social cost of possible solutions, can be carried out. Likewise, repair strategies should be studied in more detail, and future research could aim at comparing different repair strategies and categorizing which of these strategies give the best results for reinforced concrete slab bridges with large levels of shear distress.

**References**

AASHTO, 2007, *AASHTO LRFD Bridge Design Specifications*, American Association of State Highway and Transportation Officials, Washington D.C., 4086 pp.

AASHTO, 2011, *Manual for Bridge Evaluation (AASHTO LRFR)*, American Association of State Highway and Transportation Officials, Washington D.C, 538 pp.

ACI Committee 318, 2008, *Building Code Requirements for Structural Concrete (ACI 318-08) and Commentary*, American Concrete Institute, Farmington Hills, MI, USA, 465 pp.

Adebar, P., 2000, "One-way shear strength of large footings." *Canadian journal of civil engineering*, Vol. 27, pp. 553-562.

Adebar, P., Collins, M. P., 1996, "Shear strength of members without transverse reinforcement." *Canadian journal of civil engineering*, Vol. 23, No. 1, pp. 30-41.

Afhami, S., Alexander, S. D. B. and Simmonds, S. H., 1998, *Strip model for capacity of slab-column connections*, Dept. of Civil Engineering, University of Alberta, Edmonton, 231 pp.

Aktan, A. E., Zwick, M., Miller, R., Shahrooz, B., 1992, "Nondestructive and Destructive Testing of Decommissioned Reinforced Concrete Slab Highway Bridge and Associated Analytical Studies." *Transportation Research Record: Journal of the Transportation Research Board*, 1371, pp. 142-153.

Alexander, S., Simmonds, S., 1986, *Shear-Moment Transfer in Slab-Column connections*, Structural Engineering Report No. 141, University of Alberta, Edmonton, Alberta, 95 pp.

Alexander, S. D. B., Simmonds, S. H., 1986, *Shear-moment transfer in slab-column connections*, Dept. of Civil Engineering, University of Alberta, Edmonton, 116 pp.

Alexander, S. D. B., and Simmonds, S. H., 1987, "Ultimate Strength of Slab-Column connections." *ACI Structural Journal*, Vol. 84, No. 3, pp. 255-261.

Alexander, S. D. B., 1990, *Bond Model for strength of slab-column joints*. Ph.D. Thesis, University of Alberta. Dept. of Civil Engineering, 248 pp.

Alexander, S. D. B., and Simmonds, S. H., 1992, "Bond Model for Concentric Punching Shear." *ACI Structural Journal*, Vol. 89, No. 3, pp. 325-334.

Amer, A., Arockiasamy, M., Shahawy, M., 1999, "Load distribution of existing solid slab bridges based on field tests." *Journal of Bridge Engineering*, Vol. 4, No. 3, pp. 189-193.

Angelakos, D., Bentz, E. C. and Collins, M. P., 2001, "Effect of concrete strength and minimum stirrups on shear resistance of large members," *ACI Structural Journal*, V. 98, No. 3, May-June, pp. 290-300.

ASCE-ACI Committee 426 (Shear and Diagonal Tension), 1973, "The shear strength of reinforced concrete members." *Journal of the Structural Division*, Vol. 99, No. 6, pp.

## References

1091-1187.

ASCE-ACI Committee 426, 1974, "The shear strength of reinforced concrete members - slabs." *Journal of the Structural Division*, Vol. 100, No. 8, pp. 1543-1591.

ASCE-ACI Committee 445 (Shear and Torsion), 1998, "Recent approaches to shear design of structural concrete." *Journal of Structural Engineering*, Vol. 124, No. 12, pp. 1375-1417.

Aster, H., Koch, R., 1974, "Schubtragfähigkeit dicker Stahlbetonplatten." *Beton- und Stahlbetonbau*, Vol. 69, No. 11, pp. 266-270.

Azad, A. K., Baluch, M. H., Almandil, M. Y., Sharif, A. M., and Kareem, K., 1993, "Loss of punching capacity of bridge deck slabs from crack damage." *ACI Structural Journal*, Vol. 90, No. 1, pp. 37-41.

Azizinamini, A., Boothby, T. E., Shekar, Y., Barnhill, G., 1994a, "Old Concrete Slab Bridges. I: Experimental Investigation." *Journal of Structural Engineering-ASCE*, Vol. 120, No. 11, pp. 3284-3304.

Azizinamini, A., Shekar, Y., Boothby, T. E., Barnhill, G., 1994b, "Old Concrete Slab Bridges. II: Analysis." *Journal of Structural Engineering-ASCE*, Vol. 120, No. 11, pp. 3305-3319.

Baker, A. L. L., Abeles, P. W., Ashdown, A. J., Bennett, A. W., Brock, G. C., Bunn, E. W., Guest, J. E., Jones, L. L., Matthews, D. D., Regan, P. E., Smith, R. B. L., Yu, C. W., Taylor, R. (The Shear Study Group), 1969, *The shear strength of reinforced concrete beams: a report*, Institution of Structural Engineers, London, U.K, 170pp.

Balazs, G. L., 2010, "A historical review of shear." *Shear and punching shear in RC and FRC elements – Proceedings of a workshop held on 15-16 October 2010 in Salò, Lake Garda, Italy*, fib bulletin 57, pp. 1-13.

Bažant, Z. P., Kim, J. K., 1984, "Size Effect in Shear Failure of Longitudinally Reinforced Beams." *Journal of the American Concrete Institute*, Vol. 81, No. 5, pp. 456-468.

Beal, D. B., 1982, "Load capacity of concrete bridge decks." *Journal of the Structural Division-ASCE*, Vol. 108, No. 4, pp. 814-832.

Bentz, E. C., Collins, M. P., 2006, "Development of the 2004 Canadian Standards Association (CSA) A23.3 shear provisions for reinforced concrete." *Canadian Journal of Civil Engineering*, Vol. 33, No. 5, pp 521-534.

Bentz, E. C., Vecchio, F. J., Collins, M. P., 2006, "Simplified modified compression field theory for calculating shear strength of reinforced concrete elements." *ACI Structural Journal*, Vol. 103, No. 4, pp. 614-624.

Bentz, E. C., 2010, "MC2010: Shear strength of beams and implications of the new approaches," *Shear and punching shear in RC and FRC elements – Proceedings of a workshop held on 15-16 October 2010 in Salò, Lake Garda, Italy*, fib bulletin 57, pp. 15-30.

## References

- Bhide, S. B., Collins, M. P., 1989, "Influence of Axial Tension of the Shear Capacity of Reinforced-Concrete Members." *ACI Structural Journal*, Vol. 86, No. 5, pp. 570-581.
- CEN, 2003, *Eurocode 1 – Actions on Structures - Part 2: Traffic loads on bridges, NEN-EN 1991-2*, Comité Européen de Normalisation, Brussels, Belgium, 168 pp.
- CEN, 2005, *Eurocode 2 – Design of Concrete Structures: Part 1-1 General Rules and Rules for Buildings, NEN-EN 1992-1-1*, Comité Européen de Normalisation, Brussels, Belgium, 229 pp.
- Chana, P. S., 1988, "Analytical and experimental studies of shear failures in reinforced concrete beams." *Proceedings of the Institution of Civil Engineers, Structural Engineering group*, Vol. 85, No. 2, pp. 609-628.
- Chauvel, D., Thonier, H., Coin, A., and Ile, N., 2007, "*Shear Resistance of slabs not provided with shear reinforcement CEN/TC 250/SC 02 N 726*." France, 32 pp.
- Clark, A. P., 1951, "Diagonal Tension in Reinforced Concrete Beams." *ACI Journal Proceedings*, Vol. 48, No. 10, pp. 145-156.
- Coin, A., and Thonier, H., 2007, "Experiments on shear in reinforced concrete slabs (Essais sur le cisaillement des dalles en béton armé)." *Annales du bâtiment et des travaux publics*, pp. 7-16. (in French)
- Collins, M. P., 1978, "Towards a Rational Theory for RC Members in Shear." *Journal of the Structural Division-ASCE*, Vol. 104, No. 4, pp. 649-666.
- Collins, M. P., Mitchell, D., 1980, "Shear and Torsion Design of Prestressed and Non-Prestressed Concrete Beams." *Journal Prestressed Concrete Institute*, Vol. 25, No. 5, pp. 32-100.
- Collins, M. R., Bentz, E. C., Sherwood, E. G., 2008, "Where is shear reinforcement required? Review of research results and design procedures." *ACI Structural Journal*, Vol. 105, No. 5, pp. 590-600.
- Cope, R. J., 1985, "Flexural Shear Failure of Reinforced Concrete Slab Bridges." *Proceedings of the Institution of Civil Engineers Part 2-Research and Theory*, Vol. 79, 9, pp. 559-583.
- Cope, R. J., Rao, P. V., and Edwards, K. R., 1983, *Shear in skew reinforced concrete slab bridges – analytical and experimental studies – A report to the Department of Transport*. University of Liverpool, Liverpool, UK, 219 pp.
- Cortade, J., 2007, *Recommandations professionnelles*, FF Batiment, 36 pp.
- Criswell, M. E., Hawkins, N. M., 1973, "Shear Strength of Slabs: Basic Principle and Their Relation to Current Methods of Analysis." *ACI symposium March and October 1973*, pp. 641-676.
- Cullington, D. W., Daly, A. F., Hill, M. E., 1996, "Assessment of reinforced concrete bridges: Collapse tests on Thurloxton underpass." *Bridge Management*, Vol. 3, pp. 667-674.

## References

- CUR report 94-13, 1994, *Backgrounds to VBC 1990 (Achtergronden bij de VBC 1990)*, Civil Engineering Centre for Execution of Research and Standardization, Gouda, The Netherlands, 162 pp. (in Dutch)
- CUR committee 73 "High strength concrete", 2004, *Recommendation 97: High Strength Concrete (Aanbeveling 97: Hogesterktebeton)*, Gouda, The Netherlands, 20 pp. (in Dutch)
- Denton, S. R., 2001, *The Strength of Reinforced Concrete Slabs and the Implications of Limited Ductility*, PhD Thesis, University of Cambridge, pp. 332.
- Diaz de Cossio, R., Moe, J., Gould, P. L., Meason, J. G., 1962, "Shear and diagonal tension - Discussion." *ACI Journal Proceedings*, Vol. 59, No. 11, pp. 1323-1339.
- Doorgeest, J., 2012, *Transition between one-way shear and punching shear*, MSc. Thesis, Delft University of Technology, 215 pp.
- Dulacska, H., 1972, "Dowel Action of Reinforcement Crossing Cracks in Concrete." *ACI Journal Proceedings*, Vol. 69, No. 12, pp. 754-757.
- Ebeido, T., and Kennedy, J. B., 1996, "Punching Strength of Deck Slabs in Skew Composite Bridges." *Journal of Bridge Engineering*, Vol. 1, No. 2, pp. 59-66.
- Ehmann, J., 2006, "Shear resistance of concrete bridge decks in tension." *Composite construction in steel and concrete, Proceedings of the 5th international conference*, Vol. 5, pp. 67-76.
- Ekeberg, P. K., Sjurson, A., and Thorenfeldt, E., 1982, "Load-carrying capacity of continuous concrete slabs with concentrated loads." *Nordisk betong*, 2-4, pp. 153-156.
- Elstner, R., Hognestad, E., 1956, "Shearing Strength of Reinforced Concrete Slabs," *Journal of the American Concrete Institute*, Vol. 28, No. 1, pp. 29-58.
- Environment Agency, Carbon Calculator for Construction Activities Available at <http://publications.environment-agency.gov.uk/dispay.php?name=GEHO0712BWTW-E-X> Accessed 6 August, 2012
- Falbr, J., 2011, *Shear redistribution in solid concrete slabs*. MSc thesis, Delft University of Technology, Delft, 151 pp.
- Fang, I. K., Tsui, C. K. T., Burns, N. H., Klingner, R. E., 1990, "Load Capacity of Isotropically Reinforced, Cast-in-Place and Precast Panel Bridge Decks." *PCI Journal*, Vol. 35, No. 4, pp. 104-113.
- Feldman, L. R., Bartlett, F. M., 2005, "Bond strength variability in pullout specimens with plain reinforcement." *ACI Structural Journal*, Vol. 102, No. 6, pp. 860-867.
- Feldman, L. R., Bartlett, F. M., 2008, "Bond in flexural members with plain steel reinforcement." *ACI Structural Journal*, Vol. 105, No. 5, pp. 552-560.
- Fenwick, R. C., Paulay, T., 1968, "Mechanisms of Shear Resistance of Concrete Beams." *Journal of the Structural Division - ASCE*, Vol. 94, ST10, pp. 2325-2350.
- Fernandez Ruiz, M., Muttoni, A., 2007, "On development of suitable stress fields for structural concrete." *ACI Structural Journal*, Vol. 104, No. 4, pp. 495-502.

## References

- Furuuchi, H., Takahashi, Y., Ueda, T., and Kakuta, Y., 1998, "Effective width for shear failure of RC deep slabs," *Transactions of the Japan concrete institute*, Vol. 20, pp. 209-216.
- fib, 2012, *Model Code 2010 – Final Draft Vol. I*, fib Bulletin 65, 317 pp.
- fib, 2012, *Model Code 2010 - Final Draft Vol. II*, fib Bulletin 66, 311 pp.
- Furuuchi, H., Takahashi, Y., Ueda, T., Kakuta, Y., 1998, "Effective width for shear failure of RC deep slabs," *Transactions of the Japan Concrete Institute*, Vol. 20, pp.209-216.
- Gastbled, O. J., May, I. M., 2001, "Fracture mechanics model applied to shear failure of reinforced concrete beams without stirrups." *ACI Structural Journal*, Vol. 98, No. 2, pp. 184-190.
- Ghazavy-Khorasgany, M., Gopalaratnam, V., 1993, "Shear Strength of Concrete - Size and other influences." *Proceedings of the JCI International workshop on size effect in concrete structures*, oct. 31 - nov. 2, 1993, Sendai, Japan, pp. 51-62.
- Ghosn, M., Sivakumar, B., and Miao, F., 2010, "Calibration of Load and Resistance Factor Rating Methodology in New York State." *Transportation Research Record*, Vol. 2200, pp. 81-89.
- Goldbeck, A. T., 1917, "The influence of total width on the effective width of reinforced concrete slabs subjected to central concentrated loading." *ACI Journal Proceedings*, Vol. 13, No. 2, pp. 78-88.
- Goldbeck, A. T., Smith, E. B., 1916, "Tests of large reinforced concrete slabs." *ACI Journal Proceedings*, Vol. 12, No. 2, pp. 324-333.
- Graf, O., 1933, "Versuche über die Widerstandsfähigkeit von Eisenbetonplatten unter konzentrierter Last nahe einem Auflager (Tests of the strengths of reinforced concrete slabs under concentrated loads near supports)," *Deutscher Ausschuss für Eisenbeton*, Heft 73, Berlin, Germany, pp.1-16.
- Grasser, E., and Thielen, G., 1991, "Hilfsmittel zur Berechnung der Schnittgrößen unter Formänderungen von Stahlbetontragwerken." *Deutscher Ausschuss für Stahlbeton*, Heft 240, 86 pp.
- Guandalini, S., Burdet, O.L. and Muttoni, A., 2009, "Punching Tests of Slabs with Low Reinforcement Ratios," *ACI Structural Journal*, Vol. 106, No. 1, pp. 87-95.
- Gustafsson, P. J., and Hillerborg, A., 1988, "Sensitivity in Shear Strength of Longitudinally Reinforced Concrete Beams to Fracture Energy of Concrete." *ACI Structural Journal*, Vol. 85, No. 3, pp. 286-294.
- Hallgren, M., 1996, *Punching shear capacity of Reinforced High Strength Concrete Slabs*. PhD Thesis, Royal Institute of Technology, Stockholm.
- Hamadi, Y. D., Regan, P. E., 1980, "Behaviour in shear of beams with flexural cracks." *Magazine of Concrete Research*, Vol. 32, No. 111, pp. 67-78.

## References

- 't Hart, M., 2012, *Skewness analysis of slab bridges (Scheefheidsanalyse plaatviaducten)*. Report to the Dutch Ministry of Infrastructure and the Environment, 10 pp. (in Dutch).
- Hassan, A. A. A., Hossain, K. M. A., Lachemi, M., 2010, "Strength, cracking and deflection performance of large-scale self-consolidating concrete beams subjected to shear failure." *Engineering Structures*, Vol. 32, No. 5, pp. 1262-1271.
- Hawkins, N. M., Mitchell, D., 1979, "Progressive Collapse of Flat Plate Structures," *Journal of the American Concrete Institute*, Vol. 76, No. 7, pp. 775-808.
- Heger, F. J., McGrath, T. J., 1980, *Design method for reinforced concrete pipe and box sections*. Simpson Gumpertz & Heger Inc., Cambridge, Massachusetts; San Francisco, California, 251 pp.
- Hendy, C., Petty, R., 2012, "Quantification of sustainability principles in bridge projects." *Proceedings of the Sixth International Conference on Bridge Maintenance, Safety and Management*, pp. 1793-1800.
- Hewitt, B. Batchelor, B., 1975, "Punching Shear Strength of Restrained Slabs," *Journal of the Structural Division*, Vol. 101, No. 9, pp. 1837-1853.
- Hillerborg, A., 1975, *Design of reinforced concrete slabs according to the strip method*. Cement and Concrete Association, London.
- Hillerborg, A., 1996, *Strip method design handbook*, E & FN Spon, London, 302 pp.
- Hofbeck, J. A., Ibrahim, I. O., Mattock, A. H., 1969. "Shear Transfer in Reinforced Concrete." *ACI Journal Proceedings*, Vol. 66, No. 2, pp. 119-128.
- Hsu, T. T. C., 1996, "Towards a unified nomenclature for reinforced-concrete theory." *Journal of Structural Engineering*, Vol. 122, No. 3, pp. 275-283.
- Iyengar, K. T. S. R., Rangan, B. V. , Palaniswamy, R., 1988, "Some factors affecting the shear strength of reinforced concrete beams." *Indian Concrete Journal*, Vol. 42, No. 12, pp. 499-505.
- Jäger, T., 2002, "Shear Strength and Deformation Capacity of Reinforced Concrete Slabs," *Proceedings of the 4<sup>th</sup> International PhD Symposium in Civil Engineering*, Fédération Internationale du Béton , Munich, Germany, pp.280-286.
- Jäger, T., 2005, *Versuche zum Querkraftwiderstand und zum Verformungsvermögen von Stahlbetonplatten*, ETH Zurich, Zurich, Switzerland, 362pp.
- Jäger, T., 2007, *Querkraftwiderstand und Verformungsvermögen von Stahlbetonplatten*, PhD Thesis, ETH Zurich, Zurich, Switzerland, 123pp.
- Joint committee on concrete and reinforced concrete, 1916, "Final report on concrete and reinforced concrete." *Proceedings of the American Society of Civil Engineers*, Vol. 42, No. 10, pp. 167-1708.
- Joint Committee on Structural Safety, 2000, *Probabilistic Model Code. Part 1 – Basis of Design*, JCSS, 65pp.

## References

Joint Committee on Structural Safety, 2001, *Probabilistic Model Code. Part 2 – Load models*, JCSS, 73pp.

Joint Committee on Structural Safety, 2002, *Probabilistic Model Code. Part 3 – Material properties*, JCSS, 41pp.

Jung, S., Kim, K. S., 2008, "Knowledge-based prediction of shear strength of concrete beams without shear reinforcement." *Engineering Structures*, Vol. 30, No. 6, pp. 1515-1525.

Kahn, L. F., Mitchell, A. D., 2002, "Shear friction tests with high-strength concrete." *ACI Structural Journal*, Vol. 99, No. 1, pp. 98-103.

Kani, G. N. J., 1964, "The Riddle of Shear Failure and Its Solution." *ACI Journal Proceedings*, Vol. 61, No. 4, pp. 441-467.

Kani, G. N. J., 1966, "Basic Facts Concerning Shear Failure." *ACI Journal Proceedings*, Vol. 63, No. 6, pp. 675-692.

Kani, G. N. J., 1967, "How Safe Are Our Large Reinforced Concrete Beams." *ACI Journal Proceedings*, Vol. 64, No. 3, pp. 128-141.

Kani, G. N. J., 1969, "A Rational Theory for the function of Web Reinforcement." *ACI Journal Proceedings*, Vol. 66, No. 3, pp. 185-197.

Kani, M. W., Huggins, M. W., Wittkopp, R. R., 1979, *Kani on Shear in Reinforced Concrete*, University of Toronto, Dept of Civil Engineering, Toronto, 225 pp.

Kim, D., Kim, W., White, R. N., 1999, "Arch action in reinforced concrete beams - A rational prediction of shear strength." *ACI Structural Journal*, Vol. 96, No. 4, pp. 586-593.

Kim, W., Jeong, J., 2011, "Decoupling of Arch Action in Shear-Critical Reinforced Concrete Beams." *ACI Structural Journal*, Vol. 108, No. 4, pp. 395-404.

Kinnunen, S., Nylander, H., 1960, *Punching of Concrete Slabs without Shear Reinforcement*, Royal Institute of Technology, Stockholm, 112 pp.

Kirkpatrick, J., Rankin, G. I. B., Long, A. E., 1984, "Strength evaluation of M-beam bridge deck slabs." *The structural engineer*, Vol. 62B, No. 3, pp. 60-68.

König, G., Fischer, J., 1995, "Model Uncertainties concerning Design Equations for the Shear Capacity of Concrete Members without Shear Reinforcement." *CEB Bulletin 224, "Model Uncertainties and Concrete Barrier for Environmental Protection"*, pp. 49-100.

Labib, M., Moslehy, Y., Ayoub, A. S., 2009, "Behavior of Reinforced Concrete Elements Subjected to Tri-Directional Shear Using a State-of-the-Art Panel Tester." *SP-265 Thomas T.C. Hsu Symposium on Shear and Torsion in Concrete Structures*, American Concrete Institute., ed., New Orleans, LA, USA, pp. 455-476.

Lantsoght, E.O.L., 2009, *Literature review of punching shear in reinforced concrete slabs*, Research Report No. 09-10, School of Civil and Environmental Engineering – Structural Engineering, Mechanics and Materials, Georgia Institute of Technology, Atlanta, GA, USA, 93 pp.

Lantsoght, E.O.L., 2011a, *Shear tests of reinforced concrete slabs: experimental data*

## References

of undamaged slabs, Stevin Report No. 25.5-11-07, Delft University of Technology, The Netherlands, 502 pp.

Lantsoght, E.O.L., 2011b, *Shear tests of reinforced concrete slabs: experimental data of residual capacity of slabs*, Stevin Report No. 25.5-11-08, Delft University of Technology, The Netherlands, 334 pp.

Lantsoght, E.O.L., 2012a, *Progress report: Experiments on slabs in reinforced concrete: Part II: analysis of the results (Voortgangsrapportage: Experimenten op platen in gewapend beton: Deel II: analyse van de resultaten)*, Stevin Report nr. 25.5-12-10, Delft University of Technology, The Netherlands, 290 pp. (in Dutch)

Lantsoght, E.O.L., 2012b, *Shear in reinforced concrete slabs under concentrated loads close to the support – Literature review*, Stevin Report nr 25.5-12-11, Delft University of Technology, The Netherlands, 266 pp.

Lantsoght, E.O.L., 2012c, *Tests of reinforced concrete slabs subjected to a line load and a concentrated load*, Stevin Report No. 25.5-12-12, Delft University of Technology, The Netherlands, 271 pp.

Lantsoght, E., 2012d, *Progress report: Experiments on slabs in reinforced concrete subjected to a combination of loads: Part II: analysis of the result (Voortgangsrapportage: Experimenten op platen in gewapend beton onder combinatiebelasting: Deel II: analyse van de resultaten)*, Stevin Report No. 25.5-12-13, Delft University of Technology, The Netherlands, 101 pp. (in Dutch)

Lantsoght, E. 2012e, *Probabilistic approach to determine the increased shear capacity in reinforced concrete slabs under a concentrated load*, Stevin Report 25.5-12-15, Delft University of Technology, The Netherlands, 52 pp.

Lantsoght, E.O.L. 2012f, *Background to Modified Bond Model*, Stevin Report 25.5-12-16, Delft University of Technology, The Netherlands, 66 pp.

Lantsoght, E.O.L., 2012g, *Influence of skew on shear capacity – comparison Eurocode-approach to experiments by Cope et al. (Invloed van scheefheidshoek op dwarskrachtcapaciteit – Vergelijking Eurocode-aanpak met proefresultaten van Cope et al.)*." Delft University of Technology, 20 pp. (in Dutch)

Lantsoght, E.O.L., van der Veen, C., Gijsbers, F.B.J., 2012a, *Background report to spreadsheet (Achtergrondrapport bij spreadsheet)*, Stevin Report No. 25.5-12-14, Delft University of Technology, The Netherlands, 54 pp. (in Dutch)

Leonhardt, F., and Walther, R., 1962a, "Beitrage zur Behandlung der Schubprobleme in Stahlbetonbau - 2. Fortsetzung des Kapitels II - Versuchsberichte," *Beton- und Stahlbetonbau*, Vol. 57, No. 3, pp. 54-64.

Leonhardt, F., Walther, R., 1962b, *The Stuttgart shear tests, 1961; contributions to the treatment of the problems of shear in reinforced concrete construction*, Translation No. 111, Cement and Concrete Association, London, 134 pp.

## References

- Leonhardt, F., 1965, "Reducing the Shear Reinforcement in Reinforced Concrete Beams and Slabs." *Magazine of Concrete Research*, Vol. 17, No. 53, pp.187-198.
- Leonhardt, F., 1978, "Shear in concrete structures." *CEB Bulletin 126*, pp. 67-124.
- Long, A. E., 1975, "A two-phase Approach to the Prediction of the Punching Strength of Slabs." *ACI Journal Proceedings*, Vol. 72, No. 2, pp. 37-45.
- Lubell, A.S., 2006, *Shear in wide reinforced concrete members*, PhD Thesis, University of Toronto, 2006, 455pp.
- Marti, P., 1999, "How to treat shear in structural concrete." *ACI Structural Journal*, Vol. 96, No. 3, pp. 408-415.
- Massicotte, B., 2007, *Etude des causes de l'effondrement du pont du boulevard de la Concorde*. Ecole polytechnique de Montreal Groupe de recherche en genie des structures, 263 pp.,  
[http://www.cevc.gouv.qc.ca/UserFiles/File/Autres\\_pieces\\_deposees/PieceMTQ\\_6.pdf](http://www.cevc.gouv.qc.ca/UserFiles/File/Autres_pieces_deposees/PieceMTQ_6.pdf)
- Melchers, R. E., 1999, *Structural reliability : analysis and prediction*, John Wiley, Chichester, 437 pp.
- Mihashi, H., Nomura, N., 1993, "How to predict size effect in concrete structures." *Proceedings of the JCI International workshop on size effect in concrete structures*, oct. 31 - nov. 2, 1993, Sendai, Japan, pp. 235-246.
- Miller, R. A., Aktan, A. E., Shahrooz, B. M., 1994, "Destructive Testing of Decommissioned Concrete Slab Bridge." *Journal of Structural Engineering*, Vol. 120, No. 7, pp. 2176-2198.
- Ministry of Infrastructure and the Environment, 2004, "Report Mobility: Towards a reliable and predictable accessibility (Nota Mobiliteit: Naar een betrouwbare en voorspelbare bereikbaarheid)," 160 pp. (in Dutch).
- Mitchell, D., Collins, M. P., 1974, "Diagonal Compression Field Theory - A Rational Model for Structural Concrete in Pure Torsion." *ACI Journal Proceedings*, Vol. 71 , No. 8, pp. 396-408.
- Mitchell, D., Cook, W.D. Dilger, W., 2005, "Effects of size, Geometry and Material Properties on Punching Shear Resistance," *ACI Special Publication on Punching Shear in Reinforced Concrete Slabs, SP-232*, Ed. Polak, M.A., American Concrete Institute, Farmington Hills, MI, pp. 39-56.
- Moe, J., 1961, "Shearing Strength of Reinforced Concrete Slabs and Footings under Concentrated Loads," *Bulletin D47*, Portland Cement Association, Skokie, IL, 135 pp.
- Morrison, D. G., Weich, G. R., 1987., "Free-Edge and Obtuse-Corner Shear in R/C Skew Bridge Decks." *ACI Structural Journal*, Vol. 84, No. 1, pp. 3-9.
- Morrow, J., I. M. Viest, 1957, "Shear Strength of Reinforced Concrete Frame Members Without Web Reinforcement." *ACI Journal Proceedings*, Vol. 53, No. 3, pp. 833-869.
- Mörsch, E., 1908, *Der Eisenbetonbau : Seine Theorie Und Anwendung*, Verlag Von Konrad Wittwer, Stuttgart, 368 pp.

## References

Muttoni, A., 2003, "Schubfestigkeit und Durchstanzen von Platten ohne Querkraftbewehrung (Shear and punching strength of slabs without shear reinforcement)," *Beton- und Stahlbetonbau*, Vol. 98, No. 2, pp.74-84.

Muttoni, A., 2008, "Punching shear strength of reinforced concrete slabs without transverse reinforcement." *ACI Structural Journal*, Vol. 105, No. 4, pp. 440-450.

Muttoni, A., Fernández Ruiz, M., 2008a, "Shear strength in one- and two-way slabs according to the Critical Shear Crack Theory," *Proceedings of the International FIB Symposium 2008*, Fédération Internationale du Béton, Amsterdam, The Netherlands, pp. 559-563.

Muttoni, A., Fernández Ruiz, M., March- April 2008b, "Shear Strength of Members without Transverse Reinforcement as Function of Critical Shear Crack Width," *ACI Structural Journal*, Vol. 105, No. 2, pp.163-172.

Naumann, J., 2010, "Brücken und Schwerverkehr - eine Bestandsaufnahme." *Der Bauingenieur*, Vol. 85, No. 01, pp. 1-9.

Nielsen, M. P., 1984, *Limit analysis and concrete plasticity*, Prentice-Hall, Englewood Cliffs, N.J. London, 796 pp.

Nielsen, M. P. and Hoang, L. C., 2011, *Limit analysis and concrete plasticity*, 3rd ed. CRC Press, Boca Raton, FL, 816 pp.

Niwa, J., 1997, "Size effect in Shear of Concrete Beams Predicted by Fracture Mechanics." *CEB Bulletin 237*, pp. 147-158.

Normcommissie 351001, 1995, *NEN 6720:1995 Technical Foundatins of Building Codes, concrete Code TGB 1990 – Constructive requirements and design methods (VBC 1995)*, Civieltechnisch centrum uitvoering research en regelgeving, Nederlands Normalisatie-instituut, Delft, The Netherlands. (in Dutch)

Normcommissie 351001, 2011, *Assessment of existing structures in case of reconstruction and disapproval - Basic Rules, NEN 8700*, Nederlands Normalisatieinstituut, Delft, 56 pp.

Normcommissie 351001, 2011, *Assesment of constructive safety of an existing structure at repair or unfit for use - Loads, NEN 8701:2011*. Nederlands Normalisatieinstituut, Delft, 26 pp.

Olonisakin, A. A., Alexander, S. D. B., 1999, "Mechanism of shear transfer in a reinforced concrete beam." *Canadian journal of civil engineering*, Vol. 26, No. 6, pp. 810-817.

Park, R. Gamble, W., 1999, *Reinforced Concrete Slabs*, John Wiley & Sons, New York, 716 pp.

Pearson-Kirk, D., 2010, "Improving the management of bridges - the benefits of condition monitoring." *Structural Faults and Repair, 13th International Conference and Exhibition*, Edinburgh, UK, 12 pp.

## References

Prochazkova, Z., Lantsoght, E.O.L., 2011, *Material properties – Felt and Reinforcement For Shear test of Reinforced Concrete Slab*, Stevin Report No. 25.5-11-11, Delft University of Technology, The Netherlands, 28pp.

Prochazkova, Z., 2012, *FEM analyses - Shear tests of Reinforced Concrete Slabs*. Stevin Report nr. 25.5-12-02. Delft University of Technology, The Netherlands, 40 pp.

Pruijssers, A. F., 1986, *Shear resistance of beams based on the effective shear depth*. Stevinreport No. 5-86-1, Delft University of Technology, Delft, The Netherlands, 69 pp.

Rafla, K., 1971, "Empirische Formeln zur Berechnung der Schubtragfähigkeit von Stahlbetonbalken." *Strasse Brücke Tunnel*, Vol. 23, No. 12, pp. 311-320.

Rajagopalan, K. S., Ferguson, P. M., 1968, "Exploratory shear tests emphasizing percentage of longitudinal steel." *ACI Journal Proceedings*, Vol. 65, No. 8, pp. 634-638.

Ravindra, M. K., and Galambos, T. V., 1978, "Load and Resistance Factor Design for Steel." *Journal of the Structural Division-ASCE*, Vol. 104, No. 9, pp. 1337-1353.

Regan, P.E., 1982, *Shear Resistance of Concrete Slabs at Concentrated Loads close to Supports*, Engineering Structures Research Group, Polytechnic of Central London, London, United Kingdom, 24 pp.

Regan, P. E., 1971, *Shear in Reinforced Concrete – an experimental study*, Construction Industry Research and Information Association, London, Technical Note No 4.

Regan, P. E. and Braestrup, M. W., 1985, *Punching Shear in Reinforced Concrete*, CEB Bulletin 168, 241 pp.

Regan, P. E., 1987, *Shear resistance of members without shear reinforcement; proposal for CEB Model Code MC90*, Polytechnic of Central London, London, U.K., 28 pp.

Regan, P.E., Rezai-Jorabi, H., 1988, "Shear resistance of one-way slabs under concentrated loads," *ACI Structural Journal*, Vol. 85, No.2, pp.150-157.

Regan, P. E., 1998, "Enhancement of shear resistance in short shear spans of reinforced concrete - an evaluation of UK recommendations and particularly of BD44/95." University of Westminster, London, U.K., 16 pp.

Regan, P. E., 2000, "Aspects of diagonal tension in reinforced concrete." *Structural Concrete*, Vol. 1, No. 3, pp. 119-132.

Regan, P. E., Kennedy-Reid, I. L., Pullen, A. D., Smith, D. A., 2005, "The influence of aggregate type on the shear resistance of reinforced concrete." *The structural engineer*, Vol. 83, No. 23, pp. 27-32.

Reineck, K.-H., 1991, "Ultimate Shear Force of Structural Concrete Members without Transverse Reinforcement Derived from a Mechanical Model." *ACI Structural Journal*, Vol. 88, No. 5, pp. 592-602.

## References

Reineck, K.-H., 1992, "Ultimate Shear Force of Structural Concrete Members without Transverse Reinforcement Derived from a Mechanical Model - Closure" *ACI Structural Journal*, Vol. 89, No. 4, pp. 479-481.

Reineck, K.-H., 1997, "Modelling the shear behaviour and size effect of structural concrete members without transverse reinforcement." *CEB Bulletin 237*, pp. 185-197.

Reineck, K.-H., 2002, "Shear design in a consistent design concept for structural concrete based on strut-and-tie models." *Design Examples for the 1996 FIP recommendations "Practical design of structural concrete"*, fib bulletin 16, pp. 165-186.

Reineck, K.-H., Kuchma, D. A., Kim, K. S. and Marx, S., 2003, "Shear database for reinforced concrete members without shear reinforcement," *ACI Structural Journal*, Vol. 100, No. 2, pp. 240-249.

Reißen, K., and Hegger, J., 2011, "Experimental Study on the Shear Capacity of Concrete Slabs." *Proceedings of IABSE 2011*, 8 pp.

Reißen, K., and Hegger, J., 2012, " Shear Capacity of Reinforced Concrete Slabs under Concentrated Loads." *Proceedings of IABSE 2012*, 8 pp.

Richart, F. E., 1927, "An investigation of web stresses in reinforced concrete beams," *University of Illinois Engineering Experiment Station Bulletin No. 166*, Vol. 24, No. 43, University of Illinois, Urbana, 120 pp.

Richart, F. E., Kluge, R.W., 1939. "Tests of reinforced concrete slabs subjected to concentrated loads: a report of an investigation", *The engineering experiment station Bulletin*, Vol. 36, No. 85, University of Illinois, Urbana, 86 pp.

Richart, F. E., 1948, "Reinforced Concrete Wall and Column Footings: part 1" *ACI Journal Proceedings*, Vol. 45, No. 2, pp. 97-127.

Richart, F. E., 1948, "Reinforced Concrete Wall and Column Footings: part 2" *ACI Journal Proceedings*, Vol. 45, No. 3, pp. 237-260.

Rijkswaterstaat, 2012, *Guidelines for the assessment of bridges – assessment of structural safety of structural safety of existing bridges at repair or unfit for use levels. (RBK)*, 95pp. (in Dutch)

Ritter, W., 1899, "Die Bauweise Hennebique." *Schweizerische Bauzeitung*, Vol. 33, No. 7, pp. 59-61.

Rizk, E., Marzouk, H., Tiller, R., 2012., "Design of thick concrete plates using strut-and-tie model." *ACI Structural Journal*, Vol. 109, No. 5, pp. 677-686.

Rodriguez, J. J., Bianchini, A. C., Viest, I. M., Kesler, C. E., 1959, "Shear Strength of Two-Span Continuous Reinforced Concrete Beams." *ACI Journal Proceedings*, Vol. 55, No. 4, pp. 1089-1130.

Rombach, G. A., Velasco, R. R., 2005, "Schnittgrößen auskragender fahrbahnplatten infolge von radlasten nach DIN-fachbericht." *Beton- und Stahlbetonbau*, Vol. 100, No. 5, pp. 376-389.

## References

Rombach, G.A., Latte, S., 2008, "Shear resistance of bridge decks without shear reinforcement," *Proceedings of the International fib Symposium 2008*, Fédération Internationale du Béton, Amsterdam, The Netherlands, pp. 519-525.

Rombach, G., Latte, S., 2009, "Querkräfttragfähigkeit von Fahrbahnplatten ohne Querkräftbewehrung." *Beton- und Stahlbetonbau*, Vol. 104, No. 10, pp. 642-656.

Rombach, G. A., Latte, S., Steffens, R., 2009, *Querkräfttragfähigkeit von Fahrbahnplatten ohne Querkräftbewehrung*. Forschung Straßenbau under Straßenverkehrstechnik, Institut für Massivbau, Technische Universität Hamburg-Harburg, Bonn, 91pp.

Schlaich, J., Schafer, K., Jennewein, M., 1987, "Toward a Consistent Design of Structural Concrete." *Journal Prestressed Concrete Institute*, Vol. 32, No. 3, pp. 74-150.

Serna-Ros, P., Fernandez-Prada, M. A., Miguel-Sosa, P., Debb, O. A. R., 2002, "Influence of stirrup distribution and support width on the shear strength of reinforced concrete wide beams," *Magazine of Concrete Research*, Vol. 54, No. 3, pp. 181-191.

Sherwood, E.G., Lubell, A.S., Bentz, E.C, Collins, M.P., 2006, "One-way Shear Strength of Thick Slabs and Wide Beams," *ACI Structural Journal*, Vol. 103, No. 6, pp.794-802.

Sherwood, E. G., Lubell, A. S., Bentz, E.C., Collins, M.P., 2007a, "One-way shear strength of thick slabs and wide beams – Discussion and Authors' closure." *ACI Structural Journal*, Vol 104, No. 5, pp. 640-641.

Sherwood, E. G., Bentz, E. C., Collins, M. P., 2007b, "Effect of aggregate size on beam-shear strength of thick slabs." *ACI Structural Journal*, Vol. 104, No. 2, pp. 180-190.

Sherwood, E. G., 2008, *One-way shear behaviour of large, lightly-reinforced concrete beams and slabs*, PhD dissertation, University of Toronto, 547 pp.

SIA 162, 1968, *Design code for the calculation, the construction and the execution of structures in concrete, in reinforced concrete and in prestressed concrete*, Code 162, Edition 1968, Société suisse des ingénieurs et des architectes, Zurich, 1968, 84 p. (in French, also available in German).

Steenbergen, R. D. J. M., Vrouwenvelder, A. C. W. M., 2010, "Safety philosophy for existing structures and partial factors for traffic loads on bridges." *Heron*, Vol. 55, No. 2, pp. 123-140.

Steenbergen, R., Vrouwenvelder, T., Scholten, N., 2012, "Veiligheidsfilosofie bestaande bouw." *Cement*, Vol. 64, No. 4, pp. 8-16.

Steenbergen, R. D. J. M., Vervuurt, A. H. J. M., 2012, "Determining the in situ concrete strength of existing structures for assessing their structural safety." *Structural Concrete*, Vol. 13, No. 1, pp. 27-31.

Sun, S., Kuchma, D. A., 2007, *Shear Behavior and Capacity of Large-Scale Prestressed High-Strength Concrete Bulb-Tee Girders*. University of Illinois at Urbana-Champaign, 147 pp.

## References

- Swamy, R. N., Andriopoulos, A. D., 1973, "Contribution of Aggregate Interlock and Dowel Forces to the Shear Resistance of Reinforced Beams with Web Reinforcement." *ACI symposium March and October 1973*, pp. 129-166.
- Talbot, A. N., 1904, *Tests of reinforced concrete beams*. University of Illinois, Urbana, 70 pp.
- Talbot, A. N., 1905, *Tests of reinforced concrete beams*. University of Illinois, Urbana, 92 pp.
- Talbot, A. N., 1906, *Tests of reinforced concrete T-beams*. University of Illinois, Urbana, 42 pp.
- Talbot, A. N., 1908, *A test of three large reinforced concrete beams*. University of Illinois, Urbana, 42 pp.
- Talbot, A. N., 1909, *Tests of reinforced concrete beams: resistance to web stresses*, University of Illinois Engineering Experiment Station Bulletin No. 29, Vol. 6, No. 15, University of Illinois, Urbana, 90 pp.
- Talbot, A. N., 1913, *Tests of reinforced concrete buildings under load*. University of Illinois, Urbana, 118 pp.
- Talbot, A. N., Slater, W. A., 1916, *Tests of reinforced concrete flat slab structures*. University of Illinois, Urbana, 134 pp.
- Taylor, H. P. J., 1972, "Shear Strength of Large Beams." *Journal of the Structural Division - ASCE*, Vol. 98, ST11, pp. 2473-2490.
- Taylor, H. P. J., 1973, "The fundamental behavior of reinforced concrete beams in bending and shear." *ACI symposium March and October 1973*, pp. 285-303.
- Taylor, S. E., Rankin, G. I. B., Cleland, D. J., 2003, "Real strength of high-performance concrete bridge deck slabs." *Proceedings of the Institution of Civil Engineers, Bridge Engineering*, 156, Issue BE2, pp. 81-90.
- Theodorakopoulos, D. D., Swamy, R.N., 2002, "Ultimate punching shear strength analysis of slab-column connections," *Cement & Concrete Composites*, Vol. 24, No. 6, pp. 509-521.
- Theoret, P., Massicotte, B., Conciatori, D., 2012, "Analysis and Design of Straight and Skewed Slab Bridges." *Journal of Bridge Engineering*, Vol. 17, No. 2, pp. 289-301.
- Unger, C. and Empelmann, M., 2012, "Deterministic versus probabilistic reliability analysis of existing bridge structures," *Life-Cycle and Sustainability of Civil Infrastructure Systems, IALCCE 2012*, Strauss, Frangopol, D. M. and Bergmeister, eds., Vienna, Austria, pp. 2390-2397.
- van den Berg, F. J., 1962, "Shear strength of reinforced concrete beams without web reinforcement: Part 1 - Distribution of stresses over beam cross-section." *ACI Journal Proceedings*, Vol. 59, No. 10, pp. 1467-1478.

## References

- van den Berg, F. J., 1962, "Shear strength of reinforced concrete beams without web reinforcement: Part 3 - Proposed Method for Calculation of Cracking Load." *ACI Journal Proceedings*, Vol. 59, No. 12, pp. 1849-1862.
- Vaz Rodrigues, R., Muttoni, A., Olivier, O., 2006, "Large Scale Tests on Bridge Slabs Cantilevers Subjected to Traffic Loads," *Proceedings of the 2<sup>nd</sup> international Congress*, Fédération Internationale du Béton, Naples, Italy, 10 pp.
- Vaz Rodrigues, R., 2007, *Shear strength of reinforced concrete bridge deck slabs*, PhD thesis, Ecole Polytechnique Fédérale de Lausanne, Lausanne, Switzerland, 293 pp.
- Vaz Rodrigues, R., Ruiz, M. F., Muttoni, A., 2008, "Shear strength of R/C bridge cantilever slabs." *Engineering Structures*, Vol. 30, No. 11, pp. 3024-3033.
- Vecchio, F. J., Collins, M. P., 1986, "The Modified Compression-Field Theory for Reinforced-Concrete Elements Subjected to Shear." *Journal of the American Concrete Institute*, Vol. 83, No. 2, pp. 219-231.
- Vecchio, F. J., 2000, "Disturbed stress field model for reinforced concrete: Formulation." *Journal of Structural Engineering-ASCE*, Vol. 126, No. 9, pp. 1070-1077.
- Vervuurt, A., Courage, W., and Steenbergen, R., 2012, "Betonsterkte bestaande constructies." *Cement*, Vol. 64, No. 4, pp. 36-39.
- Vintzileou, E., 1997, "Shear transfer by dowel action and friction as related to size effects." *CEB Bulletin 237*, pp. 53-77.
- Vrouwenvelder, T., Holicky, M., Markova, J., 2002, *JCSS Probabilistic Model Code - Example Applications*. 19 pp.
- Waarts, P. H., 2000, *Structural reliability using Finite Element Analysis - An appraisal of DARS: Directional Adaptive Response surface Sampling*. Ph.D. Thesis, Delft University of Technology, Delft, 204 pp.
- Walraven, J.C., 1980, *Aggregate interlock: a theoretical and experimental analysis*, PhD Thesis, Delft University of Technology, Delft, The Netherlands, 197 pp.
- Walraven, J.C., 1981a, "Fundamental Analysis of Aggregate Interlock," *Journal of the Structural Division-ASCE*, Vol. 107, No. 11, pp. 2245-2270.
- Walraven, J.C., 1981b, "Aggregate Interlock (Scheurvertanding)." *Cement*, Vol. 33, No. 6, pp. 406-412. (in Dutch)
- Walraven, J., Frenay, J., Pruijssers, A., 1987, "Influence of Concrete Strength and Load History on the Shear Friction Capacity of Concrete Members." *Journal Prestressed Concrete Institute*, Vol. 32, No. 1, pp. 66-84.
- Walraven, J. C., 2002, *Background document for EC-2, Chapter 6.2 Shear*, Delft University of Technology, Delft, The Netherlands, 30 pp.
- Walraven, J. C., 2002, *Background document for EC-2, Chapter 6.4 Punching Shear*, Delft University of Technology, Delft, The Netherlands, 16 pp.
- Walraven, J. C., 2007, "Fracture mechanics of concrete and its role in explaining structural behaviour." *Fracture Mechanics of Concrete and Concrete Structures*, Vols. 1-3,

## References

pp. 1265-1275.

Walraven, J.C., Den Uijl, J., Sarkosh, R., Nguyen, T., 2012, "Long-term Loading (Langeduurbelasting)." *Cement*, Vol. 64, No. 4, pp. 56-60. (in Dutch)

Westergaard, H. M., 1930, "Computation of stresses in bridge slabs due to wheel loads." *Public roads*, Vol. 11, No. 1, pp. 1-23.

Windisch, A., Rodrigues, R. V., Muttoni, A., Ruiz, M. F., 2011, "Influence of Shear on Rotation Capacity of Reinforced Concrete Members Without Shear Reinforcement: Discussion and Authors' Closure." *ACI Structural Journal*, Vol. 108, No. 4, pp. 505-506.

Wood, J. G. M., 2008, "Implications of the collapse of the de la Concorde overpass." *The structural engineer*, Vol. 86, No. 1, pp. 16-18.

Xu, S., Reinhardt, H. W., 2005, "Shear Fracture on the basis of Fracture Mechanics." *Otto Graf Journal*, Vol. 16, No. 1, pp. 21-78.

Yang, Y., 2011. *Report of Experimental Research on Shear Capacity of Beams Close to Intermediate Supports*. Stevin Report No. 25.5-11-10, Delft University of Technology, The Netherlands, 58 pp.

Yang, Y., 2012. *Shear Capacity of Reinforced Concrete Beams under Complex Loading Conditions*. 9th fib International PhD Symposium in Civil Engineering. Karlsruhe, Germany, pp. 43-48.

Yang, Y. and den Uijl, J.A., 2012. *Shear Capacity of Concrete Structures Influenced by Concrete Strength Variation in Width Direction*. Stevin Report No. 25.5-12-07, Delft University of Technology, The Netherlands, 43 pp.

Yura, J. A., Galambos, T. V., Ravindra, M. K., 1978, "The Bending Resistance of Steel Beams." *Journal of the Structural Division-ASCE*, Vol. 104, No. 9, pp. 1355-1370.

Zararis, P. D., Papadakis, G. C., 2001, "Diagonal shear failure and size effect in RC beams without web reinforcement." *Journal of Structural Engineering-ASCE*, Vol. 127, No. 7, pp. 733-742.

Zinke, T., Ummenhofer, T., Pfaffinger, M., Mensinger, M., 2012, "The social dimension of bridge sustainability assessment - Impacts on users and the public." *Proceedings of the Sixth International Conference on Bridge Maintenance, Safety and Management*, pp. 1836-1843.

Zokaie, T., 1992, "Distribution of wheel loads on highway bridges - Final report of NCHRP Project 12-26." *Research results digest*, Number 187, pp. 1-31.

Zsutty, T., 1971, "Shear Strength Prediction for Separate Categories of Simple Beam Tests." *ACI Journal Proceedings*, Vol. 68, No. 2, pp. 138-143.

**Annex 1: Slab Shear Database**

The slab shear database contains the following information:

Ref	the author-date reference of the experiments;
Test type	the name of the experiment as used in the original reference;
slab, SS	the category of experiment:
slab, CS	a simply supported slab or wide beam;
cantilever	a continuously supported slab or wide beam;
real bridge	a cantilever slab;
n	experiment on an existing decommissioned bridge;
b	the number of loads;
$f_{c,mean}$	the specimen width;
a	the cylinder compressive strength of the concrete;
$b_r$	the centre-to-centre distance between the load and the support;
$b_{sup}$	the edge distance;
$l_{load}$	the width of the support; this distance is taken in the span direction;
$b_{load}$	the length of the load; perpendicular to the span direction
$\rho_l$	the width of the load; taken in the span direction;
$\rho_t$	the reinforcement ratio in the span direction;
$d_l$	the ratio of the transverse flexural reinforcement;
$d_t$	the effective depth to the longitudinal reinforcement;
$a_v$	the effective depth to the transverse flexural reinforcement;
$b_{eff1}$	the clear shear span;
$b_{eff2}$	the effective width based on the load spreading method from Fig. 2.16(a);
mode	the effective width based on the load spreading method from Fig. 2.16(b);
WB	the observed failure mode
P	wide beam shear failure;
nn	punching shear failure;
DT	pictures, descriptions or crack patterns are not available;
$F_{test}$	diagonal tension failure (as reported in report);
$V_{test}$	the maximum load as applied during the experiment;
	the resulting maximum sectional shear force.

In the last columns of the database, a few checks are carried out, resulting in the value “1” if true and the value “0” if not true:

- $b_{eff1} < b$ : if the effective width is larger than the specimen width, three-dimensional load spreading as in a wide beam or slab is not assumed to occur;
- $b_{eff2} < b$ : similar criterion for the other studied horizontal load spreading method;
- $a/d_l > 2,5?$ : is there an influence of direct transfer from the load to the support by means of a compressive strut?
- $e?$ : is the load placed in the middle of the slab width (0) or towards the edge (1)?

Annex 1: Slab Shear Database

Ref	Test	type	n	b (mm)	f <sub>concrete</sub> (MPa)	a (m)	b <sub>s</sub> (m)	b <sub>sp</sub> (m)	l <sub>stud</sub> (m)	b <sub>stud</sub> (mm)	ρ <sub>s</sub> (%)	ρ <sub>s</sub> (%)	d <sub>s</sub> (m)	d <sub>s</sub> (m)	a <sub>s</sub> (m)	b <sub>sp</sub> (m)	b <sub>sp</sub> (m)	mode	F <sub>max</sub> (kN)	V <sub>max</sub> (kN)	Influence b <sub>sp</sub> b <sub>stud</sub>	a/d <sub>s</sub> >2,5	e?
Reifem & Hegger 2011	50 ZTV	slab,SS	1	0,5	33,7	1	0,25	0,1	0,4	0,4	0,98	0,455	0,24	0,254	0,75	0,50	0,50	WB	204	136	0 0	1	0
	50_W 1TV	slab,SS	1	0,5	39,2	1	0,25	0,1	0,4	0,4	0,98	0,455	0,24	0,254	0,75	0,50	0,50	WB	183	137	0 0	1	0
	50_W 2TV	slab,SS	1	0,5	40,5	1	0,25	0,1	0,4	0,4	0,98	0,455	0,24	0,254	0,75	0,50	0,50	WB	215	143	0 0	1	0
	150 1 TV	slab,SS	1	1,5	37,7	1	0,75	0,1	0,4	0,4	0,98	0,455	0,24	0,254	0,75	1,50	1,50	WB	543	407	0 0	1	0
	150 2 TV	slab,SS	1	1,5	38,2	1	0,75	0,1	0,4	0,4	0,98	0,455	0,24	0,254	0,75	1,50	1,50	WB	638	425	0 0	1	0
	250 1 TV	slab,SS	1	2,5	27,9	1	1,25	0,1	0,4	0,4	0,98	0,455	0,24	0,254	0,75	1,90	2,50	WB	664	498	1 0	1	0
	250 2 TV	slab,SS	1	2,5	29,5	1	1,25	0,1	0,4	0,4	0,98	0,455	0,24	0,254	0,75	1,90	2,50	WB	780	520	1 0	1	0
	350 1 TV	slab,SS	1	3,5	35,9	1	1,75	0,1	0,4	0,4	0,98	0,455	0,24	0,254	0,75	1,90	2,70	P	985	739	1 1	1	0
	350 2 TV	slab,SS	1	3,5	38,2	1	1,75	0,1	0,4	0,4	0,98	0,455	0,24	0,254	0,75	1,90	2,70	P	1024	683	1 1	1	0
	350a1 1TV	slab,SS	1	3,5	39,6	1,3	1,75	0,1	0,4	0,4	0,98	0,455	0,24	0,254	1,05	2,50	3,30	mm	1166	787	1 1	1	0
	350a1 2TV	slab,SS	1	3,5	41,3	0,7	1,75	0,1	0,4	0,4	0,98	0,455	0,24	0,254	0,45	1,30	2,10	mm	1143	876	1 1	1	0
	350a2 1TV	slab,SS	1	3,5	29,5	1,3	1,75	0,1	0,4	0,4	0,98	0,455	0,24	0,254	1,05	2,50	3,30	P	924	624	1 1	1	0
	350a2 2TV	slab,SS	1	3,5	29,0	0,7	1,75	0,1	0,4	0,4	0,98	0,455	0,24	0,254	0,45	1,30	2,10	P	892	684	1 1	1	0
	Tb1 1TV	cantilever	1	3,5	37,0	1,14	1,75	0,28	0,4	0,4	0,98	0,446	0,24	0,254	0,80	2,00	2,80	WB	569	569	1 1	1	0
	Tb1 2TV	cantilever	1	3,5	38,4	1,14	1,75	0,28	0,4	0,4	0,98	0,584	0,207	0,22	0,80	2,00	2,80	WB	475	475	1 1	1	0
	Tb2 1TV	cantilever	1	3,5	34,3	1,14	1,75	0,28	0,4	0,4	0,98	0,446	0,24	0,254	0,80	2,00	2,80	WB/P	538	538	1 1	1	0
	Tb2 2TV	cantilever	1	3,5	34,8	1,14	1,75	0,28	0,4	0,4	0,98	0,584	0,207	0,22	0,80	2,00	2,80	WB/P	451	451	1 1	1	0

Annex 1: Slab Shear Database

Ref	Test	type	n	b (m)	f <sub>concr</sub> (MPa)	a	b <sub>p</sub> (m)	b <sub>sp</sub> (m)	l <sub>stud</sub> (m)	b <sub>stud</sub> (m)	ρ <sub>l</sub> (%)	ρ <sub>t</sub> (%)	d <sub>l</sub> (m)	d <sub>t</sub> (m)	a <sub>s</sub> (m)	b <sub>sp</sub> (m)	b <sub>sp</sub> (m)	m <sub>mode</sub>	F <sub>stud</sub> (kN)	V <sub>stud</sub> (kN)	Influence b <sub>sp</sub> b <sub>sp</sub>	a/d <sub>l</sub> >2,5	e?		
Regan 1982	1-SS	slab,CS	1	1,2	24,0	0,22	0,6	0,1	0,1	0,1	0,602	0,208	0,084	0,077	0,12	0,34	0,54	P	120	97	1	1	1	0	
	1-CS	slab,CS	1	1,2	24,0	0,245	0,6	0,15	0,1	0,1	0,602	0,208	0,084	0,077	0,12	0,34	0,54	P	150	118	1	1	1	0	
	2-SS	slab,CS	1	1,2	22,2	0,18	0,6	0,1	0,1	0,1	0,602	0,208	0,084	0,077	0,08	0,26	0,46	P	130	110	1	1	1	0	
	2-CS	slab,CS	1	1,2	22,2	0,205	0,6	0,15	0,1	0,1	0,602	0,208	0,084	0,077	0,08	0,26	0,46	P	180	148	1	1	1	0	
	3-SS	slab,CS	1	1,2	29,0	0,14	0,6	0,1	0,1	0,1	0,602	0,208	0,084	0,077	0,04	0,18	0,38	P	195	171	1	1	1	0	
	3-CS	slab,CS	1	1,2	29,0	0,165	0,6	0,15	0,1	0,1	0,602	0,208	0,084	0,077	0,04	0,18	0,38	WB	250	214	1	1	1	0	
	4-SS	slab,CS	1	1,2	33,9	0,12	0,6	0,1	0,1	0,1	0,602	0,208	0,084	0,077	0,02	0,17	0,34	P	230	206	1	1	1	0	
	5-SS	slab,CS	1	1,2	29,3	0,18	0,6	0,1	0,2	0,1	0,602	0,208	0,084	0,077	0,08	0,36	0,56	P	190	160	1	1	1	0	
	6-SS	slab,CS	1	1,2	26,6	0,23	0,6	0,1	0,1	0,2	0,602	0,208	0,084	0,077	0,08	0,26	0,66	WB	160	128	1	1	1	0	
	6-CS	slab,CS	1	1,2	26,6	0,255	0,6	0,15	0,1	0,2	0,602	0,208	0,084	0,077	0,08	0,26	0,66	WB	160	125	1	1	1	0	
	7-SS	slab,CS	1	1,2	35,4	0,14	0,6	0,1	0,2	0,1	0,602	0,208	0,084	0,077	0,04	0,28	0,48	P	200	176	1	1	1	0	
	7-CS	slab,CS	1	1,2	35,4	0,205	0,6	0,15	0,2	0,1	0,602	0,208	0,084	0,077	0,08	0,36	0,56	P	230	189	1	1	1	0	
	Regan & Rezaei & Jorabi 1988	1	slab,SS	2	0,4	31,0	0,45	0,2	0,1	0,075	0,075	1,66	0,636	0,083	0,075	0,17	0,40	0,40	WB	62,5	62,5	0	0	1	0
		2	slab,SS	2	0,6	31,0	0,45	0,3	0,1	0,075	0,075	1,58	0,636	0,083	0,075	0,26	0,60	0,60	WB	85	85	0	0	1	0
3		slab,SS	2	0,8	31,0	0,45	0,4	0,1	0,075	0,075	1,54	0,636	0,083	0,075	0,36	0,80	0,80	WB	97,5	97,5	0	0	1	0	
4		slab,SS	2	0,4	23,0	0,45	0,2	0,1	0,4	0,1	1,66	0,636	0,083	0,075	0,35	0,40	0,40	WB	54,5	54,5	0	0	1	0	
5		slab,SS	2	0,6	23,0	0,45	0,3	0,1	0,6	0,1	1,58	0,636	0,083	0,075	0,35	0,60	0,60	WB	80	80	0	0	1	0	
6		slab,SS	2	0,8	23,0	0,45	0,4	0,1	0,6	0,1	1,54	0,636	0,083	0,075	0,35	0,80	0,80	WB	96,5	96,5	0	0	1	0	
10		slab,SS	2	0,4	27,4	0,45	0,2	0,1	0,15	0,1	1,66	0,636	0,083	0,075	0,35	0,40	0,40	WB	52,5	52,5	0	0	1	0	
11		slab,SS	2	0,4	27,4	0,45	0,2	0,1	0,3	0,1	1,66	0,636	0,083	0,075	0,35	0,40	0,40	WB	55	55	0	0	1	0	
12		slab,SS	2	0,6	27,4	0,45	0,3	0,1	0,15	0,1	1,58	0,636	0,083	0,075	0,35	0,60	0,60	WB	76	76	0	0	1	0	

Annex 1: Slab Shear Database

Ref	Test	type	n	b (m)	f <sub>concr</sub> (MPa)	a (m)	b <sub>s</sub> (m)	b <sub>sp</sub> (m)	f <sub>stud</sub> (m)	b <sub>stud</sub> (m)	ρ <sub>t</sub> (%)	ρ <sub>s</sub> (%)	d <sub>t</sub> (m)	d <sub>s</sub> (m)	e <sub>s</sub> (m)	b <sub>gr</sub> (m)	b <sub>gr</sub> (m)	mode	F <sub>max</sub> (kN)	V <sub>max</sub> (kN)	Influence b <sub>gr</sub>	a/d <sub>t</sub> > 2,5	e?	
Regan & Rezaei	13	slab,SS	2	0,6	27,4	0,45	0,3	0,1	0,3	0,1	1,58	0,636	0,083	0,075	0,35	0,60	0,60	WB	79,5	79,5	0	0	1	0
	14	slab,SS	2	0,8	25,4	0,45	0,4	0,1	0,15	0,1	1,54	0,636	0,083	0,075	0,35	0,80	0,80	WB	92,5	92,5	0	0	1	0
Jorahi	15	slab,SS	2	0,8	25,3	0,55	0,4	0,1	0,15	0,1	1,54	0,636	0,083	0,075	0,45	0,80	0,80	WB	85	85	0	0	1	0
1988	16	slab,SS	2	0,8	25,6	0,45	0,4	0,1	0,8	0,1	1,54	0,636	0,083	0,075	0,35	0,80	0,80	WB	108	108	0	0	1	0
	17	slab,SS	2	1	25,4	0,45	0,5	0,1	0,1	0,075	1,51	0,636	0,083	0,075	0,36	0,83	0,98	WB	90	90	1	1	1	0
	18	slab,SS	2	1	25,6	0,45	0,5	0,1	0,3	0,1	1,51	0,636	0,083	0,075	0,35	1,00	1,00	WB	120	120	0	0	1	0
	19	slab,SS	2	1	23,8	0,45	0,5	0,1	0,15	0,1	1,51	0,636	0,083	0,075	0,35	0,85	1,00	WB	111	111	1	0	1	0
	20	slab,SS	2	1	25,3	0,45	0,5	0,1	1	0,1	1,51	0,636	0,083	0,075	0,35	1,00	1,00	WB	122,5	122,5	0	0	1	0
	21	slab,SS	2	1,2	31,3	0,45	0,6	0,1	0,07	0,1	1,64	0,663	0,08	0,072	0,35	0,77	0,97	P	117,5	117,5	1	1	1	0
	22	slab,SS	2	1,2	30,3	0,45	0,6	0,1	0,15	0,1	1,64	0,663	0,08	0,072	0,35	0,85	1,05	P/WB	121,5	121,5	1	1	1	0
	23	slab,SS	2	1,2	29,0	0,45	0,6	0,1	0,3	0,1	1,64	0,663	0,08	0,072	0,35	1,00	1,20	WB	125	125	1	0	1	0
	24	slab,SS	2	1,2	31,7	0,45	0,6	0,1	0,1	0,3	1,64	0,663	0,08	0,072	0,25	0,60	1,20	WB	150	150	1	0	1	0
	25	slab,SS	2	1,2	24,8	0,55	0,6	0,1	0,15	0,1	1,64	0,663	0,08	0,072	0,45	1,05	1,20	P2	105,8	105,8	1	0	1	0
	26	slab,SS	2	1,2	24,4	0,35	0,6	0,1	0,15	0,1	1,64	0,663	0,08	0,072	0,25	0,65	0,85	WB	137,5	137,5	1	1	1	0
14R		slab,SS	2	0,8	25,4	0,45	0,4	0,1	0,075	0,1	1,54	0,636	0,083	0,075	0,35	0,78	0,80	P	77	77	1	0	1	0
15R		slab,SS	2	0,8	25,3	0,45	0,4	0,1	0,15	0,1	1,54	0,636	0,083	0,075	0,35	0,80	0,80	P	86	86	0	0	1	0
16R		slab,SS	2	0,8	25,6	0,45	0,4	0,1	0,6	0,1	1,54	0,636	0,083	0,075	0,35	0,80	0,80	WB	116,5	116,5	0	0	1	0
17R		slab,SS	2	1	25,4	0,45	0,5	0,1	0,6	0,1	1,51	0,636	0,083	0,075	0,35	1,00	1,00	WB	137,5	137,5	0	0	1	0
19R		slab,SS	2	1	23,8	0,45	0,5	0,1	0,15	0,1	1,51	0,636	0,083	0,075	0,35	0,85	1,00	P	85	85	1	0	1	0
20R		slab,SS	2	1	25,3	0,45	0,5	0,1	0,3	0,1	1,51	0,636	0,083	0,075	0,35	1,00	1,00	P	132,5	132,5	0	0	1	0

Annex 1: Slab Shear Database

Ref	Test	type	n	b (m)	$f_{c,mean}$ (MPa)	a	$b_v$ (m)	$b_{sp}$ (m)	$l_{bar}$ (m)	$b_{bar}$ (m)	$\rho_t$ (%)	$\rho_s$ (%)	$d_t$ (m)	$d_s$ (m)	$\sigma_s$ (m)	$b_{gr}$ (m)	$b_{gr}$ (m)	mcode	$F_{ur}$ (kN)	$V_{ur}$ (kN)	Influence $b_{gr}$	$a/d_t$ >2.5	$e/t$	
Furushii Takahashi Ueda & Kakuta 1998	A-10-10	slab,SS	2	0.5	26.1	0.28	0.25	0.05	0.1	0.05	2.23	0	0.16	nn	0.23	0.50	0.50	WB/P	294	186	0	0	0	
	A-10-20	slab,SS	2	0.5	20.2	0.28	0.25	0.05	0.1	0.05	2.23	0	0.16	nn	0.23	0.50	0.50	WB	294	186	0	0	0	
	A-10-30	slab,SS	2	0.5	23.8	0.28	0.25	0.05	0.1	0.05	2.23	0	0.16	nn	0.23	0.50	0.50	WB	333	210	0	0	0	
	A-20-10	slab,SS	2	0.5	19.6	0.28	0.25	0.05	0.2	0.05	2.23	0	0.16	nn	0.23	0.50	0.50	nn	340	215	0	0	0	
	A-30-10	slab,SS	2	0.5	23.8	0.28	0.25	0.05	0.3	0.05	2.23	0	0.16	nn	0.23	0.50	0.50	nn	450	284	0	0	0	
	B-10-10	slab,SS	2	0.65	29.4	0.28	0.325	0.05	0.1	0.05	2.29	0	0.16	nn	0.23	0.56	0.65	nn	368	232	1	0	0	
	C-10-10	slab,SS	2	0.5	34.6	0.2	0.25	0.05	0.1	0.05	2.23	0	0.16	nn	0.15	0.40	0.50	WB/P	480	320	1	0	0	
	C-20-10	slab,SS	2	0.5	32.1	0.2	0.25	0.05	0.2	0.05	2.23	0	0.16	nn	0.15	0.50	0.50	WB	525	350	0	0	0	
	C-30-10	slab,SS	2	0.5	31.5	0.2	0.25	0.05	0.3	0.05	2.23	0	0.16	nn	0.15	0.50	0.50	WB	626	417	0	0	0	
	C-50-10	slab,SS	2	0.5	34.9	0.2	0.25	0.05	0.5	0.05	2.23	0	0.16	nn	0.15	0.50	0.50	WB	811	541	0	0	0	
	C-10-20	slab,SS	2	0.5	36.4	0.2	0.25	0.05	0.1	0.05	2.23	0	0.16	nn	0.15	0.40	0.50	nn	483	322	1	0	0	
	C-10-30	slab,SS	2	0.5	30.7	0.2	0.25	0.05	0.1	0.05	2.23	0	0.16	nn	0.15	0.40	0.50	nn	520	347	1	0	0	
	D-10-10	slab,SS	2	0.5	35.2	0.36	0.25	0.05	0.1	0.05	2.23	0	0.16	nn	0.31	0.50	0.50	nn	294	179	0	0	0	
	Sherwood	AT-1-East	slab,SS	1	2.016	64.0	2.7	1.008	0.15	1.2	0.152	0.76	0.018	0.916	0.906	2.55	2.02	2.02	WB	2266	1133	0	0	1
		AT-1-West	slab,SS	1	2.016	64.0	2.7	1.008	0.15	1.2	0.152	0.76	0.018	0.916	0.906	2.55	2.02	2.02	WB	2441	1221	0	0	1
		AT-2/250N	slab,SS	1	0.25	37.7	1.3	0.125	0.15	0.152	0.152	0.915	0	0.437	nn	1.15	0.25	0.25	WB	229	115	0	0	1
		AT-2/250W	slab,SS	1	0.252	38.5	1.3	0.126	0.15	0.152	0.152	0.904	0	0.439	nn	1.15	0.25	0.25	WB	224	112	0	0	1
		AT-2/1000N	slab,SS	1	1.002	37.9	1.3	0.501	0.15	0.152	0.152	0.911	0.191	0.438	0.422	1.15	1.00	1.00	WB	880	440	0	0	1
AT-2/1000W		slab,SS	1	1.002	39.0	1.3	0.501	0.15	0.152	0.152	0.909	0.19	0.439	0.423	1.15	1.00	1.00	WB	942	471	0	0	1	
AT-2/3000		slab,SS	1// 3	3.005	40.6	1.3	1.503	0.15	0.152	0.152	0.908	0.19	0.44	0.424	1.15	2.45	2.75	WB	2564	1282	1	1	1	
AT-3/N1		slab,SS	1	0.697	37.5	1.04	0.349	0.15	0.697	0.152	0.93	0	0.307	nn	0.89	0.70	0.70	WB	475	238	0	0	1	
AT-3/N2		slab,SS	1	0.706	37.1	1.04	0.353	0.15	0.706	0.152	0.93	0	0.306	nn	0.89	0.71	0.71	WB	517	259	0	0	1	
AT-3/T1		slab,SS	1	0.7	37.8	1.04	0.35	0.15	0.7	0.152	0.93	0.19	0.306	0.285	0.89	0.70	0.70	WB	506	253	0	0	1	
AT-3/T2	slab,SS	1	0.706	37.1	1.04	0.353	0.15	0.706	0.152	0.93	0.19	0.307	0.285	0.89	0.71	0.71	WB	497	249	0	0	1		

Annex 1: Slab Shear Database

Ref	Test	type	n	b (m)	$f_{c,concr}$ (MPa)	a (m)	$b_p$ (m)	$b_{sp}$ (m)	$l_{hor}$ (m)	$b_{hor}$ (m)	$\rho_t$ (%)	$\rho_l$ (%)	$\rho_t$ (%)	$d_t$ (m)	$d_l$ (m)	$a_s$ (m)	$b_{gr}$ (m)	$b_{gr}$ (m)	mode	$F_{ur}$ (kN)	$V_{ur}$ (kN)	Influence $b_{gr}$	$a/d_t$ $>2.5$	$e?$
Shawwood	AX1	slab,SS	1	0,249	40,7	1,3	0,125	0,15	0,249	0,152	0,328	0	0,434	mm	1,15	0,25	0,25	WB	170,5	85	0	0	1	0
Lubell	AX7	slab,SS	1	0,704	41,0	1,04	0,352	0,15	0,704	0,152	1,04	0,134	0,287	0,266	0,89	0,70	0,70	WB	501,1	250,6	0	0	1	0
Bentz	AX6	slab,SS	1	0,703	41,0	1,04	0,352	0,15	0,703	0,152	1,73	0,134	0,288	0,267	0,89	0,70	0,70	WB	565,0	282,5	0	0	1	0
Collins	AX8	slab,SS	1	0,705	41,0	1,04	0,353	0,15	0,152	0,152	1,72	0,133	0,289	0,268	0,89	0,71	0,71	WB	544,1	272,1	0	0	1	0
2006	AW1	slab,SS	1	1,17	36,9	1,85	0,585	0,15	0,305	0,305	0,79	0,087	0,538	0,517	1,62	1,17	1,17	WB	1170	585	0	0	1	0
	AW4	slab,SS	1	1,168	39,9	1,85	0,584	0,15	0,305	0,305	1,69	0,093	0,506	0,485	1,62	1,17	1,17	WB	1450	725	0	0	1	0
	AW8	slab,SS	1	1,169	39,4	1,85	0,585	0,15	1,169	0,152	1,69	0,093	0,507	0,486	1,70	1,17	1,17	WB	1600	800	0	0	1	0
Vaz	DR1a	cantilever	2//	10	39,1	1,395	5	0,41	0,3	0,3	0,79	0,285	0,306	0,284	1,04	2,38	2,98	P	1397	1397	1	1	1	0
Rodrigues	DR1b	cantilever	1//	10	39,9	1,505	0,95	0,41	0,3	0,3	0,79	0,285	0,309	0,287	1,15	2,25	2,55	WB	1025	1025	1	1	1	1
Muttoni	DR1c	cantilever	2	10	40,8	1,505	1,25	0,41	0,3	0,3	0,79	0,285	0,309	0,287	1,15	2,55	2,85	WB	910	910	1	1	1	1
& Olivier	DR2a	cantilever	1//	10	38,9	1,505	5	0,41	0,3	0,3	0,6	0,282	0,35	0,33	1,15	2,60	3,20	WB	961	961	1	1	1	0
2006	DR2b	cantilever	2	10	42,0	1,505	0,95	0,41	0,3	0,3	0,6	0,282	0,35	0,33	1,15	2,25	2,55	WB	857	857	1	1	1	1
	DR2c	cantilever	1	10	40,0	1,505	1,25	0,41	0,3	0,3	0,6	0,282	0,35	0,33	1,15	2,55	2,85	WB	719	719	1	1	1	1
Jaeger	A1V1	cantilever	1	0,8	52,4	0,64	0,4	0,1	0,8	0,1	1,538	1,538	0,156	0,156	0,54	0,80	0,80	WB	169,2	169	0	0	1	0
2002	A3V1	cantilever	1	0,8	58,8	0,64	0,4	0,1	0,8	0,1	1,745	0,879	0,162	0,162	0,54	0,80	0,80	WB	265,6	266	0	0	1	0
2005	A4V1	cantilever	1	0,8	46,8	0,64	0,4	0,1	0,8	0,1	0,952	0,952	0,168	0,168	0,54	0,80	0,80	WB	140,5	141	0	0	1	0
2007	A5V1	cantilever	1	0,8	56,7	0,64	0,4	0,1	0,8	0,1	1,056	0,879	0,174	0,162	0,54	0,80	0,80	WB	222,1	222	0	0	1	0
	B1V1	cantilever	1	2	52,4	1,6	1	0,1	2	0,1	1,538	1,538	0,39	0,39	1,50	2,00	2,00	WB	852	852	0	0	1	0
	B3V1	cantilever	1	2	53,7	1,6	1	0,1	2	0,1	1,745	0,879	0,405	0,405	1,50	2,00	2,00	WB	1282	1282	0	0	1	0
	B4V1	cantilever	1	2	54,2	1,6	1	0,1	2	0,1	0,952	0,952	0,42	0,42	1,50	2,00	2,00	WB	804	804	0	0	1	0
	B5V1	cantilever	1	2	51,8	1,6	1	0,1	2	0,1	1,056	0,879	0,435	0,405	1,50	2,00	2,00	WB	1170	1170	0	0	1	0

Annex 1: Slab Shear Database

Ref	Test	type	n	b (m)	$f_{c,mean}$ (MPa)	a	$b_p$ (m)	$b_{sp}$ (m)	$l_{stud}$ (m)	$b_{stud}$ (m)	$\rho_1$ (%)	$\rho_2$ (%)	$d_1$ (m)	$d_2$ (m)	$d_3$ (m)	$\alpha_s$ (m)	$b_{gr}$ (m)	$b_{gr}$ (m)	mode	$F_{test}$ (kN)	$V_{test}$ (kN)	influence $b_{gr}$ $b_{gr}$	$a/d_1$ >2,5	$e?$	
Graf 1933	1243 - a1	slab,CS	2	2	16,6	0,15	0,6	0,2	0,15	0,1	0,65	0,129	0,115	0,107	0,00	0,23	0,35	WB	314	280	1	1	0	1	
	1243 - a2	slab,CS	2	2	19,1	0,25	0,6	0,2	0,15	0,1	0,65	0,129	0,115	0,107	0,10	0,35	0,55	P	235	193	1	1	0	1	
	1243 - b1	slab,CS	1	2	19,1	0,075	0,6	0,2	0,15	0,1	0,65	0,129	0,115	0,107	-0,08	0,23	0,23	P	355	336	1	1	0	1	
	1243 - b2	slab,CS	1	2	21,6	0,175	0,6	0,2	0,15	0,1	0,65	0,129	0,115	0,107	0,03	0,23	0,40	WB	206	180	1	1	0	1	
	1244 - a1	slab,CS	2	2,004	12,7	0,2	0,6	0,2	0,15	0,1	1,14	0,145	0,104	0,095	0,05	0,25	0,45	WB	275	236	1	1	0	1	
	1244 - a2	slab,CS	2	2,004	13,3	0,25	0,6	0,2	0,15	0,1	1,14	0,145	0,104	0,095	0,10	0,35	0,55	WB	196	161	1	1	0	1	
	1244 - b1	slab,CS	1	2,004	13,3	0,175	0,6	0,2	0,15	0,1	1,14	0,145	0,104	0,095	0,03	0,21	0,40	WB	157	137	1	1	0	1	
	1244 - b2	slab,CS	1	2,004	13,9	0,225	0,6	0,2	0,15	0,1	1,14	0,145	0,104	0,095	0,08	0,30	0,50	WB	147	123	1	1	0	1	
	1245 - a1	slab,CS	2	2,404	23,7	0,2	0,6	0,2	0,15	0,1	1,52	0,142	0,106	0,097	0,05	0,25	0,45	P	333	285	1	1	0	1	
	1245 - a2	slab,CS	2	2,404	23,6	0,25	0,6	0,2	0,15	0,1	1,52	0,142	0,106	0,097	0,10	0,35	0,55	P	257	211	1	1	0	1	
	1245 - b1	slab,CS	1	2,404	23,6	0,175	0,6	0,2	0,15	0,1	1,52	0,142	0,106	0,097	0,03	0,21	0,40	P	196	172	1	1	0	1	
	1245 - b2	slab,CS	1	2,404	23,5	0,225	0,6	0,2	0,15	0,1	1,52	0,142	0,106	0,097	0,08	0,30	0,50	P/WB	206	173	1	1	0	1	
	Richart Klinge 1939	S1 - 2	slab,SS	1	6,096	25,6	0,381	2,438	0,1	0,152	0,152	0,907	0,982	0,14	0,127	0,25	0,66	0,96	P	342,5	278	1	1	1	1
		S1 - 3	slab,SS	1	6,096	25,6	0,381	1,219	0,1	0,152	0,152	0,907	0,982	0,14	0,127	0,25	0,66	0,96	P	391,4	318	1	1	1	1
S2 - 2		slab,SS	1	6,096	29,1	0,229	1,016	0,1	0,152	0,152	0,907	0,982	0,14	0,127	0,10	0,36	0,66	P	369,2	328	1	1	0	1	
Richart 1948	501a	slab,SS	1	1,829	25,4	0,914	0,915	0,1	0,356	0,356	1,38	0,53	0,254	0,241	0,69	1,73	1,83	DT	1753	877	1	0	1	0	
	501b	slab,SS	1	1,829	25,7	0,914	0,915	0,1	0,356	0,356	1,38	0,53	0,254	0,241	0,69	1,73	1,83	DT	1690	845	1	0	1	0	
	502a	slab,SS	1	1,829	24,3	0,914	0,915	0,1	0,356	0,356	0,54	0,2	0,406	0,395	0,69	1,73	1,83	DT	2464	1232	1	0	0	0	
	502b	slab,SS	1	1,829	22,6	0,914	0,915	0,1	0,356	0,356	0,54	0,2	0,406	0,395	0,69	1,73	1,83	DT	2571	1286	1	0	0	0	
	503a	slab,SS	1	1,829	24,4	0,914	0,915	0,1	0,356	0,356	0,54	0,2	0,406	0,395	0,69	1,73	1,83	DT	2607	1304	1	0	0	0	
	503b	slab,SS	1	1,829	24,0	0,914	0,915	0,1	0,356	0,356	0,54	0,2	0,406	0,395	0,69	1,73	1,83	DT	2447	1224	1	0	0	0	
	504a	slab,SS	1	1,524	24,9	0,914	0,762	0,1	0,356	0,356	1,77	0,34	0,254	0,24	0,69	1,52	1,52	DT	1446	723	0	0	1	0	
	504b	slab,SS	1	1,524	25,8	0,914	0,762	0,1	0,356	0,356	1,77	0,34	0,254	0,24	0,69	1,52	1,52	DT	1557	779	0	0	1	0	

Annex 1: Slab Shear Database

Ref	Test	type	n	b (m)	$f_{c,mean}$ (MPa)	$\alpha$	$b_p$ (m)	$b_{sp}$ (m)	$l_{sur}$ (m)	$b_{sur}$ (m)	$\rho_t$ (%)	$\rho_s$ (%)	$d_t$ (mm)	$d_s$ (mm)	$a_s$ (m)	$b_{gr}$ (m)	$b_{gr}$ (m)	mode	$F_{sur}$ (kN)	$V_{sur}$ (kN)	Influence $b_{gr}$ $b_{gr}$	$a/d_t$ >2,5	$e?$
Richart 1948	505a	slab,SS	1	1,524	25,4	0,914	0,762	0,1	0,356	0,356	0,68	0,13	0,406	0,394	0,69	1,52	1,52	DT	2438	1219	0	0	0
	505b	slab,SS	1	1,524	25,7	0,914	0,762	0,1	0,356	0,356	0,68	0,13	0,406	0,394	0,69	1,52	1,52	DT	2335	1168	0	0	0
	506a	slab,SS	1	1,524	23,1	0,914	0,762	0,1	0,356	0,356	0,68	0,13	0,406	0,394	0,69	1,52	1,52	DT	2224	1112	0	0	0
	506b	slab,SS	1	1,524	26,3	0,914	0,762	0,1	0,356	0,356	0,68	0,13	0,406	0,394	0,69	1,52	1,52	DT	2224	1112	0	0	0
Serms-Ros et al 2002	R0	slab,SS	2	0,75	29,2	0,83	0,375	0,1	0,75	0,1	2,2	0	0,206	na	0,73	0,75	0,75	WB	337	244	0	0	1
	A0	slab,SS	2	0,75	24,5	0,83	0,375	0,1	0,75	0,1	2,2	0	0,206	na	0,73	0,75	0,75	WB	259	187	0	0	1
	C0	slab,SS	2	0,75	25,2	0,83	0,375	0,1	0,75	0,1	2,2	0	0,206	na	0,73	0,75	0,75	WB	252	182	0	0	1
	D0	slab,SS	2	0,75	32,6	0,83	0,375	0,1	0,75	0,1	2,2	0	0,206	na	0,73	0,75	0,75	WB	301	218	0	0	1
		slab,SS	2	0,503	13,4	0,49	0,252	0,05	0,503	0,06	0,95	0	0,142	na	0,44	0,50	0,50	WB		76	0	0	1
		slab,SS	2	0,502	13,4	0,49	0,251	0,05	0,502	0,06	1,11	0	0,142	na	0,44	0,50	0,50	WB		81	0	0	1
Leonhardt & Walther 1962	P4	slab,SS	2	0,5	14,5	0,49	0,25	0,05	0,5	0,06	1,4	0	0,145	na	0,44	0,50	0,50	WB		101	0	0	1
	P5	slab,SS	2	0,503	13,4	0,49	0,252	0,05	0,503	0,06	1,86	0	0,145	na	0,44	0,50	0,50	WB		101	0	0	1
	P8	slab,SS	2	0,502	24,9	0,49	0,251	0,05	0,502	0,06	0,91	0	0,148	na	0,44	0,50	0,50	WB		88	0	0	1
	P9	slab,SS	2	0,5	24,9	0,491	0,25	0,05	0,5	0,06	1,86	0	0,146	na	0,44	0,50	0,50	WB		106	0	0	1
	P10	slab,SS	2	0,503	12,4	0,35	0,252	0,05	0,503	0,06	1,1	0	0,102	na	0,30	0,50	0,50	WB		59	0	0	1
	P11	slab,SS	2	0,498	13,7	0,63	0,249	0,05	0,498	0,06	1,11	0	0,183	na	0,58	0,50	0,50	WB		101	0	0	1
	P12	slab,SS	2	0,501	12,6	0,349	0,251	0,05	0,501	0,06	0,95	0	0,142	na	0,30	0,50	0,50	WB		101	0	0	0
		slab,SS	1	0,639	30,4	0,332	0,32	0,02	0,16	0,083	1,88	0	0,083	na	0,28	0,64	0,64	nn		71	0	0	1
		slab,SS	1	0,639	31,2	0,348	0,32	0,02	0,16	0,087	1,92	0	0,087	na	0,30	0,64	0,64	nn		68	0	0	1
	de Cossio 1962	64-8E	slab,SS	1	0,64	28,5	0,328	0,32	0,02	0,32	0,082	1,9	0	0,082	na	0,28	0,64	0,64	nn		85	0	0
64-8C		slab,SS	1	0,64	28,5	0,324	0,32	0,02	0,32	0,081	1,95	0	0,081	na	0,28	0,64	0,64	nn		82	0	0	1
64-8D		slab,SS	1	0,505	27,8	0,328	0,253	0,02	0,505	0,082	1,98	0	0,082	na	0,28	0,51	0,51	nn		65	0	0	1
48-8B		slab,SS	1	0,64	28,5	0,328	0,32	0,02	0,64	0,082	1,9	0	0,082	na	0,28	0,64	0,64	nn		87	0	0	1
	slab,SS	1	0,636	29,2	0,324	0,318	0,02	0,636	0,081	1,94	0	0,081	na	0,28	0,64	0,64	nn		86	0	0	1	

Annex 1: Slab Shear Database

Ref	Test	type	n	b (mm)	$f_{c,mean}$ (MPa)	a (mm)	$b_f$ (mm)	$b_{sp}$ (mm)	$l_{stud}$ (mm)	$b_{stud}$ (mm)	$\rho_1$ (%)	$\rho_2$ (%)	$\rho_3$ (%)	$d_1$ (mm)	$d_2$ (mm)	$a_s$ (mm)	$b_{gr1}$ (mm)	$b_{gr2}$ (mm)	mode	$F_{test}$ (kN)	$V_{test}$ (kN)	influence $b_{gr1}$ $b_{gr2}$	$a/d_1$ $>2.5$	$e?$	
de Cossio 1962	A50-25A	slab,SS	1	0,501	34,5	0,676	0,251	0,05	0,501	0,253	1,81	0	0	0,253	na	0,52	0,50	0,50	na	189	189	0	0	1	0
	A50-25B	slab,SS	1	0,502	34,1	0,673	0,251	0,05	0,502	0,252	1,85	0	0	0,252	na	0,52	0,50	0,50	na	171	171	0	0	1	0
Kani 1979	271	slab,SS	2	0,611	27,0	1,633	0,306	0,15	0,611	0,1	2,75	0	0	0,269	na	1,51	0,61	0,61	WB	217	217	0	0	1	0
	272	slab,SS	2	0,611	27,0	1,36	0,306	0,15	0,611	0,1	2,73	0	0	0,271	na	1,23	0,61	0,61	WB	228	228	0	0	1	0
	273	slab,SS	2	0,612	27,2	1,087	0,306	0,15	0,612	0,1	2,72	0	0	0,271	na	0,96	0,61	0,61	WB	206	206	0	0	1	0
	274	slab,SS	2	0,612	27,2	0,815	0,306	0,15	0,612	0,1	2,73	0	0	0,27	na	0,69	0,61	0,61	WB	250	250	0	0	1	0
R&F 1968	S-15	slab,SS	2	0,761	33,0	1,119	0,381	0,05	0,761	0,1	0,63	0	0	0,269	na	1,04	0,76	0,76	WB	151	151	0	0	1	0
Aster & Koch 1974	11	slab,SS	2	1	24,6	1,825	0,5	0,1	1	0,1	0,46	0	0	0,5	na	1,73	1,00	1,00	WB	267	267	0	0	1	0
	16	slab,SS	2	1	30,4	2,753	0,5	0,15	1	0,1	0,42	0	0	0,75	na	2,63	1,00	1,00	WB	407	407	0	0	1	0
	2	slab,SS	2	1	26,9	0,92	0,5	0,05	1	0,1	0,64	0	0	0,25	na	0,85	1,00	1,00	WB	218	218	0	0	1	0
	12	slab,SS	2	1	27,3	1,825	0,5	0,1	1	0,1	0,65	0	0	0,5	na	1,73	1,00	1,00	WB	330	330	0	0	1	0
	3	slab,SS	2	1	27,3	0,92	0,5	0,05	1	0,1	0,91	0	0	0,25	na	0,85	1,00	1,00	WB	223	223	0	0	1	0
	8	slab,SS	2	1	31,1	2,75	0,5	0,1	1	0,1	0,63	0	0	0,5	na	2,65	1,00	1,00	WB	287	287	0	0	1	0
	9	slab,SS	2	1	19,9	2,75	0,5	0,1	1	0,1	0,63	0	0	0,5	na	2,65	1,00	1,00	WB	261	261	0	0	1	0
	10	slab,SS	2	1	20,0	2,75	0,5	0,1	1	0,1	0,63	0	0	0,5	na	2,65	1,00	1,00	WB	262	262	0	0	1	0
	17	slab,SS	2	1	28,7	2,753	0,5	0,15	1	0,1	0,42	0	0	0,75	na	2,63	1,00	1,00	WB	364	364	0	0	1	0
	Reineck et al 1978	N8		0,5	25,8	0,791	0,25	0,01	0,5	0,1	0,79	0	0	0	0,226	na	0,74	0,50	0,50		102	102	0	0	1
N6			0,5	25,8	0,565	0,25	0,01	0,5	0,1	0,79	0	0	0	0,226	na	0,51	0,50	0,50		118	118	0	0	0	0
N7			0,5	24,6	0,563	0,25	0,01	0,5	0,1	1,39	0	0	0	0,225	na	0,51	0,50	0,50		140	140	0	0	0	0
Heger McGrath 1980	SW9-0A	slab,SS	2	0,914	48,5	0,596	0,457	0,05	0,914	0,025	0,62	0,071	0,184	0,177	0,56	0,91	0,91	0,91	WB	168	168	0	0	1	0
	SW9-0B	slab,SS	2	0,914	48,5	0,597	0,457	0,05	0,914	0,025	0,6	0,069	0,19	0,183	0,56	0,91	0,91	0,91	WB	156	156	0	0	1	0
	SW9-6A-15	slab,SS	2	0,914	48,5	0,382	0,457	0,05	0,914	0,025	0,61	0,07	0,188	0,181	0,34	0,91	0,91	0,91	WB	268	268	0	0	0	0
	SW9-0B-15	slab,SS	2	0,914	48,5	0,381	0,457	0,05	0,914	0,025	0,62	0,071	0,186	0,179	0,34	0,91	0,91	0,91	WB	271	271	0	0	0	0

Annex 1: Slab Shear Database

Ref	Test	type	n	b (mm)	$f_{c,mean}$ (MPa)	a	$b_s$ (mm)	$b_{sp}$ (mm)	$l_{stud}$ (mm)	$b_{stud}$ (mm)	$\rho_s$ (%)	$\rho_s$ (%)	$d_s$ (mm)	$d_s$ (mm)	$a_s$ (mm)	$b_{gr}$ (mm)	$b_{gr}$ (mm)	$V_{cr}$ (kN)	$F_{cr}$ (kN)	mode	Influence $b_{gr}$ $b_{sp}$	$a/d_s$ >2,5	$e?$	
Heger McGrath 1980	SW9M-0A	slab,SS	2	0,914	48,5	0,628	0,457	0,05	0,914	0,025	0,61	0,067	0,197	0,19	0,59	0,91	0,91	156	174	WB	0 0	1	0	
	SW9M-0B	slab,SS	2	0,914	48,5	0,598	0,457	0,05	0,914	0,025	0,62	0,071	0,185	0,178	0,56	0,91	0,91	300	308	WB	0 0	0	0	
	SW9M-0A-15	slab,SS	2	0,914	48,5	0,382	0,457	0,05	0,914	0,025	0,6	0,069	0,19	0,183	0,34	0,91	0,91	197	196	WB	0 0	0	0	
	SW9M-0B-15	slab,SS	2	0,914	48,5	0,381	0,457	0,05	0,914	0,025	0,66	0,076	0,174	0,167	0,34	0,91	0,91	203	223	WB	0 0	0	0	
	SW14-0A	slab,SS	2	0,914	49,0	0,598	0,457	0,05	0,914	0,025	0,93	0,069	0,191	0,183	0,56	0,91	0,91	379	390	WB	0 0	0	0	
	SW14-0B	slab,SS	2	0,914	49,0	0,597	0,457	0,05	0,914	0,025	0,96	0,071	0,186	0,178	0,56	0,91	0,91	440	700	WB	0 0	0	0	
	SW18-0A	slab,SS	2	0,914	48,3	0,598	0,457	0,05	0,914	0,025	1,24	0,072	0,184	0,175	0,56	0,91	0,91	1060	1060	WB	0 0	0	0	
	SW18-0B	slab,SS	2	0,914	48,3	0,596	0,457	0,05	0,914	0,025	1,27	0,074	0,18	0,171	0,56	0,91	0,91	257	272	P	1 1	1	0	
	SW18-0A-15	slab,SS	2	0,914	48,3	0,381	0,457	0,05	0,914	0,025	1,28	0,074	0,179	0,17	0,34	0,91	0,91	235	174	P	1 1	1	0	
	SW18-0B-15	slab,SS	2	0,914	48,3	0,382	0,457	0,05	0,914	0,025	1,3	0,076	0,176	0,167	0,34	0,91	0,91	150	306	P	1 1	1	0	
	bridge	on site	bridge	1	1	56,0	1,125	0,5	0,25	0,1	0,1	1,54	?	0,257	?	0,95	1,00	1,00	?	?	?	0 0	1	0
	Cullington et al 1996	lab 1	slab,SS	1	1	60,0	0,514	0,5	0,25	0,1	0,1	1,54	0	0,257	mm	0,34	0,78	0,98	700	620	WB	1 1	0	0
		lab 2	slab,SS	1	1	60,0	0,257	0,5	0,25	0,1	0,1	1,54	0	0,257	mm	0,08	0,51	0,51	1060	1060	WB	1 1	0	0
	Coin & Thonier	1	slab,SS	1	2,5	25,8	0,37	1,25	0,2	1	0,2	1,072	1,097	0,085	0,074	0,17	1,34	1,74	257	222	?	1 1	1	0
2		slab,SS	1	2,5	30,4	0,37	1,25	0,2	1	0,2	1,589	0,301	0,085	0,077	0,17	1,34	1,74	272	235	?	1 1	1	0	
3bis		slab,SS	1	2,5	30,4	0,37	1,25	0,2	0,4	0,2	0,776	0,22	0,085	0,077	0,17	0,74	1,14	174	150	?	1 1	1	0	
5		slab,SS	1	2,5	30,2	0,37	1,25	0,2	1	0,2	2,15	0,418	0,085	0,077	0,17	1,34	1,74	306	264	P	1 1	1	0	
5bis		slab,SS	1	2,5	30,2	0,37	1,25	0,2	1	0,2	2,15	0,418	0,085	0,077	0,17	1,34	1,74	312	269	P	1 1	1	0	
6		slab,SS	1	2,5	30,2	0,37	1,25	0,2	0,7	0,2	1,662	0,418	0,085	0,077	0,17	1,04	1,44	356	307	P	1 1	1	0	
6bis		slab,SS	1	2,5	30,2	0,37	1,25	0,2	0,7	0,2	1,662	0,418	0,085	0,077	0,17	1,04	1,44	250	216	P	1 1	1	0	
7	slab,SS	1	2,5	19,2	0,37	1,25	0,2	0,4	0,2	1,255	0,418	0,085	0,077	0,17	0,74	1,14	165	142	?	1 1	1	0		
7bis	slab,SS	1	2,5	19,2	0,37	1,25	0,2	0,4	0,2	1,255	0,418	0,085	0,077	0,17	0,74	1,14	151	130	?	1 1	1	0		

Annex 1: Slab Shear Database

Ref	Test	type	n	b (mm)	$f_{cmax}$ (MPa)	a (mm)	$b_s$ (mm)	$b_{sp}$ (mm)	$l_{stud}$ (mm)	$\rho_1$ (%)	$\rho_2$ (%)	$\rho_1$ (%)	$b_{stud}$ (mm)	$b_{gr}$ (mm)	$a_s$ (mm)	$d_1$ (mm)	$d_2$ (mm)	$d_3$ (mm)	$b_{gr}$ (mm)	$b_{gr}$ (mm)	mode	$F_{max}$ (kN)	$V_{max}$ (kN)	influence $b_{gr}$ $b_{gr}$	$a/d_1$ $>2,5$	$e?$	
Olonakin & Alexander 1999	CB1(0)	slab,SS	2	0,75	32,5	0,425	0,375	0,1	0,75	0,01	1,04	0,898	0,128	0,112	0,37	0,75	0,75	0,75	0,75	0,75	WB	258	129	0	0	1	0
		slab,SS	2	0,75	32,5	0,375	0,375	0,1	0,75	0,01	1,04	0,898	0,128	0,112	0,32	0,75	0,75	0,75	0,75	0,75	WB	260	130	0	0	1	0
		slab,SS	2	0,75	32,5	0,425	0,375	0,1	0,75	0,01	1,04	0,898	0,128	0,112	0,37	0,75	0,75	0,75	0,75	0,75	WB	246	123	0	0	1	0
		slab,SS	2	0,75	32,5	0,375	0,375	0,1	0,75	0,01	1,04	0,898	0,128	0,112	0,32	0,75	0,75	0,75	0,75	0,75	WB	256	128	0	0	1	0
Ekeberg et al 1982	1st fl-3	slab,CS	2	5	25,0	0,61	2,5	0,3	0,1	0,1	0,649	0,157	0,11	0,1	0,92	1,12	1,12	0,92	1,12	1,12	P?	371	280	1	1	1	0
		slab,CS	2	5	25,0	0,61	2,5	0,3	0,1	0,1	0,649	0,157	0,11	0,1	0,92	1,12	1,12	0,92	1,12	1,12	P?	385	291	1	1	1	0
	2nd fl-3	slab,CS	2	5	17,8	0,3	2,5	0,3	0,1	0,1	0,519	0,102	0,108	0,102	0,10	0,30	0,50	0,30	0,50	0,50	P?	465	409	1	1	1	0
		slab,CS	2	5	17,8	0,3	2,5	0,3	0,1	0,1	0,488	0,095	0,115	0,105	0,10	0,30	0,50	0,30	0,50	0,50	P?	435	383	1	1	1	0
	6	slab,CS	2	5	17,8	0,8	2,5	0,3	0,1	0,1	0,488	0,095	0,115	0,105	0,60	1,30	1,50	1,30	1,50	1,50	P?	230	156	1	1	1	0
		slab,CS	2	5	17,8	0,5	2,5	0,3	0,1	0,1	0,497	0,097	0,113	0,103	0,30	0,70	0,90	0,70	0,90	0,90	P?	340	272	1	1	1	0
	7	slab,CS	2	5	17,8	0,5	2,5	0,3	0,1	0,1	0,497	0,097	0,113	0,103	0,30	0,70	0,90	0,70	0,90	0,90	P?	315	252	1	1	1	0
		slab,CS	2	5	17,8	0,5	2,5	0,3	0,1	0,1	0,497	0,097	0,113	0,103	0,30	0,70	0,90	0,70	0,90	0,90	P?	315	252	1	1	1	0
Rombach & Lette 2008 2009	VK1V1	cantilever	1	2,4	35,0	0,85	1,2	0,28	0,4	0,4	0,81	0,638	0,224	0,21	0,51	1,42	2,22	2,22	2,22	2,22	WB	690	690	1	1	1	0
	VK2V1	cantilever	1	2,4	46,0	0,85	1,2	0,28	0,4	0,4	1,16	0,559	0,217	0,203	0,51	1,42	2,22	2,22	2,22	2,22	WB	678	678	1	1	1	0
	VK3V1	cantilever	1	2,4	46,5	0,85	1,2	0,28	0,4	0,4	1,16	0,767	0,193	0,179	0,51	1,42	2,22	2,22	2,22	2,22	WB	672	672	1	1	1	0
	VK3V3	slab,SS	1	2,4	51,5	0,85	1,2	0,28	0,4	0,4	0,52	0,767	0,174	0,16	0,51	1,42	2,22	2,22	2,22	2,22	WB/P	898	644	1	1	1	0
	VK4V1	cantilever	1	2,4	42,5	0,85	1,2	0,28	0,4	0,4	1,2	0,742	0,167	0,153	0,51	1,42	2,22	2,22	2,22	2,22	WB	487	487	1	1	1	0
Miller et al 1994	VK4V3	slab, SS	1	2,4	46,0	0,85	1,2	0,28	0,4	0,4	0,68	0,742	0,167	0,153	0,51	1,42	2,22	2,22	2,22	2,22	WB/P	935	670	1	1	1	0
		real bridge	2	11,13	54,0	3,901	5,563	0,8	2,519	1,525	0,405	0,382	0,398	0,375	2,74	8,00	11,05	8,00	11,05	11,05	P	3200	2176	1	1	1	0
Fang et al 1990	1	slab,SS	1	6,1	29,0	1,219	0,914	0,43	0,203	0,508	0,426	0,482	0,134	0,121	0,75	1,71	2,28	2,28	2,28	2,28	WB	632	569	1	1	1	1
		slab,SS	2	6,1	29,0	1,219	0,914	0,43	0,203	1,727	0,426	0,482	0,134	0,121	0,14	0,49	2,89	2,89	2,89	2,89	WB/P	907	816	1	1	1	1

*Annex 1: Slab Shear Database*

## **Annex 2: Example application of the Modified Bond Model**

The step-by-step method from §5.3.6 is now explained by using experiment S16T4 as an example. In this experiment, failure occurred in a combination of wide beam shear, beam shear and punching of the support. The maximum load was 776kN.

1. Gather the relevant information:
  - the cylinder compressive strength of the concrete: 43,9MPa;
  - the geometry of the slab:  $5\text{m} \times 2,5\text{m} \times 0,3\text{m}$  with  $l_{span} = 3,6\text{m}$ ;
  - the geometry of the load:  $200\text{mm} \times 200\text{mm}$ ;
  - the position of the load along the width and along the span:  $a = 600\text{mm}$ ,  $a_y = 360\text{mm}$ ,  $b_{r,side} = 438\text{mm}$ ;
  - the geometry of the support: 3 elastomeric bearing pads of  $280\text{mm} \times 350\text{mm}$ ;
  - whether loading occurs close to a simple or continuous support: continuous support
2. Sketch an  $xy$  plane with the load, support and slab. Draw the 4 strips that extend from the load in the  $x$ - and  $y$ -direction. This procedure is shown in Fig. A2.1.

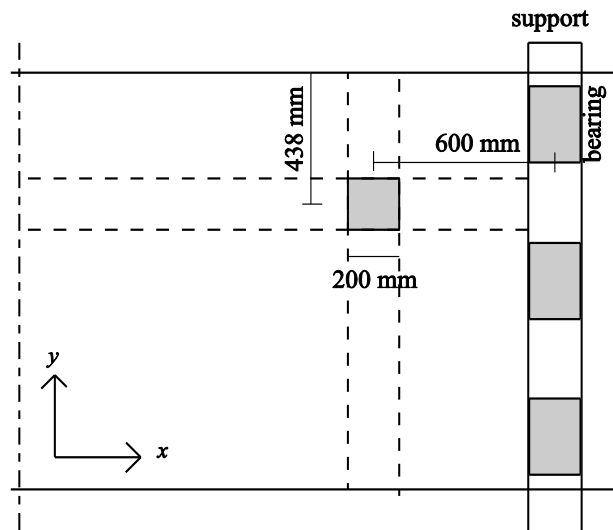


Fig. A2. 1: Sketch of the resulting strips in S16T4.

3. Study the capacity of the four (when four strips are used) resulting quadrants. If the geometric conditions do not penalize the loading that is carried in the quadrant, the quadrants carry the factors  $\alpha_{MBM}$  in two directions. If the load is placed eccentric from the middle of the width, the loading term in the quadrants between the  $x$ -direction strips and the free edge is reduced by  $\alpha_{MBM}$  with:

Annex 2: Example application of the Modified Bond Model

$$\alpha_{MBM} = \frac{2b_r}{b} = 2 \cdot \frac{438\text{mm}}{2500\text{mm}} = 0,35$$

If not the full width of the slab is supported, the loading term in the quadrants between the y-direction strips and the support is  $\alpha_{MBM}$  with:

$$\alpha_{MBM} = \frac{\sum_{i=1}^{n_{\text{bearings}}} l_{\text{bearing},i}}{b} = \frac{3 \times 350\text{mm}}{2500\text{mm}} = 0,42.$$

If a quadrant is influenced by both conditions, both factors  $\alpha_{MBM}$  can be multiplied for that quadrant, as shown in Fig A2.2 for the quadrant between the support and the free edge.

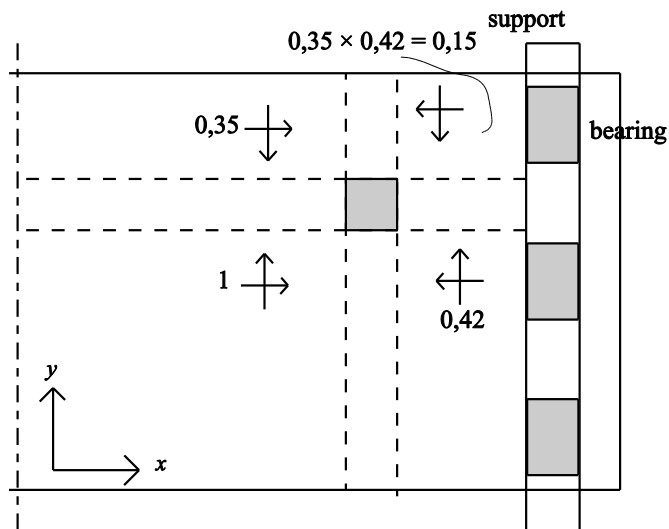


Fig. A2.2: Sketch of the reduction factors that are applied as a result of the geometry.

4. If the amount of reinforcement in the x-direction strips is considerably larger than in the y-direction strips, plastic load redistribution towards the stiff strip between the load and the support can occur, resulting in larger load coefficients on the stiffer strip and smaller load coefficient on the more flexible strip. This situation is the case for the example under study, Fig. A2.3.
5. Calculate the load on the strips by adding the  $\alpha_{MBM}$  terms into  $\chi$  on the strips, to determine  $\chi$ , the factor to quantify the influence of the geometry on the capacity of the strip. If the geometric properties do not interfere,  $\chi = 2$  for every strip, as in the original Bond Model.

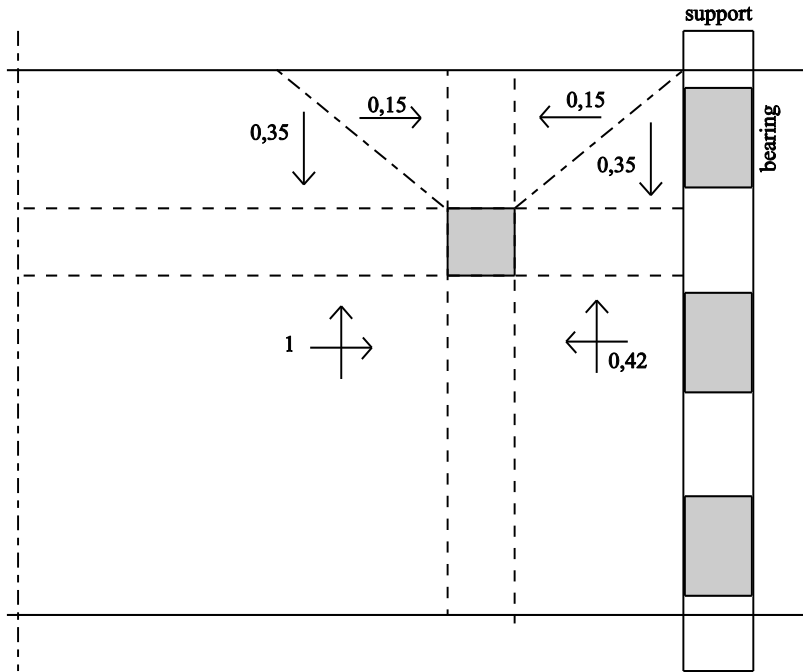


Fig. A2.3: Sketch of the reduction factors that are applied as a result of the geometry, taking into account redistribution of the load.

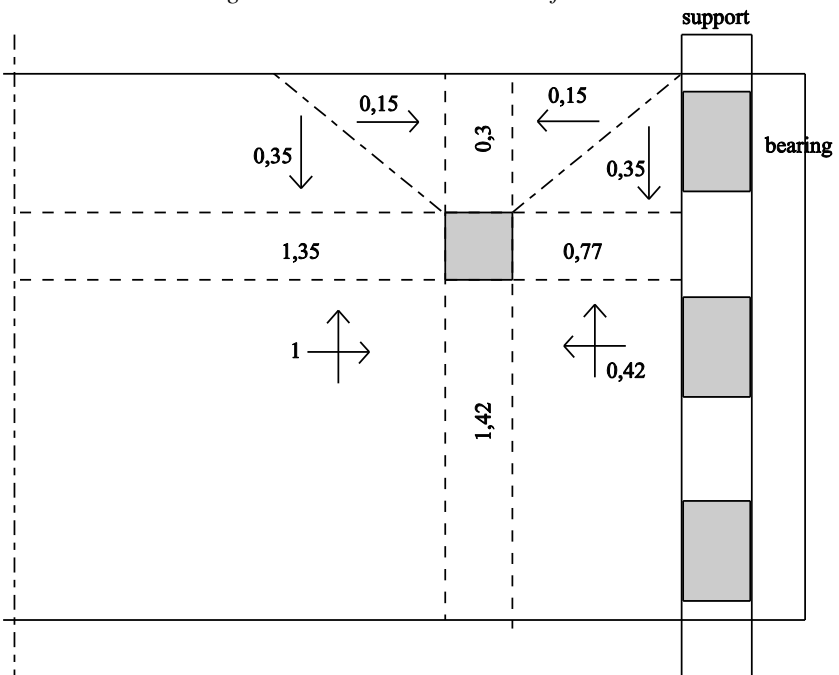


Fig. A2.4: Resulting reduction factors  $\chi$ .

Annex 2: Example application of the Modified Bond Model

6. Gather the required information about the reinforcement in the strips and the geometry of the reinforcement:
  - the effective depth to the longitudinal and transverse reinforcement:  $d_l = 0,255\text{m}$  and  $d_t = 0,233\text{m}$ ,
  - the yield strength of the bars: 537MPa for  $\phi 10\text{mm}$  and 541MPa for  $\phi 20\text{mm}$  <sup>41</sup>, and
  - the layout of the reinforcement: given in Fig A2.5.

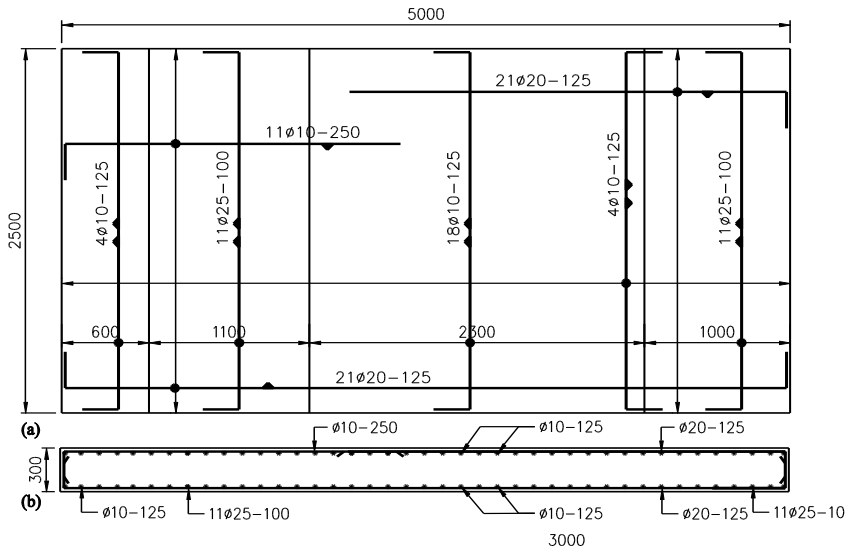


Fig. A2.5: Layout of the reinforcement for slabs S15 – S18.

7. Count the number of bars per strip, and add  $\frac{1}{2}$  bar on every side of the strip. The width between these bars is  $b_{rebar,x}$  for the longitudinal bars and  $b_{rebar,y}$  for the transverse flexural bars.
 

The strips are 200mm wide.

  - for the  $x$ -direction, bottom reinforcement: 21  $\phi 20\text{mm} - 125\text{mm}$  fits 2 bars and  $2 \times \frac{1}{2}$  bars on every side of the strip with  $b_{rebar,x} = 375\text{mm}$ ;
  - for the  $y$ -direction, bottom reinforcement 11  $\phi 25\text{mm} - 100\text{mm}$  fits 3 bars and  $2 \times \frac{1}{2}$  bars on every side of the strip with  $b_{rebar,y} = 400\text{mm}$ .
8. Determine the reinforcement area  $A_{sBx}$  and  $A_{sBy}$  of the bars over  $b_{rebar,x}$  and  $b_{rebar,y}$ . The percentage of reinforcement to be considered is determined as:

<sup>41</sup> The yield strength of the 25mm bars is not known, and therefore the smallest yield stress is used for these bars:  $f_{yk} = 537\text{MPa}$ .

Annex 2: Example application of the Modified Bond Model

$$A_{sB,x} = 3\pi \left( \frac{20\text{mm}}{2} \right)^2 = 942\text{mm}^2$$

$$A_{sB,y} = 4\pi \left( \frac{25\text{mm}}{2} \right)^2 = 1963\text{mm}^2$$

$$\rho_{neg,x} = \frac{A_{sB,x}}{b_{rebar,x} d_l} = \frac{942\text{mm}^2}{375\text{mm} \times 255\text{mm}} = 0,985\% , \text{ and}$$

$$\rho_{neg,y} = \frac{A_{sB,y}}{b_{rebar,y} d_y} = \frac{1963\text{mm}^2}{400\text{mm} \times 233\text{mm}} = 2,106\% .$$

9. The moment capacity of the longitudinal and transverse reinforcement is:

$$\begin{aligned} M_{neg,x} &= \rho_{neg,x} f_{yk} z_t d_l l_{load} \\ &= 0,00985 \times 541\text{MPa} \times 200\text{mm} \times (255\text{mm})^2 \times \left( 1 - \frac{0,00985 \times 541\text{MPa}}{1,7 \times 43,9\text{MPa}} \right) \\ &= 64,35\text{kNm} \end{aligned}$$

and

$$\begin{aligned} M_{neg,y} &= \rho_{neg,y} f_{yk} z_t d_t b_{load} \\ &= 0,0211 \times 537\text{MPa} \times 200\text{mm} \times (233\text{mm})^2 \times \left( 1 - \frac{0,0211 \times 537\text{MPa}}{1,7 \times 43,9\text{MPa}} \right) \\ &= 104\text{kNm} \end{aligned}$$

10. If the load is placed close to a continuous support, determine  $k_r$ :

$$k_r = \frac{M_{sup}}{M_{span}} = \frac{152\text{kNm}}{278\text{kNm}} = 0,548$$

with  $M_{sup}$  the moment at the support and  $M_{span}$  the moment at the location of the concentrated load. With the known forces at ultimate (concentrated load, prestressing bars, self-weight), the moment diagram can be compiled and the moments at the support and at the concentrated load are determined.

11. If the load is placed near to a continuous support, the reinforcement activated by the support moment should be taken into account as described in steps 6 to 9.

From Step 6:

- the effective depth to the longitudinal and transverse reinforcement:  $d_{l,top} = 0,255\text{m}$  and  $d_{t,top} = 0,24\text{m}$ ;
- the yield strength of the bars: 537MPa for  $\phi 10\text{mm}$  and 541MPa for  $\phi 20\text{mm}$ , and
- the layout of the reinforcement: given in Fig. A2.5.

From Step 7: The strips are 200mm wide.

- for the  $x$ -direction, top reinforcement: 21  $\phi 20\text{mm}$  - 125mm fits 2 bars and 2  $\times 1/2$  bars on every side of the strip with  $b_{rebar,x} = 375\text{mm}$ ;

*Annex 2: Example application of the Modified Bond Model*

- for the y-direction, top reinforcement 4  $\phi$ 10mm - 125mm fits 2 bars and 2  $\times$  1/2 bars on every side of the strip with  $b_{rebar,y} = 375\text{mm}$ .

From Step 8:

$$A_{sT,x} = 3\pi \left( \frac{20\text{mm}}{2} \right)^2 = 942\text{mm}^2$$

$$A_{sT,y} = 3\pi \left( \frac{10\text{mm}}{2} \right)^2 = 236\text{mm}^2$$

$$\rho_{pos,x} = \frac{A_{sT,x}}{b_{rebar,x} d_{l,top}} = \frac{942\text{mm}^2}{375\text{mm} \times 255\text{mm}} = 0,985\% , \text{ and}$$

$$\rho_{pos,y} = \frac{A_{sT,y}}{b_{rebar,y} d_{y,top}} = \frac{236\text{mm}^2}{375\text{mm} \times 240\text{mm}} = 0,262\% .$$

From Step 9:

$$\begin{aligned} M_{pos,x} &= \rho_{pos,x} f_{yk} z_{l,top} d_{l,top} l_{load} \\ &= 0,00985 \times 541\text{MPa} \times 200\text{mm} \times (255\text{mm})^2 \times \left( 1 - \frac{0,00985 \times 541\text{MPa}}{1,7 \times 43,9\text{MPa}} \right) \\ &= 64,35\text{kNm} \end{aligned}$$

and

$$\begin{aligned} M_{pos,y} &= \rho_{neg,y} f_{yk} z_{t,top} d_{t,top} b_{load} \\ &= 0,00262 \times 537\text{MPa} \times 200\text{mm} \times (240\text{mm})^2 \left( 1 - \frac{0,00262 \times 537\text{MPa}}{1,7 \times 43,9\text{MPa}} \right) \\ &= 15,9\text{kNm} \end{aligned}$$

12. If the load is placed close to a continuous support, then

$$M_{s,x} = M_{neg,x} + k_r M_{pos,x} = 64\text{kNm} + 0,548 \times 64\text{kNm} = 100\text{kNm} \text{ and}$$

$$M_{s,y} = M_{neg,y} + k_r M_{pos,y} = 105\text{kNm} + 0,548 \times 16\text{kNm} = 113\text{kNm} .$$

For loads close to the simple support,  $k_r = 0$ . The support moment and span moment influence the quadrants between the load and the support. Therefore,  $k_r$  is applied as  $> 0$  to the x-direction strip between the load and the support and the y-direction strips. This procedure is also shown in Fig. A2.6, in which the strips that are affected by the support moment are highlighted.

13. The loading term is determined to be:

$$w_{ACI,x} = 0,166 d_t \sqrt{f_{ck}} = 0,166 \times 255\text{mm} \sqrt{43,9\text{MPa}} = 280 \frac{\text{kN}}{\text{m}} \text{ in the } x\text{-direction}$$

and  $w_{ACI,y} = 0,166 d_t \sqrt{f_{ck}} = 0,166 \times 233\text{mm} \sqrt{43,9\text{MPa}} = 256 \frac{\text{kN}}{\text{m}}$  in the y-direction for ribbed bars. A reduction factor of 0,8 is applied to  $w$  for plain bars –

Annex 2: Example application of the Modified Bond Model

in S16T4, ribbed bars are used. A size effect factor can be applied as :

$$k_{MBM} = \frac{1 + \sqrt{\frac{300}{d_l}}}{2} \leq 1 \text{ with } d_l \text{ in [mm]}. \text{ The size effect factor equals } = 1 \text{ for S16T5.}$$

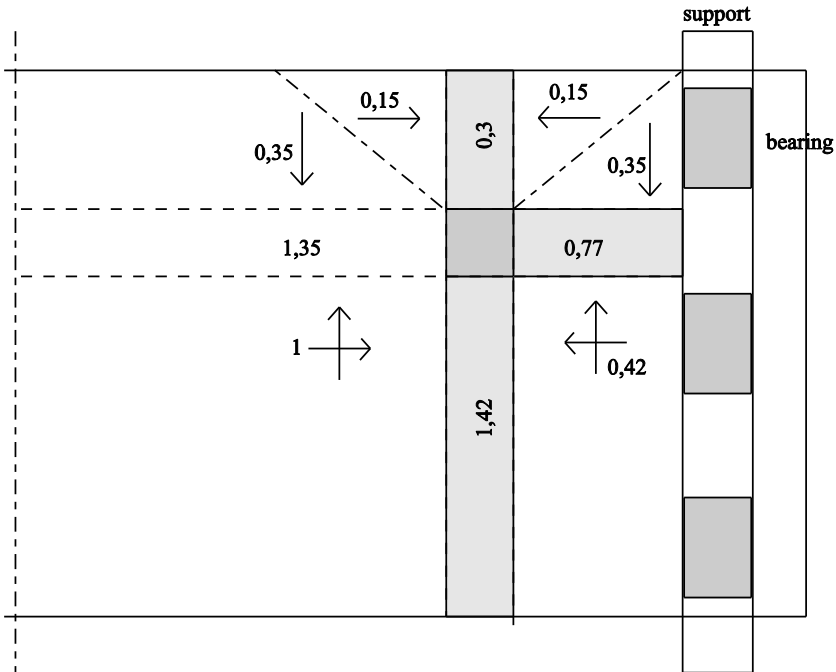


Fig. A2.6: Identification of strips on which factor  $k_r$  acts: the 3 strips are highlighted in light grey.

14. Determine the capacity of the four strips:

- for the  $x$ -direction strip from the load towards the span:

$$P_{MBM,x} = \chi_1 \sqrt{w_{ACI,x} M_{neg,x}} = 1,35 \sqrt{280 \frac{\text{kN}}{\text{m}} 64 \text{kNm}} = 181 \text{kN},$$

with  $\chi_1$  the result of the factors from the geometry for the considered strip, Fig. A2.6.

- for the  $x$ -direction strip between the load and the support:

$$P_{MBM,sup} = \chi_2 \sqrt{w_{ACI,x} M_{s,x}} \frac{2d_l}{a_v} = 0,77 \sqrt{280 \frac{\text{kN}}{\text{m}} 100 \text{kNm}} \frac{2 \times 255 \text{mm}}{360 \text{mm}} = 183 \text{kN}$$

with  $\chi_2$  the result of the factors from geometry for the considered strip.

- for the  $y$ -direction strips:

*Annex 2: Example application of the Modified Bond Model*

$$P_{MBM,y} = (\chi_3 + \chi_4) \sqrt{w_{ACI,y} M_{s,y}} = (1,42 + 0,3) \sqrt{256 \frac{\text{kN}}{\text{m}} 113 \text{kNm}} = 293 \text{kN}$$

with  $\chi_3$  and  $\chi_4$  the resulting factors from geometry for the y-direction strips.

15. The shear capacity of a slab subjected to a concentrated load close to the support according to the Modified Bond Model is:

$$P_{MBM} = P_{MBM,x} + P_{MBM,sup} + P_{MBM,y} = 181 \text{ kN} + 183 \text{ kN} + 293 \text{ kN} = 657 \text{ kN}.$$

Note that the calculation in Excel results in  $P_{MBM} = 663 \text{kN}$ , because in that calculation floating numbers are used. The ratio of the test result to the calculated result  $P_u/P_{MBM} = 776 \text{kN}/657 \text{kN} = 1,18$ . The Modified Bond Model results in a safe prediction of the experiment.

**Annex 3: Comparison between experiments and design methods**

Test	$d_i$ (m)	$a$ (m)	$b_r$ (mm)	SS/CS	$P_{exp}$ (kN)	$V_{exp,BC}$ (kN)	$V_{Re,eff1}$ (kN)	$V_{Re,eff2}$ (kN)	$V_E$ (MPa)	$V_{ps}$ (MPa)	$V_{VBC}$ (kN)	$V_{ACI}$ (kN)	$P_{Region}$ (kN)	$P_{MBM}$ (kN)
S1T1	0,265	0,60	1250	SS	954	679	252	343	1,02	0,85	309	458	839	716
S1T2	0,265	0,60	1250	CS	1023	784	252	343	1,10	0,85	301	458	923	760
S2T1	0,265	0,60	1250	SS	1374	848	249	384	1,44	0,95	393	450	957	912
S2T4	0,265	0,60	1250	CS	1421	985	249	384	1,49	0,95	294	450	1124	1014
S3T1	0,265	0,60	1250	SS	1371	851	284	439	1,43	1,21	515	550	1178	1119
S3T4	0,265	0,60	1250	CS	1337	925	284	439	1,40	1,21	385	550	1366	1239
S4T1	0,265	0,60	438	SS	1160	727	256	333	1,92	1,14	481	494	884	860
S4T2	0,265	0,60	438	SS	1110	698	256	333	1,83	1,14	481	494	884	860
S5T1	0,265	0,40	1250	CS	1804	681	177	329	2,85	2,37	233	338	1709	1700
S5T4	0,265	0,40	1250	SS	1755	573	177	329	2,77	2,37	675	338	1502	1539
S6T1	0,265	0,40	438	CS	1446	552	180	279	3,11	2,41	241	347	1429	1162
S6T2	0,265	0,40	438	CS	1423	550	180	279	3,06	2,41	241	347	1464	1185
S6T4	0,265	0,40	438	SS	1366	457	180	279	2,94	2,41	699	347	1258	1261
S6T5	0,265	0,40	438	SS	1347	442	180	279	2,90	2,41	699	347	1258	1261
S7T1	0,265	0,60	438	SS	1121	700	298	389	1,85	1,41	569	623	1058	976
S7T2	0,265	0,60	438	CS	1172	807	298	389	1,94	1,41	409	623	1188	928
S7T3	0,265	0,60	438	CS	1136	789	298	389	1,88	1,41	409	623	1215	943
S7T5	0,265	0,60	438	SS	1063	673	298	389	1,76	1,41	569	623	1058	976

Annex 3: Comparison between experiments and design methods

Test	$d_i$ (m)	$a$ (m)	$b_r$ (mm)	SS/CS	$P_{exp}$ (kN)	$V_{exp}$ (kN)	$V_{exp,EC}$ (kN)	$V_{Rc,heft1}$ (kN)	$V_{Rc,heft2}$ (kN)	$V_E$ (MPa)	$V_{pu}$ (MPa)	$V_{VBC}$ (kN)	$V_{ACI}$ (kN)	$P_{Regen}$ (kN)	$P_{MBM}$ (kN)
S8T1	0,265	0,60	1250	SS	1481	1226	923	325	502	1,55	1,38	609	672	1346	1249
S8T2	0,265	0,60	1250	CS	1356	1213	936	325	502	1,42	1,38	456	672	1550	1376
S9T1	0,265	0,40	1250	SS	1523	1355	640	211	331	2,49	2,26	640	440	1453	1287
S9T4	0,265	0,40	1250	CS	1842	1717	851	211	331	3,02	2,26	290	440	1666	1425
S10T1	0,265	0,40	438	SS	1320	1177	557	212	320	2,80	2,27	641	442	1227	1026
S10T2	0,265	0,40	438	SS	1116	994	470	212	320	2,36	2,27	642	442	1227	1026
S10T4	0,265	0,40	438	CS	1511	1422	712	212	320	3,20	2,27	290	442	1452	989
S10T5	0,265	0,40	438	CS	1454	1368	685	212	320	3,08	2,27	290	442	1445	985
S11T1	0,265	0,60	1250	SS	1194	998	848	323	441	1,28	1,23	458	567	1164	983
S11T4	0,265	0,60	1250	CS	958	886	766	323	441	1,03	1,23	448	567	1467	1077
S12T1	0,265	0,60	438	SS	931	780	663	290	349	1,54	1,22	427	509	920	663
S12T2	0,265	0,60	438	SS	1004	839	712	290	349	1,66	1,22	427	509	920	663
S12T4	0,265	0,60	438	CS	773	705	608	290	349	1,28	1,22	402	509	1053	699
S12T5	0,265	0,60	438	CS	806	735	633	290	349	1,33	1,22	402	509	1057	700
S13T1	0,265	0,40	1250	SS	1404	1253	593	202	317	2,30	2,16	605	351	1391	1252
S13T4	0,265	0,40	1250	CS	1501	1411	706	202	317	2,46	2,16	274	351	1635	1365
S14T1	0,265	0,40	438	SS	1214	1088	518	201	305	2,57	2,16	600	349	1166	842
S14T2	0,265	0,40	438	SS	1093	975	462	201	305	2,32	2,16	601	349	1166	842
S14T4	0,265	0,40	438	CS	1282	1207	605	201	305	2,72	2,16	271	349	1353	911
S14T5	0,265	0,40	438	CS	1234	1157	578	201	305	2,61	2,16	271	349	1311	896

Annex 3: Comparison between experiments and design methods

Test	$d_i$ (m)	$a$ (m)	$b_r$ (mm)	SS/CS	$P_{exp}$ (kN)	$V_{exp}$ (kN)	$V_{exp,EC}$ (kN)	$V_{Rc,leg1}$ (kN)	$V_{Rc,leg2}$ (kN)	$V_E$ (MPa)	$V_{pu}$ (MPa)	$V_{VBC}$ (kN)	$V_{ACI}$ (kN)	$P_{Regen}$ (kN)	$P_{MBM}$ (kN)
S15T1	0,255	0,60	1250	CS	1040	944	685	235	337	1,37	1,67	378	445	1471	928
S15T4	0,255	0,60	1250	SS	1127	944	670	235	337	1,49	1,67	378	445	1247	886
S16T1	0,255	0,60	438	SS	932	776	551	231	283	1,78	1,69	349	440	957	615
S16T2	0,255	0,60	438	SS	815	675	479	231	283	1,56	1,69	350	440	957	615
S16T4	0,255	0,60	438	CS	776	723	528	231	283	1,48	1,69	346	440	1191	663
S16T5	0,255	0,60	438	CS	700	653	478	231	283	1,34	1,69	346	440	1175	660
S17T1	0,255	0,40	1250	CS	1365	1285	449	133	261	3,05	3,77	242	252	1906	1159
S17T4	0,255	0,40	1250	SS	1235	1109	357	133	261	2,76	3,77	513	252	1633	1086
S18T1	0,255	0,40	438	SS	1157	1031	328	133	260	2,91	3,76	510	251	1379	799
S18T2	0,255	0,40	438	SS	1079	954	300	133	260	2,71	3,76	510	251	1379	799
S18T4	0,255	0,40	438	CS	1122	1062	375	133	260	2,82	3,76	240	251	1606	862
S18T5	0,255	0,40	438	CS	1104	1050	373	133	260	2,77	3,76	240	251	1648	874
BS1T1	0,265	0,60	250	SS	290	242	182	148	148	1,13	1,40	354	314	415	879
BS1T2	0,265	0,60	250	CS	623	562	434	148	148	2,42	1,40	204	314	529	900
BS2T1	0,265	0,40	250	SS	633	552	255	152	152	2,46	2,30	502	328	573	985
BS2T2	0,265	0,40	250	CS	976	919	461	152	152	3,79	2,30	204	328	767	1212
BS3T1	0,265	0,60	250	SS	356	293	249	154	154	1,38	1,29	270	332	403	693
BS3T2	0,265	0,60	250	CS	449	399	343	154	154	1,74	1,29	204	332	475	759
BM1T1	0,265	0,60	500	CS	923	811	622	296	296	1,79	1,40	407	628	918	1311
BM1T2	0,265	0,60	500	SS	720	591	444	296	296	1,40	1,40	820	628	830	1248

Annex 3: Comparison between experiments and design methods

Test	$d_i$ (m)	$a$ (m)	$b_r$ (mm)	SS/CS	$P_{exp}$ (kN)	$V_{exp}$ (kN)	$V_{exp,EC}$ (kN)	$V_{Rc, left}$ (kN)	$V_{Rc, right}$ (kN)	$V_E$ (MPa)	$V_{pw}$ (MPa)	$V_{VBC}$ (kN)	$V_{ACI}$ (kN)	$P_{Regen}$ (kN)	$P_{MRM}$ (kN)
BM2T1	0,265	0,40	500	SS	1212	1062	493	213	304	2,35	2,30	628	459	1146	1293
BM2T2	0,265	0,40	500	CS	1458	1354	670	213	304	2,83	2,30	285	459	1368	1423
BM3T1	0,265	0,60	500	SS	735	607	514	307	307	1,43	1,29	428	664	807	1002
BM3T2	0,265	0,60	500	CS	895	791	678	307	307	1,74	1,29	407	664	927	1058
BL1T1	0,265	0,60	750	SS	1034	844	633	326	444	1,34	1,40	598	691	1246	1248
BL1T2	0,265	0,60	750	CS	1252	1119	863	326	444	1,62	1,40	448	691	1486	1344
BL2T1	0,265	0,40	750	SS	1494	1311	610	218	343	2,45	2,35	628	474	1508	1316
BL2T2	0,265	0,40	750	CS	1708	1586	784	218	343	2,80	2,35	285	474	1769	1434
BL3T1	0,265	0,60	750	SS	1114	907	766	326	444	1,44	1,24	456	691	1166	973
BL3T2	0,265	0,60	750	CS	1153	1035	890	326	444	1,49	1,24	448	691	1407	1048
BX1T1	0,265	0,60	1000	SS	1331	1080	808	326	503	1,39	1,40	599	691	1357	1247
BX1T2	0,265	0,60	1000	CS	1596	1415	1089	326	503	1,67	1,40	448	691	1565	1324
BX2T1	0,265	0,40	1000	SS	1429	1259	588	197	310	2,34	2,13	629	409	1366	1215
BX2T2	0,265	0,40	1000	CS	1434	1332	658	197	310	2,35	2,13	285	409	1532	1292
BX3T1	0,265	0,60	1000	SS	1141	935	791	322	439	1,22	1,23	457	680	1167	965
BX3T2	0,265	0,60	1000	CS	1193	1059	908	322	439	1,28	1,23	448	680	1316	1011

Annex 3: Comparison between experiments and design methods

Test	$d_i$ (m)	$a$ (m)	$b_r$ (mm)	SS/CS	$P_{exp}$ (kN)	$P_{line}$ (kN)	$V_{exp}$ (kN)	$\tau_{exp,EC,eff1}$ (MPa)	$v_{k,c}$ (MPa)	$\tau_{exp,EC,eff2}$ (MPa)	$\tau_{VBC}$ (MPa)	$\tau_{exp,eff1}$ (MPa)	$\tau_{ACI}$ (MPa)	$P_{MBM}$ (kN)
S19T2	0,265	0,60	1250	SS	1484	0	1249	2,40	1,008	1,47	1,89	3,27	1,17	1265
S19T1	0,265	0,60	1250	CS	1568	0	1379	2,59	1,008	1,60	1,42	3,60	1,18	1356
S20T1	0,265	0,60	1250	SS	1542	603	1579	3,01	1,029	2,04	1,98	3,63	1,20	1193
S20T2b	0,265	0,60	1250	CS	1552	601	1657	3,22	1,029	2,44	1,48	4,07	1,26	1127
S20T3	0,265	0,60	438	CS	1337	601	1487	2,59	1,029	2,10	1,48	3,89	1,26	1064
S20T4	0,265	0,60	438	CS	1449	601	1569	2,76	1,029	2,22	1,48	4,15	1,26	1044
S21T1	0,265	0,60	1250	CS	1165	602	1472	2,74	1,007	2,03	1,41	2,91	1,19	1143
S21T2	0,265	0,60	1250	SS	1386	603	1544	3,00	1,007	2,16	2,19	3,15	1,17	1038
S21T5	0,265	0,87	438	SS'	853	0	678	1,99	1,007	1,61	1,41	1,62	1,14	652
S22T1	0,265	0,60	438	CS	984	602	1320	2,62	1,014	2,18	1,44	3,16	1,21	812
S22T2	0,265	0,60	438	CS	961	602	1298	2,57	1,014	2,14	1,44	3,10	1,21	810
S22T3	0,265	0,60	438	SS	978	603	1221	2,51	1,014	2,07	2,23	3,00	1,18	728
S22T4	0,265	0,60	438	SS	895	604	1143	2,34	1,014	1,94	2,23	2,78	1,18	728
S23T1	0,265	0,60	1250	CS	1386	601	1653	2,93	1,019	2,06	1,45	3,62	1,21	1289
S23T2	0,265	0,60	1250	SS	1132	602	1343	2,44	1,019	1,73	2,01	2,95	1,19	1183
S24T1	0,265	0,60	438	CS	1358	601	1629	2,94	1,019	2,38	1,45	4,32	1,21	896
S24T2	0,265	0,60	438	CS	1182	601	1477	2,65	1,019	2,16	1,45	3,85	1,21	896
S24T3	0,265	0,60	438	SS	995	602	1235	2,27	1,019	1,86	1,94	3,22	1,19	822
S24T4	0,265	0,60	438	SS	784	602	1048	1,91	1,019	1,59	1,94	2,65	1,19	822

Annex 3: Comparison between experiments and design methods

Test	$d_i$ (m)	$a$ (m)	$b_r$ (mm)	SS/CS	$P_{exp}$ (kN)	$P_{lim}$ (kN)	$V_{exp}$ (kN)	$\tau_{exp,RC,eff}$ (MPa)	$v_{l,c}$ (MPa)	$\tau_{exp,RC,eff2}$ (MPa)	$\tau_{VBC}$ (MPa)	$\tau_{exp,eff}$ (MPa)	$\tau_{ACI}$ (MPa)	$P_{MBM}$ (kN)
S25T1	0,265	0,60	1250	SS	1461	0	1214	2,53	1,018	1,64	2,25	3,04	1,18	1143
S25T2	0,265	0,40	1250	CS	1620	601	1945	3,08	1,018	1,99	1,45	4,94	1,27	1732
S25T3	0,265	0,40	438	CS	1563	602	1893	2,99	1,018	2,19	1,45	5,58	1,27	1195
S25T4	0,265	0,87	438	SS'	854	0	678	1,99	1,018	1,62	1,45	1,62	1,16	695
S25T5	0,265	1,13	438	SS'	968	0	695	1,70	1,018	1,43	1,45	1,43	1,15	695
S26T1	0,265	0,42	438	SS	1448	602	1686	2,80	1,018	2,08	3,90	4,97	1,22	983
S26T2	0,265	0,42	438	SS	1324	602	1568	2,60	1,018	1,94	3,36	4,58	1,22	983
S26T3	0,265	0,40	1250	CS	1555	602	1896	2,99	1,018	1,95	1,45	4,79	1,28	1778
S26T4	0,265	0,40	438	CS	1363	602	1725	2,71	1,018	2,01	1,45	4,98	1,29	1256
S26T5	0,265	0,40	438	CS	1451	602	1804	2,84	1,018	2,09	1,45	5,25	1,29	1244

**Annex 4: Comparison between experiments from slab shear database and NEN-EN 1992-1-1:2005**

Reference	Test	$b_{eff1}$	$b_{eff2}$	mode	$V_{exp}$	$k$	$V_{R,c}$	$V_{R,c,eff}$	$\beta$	$V_{exp,EC}$	$V_{exp,EC}/V_{R,c}$	$V_{exp,EC}/V_{R,c,eff}$
		(m)	(m)									
Reißen & Hegger 2011	50 2TV	0,50	0,50	WB	136	1,91	110	110	1,00	136	1,231	1,231
	50_W 1TV	0,50	0,50	WB	137	1,91	116	116	1,00	137	1,181	1,181
	50_W 2TV	0,50	0,50	WB	143	1,91	117	117	1,00	143	1,220	1,220
	150 1 TV	1,50	1,50	WB	407	1,91	344	344	1,00	407	1,184	1,184
	150 2 TV	1,50	1,50	WB	425	1,91	346	346	1,00	425	1,231	1,231
	250 1 TV	1,90	2,50	WB	498	1,91	394	519	1,00	498	1,263	0,960
	250 2 TV	1,90	2,50	WB	520	1,91	402	528	1,00	520	1,295	0,984
	350 1 TV	1,90	2,70	P	739	1,91	429	609	1,00	739	1,723	1,213
	350 2 TV	1,90	2,70	P	683	1,91	438	622	1,00	683	1,560	1,098
	350a1 1TV	2,50	3,30	nn	787	1,91	583	769	1,00	787	1,350	1,023
	350a1 2TV	1,30	2,10	nn	876	1,91	307	497	0,94	822	2,673	1,655
	350a2 1TV	2,50	3,30	P	624	1,91	528	697	1,00	624	1,180	0,894
	350a2 2TV	1,30	2,10	P	684	1,91	273	441	0,94	641	2,347	1,453
	Tb1 1TV	2,00	2,80	WB	569	1,91	456	638	1,00	569	1,248	0,892
	Tb1 2TV	2,00	2,80	WB	475	1,98	412	577	1,00	475	1,152	0,823
Tb2 1TV	2,00	2,80	WB/P	538	1,91	444	622	1,00	538	1,210	0,865	
Tb2 2TV	2,00	2,80	WB/P	451	1,98	399	558	1,00	451	1,131	0,808	
Regan 1982	1-SS	0,34	0,54	P	97	2,00	21	33	0,72	70	3,360	2,116
	1-CS	0,34	0,54	P	118	2,00	21	33	0,72	85	4,088	2,574
	2-SS	0,26	0,46	P	110	2,00	15	27	0,48	53	3,397	1,920
	2-CS	0,26	0,46	P	148	2,00	15	27	0,48	71	4,583	2,590
	3-SS	0,18	0,38	P	171	2,00	12	25	0,25	43	3,659	1,733
	3-CS	0,18	0,38	WB	214	2,00	12	25	0,25	54	4,575	2,167
	4-SS	0,17	0,34	P	206	2,00	11	23	0,25	52	4,506	2,213
	5-SS	0,36	0,56	P	160	2,00	23	37	0,48	77	3,271	2,103
	6-SS	0,26	0,66	WB	128	2,00	16	42	0,48	61	3,737	1,472
	6-CS	0,26	0,66	WB	125	2,00	16	42	0,48	60	3,635	1,432
	7-SS	0,28	0,48	P	176	2,00	19	33	0,25	44	2,258	1,317
7-CS	0,36	0,56	P	189	2,00	25	39	0,48	91	3,620	2,327	
Sherwood Lubell Bentz Collins 2006	AT-1-East	2,02	2,02	WB	1133	1,47	1484	1484	1,00	1133	0,764	0,764
	AT-1-West	2,02	2,02	WB	1221	1,47	1484	1484	1,00	1221	0,823	0,823
	AT-2/250N	0,25	0,25	WB	115	1,68	89	89	1,00	115	1,280	1,280
	AT-2/250W	0,25	0,25	WB	112	1,67	91	91	1,00	112	1,234	1,234
	AT-2/1000N	1,00	1,00	WB	440	1,68	359	359	1,00	440	1,225	1,225
	AT-2/1000W	1,00	1,00	WB	471	1,67	363	363	1,00	471	1,297	1,297
	AT-2/3000	2,45	2,75	WB	1282	1,67	900	1012	1,00	1282	1,424	1,267
AT-3/N1	0,70	0,70	WB	238	1,81	190	190	1,00	238	1,253	1,253	

*Annex 4: Comparison between experiments from slab shear database and NEN-EN 1992-1-1:2005*

Reference	Test	$b_{eff1}$	$b_{eff2}$	mode	$V_{exp}$	$k$	$V_{R,c}$	$V_{R,c,eff}$	$\beta$	$V_{exp,EC}$	$V_{exp,EC}/V_{R,c}$	$V_{exp,EC}/V_{R,c,eff}$
		(m)	(m)									
Sherwood	<b>AT-3/N2</b>	0,71	0,71	WB	259	1,81	191	191	1,00	259	1,355	1,355
Lubell	<b>AT-3/T1</b>	0,70	0,70	WB	253	1,81	190	190	1,00	253	1,329	1,329
Bentz	<b>AT-3/T2</b>	0,71	0,71	WB	249	1,81	191	191	1,00	249	1,299	1,299
Collins	<b>AY1</b>	0,25	0,25	WB	85	1,68	65	65	1,00	85	1,321	1,321
2006	<b>AX7</b>	0,70	0,70	WB	250,6	1,83	194	194	1,00	251	1,290	1,290
	<b>AX6</b>	0,70	0,70	WB	282,5	1,83	230	230	1,00	283	1,226	1,226
	<b>AX8</b>	0,71	0,71	WB	272,1	1,83	231	231	1,00	272	1,176	1,176
	<b>AW1</b>	1,17	1,17	WB	585	1,61	468	468	1,00	585	1,251	1,251
	<b>AW4</b>	1,17	1,17	WB	725	1,63	588	588	1,00	725	1,234	1,234
	<b>AW8</b>	1,17	1,17	WB	800	1,63	587	587	1,00	800	1,364	1,364
Vaz Rodrigues	<b>DR1a</b>	2,38	2,98	P	1397	1,81	620	776	1,00	1397	2,254	1,800
Muttoni	<b>DR1b</b>	2,25	2,55	WB	1025	1,80	594	674	1,00	1025	1,724	1,521
& Olivier	<b>DR1c</b>	2,55	2,85	WB	910	1,80	679	759	1,00	910	1,341	1,200
2006	<b>DR2a</b>	2,60	3,20	WB	961	1,76	685	843	1,00	961	1,403	1,140
	<b>DR2b</b>	2,25	2,55	WB	857	1,76	608	689	1,00	857	1,409	1,243
	<b>DR2c</b>	2,55	2,85	WB	719	1,76	678	758	1,00	719	1,060	0,949
Jaeger	<b>A1V1</b>	0,80	0,80	WB	169	2,00	162	162	1,00	169	1,046	1,046
2002	<b>A3V1</b>	0,80	0,80	WB	266	2,00	182	182	1,00	266	1,459	1,459
2005	<b>A4V1</b>	0,80	0,80	WB	141	2,00	143	143	1,00	141	0,983	0,983
2007	<b>A5V1</b>	0,80	0,80	WB	222	2,00	163	163	1,00	222	1,359	1,359
	<b>B1V1</b>	2,00	2,00	WB	852	1,72	867	867	1,00	852	0,982	0,982
	<b>B3V1</b>	2,00	2,00	WB	1282	1,70	940	940	1,00	1282	1,364	1,364
	<b>B4V1</b>	2,00	2,00	WB	804	1,69	793	793	1,00	804	1,014	1,014
	<b>B5V1</b>	2,00	2,00	WB	1170	1,68	831	831	1,00	1170	1,407	1,407
Graf	<b>1243 - a1</b>	0,23	0,35	WB	306	2,00	18	27	0,25	76	4,357	2,863
1933	<b>1243 - a2</b>	0,35	0,55	P	212	2,00	28	44	0,43	92	3,295	2,097
	<b>1243 - b1</b>	0,23	0,23	P	336	2,00	18	18	0,25	84	4,572	4,572
	<b>1243 - b2</b>	0,23	0,40	WB	180	2,00	19	33	0,25	45	2,354	1,354
	<b>1244 - a1</b>	0,25	0,45	WB	258	2,00	19	34	0,25	64	3,390	1,884
	<b>1244 - a2</b>	0,35	0,55	WB	177	2,00	27	42	0,48	85	3,144	2,001
	<b>1244 - b1</b>	0,21	0,40	WB	137	2,00	16	31	0,25	34	2,138	1,112
	<b>1244 - b2</b>	0,30	0,50	WB	123	2,00	24	39	0,36	44	1,892	1,135
	<b>1245 - a1</b>	0,25	0,45	P	312	2,00	26	47	0,25	78	2,973	1,651
	<b>1245 - a2</b>	0,35	0,55	P	232	2,00	37	58	0,47	109	2,978	1,895
	<b>1245 - b1</b>	0,21	0,40	P	172	2,00	22	42	0,25	43	1,928	1,022
	<b>1245 - b2</b>	0,30	0,50	P/WB	173	2,00	31	52	0,35	61	1,947	1,168

*Annex 4: Comparison between experiments from slab shear database and NEN-EN 1992-1-1:2005*

Reference	Test	$b_{eff1}$ (m)	$b_{eff2}$ (m)	mode	$V_{exp}$ (kN)	$k$ (kN)	$V_{R,c}$ (kN)	$V_{R,c,eff}$ (kN)	$\beta$	$V_{exp,EC}$ (kN)	$V_{exp,EC}/V_{R,c}$	$V_{exp,EC}/V_{R,c,eff}$
Richart Kluge 1939	<b>S1 - 2</b>	0,66	0,96	P	278	2,00	79	115	0,91	253	3,206	2,196
	<b>S1 - 3</b>	0,66	0,96	P	318	2,00	79	115	0,91	289	3,664	2,509
	<b>S2 - 2</b>	0,36	0,66	P	328	2,00	44	82	0,37	120	2,694	1,454
de Cossio 1962	<b>A50-25A</b>	0,50	0,50	nn	189	1,89	142	142	1,00	189	1,324	1,324
	<b>A50-25B</b>	0,50	0,50	nn	171	1,89	143	143	1,00	171	1,199	1,199
R&F 1968	<b>S-15</b>	0,76	0,76	WB	151	1,86	157	157	1,00	151	0,959	0,959
Aster & Koch 1974	<b>11</b>	1,00	1,00	WB	267	1,63	275	275	1,00	267	0,973	0,973
	<b>16</b>	1,00	1,00	WB	407	1,52	399	399	1,00	407	1,020	1,020
	<b>2</b>	1,00	1,00	WB	218	1,89	183	183	1,00	218	1,188	1,188
	<b>12</b>	1,00	1,00	WB	330	1,63	319	319	1,00	330	1,034	1,034
	<b>3</b>	1,00	1,00	WB	223	1,89	207	207	1,00	223	1,073	1,073
	<b>8</b>	1,00	1,00	WB	287	1,63	330	330	1,00	287	0,870	0,870
	<b>9</b>	1,00	1,00	WB	261	1,63	284	284	1,00	261	0,916	0,916
	<b>10</b>	1,00	1,00	WB	262	1,63	285	285	1,00	262	0,918	0,918
	<b>17</b>	1,00	1,00	WB	364	1,52	391	391	1,00	364	0,929	0,929
Heger McGrath 1980	<b>SW9-0A</b>	0,91	0,91	WB	168	2,00	157	157	1,00	168	1,068	1,068
	<b>SW9-0B</b>	0,91	0,91	WB	156	2,00	160	160	1,00	156	0,970	0,970
	<b>SW9-6A-15</b>	0,91	0,91	WB	268	2,00	159	159	0,91	245	1,536	1,536
	<b>SW9-0B-15</b>	0,91	0,91	WB	271	2,00	159	159	0,92	250	1,577	1,577
	<b>SW9M-0A</b>	0,91	0,91	WB	156	2,00	167	167	1,00	156	0,932	0,932
	<b>SW9M-0B</b>	0,91	0,91	WB	174	2,00	158	158	1,00	174	1,105	1,105
	<b>SW9M-0A-15</b>	0,91	0,91	WB	300	2,00	160	160	0,91	272	1,695	1,695
	<b>SW9M-0B-15</b>	0,91	0,91	WB	308	2,00	151	151	0,99	304	2,007	2,007
	<b>SW14-0A</b>	0,91	0,91	WB	197	2,00	187	187	1,00	197	1,054	1,054
	<b>SW14-0B</b>	0,91	0,91	WB	196	2,00	184	184	1,00	196	1,064	1,064
	<b>SW18-0A</b>	0,91	0,91	WB	203	2,00	197	197	1,00	203	1,026	1,026
	<b>SW18-0B</b>	0,91	0,91	WB	223	2,00	195	195	1,00	223	1,145	1,145
	<b>SW18-0A-15</b>	0,91	0,91	WB	379	2,00	194	194	0,96	364	1,874	1,874
	<b>SW18-0B-15</b>	0,91	0,91	WB	390	2,00	192	192	0,98	382	1,989	1,989
Cullington et al 1996	<b>on site</b>	1,00	1,00	?	330	1,88	321	321	1,00	330	1,031	1,031
	<b>lab 1</b>	0,78	0,98	WB	620	1,88	255	321	0,66	409	1,603	1,275
	<b>lab 2</b>	0,51	0,51	WB	1000	1,88	169	169	0,25	250	1,482	1,482
Coin & Thonier	<b>3bis</b>	0,74	1,14		150	2,00	54	83	1,00	150	2,775	1,801
	<b>6bis</b>	1,04	1,44	P	216	2,00	98	135	1,00	216	2,205	1,593
	<b>7</b>	0,74	1,14		142	2,00	55	84	1,00	142	2,612	1,696
	<b>7bis</b>	0,74	1,14		130	2,00	55	84	1,00	130	2,391	1,552

*Annex 4: Comparison between experiments from slab shear database and NEN-EN 1992-1-1:2005*

Reference	Test	$b_{eff1}$	$b_{eff2}$	mode	$V_{exp}$ (kN)	$k$	$V_{R,c}$ (kN)	$V_{R,c,eff}$ (kN)	$\beta$	$V_{exp,EC}$ (kN)	$V_{exp,EC}/V_{R,c}$	$V_{exp,EC}/V_{R,c,eff}$	
		(m)	(m)										
Olonisakin & Alexander 1999	<b>CB1(b)</b>	0,75	0,75	WB	129	2,00	93	93	1,00	129	1,385	1,385	
	<b>CB2</b>	0,75	0,75	WB	130	2,00	93	93	1,00	130	1,396	1,396	
	<b>RB1</b>	0,75	0,75	WB	123	2,00	93	93	1,00	123	1,321	1,321	
	<b>RB2</b>	0,75	0,75	WB	128	2,00	93	93	1,00	128	1,375	1,375	
Rombach & Latte 2008 2009	<b>VK1V1</b>	1,42	2,22	WB	690	1,94	283	443	1,00	690	2,437	1,558	
	<b>VK2V1</b>	1,42	2,22	WB	678	1,96	341	533	1,00	678	1,988	1,272	
	<b>VK3V1</b>	1,42	2,22	WB	672	2,00	311	486	1,00	672	2,160	1,381	
	<b>VK3V3</b>	1,42	2,22	WB/P	644	2,00	222	347	1,00	644	2,901	1,855	
	<b>VK4V1</b>	1,42	2,22	WB	487	2,00	264	412	1,00	487	1,846	1,181	
											AVG	1,837	1,404
											STD	0,983	0,518
											COV	0,535	0,369
											CHAR	0,224	0,555

Reference	Test	mode	$P_{exp}$	$u$	$W$	$e_{pu}$	$k_{pu}$	$v_E$	$k$	$v_{min}$ (MPa)	$v_{pu}$ (MPa)	$v_E/v_{pu}$
			(kN)	(m)	(m <sup>2</sup> )	(m)	Mpa					
Reißen & Hegger 2011	<b>50 2TV</b>	WB	204	1,00	2,23	0,00	0,60	0,826	1,90	0,53	0,97	0,855
	<b>50_W 1TV</b>	WB	183	1,00	2,23	0,00	0,60	0,741	1,90	0,57	1,02	0,730
	<b>50_W 2TV</b>	WB	215	1,00	2,23	0,00	0,60	0,870	1,90	0,58	1,03	0,848
	<b>150 1 TV</b>	WB	543	3,00	2,23	0,00	0,60	0,733	1,90	0,56	1,00	0,731
	<b>150 2 TV</b>	WB	638	3,00	2,23	0,00	0,60	0,861	1,90	0,57	1,01	0,855
	<b>250 1 TV</b>	WB	664	4,70	2,23	0,00	0,60	0,571	1,90	0,48	0,91	0,630
	<b>250 2 TV</b>	WB	780	4,70	2,23	0,00	0,60	0,671	1,90	0,5	0,92	0,727
	<b>350 1 TV</b>	P	985	4,70	2,23	0,00	0,60	0,848	1,90	0,55	0,99	0,860
	<b>350 2 TV</b>	P	1024	4,70	2,23	0,00	0,60	0,881	1,90	0,57	1,01	0,876
	<b>350a1 1TV</b>	nn	1166	4,70	2,23	0,00	0,60	1,005	1,90	0,58	1,02	0,986
	<b>350a1 2TV</b>	nn	1143	4,43	1,98	0,00	0,60	1,046	1,90	0,59	1,13	0,923
	<b>350a2 1TV</b>	P	924	4,70	2,23	0,00	0,60	0,797	1,90	0,5	0,92	0,862
	<b>350a2 2TV</b>	P	892	4,43	1,98	0,00	0,60	0,816	1,90	0,49	1,01	0,811
	<b>Tb1 1TV</b>	WB	569	4,70	2,23	0,00	0,60	0,491	1,90	0,56	0,99	0,494
	<b>Tb1 2TV</b>	WB	475	4,28	1,85	0,00	0,60	0,520	1,97	0,6	1,09	0,477
<b>Tb2 1TV</b>	WB/P	538	4,70	2,23	0,00	0,60	0,463	1,90	0,54	0,97	0,478	
<b>Tb2 2TV</b>	WB/P	451	4,28	1,85	0,00	0,60	0,493	1,97	0,57	1,05	0,468	
Regan 1982	<b>1-SS</b>	P	120	1,15	0,13	0,00	0,60	1,300	2,00	0,49	0,98	1,327
	<b>1-CS</b>	P	150	1,15	0,13	0,00	0,60	1,625	2,00	0,49	0,98	1,659
	<b>2-SS</b>	P	130	0,90	0,08	0,00	0,60	1,800	2,00	0,47	1,43	1,257
	<b>2-CS</b>	P	180	0,90	0,08	0,00	0,60	2,493	2,00	0,47	1,43	1,741
	<b>3-SS</b>	P	195	0,65	0,04	0,00	0,60	3,742	2,00	0,53	3,13	1,196
	<b>3-CS</b>	WB	250	0,65	0,04	0,00	0,60	4,798	2,00	0,53	3,13	1,533
	<b>4-SS</b>	P	230	0,47	0,04	0,00	0,60	6,174	2,00	0,58	3,30	1,874

Annex 4: Comparison between experiments from slab shear database and NEN-EN 1992-1-1:2005

Reference	Test	mode	$P_{exp}$ (kN)	$u$ (m)	$W$ (m <sup>2</sup> )	$e_{pu}$ (m)	$k_{pu}$	$v_E$ Mpa	$k$	$v_{min}$ (MPa)	$v_{pu}$ (MPa)	$v_E/v_{pu}$
	5-SS	P	190	1,10	0,13	0,00	0,70	2,154	2,00	0,54	1,57	1,372
	6-SS	WB	160	1,10	0,11	0,00	0,45	1,814	2,00	0,51	1,52	1,194
	6-CS	WB	160	1,10	0,11	0,00	0,45	1,814	2,00	0,51	1,52	1,194
	7-SS	P	200	0,85	0,08	0,00	0,70	2,937	2,00	0,59	3,35	0,878
	7-CS	P	230	1,10	0,13	0,00	0,70	2,607	2,00	0,59	1,67	1,559
Sherwood	AT-1-East	WB	2266	4,03	21,60	0,00	0,80	0,617	1,47	0,5	0,52	1,193
Lubell	AT-1-West	WB	2441	4,03	21,60	0,00	0,80	0,665	1,47	0,5	0,52	1,285
Bentz	AT-2/250N	WB	229	0,50	3,77	0,00	0,60	1,048	1,68	0,47	0,47	2,247
Collins	AT-2/250W	WB	224	0,50	3,80	0,00	0,60	1,012	1,67	0,47	0,47	2,151
2006	AT-2/1000N	WB	880	2,00	3,67	0,00	0,60	1,021	1,68	0,47	0,76	1,344
	AT-2/1000W	WB	942	2,00	3,68	0,00	0,60	1,091	1,68	0,48	0,77	1,424
	AT-2/3000	WB	2564	6,01	3,70	0,00	0,60	0,988	1,68	0,49	0,78	1,273
	AT-3/N1	WB	475	1,39	3,39	0,00	0,80	1,110	1,81	0,52	0,52	2,132
	AT-3/N2	WB	517	1,41	3,40	0,00	0,80	1,197	1,81	0,52	0,52	2,308
	AT-3/T1	WB	506	1,40	3,23	0,00	0,80	1,223	1,82	0,53	0,82	1,483
	AT-3/T2	WB	497	1,41	3,25	0,00	0,80	1,189	1,82	0,52	0,82	1,451
	AY1	WB	170,5	0,50	4,03	0,00	0,66	0,789	1,68	0,49	0,49	1,624
	AX7	WB	501,1	1,41	2,97	0,00	0,80	1,287	1,85	0,56	0,83	1,556
	AX6	WB	565,02	1,41	2,98	0,00	0,80	1,448	1,85	0,56	0,90	1,610
	AX8	WB	544,1	1,41	1,71	0,00	0,60	1,386	1,85	0,56	0,90	1,545
	AW1	WB	1170	2,34	6,25	0,00	0,60	0,948	1,62	0,44	0,62	1,529
	AW4	WB	1450	2,34	5,62	0,00	0,60	1,253	1,64	0,46	0,74	1,695
	AW8	WB	1600	2,34	8,75	0,00	0,80	1,378	1,63	0,46	0,74	1,875
Vaz Rodrigues	DR1a	P	1397	4,91	2,44	0,00	0,60	0,965	1,82	0,54	0,87	1,111
Muttoni	DR1b	WB	1025	4,37	2,48	0,26	0,60	1,006	1,82	0,54	0,87	1,153
& Olivier	DR1c	WB	910	4,94	2,48	0,12	0,60	0,709	1,82	0,55	0,88	0,807
2006	DR2a	WB	961	5,47	3,03	0,00	0,60	0,516	1,77	0,51	0,80	0,644
	DR2b	WB	857	4,64	3,03	0,28	0,60	0,684	1,77	0,53	0,82	0,831
	DR2c	WB	719	5,24	3,03	0,14	0,60	0,463	1,77	0,52	0,81	0,572
Jaeger	A1V1	WB	169,2	1,60	1,64	0,00	0,80	0,678	2,00	0,72	1,56	0,436
2002	A3V1	WB	265,6	1,60	1,70	0,00	0,80	1,025	2,00	0,76	1,50	0,682
2005	A4V1	WB	140,5	1,60	1,76	0,00	0,80	0,523	2,00	0,68	1,28	0,410
2007	A5V1	WB	222,1	1,60	1,76	0,00	0,80	0,826	2,00	0,75	1,37	0,605
	B1V1	WB	852	4,00	9,69	0,00	0,80	0,546	1,72	0,57	1,33	0,409
	B3V1	WB	1282	4,00	10,08	0,00	0,80	0,791	1,70	0,57	1,24	0,637
	B4V1	WB	804	4,00	10,47	0,00	0,80	0,479	1,69	0,57	1,13	0,423
	B5V1	WB	1170	4,00	10,47	0,00	0,80	0,696	1,69	0,55	1,12	0,622

*Annex 4: Comparison between experiments from slab shear database and NEN-EN 1992-1-1:2005*

Reference	Test	mode	$P_{exp}$ (kN)	$u$ (m)	$W$ (m <sup>2</sup> )	$e_{pu}$ (m)	$k_{pu}$	$v_E$ Mpa	$k$	$v_{min}$ (MPa)	$v_{pu}$ (MPa)	$v_E/v_{pu}$
Graf 1933	<b>1243 - a1</b>	WB	314	0,54	0,08	0,43	0,65	15,616	2,00	0,4	2,43	6,426
	<b>1243 - a2</b>	P	235	1,13	0,13	0,36	0,65	5,589	2,00	0,43	1,41	3,964
	<b>1243 - b1</b>	P	355	0,54	0,08	0,43	0,65	17,655	2,00	0,43	2,55	6,933
	<b>1243 - b2</b>	WB	206	0,57	0,08	0,43	0,65	10,066	2,00	0,46	2,65	3,794
	<b>1244 - a1</b>	WB	275	0,81	0,07	0,44	0,65	14,765	2,00	0,35	2,47	5,977
	<b>1244 - a2</b>	WB	196	1,13	0,13	0,36	0,65	5,202	2,00	0,36	1,25	4,147
	<b>1244 - b1</b>	WB	157	0,56	0,07	0,44	0,65	9,384	2,00	0,36	2,53	3,713
	<b>1244 - b2</b>	WB	147	0,97	0,10	0,39	0,65	5,314	2,00	0,37	1,70	3,131
	<b>1245 - a1</b>	P	333	0,61	0,07	0,44	0,65	18,709	2,00	0,48	3,20	5,840
	<b>1245 - a2</b>	P	257	1,13	0,13	0,36	0,65	6,686	2,00	0,48	1,62	4,128
	<b>1245 - b1</b>	P	196	0,56	0,07	0,44	0,65	11,296	2,00	0,48	3,20	3,531
<b>1245 - b2</b>	P/WB	206	0,97	0,10	0,39	0,65	7,299	2,00	0,48	2,16	3,385	
Richart	<b>S1 - 2</b>	P	342,5	2,21	0,49	0,54	0,60	2,851	2,00	0,5	1,09	2,611
Kluge	<b>S1 - 3</b>	P	391,4	2,21	0,49	0,06	0,60	1,530	2,00	0,5	1,09	1,401
1939	<b>S2 - 2</b>	P	369,2	1,25	0,16	0,22	0,60	4,559	2,00	0,53	2,83	1,608
de Cossio 1962	<b>A50-25A</b>	nn	283,23	1,00	2,33	0,00	0,70	1,117	1,89	0,53	0,53	2,093
	<b>A50-25B</b>	nn	256,96	1,00	2,32	0,00	0,70	1,016	1,89	0,53	0,53	1,911
R&F 1968	<b>S-15</b>	WB	151	1,52	2,92	0,00	0,80	0,369	1,86	0,51	0,51	0,722
Aster & Koch 1974	<b>11</b>	WB	267	2,00	7,94	0,00	0,80	0,267	1,63	0,36	0,36	0,739
	<b>16</b>	WB	406,7	2,00	14,61	0,00	0,80	0,271	1,52	0,36	0,36	0,752
	<b>2</b>	WB	218	2,00	3,27	0,00	0,80	0,436	1,89	0,47	0,47	0,921
	<b>12</b>	WB	330,2	2,00	7,94	0,00	0,80	0,330	1,63	0,38	0,38	0,866
	<b>3</b>	WB	222,5	2,00	3,27	0,00	0,80	0,445	1,89	0,48	0,48	0,933
	<b>8</b>	WB	287,1	2,00	7,94	0,00	0,80	0,287	1,63	0,41	0,41	0,705
	<b>9</b>	WB	260,6	2,00	7,94	0,00	0,80	0,261	1,63	0,33	0,33	0,800
	<b>10</b>	WB	261,6	2,00	7,94	0,00	0,80	0,262	1,63	0,33	0,33	0,801
<b>17</b>	WB	363,5	2,00	14,61	0,00	0,80	0,242	1,52	0,35	0,35	0,692	
Heger McGrath 1980	<b>SW9-0A</b>	WB	168	1,83	2,02	0,00	0,80	0,508	2,00	0,69	0,78	0,651
	<b>SW9-0B</b>	WB	155,5	1,83	2,09	0,00	0,80	0,456	2,00	0,69	0,77	0,591
	<b>SW9-6A-15</b>	WB	267,7	1,83	1,92	0,00	0,80	0,794	2,00	0,69	0,83	0,954
	<b>SW9-0B-15</b>	WB	270,7	1,83	1,92	0,00	0,80	0,812	2,00	0,69	0,83	0,981
	<b>SW9M-0A</b>	WB	155,7	1,83	2,17	0,00	0,80	0,440	2,00	0,69	0,77	0,572
	<b>SW9M-0B</b>	WB	174,3	1,83	2,03	0,00	0,80	0,526	2,00	0,69	0,78	0,674
	<b>SW9M-0A-15</b>	WB	299,8	1,83	1,92	0,00	0,80	0,880	2,00	0,69	0,84	1,052
	<b>SW9M-0B-15</b>	WB	308,1	1,83	1,90	0,00	0,80	0,989	2,00	0,69	0,80	1,241
	<b>SW14-0A</b>	WB	197,2	1,83	2,09	0,00	0,80	0,577	2,00	0,69	0,83	0,693
	<b>SW14-0B</b>	WB	195,9	1,83	2,03	0,00	0,80	0,589	2,00	0,69	0,84	0,700
	<b>SW18-0A</b>	WB	202,6	1,83	2,01	0,00	0,80	0,617	2,00	0,69	0,88	0,704
<b>SW18-0B</b>	WB	222,8	1,83	1,96	0,00	0,80	0,694	2,00	0,69	0,88	0,786	

*Annex 4: Comparison between experiments from slab shear database and NEN-EN 1992-1-1:2005*

Reference	Test	mode	$P_{exp}$	$u$	$W$	$e_{pu}$	$k_{pu}$	$v_E$	$k$	$v_{min}$	$v_{pu}$	$v_E/v_{pu}$
			(kN)	(m)	(m <sup>2</sup> )	(m)	Mpa	(MPa)	(MPa)			
Heger	<b>SW18-0A-15</b>	WB	378,9	1,83	1,92	0,00	0,80	1,187	2,00	0,69	0,90	1,319
McGrath	<b>SW18-0B-15</b>	WB	390,2	1,83	1,91	0,00	0,80	1,244	2,00	0,69	0,89	1,397
Cullington et al 1996	<b>on site</b>	?	440	2,00	1,34	0,00	0,60	0,856	1,88	0,68	0,68	1,266
	<b>lab 1</b>	WB	700	2,00	0,65	0,00	0,60	1,362	1,88	0,7	1,06	1,283
	<b>lab 2</b>	WB	1060	0,87	0,15	0,00	0,60	4,753	1,88	0,7	2,80	1,698
	<b>3bis</b>		174	2,22	0,53	0,00	0,70	0,969	2,00	0,55	0,84	1,157
	<b>6bis</b>	P	250	2,82	0,91	0,00	0,80	1,095	2,00	0,54	1,05	1,038
	<b>7</b>		165	2,22	0,53	0,00	0,70	0,918	2,00	0,43	0,87	1,061
	<b>7bis</b>		151	2,22	0,53	0,00	0,70	0,841	2,00	0,43	0,87	0,971
Olonisakin & Alexander 1999	<b>CB1(b)</b>	WB	258	1,50	1,09	0,00	0,80	1,433	2,00	0,56	1,14	1,262
	<b>CB2</b>	WB	260	1,50	1,09	0,00	0,80	1,444	2,00	0,56	1,14	1,272
	<b>RB1</b>	WB	246	1,50	1,09	0,00	0,80	1,367	2,00	0,56	1,14	1,203
	<b>RB2</b>	WB	256	1,50	1,09	0,00	0,80	1,422	2,00	0,56	1,14	1,252
Rombach & Latte 2008 2009	<b>VK1V1</b>	WB	690	4,33	1,89	0,00	0,60	0,733	1,96	0,57	1,03	0,710
	<b>VK2V1</b>	WB	678	4,24	1,81	0,00	0,60	0,762	1,98	0,66	1,19	0,642
	<b>VK3V1</b>	WB	672	3,94	1,56	0,00	0,60	0,915	2,00	0,68	1,27	0,721
	<b>VK3V3</b>	WB/P	898	3,70	1,37	0,00	0,60	1,453	2,00	0,71	1,15	1,264
	<b>VK4V1</b>	WB	487	3,61	1,31	0,00	0,60	0,843	2,00	0,65	1,23	0,684
										AVG	1,447	
										STD	1,220	
										COV	0,843	
										Char	-0,553	

*Annex 4: Comparison between experiments from slab shear database and NEN-EN 1992-1-1:2005*

**Annex 5: Results of North American slab bridges checked by the Quick Scan**

Section	$b$ (m)	$d_i$ (m)	$l_{span}$ (m)	$f_{ck,cube}$ (MPa)	$\rho_l$ (%)	$\nu_{Ed}$ (MPa)	$\nu_{Rd,c}$ (MPa)	uc EC	$\nu_{w,ASHTO}$ (MPa)	$\nu_{c,ASHTO}$ (MPa)	uc AASHTO
1 sup 1-2	9,574	0,317	10,287	21,021	1,122	0,765	0,578	1,325	0,332	0,783	0,424
1 sup 2-1	9,574	0,749	10,287	21,021	0,604	0,396	0,397	0,996	0,419	0,593	0,706
1 sup 2-3	9,574	0,711	14,021	21,021	0,604	0,399	0,398	1,004	0,422	0,572	0,738
2 sup 1-1	10,973	0,238	9,373	21,021	1,076	0,929	0,642	1,447	0,29	0,783	0,37
2 sup 2-1	10,973	0,786	9,373	21,021	0,628	0,323	0,399	0,808	0,356	0,715	0,498
2 sup 2-3	10,973	0,786	15,24	21,021	0,628	0,382	0,399	0,956	0,413	0,511	0,808
3 sup 1-2	10,973	1,486	22,86	21,021	0,171	0,309	0,259	1,193	0,399	0,329	1,214
4 sup 1-2	19,202	0,292	9,144	21,021	0,884	0,795	0,544	1,462	0,351	0,783	0,449
4 sup 2-1	19,202	0,648	9,144	21,021	0,187	0,439	0,314	1,399	0,431	0,465	0,927
4 sup 2-3	19,202	0,648	12,497	21,021	0,187	0,461	0,314	1,469	0,451	0,393	1,147
5 sup 1-2	11,43	0,699	19,298	21,021	0,645	0,575	0,411	1,399	0,4	0,501	0,799
5 sup 2-1	11,43	1,461	19,298	21,021	0,405	0,405	0,314	1,288	0,529	0,422	1,254
6 sup 1-2	18,898	0,699	20,282	21,021	0,762	0,625	0,435	1,439	0,425	0,615	0,692
6 sup 2-1	18,898	1,461	20,282	21,021	0,6	0,445	0,358	1,241	0,566	0,501	1,13
7 sup 1-2	9,754	0,446	13,153	21,021	0,66	0,655	0,451	1,453	0,394	0,715	0,552
7 sup 2-1	9,754	0,918	13,153	21,021	0,367	0,43	0,326	1,321	0,496	0,408	1,217
7 sup 2-3	9,754	0,918	17,678	21,021	0,367	0,412	0,326	1,266	0,476	0,34	1,401

Section	<i>b</i> (m)	<i>d<sub>i</sub></i> (m)	<i>l<sub>span</sub></i> (m)	<i>f<sub>ck,cube</sub></i> (MPa)	$\rho_l$ (%)	<i>v<sub>Ed</sub></i> (MPa)	<i>v<sub>Ed,c</sub></i> (MPa)	uc EC	<i>v<sub>n,AASHTO</sub></i> (MPa)	<i>v<sub>c,AASHTO</sub></i> (MPa)	uc AASHTO
8 sup 1-2	9,754	0,47	14,122	21,021	0,958	0,652	0,505	1,291	0,363	0,715	0,507
8 sup 2-1	9,754	1,08	14,122	21,021	0,558	0,385	0,365	1,054	0,462	0,501	0,924
8 sup 2-3	9,754	1,08	20,422	21,021	0,558	0,395	0,365	1,082	0,473	0,329	1,439
9 sup 1-2	12,04	0,66	17,732	21,021	0,585	0,586	0,402	1,457	0,38	0,501	0,758
9 sup 2-1	12,04	1,384	17,762	21,021	0,310	0,406	0,29	1,401	0,498	0,329	1,513
10 sup 1-2	12,497	0,293	9,347	21,021	0,89	0,802	0,544	1,474	0,374	0,783	0,478
10 sup 2-1	12,497	0,613	9,347	21,021	0,563	0,478	0,402	1,189	0,46	0,658	0,7
10 sup 2-3	12,497	0,613	12,497	21,021	0,563	0,493	0,402	1,226	0,48	0,572	0,839
11 sup 1-2	12,192	0,317	9,754	25,22	1,12	0,791	0,614	1,29	0,364	0,847	0,43
11 sup 2-1	12,192	0,699	9,754	25,22	0,565	0,451	0,418	1,079	0,446	0,711	0,627
11 sup 2-3	12,192	0,699	12,192	25,22	0,565	0,437	0,418	1,047	0,432	0,711	0,607
12 sup 1-2	13,868	0,419	5,969	21,02	0,38	0,406	0,38	1,069	0,378	0,88	0,429
12 sup 2-1	13,868	0,419	5,969	21,02	0,811	0,547	0,489	1,119	0,491	0,879	0,559
12 sup 2-3	13,868	0,419	7,62	21,02	0,811	0,592	0,489	1,212	0,513	0,879	0,584
13 sup 1-2	9,944	0,317	9,982	25,22	2,173	0,805	0,765	1,052	0,368	1,09	0,338
13 sup 2-1	9,944	0,699	9,982	25,22	0,846	0,462	0,478	0,966	0,451	0,846	0,532
13 sup 2-3	9,944	0,699	13,716	25,22	0,846	0,476	0,478	0,994	0,466	0,711	0,656

Total: QS-EC: 29 sections in 13 (all) bridges; QS-AASHTO: 8 sections in 7 bridges

## **Acknowledgements**

Obtaining a doctoral degree marks the end of my formal education, and therefore I am grateful for all individuals and institutions that have educated me. From the Stedelijke Academie voor Muziek, Woord en Dans in Lier, to my alma mater Vrije Universiteit Brussel, and on to the Georgia Institute of Technology – all have fostered my curiosity and supported my learning.

The research in this thesis was carried out at Delft University of Technology, in the research group of Concrete Structures of Civil Engineering and Geosciences. Funding for this project was provided by the Dutch Ministry of Infrastructure and the Environment. I gratefully acknowledge their support.

I would like to express my gratitude to my supervisor Prof. Joost Walraven for giving me the opportunity to carry out this research project and his guidance in writing this dissertation. My thesis committee members guided and helped me to improve the manuscript of this thesis. I would like to especially thank Prof. Regan for all time and effort spent at helping me sharpen my ideas concerning the Modified Bond Model, the description of the experiments and the analysis of the experiments with respect to the Eurocodes, and Prof. Vrouwenvelder for his guidance with regard to the reliability analysis and the mechanics behind the Bond Model.

This work would not have been possible without two persons that were most crucial to its success: my daily supervisor and copromotor Dr. Cor van der Veen and technician Albert Bosman. It's been a joy and honour to work with you.

From the laboratory, I would also like to acknowledge Edwin and Ton for preparing the cube specimens from the concrete casts and testing these, and Ruben for making the formwork. Moreover, many colleagues rolled up their sleeves and helped me out during the casts, and I truly appreciate their time and effort.

For the application of the experimental results to practice, I had the opportunity to implement my findings into the deliverables of the project on the Existing Bridges in which TNO and the Ministry of Infrastructure and the Environment are involved. I'm grateful for all their suggestions and critical questions. Special thanks go to Dr. Ane de Boer for his input and thoughts on the practical application, and to Jan Gijbbers for the interpretation of the experimental results with regard to the codes.

My colleagues, fellow PhD students and lab technicians from the Stevin II Laboratory will be remembered for all the lunches, cake times and coffee breaks. To Yuguang, Sonja, Kees, Albert and Patrick: thanks for turning the lunch breaks into a real break. I also enjoyed discussing the topic of shear with my fellow PhD students very much. Moreover, I had the pleasure to share office with René Braam who brought stories from practice, lessons learned in teaching, interesting papers and art history books.

### *Acknowledgements*

I am grateful for having had the opportunity to travel to conferences and learn from the international experts in my field. My personal learning network consists of the international concrete research community with whom I interacted at conferences as well as of fellow PhD students from various disciplines who shared their best practices with me online through blogs and Twitter discussions – you are too many to name, but you all have my sincerest gratitude and appreciation.

To my friends and family, especially to my parents and my sister Olivia, I want to apologize for not spending enough time with you while I was completely buried in my research, but know that your support has been the foundation of all my endeavours. Special thanks to Karen and Kathleen for always being there for me. Last but not least, I would like to thank my husband Andres for his patience while I was abroad for four years, his encouragement and unwavering love.

## Curriculum Vitae

Name: Eva Olivia Leontien Lantsoght  
Date of birth: August 10, 1985  
Place of birth: Lier, Belgium



1997 - 2003 Secondary School: Regina Pacis Hove, Hove, Belgium  
ASO Diploma (Latin-Mathematics), 2003, magna cum laude

2003 - 2008 Vrije Universiteit Brussel, Brussels, Belgium  
Thesis on buckling of reinforced concrete columns  
Degree of Engineer, 2008, magna cum laude

2008 - 2009 Georgia Institute of Technology, Atlanta, GA, USA  
Research project on punching in reinforced concrete slabs  
MS in Structural Engineering, 2008. GPA = 3,87

2008 - 2009 Fulbright Fellowship

2008 - 2009 Belgian American Educational Foundation Fellowship

2009 - 2013 Concrete Structures, Faculty of Civil Engineering and Geosciences, Delft  
University of Technology, the Netherlands  
PhD research on shear in reinforced concrete slabs

### Scientific output of this research project

Kalsbeek, I., Arragon, M. v., Vries, R. d., Ghossein, A., Lourens, K., Plas, A. v. d., Heinsbroek, A., Yip, C., Semiari, A., Tian, K., Kabos, M., Griemink, A., Oortmerssen, L. v., Autar, N., Kraus, J., Reenen, K. v., Smaling, H., Gemeren, W. v., Straten, R. v., Teeuwen, B., Joosten, S., Altinga, N., Markerink, S., Vries, W. d., Lantsoght, E.O.L., and Hoogenboom, P., 2011, "Staafwerkmodellen getoetst." *Cement*, 7(2011), 9 pp.

Lantsoght, E.O.L., van der Veen, C., and Walraven, J., 2010, "Shear tests of reinforced concrete slabs with concentrated loads near to supports." *8th fib international PhD Symposium in Civil Engineering*, G. Fisher, M. Geiker, O. Hededal, L. Ottosen, and H. Stang, eds., DTU Byg, Technical University of Denmark, Kgs. Lyngby, Denmark, pp. 81-86.

Lantsoght, E.O.L., van der Veen, C., and Walraven, J., 2010, "Experimental study of reinforced concrete bridge decks under concentrated loads near to supports." *Structural Faults and Repair, 13th International Conference and Exhibition*, Edinburgh, UK, 12 pp.

## Curriculum Vitae

Lantsoght, E.O.L., van der Veen, C., and Walraven, J., 2011, "Experimental Study of Shear Capacity of Reinforced Concrete Slabs." *ASCE Structures Congress*, Las Vegas, NV, pp. 152-164.

Lantsoght, E.O.L., van der Veen, C., and Walraven, J., 2011, "Experimental Study of Shear in Reinforced Concrete One-Way Slabs subjected to Concentrated Loads." *fib symposium Prague*, pp. 551-554 or 10 pp. (long digital version)

Lantsoght, E.O.L., 2011, *Shear tests of reinforced concrete slabs: experimental data of undamaged slabs*, Stevin Report 25.5-11-07, Delft University of Technology, The Netherlands, 502 pp.

Lantsoght, E.O.L., 2011, *Shear tests of reinforced concrete slabs: experimental data of residual capacity of slabs*, Stevin Report 25.5-11-08, Delft University of Technology, The Netherlands, 334 pp.

Lantsoght, E.O.L., 2012, *Tests of reinforced concrete slabs subjected to a line load and a concentrated load*, Stevin Report 25.5-12-12, Delft University of Technology, The Netherlands, 271 pp.

Lantsoght, E.O.L., 2012, *Voortgangsrapportage: Experimenten op platen in gewapend beton onder combinatiebelasting: Deel II: analyse van de resultaten*, Stevin Report 25.5-12-13, Delft University of Technology, The Netherlands, 98 pp.

Lantsoght, E.O.L., 2012, *Voortgangsrapportage: Experimenten op platen in gewapend beton: Deel II: analyse van de resultaten*, Stevin Report 25.5-12-10, Delft University of Technology, The Netherlands, 289 pp.

Lantsoght, E.O.L., 2012, *Shear in reinforced concrete slabs under concentrated loads close to the support – Literature review*, Stevin Report 25.5-12-11, Delft University of Technology, The Netherlands, 260 pp.

Lantsoght, E.O.L., van der Veen, C., Gijsbers, F.B.J., 2012, *Achtergrondrapport bij spreadsheet*, Stevin Report 25.5-12-14, Delft University of Technology, The Netherlands, 50 pp.

Lantsoght, E.O.L. 2012, *Probabilistic approach to determine the increased shear capacity in reinforced concrete slabs under a concentrated load*, Stevin Report 25.5-12-15, Delft University of Technology, The Netherlands, 48 pp.

Lantsoght, E.O.L. 2012, *Background to Modified Bond Model*, Stevin Report 25.5-12-16, Delft University of Technology, The Netherlands, 66 pp.

Lantsoght, E.O.L., van der Veen, C., Walraven, J., 2012, "Shear capacity of slabs and slab strips loaded close to the support." *ACI SP287 – Recent Developments in Reinforced Concrete Slab Analysis, Design and Serviceability*, pp. 5.1-5.17.

Lantsoght, E.O.L., van der Veen, C., and Walraven, J., 2012, "Residual Capacity from aggregate interlock of cracked reinforced concrete slab bridge." *IABMAS 2012, 6<sup>th</sup> international conference on Bridge Maintenance, Safety and Management*, Villa Erba, Lake Como, Italy, pp. 3368-3375

Lantsoght, E.O.L., 2012, "Shear tests of reinforced concrete slabs and slab strips under concentrated loads." *9<sup>th</sup> fib International PhD Symposium in Civil Engineering*, Karlsruhe, Germany, pp. 3-8.

Lantsoght, E.O.L., van der Veen, C., and Walraven, J., 2012, "Shear assessment of solid slab bridges." *ICCRRR 2012, 3rd International Conference on Concrete Repair, Rehabilitation and Retrofitting*, Cape Town, South Africa, pp. 827-833.

Lantsoght, E.O.L., van der Veen, C., Walraven, J., de Boer, A., 2012, "Spreiding puntlasten plaatviaducten." *Cement* 4(2012), pp. 46-50.

Lantsoght, E.O.L., van der Veen, C., Walraven, J., de Boer, A., 2013, "Shear assessment of reinforced concrete slab bridges" *Transportation Research Board 92<sup>nd</sup> Annual Meeting Compendium of Papers*, Washington DC, 17 pp.

Lantsoght, E.O.L., van der Veen, C., Walraven, J., 2013, "Shear capacity of slabs under a combination of loads." *fib Symposium 2013 Engineering a Concrete Future Technology, Modeling & Construction*, Tel Aviv, Israel, pp. 297-300.

Lantsoght, E.O.L., van der Veen, C., Walraven, J., de Boer, A., 2013 "Shear assessment of reinforced concrete slab bridges" *International IABSE Conference, Assessment, Upgrading and Refurbishment of Infrastructures*, Rotterdam, The Netherlands, pp. 76-77.

Lantsoght, E.O.L., van der Veen, C., Walraven, J., 2013, "Shear capacity of reinforced concrete solid slabs subjected to a combination of loads" *International IABSE Conference, Assessment, Upgrading and Refurbishment of Infrastructures*, Rotterdam, The Netherlands, pp. 526-527.

Lantsoght, E.O.L., van der Veen, C., Walraven, J., 2013, "Prolonging the service life of existing reinforced concrete slab bridges through experimental studies on the shear capacity", *First International Conference on Concrete Sustainability, ICCS 2013*, Tokyo, Japan (in press)

Lantsoght, E.O.L., van der Veen, C., Walraven, J., de Boer, A., 2013, "Shear assessment practice for reinforced concrete slab bridges in the Netherlands " *30<sup>th</sup> International Bridge Conference*, Pittsburgh, USA (in press)

Lantsoght, E.O.L., de Boer, A., van der Veen, C., Walraven, J., 2013, "Distribution of peak shear stresses in finite element models of reinforced concrete slabs," *SEMC 2013, Fifth International Conference on Structural Engineering, Mechanics and Computation*, Cape Town, South Africa (in press)

Lantsoght, E.O.L., van der Veen, C., Walraven, J., de Boer, A., 2013, "Applying Experimental Results to the Shear Assessment Method for Solid Slab Bridges" *Concrete 2013*, Brisbane, Australia (in review)

Lantsoght, E.O.L., Van der Veen, C., Walraven, J., 2013, "Shear in One-way Slabs under a Concentrated Load close to the support." *ACI Structural Journal*, Vol. 110, No. 2, p. 275-284.

### *Curriculum Vitae*

Lantsoght, E.O.L., van der Veen, C., Walraven, J., de Boer, A. 2013 “Shear Assessment of Reinforced Concrete Slab Bridges”. *Structural Engineering International*, Issue 4 (in press).

Lantsoght, E.O.L., van der Veen, C., Walraven, J., 2013 “Transverse Load Redistribution and Effective Shear Width in Reinforced Concrete Slabs”. *Heron* (in progress).

Lantsoght, E.O.L., van der Veen, C., Walraven, J., de Boer, A., 2014, “Recommendations for the Shear Assessment of Reinforced Concrete Solid Slab Bridges” *IABMAS 2014*, Shanghai, China (in progress)

Prochazkova, Z., Lantsoght, E.O.L., 2011, *Material properties – Felt and Reinforcement For Shear test of Reinforced Concrete Slab*. Stevin Report 25.5-11-11, Delft University of Technology, The Netherlands, 28pp.

van der Veen, C., Lantsoght, E.O.L., 2010, *Opinie TU Delft betreffende draagvermogen St. Sebastiaansbrug*, Stevin Report 25.5-10-14. Delft University of Technology, The Netherlands, 47pp.